Coordination Cages for Fullerene Encapsulation

This dissertation is submitted for the degree of

“Doctor rerum naturalium”

TU Dortmund

Fakultät für Chemie und Chemische Biologie

Shota Hasegawa

Dortmund, November 2022

Principal advisor: **Prof. Dr. Guido H. Clever**
Department of Chemistry and Chemical Biology,
TU Dortmund University

Coexaminer: **Junior. Prof. Dr. Max M. Hansmann**
Department of Chemistry and Chemical Biology,
TU Dortmund University

Submission Date: 16.11.2022

オヤジの栄光時代はいつだよ…全日本の時か？

俺は……俺は今なんだよ!!

桜木花道, SLAM DUNK

Abstract

Since the discovery of Buckminster fullerene C_{60} in 1985, carbon materials have been intensively studied. Carbon allotropes such as fullerenes, carbon nanotubes, diamonds, and graphite have been proven to have a splendid potential for applications in many kinds of devices such as quantum computers, organic solar cells, and transistors.

Among those carbon allotropes, fullerenes stand out by their uniform sizes which allow for precise structural control at the molecular level. In addition to the versatility in molecular engineering, the small size of fullerenes allows to study them inside a nanoscopic object, e.g. carbon nanotubes.

Fullerenes under nano-confinement are known to show different physical and chemical properties such as chain-like polymer formation inside carbon nanotubes. In addition, research on assembled fullerenes is of great interest across a variety of fields. The assembly of fullerenes in various forms such as (liquid)crystals, films and solutions contributes to the development of materials with tunable properties.

Furthermore, incorporation of guests in between the assembled fullerenes endows the assembly with electronic perturbation. To name an example, fullerides are known to show superconductivity at relatively high temperature. Fullerides are crystals of a salt comprised of fullerene radical anions and alkali metals. The latter occupy the vacant sites in between the fullerene radical anions which are arranged in a face-centered cubic packing pattern.

To gain comprehensive understanding of both nano-confinement effects and incorporation of guests in between C_{60}s, coordination cages are one of the most appropriate host candidates. Coordination cages are synthesized via metal-mediated self-assembly of organic ligands. The properties of the inner cavities are often inherited from the properties of the organic ligands. Besides, some coordination cages can encapsulate multiple guest molecules. Owing to those features, coordination cages are well suited hosts for the investigation of fullerenes under nano-confinement as well as guest-incorporation in between well-aligned C_{60} assemblies. Therefore, this work has been focusing on the development of coordination cages designed for fullerene(s) C_{60} encapsulation and the investigation of the physical and chemical properties of the encapsulated fullerene(s) based on two keywords, nano-confinement and hierarchical assembly.

In this dissertation, the synthesis of triptycene-based organic ligands and the self-assembly of the ligands and Pd(II), as well as encapsulation of C_{60} molecule(s) inside

the resulting cages are shown. A cationic Pd_2L_4 coordination cage can encapsulate C_{60} quantitatively inside the cavity surrounded by the triptycene backbone. The coordination cage was found to stabilize rather unstable C_{60} radical anion for a longer period (up to 1 month) inside its cavity.

Furthermore, the guest encapsulation scope of the Pd_2L_4 coordination cage has been investigated. The coordination cage was found to encapsulate not only C_{60}, but also two corannulene molecules and various C_{60} derivatives. The simple addition of CS_2 was found to liberate the entrapped C_{60} derivative, $PC_{61}BM$, in a non-disruptive manner. A repetitive uptake and release of $PC_{61}BM$ using the coordination cage was demonstrated.

In addition to the host-guest capability, the Pd_2L_4 coordination cage was found to act as a protecting group to synthesize [η^2-$C_{60}(Pd(0)L)_n$] (n=1,2) complexes. In the confined environment, [η^2-$C_{60}(Pd(0)L)_n$] is prevented from polymerization, inevitable in the free form. In order to stabilize the resulted unstable [η^2-$C_{60}(Pd(0)L)_n$], an organic ligand based on thianthrene was synthesized. The thianthrene-based ligand was found to undergo cage-to-cage transformation from a Pd_3L_6 ring to a Pd_2L_4 cage upon encapsulation of C_{60}.

Beside such Pd_2L_4 coordination cage, a pill-shaped coordination cage capable of encapsulating two molecules of C_{60} within its cavities has been synthesized. The pill-shaped coordination cage was synthesized by bridging two bowl-shaped coordination cages with two 2,6-naphthalene dicarboxylates. Owing to the good alignment of two C_{60}s inside the coordination cage, investigations of the chemistry within a nanoscopic space surrounded by the *outer* surface of the encapsulated C_{60}s were performed. That nanoscopic space can accommodate a single corannulene molecule resulting in the formation of a charge-transfer complex between the entrapped C_{60} and corannulene. In addition, within the nanoscopic space, the Diels-Alder reaction between C_{60} and anthracene takes place quantitatively at a higher reaction rate compared to naked C_{60} and anthracene. Further, we elucidated the unique topochemical-like reaction inside the pill-shaped cage initiated by the Diels-Alder and retro Diels-Alder reactions with 9,10-dimethylanthracene and the encapsulated C_{60}s.

Up to now, a variety of coordination cages which can encapsulate fullerene(s) have been synthesized. Based on such well-established molecular designs and knowledges, the investigations of the encapsulated C_{60}(s) could be conducted such as stabilization of $C_{60}^{\bullet-}$, recycling encapsulation and release of $PC_{61}BM$, synthesis of [η^2-$C_{60}(Pd(0)L)_n$] (n=1,2) complexes, and host-guest chemistry in between the well-aligned C_{60}s.

Zusammenfassung

Seit der Entdeckung von Buckminster-Fulleren C_{60} im Jahr 1985 werden Kohlenstoffmaterialien intensiv untersucht. Kohlenstoffallotrope wie Fullerene, Kohlenstoff-Nanoröhren, Diamant und Graphit haben sich für die Anwendung in vielen Arten von Geräten und elektronischen Bauteilen wie Quantencomputern, organischen Solarzellen und Transistoren als hervorragend geeignet erwiesen.

In der Familie der Kohlenstoff-Allotrope zeichnen sich die Fullerene durch ihre einheitliche Größe aus, die eine präzise Strukturkontrolle bei Reaktionen auf molekularer Ebene ermöglicht. Neben der Vielseitigkeit ihres Einsatzes in der Molekulartechnik kann wegen der geringen Größe der Fullerene auch ihr Verhalten innerhalb nanoskopischer Objekte, wie z. B. Kohlenstoff-Nanoröhren, untersucht werden.

Es ist bekannt, dass Fullerene im nano-begrenzten Raum unterschiedliche physikalische und chemische Eigenschaften aufweisen. Beispielsweise bilden sie innerhalb von Kohlenstoff-Nanoröhren kettenartige Polymere. Darüber hinaus ist die Forschung an assemblierten Fullerenen in unterschiedlichsten Bereichen von großem Interesse. Die Assemblierung von Fullerenen zu verschiedenartigen Systemen, wie (Flüssig-)Kristallen, Filmen und Lösungen, trägt zur Entwicklung von Geräten bei, die diese Eigenschaften der Fullerene nutzen.

Darüber hinaus können durch den Einbau von „Gästen“ zwischen die assemblierten Fullerene die Eigenschaften dieser Assemblierungen moduliert werden. Beispielsweise sind die sog. Fulleride dafür bekannt, dass sie bei relativ hohen Temperaturen Supraleitfähigkeit zeigen. Fulleride sind Kristalle eines Salzes, das aus Fulleren-Radikalanionen und Alkalimetallen besteht. Letztere besetzen die freien Plätze zwischen den Fulleren-Radikalanionen, die in einem kubisch flächenzentrierten Gitter angeordnet sind.

Um ein umfassendes Verständnis sowohl für Effekte im nano-begrenzten Raum als auch für den Einbau von Gästen zwischen geordneten C_{60}-Fullerenen zu erlangen, zählen Koordinationskäfige zu den sehr gut geeigneten Kandidaten für Wirt-Systeme. Koordinationskäfige werden durch die metallvermittelte Selbstassemblierung von organischen Liganden und Metallen synthetisiert. Die Eigenschaften der Kavitäten der Käfige entsprechen häufig denen der organischen Liganden. Einige Koordinationskäfige können auch mehrere Gastmoleküle aufnehmen. Aufgrund dieser Eigenschaften sind Koordinationskäfige sowohl für Untersuchungen von Fullerenen im nano-begrenzten Raum als auch hinsichtlich ihrer Assemblierung geeignet. Daher konzentriert sich diese Arbeit auf die Entwicklung von Koordinationskäfigen, die Fulleren(e) (C_{60}) einlagern können und auf die Untersuchung der physikalischen und

chemischen Eigenschaften von eingelagertem/eingelagerten Fulleren(en) (C_{60}), unter dem Blickwinkel „Nano-Begrenzung“ und „Assemblierung“.

In dieser Dissertation werden die Synthese von organischen Liganden auf Triptycenbasis, die Selbstassemblierung der Liganden mit Pd(II) sowie die Einkapselung von C_{60}-Molekülen innerhalb der Kavitäten der resultierenden Käfige beschrieben. Es zeigte sich, dass ein kationischer Pd_2L_4-Koordinationskäfig das eher instabile C_{60}-Radikalanion über einen längeren Zeitraum (bis zu einem Monat) in seinem Hohlraum stabilisieren kann. Darüber hinaus wurde die Kapazität des Pd_2L_4-Koordinationskäfigs bzgl. der Einlagerung von Gästen untersucht. Es konnte gezeigt werden, dass der Koordinationskäfig nicht nur C_{60} sondern auch zwei Corannulen Moleküle sowie diverse Fulleren-Derivate einlagert. Die Zugabe von CS_2 führte zur Freisetzung des eingelagerten Fulleren-Derivats $PC_{61}BM$ unter Beibehaltung der Integrität des Käfigs. Es konnte gezeigt werden, dass die Aufnahme von $PC_{61}BM$ in den Käfig und seine Freisetzung wiederholbar sind.

Ferner wurde festgestellt, dass der Pd_2L_4-Koordinationskäfig als Schutzgruppe bei der Synthese von [η^2-$C_{60}(Pd(0)L)_n$] (n=1,2) -Komplexen fungiert. Im begrenzten Raum wird dadurch die Polymerisation von η^2-$C_{60}Pd(0)_n$ verhindert, die ohne die Käfig-Schutzgruppe nicht zu vermeiden ist. Um das dabei gebildete η2-$C_{60}Pd(0)_n$ zu stabilisieren, wurde ein organischer Ligand auf Thianthren-Basis synthetisiert. Bei Zugabe von Pd(II) bildet sich ein Pd_3L_6 Ring, welcher bei Einlagerung von C_{60} infolge einer Käfig-zu-Käfig-Transformation in Pd_2L_4 umgewandelt wird.

Neben den beschriebenen Pd_2L_4 Koordinationskäfigen gelang die Synthese eines pillenförmigen Käfigs, der in der Lage ist, zwei C_{60}-Moleküle einzulagern. In diesem Käfig sind zwei schüsselförmige Koordinationskäfige durch zwei 2,6-Naphthalen-dicarboxylat-Linker-Einheiten verbunden. Dank der geeigneten Ausrichtung von zwei C_{60}-Molekülen innerhalb des Koordinationskäfigs konnten Untersuchungen zur Chemie in einem nanoskopischen Raum, der von den Außenflächen der eingelagerten C_{60}-Moleküle umgeben ist, durchgeführt werden. In diesem nanoskopischen Raum kann ein einzelnes Corannulen-Molekül binden, wobei sich ein Charge-Transfer-Komplex zwischen dem eingekapselten C_{60} und Corannulen bildet. Zusätzlich wurde gezeigt, dass im nanoskopischen Raum die Diels-Alder-Reaktion zwischen C_{60} und Anthracen quantitativ und mit höherer Reaktionsgeschwindigkeit abläuft als bei der Reaktion von freiem C_{60} mit Anthracen.

Bisher wurde bereits eine Vielzahl von Koordinationskäfigen synthetisiert, die Fullerene einlagern können. Die meisten Untersuchungen zu solchen Koordinationskäfigen konzentrierten sich jedoch nur auf das Phänomen der Einkapselung. Daher können die in dieser Arbeit gezeigten Forschungsergebnisse den Weg für die Untersuchung von Wirt-Gast-Komplexen mit Fullerenen ebnen, die über deren bloße Einlagerung hinausgehen.

TABLE OF CONTENTS

1 General Introduction

1.1 The Era of Carbon

Carbon is one of the most prevalent elements in a variety of molecules. Modern society produces energy by burning fossil fuels comprised of (hydro)carbons. Meanwhile, as a result of the production of the energy, carbon atoms are transformed into carbon dioxide (CO_2) which causes global warming, the biggest issues mankind is facing. Carbon can generate sp, sp^2 and sp^3 hybridized orbitals by forming covalent bonds. Owing to the diverse hybridization modes, carbon can form many different allotropes e.g. diamond, fullerene, carbon nanotube, and graphene (**Figure 1.1.1**). Carbon allotropes are studied for their potential use in a variety of devices in the future. From both aspects of global warming and the potential of carbon materials, the 21st century may be named the era of carbon.

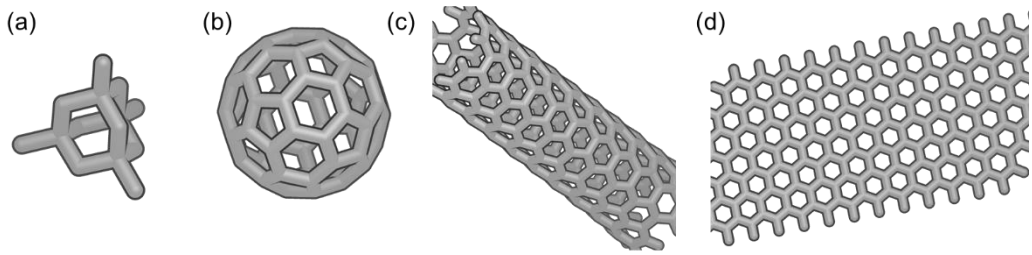

Figure 1.1.1 Structures of representative allotropes of carbon (a) diamond (b) fullerene C_{60} (c) carbon nanotube and (d) graphene

Because of the peculiar abilities such as electrical and thermal conductivities, carbon allotropes have become an appealing field of research for both synthetic and material chemists.[1,2] The intense research about carbon materials has begun since the discovery of Buckminster-fullerene C_{60}.[3] Fullerenes and their derivatives show electron accepting and transporting abilities which have been exploited in organic photovoltaics.[4,5] Stimulated by the discovery of C_{60}, carbon nanotubes were later discovered by an arc-discharge evaporation method in 1991.[6] The carbonaceous tubes are light yet extremely strong materials.[7,8] In 2004, single graphite layers, so called graphene, were prepared and the physical properties have been extensively investigated since then.[9] Graphene is known for its ambipolar field effect, quantum Hall effect and so forth.[10] As strongly represented by the attribution of the Nobel prizes

in 1996 and 2010 for the discoveries of fullerene C_{60} and graphene, respectively, countless attention has been paid to those novel materials consisting of carbon atoms only. In fact, new synthetic carbon materials have been continuously reported.[11]

1.2 Fullerenes

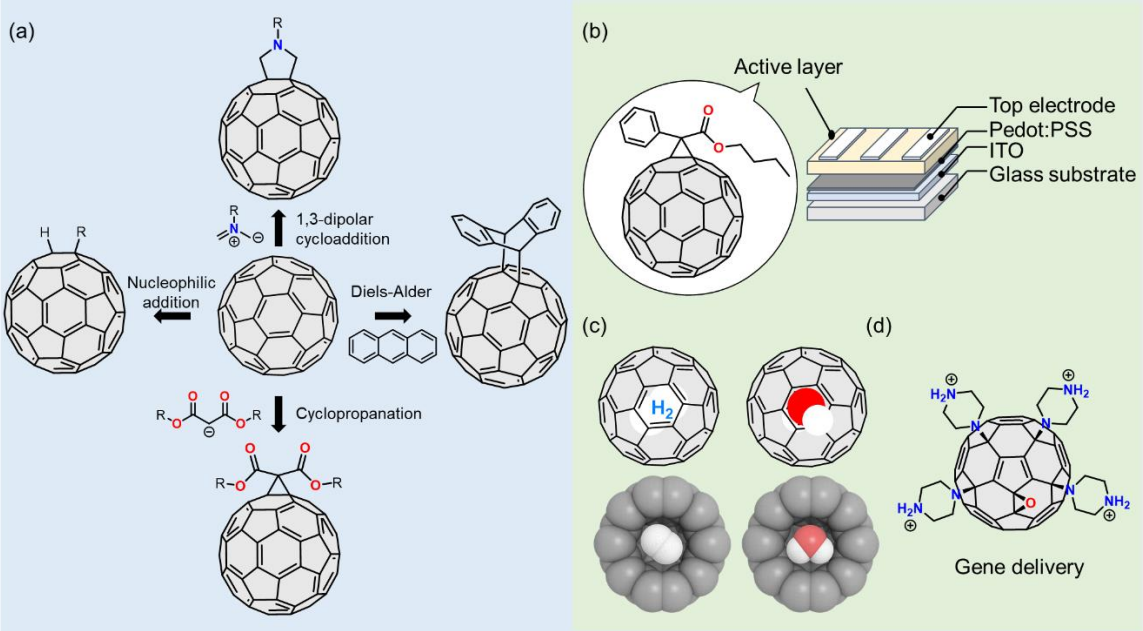

Figure 1.2.1 (a) Variety of examples of functionalization of C_{60}, (b) Structure of bulk heterojunction organic solar cell devices[12] with $PC_{61}BM$ as an electron accepting material, (c) Structures of endohedral-fullerene C_{60} encapsulating H_2[13] and H_2O[14], (d) Structure of C_{60} derivative utilized for gene delivery[15]

One of the biggest differences of fullerenes from the other carbon allotropes is the facileness of its molecular engineering. Unlike other carbon materials such as carbon nanotubes or graphene, fullerenes can be obtained in a uniform size and structure.[16] In addition, fullerenes can be solubilized in organic solvents in contrast to graphene or carbon nanotubes. While control of the length and the diameter of carbon nanotubes is hard, separation methods for many different fullerenes have been already reported.[17] Among fullerenes, C_{60} is the most abundant, and thus, best studied fullerenes so far. C_{60} can be handled as a single molecule which is beneficial for a better understanding of its physical and chemical properties. Furthermore, many chemical modifications of C_{60} have been reported so far which opened the access to functionalized C_{60} derivatives (**Figure 1.2.1a**).[18–20] Owing to the development of

functionalization of C_{60}, applications of C_{60} derivatives varied into photovoltaics,[4,12,21] single molecular storage,[13,14] and even biomedicine (**Figure 1.2.1b-d**).[22] Beside the aspect of molecular engineering, C_{60} presents an ideal size to be investigated under confinement contrary to carbon nanotubes or graphene. Upon the establishment of the mass production of C_{60} by Krätschmer and Hoffman[23], encapsulation of C_{60} inside a variety of hosts have been investigated.

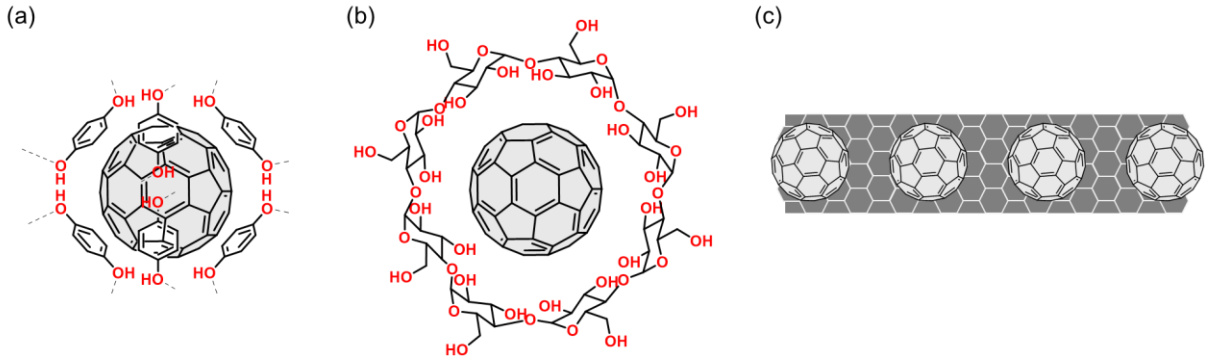

Figure 1.2.2 (a) 3:1 complex of hydroquinones and C_{60} (b) host-guest complex of C_{60} and γ-cyclodextrin and (c) illustration of carbon nano-peapod [24]

The first example of C_{60} adsorption inside a host was reported by Ermer et al..[25] Ermer co-crystalized hydroquinone and C_{60} to obtain such a host-guest complex in which C_{60} sits in a space surrounded by six hydroquinones connected via a hydrogen-bonding network (**Figure 1.2.2a**). A subsequent example of encapsulation of C_{60} was reported in 1992 by Wennerström.[26] Wennerström utilized *γ*-cyclodextrin to capture C_{60} into the hydrophobic cavity of the host (**Figure 1.2.2b**). Among many reports on encapsulation of C_{60}, one of the biggest achievements was the observation of a carbon peapod, a molecular composite of C_{60} and single walled carbon nanotube, reported by Luzzi and Smith (**Figure 1.2.2c**).[24] In the structure of the carbon peapod, C_{60}s are filling the hollow cavity of the carbon nanotube. Carbon peapods can be considered as a new class of carbon material as some of them display different physical properties from both the carbon nanotube and C_{60}. In addition, some reports have shown that trapped C_{60}s inside a carbon nanotube display different physical and chemical properties.[27] For instance, a linear chain of C_{60}s connected via covalent bonds displaying metallic characters have been reported by Achiba and co-workers.[28] The C_{60}-chain can be synthesized by doping potassium to nano-peapods and exists only in the carbon nanotube. Note, that the topology of the C_{60}-chains should be defined by the inner environment of the carbon nanotube. Such control of the topology would

have been difficult without the template effect by the carbon nanotube owing to the spherical structure of C_{60} with the same reactivity of all the bonds.[29] As can be seen in those examples, C_{60} under nano-confinement is an intriguing object to be investigated.

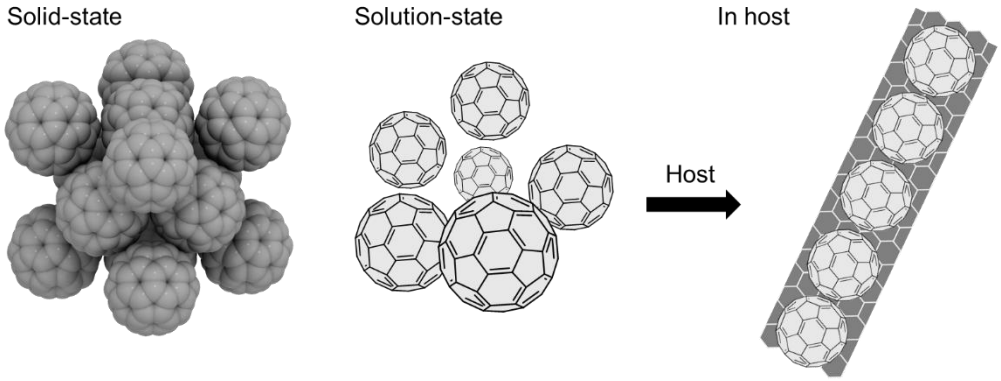

Figure 1.2.3 C_{60} arrays in solid-state, solution-state, and inside host

In addition, aligned C_{60}s are of great interest as well. Due to the electron accepting and transporting abilities of C_{60}, assemblies of C_{60} have gained attentions to develop various functional arrays.[30–32] For instance, an embedded manner of C_{60}/C_{60} derivatives plays a crucial role to achieve higher electron mobility and efficiency in electronic devices.[33,34] A key feature resulting from such a morphological control of fullerenes is to manipulate weak interactions. Self-assembled pristine C_{60} and its derivatives have been investigated in various forms such as (liquid)crystals, films, fibres and so forth.[30-32] Introduction of chemical pendants on C_{60} is often required to realize such assemblies due to scarce interactions between pristine C_{60}s. Thus, investigations of intact C_{60}s in an ordered-form have been done mostly in the solid state.[35] Pristine C_{60} is known to crystalize into face-centered-cubic Bravais lattice (**Figure 1.2.3**).[36] When C_{60} is treated with an alkali metal, a material showing superconductivity can be obtained. The resulting material in the crystalline state is called fulleride. Fullerides can be regarded as salts composed of C_{60} anions and alkali metal cations as a result of electron transfer from the doped alkali metals to C_{60}. In the solid-state structure of fullerides, alkali metal cations occupy the vacant sites of C_{60} crystals in the cubic crystal system.[37] Furthermore, some fullerides are superconductive at a relatively high temperature.[38] Thus, fullerides shed light on the potential of incorporation of guests in between aligned C_{60}s for material development. Spurred by these properties, examples of incorporation of guest molecules, such as

haloform, ethylene, carbon disulphide and so on, within assembled C_{60}s have been reported.[39–46] However, such investigation is, again, limited in the solid-state in most of the cases. Assembling C_{60} in solution has been hampered by the scarce interactions between C_{60}s. One possibility to deploy C_{60}s in a precise arrangement in solution could be the utilization of host molecules like molecular peapods (**Figure 1.2.3**). Therefore, it is an intriguing topic to synthesize a host enabling to conduct research on guest incorporation in between C_{60}-assembly in solution. Amongst host molecules enabling investigations of C_{60}(s) both under “nano-confinement” and “assembly”, coordination cages are one of the most suitable candidates.

1.3 Coordination Cages

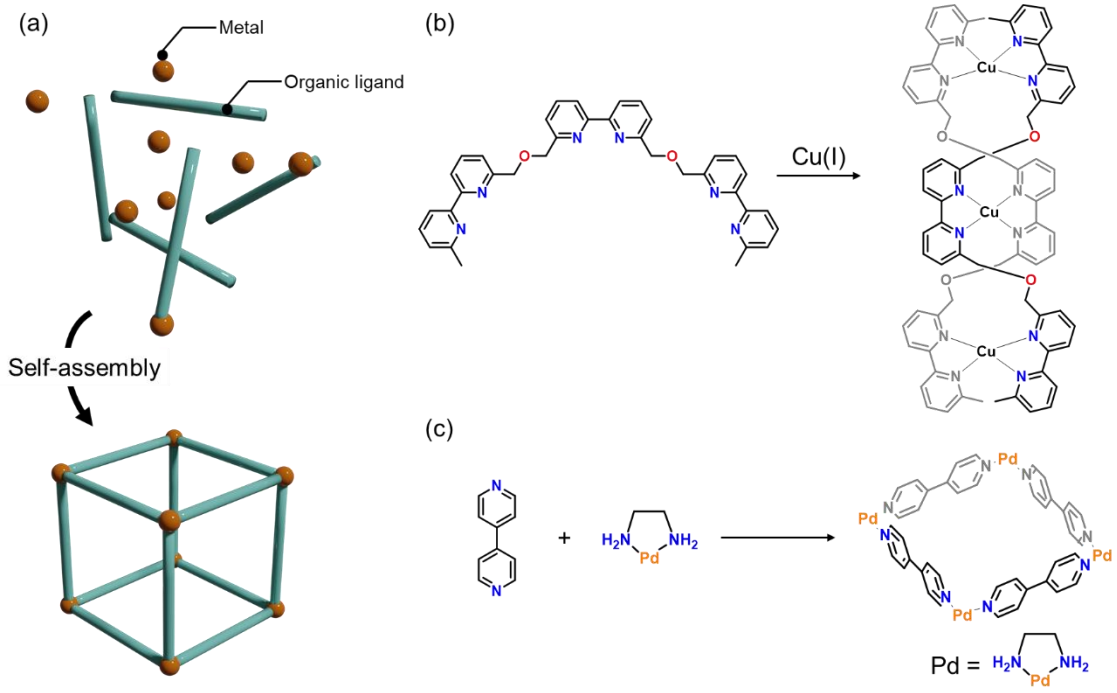

Figure 1.3.1 (a) concept of metal-mediated self-assembly (b) Synthesis of double-stranded helicate templated by Cu(I)[47] (c) Synthesis of square-shaped coordination ring[48]

Coordination rings and cages are a compound class having discrete structures formed via metal-mediated self-assembly of organic ligands and metals (**Figure 1.3.1a**). Jean-Marie Lehn first demonstrated the power and the versatility of metal-mediated self-assembly by the synthesis of double stranded helicates (**Figure 1.3.1b**).[47] Two of oligo-bipyridine ligands form the double stranded helicates hinged by Cu(I) metals. As can be seen in the example, by mixing organic ligands and metals, if necessary under heating, a precise discrete structure is assembled as the thermodynamic species. Based on this concept, Fujita and co-workers reported the quantitative synthesis of a square-shaped coordination complex by self-assembly of 4,4´-bipyridins and *cis*-protected Pd(II) (**Figure 1.3.1c**).[48] The utilization of the metals as the nodes of the structure introduces angles which cannot be provided by bonds of organic elements. In fact, numerous topologies can be created in coordination cages.[49] Depending on the bite-angle and the coordination geometry of the metal, structure of coordination cages can be quite diversified compared with organic cages. The various topologies in coordination cages broadens the utility of these assemblies in several fields. One of the most important structural features of coordination cages is their cavities inside.[50]

Supramolecular chemistry has been flourished since the synthesis of crown ethers and their encapsulation capability toward alkali metal ions were showcased by Pederson.[51] Molecular recognition and encapsulation as well as subsequent host-guest chemistry is a center of the supramolecular chemistry field. Coordination cages can be used to encapsulate various molecules within their cavities. Coordination cages are often charged owing to the metal nodes and thus possess a hydrophilic outer shell while their inner space is hydrophobic, which allows encapsulation of hydrophobic organic molecules. The inner cavities can store reactive species,[52,53] catalyze reactions,[54] recognize subtle structural difference[55–57] and so forth.[58–60] Furthermore, the size and number of cavities can be finely controlled by a proper choice of organic ligands.[61]

In the Clever group, where this doctoral research was conducted, coordination cages comprised of banana-shaped organic ligands and Pd(II) have been intensively studied (**Figure 1.3.2**).[59,62–64] One of the greatest achievements of the group is a systematic study of self-assembly of such coordination cages bringing multiple organic ligands and Pd(II) together. In the course of the exploration, the group has suggested and demonstrated a concept of rational syntheses of heteroleptic coordination cages in which more than two different organic ligands are joined to form the structures. For synthesizing heteroleptic coordination cages, contributions of both entropy and enthalpy must be considered to achieve a stable assembly. The strategies the Clever group has suggested are namely "*Shape Complementarity Assembly*" (SCA) and "*Coordination Sphere Engineering*" (CSE). In the first concept, our group has demonstrated the synthesis of heteroleptic coordination cages by bringing two different organic ligands having different bite angles together (**Figure 1.3.2b**). The different bite angles complement each other so that Pd(II) can adopt a square planar coordination geometry, which helps coordination cages to have less strain energy.[65,66] In the latter concept, the introduction of steric bulk directly around the coordination sites can control the topology of resulting coordination cages (**Figure 1.3.2c**).[64,67,68] For example, organic ligands **4** and **5** having pycolyl coordination-sites yield heteroleptic coordination cage $Pd_2\mathbf{4}_2\mathbf{5}_2$ by self-assembly with Pd(II). The steric bulk around the coordination-sites disfavors narcissistic self-sorting. Based on the concepts explained above, various coordination cages showing unique physical properties have been reported by the group.[59,62–64] The synthesized cationic coordination cages enable encapsulation of anionic guests within the cavities.[69]

However, examples of encapsulation of neutral guest molecules are still quite limited.[70] For encapsulation of neutral guest molecules, a well-isolated space surrounded by motifs which allow multiple weak interactions with the guest is required to overcome solvation effects. In light of this, organic ligand **6** has been synthesized and its behavior in the self-assembly with Pd(II) has been investigated (**Figure 1.3.3**).[71] **6** has a structural resemblance to triptycene which is known for convex-concave interactions with fullerene.[72]

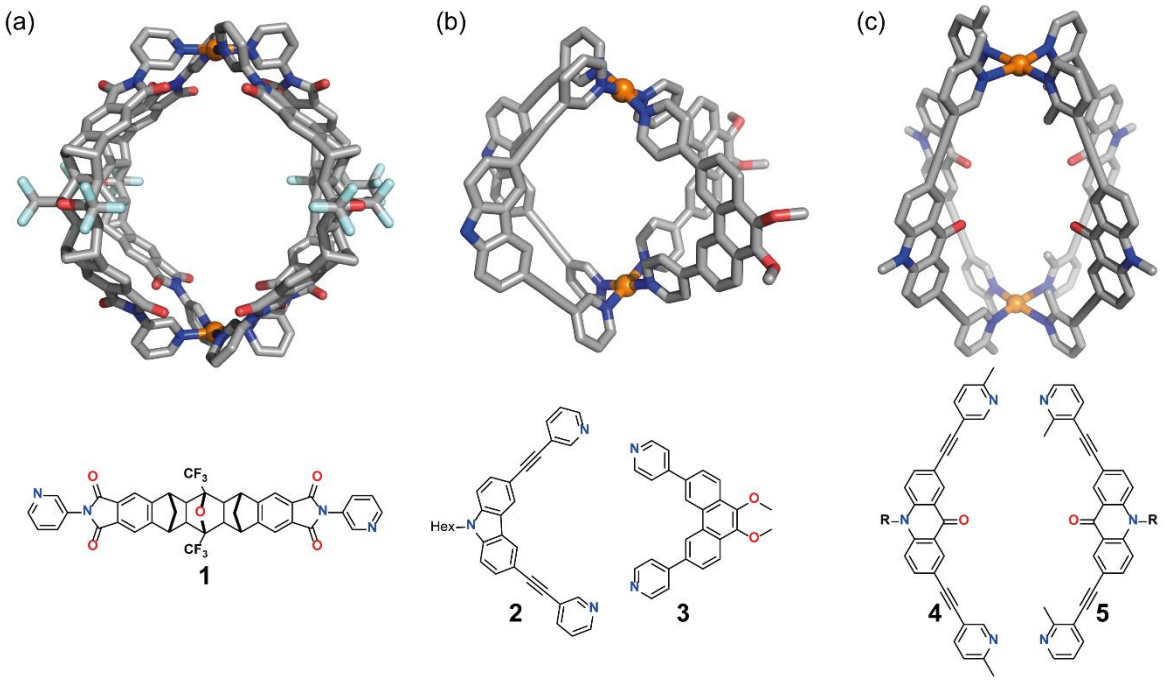

Figure 1.3.2 X-ray structure of a Pd_2**1**$_4$ coordination cage[69], (b) X-ray structure of a heteroleptic coordination cage Pd_2**2**$_2$**3**$_2$[66], where the hexyl chains are omitted for clarity, and (b) model structure of Pd_2**4**$_2$**5**$_2$.[67] In the X-ray structures, solvent molecules, counter anions, disorders are omitted for clarity unless otherwise stated.

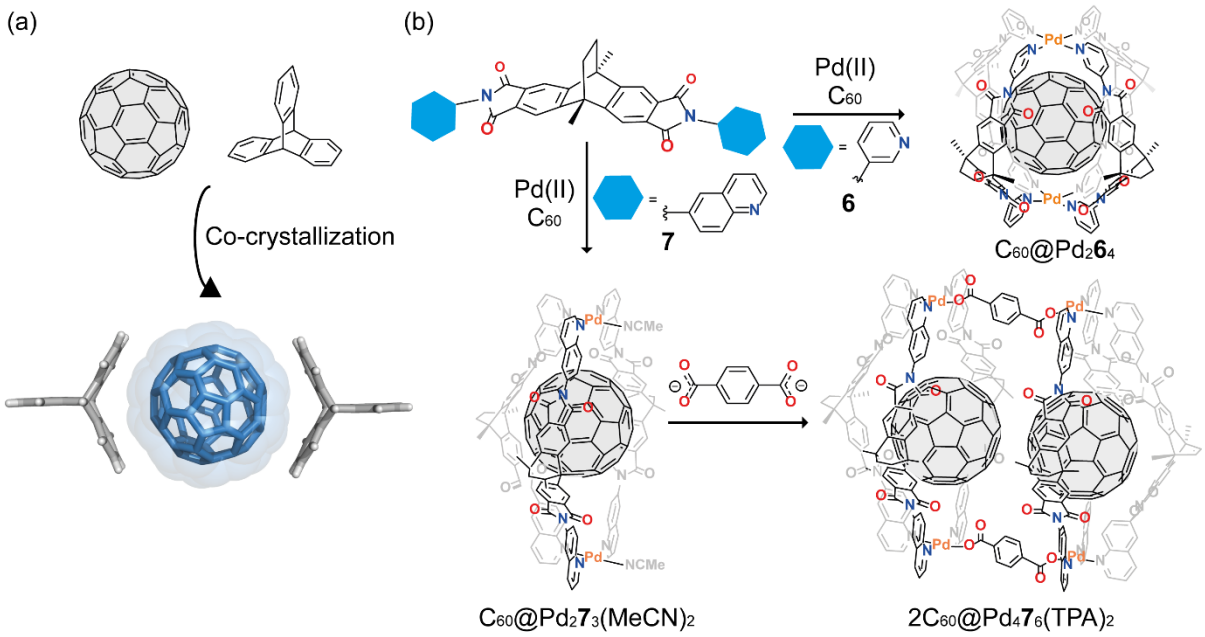

Figure 1.3.3 (a) Secondary structure of C_{60} and triptycene in the solid state[72], (b) syntheses of $C_{60}@Pd_2\mathbf{6}_4$, $C_{60}@Pd_2\mathbf{7}_3(MeCN)_2$, and $2C_{60}@Pd_4\mathbf{7}_6(TPA)_2$

Pd(II)-mediated self-assembly of **6** brings four of the ligands together to create a nanoscopic space which is suitable for the encapsulation of a single fullerene C_{60} inside. In addition, self-assembly of **7** and Pd(II) leads to the formation of coordination bowl $Pd_2\mathbf{7}_3(MeCN)_2$. The coordination bowl can also encapsulate C_{60} as well as C_{70} within the cavity. Instead of the fourth ligand, two acetonitrile molecules are coordinated to the Pd(II) centers. The weakly bound acetonitrile molecules can be replaced by anionic carboxylate linkers, such as terephthalate (TPA), yielding a pill-shaped coordination cage. The elongated cavities of the pill-shaped coordination cage can be filled with two fullerenes C_{60} or C_{70}. These examples show the potential of coordination cages as a platform for investigating nano-confinement effects and assembly of more than two C_{60}s. Note that, coordination cages are soluble in polar organic solvents thanks to their charges making the investigations in the solution-state possible.

To point out what has been achieved and what is next in this research field, host molecules including coordination cages for C_{60} encapsulation, will be described in the next section.

1.4 Encapsulation of Fullerene

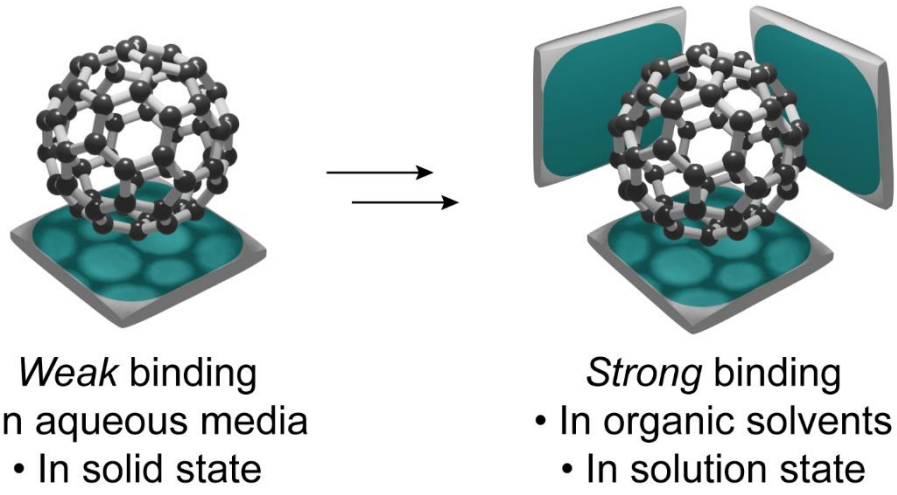

Figure 1.4.1 Comparison of weak binding and strong binding of C_{60} encapsulation

1.4.1 The dawn of fullerene-binders

At the dawn of fullerene-binders, a few numbers of compounds were mainly applied to capture fullerene C_{60} or C_{70}. The first host-guest complex accommodating C_{60} was reported by Ermer in 1991 (**Figure 1.2.2a**).[25] Intermolecular hydrogen-bonding networks bring hydroquinones to form a clathrate with C_{60} and also C_{70}. The nanoscopic space surrounded by six hydroquinones accommodates C_{60}/C_{70} via π–π interactions. A subsequent example of fullerene encapsulation was reported in 1992 by Wennerström and co-workers. They employed γ-cyclodextrin to capture and solubilize C_{60} in water (**Figure 1.2.2b**).[26] This result implied that the solubility of C_{60} is inherited from the host. From these two reports, two implicit criteria to encapsulate fullerene can be extracted. First, hosts should be composed of a moiety which allows weak interactions, i.e.π–π interactions, with the surface of fullerene. Second, host-molecules should be able to provide a nanoscopic space to the globular shape of fullerene. Calix[n]arenes are ideal molecules fulfilling the prerequisites as they are composed of a certain number of phenol molecules and their concave structure fits the convex fullerene-surface. In fact, a number of fullerene-binders based on calix[n]arenes have been reported.[73] In 1994, the groups of Atwood and Shinkai simultaneously discovered that para-*tert*-butyl-[8]-calixarene can selectively bind C_{60} in 1:1 ratio, which is beneficial for a facile C_{60} purification.[74,75] Since calix[n]arenes present diverse and dynamic structural features depending on the number of phenols

contributing to form the macrocycle, encapsulation behavior widely varies especially in the solid state.[35] For instance, a calix[5]arene derivative prefers to form a 2:1 complex with fullerene C_{60} in the solid state, while a 1:1 complex is formed in the solution state.[76]

Two of the most famous substructures of fullerenes are namely corannulene[77] and sumanene.[78] In 1993, Bohne and co-workers showcased a reaction between corannulene and C_{60} in the gas phase.[79] An adduct ion of C_{60} and corannulene is formed by reacting either corannulene radical cation with C_{60} or C_{60} radical cation with corannulene molecule. A pristine corannulene molecule does not have enough binding ability to form a molecular complex with C_{60} in the solution state most likely because of its π–surface.[80] Cyclotriveratrylene is another bowl-shaped molecule which is able to form a host-guest complex with C_{60} in the solid state, firstly reported by Atwood and Raston.[81] Not only bowl- or cup-shaped molecules but also saddle-shaped molecules can form a molecular complex with fullerenes C_{60} and C_{70} in the solid state. A nickel macrocycle 5,7,12,14-tetramethyldibenzo[b,i]-1,4,8,11]tetraazacyclotetradecinenickel(II), having two concave surfaces, is a versatile host for formation of supramolecular arrays in the solid state with fullerene.[82] Derivatives of the Ni(II)macrocycle assemble into various supramolecular arrays with C_{60} in several packing modes.[35]

Porphyrin is a flat molecule, however, the electron-rich aromatic molecule is often good at fetching fullerenes thanks to their good electron accepting ability.[83–85] One of the earliest pioneering works of molecular complexes between C_{60} and a metalloporphyrin derivative, Cr(II)tetraphenylporphyrin (Cr(II)TPP), was prepared in both solid and solution states by Wudl, Reed and co-workers.[86] C_{60} is reduced to $C_{60}^{\bullet-}$ upon complexation. Combinations of fullerene and porphyrin derivatives are widely utilized in, for example, crystal-engineering,[87,88] supramolecular chemistry,[85] and artificial photosynthesis.[89,90] Co-crystallization of fullerene and a porphyrin derivative often simplifies crystallographic analyses of fullerenes.[14,91] In 1999, Feringa and co-workers showcased encapsulation of C_{60} inside a nano-space furnished in between triptycenes.[72] The triangular molecule, triptycene, with three concave surfaces, co-crystalizes with C_{60} by sandwiching from two opposite sides. Introducing an N atom into triptycene substituting one of the sp^3 carbons leads to a different crystal packing due to the electronic perturbation.

1.4.2 Strategy for fullerene encapsulation in organic solvents

Due to the weak binding ability of the host-molecules with fullerenes aforementioned, encapsulation of fullerene was largely limited either to the crystalline state or to aqueous media as hydrophobic fullerenes prefer to be isolated within a hydrophobic inner cavity of the host in aqueous media through the hydrophobic effect (**Figure 1.4.1**). The weak binding constants had been hindering further investigations of encapsulation of fullerenes in organic solvents. To strongly encapsulate fullerene not only in the solid state or in aqueous media but also in organic solvents, manipulation of weak-interactions, i.e. π–π interactions and C–H•••π interactions, is one of the most important factors.[92,93] Fullerene-binders have evolved based on the promising backbones shown in the previous section to obtain a higher binding constant in organic solvents at the early stage. In this section, how fullerene-binders have been improved in terms of binding-constant in the last decades will be described. Fullerene-binders based on calix[n]arenes, buckybowls, porphyrins and carbon-nanohoops will be mainly depicted here.

Fukazawa and co-workers discovered that calix[5]arene derivative **8** strongly binds C_{60} in several organic solvents such as toluene, CS_2, benzene, and *o*-dichlorobenzene with binding constant being 2.12 ×10^3 M^{-1} in a toluene solution (**Figure 1.4.2a**).[76] This study also showed that the binding constant decreased inversely against solubility of C_{60} in the organic solvents (*cf*. K_a = 3.08 ± 0.41 × 10^2 M^{-1} in *o*-dichlorobenzene, 2.12 ± 0.11 × 10^3 M^{-1} in toluene). This indicates that solvation and binding of C_{60} are in competition. Therefore, to cover the surface of fullerene is important to realize a stronger binding of fullerene within a host in order to maximize the contacted surface between fullerene and the host alongside decreasing the contact to solvent molecules. Fukazawa and co-workers synthesized bridged bis-calix[5]arenes **9-11** and investigated the binding behavior of the hosts toward C_{60} and C_{70} in organic solvents.[94] In fact, **9** encapsulates single C_{60} with a ca. 30 times larger binding constant, K_a = 76 ± 5 ×10^3 M^{-1}, in toluene than **8**. **9** can encapsulate also larger fullerene C_{70} with a higher binding constant, K_a = 163 ± 16 ×10^3 M^{-1}, compared to the K_a toward C_{60} in toluene. The tight encapsulation prevents C_{60} from being solvated.

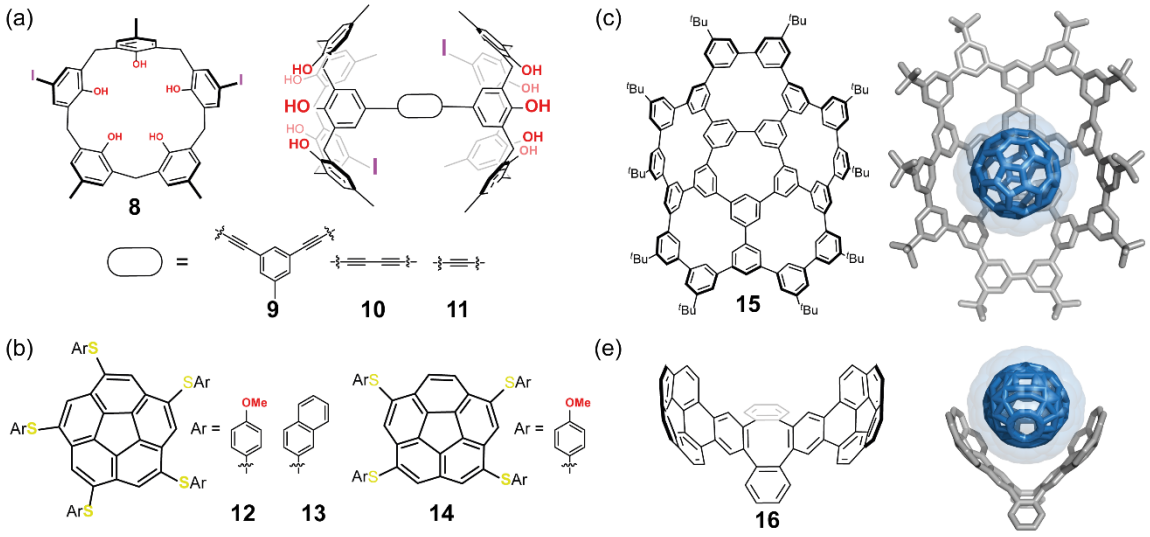

Figure 1.4.2 Structure of covalently bonded fullerene-binders (a) **8**-**11** (b) **12**-**14** (c) **15** and X-ray structure of C_{60}@**15** and (d) **16** and C_{60}@**16** with disorder of C_{60}

As mentioned in the previous section, a simple corannulene molecule shows only neglectable association with a neutral fullerene in the solution state. However, similar to calix[n]arenes, either to bridge two buckybowls or to expand the contacting surface with fullerene enhances the binding-ability and to form a host-guest complex with fullerene (**Figure 1.4.2b**). Scott and co-workers synthesized corannulene derivatives **12**-**14** by nucleophilic aromatic substitution reactions of a chlorinated corannulene derivative with the corresponding thiolates.[95] The aromatic chemical pendants attached on the edge of corannulene endow **12**-**14** to form a 1:1 molecular complex with C_{60}. Isobe and co-workers have reported gigantic buckybowl **15** (**Figure 1.4.2c**).[96] **15** can be regarded as a molecule in which all the carbon atoms of corannulene are replaced by benzene rings. The large surface of **15** covers almost half of the sphere of C_{60} and a 1:1 molecular complex is formed in benzene with a binding-constant of $3.4 \pm 0.1 \times 10^4$ M^{-1}.[97]

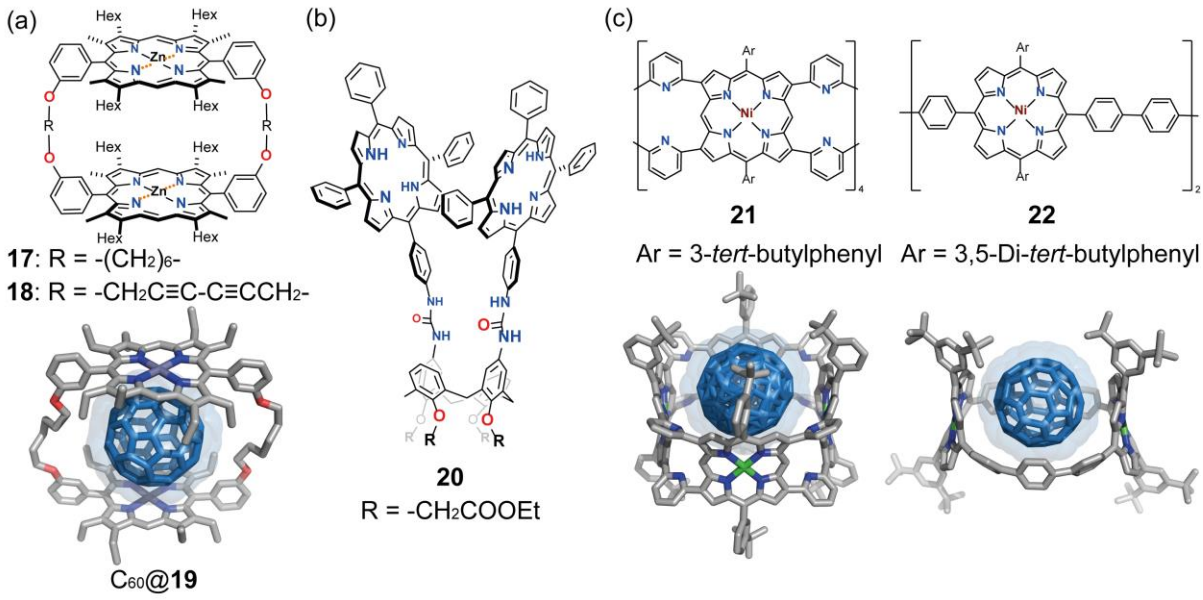

Figure 1.4.3 Structure of covalently bonded fullerene-binders (a) **17**-**19** and X-ray structure of C_{60}@**19** (b) **20** and (c) **21** and **22** and X-ray structure of C_{60}@**21** with disordered C_{60} and C_{60}@**22**

Nowadays, hosts which are composed of bridged aromatic compounds, so called molecular tweezers, are of great interest for the sake of fullerene-binding and their structural uniqueness. Molecular tweezers serve a well-defined nanoscopic space which is suitable to capture fullerenes. Sygula and co-workers reported first molecular tweezer **16** composed of two corannulene molecules in 2007 (**Figure 1.4.2d**).[98] **16** forms a molecular complex with C_{60} in 1:1 ratio in the crystalline state as well as the solution state. The NMR titration experiment revealed that molecular tweezer **16** binds C_{60} with K_a =8.6 ± 0.5 × 10^3 M^{-1}. Regarding porphyrin-based fullerene-binders, despite the preferable donor-acceptor relations between porphyrin and fullerenes, the planar structure is a disadvantage to prevent fullerene from solvation. Thus, the bridging strategy has been applied to porphyrins as well to increase binding ability toward fullerene. Covalently-bridged porphyrins **17** and **18** have been reported by Aida and co-workers (**Figure 1.4.3a**).[99] Bridged-porphyrin dimer **17**, in which two porphyrins located in a face-to-face manner, encapsulates one molecule of fullerene C_{60} in between the two panels in a benzene solution with a K_a value being 6.7 × 10^5 M^{-1}. The solid-state structure of **19** encapsulating C_{60}, in which the hexyl chains and the methyl groups on the porphyrins of **17** are replaced with ethyl groups, was elucidated by single crystal X-ray structure analysis two years later.[100]

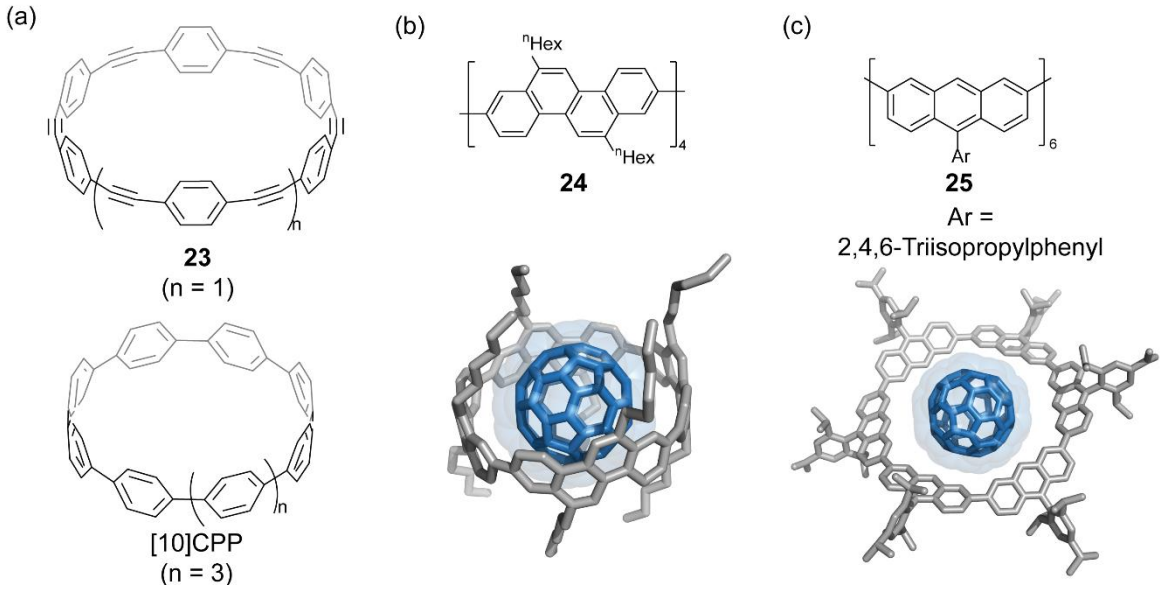

Figure 1.4.4 Structure of macrocyclic fullerene-binders (a) **23** and [10]CPP (b) **24** and X-ray structure of C_{60}@**24** (c) **25** and X-ray structure of C_{60}@**25**

Lang, Lhoták and co-workers have synthesized calix[4]arene-based molecular tweezer **20** and demonstrated that **20** captures fullerene C_{70} as well as C_{60} in between the two porphyrin panels (**Figure 1.4.3b**).[101] A 1:1 C_{70}-inclusion molecular complex is formed by mixing C_{70} and **20** in toluene, and an association constant K_a was determined to be 1.45×10^4 M^{-1} by ^1H NMR titration. **20** displays preferable encapsulation towards C_{70} rather than C_{60}. In addition to these porphyrin-based hosts, tubular macrocycles composed of metalloporphyrins also display a good binding ability toward C_{60}. Osuka and co-workers synthesized **21** (**Figure 1.4.3c**). With an inner diameter of about 14 Å, **21** binds C_{60} within the tubular structure with an association constant of $5.3 \pm 0.1 \times 10^5$ M^{-1}.[102] Recently von Delius and co-workers reported highly strained tubular porphyrin-macrocycle **22** showing a10^3-fold higher association constant for C_{60} than **21**. The encapsulated C_{60} is located off-center of the tube (**Figure 1.4.3d**).[103]

Molecular complexes of carbon allotropes such as molecular peapods have been attracting attention due to their physical properties.[104] For systematic understanding into hidden properties of such carbon composites, investigation at the molecular level is important. In this context, Kawase, Oda and co-workers investigated C_{60} encapsulation into [6]-cycloparaphenyleneacetylene **23** (**Figure 1.4.4a**).[105] The association constant between **23** and C_{60} was estimated to be $1.6 \pm 0.3 \times 10^4$ M^{-1} in

benzene.[106] A substructure of CNTs, [n]cycloparaphenylenes ([n]CPPs), was independently synthesized by the groups of Bertozzi,[107] Itami,[108] and Yamago[109] through different approaches. [n]CPPs can be seen as a molecular model to investigate molecular peapods. Yamago and co-workers found that C_{60} can be selectively encapsulated in [10]CPP out of other [n]CPPs due to size-matching. The association constant was determined to be $2.79 \pm 0.03 \times 10^6$ M^{-1} by fluorescence spectroscopy.[110] The highest binding constant toward C_{60} so far was achieved by Isobe and co-workers.[111,112] Macrocyclic hydrocarbon **24** encapsulates C_{60} with the highest association constant in the order of 10^{12} in benzene(**Figure 1.4.4b**). The binding-constant increases as the solubility of C_{60} becomes lower similar to most of other fullerene-binders. Solid-state dynamics of C_{60}@**24** and its enantiomer have been also investigated.[113,114] These researches show that host-guest complexes encapsulating fullerene are not merely of aesthetic appeal but that they can be a platform to investigate solid-state physics of fullerenes for instance. Macrocyclic hydrocarbons can encapsulate fullerene not only through π–π interactions but also CH–π interactions. Toyota and co-workers reported macrocyclic host **25** composed of anthracenes (**Figure 1.4.4c**). The hydrogens pointing inward interact with the π–surface of C_{60}/C_{70} and thus **25** entraps fullerene within the macrocycle to form the Saturn-shaped host-guest complex.[115,116]

1.4.3 Fullerene-binders based on coordination cages

1.4.3.1 Designs and syntheses

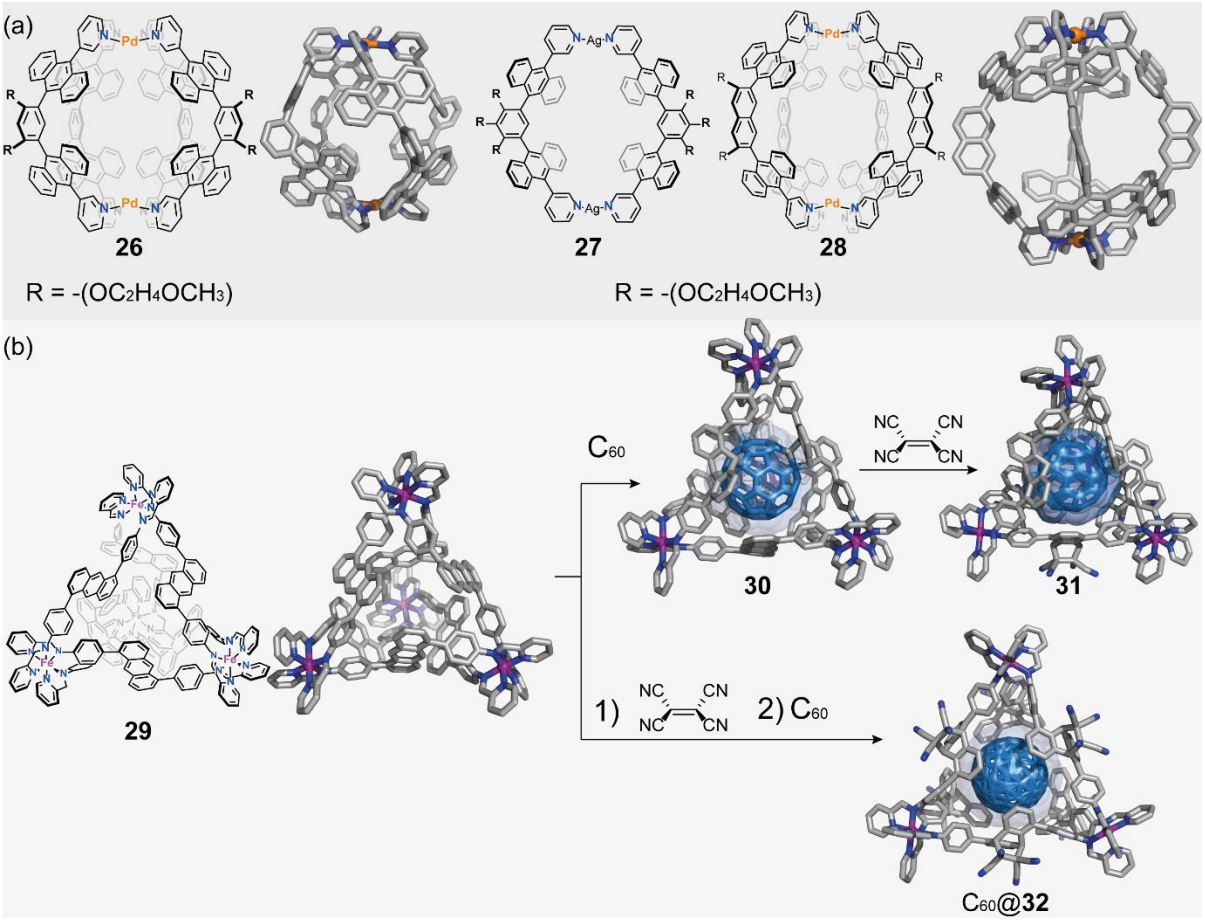

Figure 1.4.5 Structure of coordination cages (a) **26**-**28** and X-ray structures of **26** and **28** (b) **29**-C_{60}@**32** and X-ray structure of **29**, **30**, and C_{60}@**32**. A modelled structure is shown for **31**.

In the previous section, the history of fullerene-binders based on covalently-bonded host-molecules was briefly covered. To strongly bind fullerenes, host-molecules must be able to interact with the globular surface. As organic syntheses have been advancing over the decades, many covalently-bonded hosts designed for encapsulation of fullerene have been synthesized. The host-molecules have been extended, bridged, or hooped to provide a well-defined and isolated space to accommodate fullerene even in organic solvents. Hence, the synthetic routes tend to become more complicated and time-consuming. On the other hand, it has become easier to construct an isolated space to store unstable compounds,[52,53] to create a reaction field,[50] separate molecules by their structures[55,56] thanks to metal-mediated

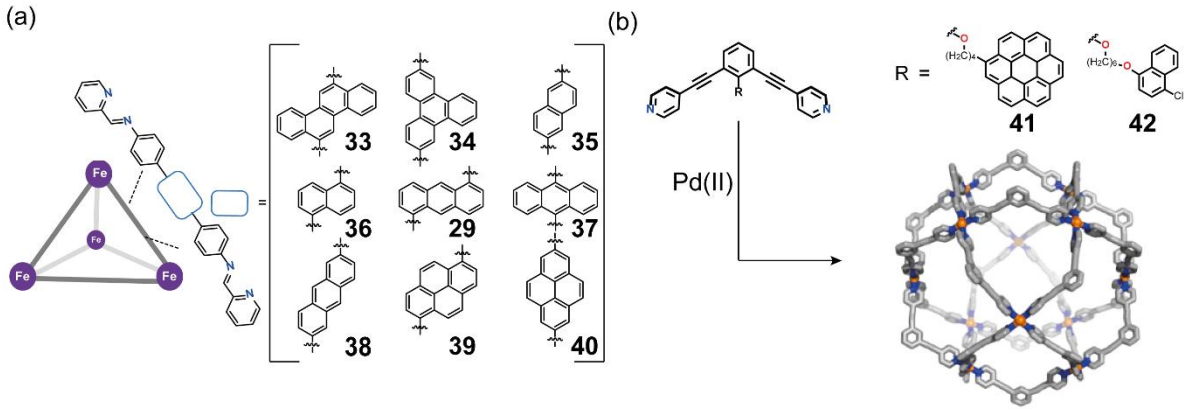

Figure 1.4.6 Schematic structure of (a) **29**, **33**-**40** and (b) model structure of **41** and **42** without coronene pendants

self-assembly. In addition, a rational choice of organic ligands and metal centers makes it possible to assemble supramolecular complexes with a larger variety of topologies without laborious syntheses.[117,118] Recently, a number of coordination cages designed for fullerene encapsulation have been reported. Covalently-bonded fullerene-binders are a good model to learn how to design organic ligands to capture fullerene. Following these experiences, the organic ligands should be based on a moiety which offers weak-interactions with globular fullerene. In addition, the assembled cages must possess a well-defined nanoscopic space for fullerene. Flat aromatic compounds are attractive molecules for this sake because their π–extended panels can induce favorable interactions with fullerene. Further, aromatic compounds are prone to halogenation reaction which is ideal for following with coupling reactions to attach coordination-sites. For example, Yoshizawa and co-workers reported Pd_2L_4 cage **26** whose inner space is surrounded by eight anthracene panels (**Figure 1.4.5a**).[119] Sheer anthracene molecule does not have ability of accommodating other molecules, however, self-assembly brings anthracenes together and constructs the isolated space which shows outstanding encapsulation capability for a variety of guest-molecules in aqueous media.[120] **26** can encapsulate C_{60} quantitatively via multiple weak interactions. It is important to note that the encapsulation of C_{60} in **26** was performed heterogeneously. Yoshizawa and co-workers have also reported confinement of C_{60} in tubular coordination cage **27**.[121] The coordination numbers of the metal center is a decisive factor to determine the topology of coordination cages. In this study, Ag(I) was used as metal centers in lieu of Pd(II). Two pyridine coordination-sites of the ligand coordinate to Ag(I) center in a linear fashion and

tubular **27** is assembled. Although **27** provides a less isolated-space due to its tubular structure, **27** fetches C_{60} and forms C_{60}@**27** with an encapsulation yield of 88%. The open structure also makes it possible to encapsulate C_{60} derivatives in a good yield. In addition to encapsulation, the tubular structure disassembles and releases the encapsulated C_{60} as well as the C_{60} derivatives upon irradiation. The same group has shown anisotropic-expansion of cage **26** by replacement of the phenylene backbone with naphthalene.[122] As a consequence of self-assembly of the elongated ligand with Pd(II), M_2L_4 capsule **28** is assembled. The larger and anisotropic cavity is capable of accommodating anisotropic fullerene C_{70}. The anisotropic expansion of the inner cavity also facilitates the formation of apertures which are beneficial for incorporation of a C_{60} derivative. In a similar manner, Nitschke and co-workers constructed M_4L_6 tetrahedron **29** from an anthracene-based organic ligand (**Figure 1.4.5b**).[123] Tetrahedral coordination cage **29** is constructed via multi-component self-assembly with Fe(II). The key feature of this reaction is the formation of the dynamic imine bonds during the self-assembly process. Dispersing C_{60} in an acetonitrile solution of **29** results not only in mere encapsulation of C_{60} but also in the intramolecular cycloadditions of three anthracenes on the confined C_{60} yielding **30**. Interestingly, the regio-selectivity of the cycloaddition is higher than 95%. In this study, the authors also performed post-assembly modification. Once **30** is treated with excess amounts of tetracyanoethylene (TCNE), three unreacted anthracene-panels undergo Diels-Alder reaction with TCNE followed by formation of **31** with C_3-symmmetry. On the other hand, Diels-Alder reaction of **29** with TCNE transforms *T*-symmetrical **29** to **32** as a mixture of diastereomers. Subsequent encapsulation of C_{60} inside **32** gives *T*-symmetry to maximize the contacted surfaces with C_{60}. Intriguingly, when both encapsulation and Diels-Alder reactions are taken place in one-pot, **32** is dominantly formed because the Diels-Alder reaction is faster than the encapsulation of C_{60}. Following this work, Nitschke and co-workers also systematically and broadly examined the accommodation capability of coordination cages **33-40** possessing various aromatic moieties on the vertices instead of anthracene (**Figure 1.4.6a**).[124]

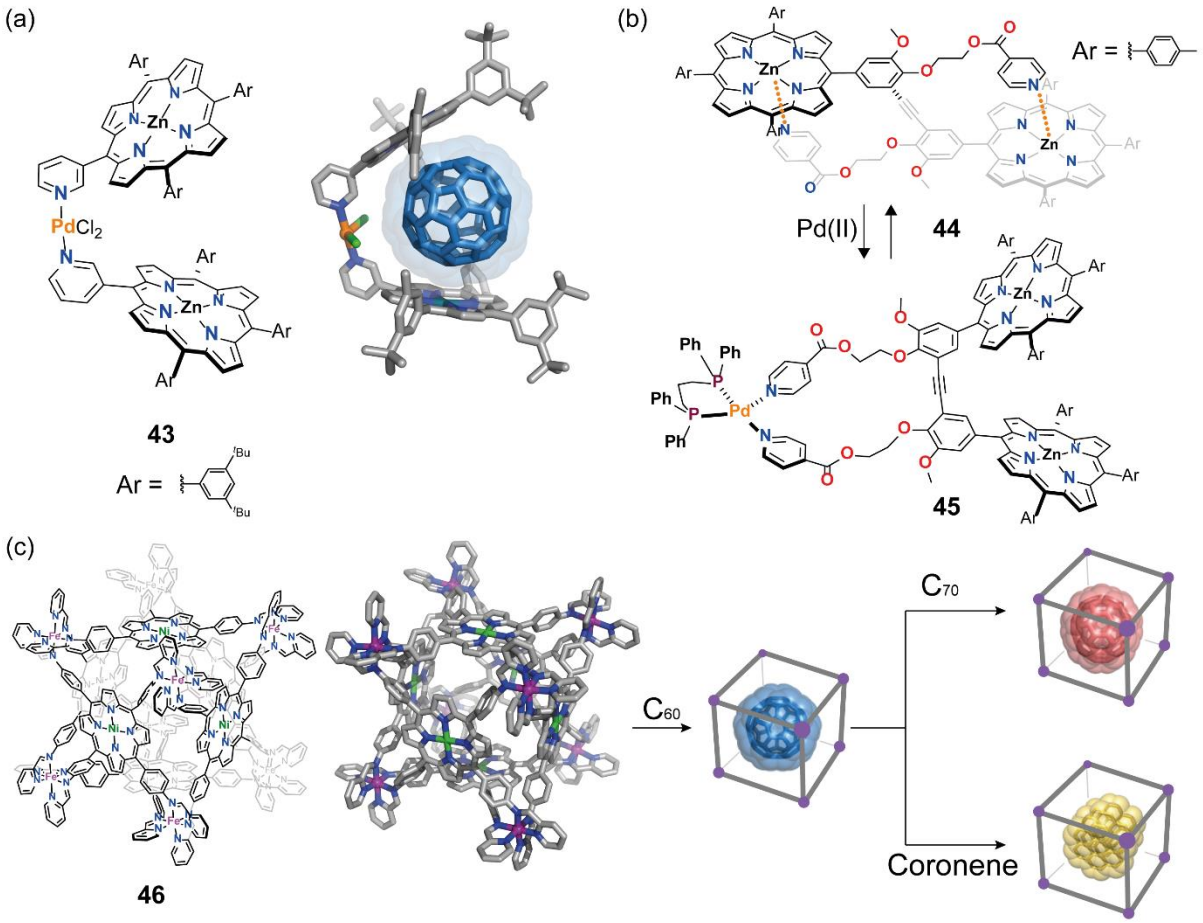

Figure 1.4.7 Structure of molecular tweezers (a) **43** with X-ray structure of C_{60}@**43** (b) **44** for *off-state* and **45** for *on*-state (c) coordination cage **46** and schematic illustration of guest-exchange behaviour

According to the report, they found that the way the aromatic moieties are lying on the vertices is important to entrap neutral molecules inside the tetrahedral cages. Fujita and co-workers have shown endohedral functionalization of a $M_{12}L_{24}$ nanoscopic sphere.[125] Chemical modifications of the organic ligand can change the environment of the inner sphere. For instance, an organic ligand strapped with coronene forms nanoscopic cage **41** by self-assembly with Pd(II) and its hydrophobic environment inside **41** is almost fully occupied with coronenes (**Figure 1.4.7b**).[126] The inner cavity of **41** provides a pseudo-solvating environment for guest molecules. Owing to the ubiquitously existing coronene inside **41**, C_{60} is *solubilized* within the cage. On the other hand, cage **42** whose inner space is decorated with chloronaphthalenes does not show a strong binding toward C_{60}.

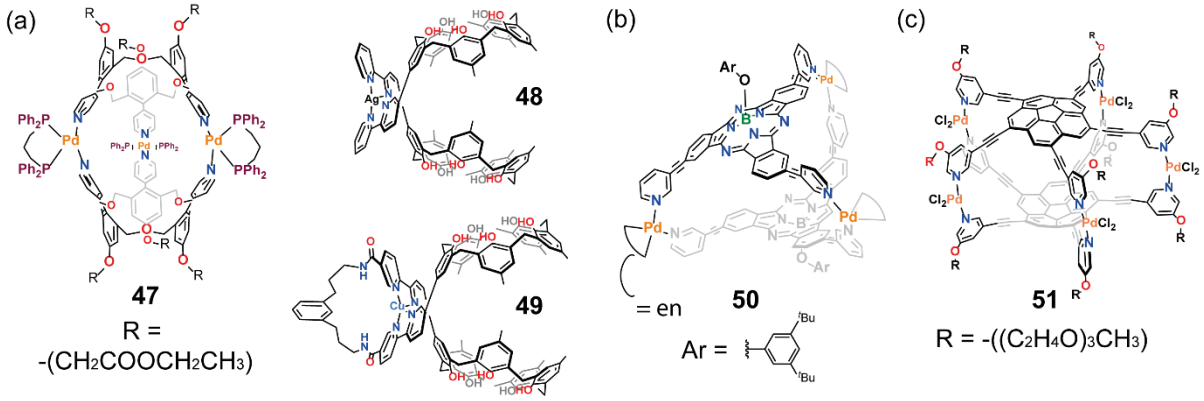

Figure 1.4.8 Structure of coordination capsules (a) **47**-**49** (b) **50** and (c) **51**

Porphyrin is one of the mostly used moieties among covalently-bonded fullerene-binders because of its electronic affinity with fullerene. Reed, Boyd and co-workers reported inclusion of fullerene C_{60} and C_{70} inside **43**, in which two porphyrins are facing each other (**Figure 1.4.7a**).[127] The binding constant of **43** toward C_{60} was determined to be 5.2×10^3 M^{-1} in toluene by ^{13}C NMR titration. Shinkai and co-workers constructed a Pd(II)-responsive bis-porphyrin C_{60} binder **44** and investigated its C_{60} encapsulation behavior (**Figure 1.4.7b**).[128] The attached two pyridine coordination-sites coordinate to Zn(II) centers of the two metalloporphyrins in the "off" state. Upon addition of Pd(II), **44** turns into the "on" state **45** where the porphyrins form a sandwich-like structure similar to **20**. In the "on" state, **45** is able to encapsulate C_{60} in a toluene/CH_2Cl_2 solution (50:1) with an association constant of 5.1×10^3 M^{-1}, while **44** does not encapsulate C_{60} when it is in the "off" state. Nitschke and co-workers synthesized cubic M_8L_6 supramolecular coordination cage **46** composed of six tetrakis-bidentate ligands and eight Fe(II) centers (**Figure 1.4.7c**).[129] **46** encapsulates coronenes, C_{60} and C_{70} owing to six porphyrin panels offering π–π interactions with those guests. Guest-exchange takes place from C_{60} to coronenes and from C_{60} to C_{70} because the cavity size of **46** is more suitable to accommodate guests of higher volume than C_{60}.

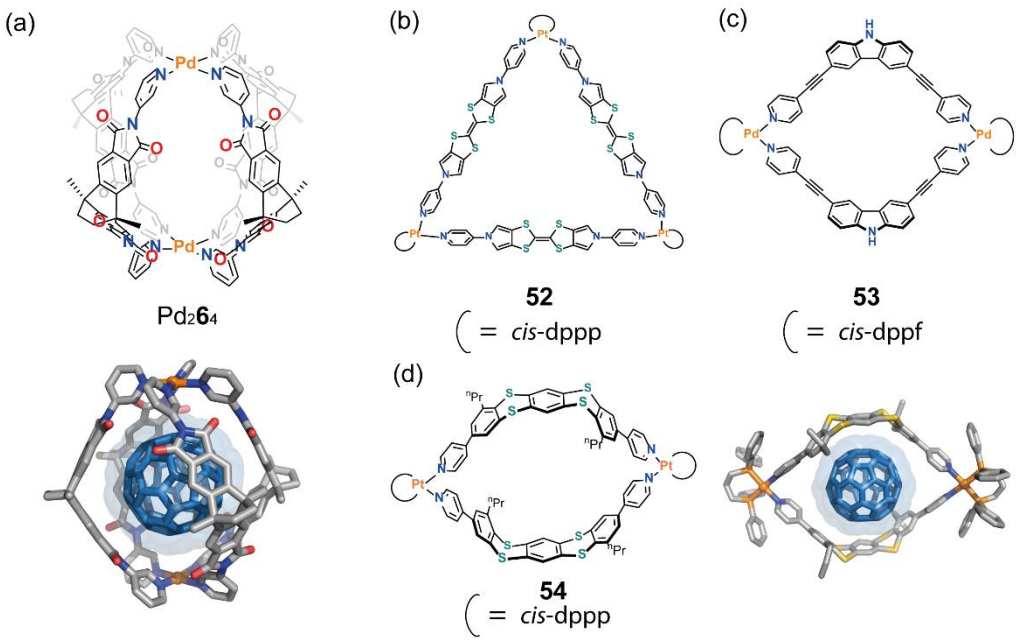

Figure 1.4.9 Structure of coordination cages (a) Pd_2**6**$_4$ with X-ray structure of C_{60}@Pd_2**6**$_4$ and rings (b) **52** (c) **53** (d) **54** and its X-ray structure encapsulating C_{60} inside

Not only planar molecules but also curved molecules are suitable moieties for the sake of fullerene-binding thanks to convex-concave interactions. Shinkai and co-workers reported in a pioneering work for coordination cages, the encapsulation of C_{60} utilizing calix[3]arene in 1999 (**Figure 1.4.8a**).[130] Self-assembly of a calix[3]arene derivative and *cis*-protected Pd(II) yields a M_3L_2 molecular capsule **47**. **47** forms a 1:1 C_{60}-inclusion complex in 1,2-tetrachloroethane solution with an association constant of 54 M^{-1}. Fukazawa and co-workers have reported the complexation of calix[5]arene derivatives and metals (**Figure 1.4.8a**).[131,132] Ag(I) center brings two mono-2,2'-bispyridyl-functionalized tetra-*p*-methylcalix[5]arene to create **48** having a cavity for single C_{60}/C_{70} encapsulation.[81] They also demonstrated that Cu(I) as a template alters the complexation behavior between **49** and C_{60} from 1:2 to 1:1 fashion. On the other hand, an enhancement of the binding constant was observed for C_{70} in a tetrachloroethane solution.[82] In 2004, Torres and Classen have reported subphthalocyanine-based M_3L_2 coordination cage **50** and showed encapsulation of C_{60} (**Figure 1.4.8b**).[133] Jiang and co-workers have constructed M_5L_2 capsule **51** (**Figure 1.4.8c**).[134] Generally, corannulene is a difficult molecule to use as a ligand because of limited possibilities of chemical modifications and its bowl inversion.[135] The authors utilized a corannulene-based ligand having five pyridine coordination-

sites to construct cage **51**. $PdCl_2$ centers help to form the cage thanks to the *trans*-configuration of the vacant coordination sites. **51** preferentially encapsulates C_{60} over C_{70} in 1,2-tetrachloroethane upon heating to 130 °C. Clever and co-workers utilized a bent-shaped ligand to construct Pd_2L_4 lantern-shaped coordination cage Pd_2**6**$_4$ for fullerene encapsulation (**Figure 1.4.9a**).[71] The bent ligand has a nearly identical angle to triptycene which shows a good geometrical complementarity to C_{60}.[72] Dispersing C_{60} solid in an acetonitrile solution of Pd_2**6**$_4$ results in quantitative C_{60} encapsulation. The authors made use of coordination-sphere-engineering by exploring ligands having a variety of coordination-sites and thus varied steric hinderance as discussed later. Recently, some metallacycles showing fullerene-encapsulation capability have been reported. For instance, metallacycle **52** having tetrathiafulvalene-backbone shows a binding constant of 1.5×10^4 M^{-1} with C_{60} (**Figure 1.4.9b**).[136] As another example, **53** composed of carbazole-based ligands and *cis*-(dppf)Pd$(OTf)_2$ shows 1:1 molecular complex formation with C_{60} via π–π interactions with the carbazole ligands and C_{60} (**Figure 1.4.9c**). The association constant was determined to be $K_a = 1.0 \times 10^5$ M^{-1} in an acetonitrile-tetrachloroethane mixture.[137] Very recently, belt-shaped coordination cage **54** has been reported (**Figure 1.4.9d**). **54** is formed via metal-mediated self-assembly of *cis*-Pt(dppp)$(OTf)_2$ and organic ligands having an electron-rich thianthrene backbone. **54** efficiently binds C_{60} as well as C_{70} with binding constant of 5.1×10^6 M^{-1} and 3.7×10^6 M^{-1} in CH_2Cl_2 in the excited states respectively determined by fluorescence spectroscopy. [138]

1.4.3.2 Template-effects

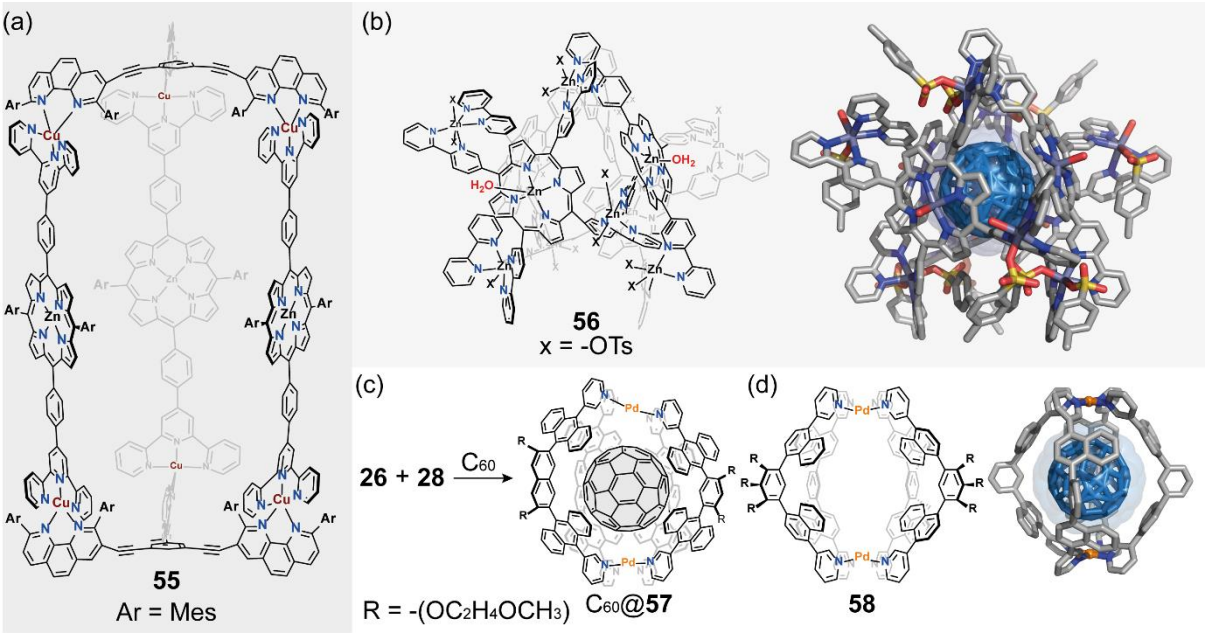

Figure 1.4.10 Structure of coordination cages (a) **55** (b) **56** with X-ray structure of C_{60}@**56** (c) formation of **57** (d) **58** and its X-ray structure encapsulating C_{60} inside

One of the most intriguing features of fullerene encapsulation inside coordination cages is unprecedented template effects. Only in the presence of fullerene as a guest, a specific topology will be formed to maximize the contacting surface between cages and fullerene via an induced fit phenomenon. As a result of repeated coordination and dissociation processes, the thermodynamically most stable host-guest complex will be obtained. Therefore, fullerene-encapsulation sometimes gives the opportunity to provide deeper insights into the thermodynamics of molecular complexes. In 2008, Schmittel and co-workers reported the synthesis of prism-shaped heteroleptic coordination cages assembled by two different organic ligands and Cu(I) metal centers (**Figure 1.4.10a**).[139] In addition to the prism-shaped coordination cages, oligomeric compounds were formed. However, the formation of undesired oligomers can be suppressed in the presence of C_{60} as a guest molecule thanks to π–π interactions with C_{60} and zinc-porphyrins stabilizing cage **55**. Template-effects of C_{60} on the formation of barrel-like coordination cage **56** was reported by Shionoya and co-workers (**Figure 1.4.10b**).[140] The ligand based on metalloporphyrins carrying four bipyridyl donor-sites assembles to form a mixture of trimer and tetramer **56** upon addition of $Zn(OTs)_2$ in a $CDCl_3/CD_3OD$ (1:1) solution. By heating the solution in presence of C_{60}, the

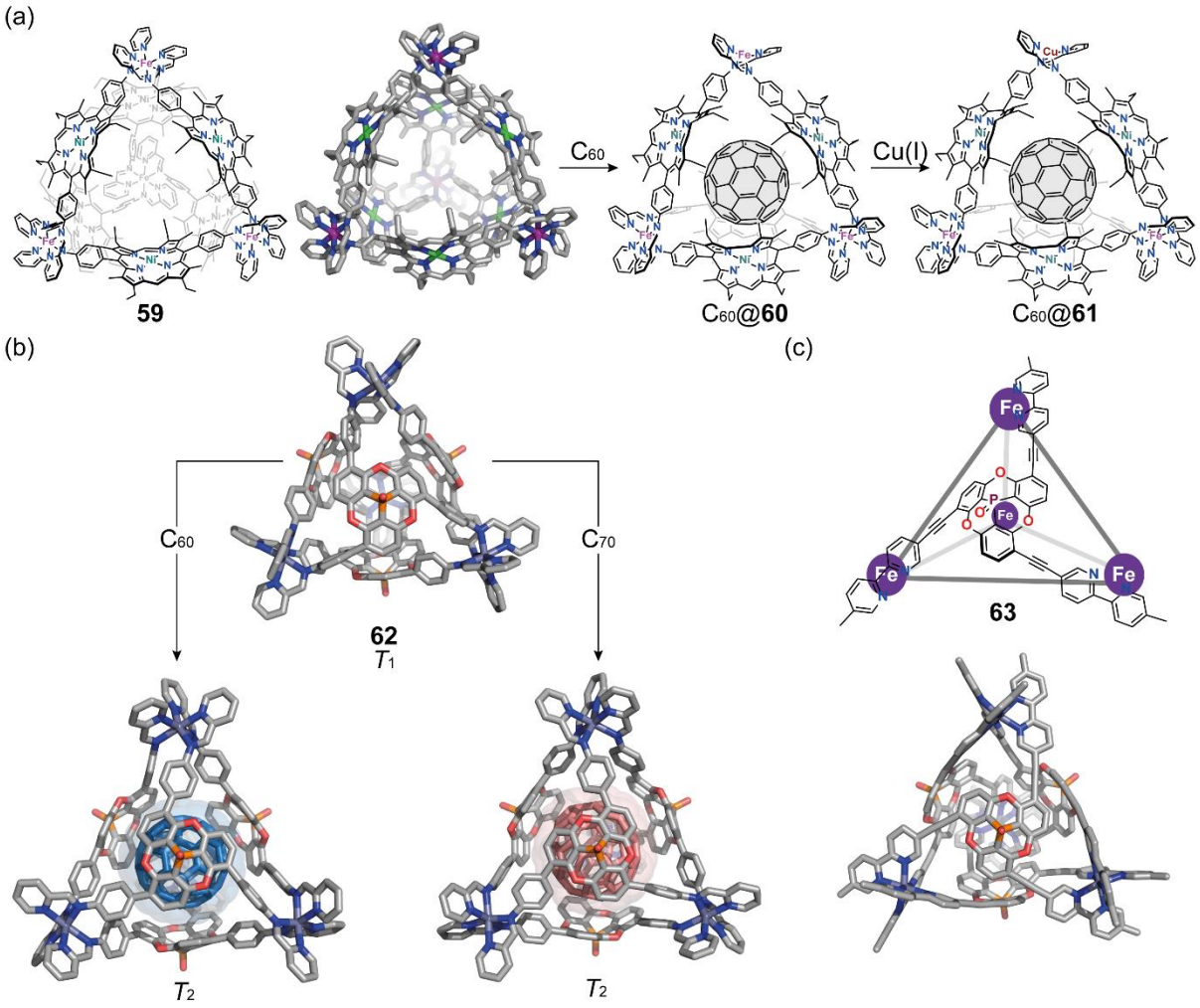

Figure 1.4.11 (a) Transformation from **59** to C_{60}@**60** to C_{60}@**61**. X-ray structure of **59** is shown (b) Isomerization of **62** by template effect. X-ray structures of **62**, C_{60}@**62**-T_2 and C_{70}@**62**-T_2 are shown (c) schematic illustration of **63** with its X-ray structure

equilibrium between those two conformers leans to tetramer **56** encapsulating C_{60} owing to the stabilization by weak interactions between C_{60} and the ligands. Yoshizawa and co-workers reported a C_{60}-templated self-assembly leading to formation of a heteroleptic cage (**Figure 1.4.10c**). By mixing acetonitrile solutions of cage **26** and cage **28** with solid C_{60}, the construction of heteroleptic coordination cage **57** was achieved, while only statistical mixtures are obtained without the C_{60} template.[122] The same group has reported a template-effect of C_{60} on cage **58** (**Figure 1.4.10d**). Empty **58** is obtained as a mixture of regio-isomers in solution upon reacting the atropisomeric ligand with Pd(II).[141] However, upon encapsulation of C_{60}, **58** gives a single regio-isomer where all the ligands adopt a *syn*-configuration via the template-

effect. This result indicates that the C_{60}-templation can influence the equilibrium between different species but also between different regio-isomers. Nitschke and co-workers have reported the synthesis of heterometallic M_3L_4 coordination cage **59** with the help of a template-effect by C_{60}/C_{70} encapsulation (**Figure 1.4.11a**).[142] A sequential reaction of the subcomponents leads to the construction of supramolecular M_4L_6 coordination cage **59** as a mixture of all possible diastereomers. Tetrahedral **59** transforms into cone-shaped **60** upon encapsulating fullerene, presumably due to the release of the distortion observed in the X-ray structure of **58** and weak-interactions between the ligands and the entrapped C_{60}/C_{70}. It should be noted that multi-point bonding is an essential factor to stabilize coordination cages, often seen in coordination polymer chemistry, however, one out of three Fe(II) centers loses hexa-coordination while the structure undergoes reconfiguration from **59** to **60**. This result indicates existence of a template-effect. The unsaturated Fe(II) center is further replaceable with a Cu(I) center. Treatment of C_{60}/C_{70}@**60** with $Cu(MeCN)_4$•(NTf) yields heterometallic coordination cage **61**. Phosphangulene has a bowl-shaped structure thanks to the phosphorous atom in the center.[143] A couple of coordination cages based on phosphangulene have been reported so far.[144,145] Due to the hindered bowl-inversion, the ligands are chiral, so are the coordination cages. Nitschke and co-workers reported M_4L_4 tetrahedral cage **62** by multi-component metal-mediated self-assembly (**Figure 1.4.11b**).[144] **62** is obtained as one of the possible diasteromers, T_1, with *P* and *M* chirality. Without any templates, T_1-**62** is selectively formed, however, the other diastereomer T_2-**62** is selectively obtained by adding C_{60} or C_{70} as a template. Nabeshima and co-workers recently discovered chirogenesis on the encapsulated C_{60} within chiral M_4L_4 cage **63** composed of the chiral phosphangulene ligand and Zn(II) by chirality-transfer from the cage to the encapsulated C_{60} (**Figure 1.4.11c**).[145] Clever and co-workers have reported a systematic study on heteroleptic assemblies by a coordination-sphere-engineering approach based on cooperative steric bulk and H-bonding around metal centers.[146] The group has investigated self-assembly of a ligand library in which coordination-sites are diversified (**Figure 1.4.12**). The ligand having the quinoline coordination-sites forms bowl-shaped compound Pd_2**7**$_3(MeCN)_2$ by mixing with Pd(II). The steric bulk around the Pd(II)-centers prevents a fourth quinoline-ligand from coordination. On the other hand, a ligand possessing naphthyridine coordination-sites yields cage Pd_2**64**$_4$ via self-assembly with Pd(II). The coordination sites are stabilized so that the

electronic repulsion becomes minimum as can be seen in the X-ray structure. Further introduction of steric bulk around the metal centers leads to fewer ligands to coordinate.

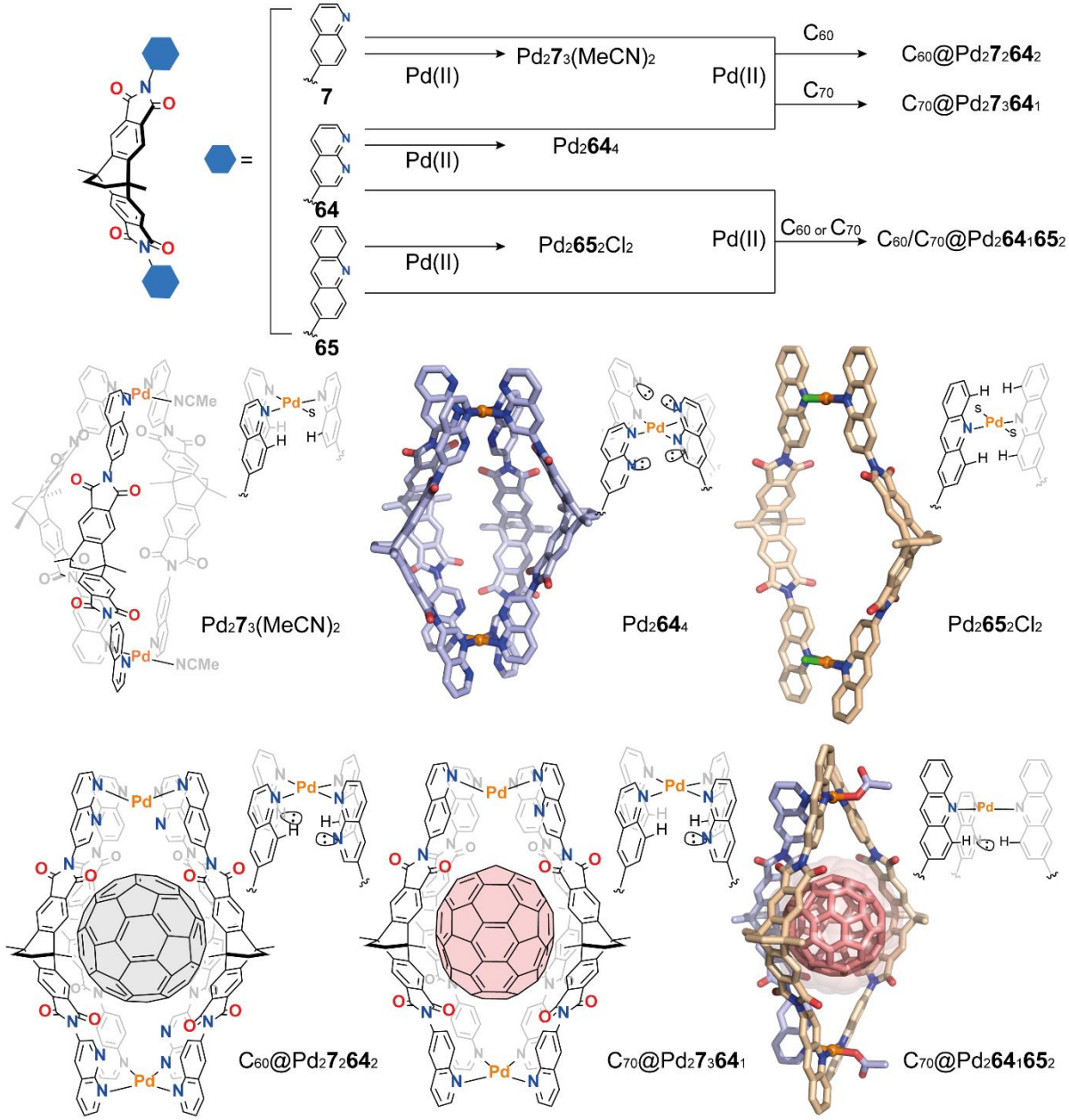

Figure 1.4.12 Syntheses of $Pd_2\mathbf{7}_3(MeCN)_2$-$C_{70}@Pd_2\mathbf{64}_1\mathbf{65}_2(OAc)_2$. Structures of $Pd_2\mathbf{7}_3(MeCN)_2$, $C_{60}@Pd_2\mathbf{7}_2\mathbf{64}_2$, $C_{70}@Pd_2\mathbf{7}_3\mathbf{64}_2$, X-ray structures of $Pd_2\mathbf{64}_4$, $Pd_2\mathbf{64}_2(Cl)_2$, $C_{70}@Pd_2\mathbf{64}_1\mathbf{65}_2(OAc)_2$ are shown

Self-assembly of the ligand with acridine coordination-sites and Pd(II) forms coordination ring $Pd_2\mathbf{65}_2(MeCN)_4$. $Pd_2\mathbf{65}_2(MeCN)_4$ shows a weak binding toward C_{60}.[147] When an equimolar amount of ligands **7** and **64** are mixed with Pd(II) in

acetonitrile, an unidentifiable mixture is obtained while heteroleptic coordination cage Pd_2**7**$_2$**64**$_2$ is cleanly assembled by the template-effect with C_{60} in the *trans*-configuration. The ratio of **7** and **64** can be varied from 2:2 to 3:1. For instance, heteroleptic cage Pd_2**7**$_3$**64**$_1$ can be synthesized by combining a mixture of C_{70}@Pd_2**7**$_3$ and C_{70}@Pd_2**7**$_4$ and **64**. H-bonding between the lone-pairs from the naphthyridine coordination-sites and the hydrogen atoms from the quinoline coordination-sites around the metal centers is essential for the formation of Pd_2**7**$_3$**64**$_1$ and Pd_2**7**$_2$**64**$_2$. The hydrogen atoms around Pd(II) in Pd_2**65**$_2$(MeCN)$_4$ further introduce steric bulk, preventing a third ligand to coordinate. On the contrary, the hydrogen atoms of ligand **65** together with naphthyridine ligand **64** allowed to form the first example of a heteroleptic coordination bowl Pd_2**64**$_1$**65**$_2$. Pd_2**64**$_1$**65**$_2$ can be yielded by mixing Pd_2**65**$_2$(MeCN)$_4$ and ligand **64**.

1.4.3.3 Encapsulation of multiple fullerenes

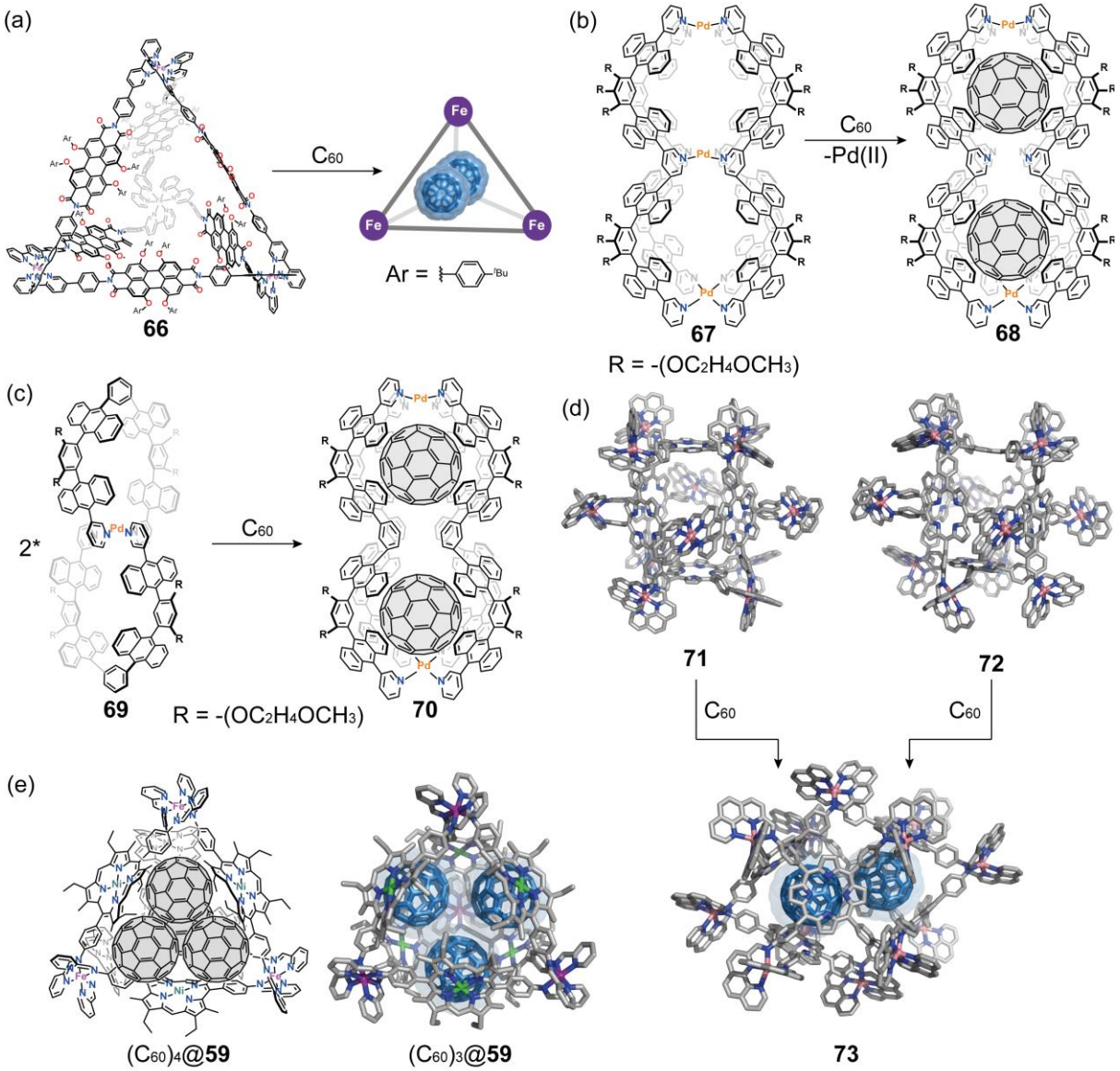

Figure 1.4.13 Encapsulation of more than one fullerene inside coordination cages (a) **66** (b) **67** yielding $(C_{60})_2$@**68** and (c) **69** forming $(C_{60})_2$@**70** (d) Template effect leading to formation of multiple C_{60} molecules encapsulating cage $(C_{60})_2$@**73** from **71** and **72**. X-ray structures of **71**, **72**, and $(C_{60})_2$@**73** are shown (e) structure of $(C_{60})_4$@**59** on the left side and X-ray structure of $(C_{60})_3$@**59**

Multi-substrate encapsulation is a ubiquitous and important function in biological systems.[61] To understand this phenomenon, mimicking and developing a molecular system accommodating multiple guest molecules are of importance.[61] Furthermore, fullerenes trapped and well-aligned in close proximity is of great interest in solid-state physics.[24,27] Until recently, only few coordination cages incarcerating more than one

C_{60}s have been reported. The first example of encapsulating multiple C_{60}s within a coordination cage was reported by Würthner and co-workers (**Figure 1.4.13a**).[148] They have chosen a perylene bisimide (PBI) based organic ligand in order to construct a supramolecular coordination cage. Tetrahedral M_4L_6 cage **66** is formed by reacting the organic ligand and Fe(II) metal source in an acetonitrile/$CHCl_3$ (1:1) solution. The inner cavity volume of cage **66** was calculated to be 950–2150 $Å^3$ while the volume of C_{60} is estimated to be 597 $Å^3$. The large and hollow cavity of **66** is therefore suitable to accommodate several counts of C_{60}. After mixing **66** and an excess amount of C_{60} in acetonitrile/$CHCl_3$ (9:1), according to ^{13}C NMR analysis of C_{60}@**66** in an acetonitrile solution, encapsulation of one molecule of C_{60} was observed. On the other hand, an ESI-MS spectrum showed not only C_{60}@**66** but also $(C_{60})_2$@**66**, which is indicative of accommodation of two C_{60}s in the gas phase. Considering the empirical "55% occupancy theory" postulated by Rebek,[149] encapsulation of two C_{60} molecules is in agreement with this theory. Yoshizawa and co-workers reported encapsulation of two molecules inside M_3L_4 coordination cage **67** (**Figure 1.4.13b**).[150] The ligand having three pyridine coordination-sites and four anthracene panels yields assembly **67** by treatment with Pd(II) in DMSO at 110 °C. **67** provides two independent isolated spaces, and therefore, two C_{60} molecules were assumed to be encapsulated in these voids. Intriguingly, coordinate bonds at the central Pd(II) center spontaneously break to expand the isolated spaces in order to accommodate two C_{60}s and form peanut-shape coordination cage **68** after release of a Pd(II) cation. These expanded inner cavities can incarcerate not only two C_{60}s but also two C_{70}s and two Sc_3N@C_{80}s. These results demonstrate the flexibility of the cavities. Notably, the flexible cavities make it possible to encapsulate two different guest-molecules with a different size, in which a smaller cavity is occupied with adamantane while a larger cavity is occupied by two phenanthrene molecules. By replacing the central pyridine group with benzene, another supramolecular array was further obtained.[151] In contrast to **67**, M_2L_4 peanut-shaped coordination cage **70** can be synthesized at room temperature. The W-shaped organic ligand displays a solvent-dependent assembly. In DMSO in the presence of Pd(II), a mononuclear ML_2 coordination compound **69** forms with both ligands folding back to coordinate the single Pd(II) in a chelating mode, while M_2L_4 cage **70** forms in an acetonitrile/H_2O (9:1) solution (**Figure 1.4.13c**). M_2L_4 cage **70** can encapsulate two C_{60} molecules at room temperature, whilst addition of C_{60} into the DMSO solution of **69** yields the formation of the same $(C_{60})_2$@**70** in virtue of a template effect.

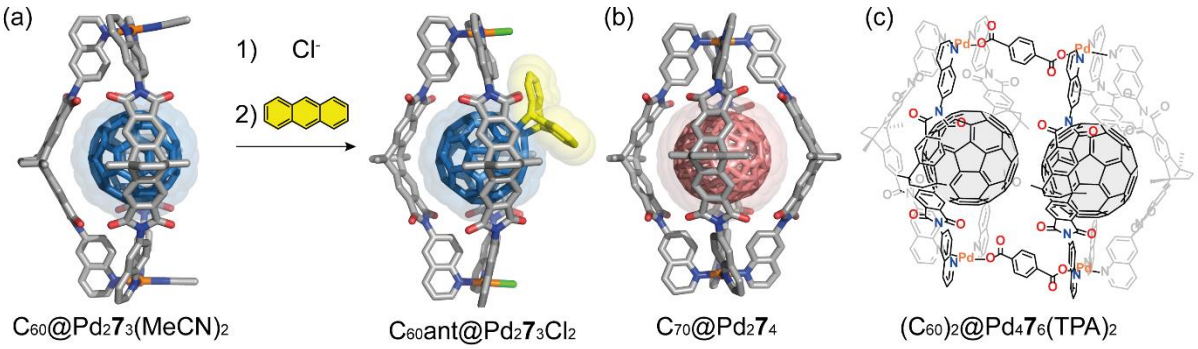

Figure 1.4.14 (a) Diels-Alder reaction between encapsulated C_{60} inside Pd_2**7**$_3(MeCN)_2$; X-ray structures are shown for C_{60}@Pd_2**7**$_3(MeCN)_2$ and C_{60}ant@Pd_2**7**$_3Cl_2$ (b) X-ray structure of C_{70}@Pd_2**7**$_4$ and (c) $(C_{60})_2$@Pd_4**7**$_6(TPA)_2$

Cyclic voltammetry highlighted that each encapsulated C_{60}s within an analogue of **70** show different reduction potentials although they are not in direct contact. Nitschke and co-workers reported incorporation of two C_{60}s inside *S*$_6$-symmetric polyhedral **73** (**Figure 1.4.13d**).[152] In this study, a template-effect helps re-organization of $(C_{60})_2$@**73** from either *O*-symmetric polyhedral **71** or *D*$_4$-symmetric polyhedral **72**. Notably, in the *O*-symmetric structure, **71** shows negative cooperativity in binding of $B_{12}F_{12}^{2-}$, whilst $(C_{60})_2$@**73** showcases the cage-to-cage transformation and the allosteric binding behavior with a C_{70}s encapsulating species as well. The same group reported encapsulation of up to four molecules of fullerene into **59** and investigated electronic properties of the confined C_{60}s closely contacting each other.[153] **59** was shown to undergo reconstitution to cone-shaped **60** templated by C_{60}[142] in acetonitrile, yet, the M_4L_6 structure is maintained in less coordinative solvents such as $MeNO_2$ or $PhNO_2$. The encapsulation behavior was also found to be different in both solvents. Up to three C_{60}s can be accommodated in **59** in $MeNO_2$, while up to four C_{60}s can be accommodated in **59** in $PhNO_2$. Cyclic voltammetry revealed the existence of electronic communication between the closely packed C_{60}s. In another work, Clever and co-workers constructed a pill-shaped coordination cage encapsulating two C_{60} molecules. Coordination-sphere engineering enables the formation of bowl-shaped Pd_2**7**$_3(MeCN)_2$ in which acetonitrile molecules are coordinating one of the coordination sites of each Pd(II) cation (**Figure 1.4.14**). Treatment of Pd_2**7**$_3(MeCN)_2$ with two equivalents of terephthalate (TPA) creates pill-shaped cage Pd_4**7**$_6(TPA)_2$ whilst addition of C_{70} leads to a mixture of

C_{70}@Pd_2**7**$_3$$(MeCN)_2$ and C_{70}@Pd_2**7**$_4$. C_{60}@Pd_2**7**$_3$$(MeCN)_2$ also shows the same dimerization behavior. As a result of the dimerization of C_{60}@Pd_2**7**$_3$$(MeCN)_2$, $(C_{60})_2$@Pd_4**7**$_6$$(TPA)_2$ is assembled.[71]

1.4.3.4 Selective encapsulation of fullerenes

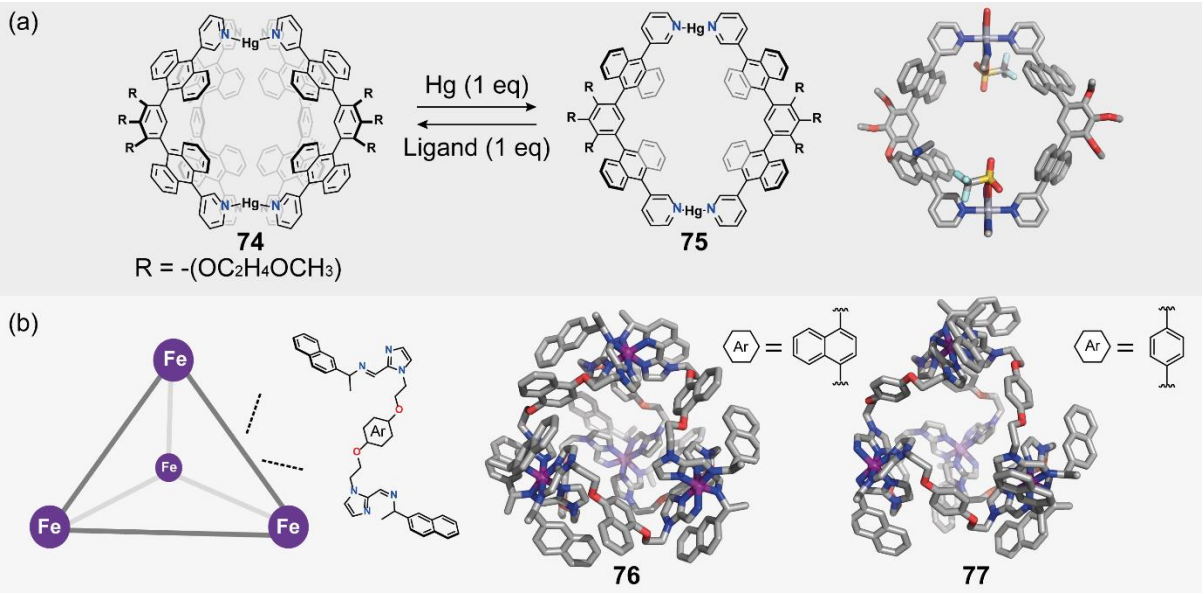

Figure 1.4.15 Cage-to-cage transformation between **74** and **75** by addition of metal/ligand. X-ray structure of **75**, (b) X-ray structure of **76** and **77**

On account of a demand for facile and environment friendly fullerene purification methods, size selective encapsulation of fullerenes is of great interest. Some of the state-of-the-art molecular designs of covalently-bonded fullerene-binders showing selectivity for specific fullerenes have been introduced already in above sections. A geometrical and spatial matching is one of the most important factors to determine if fullerene-binders have special preferences for selected fullerenes. Among the coordination cages introduced already, for instance, Yoshizawa's molecular capsule **27** selectively binds C_{60} out of carbon-soot and releases the captured C_{60} upon light irradiation.[121]

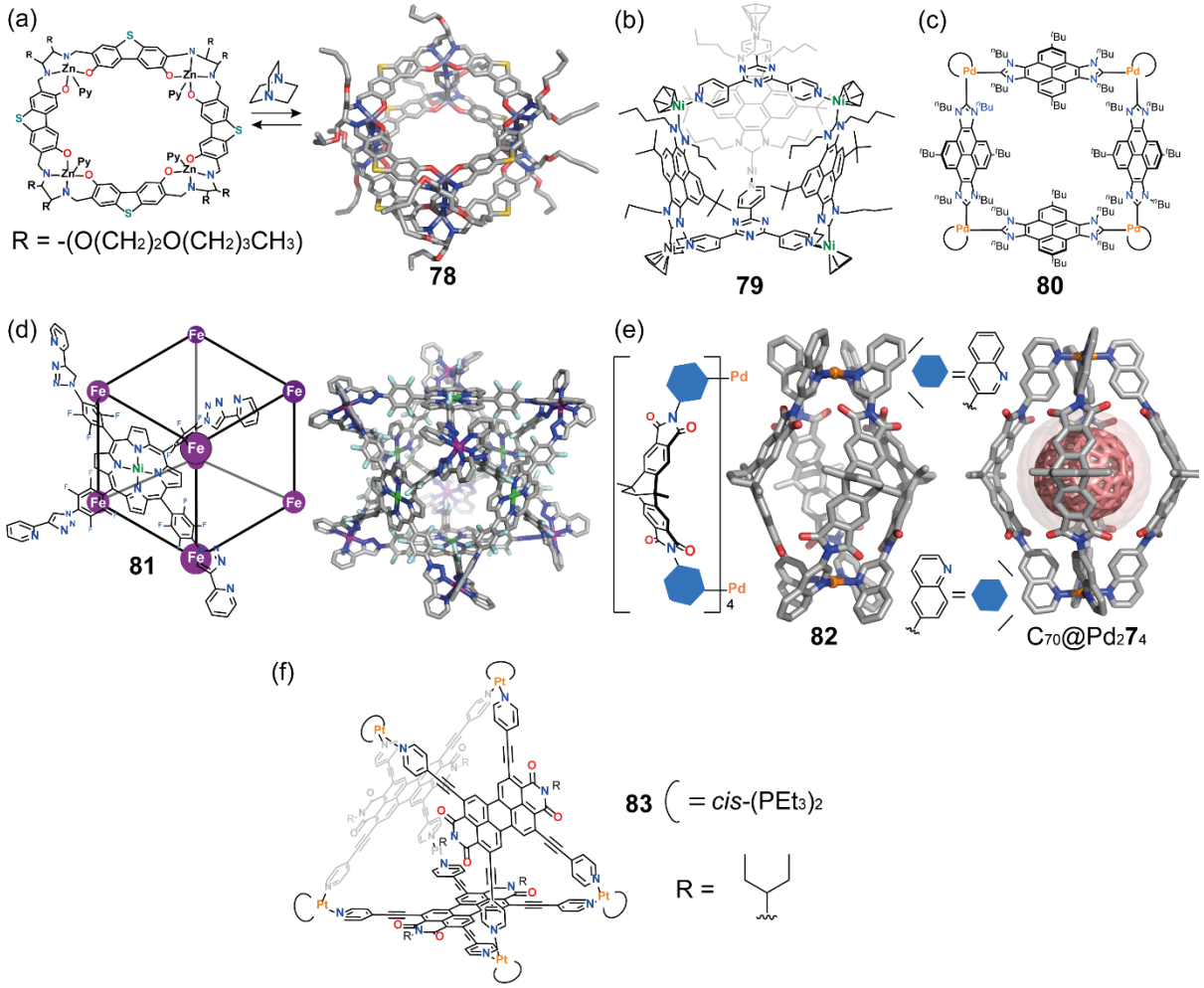

Figure 1.4.16 (a) Dimerization of macrocycles to form **78** (b) structures of **79** (c) **80** (d) and **81** with its X-ray structure (e) X-ray structures of **82** and $C_{70}@Pd_2$**7**$_4$ (f) structure of **83**

In addition, the anthracene ligand mixed in 2:1 ratio with Hg(II) gives Hg_2L_4 capsule **74** while ring-shaped **75** is formed when the ratio is 1:1 (**Figure 1.4.15a**).[154] While **74** can bind either C_{60} or C_{70}, **75** cannot. In addition, **74** preferably encapsulates C_{60} over C_{70}. By exploiting these features, uptake and release of C_{60}/C_{70} can be performed by changing the Hg(II)-to-ligand ratio. Cubic coordination cage **46** reported by Nitschke's group shows a preference to bind larger fullerenes, e.g., C_{70}, C_{76} and C_{84}, over C_{60} according to ESI-MS analyses.[129] Corannulene-based coordination cage **51** reported by Jiang shows selective encapsulation of C_{60} over C_{70} upon temperature increase as introduced before.[134] In addition to those works, Gu and co-workers have reported selective encapsulation of C_{60} in M_4L_6 coordination cages **76** and **77** composed of Fe(II) centers and flexible organic ligands (**Figure 1.4.15b**).[155] Recently C–H•••π

interactions have been found to be versatile weak interactions to create unique supramolecular arrays. An elaborate molecular design even makes the construction of fullerene-inclusion molecular complexes possible utilizing C–H•••π interactions.[115,116,156] As an example of such supramolecular complexes, Tanaka and co-workers reported double-decker type coordination cage **78** (**Figure 1.4.16a**).[157] Bridging two macrocycles by DABCO gives **78** in $CDCl_3$. **78** can encapsulate C_{70} within the central hole of the macrocycles via C–H•••π interactions. **78** forms a 1:1 molecular complex with C_{70} in a $CHCl_3/CS_2$ (5:2) solution with an encapsulation yield of 22%. The K_a value was determined to be 180 M^{-1} by a ^1H NMR study. The authors claimed that multiple C–H•••π interactions should be the key for encapsulation. Peris and co-workers have shown preferable encapsulation of C_{70} within prism-shaped coordination cage **79** via π–π interactions (**Figure 1.4.16b**).[158] Self-assembly of a bis-nickel-pyrene-di-imidazolylidene complex and 1,3,5-tripyridyl-triazine in the presence of $AgBF_4$ yields the prism-shaped cage. The pillars possessing aromatic pyrene moieties enable π–π interactions with fullerenes. **79** is capable of encapsulating C_{60} and C_{70}, however, C_{70} shows more favorable interactions compare to C_{60}. DFT calculations suggest that the replacement from C_{60}@**79** to C_{70}@**79** should be an exergonic process. The pyrene-di-imidazolylidene ligand also forms box-shaped complex **80** upon reaction with allylpalladium(II) chloride dimer (**Figure 1.4.16c**).[159,160] **80** displays selective encapsulation of C_{70} thanks to the one order of magnitude higher association constant with C_{70} over C_{60}. **80** shows the adjustment of the size of the cavity depending on the guest molecules in the solid state. C_{60} and C_{70} are known to have a property to generate $^1O_2$ by triplet-triplet energy transfer from $^3C_{60}/^3C_{70}$ to $^3O_2$.[161] The encapsulated C_{60}/C_{70} within **80** has the inherited property even under confinement and promotes a hetero Diels-Alder reaction with *in situ* generated $^1O_2$. The adaptability of the cage was further investigated also in the gas-phase using ion mobility mass spectrometry.[162] Based on their previous works, Nitschke and co-workers synthesized cubic coordination cage **81** composed of six Ni(II)-porphyrin based ligands and eight Fe(II) ions (**Figure 1.4.16d**).[163] Single crystal X-ray structural analysis confirms the pseudo-*O*-symmetric structure with a large cavity of 3183 $Å^3$. In virtue of the large inner cavity and the large deviation from the Rebek's 55% rule, mere C_{60} as well as some large anions are not suitable as guest molecules. The encapsulation of fullerene adducts synthesized via Diels-Alder reaction with either anthracene or indene were tested in an acetonitrile solution of the cage by suspending

the adducts. The experiments showed that only the bis-adduct could be encapsulated within **81**. Clever and co-workers have reported size-selective encapsulation of C_{60} and C_{70} inside Pd_2L_4 cavities by coordination-sphere engineering.[71,147] Depending on the coordination-sites, the size of a cavity can be modified. For instance, cage Pd_2**6**$_4$ selectively binds C_{60}, however, cage Pd_2**7**$_4$ possessing a larger cavity can bind C_{70} (**Figure 1.4.16e**). These results imply that the position of the N-atoms on the quinoline coordination-sites also influences the encapsulation ability. **82** encapsulates neither C_{60} nor C_{70} due to its relatively small cavity. Stang and co-workers have recently reported prism-shaped coordination cage **83** by metal-mediated self-assembly of a PDI-based ligand and *cis*-$(PEt_3)_2Pt(OTf)_2$ (**Figure 1.4.16f**).[164] **83** selectively encapsulates C_{70} out of a C_{60} and C_{70} mixture.

1.4.3.5 Purification of fullerenes

One of the ultimate goals of the selective binding of a specific fullerene is to develop a purification system. The first example of fullerene-purification using a supramolecular approach was reported by Shinkai and Atwood.[74,75] In their approach, a calix[8]arene derivative can selectively encapsulate C_{60} out of other higher fullerenes and the encapsulated C_{60} can be released by a simple solvent treatment. Coordination cages which can selectively encapsulate a specific fullerene have attracted attention in terms of fullerene purification as coordination cages are relatively easy to synthesize and are assembled via rather labile coordinative bonds which are advantageous for uptake-and-release. Shinkai and co-workers reported metallo-supramolecular fullerene-binder **47** in 1999,[130] and nano-capsule **47** has been proven to exhibit alkali-metal responsive C_{60} uptake/release behavior.[165] The K_a value for the formation of the 1:1 host-guest complex C_{60}@**47** is 54 M^{-1} in 1,2-dichloroethane at 298 K. Besides the binding abilities of the central cavity, the peripheral ester chains in proximity capture small cations such as Li^+ and Na^+. Addition of Li^+ cations induce the adjacent of phenyl groups to become more flattened, thus altering the shape and size of the central cavity.

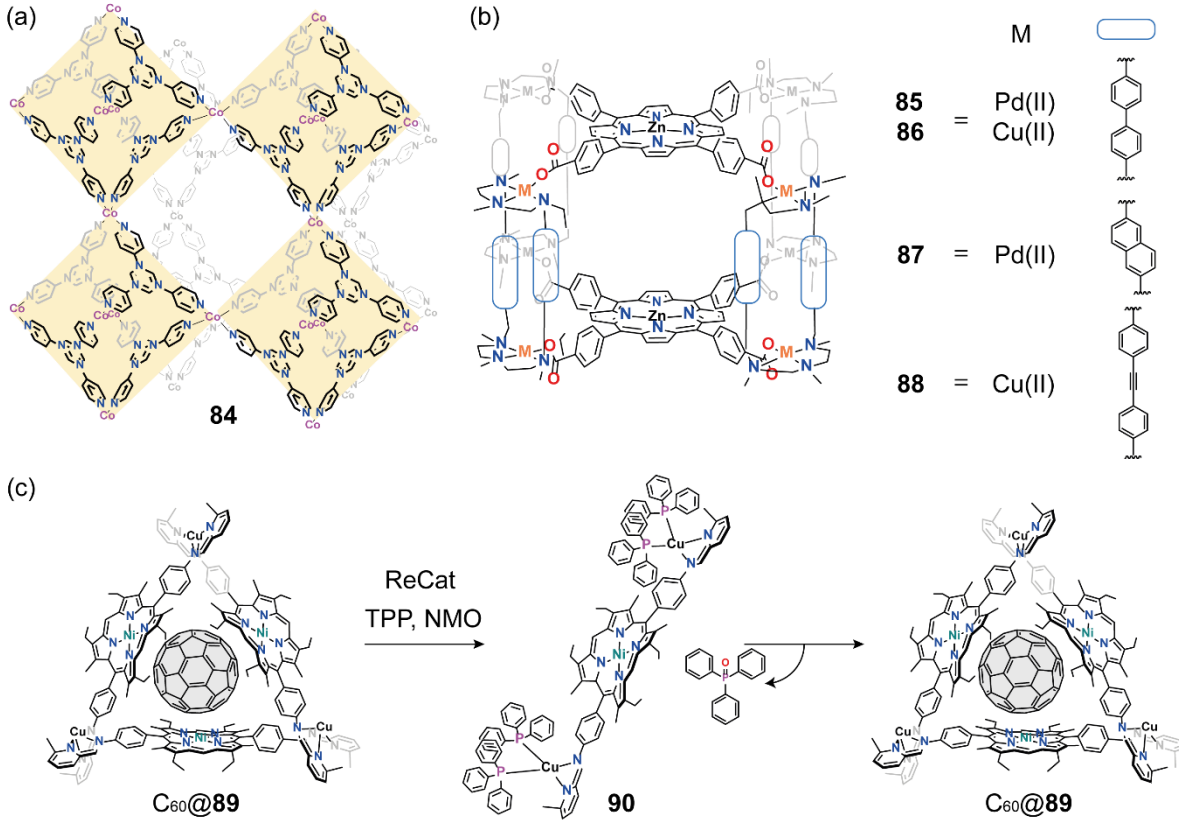

Figure 1.4.17 (a) partial structure of coordination polymer **84** (b) structure of **85**-**88** (c) ejection and encapsulation of C_{60} through formation and deformation of C_{60}@**89** and **90**

The resulting cavity of $2Li^{+}$•**47** is more suitable for the encapsulation of globular C_{60}, resulting in the enhanced K_a values up to 2100 M^{-1}. In stark contrast, when the larger cations, Na^{+}, are bound to the ester pockets, a significant decrease of K_a value is observed. Accordingly, the cation-induced adjustment on binding affinities of this host is employed to realize C_{60} uptake/release in a reversible fashion. Note that **47** does not show encapsulation toward C_{70} which is a criterion for purification of C_{60}. Fujita and co-workers showcased accommodation of fullerenes into the 3D network of porous coordination polymer **84**, hinged by Co(II) centers (**Figure 1.4.17a**).[166] Single crystal X-ray structure analysis revealed that **84** has a cuboctahedral unit. Owing to the hierarchical structure, coordination polymer **84** has large apertures allowing encapsulation of fullerene in the crystalline state by soaking a toluene solution of fullerenes. Acid treatment of the host-guest crystals is required to recover the stored fullerenes. Due to the huge cavities, larger fullerenes are more prone to be captured than smaller ones enabling enrichment of C_{70} from commercially available carbon-

soot. Ribas and co-workers have also developed a C_{60} purification method out of crude carbon-soot containing higher fullerenes by washing solids of C_{60}-inclusion coordination cage **85** with an organic solvent (**Figure 1.4.17b**).[167] Tetragonal prism-shaped coordination cage **85** is synthesized via self-assembly of two molecules of tetracarboxylate Zn(II)-porphyrin and four molecules of a readily prepared Pd(II)-based macrocyclic synthone in acetonitrile. Large apertures allowing solvation of confined fullerenes often result in small binding constants, however, a strong affinity of the metalloporphyrins with fullerene compensates the poor binding ability.[99] In fact, **85** forms 1:1 molecular complex with C_{60} with K_a value of 2.8×10^7 M^{-1}, although **85** has four apertures allowing solvent molecules to reach the confined C_{60}. A variety of fullerenes including C_{60}, $PC_{61}BM$, C_{70} and C_{84} can be bound within prismatic cage **85** in 1:1 ratio and the larger fullerene tends to display a higher affinity with **85**. The accommodation of a fullerene causes a shrinkage of the cage to maximize contacting surfaces. The lower binding ability of **85** for C_{60} relatively to larger fullerenes realizes a facile and selective release of the encapsulated C_{60} by a washing process. Solid sample of fullerenes encapsulating **85** are precipitated by addition of diethylether to an acetonitrile/toluene (1:1) solution of **85** and fullerene-extracts from carbon-soot. By washing the solid sample with CS_2/*o*-dichlorobenzen (1:1), only C_{60} is liberated while the other encapsulated higher fullerenes can be released by acid treatment. This encapsulating-washing protocol is repeatable with the same sample and the strategy has potential to simplify fullerene-purification. Not only the solvent-washing strategy is applicable to release the confined C_{60} but also competitive guest-uptake can release the C_{60} as following.[168] The same group demonstrated recovery of the encapsulated C_{60} in **85** by encapsulation of a two-electron-oxidation active compound, tetrapyridyl-extended-tetrathiafulvalene (exTTF)-based ligand (*m*-Py)exTTF. In a neutral state (*m*-Py)exTTF is in a bent-shape and is able to anchor Zn(II) centers from inside the cage. Upon two-electron oxidation, (*m*-Py)exTTF becomes flat and escapes outside. C_{60} uptake and release can be performed accompanying the reduction/oxidation process. The size of the prismatic cage can be tuned by changing linkers. Replacement of the biphenyl linkers to naphthalene linkers changes the Zn-Zn distance of the porphyrin from 14.1 Å to 8.2 Å according to the X-ray structures.[169] Although the Zn-Zn distance is smaller than the diameter of C_{60}, **87** can encapsulate C_{60} and even C_{70}. MD simulations suggest the adaptability of **87** derives from the flexibility of the cage. Contrary to cage **85**, naphthalene-linked cage **87** shows exclusive encapsulation of

C_{60} out of a fullerene mixture containing C_{60}, C_{70} and other bigger fullerenes. **87** can also encapsulate fullerene C_{60} derivatives, $PC_{61}BM$ and N-pyrrolidine-C_{60}, in a 1:1 ratio. Interestingly, cage **87** shows a slightly lower K_a value towards both C_{60} derivatives compared to C_{60}. Only weakly bound N-pyrrolidine-C_{60} can be liberated by the solvent-washing strategy. The strong binding ability of cage **85** to higher fullerenes realizes a simple purification of C_{60}, higher fullerenes, and even endohedral metallofullerenes (EMFs). In this study, Ribas and co-workers tried purification of endohedral metallofullerenes (EMFs) by utilizing **86**, an Cu(II) analogue of **85**. [170] When the encapsulation of fullerenes extracted from carbon-soot containing C_{60}, C_{70}, $Sc_3N@C_{68}$, $Sc_3N@C_{78}$, $Sc_3N@C_{80}$ and other fullerenes is performed in a toluene/acetonitrile (9:1) solution, 1:1 complexes of **86** incarcerating C_{60}, C_{70}, $Sc_3N@C_{68}$, $Sc_3N@C_{78}$, $Sc_3N@C_{80}$ are mainly obtained. Notably, all encapsulated species can be liberated through the solvent-washing protocol. In stark contrast, **86** shows a preferential encapsulation-behavior for smaller fullerenes when solid **86** is soaked into the fullerene mixture in a toluene solution. By taking advantage of this, $Sc_3N@C_{80}$ can be selectively obtained by capturing other smaller fullerenes. As a result, only $Sc_3N@C_{80}$ remains in the toluene solution, whilst the other smaller fullerenes are entrapped in **86**. Surprisingly, **86** is also able to purify $U_2@I_h$-C_{80} and $Sc_2CU@I_h$-C_{80} from carbon-soot one by one each.[171] In stark contrast to $Sc_3N@C_{80}$, both $U_2@I_h$-C_{80} and $Sc_2CU@I_h$-C_{80} are extracted by mixing solid-state **86** and a toluene solution of EMFs and empty fullerenes mixture. When crystalline **86** is soaked in a toluene solution of a carbon-soot containing $U_2@C_{80}$, $Sc_2CU@I_h$-C_{80} and other fullerenes, $U_2@C_{80}$ is selectively encapsulated. Repetitive soaking of **87** to the remaining supernatant results in the removal of $Sc_2CU@I_h$-C_{80} as $Sc_2CU@I_h$-C_{80} is entrapped within the cage. **87** even shows the selective encapsulation for $U_2@I_h$-C_{80} over $Sc_2CU@I_h$-C_{80}. **86** also shows a favorable encapsulation behavior to EMFs, $U_2@C_{78}$ and $U_2C@C_{78}$, possessing a slightly different carbon cage from $U_2@I_h$-C_{80}.[172] The adaptability of **86** allows specific molecular recognition. **86** can tell apart from $U_2@C_{78}$ and $U_2C@C_{78}$ depending on the encapsulated species within the fullerene. The trapped guest molecules can be released by washing the crystalline host-guest complex with CS_2. Elongation of the cavity size by replacing the biphenyl linkers by diphenylacetylene linkers makes the selective encapsulation of C_{84} possible.[173] The content of C_{84} in the recovered guests can be increased ~125-fold compared with the one in the initial carbon-soot by purification utilizing **88**. The

detailed dynamic behavior of the adaptability of cage **85** was investigated by combination of $^{1}H-^{1}H$ exchange spectroscopy (2D-EXSY) NMR experiments, long time-scale Molecular Dynamics (MD) and accelerated Molecular Dynamics (aMD) simulations.[174] Nitschke and co-workers reported fuel-controlled reassembly of macrocycle **89** accompanied by C_{60} uptake and release (**Figure 1.4.17c**).[175] When **89** is mixed with triphenylphosphine (TPP), TPP coordinates Cu(I) and thus replaces the Ni-porphyrin ligands to yield **90**. As a consequence of the ligand exchange, the encapsulated C_{60} is released from the macrocycle. In the presence of a rhenium catalyst and pyridine *N*-oxide, TPP is oxidized to triphenylphosphineoxide presenting lower coordination ability than TPP. Thus, **91** gradually transforms into **89** over time and encapsulates C_{60} inside the macrocycle when **90** is treated under oxidation conditions.

1.4.3.6 Reaction of C_{60} inside coordination cages

Fullerene derivatives have been utilized in the field of photovoltaics and molecular electronics. The electron-accepting ability and the unique structure are a great advantage as an electron-accepting material.[176–178] However, regio-selective chemical modification of C_{60} require a special strategy.[29,179,180] Fullerene-binders such as coordination cages can help regioselective modifications of C_{60} as a supramolecular mask as nicely summarized in the literature.[180] Clever and co-workers have showcased a Diels-Alder reaction between confined C_{60} and anthracene.[71] Bowl-shaped $Pd_2\mathbf{7}_3(MeCN)_2$ covers ca. 75% of the surface of the incarcerated C_{60}, and thus, Diels-Alder reaction takes place only on the uncovered surface to give only the mono-adduct. Mixing $C_{60}@Pd_2\mathbf{7}_3(MeCN)_2$ and 10 equivalents of anthracene in acetonitrile gives only mono-adduct of fullerene (**Figure 1.4.14**). As mentioned above, Nitschke and co-workers have demonstrated the chemo-selective formation of the bis-adduct of C_{60} and anthracene/indene using **81** (**Figure 1.4.18a**). Stimulated by this work, a metal-organic framework which catalyzes the same Diels-Alder reaction with C_{60} and anthracene yielding only C_{60}-anthracene bis-adduct was developed.[181] Ribas and co-workers reported a regio-selective Bingel-Hirsch reaction by utilizing metallo-supramolecular complex **85** as a supramolecular mask.[182,183] The structure of **85** possessing four large apertures allows nucleophiles to access the bound C_{60} and controls the regio-selectivity.

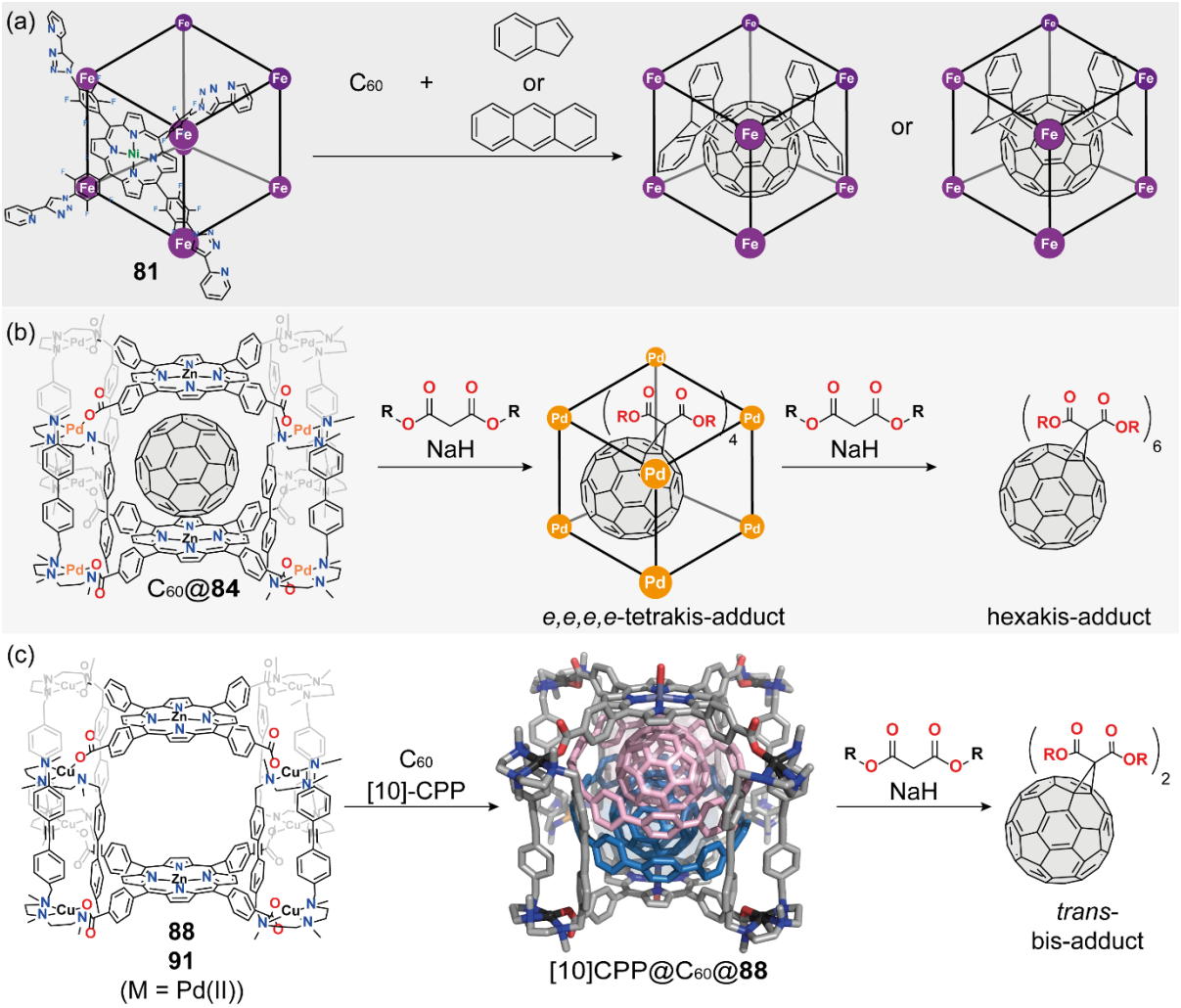

Figure 1.4.18 (a) Selective formation and encapsulation of C_{60} Diels-Alder bis-adducts inside **81**, (b) Regio-selective Bingel-Hirsch reaction on the encapsulated C_{60} inside C_{60}@**85**, (c) X-ray structure of [10]CPP@C_{60}@**88** and utilization of the molecular complex for regio-selective synthesis of C_{60} *trans*-bis-adduct.

When C_{60} encapsulating coordination cage **85** is treated in the Bingel-Hirsch reaction condition, cage **85** serves as a protecting group leading to the regioselective multi-addition reaction on the encapsulated C_{60} (**Figure 1.4.18b**). As a consequence, four malonate substituents are introduced on the equator of the encapsulated C_{60}. It was elucidated that the Bingel-Hirsch reaction takes place step-by-step by ESI-MS analysis. This stepwise process realizes a one-pot synthesis of hetero-tetrakis adducts and hetero-hexakis adducts. The regioselective functionalization reaction can be performed under cyclic turnover conditions. Addition of excess amounts of sulfate triggers anion metathesis and the transfer of the cage into the water layer of a reaction

mixture takes place. Then after, the Bingel-Hirsch reaction proceeds in the aqueous phase. Once the reaction finished, the host-guest complex is carried back to the organic layer by the addition of tetraarylborates. In the organic layer, the tetrakis-adduct is replaced by intact C_{60}. It should also be noted that all the reactions introduced in this section can be performed in polar media, which are usually not employed for chemical reactions of C_{60} due to its poor solubility. Very recently, Ribas, von Delius and co-workers further extended the regio-selective Bingel-Hirsch reaction (**Figure 1.4.18c**). A Russian-doll like molecular complex was synthesized by encapsulation of a molecular complex of C_{60} and [10]CPP inside **88**/**91**.[184] The solid-state structure of C_{60}@[10]CPP@**88** was elucidated by single crystal X-ray structure analysis. The encapsulated C_{60}@[10]CPP complex was found to tilt against the Zn-Zn axis. The introduction of further molecular hindrance around C_{60} together with the tilted geometry leads the exclusive formation of *trans*-bis-adducts. In addition to those examples, a couple of advanced reactions of C_{60} inside coordination cages have been reported.[185,186]

1.4.3.7 Electronic/Magnectic interactions

Electronic/Magnetic communication within supramolecular systems including fullerenes is one of the greatest interests as it plays a significant role in artificial photosynthesis,[187,188] molecular magnetism,[155,189] and charge separation.[190] Electronic properties of organic ligands may give rise to perturbations on confined fullerenes and thus, physical properties of fullerenes are tunable by a nano-confinement effect. Nitschke and co-workers have demonstrated an enhanced catalytic activity of **92** for oxidative coupling of arylborates by incarceration of C_{60} (**Figure 1.4.19a**).[191] The redox-activity of **92** is inherited from the redox-active NDI ligand incorporated in the cage structure. Redox-active **92** catalyzes oxidative coupling of a tetraarylborate to give a homo-coupling product. Addition of C_{60} improves the catalytic efficiency. The author concluded that the improvement should derive from the stabilization of radical species of the ligand by the encapsulated C_{60}. On the other hand, cationic NDI-based coordination cage **93** does not entrap neutral C_{60} due to electronic repulsions.[192] However, reduction of the NDI-backbone decreases the

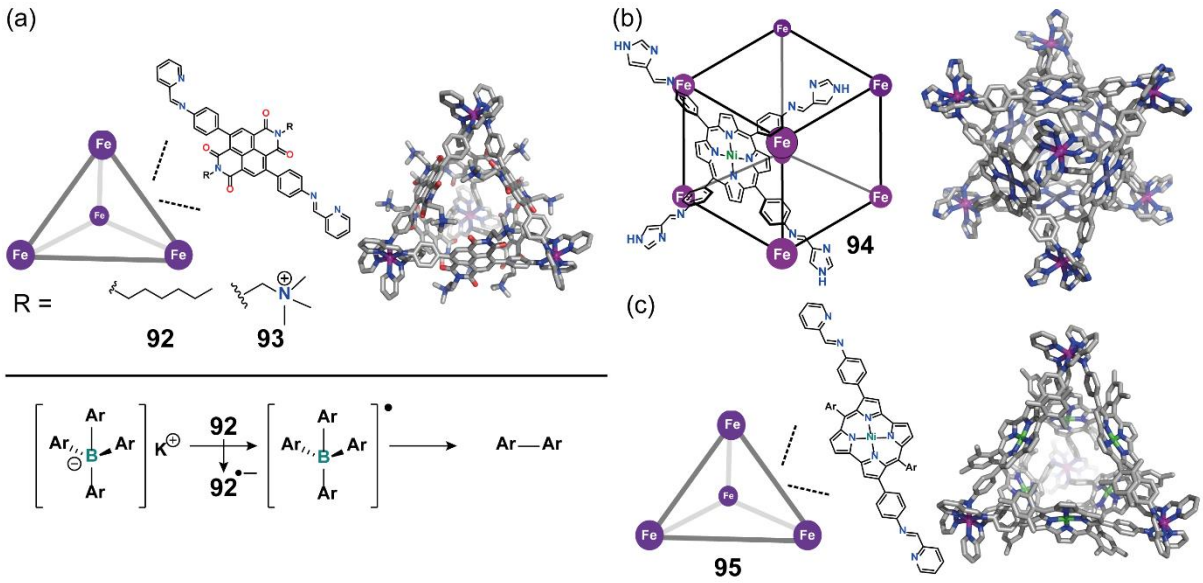

Figure 1.4.19 (a) Structures of **92** and **93**; X-ray structure of **93** is shown. Reaction catalysed by **92** is shown below the structures (b) Structure of **94** and its X-ray structure (c) X-ray structure of **95**

repulsion with C_{60} and thus C_{60} can be incarcerated only in the reduced-state. When **93** is treated with Cp_2Co, the reduced cage encapsulates C_{60}. Addition of Ag(NTf) oxidizes reduced **93** leading to ejection of C_{60} from the cage over time. Phase-transfer from the acetonitrile solution to water by anion-metathesis also initiates the ejection of C_{60} from **93**. Lützen and co-workers have reported stabilized high-spin state Fe(II) centers by accommodation of C_{70} inside cage **94** (**Figure 1.4.19b**).[155,189] As a result of the stabilized high-spin state in virtue of C_{70} inside, the phase-transition temperature of the spin-crossover becomes lower. The authors attributed the stability to entropic effects. Cages **76** and **77**, reported by Gu and co-workers, also show the stabilized high-spin state of the Fe(II) centers by inclusion of C_{60} in the solid-state. Nitschke and co-workers reported coordination cage **95** consisting of an antiaromatic building block, Ni(II)-norcorrole (**Figure 1.4.19c**).[193] In stark contrast to nanoscopic space composed of aromatic building blocks which shows shielding effect in NMR, the unique inner space surrounded with the antiaromatic building blocks displayed an antiaromatic deshielding effect.[194] Guest compounds incarcerated within **95** show uncommon downfield shifts of up to +14.9 ppm in ^{1}H NMR relative to the free guest.

1.4.4 References

[1] E. H. Falcao, F. Wudl, *J. Chem. Technol. Biot.* **2007**, *82*, 524–531.

[2] V. Georgakilas, J. A. Perman, J. Tucek, R. Zboril, *Chem. Rev.* **2015**, *115*, 4744–4822.

[3] H. W. Kroto, J. R. Heath, S. C. O'Brien, R. F. Curl, R. E. Smalley, *Nature* **1985**, *318*, 162–163.

[4] S. Collavini, J. L. Delgado, *Sustain. Energy Fuels* **2018**, *2*, 2480–2493.

[5] R. Ganesamoorthy, G. Sathiyan, P. Sakthivel, *Sol. Energy Mater. Sol. Cells* **2017**, *161*, 102–148.

[6] S. Iijima, *Nature* **1991**, *354*, 56–58.

[7] A. Takakura, K. Beppu, T. Nishihara, A. Fukui, T. Kozeki, T. Namazu, Y. Miyauchi, K. Itami, *Nat. Commun.* **2019**, *10*, 3040.

[8] J. N. Coleman, U. Khan, W. J. Blau, Y. K. Gun'ko, *Carbon* **2006**, *44*, 1624–1652.

[9] K. S. Novoselov, A. K. Geim, S. V. Morozov, D. Jiang, Y. Zhang, S. V. Dubonos, I. V. Grigorieva, A. A. Firsov, *Science* **2004**, *306*, 666–669.

[10] Z. Li, Z. Liu, H. Sun, C. Gao, *Chem. Rev.* 2015, *115*, 7046–7117.

[11] Y. Segawa, D. R. Levine, K. Itami, *Acc. Chem. Res.* **2019**, *52*, 2760–2767.

[12] E. von Hauff, V. Dyakonov, J. Parisi, *Sol. Energy Mater. Sol. Cells* **2005**, *87*, 149–156.

[13] K. Komatsu, M. Murata, Y. Murata, *Science* **2005**, *307*, 238–240.

[14] K. Kurotobi, Y. Murata, *Science* **2011**, *333*, 613–616.

[15] R. Maeda-Mamiya, E. Noiri, H. Isobe, W. Nakanishi, K. Okamoto, K. Doi, T. Sugaya, T. Izumi, T. Homma, E. Nakamura, *Proc. Natl. Acad. Sci.* **2010**, *107*, 5339–5344.

[16] F. Diederich, R. L. Whetten, *Acc. Chem. Res.* **1992**, *25*, 119–126.

[17] A. A. Popov, S. Yang, L. Dunsch, *Chem. Rev.* **2013**, *113*, 5989–6113.

[18] J. L. Segura, N. Martín, *Chem. Soc. Rev.* **2000**, *29*, 13–25.

[19] K. Itami, *Chem. Rec.* **2011**, *11*, 226–235.

[20] W. Yan, S. M. Seifermann, P. Pierrat, S. Bräse, *Org. Biomol. Chem.* **2014**, *13*, 25–54.

[21] N. S. Sariciftci, L. Smilowitz, A. J. Heeger, F. Wudl, *Science* **1992**, *258*, 1474–1476.

[22] J. Conyers, *Int. J. Nanomed.* **2009**, 261.

[23] W. Krätschmer, L. D. Lamb, K. Fostiropoulos, D. R. Huffman, *Nature* **1990**, *347*, 354–358.

[24] B. W. Smith, M. Monthioux, D. E. Luzzi, *Nature* **1998**, *396*, 323–324.

[25] O. Ermer, *Helv. Chim. Acta.* **1991**, *74*, 1339–1351.

[26] T. Andersson, K. Nilsson, M. Sundahl, G. Westman, O. Wennerström, *J. Chem. Soc. Chem. Commun.* **1992**, *0*, 604–606.

[27] I. V. Krive, R. I. Shekhter, M. Jonson, *Low. Temp. Phys.* **2006**, *32*, 887–905.

[28] T. Pichler, H. Kuzmany, H. Kataura, Y. Achiba, *Phys. Rev. Lett.* 2001, *87*, 267401.

[29] C. Thilgen, F. Diederich, *Cr. Chim.* **2006**, *9*, 868–880.

[30] D. M. Guldi, F. Zerbetto, V. Georgakilas, M. Prato, *Acc. Chem. Res.* **2005**, *38*, 38–43.

[31] S. S. Babu, H. Möhwald, T. Nakanishi, *Chem. Soc. Rev.* **2010**, *39*, 4021.

[32] T. Hasobe, *Phys. Chem. Chem. Phys.* **2009**, *12*, 44–57.

[33] H. Li, B. C.-K. Tee, J. J. Cha, Y. Cui, J. W. Chung, S. Y. Lee, Z. Bao, *J. Am. Chem. Soc.* **2012**, *134*, 2760–2765.

[34] Y. Liu, J. Zhao, Z. Li, C. Mu, W. Ma, H. Hu, K. Jiang, H. Lin, H. Ade, H. Yan, *Nat. Commun.* **2014**, *5*, 5293.

[35] M. Makha, A. Purich, C. L. Raston, A. N. Sobolev, *Eur. J. Inorg. Chem.* **2006**, *2006*, 507–517.

[36] W. I. F. David, R. M. Ibberson, J. C. Matthewman, K. Prassides, T. J. S. Dennis, J. P. Hare, H. W. Kroto, R. Taylor, D. R. M. Walton, *Nature* **1991**, *353*, 147–149.

[37] A. F. Hebard, M. J. Rosseinsky, R. C. Haddon, D. W. Murphy, S. H. Glarum, T. T. M. Palstra, A. P. Ramirez, A. R. Kortan, *Nature* **1991**, *350*, 600–601.

[38] Y. Takabayashi, K. Prassides, *Philos. Trans. A. Math. Phys. Eng. Sci.* **2016**, *374*, 20150320.

[39] C. Bousige, S. Rols, J. Cambedouzou, B. Verberck, S. Pekker, É. Kováts, G. Durkó, I. Jalsovsky, É. Pellegrini, P. Launois, *Phys. Rev. B.* **2010**, *82*, 195413.

[40] M. Gu, T. B. Tang, C. Hu, D. Feng, *Phys. Rev. B.* **1998**, *58*, 659–663.

[41] J. E. Fischer, P. A. Heiney, A. B. Smith, *Acc. Chem. Res.* **1992**, *25*, 112–118.

[42] B. Renker, H. Schober, M. T. Fernandez-Diaz, R. Heid, *Phys. Rev. B.* **2000**, *61*, 13960–13968.

[43] R. E. Dinnebier, O. Gunnarsson, H. Brumm, E. Koch, P. W. Stephens, A. Huq, M. Jansen, *Science* **2002**, *296*, 109–113.

[44] A. O'Neil, C. Wilson, J. M. Webster, F. J. Allison, J. A. K. Howard, M. Poliakoff, *Angew. Chem. Int. Ed.* **2002**, *41*, 3796–3799.

[45] M. Riccò, M. Belli, M. Mazzani, D. Pontiroli, D. Quintavalle, A. Jánossy, G. Csányi, *Phys. Rev. Lett.* **2009**, *102*, 145901.
[46] A. Y. Ganin, Y. Takabayashi, P. Jeglič, D. Arčon, A. Potočnik, P. J. Baker, Y. Ohishi, M. T. McDonald, M. D. Tzirakis, A. McLennan, G. R. Darling, M. Takata, M. J. Rosseinsky, K. Prassides, *Nature* **2010**, *466*, 221–225.
[47] J. M. Lehn, A. Rigault, J. Siegel, J. Harrowfield, B. Chevrier, D. Moras, *Proc. Natl. Acad. Sci.* **1987**, *84*, 2565–2569.
[48] M. Fujita, J. Yazaki, K. Ogura, *J. Am. Chem. Soc.* **1990**, *112*, 5645–5647.
[49] M. Fujita, M. Tominaga, A. Hori, B. Therrien, *Acc. Chem. Res.* **2005**, *38*, 369–378.
[50] M. Yoshizawa, J. K. Klosterman, M. Fujita, *Angew. Chem. Int. Ed.* **2009**, *48*, 3418–3438.
[51] C. J. Pedersen, *J. Am. Chem. Soc.* **1967**, *89*, 2495–2496.
[52] P. Mal, B. Breiner, K. Rissanen, J. R. Nitschke, *Science* **2009**, *324*, 1697–1699.
[53] M. Yamashina, Y. Sei, M. Akita, M. Yoshizawa, *Nat. Commun.* **2014**, *5*, 4662.
[54] Y. Fang, J. A. Powell, E. Li, Q. Wang, Z. Perry, A. Kirchon, X. Yang, Z. Xiao, C. Zhu, L. Zhang, F. Huang, H.-C. Zhou, *Chem. Soc. Rev.* **2019**, *48*, 4707–4730.
[55] M. Yamashina, M. Akita, T. Hasegawa, S. Hayashi, M. Yoshizawa, *Sci. Adv.* **2017**, *3*, e1701126.
[56] M. Yamashina, T. Tsutsui, Y. Sei, M. Akita, M. Yoshizawa, *Sci. Adv.* **2019**, *5*, eaav3179.
[57] T. R. Schulte, J. J. Holstein, G. H. Clever, *Angew. Chem. Int. Ed.* **2019**, *58*, 5562–5566.
[58] Y. Inokuma, S. Yoshioka, J. Ariyoshi, T. Arai, Y. Hitora, K. Takada, S. Matsunaga, K. Rissanen, M. Fujita, *Nature* **2013**, *495*, 461.
[59] M. Han, D. M. Engelhard, G. H. Clever, *Chem. Soc. Rev.* **2014**, *43*, 1848–1860.
[60] E. G. Percástegui, T. K. Ronson, J. R. Nitschke, *Chem. Rev.* **2020**, *120*, 13480–13544.
[61] F. J. Rizzuto, L. K. S. von Krbek, J. R. Nitschke, *Nat. Rev. Chem.* **2019**, *3*, 204–222.
[62] S. Saha, I. Regeni, G. H. Clever, *Coord. Chem. Rev.* **2018**, *374*, 1–14.
[63] S. Pullen, G. H. Clever, *Acc. Chem. Res.* **2018**, *51*, 3052–3064.
[64] S. Pullen, J. Tessarolo, G. H. Clever, *Chem. Sci.* **2021**, *12*, 7269–7293.
[65] G. H. Clever, S. Tashiro, M. Shionoya, *Angew. Chem. Int. Ed.* **2009**, *48*, 7010–7012.
[66] W. M. Bloch, J. J. Holstein, W. Hiller, G. H. Clever, *Angew. Chem. Int. Ed.* **2017**, *56*, 8285–8289.
[67] R. Zhu, W. M. Bloch, J. J. Holstein, S. Mandal, L. V. Schäfer, G. H. Clever, *Chem. Eur. J.* **2018**, *24*, 12976–12982.
[68] W. M. Bloch, Y. Abe, J. J. Holstein, C. M. Wandtke, B. Dittrich, G. H. Clever, *J. Am. Chem. Soc.* **2016**, *138*, 13750–13755.
[69] J. Tessarolo, H. Lee, E. Sakuda, K. Umakoshi, G. H. Clever, *J. Am. Chem. Soc.* **2021**, *143*, 6339–6344.
[70] S. Löffler, J. Lübben, L. Krause, D. Stalke, B. Dittrich, G. H. Clever, *J. Am. Chem. Soc.* **2015**, *137*, 1060–1063.
[71] B. Chen, J. J. Holstein, S. Horiuchi, W. G. Hiller, G. H. Clever, *J. Am. Chem. Soc.* **2019**, *141*, 8907–8913.
[72] E. M. Veen, B. L. Feringa, P. M. Postma, H. T. Jonkman, A. L. Spek, *Chem. Commun.* **1999**, *0*, 1709–1710.
[73] P. E. Georghiou, in *Calixarenes and Beyond* (Eds.: P. Neri, J. L. Sessler, M.-X. Wang), Springer, Cham, **2016**, Ch. 33, pp. 879–919.
[74] T. Suzuki, K. Nakashima, S. Shinkai, *Chem. Lett.* **1994**, *23*, 699–702.
[75] J. L. Atwood, G. A. Koutsantonis, C. L. Raston, *Nature* **1994**, *368*, 229–231.
[76] T. Haino, M. Yanase, Y. Fukazawa, *Angew. Chem. Int. Ed.* **1997**, *36*, 259–260.
[77] R. G. Lawton, W. E. Barth, *J. Am. Chem. Soc.* **1971**, *93*, 1730–1745.
[78] H. Sakurai, T. Daiko, T. Hirao, *Science* **2003**, *301*, 1878–1878.
[79] H. Becker, G. Javahery, S. Petrie, P. C. Cheng, H. Schwarz, L. T. Scott, D. K. Bohme, *J. Am. Chem. Soc.* **1993**, *115*, 11636–11637.
[80] M. Yamada, K. Ohkubo, M. Shionoya, S. Fukuzumi, *J. Am. Chem. Soc.* **2014**, *136*, 13240–13248.
[81] J. W. Steed, P. C. Junk, J. L. Atwood, M. J. Barnes, C. L. Raston, R. S. Burkhalter, *J. Am. Chem. Soc.* **1994**, *116*, 10346–10347.
[82] P. C. Andrews, J. L. Atwood, L. J. Barbour, P. J. Nichols, C. L. Raston, *Chem. Eur. J.* **1998**, *4*, 1384–1387.
[83] P. D. W. Boyd, M. C. Hodgson, C. E. F. Rickard, A. G. Oliver, L. Chaker, P. J. Brothers, R. D. Bolskar, F. S. Tham, C. A. Reed, *J. Am. Chem. Soc.* **1999**, *121*, 10487–10495.
[84] P. D. W. Boyd, C. A. Reed, *Acc. Chem. Res.* **2005**, *38*, 235–242.

[85] K. Tashiro, T. Aida, *Chem. Soc. Rev.* **2006**, *36*, 189–197.
[86] A. Penicaud, J. Hsu, C. A. Reed, A. Koch, K. C. Khemani, P. M. Allemand, F. Wudl, *J. Am. Chem. Soc.* **1991**, *113*, 6698–6700.
[87] M. M. Olmstead, D. A. Costa, K. Maitra, B. C. Noll, S. L. Phillips, P. M. V. Calcar, A. L. Balch, *J. Am. Chem. Soc.* **1999**, *121*, 7090–7097.
[88] X. Yu, B. Wang, Y. Kim, J. Park, S. Ghosh, B. Dhara, R. D. Mukhopadhyay, J. Koo, I. Kim, S. Kim, I.-C. Hwang, S. Seki, D. M. Guldi, M.-H. Baik, K. Kim, *J. Am. Chem. Soc.* **2020**, *142*, 12596–12601.
[89] D. M. Guldi, *Chem. Soc. Rev.* 2001, *31*, 22–36.
[90] H. Imahori, *Org. Biomol. Chem.* **2004**, *2*, 1425–1433.
[91] K. B. Ghiassi, X. B. Powers, J. Wescott, A. L. Balch, M. M. Olmstead, *Cryst. Growth. Des.* **2016**, *16*, 447–455.
[92] T. Kawase, H. Kurata, *Chem. Rev.* **2006**, *106*, 5250–5273.
[93] E. M. Pérez, N. Martín, *Chem. Soc. Rev.* **2008**, *37*, 1512–9.
[94] T. Haino, M. Yanase, Y. Fukazawa, *Angew. Chem. Int. Ed.* **1998**, *37*, 997–998.
[95] S. Mizyed, P. E. Georghiou, M. Bancu, B. Cuadra, A. K. Rai, P. Cheng, L. T. Scott, *J. Am. Chem. Soc.* **2001**, *123*, 12770–12774.
[96] K. Ikemoto, R. Kobayashi, S. Sato, H. Isobe, *Angew. Chem. Int. Ed.* **2017**, *56*, 6511–6514.
[97] K. Ikemoto, R. Kobayashi, S. Sato, H. Isobe, *Org. Lett.* **2017**, *19*, 2362–2365.
[98] A. Sygula, F. R. Fronczek, R. Sygula, P. W. Rabideau, M. M. Olmstead, *J. Am. Chem. Soc.* **2007**, *129*, 3842–3843.
[99] K. Tashiro, T. Aida, J.-Y. Zheng, K. Kinbara, K. Saigo, S. Sakamoto, K. Yamaguchi, *J. Am. Chem. Soc.* **1999**, *121*, 9477–9478.
[100] J. Zheng, K. Tashiro, Y. Hirabayashi, K. Kinbara, K. Saigo, T. Aida, S. Sakamoto, K. Yamaguchi, *Angew. Chem. Int. Ed.* **2001**, *40*, 1857–1861.
[101] M. Dudič, P. Lhoták, I. Stibor, H. Petříčková, K. Lang, *New. J. Chem.* **2003**, *28*, 85–90.
[102] J. Song, N. Aratani, H. Shinokubo, A. Osuka, *J. Am. Chem. Soc.* **2010**, *132*, 16356–16357.
[103] Y. Xu, S. Gsänger, M. B. Minameyer, I. Imaz, D. Maspoch, O. Shyshov, F. Schwer, X. Ribas, T. Drewello, B. Meyer, M. von Delius, *J. Am. Chem. Soc.* **2019**, *141*, 18500–18507.
[104] M.-M. Titirici, R. J. White, N. Brun, V. L. Budarin, D. S. Su, F. del Monte, J. H. Clark, M. J. MacLachlan, *Chem. Soc. Rev.* **2014**, *44*, 250–290.
[105] T. Kawase, H. R. Darabi, M. Oda, *Angew. Chem. Int. Ed.* **1996**, *35*, 2664–2666.
[106] T. Kawase, K. Tanaka, N. Fujiwara, H. R. Darabi, M. Oda, *Angew. Chem. Int. Ed.* **2003**, *42*, 1624–1628.
[107] R. Jasti, J. Bhattacharjee, J. B. Neaton, C. R. Bertozzi, *J. Am. Chem. Soc.* **2008**, *130*, 17646–17647.
[108] H. Omachi, S. Matsuura, Y. Segawa, K. Itami, *Angew. Chem. Int. Ed.* **2010**, *49*, 10202–10205.
[109] S. Yamago, Y. Watanabe, T. Iwamoto, *Angew. Chem. Int. Ed.* **2010**, *49*, 757–759.
[110] T. Iwamoto, Y. Watanabe, T. Sadahiro, T. Haino, S. Yamago, *Angew. Chem. Int. Ed.* **2011**, *50*, 8342–8344.
[111] H. Isobe, S. Hitosugi, T. Yamasaki, R. Iizuka, *Chem. Sci.* **2013**, *4*, 1293.
[112] S. Hitosugi, W. Nakanishi, T. Yamasaki, H. Isobe, *Nat. Commun.* **2011**, *2*, 492.
[113] S. Sato, T. Yamasaki, H. Isobe, *Proc. Natl. Acad. Sci.* **2014**, *111*, 8374–8379.
[114] T. Matsuno, Y. Nakai, S. Sato, Y. Maniwa, H. Isobe, *Nat. Commun.* **2018**, *9*, 1907.
[115] S. Toyota, Y. Yamamoto, K. Wakamatsu, E. Tsurumaki, A. Muñoz-Castro, *Bull. Chem. Soc. Jpn.* **2019**, *92*, 1721–1728.
[116] Y. Yamamoto, E. Tsurumaki, K. Wakamatsu, S. Toyota, *Angew. Chem. Int. Ed.* **2018**, *57*, 8199–8202.
[117] M. Han, D. M. Engelhard, G. H. Clever, *Chem. Soc. Rev.* **2014**, *43*, 1848–1860.
[118] S. Saha, I. Regeni, G. H. Clever, *Coordin. Chem. Rev.* **2018**, *374*, 1–14.
[119] N. Kishi, Z. Li, K. Yoza, M. Akita, M. Yoshizawa, *J. Am. Chem. Soc.* **2011**, *133*, 11438–11441.
[120] M. Yoshizawa, L. Catti, *Acc. Chem. Res.* **2019**, *52*, 2392–2404.
[121] N. Kishi, M. Akita, M. Kamiya, S. Hayashi, H.-F. Hsu, M. Yoshizawa, *J. Am. Chem. Soc.* **2013**, *135*, 12976–9.
[122] M. Yamashina, T. Yuki, Y. Sei, M. Akita, M. Yoshizawa, *Chem. Eur. J.* **2015**, *21*, 4200–4204.
[123] T. K. Ronson, B. S. Pilgrim, J. R. Nitschke, *J. Am. Chem. Soc.* **2016**, *138*, 10417–10420.
[124] T. K. Ronson, W. Meng, J. R. Nitschke, *J. Am. Chem. Soc.* **2017**, *139*, 9698–9707.
[125] K. Harris, D. Fujita, M. Fujita, *Chem. Commun.* **2013**, *49*, 6703–6712.
[126] K. Suzuki, K. Takao, S. Sato, M. Fujita, *J. Am. Chem. Soc.* **2010**, *132*, 2544–2545.

[127] D. Sun, F. S. Tham, C. A. Reed, L. Chaker, M. Burgess, P. D. W. Boyd, *J. Am. Chem. Soc.* **2000**, *122*, 10704–10705.
[128] M. Ayabe, A. Ikeda, S. Shinkai, S. Sakamoto, K. Yamaguchi, *Chem. Commun.* **2002**, *0*, 1032–1033.
[129] W. Meng, B. Breiner, K. Rissanen, J. D. Thoburn, J. K. Clegg, J. R. Nitschke, *Angew. Chem. Int. Ed.* **2011**, *50*, 3479–3483.
[130] A. Ikeda, M. Yoshimura, H. Udzu, C. Fukuhara, S. Shinkai, *J. Am. Chem. Soc.* **1999**, *121*, 4296–4297.
[131] T. Haino, H. Araki, Y. Yamanaka, Y. Fukazawa, *Tetrahedron Lett.* **2001**, *42*, 3203–3206.
[132] T. Haino, Y. Yamanaka, H. Araki, Y. Fukazawa, *Chem. Commun.* **2002**, *0*, 402–403.
[133] C. G. Claessens, T. Torres, *Chem. Commun.* **2004**, *0*, 1298–1299.
[134] W. Sun, Y. Wang, L. Ma, L. Zheng, W. Fang, X. Chen, H. Jiang, *J. Org. Chem.* **2018**, *83*, 14667–14675.
[135] M. Saito, H. Shinokubo, H. Sakurai, *Mater. Chem. Front.* **2018**, *2*, 635–661.
[136] S. Goeb, S. Bivaud, P. I. Dron, J.-Y. Balandier, M. Chas, M. Sallé, *Chem. Commun.* 2012, *48*, 3106–3108.
[137] S. Shanmugaraju, V. Vajpayee, S. Lee, K.-W. Chi, P. J. Stang, P. S. Mukherjee, *Inorg. Chem.* 2012, *51*, 4817–4823.
[138] J. Yuan, W. Lv, A. Li, K. Zhu, *Chem. Commun.* 2021, DOI 10.1039/d1cc05581j.
[139] M. Schmittel, B. He, P. Mal, *Org Lett* 2008, *10*, 2513–2516.
[140] T. Nakamura, H. Ube, R. Miyake, M. Shionoya, *J. Am. Chem. Soc.* 2013, *135*, 18790–18793.
[141] T. Tsutsui, L. Catti, K. Yoza, M. Yoshizawa, *Chem. Sci.* 2020, DOI 10.1039/d0sc03223a.
[142] D. M. Wood, W. Meng, T. K. Ronson, A. R. Stefankiewicz, J. K. M. Sanders, J. R. Nitschke, *Angew. Chem. Int. Ed.* 2015, *54*, 3988–3992.
[143] F. C. Krebs, P. S. Larsen, J. Larsen, C. S. Jacobsen, C. Boutton, N. Thorup, *J. Am. Chem. Soc.* 1997, *119*, 1208–1216.
[144] Y. Yang, T. K. Ronson, Z. Lu, J. Zheng, N. Vanthuyne, A. Martinez, J. R. Nitschke, *Nat. Commun.* 2021, *12*, 4079.
[145] M. Yamamura, T. Saito, T. Hasegawa, E. Nishibori, T. Nabeshima, *Chem. Commun.* 2021, *57*, 8754–8757.
[146] B. Chen, J. J. Holstein, A. Platzek, L. Schneider, K. Wu, G. H. Clever, *Chem. Sci.* 2022, DOI 10.1039/d1sc06931d.
[147] B. Chen, S. Horiuchi, J. J. Holstein, J. Tessarolo, G. H. Clever, *Chem. Eur. J.* **2019**, *25*, 14921–14927.
[148] K. Mahata, P. D. Frischmann, F. Würthner, *J. Am. Chem. Soc.* **2013**, *135*, 15656–15661.
[149] S. Mecozzi, J. R. Jr., *Chem. Eur. J.* **1998**, *4*, 1016–1022.
[150] K. Yazaki, M. Akita, S. Prusty, D. K. Chand, T. Kikuchi, H. Sato, M. Yoshizawa, *Nat. Commun.* **2017**, *8*, ncomms15914.
[151] K. Matsumoto, S. Kusaba, Y. Tanaka, Y. Sei, M. Akita, K. Aritani, M. Haga, M. Yoshizawa, *Angew. Chem. Int. Ed.* **2019**, *58*, 8463–8467.
[152] F. J. Rizzuto, J. R. Nitschke, *Nat. Chem.* **2017**, *9*, 903–908.
[153] F. J. Rizzuto, D. M. Wood, T. K. Ronson, J. R. Nitschke, *J. Am. Chem. Soc.* **2017**, *139*, 11008–11011.
[154] N. Kishi, M. Akita, M. Yoshizawa, *Angew. Chem. Int. Ed.* **2014**, *53*, 3604–3607.
[155] W.-K. Han, H.-X. Zhang, Y. Wang, W. Liu, X. Yan, T. Li, Z.-G. Gu, *Chem. Commun.* **2018**, *54*, 12646–12649.
[156] K. Kajiyama, E. Tsurumaki, K. Wakamatsu, G. Fukuhara, S. Toyota, *Chempluschem* **2021**, *86*, 716–722.
[157] S. Kawano, T. Fukushima, K. Tanaka, *Angew. Chem. Int. Ed.* **2018**, *57*, 14827–14831.
[158] V. Martínez‐Agramunt, D. G. Gusev, E. Peris, *Chem. Eur. J.* **2018**, *24*, 14802–14807.
[159] V. Martínez-Agramunt, E. Peris, *Chem. Commun.* **2019**, *55*, 14972–14975.
[160] V. Martínez‐Agramunt, T. Eder, H. Darmandeh, G. Guisado‐Barrios, E. Peris, *Angew. Chem. Int. Ed.* **2019**, *58*, 5682–5686.
[161] V. Martínez-Agramunt, E. Peris, *Inorg. Chem.* **2019**, *58*, 11836–11842.
[162] E. V. Peris, C. Vicent, V. Martinez-Agramunt, V. Gandhi, C. Larriba-Andaluz, D. Gusev, *Angew. Chem. Int. Ed.* **2021**, *60*, 15412–15417.
[163] W. Brenner, T. K. Ronson, J. R. Nitschke, *J. Am. Chem. Soc.* **2016**, *139*, 75–78.
[164] X. Chang, S. Lin, G. Wang, C. Shang, Z. Wang, K. Liu, Y. Fang, P. J. Stang, *J. Am. Chem. Soc.* **2020**, *142*, 15950–15960.
[165] A. Ikeda, H. Udzu, M. Yoshimura, S. Shinkai, *Tetrahedron* **2000**, *56*, 1825–1832.
[166] Y. Inokuma, T. Arai, M. Fujita, *Nat. Chem.* **2010**, *2*, 780.
[167] C. García-Simón, M. Garcia-Borràs, L. Gómez, T. Parella, S. Osuna, J. Juanhuix, I. Imaz, D.

Maspoch, M. Costas, X. Ribas, *Nat. Commun.* **2014**, *5*, 5557.
[168] C. Colomban, G. Szalóki, M. Allain, L. Gómez, S. Goeb, M. Sallé, M. Costas, X. Ribas, *Chem. Eur. J.* **2017**, *23*, 3016–3022.
[169] C. García-Simón, A. Monferrer, M. Garcia-Borràs, I. Imaz, D. Maspoch, M. Costas, X. Ribas, *Chem. Commun.* **2019**, *55*, 798–801.
[170] C. Fuertes‐Espinosa, C. García‐Simón, E. Castro, M. Costas, L. Echegoyen, X. Ribas, *Chem. Eur. J.* **2017**, *23*, 3553–3557.
[171] C. Fuertes‐Espinosa, A. Gómez‐Torres, R. Morales‐Martínez, A. Rodríguez‐Fortea, C. García‐Simón, F. Gándara, I. Imaz, J. Juanhuix, D. Maspoch, J. M. Poblet, L. Echegoyen, X. Ribas, *Angew. Chem. Int. Ed.* **2018**, *57*, 11294–11299.
[172] C. Fuertes-Espinosa, J. Murillo, M. E. Soto, M. R. Ceron, R. Morales-Martínez, A. Rodríguez-Fortea, J. M. Poblet, L. Echegoyen, X. Ribas, *Nanoscale* **2019**, *11*, 23035–23041.
[173] E. Ubasart, C. García-Simón, M. Pujals, K. Asad, N. Chronakis, T. Parella, X. Ribas, *Org. Chem. Front.* **2021**, *8*, 4101–4105.
[174] C. García-Simón, C. Colomban, Y. A. Çetin, A. Gimeno, M. Pujals, E. Ubasart, C. Fuertes-Espinosa, K. Asad, N. Chronakis, M. Costas, J. Jiménez-Barbero, F. Feixas, X. Ribas, *J. Am. Chem. Soc.* **2020**, *142*, 16051–16063.
[175] C. S. Wood, C. Browne, D. M. Wood, J. R. Nitschke, *ACS Cent. Sci.* **2015**, *1*, 504–509.
[176] P. W. M. Blom, V. D. Mihailetchi, L. J. A. Koster, D. E. Markov, *Adv. Mater.* **2007**, *19*, 1551–1566.
[177] G. Dennler, M. C. Scharber, C. J. Brabec, *Adv. Mater.* **2009**, *21*, 1323–1338.
[178] B. C. Thompson, J. M. J. Fréchet, *Angew. Chem. Int. Ed.* **2008**, *47*, 58–77.
[179] V. Leonhardt, S. Fimmel, A.-M. Krause, F. Beuerle, *Chem. Sci.* 2020, *11*, 8409–8415.
[180] S. Beil, M. von Delius, *Org. Mater.* **2021**, *03*, 146–154.
[181] N. Huang, K. Wang, H. Drake, P. Cai, J. Pang, J. Li, S. Che, L. Huang, Q. Wang, H.-C. Zhou, *J. Am. Chem. Soc.* **2018**, *140*, 6383–6390.
[182] C. Fuertes-Espinosa, C. García-Simón, M. Pujals, M. Garcia-Borràs, L. Gómez, T. Parella, J. Juanhuix, I. Imaz, D. Maspoch, M. Costas, X. Ribas, *Chem* **2019**, *6*, 169–186.
[183] S. Hasegawa, G. H. Clever, *Chem* **2020**, *6*, 5–7.
[184] E. Ubasart, O. Borodin, C. Fuertes-Espinosa, Y. Xu, C. García-Simón, L. Gómez, J. Juanhuix, F. Gándara, I. Imaz, D. Maspoch, M. von Delius, X. Ribas, *Nat. Chem.* **2021**, *13*, 420–427.
[185] Z. Lu, T. Ronson, A. Heard, S. Feldmann, N. Vanthuyne, A. Martinez, J. Nitschke, DOI 10.26434/chemrxiv-2022-l5zk8.
[186] M. Pujals, T. Pèlachs, C. Fuertes-Espinosa, T. Parella, M. Garcia-Borràs, X. Ribas, DOI 10.26434/chemrxiv-2022-ckrjp.
[187] H. Imahori, Y. Mori, Y. Matano, *J. Photochem. Photobiol. C: PhotoChem. Rev.* **2003**, *4*, 51–83.
[188] D. Gust, T. A. Moore*, A. L. Moore, *J Photochem. Photobiol. B: Biol.* **2000**, *58*, 63–71.
[189] N. Struch, C. Bannwarth, T. K. Ronson, Y. Lorenz, B. Mienert, N. Wagner, M. Engeser, E. Bill, R. Puttreddy, K. Rissanen, J. Beck, S. Grimme, J. R. Nitschke, A. Lützen, *Angew. Chem. Int. Ed.* **2017**, *56*, 4930–4935.
[190] T. A. Barendt, W. K. Myers, S. P. Cornes, M. A. Lebedeva, K. Porfyrakis, I. Marques, V. Félix, P. D. Beer, *J. Am. Chem. Soc.* **2019**, *142*, 349–364.
[191] Z. Lu, R. Lavendomme, O. Burghaus, J. R. Nitschke, *Angew. Chem. Int. Ed.* **2019**, *58*, 9073–9077.
[192] Z. Lu, T. K. Ronson, J. R. Nitschke, *Chem. Sci.* **2019**, *11*, 1097–1101.
[193] T. Ito, Y. Hayashi, S. Shimizu, J. Shin, N. Kobayashi, H. Shinokubo, *Angew. Chem. Int. Ed.* **2012**, *51*, 8542–8545.
[194] M. Yamashina, Y. Tanaka, R. Lavendomme, T. K. Ronson, M. Pittelkow, J. R. Nitschke, *Nature* **2019**, *574*, 511–515.

2 Scope of this thesis

Previous examples of fullerene-binders inspired us for rational molecular designs for construction of fullerene-binders with certain properties and functions. Among those fullerene-binders, coordination cages are powerful and versatile hosts which can provide a discrete and isolated space which is suitable to accommodate fullerenes. Until now, many coordination cages which can encapsulate fullerene have been reported as well as their unique behavior in self-assembly and physical properties. As discussed in the *General Introduction*, C_{60} is known to show intriguing physical and chemical properties under “Nano-confinement” & “Hierarchical Assembly”. In light of these perspectives, I have chosen to investigate physical and chemical properties of C_{60}(s) inside coordination cages based on the established design and concept by our group as a main subject of this dissertation. In this Ph.D. dissertation, the following is described:

C_{60} in
“Nano-confinement”

• Generation and stabilization of C_{60} radical anion inside a cationic triptycene-based coordination cage
• Encapsulation capability of a triptycene-based coordination cage towards C_{60} derivatives and a curved polyaromatic hydrocarbon
• Synthesis of $C_{60}Pd(0)_n$ (n=1, 2) by utilizing a triptycene-based coordination cage as a supramolecular mask

C_{60} in
“Hierarchical Assembly”

• Synthesis of a pill-shaped coordination cage encapsulating two C_{60} molecules and guest-uptake and reaction in between two confined C_{60}s

3 Generation and stabilization of C_{60} radical anion inside a cationic coordination cage

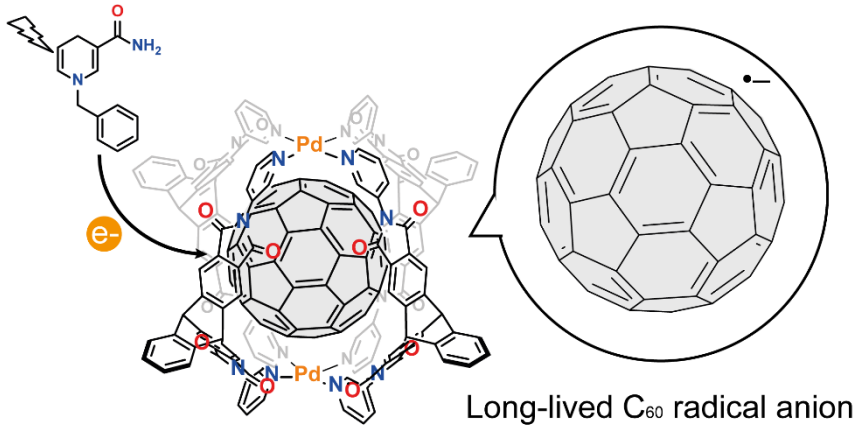

Abstract:

The C_{60} radical anion ($C_{60}^{\bullet-}$) is a component of fullerides, which is a superconductive material at a relatively high temperature. Further, $C_{60}^{\bullet-}$ and further reduced species are supposed to be the actual electron transporters in organic photovoltaics containing C_{60}. Thus, $C_{60}^{\bullet-}$ is an intriguing radical species to be investigated to further gain insights for material development. However, $C_{60}^{\bullet-}$ is a rather unstable species, and thus, a special set up is required to investigate $C_{60}^{\bullet-}$. In this chapter, the synthesis of a triptycene-based ligand and its behavior in self-assembly with Pd(II) to a Pd_2L_4 cage is described. The self-assembled cage has a cavity suitable to accommodate a single C_{60} molecule. Selective one electron reduction of the confined C_{60} was performed yielding $C_{60}^{\bullet-}$ inside the cavity characterized by ESI MS, EPR, and UV-Vis NIR spectroscopy. The generated $C_{60}^{\bullet-}$ inside the cage was found to have a long lifetime up to 1 month most likely due to the confinement effect inside the cationic cage via electrostatic interactions and kinetic protection.

Contents of this chapter were published in:

S. Hasegawa, S. L. Meichsner, J. J. Holstein, A. Baksi, M. Kasanmascheff, G H. Clever* *J. Am. Chem. Soc*. **2021**, *143*, 9718.

3.1 Introduction

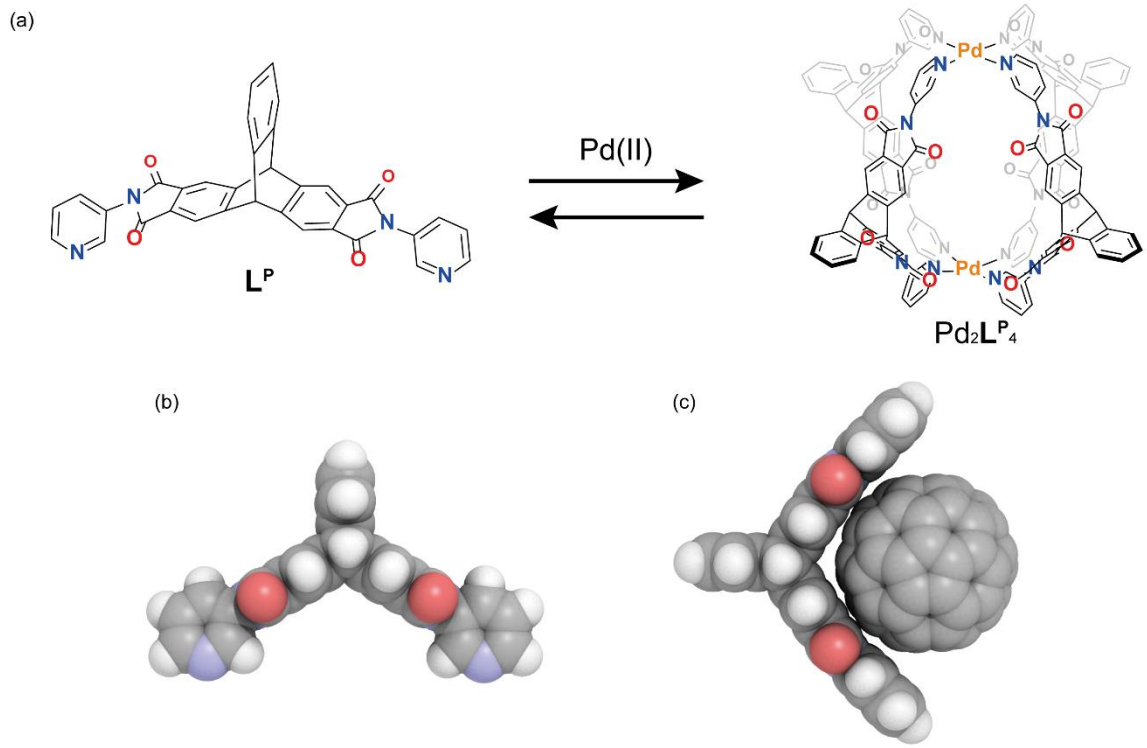

Figure 3.1.1 (a) Self-assembly of $\mathbf{L^P}$ with Pd(II) to form $Pd_2\mathbf{L^P}_4$ (b) CPK model of $\mathbf{L^P}$ (c) MM2 calculated geometry of $\mathbf{L^P}$ in complex with C_{60}

Since the discovery of fullerene C_{60} by Kroto, Smalley and Curl,[1] the globular-shaped molecule has inspired scientists across a variety of fields to investigate its physical properties, host-guest ability towards single molecule,[2–4] derivatization,[5,6] material development and so forth.[7] Especially, C_{60} and its derivatives have been widely utilized in organic devices as an electron-accepting/-transporting material.[8] In such organic devices, one-electron transfer from the donor occurs and the reduced species, C_{60} radical anion ($C_{60}^{\bullet-}$) and further reduced species are generated. The generated radical species are the actual electron-transporters in the devices and play a key role to harvest charges efficiently. In addition, $C_{60}^{\bullet-}$ has absorption bands in the NIR region, which provides potential for applications in bioimaging and photodynamic therapy.[9] However, naked $C_{60}^{\bullet-}$ has a rather short lifetime in general, especially at ambient temperatures and in solution.[10] Therefore, spectroscopic techniques after bulk-electrolysis conditions or electron donation from a chemical reductant pool are often required for investigating naked $C_{60}^{\bullet-}$.[11–15] Hence, the development of a facile method to stabilize generated $C_{60}^{\bullet-}$ species in solution is meaningful. As introduced in *General*

Introduction, coordination-driven self-assembly is a versatile method to construct nanoscopic molecular entities.[16] One of the most important features of coordination cages is their inner space which offers a unique reaction field,[17,18] structural recognition ability,[19,20] stabilization of reactive species[21,22] and so forth.[23] Encapsulation of a specific molecule, i.e. C_{60}, is possible by a rational molecular design as introduced in *General Introduction*. Further, in many cases, coordination cages possess a charge owing to the metal ions connecting the organic ligands.[24] This electronic property enhances encapsulation of charged species via electrostatic interactions.

Confined C_{60} inside some cationic coordination cages tends to show a positive shift of the first reduction potential of the encapsulated C_{60} [25,26] compared to pristine C_{60}.[27] Therefore, electronic interactions between cationic coordination cages and encapsulated $C_{60}^{\bullet-}$ can be anticipated. According to those facts, triptycene-based organic ligand $\mathbf{L^P}$ for construction of a coordination cage enabling efficient C_{60} encapsulation was synthesized (**Figure 3.1.1a**). In addition, generation of $C_{60}^{\bullet-}$ within the formed cationic coordination cage via self-assembly of the synthesized ligand and Pd(II) has been investigated. Our approaches to construct a coordination cage for C_{60} encapsulation is based on geometrical matching. Dr. Bin Chen, a former Ph.D. student of our group, has synthesized organic ligands having a curved π-surface.[28–30] Despite of the rather small surface area, a coordination cage consisted of the curved ligands and Pd(II) shows quantitative encapsulation of C_{60} within its cavity most likely via convex-concave interactions. Based on this report, a similar, yet, new ligand having triptycene-backbone has been synthesized aiming for C_{60} encapsulation. Triptycene is known for attractive interactions with C_{60} due to the geometrical matching (**Figure 3.1.1b** and **c**).[31]

3.2 Results and discussion

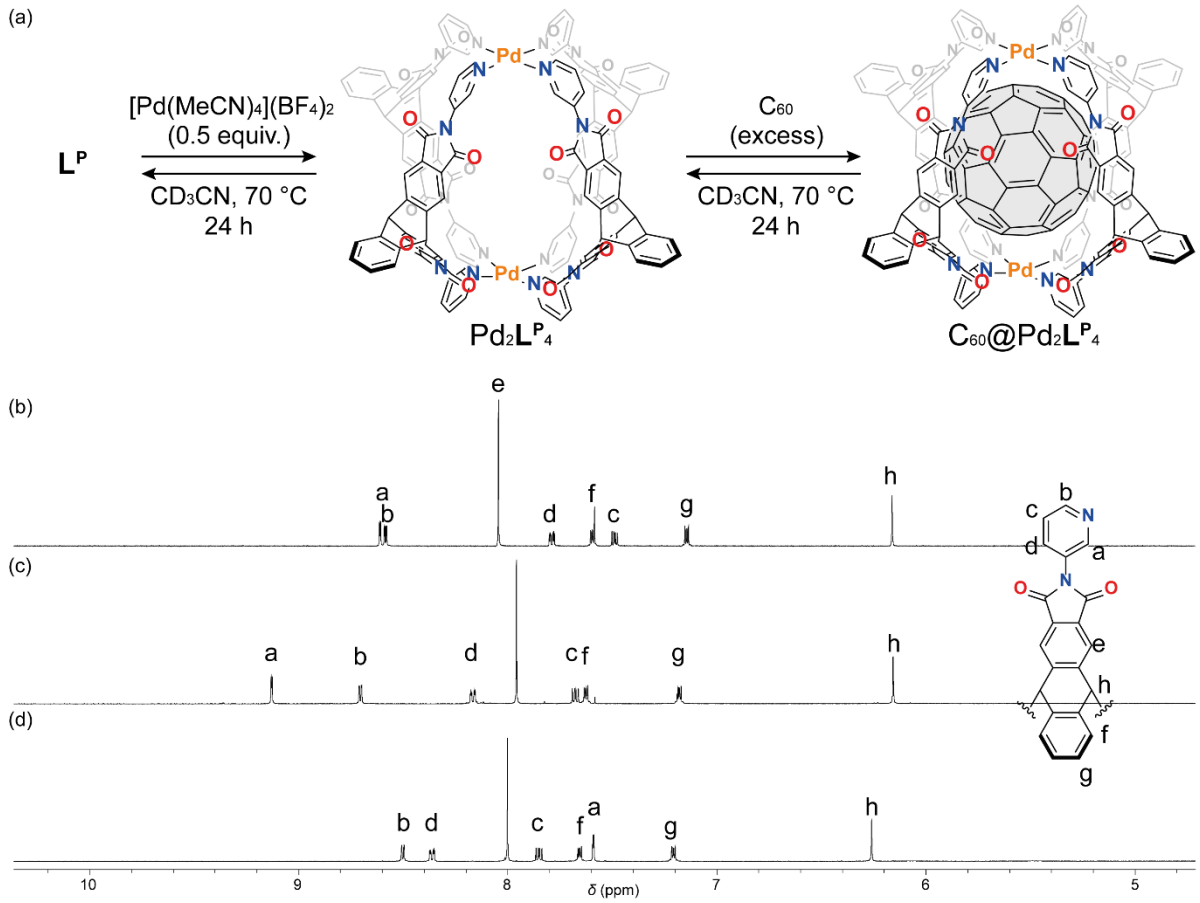

Figure 3.2.1 (a) Synthesis of $Pd_2\mathbf{L}^{\mathbf{P}}_4$ and encapsulation of $C_{60}@Pd_2\mathbf{L}^{\mathbf{P}}_4$ (b) ^{1}H NMR spectrum of $\mathbf{L}^{\mathbf{P}}$ (CD_3CN, 500 MHz, 298 K) (c) $Pd_2\mathbf{L}^{\mathbf{P}}_4$ (CD_3CN, 0.70 mM, 500 MHz, 298 K) and (d) $C_{60}@Pd_2\mathbf{L}^{\mathbf{P}}_4$ (CD_3CN, 0.70 mM, 500 MHz, 298 K)

Synthesis of $\mathbf{L}^{\mathbf{P}}$ has been conducted following the literature.[32] The dianhydride precursor was synthesized via 4 steps from *o*-dichlorobenzene. The condensation reaction to synthesize the desired ligand was performed under a neat condition. After mixing $\mathbf{L}^{\mathbf{P}}$ and 0.5 equiv. of $[Pd(MeCN)_4](BF_4)_2$ at 70 °C for 24 h, quantitative formation of $Pd_2\mathbf{L}^{\mathbf{P}}_4$ took place (**Figure 3.2.1a** and **c**). Similar to other Pd(II)-coordination cages, downfield shifts of the pyridine-coordination sites were observed (**Figure 3.2.1b** and **c**).[33,34] The formation of $Pd_2\mathbf{L}^{\mathbf{P}}_4$ was further confirmed by ESI MS, and DOSY (**Figure 3.4.10** and **Figure 3.4.12**). The VOIDOO calculations suggested a sufficient size of the cavity for single C_{60} encapsulation (**Figure 3.4.25**). Thus, incarceration of C_{60} inside the coordination cage was performed by stirring solid C_{60} in an acetonitrile solution of $Pd_2\mathbf{L}^{\mathbf{P}}_4$. After filtration of the remaining powdered C_{60}, a purple solution was obtained, which is a characteristic color of C_{60}.

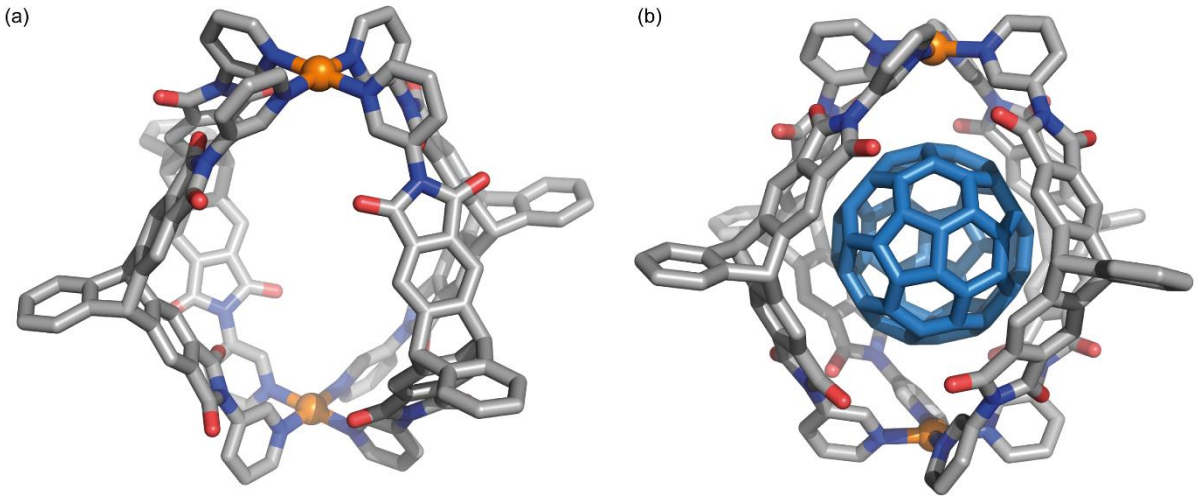

Figure 3.2.2 X-ray structure of (a) $Pd_2\mathbf{L}^{\mathbf{P}}_4$ and (b) $C_{60}@Pd_2\mathbf{L}^{\mathbf{P}}_4$; color legend: gray, blue, red, orange, skyblue for C, N, O, Pd, and C_{60} respectively

A ^{1}H NMR spectrum was measured for the purple filtrate. In the ^{1}H NMR spectrum, an upfield shift of the protons H^a which are supposed to be pointing inward the cavity was observed (**Figure 3.2.1d**), which is in line with the previous study.[28–30] This upfield shift is most likely due to interactions between the protons and the encapsulated C_{60}. The encapsulation was further supported by ESI MS analysis (**Figure 3.4.19**).

The solid-state structure of $Pd_2\mathbf{L}^{\mathbf{P}}_4$ and $C_{60}@Pd_2\mathbf{L}^{\mathbf{P}}_4$ was unambiguously elucidated by single crystal X-ray structural analysis (**Figure 3.2.2**). Plate-like crystals of $Pd_2\mathbf{L}^{\mathbf{P}}_4$ suitable for crystallographic analysis were obtained by slow vapor diffusion of diisopropylether into an acetonitrile solution of the cage. Single crystals of $C_{60}@Pd_2\mathbf{L}^{\mathbf{P}}_4$ were grown by slow vapor diffusion of benzene into an acetonitrile solution of $C_{60}@Pd_2\mathbf{L}^{\mathbf{P}}_4$. In comparison to $Pd_2\mathbf{L}^{\mathbf{P}}_4$, shrinkage of the Pd•••Pd was observed in the structure of $C_{60}@Pd_2\mathbf{L}^{\mathbf{P}}_4$ by 0.435(9) Å, probably to enlarge π–π interactions between the cage and the confined C_{60} (**Figure 3.4.20** and **Figure 3.4.21**).

Next, the electron-deficient character of the cage together with the cationic charge originated from the Pd(II) centers stimulated me to investigate the electronic properties of the encapsulated C_{60}. In general, pristine C_{60} shows a first reduction potential around ca. –1.0 V in various organic solvents versus Fc/Fc^+.[27] A cyclic voltammogram of $Pd_2\mathbf{L}^{\mathbf{P}}_4$ showcased a first reduction wave at –1.78 V against the Fc/Fc^+ reference, which should belong to reduction of the ligands (**Figure 3.2.3a**). Meanwhile, the cyclic voltammogram of $C_{60}@Pd_2\mathbf{L}^{\mathbf{P}}_4$ showed irreversible

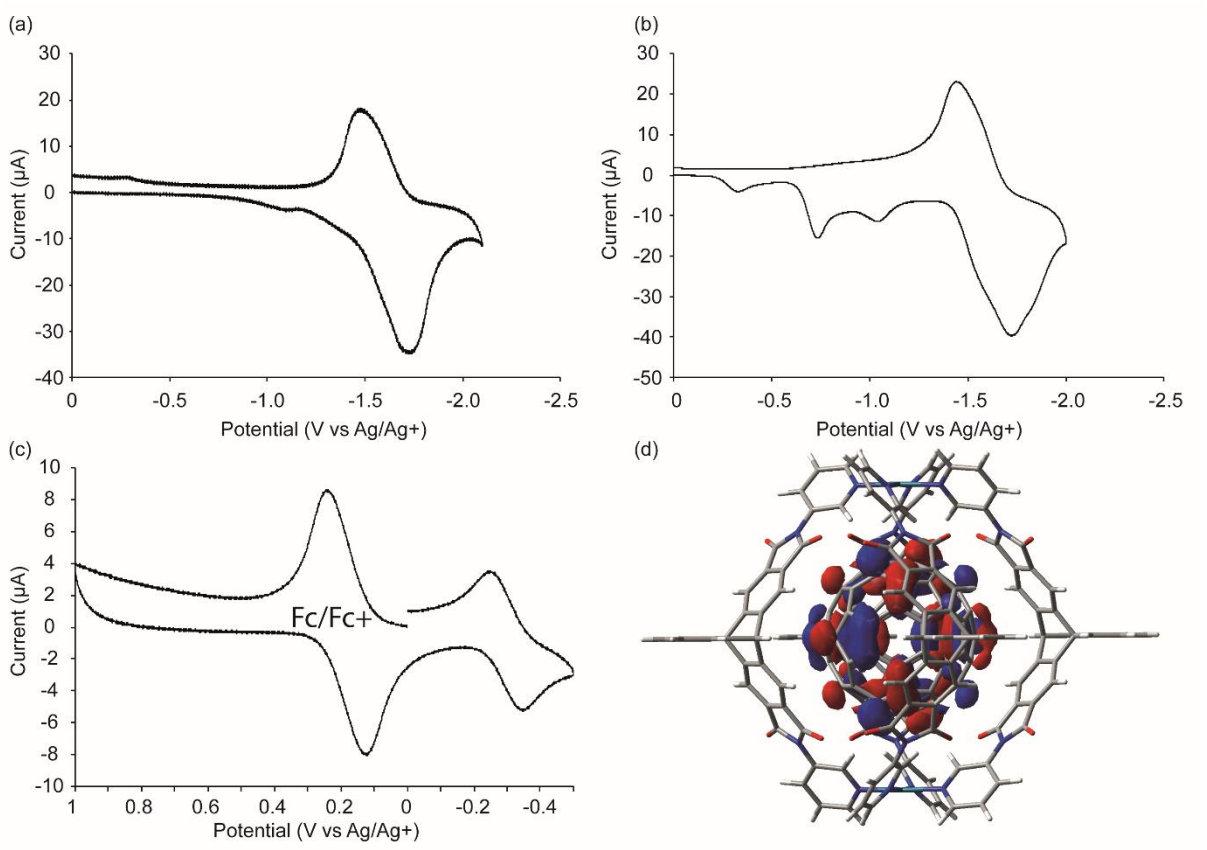

Figure 3.2.3 Cyclic voltammograms of (a) $Pd_2\mathbf{L}^{\mathbf{P}}_4$ (b) $C_{60}@Pd_2\mathbf{L}^{\mathbf{P}}_4$ (c) and only the first reduction wave of $C_{60}@Pd_2\mathbf{L}^{\mathbf{P}}_4$ with oxidation wave of Fc/Fc^+; scan rate: 100 mV/s, electrolyte: $TBAPF_6$ in acetonitrile

reduction waves at more cathodic potentials in addition to the quasi-reversible cage reduction at –1.79 V (vs. Fc/Fc+; **Figure 3.2.3b**). These newly observed waves should be assignable to progressive reduction steps of the encapsulated C_{60} molecule. DFT calculations implied that the LUMO should be localized on the encapsulated C_{60} molecule inside the cavity, supporting those observations (**Figure 3.2.3d**). The first reduction potential for the encapsulated C_{60} molecule appeared at –0.48 V vs Fc/Fc^+ as a reversible wave when the measurement was performed in a narrower range (**Figure 3.2.3c**). Note, this value is the most cathodic for C_{60} encapsulated in coordination cages reported so far.[25,26] This result implies interactions between the reduced anionic species $C_{60}^{\bullet-}$ and the cationic cage. DFT calculations in the gas-phase further indicate the possible stronger interactions between the cage and $C_{60}^{\bullet-}$ than C_{60} (**Table 3.4.6.1**).

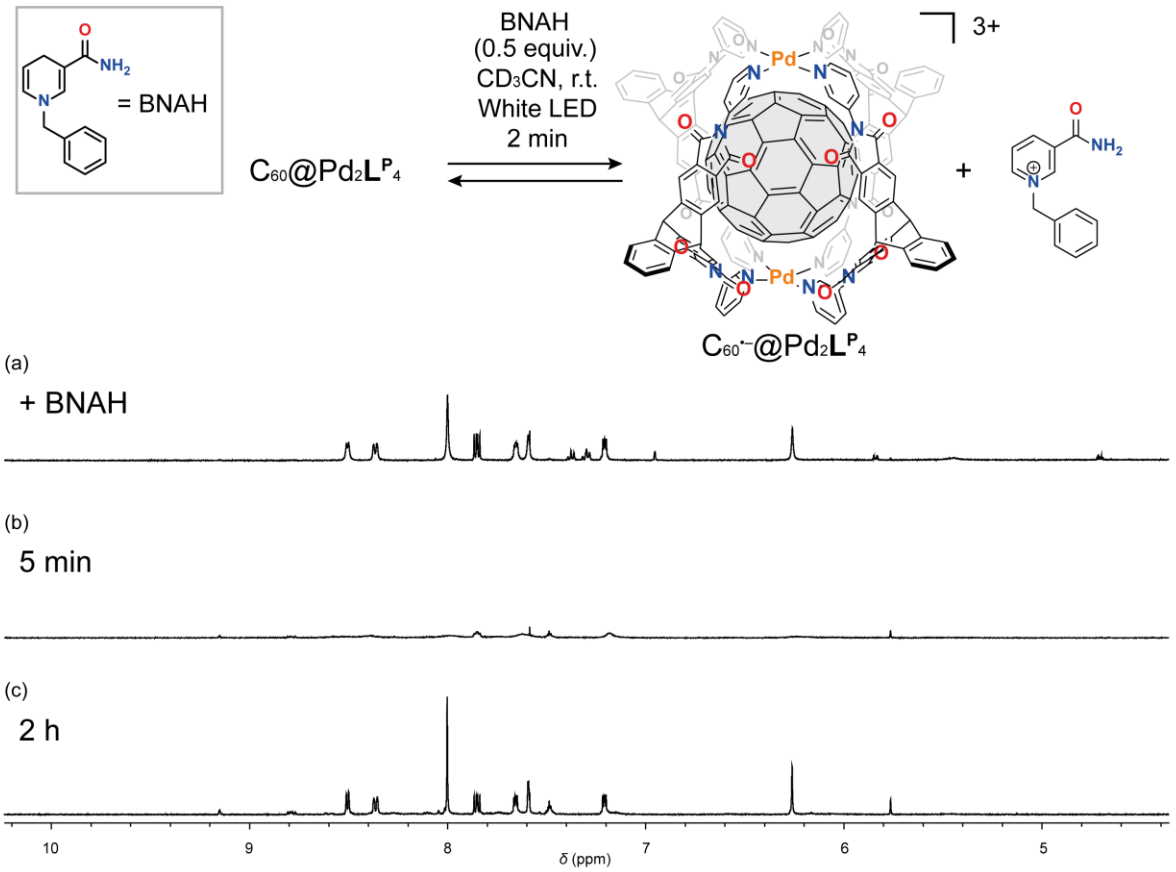

Figure 3.2.4 ^{1}H NMR spectrum of C_{60}@Pd_2**L**$^{P}_4$ in the presence of BNAH (CD_3CN, 500 MHz, 298 K) (b) C_{60}@Pd_2**L**$^{P}_4$ 5 mins after irradiation with the white LED light source with BNAH (CD_3CN, 500 MHz, 298 K) (c) 2 h after irradiation showing regeneration of original C_{60}@Pd_2**L**$^{P}_4$ (CD_3CN, 500 MHz, 298 K)

Encouraged by these results, the generation of $C_{60}^{\bullet-}$ inside the coordination cage was investigated. Amongst several possible reductants, 1-benzyl-1,4-dihydronicotinamide (BNAH) has been chosen for this study due to the controllability of one-electron reduction by light irradiation (**Figure 3.2.4**). Fukuzumi and co-workers have reported one-electron reduction of C_{60} using BNAH as a reductant.[35] In the reaction mechanism they proposed, energy transfer from C_{60} in triplet excited states to BNAH triggers this chemical reduction process. From one BNAH, two molecular C_{60} should be reduced in theory. Therefore, 0.5 equiv. of BNAH was added into C_{60}@Pd_2**L**$^{P}_4$ in acetonitrile and irradiated with a white LED source. As a result, the ^{1}H NMR signals became broadened which is implying encapsulation of paramagnetic species (**Figure 3.2.4b**).[36] The broadened signals became sharper over time (**Figure 3.2.4c**), suggesting deactivation of the encapsulated radical species. In the ESI MS spectrum

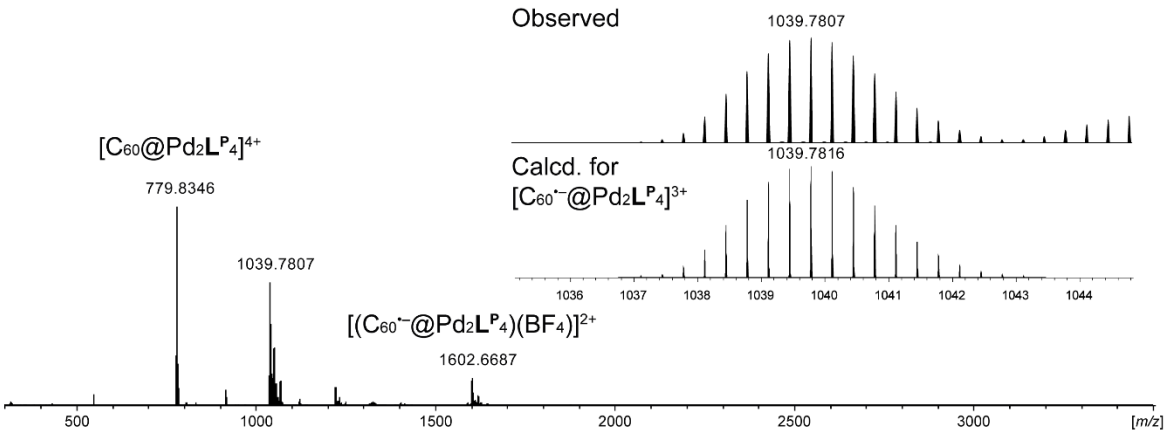

Figure 3.2.5 ESI MS spectrum of $C_{60}^{\bullet-}$@$Pd_2\mathbf{L}^{\mathbf{P}}_4$ (positive mode)

measured immediately after the photochemical reduction, a prominent signal assignable to $[C_{60}^{\bullet-}@Pd_2\mathbf{L}^{\mathbf{P}}_4]^{3+}$ was observed (**Figure 3.2.5**). In addition, a UV-vis-NIR spectrum was measured right after photochemical reduction process. In the absorption spectrum, new absorption bands at 975 and 1111 nm were observed whilst the encapsulated C_{60} showed absorption at 546 and 599 nm (**Figure 3.2.6a**-**b**). The absorption bands in the NIR region are in good accordance with the absorption spectrum of $C_{60}^{\bullet-}$ reported before, further evidencing generation of $C_{60}^{\bullet-}$ inside the cage.[11] Among the observed NIR absorptions, the absorption band at the longer wavelength showed a red-shift by approximately 20-30 nm compared to the reported absorption band of naked $C_{60}^{\bullet-}$ (*cf*. 1080 nm vs. 1111 nm). On the other hand, the shorter absorption wavelength is comparable to previous reports. It is reported that the NIR absorptions are originated from an electron transition from SOMO to an unoccupied orbital.[37] Based on resonance Raman spectroscopy studies, two symmetric A_g vibrational modes cause the observed splitting.[37] The vibrational mode with higher wavenumber is a so-called “pentagonal-pitch” mode and the other mode is a so called “breathing” mode. Hence, perturbation of the breathing mode is presumed as a potential reason for the bathochromic shift observed in the absorption spectrum, most likely due to the confinement of the radical anion within the cavity of the cationic cage $Pd_2\mathbf{L}^{\mathbf{P}}_4$.

Control experiments using the empty host showed that the photochemical reduction does not occur (**Figure 3.4.36**). Further, when the mixture of $C_{60}@Pd_2\mathbf{L}^{\mathbf{P}}_4$ and $Pd_2\mathbf{L}^{\mathbf{P}}_4$ was applied to the photochemical reduction, only $C_{60}@Pd_2\mathbf{L}^{\mathbf{P}}_4$ gave broadened ^{1}H

NMR signals (**Figure 3.4.35**). These results strongly support the generation of $C_{60}^{\bullet-}$ within the cage.

The decay of generated $C_{60}^{\bullet-}$ inside the cage was investigated by EPR, in collaboration by Shari Meichsner in the Kasanmaschef group, and UV-Vis NIR absorption studies (**Figure 3.2.6**). The decay of the absorption intensity in the NIR region was observed over time due to deactivation of generated $C_{60}^{\bullet-}$ (**Figure 3.2.6a**). The half-lifetime of $C_{60}^{\bullet-}$ inside the cage was estimated to be 13 mins from the decay of the 1111 nm absorption band in acetonitrile at 295 K under ambient conditions. Generated $C_{60}^{\bullet-}$ within the coordination cage can be chemically oxidized back to original C_{60} by tetracyanoethylene (TCNE). The absorbance in the NIR region instantly vanished after addition of TCNE and gave the almost identical absorption spectrum to $C_{60}@Pd_2\mathbf{L}^{\mathbf{P}}_4$ after 1 h (**Figure 3.4.43**). The clean oxidation process was further investigated by an ^{1}H NMR study as well (**Figure 3.4.44**). This reduction-oxidation process suggests a potential use of the host-guest complex for photoredox catalysis.

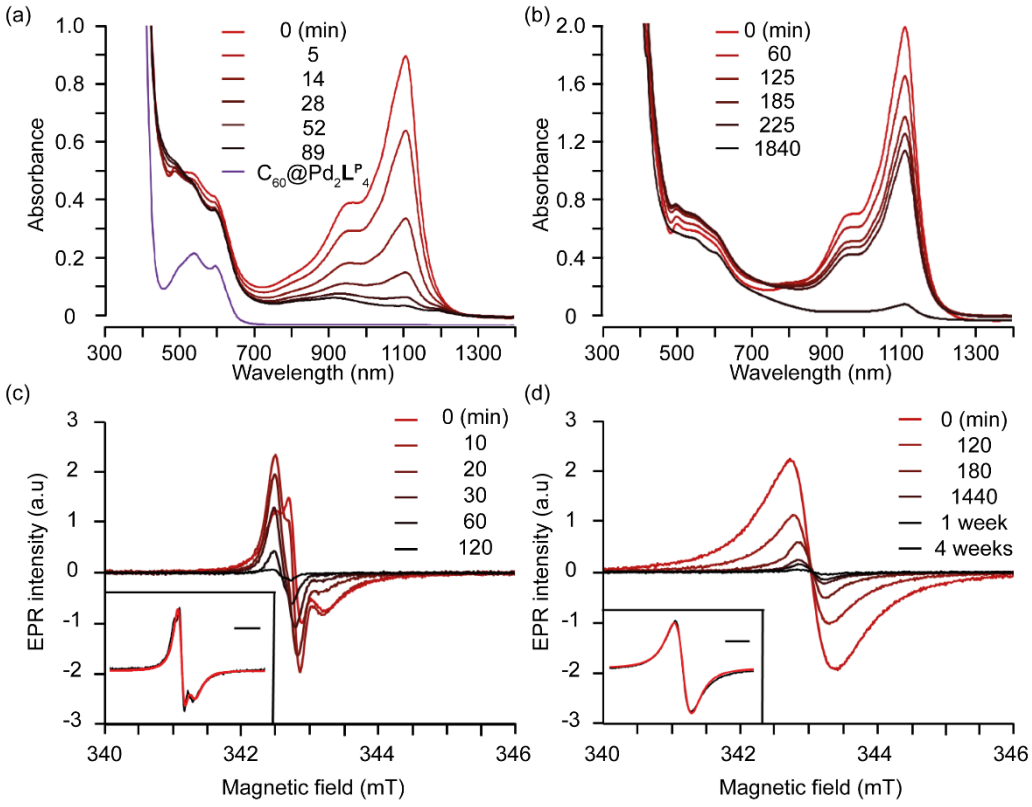

Figure 3.2.6 UV-Vis NIR absorption spectrum (acetonitrile, 0.35 mM, 295 K) of (a) $C_{60}^{\bullet-}@Pd_2\mathbf{L}^{\mathbf{P}}_4$ in the air (b) $C_{60}^{\bullet-}@Pd_2\mathbf{L}^{\mathbf{P}}_4$ prepared inert condition; EPR spectra of (c) $C_{60}^{\bullet-}@Pd_2\mathbf{L}^{\mathbf{P}}_4$ in the air and (d) $C_{60}^{\bullet-}@Pd_2\mathbf{L}^{\mathbf{P}}_4$ prepared under inert condition; both EPR spectra were measured at X-band at 100 K. The corresponding simulations are shown in the inset as red line. The figure is reproduced from the data published[51]

The lifetime of $C_{60}^{\bullet-}$ inside $Pd_2\mathbf{L^P}_4$ was further investigated in inert atmosphere (**Figure 3.2.6b**). Absorption bands with higher intensity were observed at the same wavelength in the NIR region but their decline was found to be dramatically elongated by removing oxygen, a potential oxidant in the system.[10] In addition, X-band EPR spectra were measured for $C_{60}^{\bullet-}$@$Pd_2\mathbf{L^P}_4$ prepared in air or inert condition at 100 K (**Figure 3.2.6c-d**). For the measurement under inert condition, the sample was prepared in the glovebox filled with N_2. The EPR signal originating from $C_{60}^{\bullet-}$, having a *g* value of 1.999, was observed in both samples (**3.4.8** for details).[12] On the other hand, an additional signal with g_{iso} = 2.001 assignable to an oxygenated species was observed in the case of the sample prepared in air (**Figure 3.2.6c**).[38] The presence of such an oxygenated species was also evidenced by ESI-MS analysis (**Figure 3.4.33**). Contrary, encapsulated $C_{60}^{\bullet-}$ was the only paramagnetic species observed in the sample prepared under inert atmosphere (**Figure 3.4.45**). The half-lifetime of $C_{60}^{\bullet-}$ was estimated to be 14 min under aerobic conditions by these EPR studies, while the comparable value obtained by the UV-Vis NIR absorption (13 min). Meanwhile, the EPR investigations of the sample prepared under inert condition showed a half-lifetime of 893 min, while a half-lifetime of about 300 min was estimated by UV-Vis NIR spectroscopy-based analysis (**3.4.8.3**). A potential reason for the large distribution would be how the samples were handled for the absorption and EPR studies. Both samples were prepared in the glovebox. While the samples could be stored in the glovebox for the aliquot-based EPR studies until the measurement time, the sample for the absorption study was let stand outside the glovebox once the measurement has started. Therefore, it can be assumed that more contamination of oxygen occurred for the sample used for the absorption study. It should be noted that the sample prepared under inert atmosphere showed the EPR signal even after one month, which clearly showing a stabilization of $C_{60}^{\bullet-}$ by nano-confinement inside the coordination cage.[12, 52] Nano-confinement inside the coordination cage provides the electrostatic interactions between $C_{60}^{\bullet-}$ and the cationic cage as well as protection of the encapsulated $C_{60}^{\bullet-}$ preventing access of oxidants.

3.3 Conclusion

In conclusion, the synthesis of the triptycene-based coordination cage and its accommodation capability towards C_{60} has been investigated. Owing to the molecular

design, taking advantage of convex-concave interactions between the curved π-surface of the ligand and C_{60}, encapsulation of C_{60} proceeds quantitatively. The formation of the empty host and the host-guest complex was fully characterized by NMR, ESI MS, and their structures in the solid-state were revealed by single crystal X-ray structure analysis. The photochemical reduction using BNAH was performed to generate $C_{60}^{\bullet-}$ inside the coordination cage. Generation of $C_{60}^{\bullet-}$ has been characterized by NMR, ESI MS, UV-Vis NIR, and EPR spectroscopy. To my surprise, generated $C_{60}^{\bullet-}$ has a long lifetime of utmost 1 month under inert atmosphere. The stabilization effect is probably due to confinement effects within the cationic coordination cage via electrostatic interactions between the anionic guest and the cationic host as well as steric protection provided by the cage hampering access of oxidants.

3.4 Appendix

3.4.1 Material and method

Unless otherwise stated, all chemicals were purchased from commercial sources and used as received. $[Pd(MeCN)_4](BF_4)_2$ and 3-aminopyridine were purchased from Sigma-Aldrich. Precursors to ligand **L^P** were prepared according to literature procedures.[30,32] Electrospray ionization (ESI) mass spectra were recorded using Bruker ESI-timsTOF and compact mass spectrometers using Agilent tune mix as calibrant. NMR experiments were performed using Bruker AV 500 Avance NEO FT NMR and Bruker Avance III HD 700 MHz spectrometers. EPR experiments were performed using a Bruker EMX-Nano Benchtop spectrometer equipped with a continuous-flow nitrogen cryostat. 1H and 13C signals were referenced to the residual solvent peak: acetonitrile (1.94 ppm, 118.26 ppm). DFT calculations were performed using Gaussian Gaussian 16, Revision B.01.[39] Hydrodynamic radii of compounds were calculated from the Stokes-Einstein equation (eq 1) where D is a diffusion coefficient, k_B is Boltzman constant, T is a temperature, η is a viscosity of the solvent, and r_H is a hydrodynamic radius of interest.

$$D = \frac{k_B T}{6\pi\eta r_H} \quad \text{(eq 1)}$$

3.4.2 Synthesis of L^P

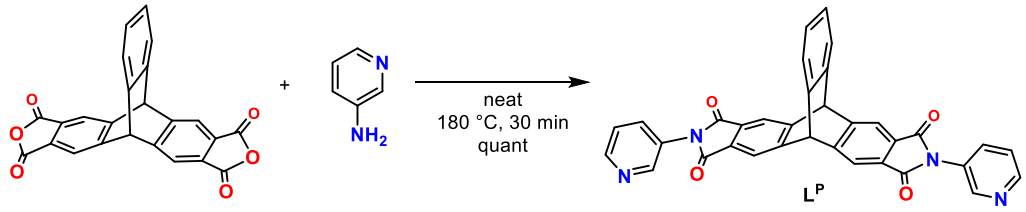

Figure 3.4.1 Synthesis of L^P

Triptycene-2,3,6,7-tetracarboxylic dianhydride (39.2 mg, 0.1 mmol) and 3-aminopyridine (282.2 mg, 3.0 mmol) were placed in a 10 mL vial and Ar gas was purged into the vial. The sealed vial was heated at 180 °C for 30 min while stirring and the resulting mixture was cooled to ambient temperature. The crude material was purified by silica-gel column chromatography ($CHCl_3$/MeOH=50:1). After evaporating organic solvents, the obtained compound was dissolved in 1.0 mL of $CHCl_3$ and precipitated by addition of Et_2O (5 mL). After filtration, desired compound **1** was obtained as a pale-yellow powder in quantitative yield. (54.6 mg, 100%)

^{1}H NMR (500 MHz, CD_3CN, 298 K): δ (ppm) **a** 8.61 (d, J = 2.5, 2H), **b** 8.56 (dd, J = 1.6, 5.5 Hz, 2H), **e** 8.04 (s, 4H), **d** 7.78 (ddd, J = 8.5, 2.5, 1.6 Hz, 2H), **f** 7.59 (dd, J = 5.5, 3.3 Hz, 2H), **c** 7.48 (ddd, J = 8.5, 5.5, 0.7 Hz, 2H), **g** 7.14 (dd, J = 5.5, 3.3 Hz,2H), **h** 6.16 (s, 2H)

^{13}C NMR (175 MHz, CD_3CN, 298 K): δ (ppm) 167.76, 152.52, 149.78, 148.55, 143.57, 135.05, 131.24, 130.02, 127.36, 125.81, 124.68, 120.31, 54.73

While 13 signals must be observed in theory, 13 signals were found.

ESI MS (positive mode): found: 547.1373; calculated for $[(C_{34}H_{19}N_4O_4)]^{1+}$ to be 547.1401

3.4.2.1 ^{1}H NMR spectra of $L^{P,}$

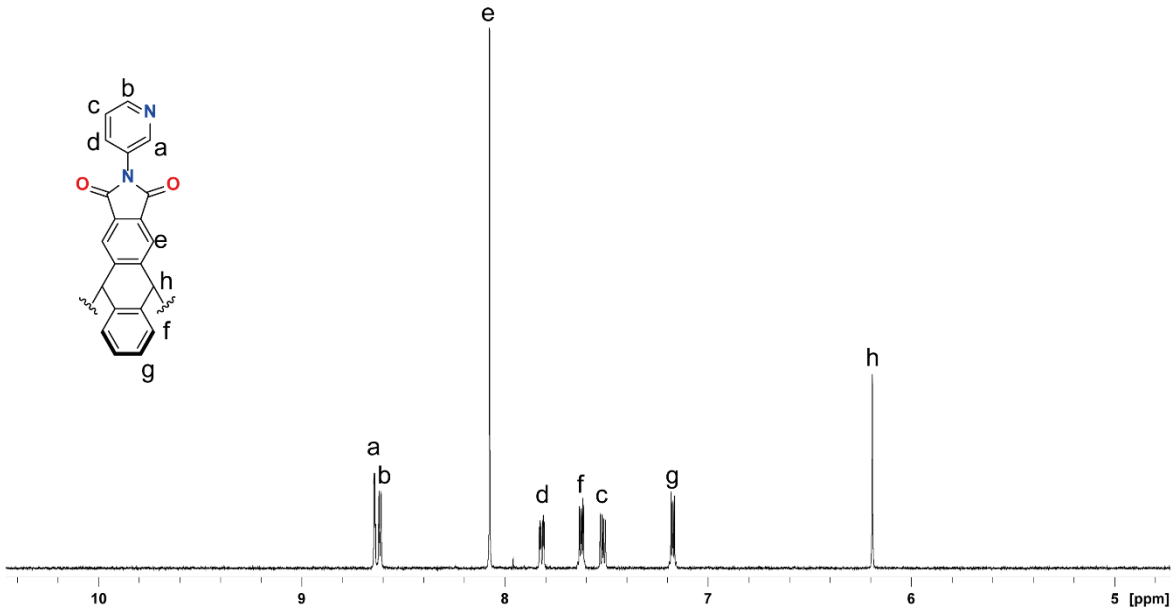

Figure 3.4.2 ^{1}H NMR spectrum of $\mathbf{L^{P}}$ (CD_3CN, 500 MHz, 298 K)

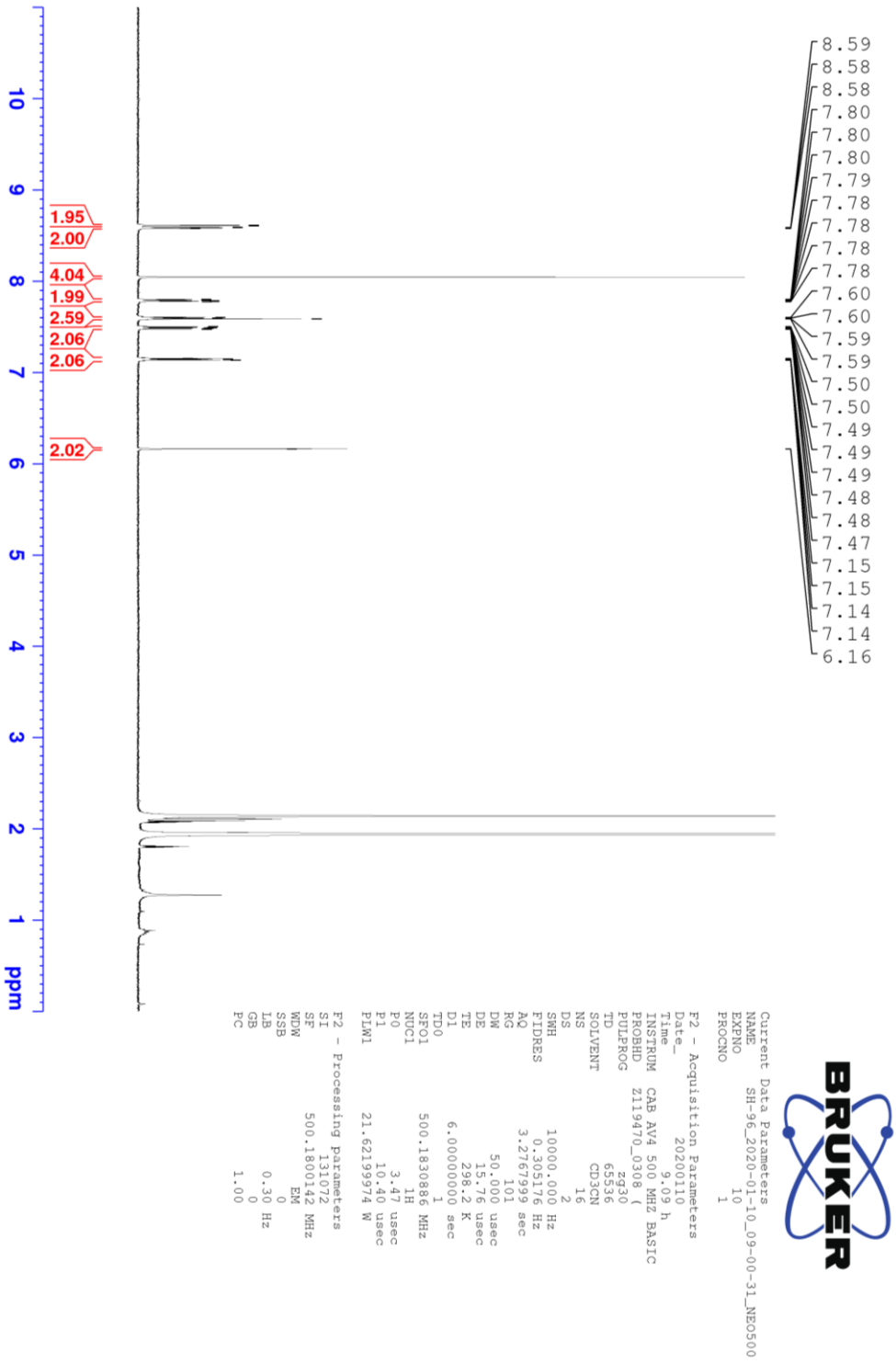

Figure 3.4.3 ^{1}H NMR spectrum of **L^{P}** (CD_3CN, 500 MHz, 298 K)

3.4.2.2 ^{13}C NMR spectrum of L^P

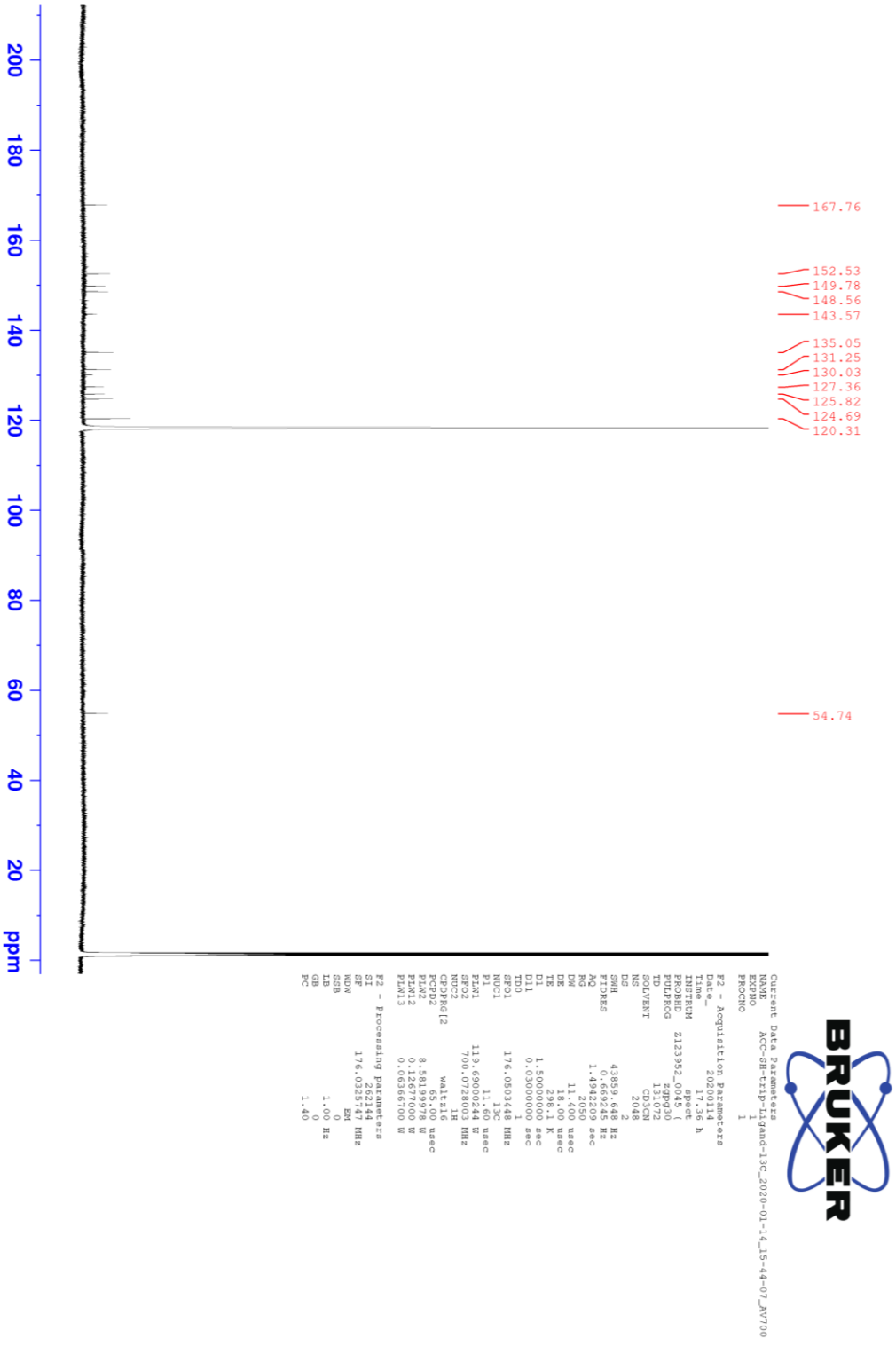

Figure 3.4.4 ^{13}C NMR spectrum of **L^P** (CD_3CN, 176 MHz, 298 K)

3.4.2.3 ESI MS spectrum of L^P

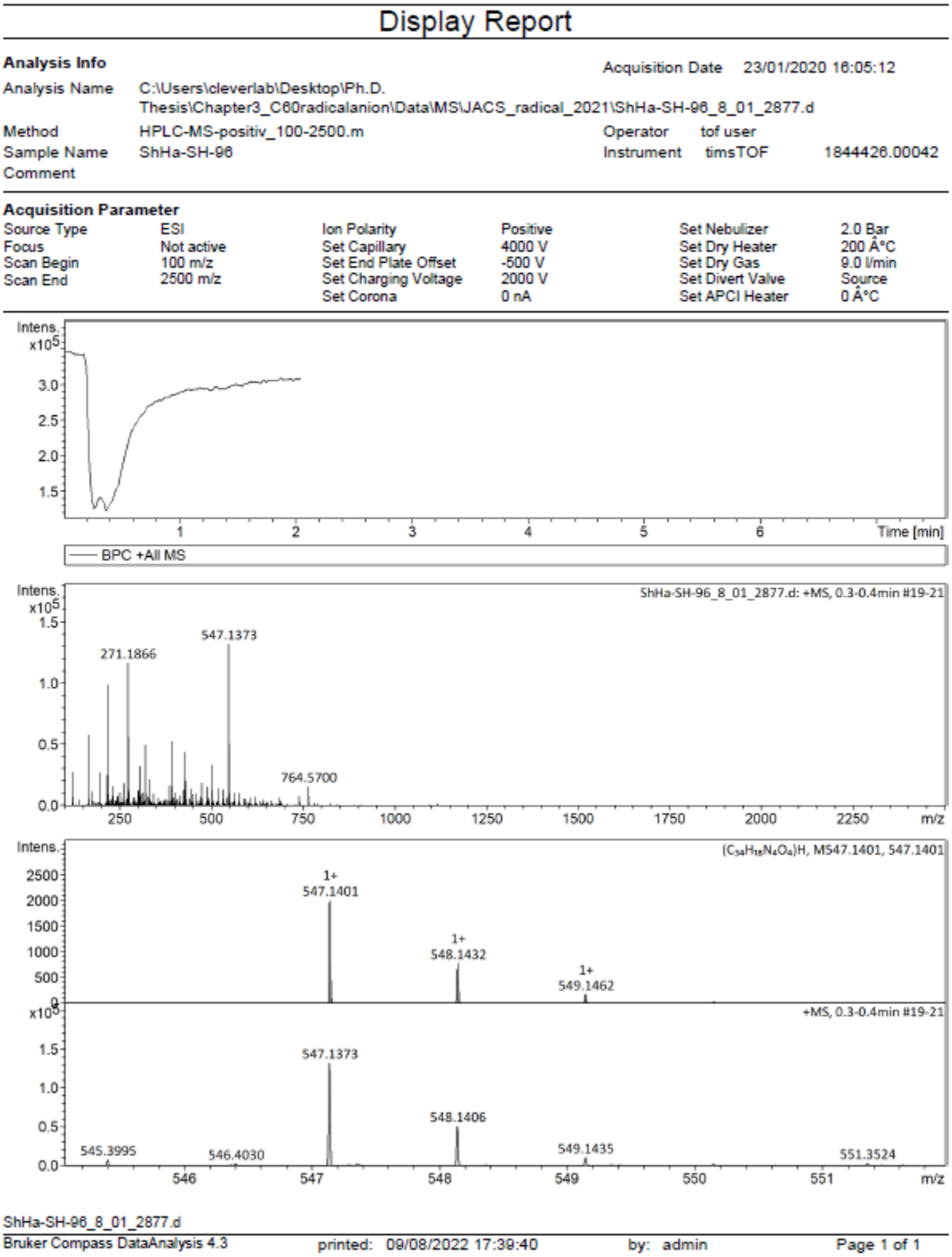

Figure 3.4.5 ESI MS spectrum of **L^P** (positive mode)

3.4.3 Synthesis of $Pd_2L^P_4$

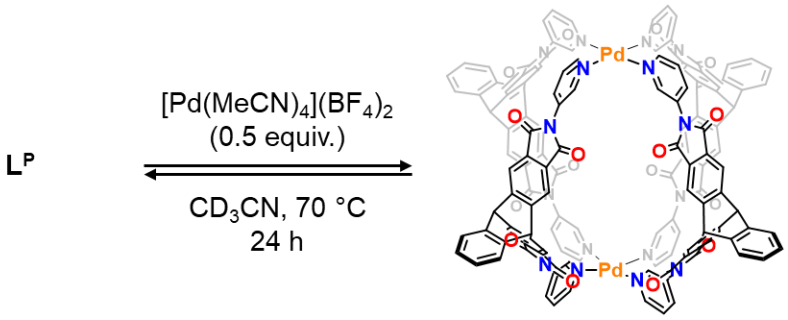

Figure 3.4.6 Synthesis of $Pd_2L^P_4$

To a suspension of L^P(1.52 mg, 2.8 µmol) in acetonitrile (1.00 mL, 0.70 mM), a solution of $[Pd(MeCN)_4](BF_4)_2$ in acetonitrile (70.0 µL, 20.0 mM, 1.4 µmol) was added. The mixture was heated at 70 °C for 24 h and the desired complex was obtained quantitatively.

^{1}H NMR (500 MHz, CD_3CN, 298 K): δ (ppm) **a** 9.12 (d, J = 2.5, 8H), **b** 8.70 (dd, J = 5.5, 1.3 Hz, 8H), **d** 8.16 (ddd, J = 8.5, 2.5, 1.3 Hz, 8H), 7.95 (s, 16H), **c** 7.67 (dd, J = 8.5, 5.5 Hz, 8H), **f** 7.62 (dd, J = 5.5, 3.3 Hz, 8H), **g** 7.17 (dd, J = 5.5, 3.3 Hz, 8H), **h** 6.15 (s, 8H)

^{13}C NMR (150 MHz, CD_3CN, 298 K): δ (ppm) 166.17, 153.11, 150.26, 148.67, 142.99, 138.05, 132.50, 130.39, 128.39, 127.55, 125.97, 120.72, 54.66

While 13 signals must be observed in theory, 13 signals were found.

DOSY: Diffusion coefficient D = 5.61 × 10^{-10} m^2s^{-1}, hydrodynamic radius r_H was calculated to be 11.6 Å

ESI MS (positive mode): found: 828.4497 and 1286.1774; calculated for $[(C_{34}H_{18}N_4O_4)_4Pd_2(BF_4)]^{3+}$ and $[(C_{34}H_{18}N_4O_4)_4Pd_2(BF_4)_2]^{2+}$ to be 828.4486 and 1286.1751 respectively

3.4.3.1 ^{1}H NMR spectra of $Pd_2L^{P}_4$

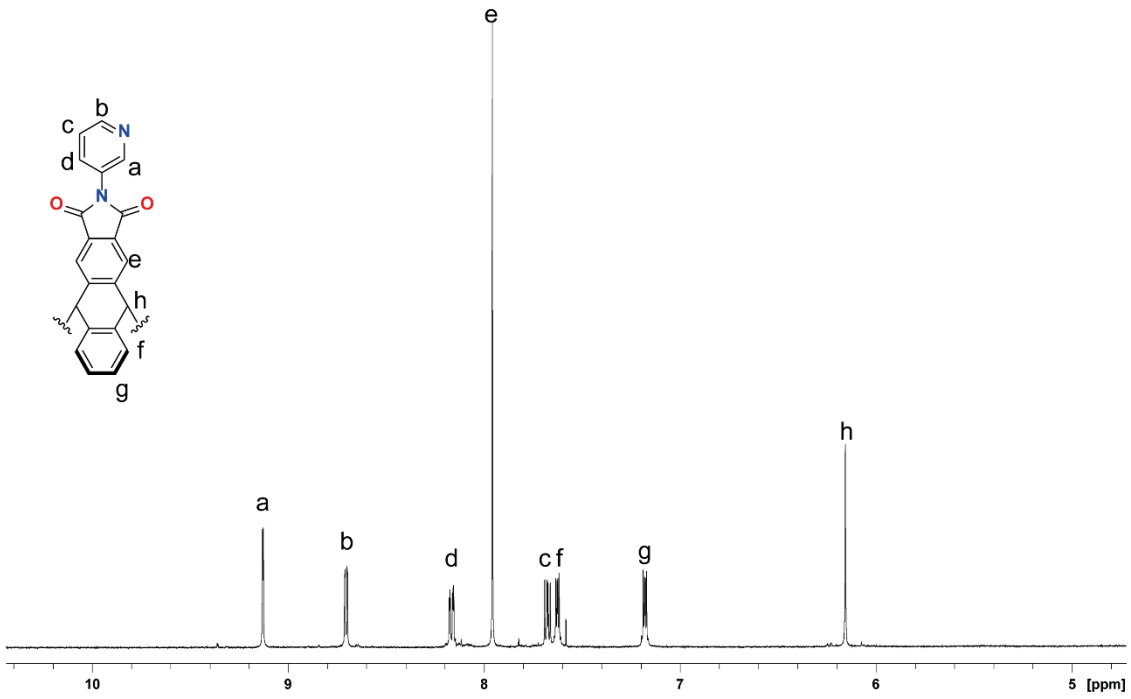

Figure 3.4.7 ^{1}H NMR spectrum of $Pd_2\mathbf{L}^{P}_4$ (CD_3CN, 0.70 mM, 500 MHz, 298 K)

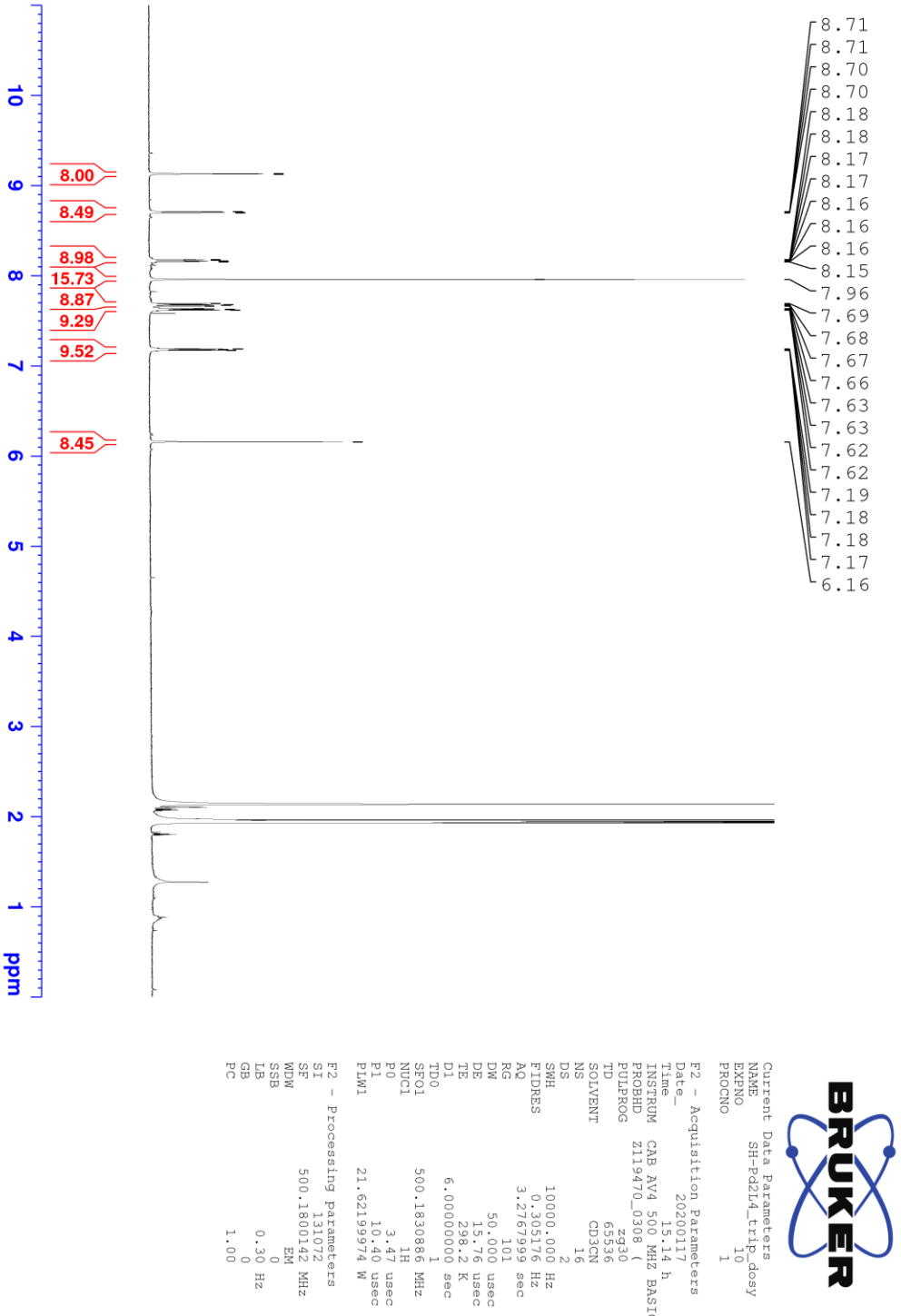

Figure 3.4.8 ^{1}H NMR spectrum of $Pd_2\mathbf{L}^{\mathbf{P}}_4$ (CD_3CN, 0.70 mM, 500 MHz, 298 K)

3.4.3.2 ^{1}H-^{1}H COSY NMR spectrum of $Pd_2L^P_4$

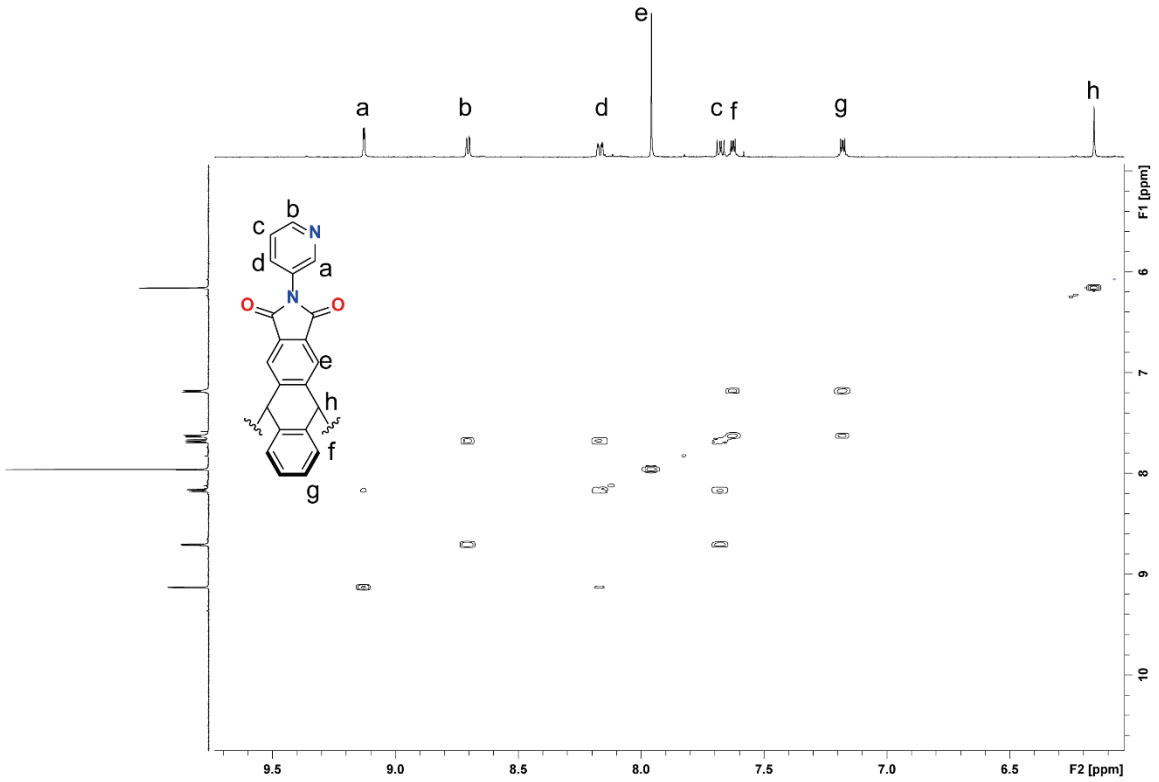

Figure 3.4.9 ^{1}H-^{1}H COSY NMR spectrum of $Pd_2\mathbf{L}^{P}_4$ (CD_3CN, 0.70 mM, 500 MHz, 298 K)

3.4.3.3 ^{1}H DOSY NMR spectrum of $Pd_2L^{P}_4$

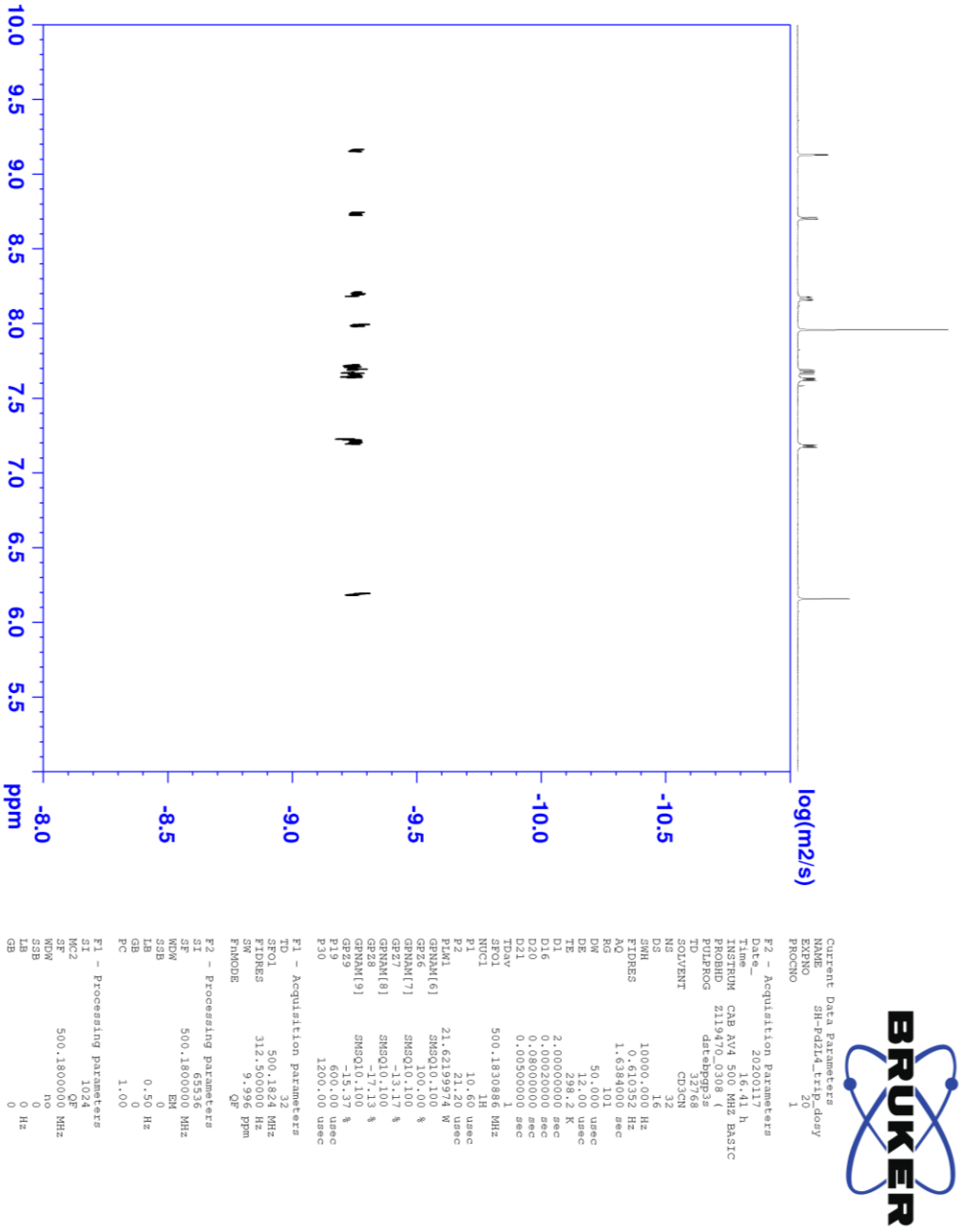

Figure 3.4.10 ^{1}H DOSY NMR spectrum of $Pd_2\mathbf{L}^{P}_4$ (CD_3CN, 0.70 mM, 500 MHz, 298 K)

3.4.3.4 ^{13}C NMR spectrum of $Pd_2L^P_4$

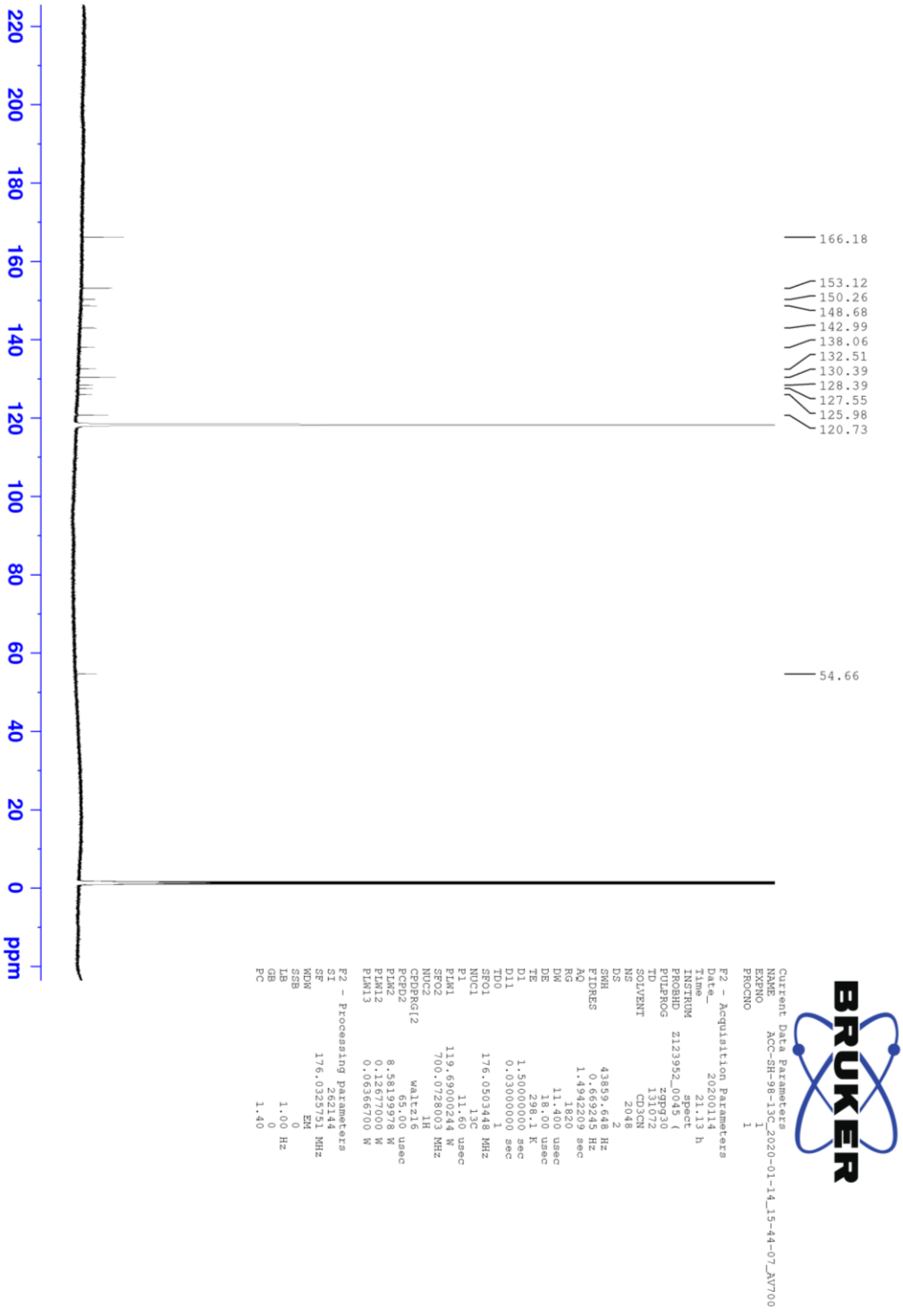

Figure 3.4.11 ^{13}C NMR spectrum of $Pd_2\mathbf{L}^{\mathbf{P}}_4$ (CD_3CN, 0.70 mM, 176 MHz, 298 K)

3.4.3.5 ESI MS spectrum of $Pd_2L^P_4$

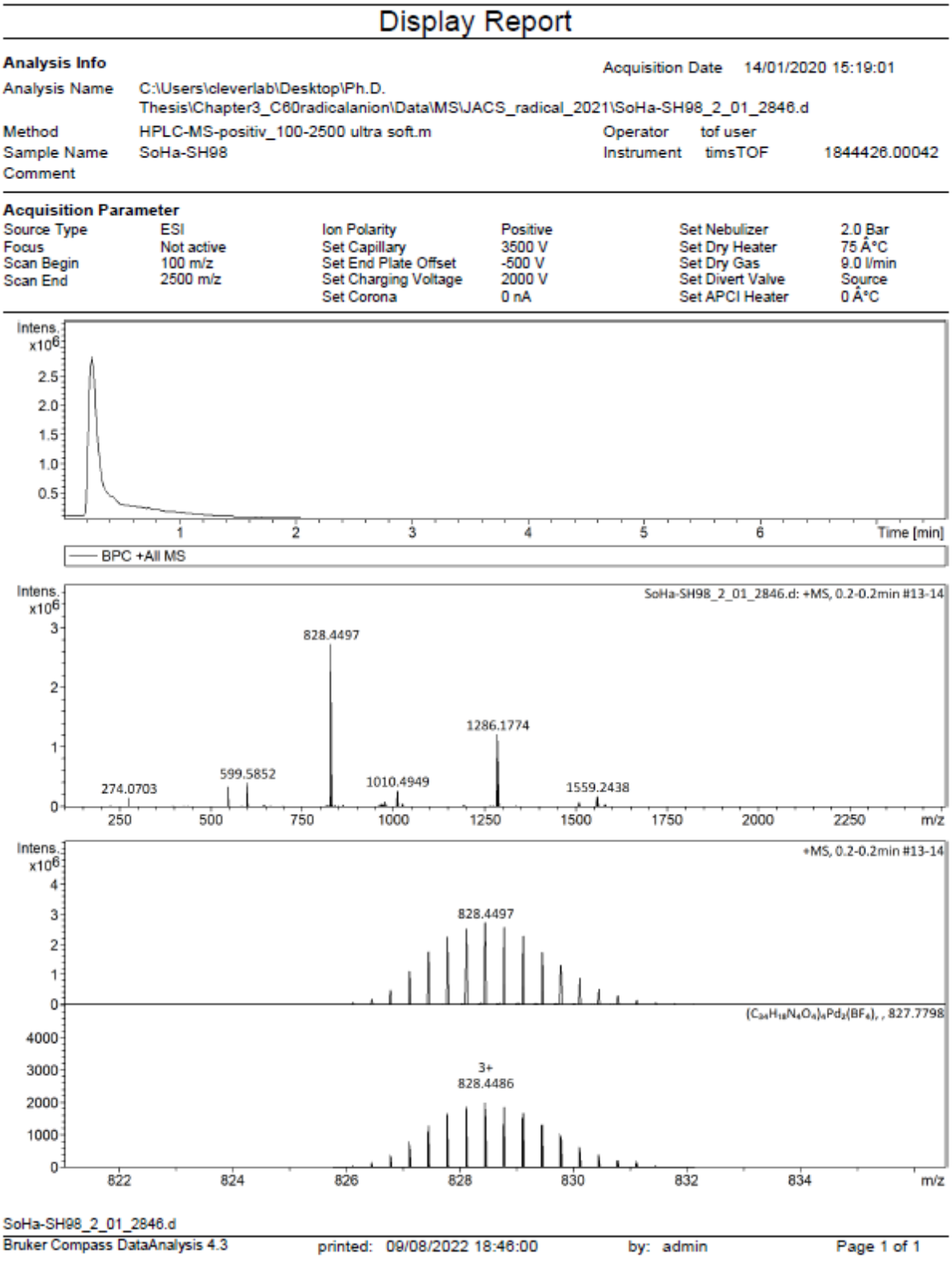

Figure 3.4.12 ESI MS spectrum of $Pd_2L^P_4$ (positive mode)

3.4.4 Synthesis of $C_{60}@Pd_2L^P_4$

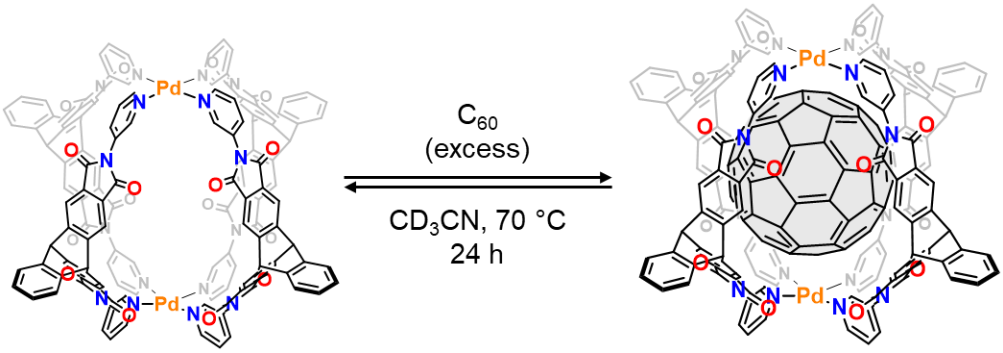

Figure 3.4.13 Synthesis of $C_{60}@Pd_2L^P_4$

To an acetonitrile solution of $Pd_2L^P_4$ (0.70 mM, 1.00 mL), 5 mg of powdered C_{60} was added and the suspension was heated at 70 °C for 24 h. The remained C_{60} powder was filtrated off. The desired complex was obtained quantitatively as a purple solution.

^{1}H NMR (500 MHz, CD_3CN, 298 K): δ (ppm) **b** 8.50 (d, J = 5.5 Hz, 8H), **d** 8.36 (ddd, J = 8.5, 2.5, 1.2 Hz, 8H), **e** 8.00 (s, 16H), **c** 7.85 (dd, J = 8.5, 5.5 Hz, 8H), **f** 7.65 (dd, J = 5.5, 3.3 Hz, 8H), **a** 7.59 (d, J = 2.5, 8H), **g** 7.20 (dd, J = 5.5, 3.3 Hz, 8H), 6.26 (s, 8H);

^{13}C NMR (150 MHz, CD_3CN, 298 K): δ (ppm) 165.90, 153.70, 152.36, 147.51, 142.87, 142.14 (C_{60}), 140.33, 132.59, 130.89, 129.52, 127.71, 126.16, 121.54, 54.59

While 14 signals must be observed in theory, 14 signals were found.

DOSY: Diffusion coefficient D = 5.40 × 10^{-10} m^2s^{-1}, hydrodynamic radius r_H was calculated to be 12.1 Å

ESI MS (positive mode): found: 779.8370 and 1068.7848; calculated for $[(C_{34}H_{18}N_4O_4)_4\ C_{60}Pd_2]^{4+}$ and $[(C_{34}H_{18}N_4O_4)_4C_{60}Pd_2(BF_4)]^{3+}$ to be 779.8360 and 1068.7828 respectively

3.4.4.1 ^{1}H NMR spectra of $C_{60}@Pd_2L^{P}_4$

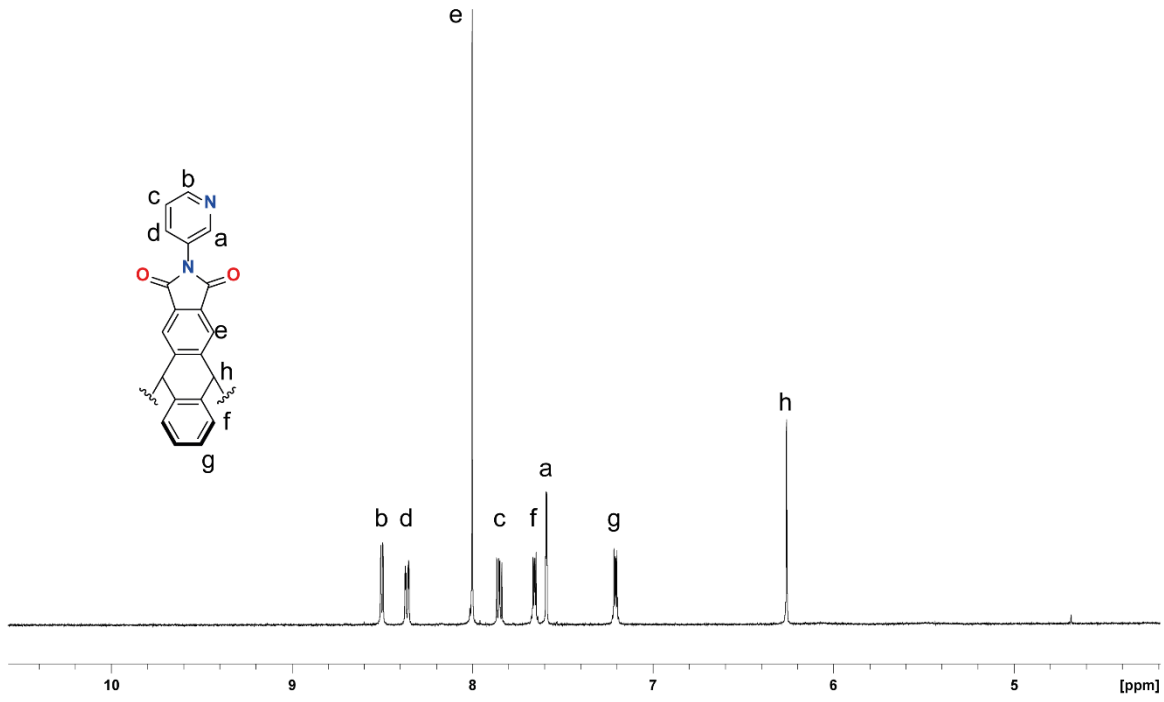

Figure 3.4.14 ^{1}H NMR spectrum of $C_{60}@Pd_2\mathbf{L}^{P}_4$ (CD_3CN, 0.70 mM, 500 MHz, 298 K)

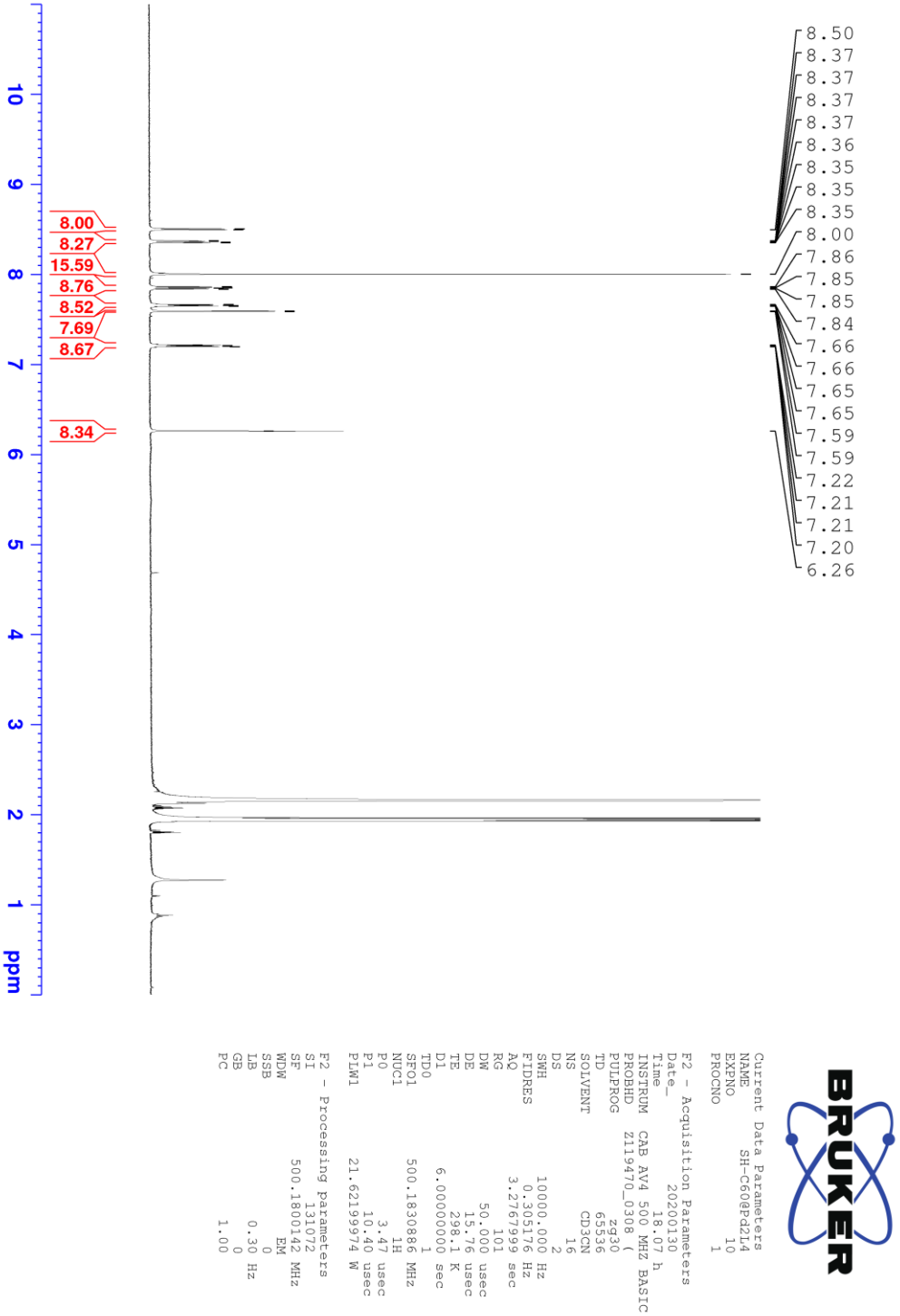

Figure 3.4.15 ^{1}H NMR spectrum of $C_{60}@Pd_2\mathbf{L}^{P}_4$ (CD_3CN, 0.70 mM, 500 MHz, 298 K)

3.4.4.2 ^{1}H-^{1}H COSY NMR spectrum of $C_{60}@Pd_2L^{P}_4$

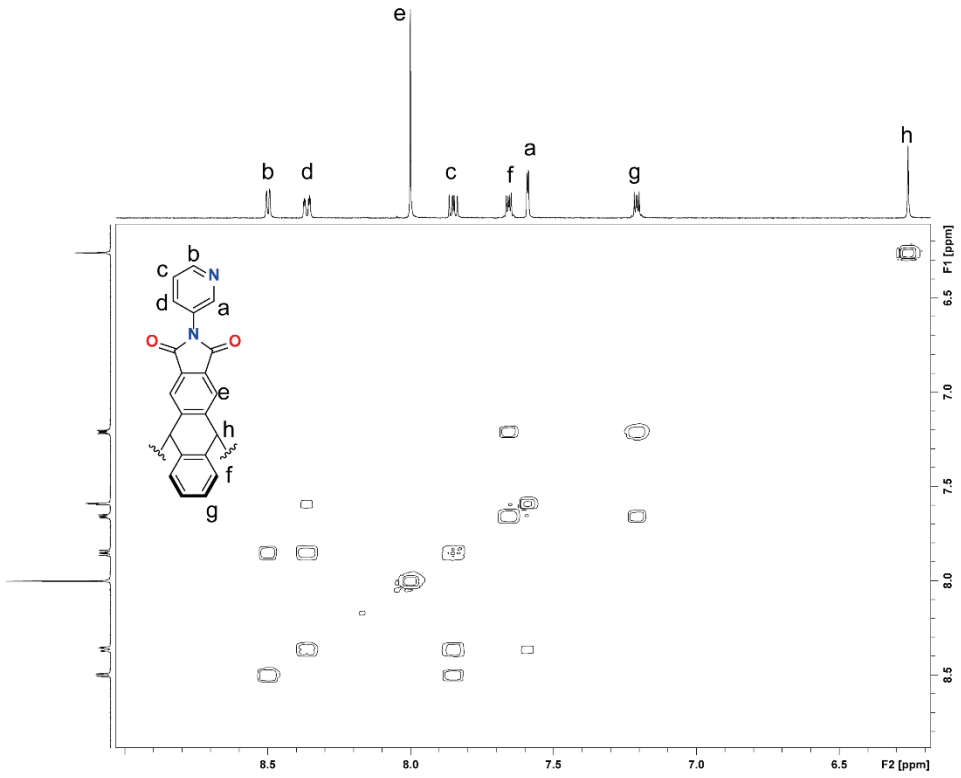

Figure 3.4.16 ^{1}H-^{1}H COSY NMR spectrum of $C_{60}@Pd_2\mathbf{L}^{P}_4$ (CD_3CN, 0.70 mM, 500 MHz, 298 K)

3.4.4.3 ^{1}H DOSY NMR spectrum of $C_{60}@Pd_2L^{P}_4$

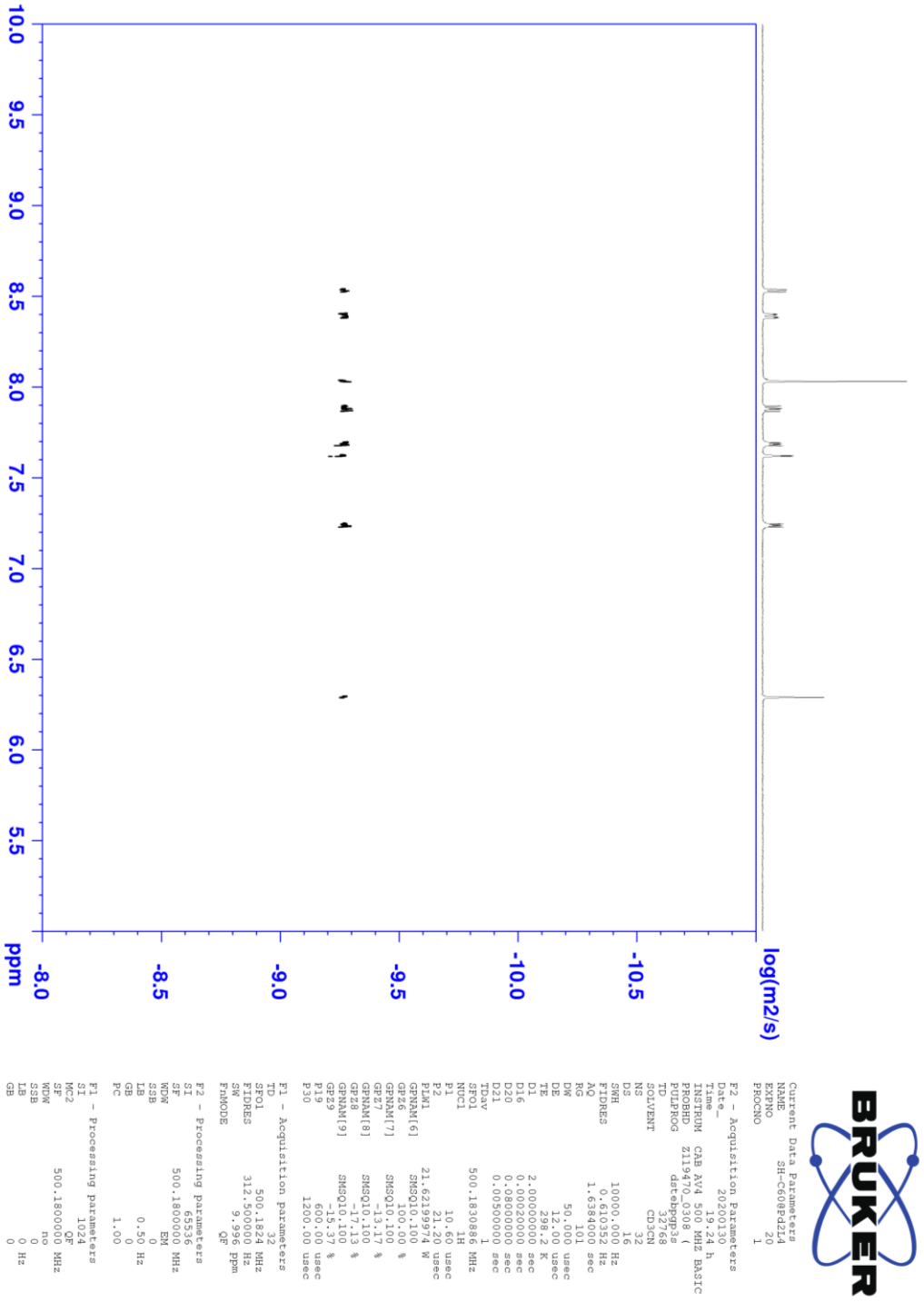

Figure 3.4.17 ^{1}H DOSY NMR spectrum of $C_{60}@Pd_2\mathbf{L}^{P}_4$ (CD_3CN, 0.70 mM, 500 MHz, 298 K)

3.4.4.4 ^{13}C NMR spectrum of $C_{60}@Pd_2L^P_4$

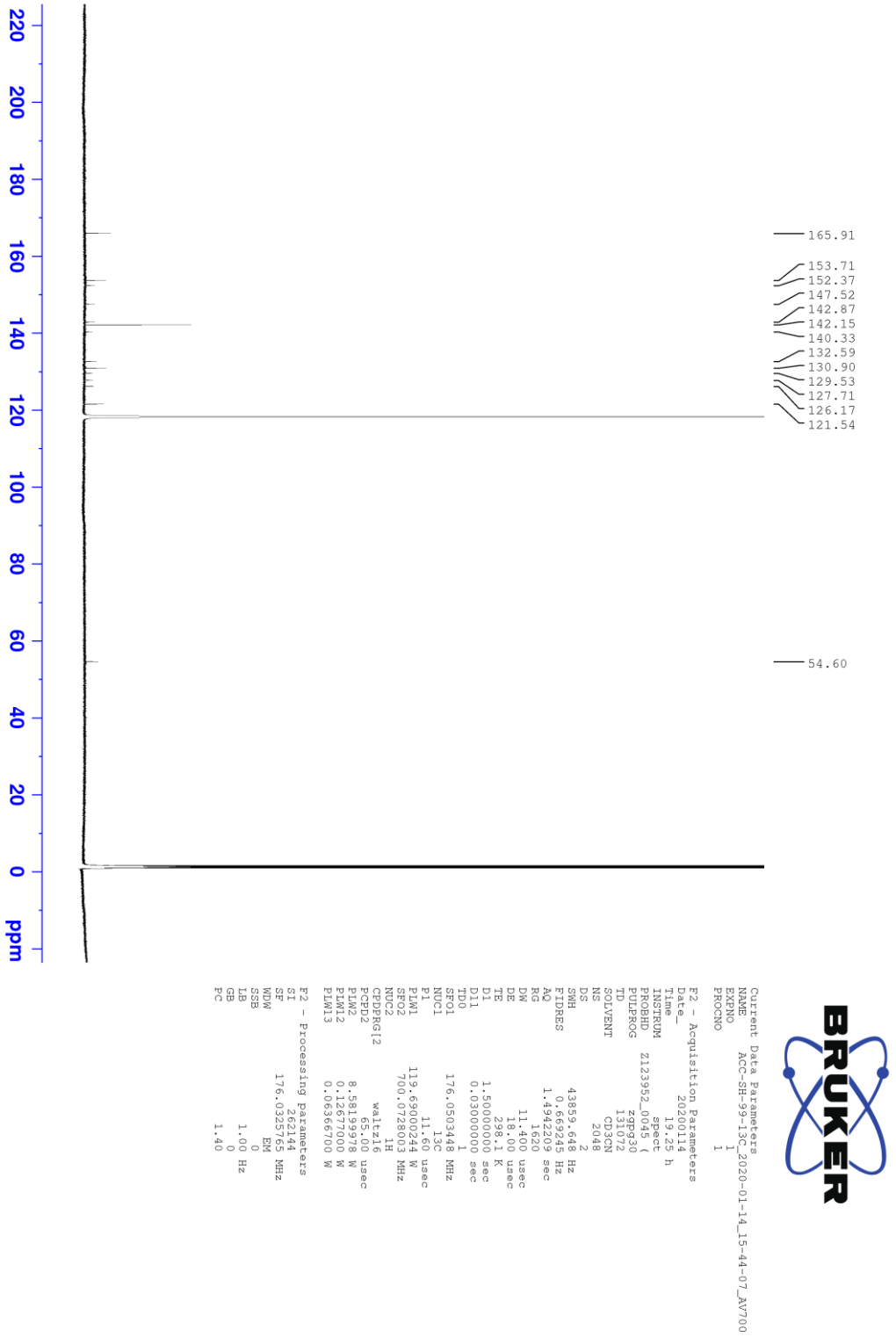

Figure 3.4.18 ^{13}C NMR spectrum of $C_{60}@Pd_2\mathbf{L}^P_4$ (CD_3CN, 0.70 mM, 176 MHz, 298 K)

3.4.4.5 ESI MS spectrum of $C_{60}@Pd_2L^P_4$

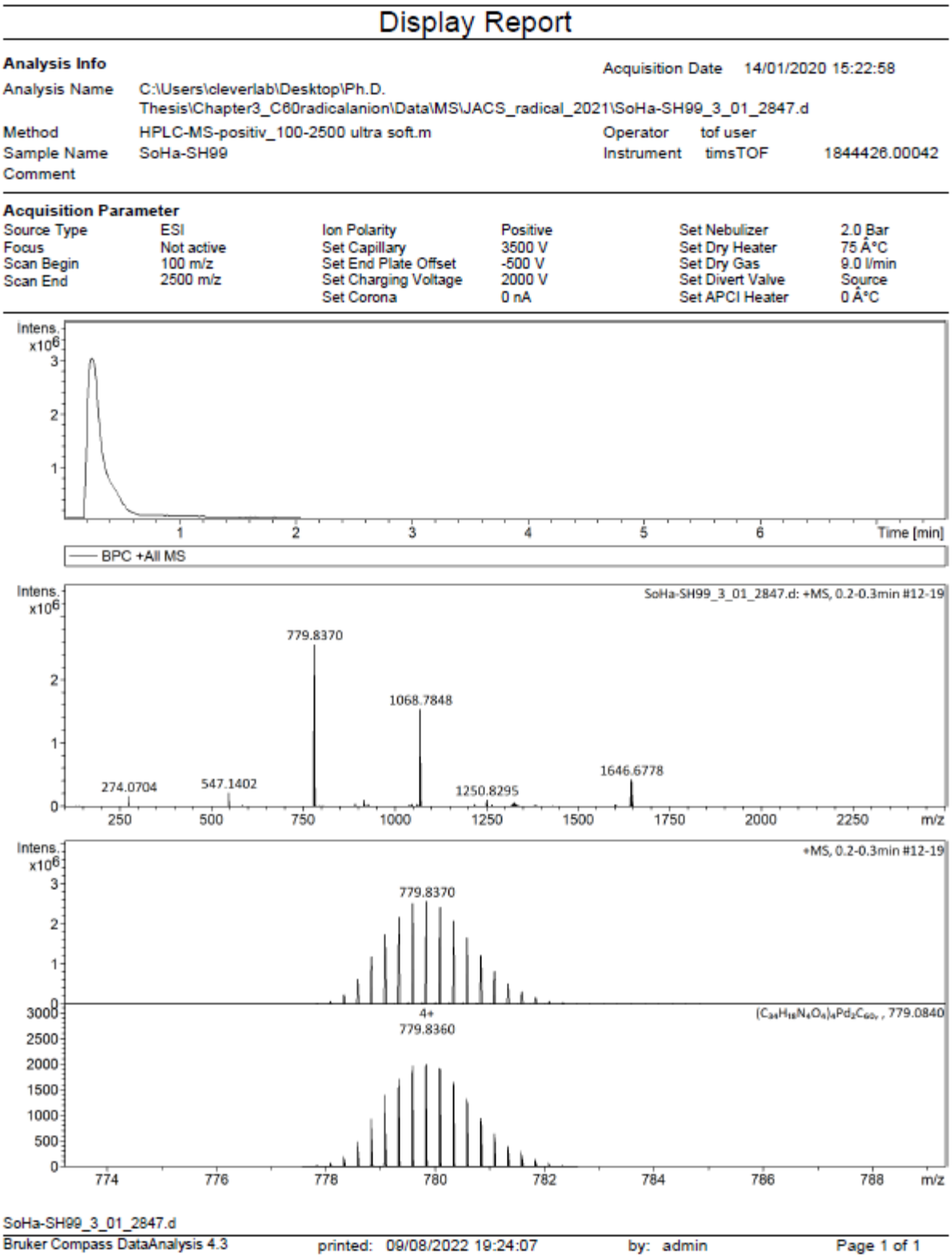

Figure 3.4.19 ESI MS spectrum of $C_{60}@Pd_2L^P_4$ (positive mode)

3.4.5 Single crystal X-ray structure analysis

3.4.5.1 X-ray Crystallography

$Pd_2\mathbf{L}^{\mathbf{P}}_4$ and $C_{60}@Pd_2\mathbf{L}^{\mathbf{P}}_4$ were studied using single-crystal X-ray diffraction. Due to very thin plate or needle-shaped crystals, the analysis was hampered by the limited scattering power of the samples not allowing to reach the desired (sub-)atomic resolution using our modern in-house micro-focused X-ray Cu-K_α source. Gaining detailed structural insight thus required cryogenic crystal handling and highly brilliant synchrotron radiation. Hence, diffraction data of both of supramolecular assemblies was collected during two beamtime shifts at macromolecular synchrotron beamline P11, PETRA III, DESY.[40] Counterion and solvent flexibility required carefully adapted macromolecular refinement protocols employing geometrical restraint dictionaries, similarity restraints and restraints for anisotropic displacement parameters (ADPs). The crystal structures were refined and deposited on the CCDC database by Dr. Julian J. Holstein. In addition, the following detail description of the refinement was contributed by Dr. Julian J. Holstein.

Compound	$Pd_2\mathbf{L}^{\mathbf{P}}_4$	$C_{60}@Pd_2\mathbf{L}^{\mathbf{P}}_4$
CIF ID	**sha3j**	**sha3b**
CCDC number	**2063154**	**2063155**
Empirical formula	$C_{148}H_{100}B_4F_{16}N_{16}O_{18}Pd_2$	$C_{262}H_{139}B_4F_{16}N_{16}O_{16}Pd_2$
Formula weight	2950.47	4326.92
Temperature [K]	80(2)	80(2)
Crystal system	triclinic	triclinic
Space group (number)	$P\bar{1}$ (2)	$P\bar{1}$ (2)
a [Å]	16.077(5)	20.306(2)
b [Å]	17.208(5)	23.077(4)
c [Å]	17.267(3)	23.8270(13)
α [Å]	65.05(6)	108.88(3)
β [Å]	75.44(2)	95.01(4)
γ [Å]	78.11(3)	96.18(6)
Volume [Å^3]	4165(3)	10414(3)
Z	1	2
ρ_{calc} [g/cm^3]	1.176	1.380
μ [mm^{-1}]	0.267	0.237
F(000)	1500	4414
Crystal size [mm^3]	0.020×0.020×0.005	0.180×0.030×0.015
Crystal colour	colourless	purple
Crystal shape	plate	plate
Radiation	synchrotron (λ=0.6888 Å)	synchrotron (λ=0.6888 Å)
2Θ range [°]	2.55 to 51.00 (0.80 Å)	1.77 to 58.94 (0.70 Å)
Index ranges	-20 ≤ h ≤ 20 -21 ≤ k ≤ 21 -21 ≤ l ≤ 21	-28 ≤ h ≤ 29 -32 ≤ k ≤ 32 -33 ≤ l ≤ 33
Reflections collected	54772	165384
Independent reflections	15968 R_{int} = 0.0570 R_{sigma} = 0.0521	49451 R_{int} = 0.0303 R_{sigma} = 0.0281
Completeness	94.3 %	93.3 %
Data / Restraints / Parameters	15968/1930/915	49451/6146/2935
Goodness-of-fit on F^2	1.339	2.147
Final *R* indexes [$I \geq 2\sigma(I)$]	R_1 = 0.1067 wR_2 = 0.3319	R_1 = 0.1131 wR_2 = 0.4303
Final *R* indexes [all data]	R_1 = 0.1279 wR_2 = 0.3462	R_1 = 0.1176 wR_2 = 0.4360
Largest peak/hole [eÅ^3]	2.49/-0.86	4.53/-1.70

3.4.5.2 $Pd_2L^P_4$

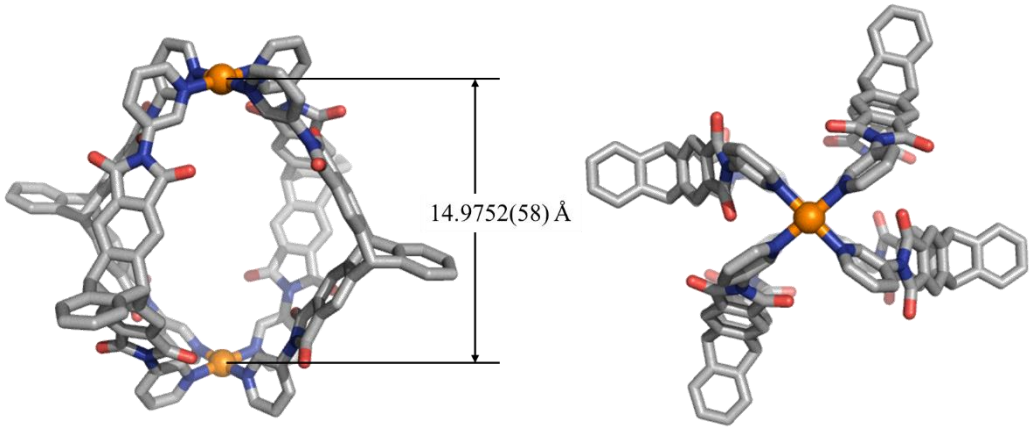

Figure 3.4.20 X-ray structure of $Pd_2\mathbf{L}^P_4$. Hydrogen atoms, counter anions, solvent molecules are omitted for clarity. Color scheme: C (gray), N (blue), O (red), and Pd (orange)

Single crystals were grown by slow diffusion of diisopropyl ether into a solution of $Pd_2\mathbf{L}^P_4$ in acetonitrile. A single crystal of $Pd_2\mathbf{L}^P_4$ in mother liquor was pipetted onto a glass slide containing NVH oil. To avoid cracking of the crystal, the crystal was quickly mounted onto a 0.04 mm nylon loop and immediately flash cooled in liquid nitrogen. Crystals were stored at cryogenic temperature in dry shippers, in which they were safely transported to macromolecular beamline P11 at Petra III,[40] DESY, Germany. A wavelength of λ = 0.6888 Å was chosen using a liquid N_2 cooled double crystal monochromator. Single crystal X-ray diffraction data was collected at 80(2) K on a single axis goniometer, equipped with an Oxford Cryostream 800 open flow cooling device and a Pilatus 6M fast detector. 3600 diffraction images were collected in a 360° φ sweep at a detector distance of 170 mm, 100% filter transmission, 0.1° step width and 0.1 seconds exposure time per image. Data integration and reduction were undertaken using XDS.[41] The structure was solved by intrinsic phasing/direct methods using SHELXT[42] and refined with SHELXL[43] using 22 CPU cores for full-matrix least-squares routines on F^2 and ShelXle[44] as a graphical user interface and the DSR program plugin was employed for modeling.[45,46] The asymmetric unit contains half a cage. One of the two co-crystallized tetrafluoroborate anions was modelled with two discrete positions refining their occupancy factor to 56:44 using a free variable. Despite reaching 0.8 Å resolution, disorder and poor crystal quality

required stereochemical restraints to be employed for ensuring a sensible geometry of the organic part of the structure.

Stereochemical restraints for the ligands **L^P** (residue class TRP) and co-crystallized diisolpropylether solvent molecule (residue class DIP) were generated by the GRADE program using the GRADE Web Server (http://grade.globalphasing.org) and applied in the refinement. A GRADE dictionary for SHELXL contains target values and standard deviations for 1,2-distances (DFIX) and 1,3-distances (DANG), as well as restraints for planar groups (FLAT). All displacements for non-hydrogen atoms were refined anisotropically. The refinement of ADPs for carbon, nitrogen and oxygen atoms was enabled by a combination of similarity restraints (SIMU) and rigid bond restraints (RIGU).[47] The contribution of the electron density from disordered counterions and solvent molecules, which could not be modeled with discrete atomic positions, were handled using the SQUEEZE[48] routine in PLATON.[49] The solvent mask file (.fab) computed by PLATON were included in the SHELXL refinement via the ABIN instruction leaving the measured intensities untouched.

3.4.5.3 C_{60}@$Pd_2L^P_4$

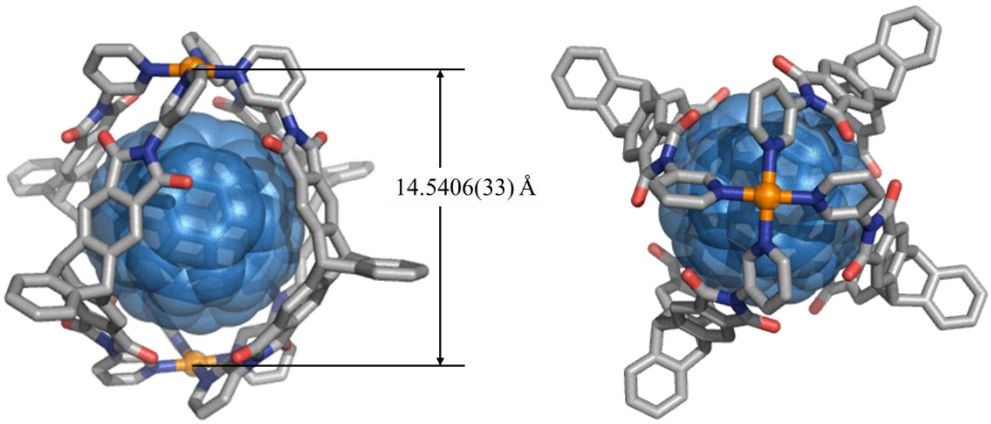

Figure 3.4.21 X-ray structure of C_{60}@Pd_2**L$^P_4$**. Hydrogen atoms, counter anions, solvent molecules are omitted for clarity. Color scheme: C (gray), N (blue), O (red), Pd (orange), C_{60} (light blue)

Single crystals were grown by slow diffusion of benzene into a solution of C_{60}@Pd_2**L$^P_4$** in acetonitrile. A single crystal of C_{60}@Pd_2**L$^P_4$** in mother liquor was pipetted onto a glass slide containing NVH oil. To avoid cracking of the crystal, the crystal was quickly mounted onto a 0.2 mm nylon loop and immediately flash cooled in liquid nitrogen.

Crystals were stored at cryogenic temperature in dry shippers, in which they were safely transported to macromolecular beamline P11 at Petra III[3], DESY, Germany. A wavelength of λ = 0.6888 Å was chosen using a liquid N_2 cooled double crystal monochromator. Single crystal X-ray diffraction data was collected at 80(2) K on a single axis goniometer, equipped with an Oxford Cryostream 800 open flow cooling device and a Pilatus 6M fast detector. 3600 diffraction images were collected in a 360° φ sweep at a detector distance of 170 mm, 100% filter transmission, 0.1° step width and 0.1 seconds exposure time per image. Data integration and reduction were undertaken using XDS.[40] The structure was solved by intrinsic phasing/direct methods using SHELXT[41] and refined with SHELXL[42] using 22 CPU cores for full-matrix least-squares routines on F^2 and ShelXle[43] as a graphical user interface and the DSR program plugin was employed for modeling.[44,45]

The asymmetric unit contains one full cage with C_{60} encapsulated. Three of seven co-crystallized benzene solvent molecules were modelled with two discrete positions refining their occupancy factor for two of which to 67:33 and 42:58 for the other using a free variable. One of the four co-crystallized tetrafluoroborates was modelled with two discrete positions refining their occupancy factor to 70:30 using a free variable. Despite reaching 0.7 Å resolution, disorder and poor crystal quality required stereochemical restraints to be employed for ensuring a sensible geometry of the organic part of the structure.

Stereochemical restraints for the ligands **1** (residue class TRP) and co-crystallized benzene solvent molecules (residue class BEN) were generated by the GRADE program using the GRADE Web Server (http://grade.globalphasing.org) and applied in the refinement. A GRADE dictionary for SHELXL contains target values and standard deviations for 1,2-distances (DFIX) and 1,3-distances (DANG), as well as restraints for planar groups (FLAT). All displacements for non-hydrogen atoms were refined anisotropically. The refinement of ADPs for carbon, nitrogen and oxygen atoms was enabled by a combination of similarity restraints (SIMU) and rigid bond restraints (RIGU).[46] The contribution of the electron density from disordered counterions and solvent molecules, which could not be modeled with discrete atomic positions were handled using the SQUEEZE[47] routine in PLATON.[48] The solvent mask file (.fab) computed by PLATON were included in the SHELXL refinement via the ABIN instruction leaving the measured intensities untouched.

3.4.6 Electronic properties

3.4.6.1 Cyclic voltammetry

Cyclic voltammetry was performed using an Metrohm Autolab PGSTAT101 potentiostat and analyzed by using NOVA software ver. 2.1. All experiments were carried out in 0.1 M acetonitrile solutions of tetrabutylammonium hexafluorophosphate ($TBAPF_6$, 99.9% purity). To an acetonitrile solution of each cage, an appropriate amount of $TBAPF_6$ was added so that the concentration of $TBAPF_6$ became 0.1 M. The voltammograms were measured using a glassy carbon working electrode, $Ag/AgNO_3$ (0.01 M in 0.1 M $TBAPF_6$ acetonitrile solution) as a reference electrode, and a Pt wire as a counter electrode under 100 mV/s scan rate under N_2 atmosphere.

3.4.6.2 Theoretical studies

All calculations were conducted using the Gaussian 16 program. The single point calculation was performed using the optimized geometry to calculate molecular orbitals.

3.4.6.2.1 $C_{60}@Pd_2L^P_4$

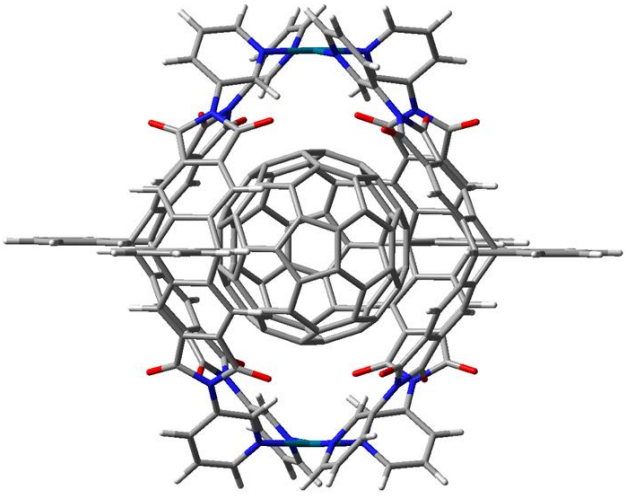

Figure 3.4.22 Gas-phase DFT-optimized geometry of $[C_{60}@Pd_2\mathbf{L}^{\mathbf{P}}_4]^{4+}$ (M06-2X/Lanl2dz)

Standard orientation:

Center Number	Atomic Number	Atomic Type	Coordinates (Angstroms) X	Y	Z
1	6	0	-3.192340	-4.982860	3.858819
2	6	0	-3.230918	-3.685181	4.381004
3	6	0	-2.251275	-3.216839	5.259927
4	6	0	-1.216447	-4.105133	5.578309
5	6	0	-0.000049	-3.795318	6.456971
6	6	0	1.216538	-4.104892	5.578477
7	6	0	2.251212	-3.216383	5.260213
8	6	0	3.231116	-3.684564	4.381493
9	6	0	3.192953	-4.982283	3.859400
10	6	0	2.196845	-5.892360	4.203288
11	6	0	1.204602	-5.430486	5.072986
12	6	0	0.000266	-6.240936	5.544601
13	6	0	-1.204138	-5.430703	5.072779
14	6	0	-2.196107	-5.892740	4.202852
15	6	0	-4.388983	-2.971455	3.786418
16	6	0	-4.306728	-5.150875	2.896789
17	6	0	4.389033	-2.970554	3.786971
18	6	0	-0.000028	-4.852853	7.569302
19	6	0	0.000136	-6.170299	7.075685
20	6	0	4.307531	-5.150075	2.897550
21	7	0	5.000721	-3.891593	2.883528
22	7	0	-5.000230	-3.892580	2.882761
23	8	0	-4.600741	-6.123006	2.204259
24	8	0	-4.771919	-1.810069	3.974007
25	8	0	4.601876	-6.122192	2.205141
26	8	0	4.771541	-1.809008	3.974462
27	6	0	-6.069809	-3.592024	2.009798
28	6	0	6.070364	-3.590802	2.010711
29	6	0	-6.953621	-4.585310	1.547592
30	6	0	-7.962154	-4.225973	0.645931
31	6	0	-8.074825	-2.900579	0.222970
32	7	0	-7.222882	-1.951241	0.686440
33	6	0	-6.240746	-2.275452	1.559715
34	6	0	6.241199	-2.274152	1.560783
35	7	0	7.223357	-1.949750	0.687600
36	6	0	8.075459	-2.898938	0.224118
37	6	0	7.962932	-4.224376	0.646970
38	6	0	6.954359	-4.583928	1.548498
39	6	0	-0.000169	-4.605847	8.940315
40	6	0	-0.000139	-5.700879	9.826383
41	6	0	0.000028	-7.014054	9.334474
42	6	0	0.000168	-7.257234	7.947105
43	6	0	-0.000033	7.257842	-7.947240

44	6	0	0.000127	7.014759	-9.334626	102	6	0	-0.001365	7.736200	4.681283
45	6	0	0.000275	5.701619	-9.826626	103	6	0	-0.001404	7.260028	6.004970
46	6	0	0.000263	4.606525	-8.940636	104	6	0	4.249121	2.999287	5.041512
47	6	0	6.953433	4.585436	-1.547616	105	7	0	4.960108	2.972872	3.796405
48	6	0	7.961924	4.226096	-0.645912	106	7	0	-4.961671	2.971884	3.795736
49	6	0	8.074677	2.900670	-0.223091	107	8	0	-4.513336	2.296881	6.015991
50	7	0	7.222889	1.951296	-0.686775	108	8	0	-4.808953	4.081660	1.717758
51	6	0	6.240824	2.275487	-1.560143	109	8	0	4.511408	2.297556	6.016495
52	6	0	-6.241036	2.274296	-1.561134	110	8	0	4.807628	4.082802	1.718500
53	7	0	-7.223087	1.949845	-0.687846	111	6	0	-6.025093	2.083253	3.524326
54	6	0	-8.075063	2.899032	-0.224112	112	6	0	6.023778	2.084491	3.525163
55	6	0	-7.962513	4.224516	-0.646798	113	6	0	-6.909890	1.662097	4.535190
56	6	0	-6.954027	4.584127	-1.548400	114	6	0	-7.918359	0.746776	4.214373
57	6	0	6.069763	3.592121	-2.010039	115	6	0	-8.035674	0.278882	2.904453
58	6	0	-6.070156	3.591012	-2.010875	116	7	0	-7.183705	0.703400	1.937972
59	8	0	4.771877	1.810306	-3.974398	117	6	0	-6.190065	1.577645	2.228299
60	8	0	4.600661	6.123124	-2.204352	118	6	0	6.189133	1.578905	2.229173
61	8	0	-4.771536	1.809428	-3.974968	119	7	0	7.183093	0.704934	1.939072
62	8	0	-4.601661	6.122419	-2.205199	120	6	0	8.034982	0.280671	2.905733
63	7	0	-5.000595	3.891885	-2.883773	121	6	0	7.917269	0.748535	4.215625
64	7	0	5.000216	3.892743	-2.883030	122	6	0	6.908486	1.663582	4.536211
65	6	0	4.306711	5.151044	-2.896985	123	6	0	-0.001569	9.103852	4.416048
66	6	0	-0.000041	6.170847	-7.075896	124	6	0	-0.001817	10.004262	5.499212
67	6	0	0.000103	4.853435	-7.569605	125	6	0	-0.001857	9.529767	6.818794
68	6	0	4.388975	2.971696	-3.786768	126	6	0	-0.001649	8.145784	7.080355
69	6	0	-4.307390	5.150366	-2.897730	127	6	0	0.001682	-8.147409	-7.078623
70	6	0	-4.389005	2.970949	-3.787382	128	6	0	0.001891	-9.531312	-6.816642
71	6	0	-2.196764	5.892741	-4.203505	129	6	0	0.001832	-10.005409	-5.496917
72	6	0	-1.204545	5.430917	-5.073258	130	6	0	0.001563	-9.104672	-4.414027
73	6	0	-0.000189	6.241376	-5.544809	131	6	0	6.909689	-1.662756	-4.535183
74	6	0	1.204195	5.431087	-5.073032	132	6	0	7.918177	-0.747368	-4.214622
75	6	0	2.196159	5.893044	-4.203060	133	6	0	8.035558	-0.279181	-2.904812
76	6	0	3.192374	4.983123	-3.859082	134	7	0	7.183614	-0.703454	-1.938207
77	6	0	3.230944	3.685484	-4.381357	135	6	0	6.189923	-1.577728	-2.228293
78	6	0	2.251297	3.217215	-5.260319	136	6	0	-6.188861	-1.578946	-2.229289
79	6	0	1.216486	4.105550	-5.578653	137	7	0	-7.182818	-0.704935	-1.939327
80	6	0	0.000083	3.795822	-6.457349	138	6	0	-8.034799	-0.280939	-2.906027
81	6	0	-1.216511	4.105363	-5.578852	139	6	0	-7.917198	-0.749156	-4.215805
82	6	0	-2.251214	3.216858	-5.260660	140	6	0	-6.908456	-1.664312	-4.536227
83	6	0	-3.231096	3.684989	-4.381888	141	6	0	6.024914	-2.083652	-3.524189
84	6	0	-3.192882	4.982656	-3.859672	142	6	0	-6.023648	-2.084911	-3.525142
85	6	0	-3.162610	3.985578	4.857741	143	8	0	4.808803	-4.081621	-1.717109
86	6	0	-3.226596	4.508185	3.560678	144	8	0	4.513178	-2.297940	-6.015798
87	6	0	-2.263420	5.403676	3.085068	145	8	0	-4.807517	-4.082681	-1.717941
88	6	0	-1.221190	5.735326	3.961407	146	8	0	-4.511363	-2.298729	-6.016472
89	6	0	-0.001124	6.609736	3.638974	147	7	0	-4.959999	-2.973371	-3.796172
90	6	0	1.219109	5.735639	3.961599	148	7	0	4.961492	-2.972346	-3.795360
91	6	0	2.261562	5.404250	3.085427	149	6	0	4.250759	-2.999321	-5.040601
92	6	0	3.224828	4.508911	3.561149	150	6	0	0.001416	-7.261325	-6.003506
93	6	0	3.160695	3.986198	4.858162	151	6	0	0.001357	-7.737101	-4.679678
94	6	0	2.168957	4.354476	5.762218	152	6	0	4.388892	-3.893613	-2.864483
95	6	0	1.198169	5.242019	5.292020	153	6	0	-4.249025	-3.000146	-5.041279
96	6	0	-0.001210	5.730851	6.096855	154	6	0	-4.387415	-3.894573	-2.865227
97	6	0	-1.200365	5.241750	5.291846	155	6	0	-2.168920	-4.355641	-5.761620
98	6	0	-2.171081	4.354072	5.761938	156	6	0	-1.198169	-5.243092	-5.291170
99	6	0	-4.389064	3.893390	2.865098	157	6	0	0.001215	-5.732174	-6.095850
100	6	0	-4.250932	2.998527	5.040981	158	6	0	1.200343	-5.242807	-5.290956
101	6	0	4.387537	3.894373	2.865738	159	6	0	2.171018	-4.355198	-5.761265

160	6	0	3.162485	-3.986380	-4.857131	217	1	0	5.545844	1.894715	1.416373
161	6	0	3.226461	-4.508626	-3.559922	218	1	0	8.800588	-0.428580	2.616787
162	6	0	2.263334	-5.404054	-3.084098	219	1	0	8.610916	0.404430	4.971865
163	6	0	1.221153	-5.736002	-3.960375	220	1	0	6.802752	2.033123	5.547979
164	6	0	0.001097	-6.610330	-3.637706	221	1	0	-0.001544	9.474907	3.395832
165	6	0	-1.219118	-5.736316	-3.960602	222	1	0	-0.001983	11.072156	5.312238
166	6	0	-2.261534	-5.404614	-3.084512	223	1	0	-0.002055	10.233333	7.643543
167	6	0	-3.224745	-4.509351	-3.560477	224	1	0	-0.001686	7.781964	8.103024
168	6	0	-3.160616	-3.987033	-4.857651	225	1	0	0.001733	-7.783900	-8.101402
169	46	0	7.266888	0.000789	0.000417	226	1	0	0.002104	-10.235127	-7.641179
170	46	0	-7.266755	-0.000715	-0.000728	227	1	0	0.002000	-11.073246	-5.309619
171	1	0	-2.291628	-2.209534	5.662871	228	1	0	0.001523	-9.475415	-3.393698
172	1	0	-0.000174	-2.772932	6.840167	229	1	0	6.804217	-2.032544	-5.546889
173	1	0	2.291270	-2.209043	5.663097	230	1	0	8.611858	-0.403249	-4.970825
174	1	0	2.194066	-6.901345	3.803827	231	1	0	8.800932	0.430330	-2.615894
175	1	0	0.000391	-7.263467	5.163890	232	1	0	5.546571	-1.893511	-1.415539
176	1	0	-2.193039	-6.901703	3.803340	233	1	0	-5.545409	-1.894462	-1.416497
177	1	0	-6.847332	-5.611962	1.872871	234	1	0	-8.800377	0.428390	-2.617202
178	1	0	-8.656846	-4.967506	0.273044	235	1	0	-8.610905	-0.405252	-4.972082
179	1	0	-8.835263	-2.586302	-0.481007	236	1	0	-6.802818	-2.034151	-5.547897
180	1	0	-5.608060	-1.474012	1.914905	237	1	0	-2.152491	-3.958635	-6.771392
181	1	0	5.608436	-1.472808	1.916063	238	1	0	0.001262	-5.365057	-7.123292
182	1	0	8.835916	-2.584500	-0.479766	239	1	0	2.154702	-3.958238	-6.771056
183	1	0	8.657756	-4.965788	0.274089	240	1	0	2.313127	-5.797384	-2.073353
184	1	0	6.848182	-5.610627	1.873657	241	1	0	0.001051	-6.979786	-2.610277
185	1	0	-0.000300	-3.590641	9.324894	242	1	0	-2.311432	-5.797983	-2.073787
186	1	0	-0.000248	-5.528072	10.896664	243	6	0	-2.610570	1.437350	1.953184
187	1	0	0.000048	-7.848046	10.027075	244	6	0	-1.428362	1.761948	2.750228
188	1	0	0.000295	-8.274984	7.569719	245	6	0	-0.731460	0.747625	3.405694
189	1	0	-0.000145	8.275566	-7.569783	246	6	0	-1.181629	-0.637425	3.295911
190	1	0	0.000138	7.848800	-10.027169	247	6	0	-2.306649	-0.945159	2.534309
191	1	0	0.000400	5.528886	-10.896920	248	6	0	-3.042160	0.113843	1.851921
192	1	0	0.000377	3.591345	-9.325286	249	6	0	-0.696230	2.818774	2.057389
193	1	0	6.847079	5.612118	-1.872768	250	6	0	0.729977	0.747531	3.406006
194	1	0	8.656506	4.967657	-0.272877	251	6	0	-0.000853	-1.495156	3.232015
195	1	0	8.835072	2.586380	0.480925	252	6	0	-2.310698	-2.127291	1.677469
196	1	0	5.608345	1.473996	-1.915608	253	6	0	-3.496431	-0.410705	0.563789
197	1	0	-5.608446	1.472936	-1.916703	254	6	0	-2.604890	2.293539	0.768589
198	1	0	-8.835440	2.584550	0.479838	255	6	0	-1.183270	-2.949004	1.617880
199	1	0	-8.657250	4.965919	-0.273736	256	6	0	-0.000755	-2.627561	2.415660
200	1	0	-6.847836	5.610864	-1.873431	257	6	0	-0.731856	-3.470222	0.330795
201	1	0	-2.193946	6.901687	-3.803948	258	6	0	1.182048	-2.949158	1.618381
202	1	0	-0.000296	7.263880	-5.164024	259	6	0	0.695597	2.818673	2.057679
203	1	0	2.193101	6.901975	-3.803467	260	6	0	1.180006	-0.637578	3.296406
204	1	0	2.291630	2.209934	-5.663325	261	6	0	0.731122	-3.470322	0.331105
205	1	0	0.000191	2.773463	-6.840619	262	6	0	2.305298	-0.945454	2.535277
206	1	0	-2.291296	2.209548	-5.663620	263	6	0	1.427294	1.761759	2.750837
207	1	0	-2.313225	5.797298	2.074437	264	6	0	-3.042495	-1.796709	0.457691
208	1	0	-0.001092	6.979501	2.611656	265	6	0	-3.496110	0.411694	-0.565752
209	1	0	2.311460	5.797929	2.074824	266	6	0	1.425604	3.148721	0.834456
210	1	0	2.152536	3.957175	6.771874	267	6	0	-3.042047	1.797642	-0.459472
211	1	0	-0.001243	5.363429	7.124189	268	6	0	-1.425669	3.148929	0.833854
212	1	0	-2.154761	3.956836	6.771621	269	6	0	-3.041374	-0.112926	-1.853684
213	1	0	-6.804457	2.031640	5.546989	270	6	0	-2.309667	2.128098	-1.678926
214	1	0	-8.612069	0.402477	4.970467	271	6	0	-0.731243	3.470837	-0.331584
215	1	0	-8.801012	-0.430591	2.615348	272	6	0	2.309552	-2.127590	1.678448
216	1	0	-5.546719	1.893696	1.415653	273	6	0	-2.604883	-2.292674	-0.770186
						274	6	0	2.609806	1.437001	1.954299

275	6	0	-2.305418	0.945961	-2.535754
276	6	0	-1.182171	2.949672	-1.618861
277	6	0	0.731729	3.470737	-0.331275
278	6	0	1.183138	2.949514	-1.618359
279	6	0	2.604750	2.293185	0.769708
280	6	0	3.041250	0.113435	1.853206
281	6	0	3.495994	-0.411181	0.565274
282	6	0	0.000630	2.628071	-2.416142
283	6	0	0.000728	1.495664	-3.232495
284	6	0	1.181502	0.637932	-3.296389
285	6	0	-1.180131	0.638085	-3.296887
286	6	0	-1.425731	-3.148204	-0.834933
287	6	0	3.496299	0.411226	-0.564265
288	6	0	-2.609937	-1.436496	-1.954782
289	6	0	-1.427424	-1.761259	-2.751322
290	6	0	3.042356	1.797225	-0.458169
291	6	0	3.041927	-1.797127	0.458990
292	6	0	2.604782	-2.293030	-0.769078
293	6	0	2.310557	2.127794	-1.677943
294	6	0	2.306516	0.945666	-2.534785
295	6	0	-0.730100	-0.747026	-3.406485
296	6	0	0.731334	-0.747120	-3.406174
297	6	0	3.042036	-0.113328	-1.852396
298	6	0	-0.695722	-2.818162	-2.058159
299	6	0	1.425546	-3.148408	-0.834330
300	6	0	2.610456	-1.436842	-1.953668
301	6	0	0.696107	-2.818264	-2.057870
302	6	0	1.428242	-1.761446	-2.750711

3.4.6.2.2

The single point calculations were performed at DFT-M06-2X level of theory using basis-set 6-31G(d,p) for H, C, N, O atoms and Lanl2dz as basis-set for Pd atoms considering solvation effects by the Polarizable Continuum Model (PCM). As the input, the optimized geometry calculated at M06-2X/Lanl2dz level of theory was used.

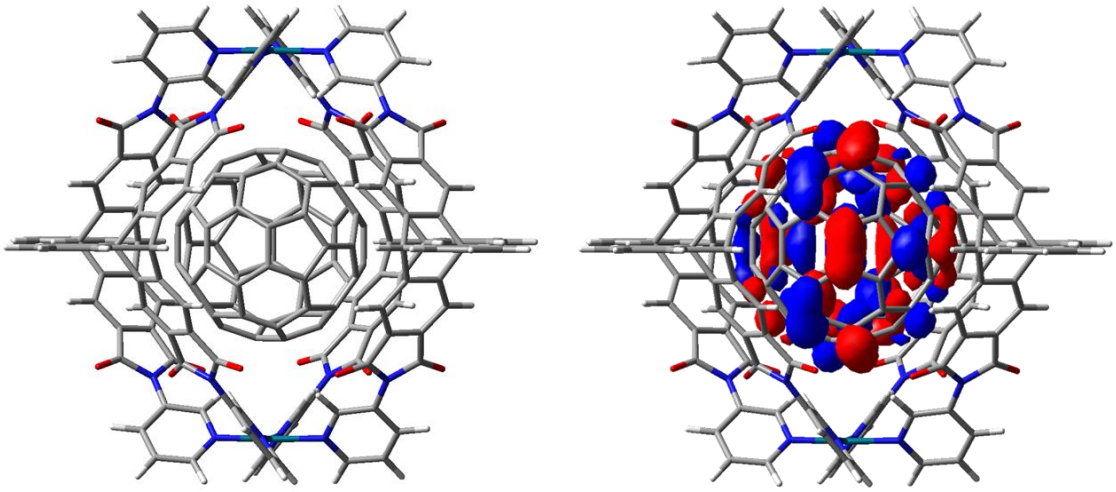

Figure 3.4.23 Geometry of $[C_{60}@Pd_2\mathbf{L}^{\mathbf{P}}_4]^{4+}$ (M06-2X/6-31G(d,p) for H, C, N, O atoms and Lanl2dz for Pd atoms) and visualization of the LUMO

3.4.6.2.3 $Pd_2L^P_4$

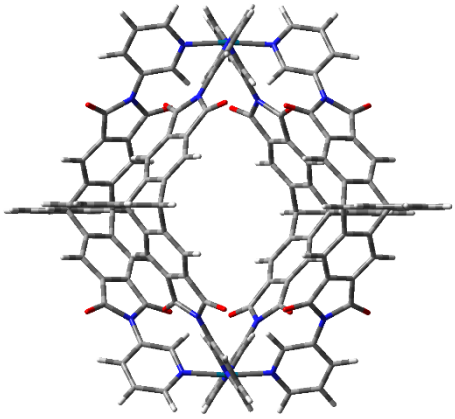

Figure 3.4.24 Gas-phase optimized geometry of $[Pd_2\mathbf{L}^P_4]^{4+}$ (M06-2X/Lanl2dz)

Standard orientation:

Center Number	Atomic Number	Atomic Type	X	Y	Z
1	6	0	3.236525	5.061884	3.323589
2	6	0	3.229923	3.760920	3.838018
3	6	0	2.227006	3.313730	4.699595
4	6	0	1.212447	4.225195	5.008248
5	6	0	0.000062	3.943742	5.897502
6	6	0	-1.212256	4.225274	5.008182
7	6	0	-2.226859	3.313875	4.699473
8	6	0	-3.229705	3.761134	3.837850
9	6	0	-3.236205	5.062104	3.323437
10	6	0	-2.236928	5.985485	3.633167
11	6	0	-1.213774	5.541943	4.478037
12	6	0	0.000166	6.362944	4.918069
13	6	0	1.214071	5.541860	4.478094
14	6	0	2.237288	5.985328	3.633260
15	6	0	4.390886	3.021272	3.284475
16	6	0	4.415670	5.218986	2.434971
17	6	0	-4.390690	3.021567	3.284247
18	6	0	0.000067	5.030754	6.979668
19	6	0	0.000126	6.334879	6.451572
20	6	0	-4.415299	5.219290	2.434765
21	7	0	-5.088923	3.945937	2.448341
22	7	0	5.089176	3.945579	2.448534
23	8	0	4.778200	6.196211	1.784501
24	8	0	4.711681	1.839003	3.459259
25	8	0	-4.777764	6.196579	1.784355
26	8	0	-4.711598	1.839328	3.459021
27	6	0	6.244869	3.645980	1.690043
28	6	0	-6.244660	3.646375	1.689902
29	6	0	7.165213	4.640178	1.302762
30	6	0	8.276864	4.272144	0.535497
31	6	0	8.463508	2.935699	0.174018
32	7	0	7.576506	1.987831	0.564081
33	6	0	6.487659	2.322094	1.297594
34	6	0	-6.487473	2.322480	1.297505
35	7	0	-7.576339	1.988205	0.564027
36	6	0	-8.463349	2.936067	0.173966
37	6	0	-8.276689	4.272520	0.535402
38	6	0	-7.165013	4.640571	1.302619
39	6	0	0.000019	4.821066	8.356990
40	6	0	0.000033	5.939243	9.213743
41	6	0	0.000092	7.238842	8.686997
42	6	0	0.000140	7.444831	7.293594
43	6	0	-0.000182	-7.444851	-7.292900
44	6	0	-0.000180	-7.238969	-8.686319
45	6	0	-0.000181	-5.939410	-9.213166
46	6	0	-0.000183	-4.821168	-8.356497
47	6	0	-7.164973	-4.639786	-1.301654
48	6	0	-8.276637	-4.271643	-0.534468
49	6	0	-8.463391	-2.935120	-0.173347
50	7	0	-7.576483	-1.987282	-0.563693
51	6	0	-6.487650	-2.321631	-1.297191
52	6	0	6.487441	-2.321820	-1.297082
53	7	0	7.576361	-1.987633	-0.563642
54	6	0	8.463223	-2.935587	-0.173472
55	6	0	8.276340	-4.272055	-0.534733
56	6	0	7.164597	-4.640019	-1.301896
57	6	0	-6.244744	-3.645609	-1.689278
58	6	0	6.244422	-3.645729	-1.689328
59	8	0	-4.711712	-1.838840	-3.458817
60	8	0	-4.777914	-6.195855	-1.783491
61	8	0	4.711389	-1.838861	-3.458906
62	8	0	4.777527	-6.195805	-1.783414
63	7	0	5.088681	-3.945295	-2.447762
64	7	0	-5.089075	-3.945294	-2.447775
65	6	0	-4.415541	-5.218693	-2.434147
66	6	0	-0.000186	-6.334836	-6.450961
67	6	0	-0.000186	-5.030753	-6.979159

68	6	0	-4.390875	-3.021075	-3.283886	126	6	0	-0.000156	-7.300625	7.436564
69	6	0	4.415076	-5.218642	-2.434022	127	6	0	0.000232	7.299270	-7.438462
70	6	0	4.390466	-3.021054	-3.283844	128	6	0	0.000246	8.692498	-7.231291
71	6	0	2.236831	-5.985095	-3.632498	129	6	0	0.000253	9.218140	-5.931244
72	6	0	1.213710	-5.541696	-4.477482	130	6	0	0.000247	8.360435	-4.813792
73	6	0	-0.000192	-6.362786	-4.917455	131	6	0	-7.164594	1.305199	-4.639280
74	6	0	-1.214104	-5.541702	-4.477498	132	6	0	-8.276064	0.537341	-4.271931
75	6	0	-2.237243	-5.985112	-3.632541	133	6	0	-8.462889	0.174955	-2.935755
76	6	0	-3.236466	-5.061654	-3.322868	134	7	0	-7.576187	0.564696	-1.987490
77	6	0	-3.229937	-3.760748	-3.837434	135	6	0	-6.487465	1.298709	-2.321102
78	6	0	-2.227105	-3.313619	-4.699141	136	6	0	6.487705	1.298419	-2.321050
79	6	0	-1.212537	-4.225081	-5.007763	137	7	0	7.576352	0.564286	-1.987450
80	6	0	-0.000190	-3.943662	-5.897079	138	6	0	8.462947	0.174364	-2.935740
81	6	0	1.212152	-4.225081	-5.007759	139	6	0	8.276081	0.536667	-4.271931
82	6	0	2.226723	-3.313620	-4.699139	140	6	0	7.164687	1.304636	-4.639272
83	6	0	3.229533	-3.760736	-3.837399	141	6	0	-6.244504	1.692132	-3.644678
84	6	0	3.236041	-5.061632	-3.322803	142	6	0	6.244712	1.691778	-3.644644
85	6	0	3.236218	-3.327796	5.058376	143	8	0	-4.711529	3.460272	-1.836143
86	6	0	3.229738	-3.840728	3.756824	144	8	0	-4.777782	1.789143	-6.194791
87	6	0	2.226844	-4.701811	3.308595	145	8	0	4.711877	3.460152	-1.836145
88	6	0	1.212208	-5.011505	4.219637	146	8	0	4.778031	1.788922	-6.194761
89	6	0	-0.000170	-5.900439	3.937104	147	7	0	5.089218	2.450923	-3.943543
90	6	0	-1.212530	-5.011488	4.219653	148	7	0	-5.088913	2.451127	-3.943561
91	6	0	-2.227169	-4.701770	3.308621	149	6	0	-4.415296	2.438697	-5.216945
92	6	0	-3.230053	-3.840685	3.756869	150	6	0	0.000225	6.456306	-6.329229
93	6	0	-3.236518	-3.327770	5.058427	151	6	0	0.000232	6.983293	-5.024655
94	6	0	-2.237251	-3.638556	5.981450	152	6	0	-4.390651	3.286326	-3.018523
95	6	0	-1.214073	-4.482884	5.536936	153	6	0	4.415646	2.438588	-5.216952
96	6	0	-0.000146	-4.923851	6.357447	154	6	0	4.391059	3.286266	-3.018550
97	6	0	1.213775	-4.482898	5.536919	155	6	0	2.237310	3.637623	-5.982186
98	6	0	2.236964	-3.638574	5.981416	156	6	0	1.214126	4.482098	-5.537957
99	6	0	4.390801	-3.286350	3.017934	157	6	0	0.000205	4.922825	-6.358616
100	6	0	4.415278	-2.439274	5.216578	158	6	0	-1.213727	4.482131	-5.537955
101	6	0	-4.391118	-3.286290	3.017995	159	6	0	-2.236936	3.637688	-5.982184
102	6	0	-0.000170	-6.983894	5.022850	160	6	0	-3.236187	3.327208	-5.059035
103	6	0	-0.000157	-6.457319	6.327589	161	6	0	-3.229660	3.840521	-3.757640
104	6	0	-4.415575	-2.439250	5.216654	162	6	0	-2.226776	4.701758	-3.309695
105	7	0	-5.089225	-2.451268	3.943294	163	6	0	-1.212156	5.011167	-4.220844
106	7	0	5.088969	-2.451390	3.943243	164	6	0	0.000221	5.900181	-3.938582
107	8	0	4.777765	-1.790030	6.194629	165	6	0	1.212576	5.011139	-4.220847
108	8	0	4.711772	-3.459905	1.835522	166	6	0	2.227195	4.701711	-3.309704
109	8	0	-4.777996	-1.789952	6.194694	167	6	0	3.230059	3.840454	-3.757655
110	8	0	-4.712037	-3.459736	1.835551	168	6	0	3.236561	3.327127	-5.059043
111	6	0	6.244556	-1.692297	3.644619	169	46	0	-7.691900	0.000476	0.000136
112	6	0	-6.244731	-1.692070	3.644631	170	46	0	7.692059	0.000105	0.000194
113	6	0	7.164736	-1.305826	4.639310	171	1	0	2.239843	2.306222	5.102299
114	6	0	8.276181	-0.537823	4.272190	172	1	0	0.000018	2.932892	6.309170
115	6	0	8.462906	-0.174912	2.936139	173	1	0	-2.239777	2.306364	5.102168
116	7	0	7.576130	-0.564248	1.987779	174	1	0	-2.258626	6.992765	3.229961
117	6	0	6.487387	-1.298314	2.321199	175	1	0	0.000212	7.374886	4.509928
118	6	0	-6.487465	-1.298076	2.321198	176	1	0	2.259071	6.992604	3.230049
119	7	0	-7.576122	-0.563909	1.987722	177	1	0	7.009441	5.674391	1.580412
120	6	0	-8.462912	-0.174488	2.936035	178	1	0	8.998330	5.016304	0.223199
121	6	0	-8.276290	-0.537415	4.272096	179	1	0	9.308536	2.614191	-0.421883
122	6	0	-7.164928	-1.305514	4.639276	180	1	0	5.820201	1.524314	1.590245
123	6	0	-0.000181	-8.360970	4.811562	181	1	0	-5.820000	1.524706	1.590153
124	6	0	-0.000181	-9.219023	5.928750	182	1	0	-9.308391	2.614547	-0.421909
125	6	0	-0.000169	-8.693787	7.228960	183	1	0	-8.998160	5.016675	0.223102

184	1	0	-7.009230	5.674791	1.580227	214	1	0	8.997461	-0.226072	5.016759
185	1	0	-0.000028	3.816466	8.768528	215	1	0	9.307817	0.421535	2.615336
186	1	0	-0.000002	5.795007	10.288256	216	1	0	5.820050	-1.590242	1.523059
187	1	0	0.000101	8.091096	9.357011	217	1	0	-5.820111	-1.590068	1.523093
188	1	0	0.000188	8.452139	6.889154	218	1	0	-9.307752	0.422033	2.615187
189	1	0	-0.000183	-8.452130	-6.888386	219	1	0	-8.997579	-0.225599	5.016629
190	1	0	-0.000177	-8.091274	-9.356267	220	1	0	-7.009271	-1.584331	5.673185
191	1	0	-0.000179	-5.795254	-10.287689	221	1	0	-0.000191	-8.771350	3.806489
192	1	0	-0.000182	-3.816599	-8.768110	222	1	0	-0.000190	-10.293367	5.783264
193	1	0	-7.009120	-5.674063	-1.579004	223	1	0	-0.000169	-9.364785	8.080439
194	1	0	-8.998033	-5.015783	-0.221961	224	1	0	-0.000145	-6.897350	8.444339
195	1	0	-9.308432	-2.613528	0.422490	225	1	0	0.000226	6.895686	-8.446114
196	1	0	-5.820314	-1.523855	-1.590135	226	1	0	0.000251	9.363231	-8.082978
197	1	0	5.820128	-1.523964	-1.589851	227	1	0	0.000264	10.292530	-5.786092
198	1	0	9.308336	-2.614126	0.422334	228	1	0	0.000252	8.771123	-3.808843
199	1	0	8.997697	-5.016286	-0.222355	229	1	0	-7.008779	1.583563	-5.673287
200	1	0	7.008635	-5.674251	-1.579374	230	1	0	-8.997287	0.225302	-5.016434
201	1	0	2.258548	-6.992327	-3.229173	231	1	0	-9.307807	-0.421381	-2.614774
202	1	0	-0.000192	-7.374699	-4.509244	232	1	0	-5.820270	1.591057	-1.523002
203	1	0	-2.258972	-6.992349	-3.229231	233	1	0	5.820605	1.590914	-1.522927
204	1	0	-2.239989	-2.306145	-5.101930	234	1	0	9.307815	-0.422048	-2.614765
205	1	0	-0.000188	-2.932842	-6.308824	235	1	0	8.997214	0.224476	-5.016458
206	1	0	2.239621	-2.306154	-5.101948	236	1	0	7.008842	1.582930	-5.673293
207	1	0	2.239752	-5.103387	2.300637	237	1	0	2.259028	3.235234	-6.989792
208	1	0	-0.000179	-6.310936	2.925777	238	1	0	0.000199	4.515575	-7.370915
209	1	0	-2.240088	-5.103335	2.300658	239	1	0	-2.258672	3.235307	-6.989792
210	1	0	-2.258953	-3.236479	6.989180	240	1	0	-2.239656	5.103618	-2.301848
211	1	0	-0.000134	-4.516915	7.369872	241	1	0	0.000226	6.310993	-2.927382
212	1	0	2.258682	-3.236490	6.989143	242	1	0	2.240094	5.103581	-2.301862
213	1	0	7.009002	-1.584638	5.673210	----------					

3.4.6.2.4 VOIDOO calculations

The size of inner cavity was calculated with VOIDOO using the optimized geometry for $Pd_2\mathbf{L^P}_4$ calculated at M06-2X/Lanl2dz using a primary grid and plot grid spacing of 0.1 Å and 10 cycles of volume refinement with the probe size radius of 3.0 Å, the minimum radius such that it would not exit the cavity of the structures. Molecular visualization was done using Pymol.[15]

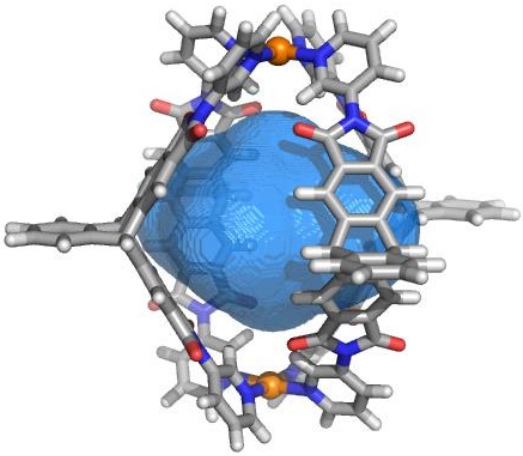

Figure 3.4.25 Calculated void space as shown (blue mesh) within $Pd_2\mathbf{L}^{\mathbf{P}}_4$ (651 $Å^3$). Color scheme: C, dark gray; N, blue; O, red; Pd, orange.

3.4.6.2.5 $C_{60}^{\bullet-}$@$Pd_2L^P_4$

At first, geometry optimization was performed at UB3LYP/Lanl2dz level of theory. Subsequently, a single point calculation was performed with SCRF (PCM=acetonitrile) at UB3LYP/6-31G(d,p) for H, C, N, O atoms and Lanl2dz for Pd atom.

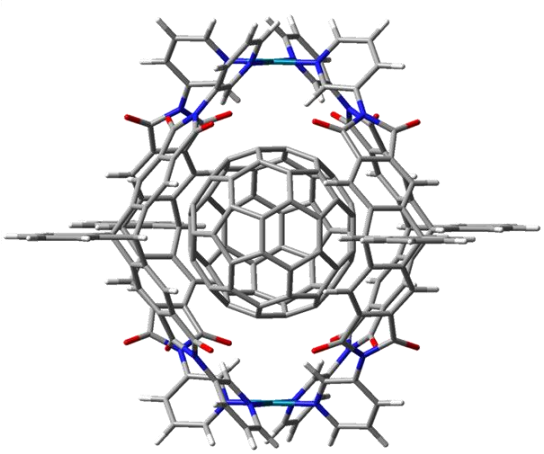

Figure 3.4.26 The gas-phase optimized geometry of $[C_{60}^{\bullet-}@Pd_2\mathbf{L}^{\mathbf{P}}_4]^{3+}$ (UB3LYP/Lanl2dz)

Standard orientation:

Center Number	Atomic Number	Atomic Type	Coordinates (Angstroms) X	Y	Z
1	6	0	3.261741	-0.019479	6.492130
2	6	0	3.273940	-1.266191	5.839412
3	6	0	2.264353	-2.215718	6.053786

4	6	0	1.225420	-1.859235	6.929153
5	6	0	-0.002809	-2.718035	7.275058
6	6	0	-1.227929	-1.854600	6.929669
7	6	0	-2.268580	-2.207158	6.054751
8	6	0	-3.274679	-1.253832	5.840831
9	6	0	-3.257489	-0.007180	6.493547
10	6	0	-2.242050	0.342857	7.392404
11	6	0	-1.220102	-0.596953	7.596958
12	6	0	0.001813	-0.410673	8.508019
13	6	0	1.222639	-0.601574	7.596455
14	6	0	2.248033	0.334378	7.391446
15	6	0	4.435874	-1.310348	4.913989
16	6	0	4.410759	0.789862	6.015935
17	6	0	-4.437192	-1.293609	4.915934
18	6	0	-0.002744	-2.855313	8.809571
19	6	0	-0.000256	-1.609197	9.474946
20	6	0	-4.403656	0.806492	6.017863
21	7	0	-5.076601	-0.006282	5.026666
22	7	0	5.080098	-0.025393	5.024335
23	8	0	4.759993	1.933185	6.342238
24	8	0	4.825283	-2.224682	4.168593
25	8	0	-4.748496	1.951078	6.344408
26	8	0	-4.830374	-2.206479	4.170721
27	6	0	6.143569	0.431343	4.204404
28	6	0	-6.138868	0.454427	4.207392
29	6	0	7.110504	1.336842	4.692333
30	6	0	8.107957	1.800666	3.819538
31	6	0	8.124009	1.372384	2.488516
32	7	0	7.185853	0.497550	2.020021
33	6	0	6.220507	0.024088	2.854175
34	6	0	-6.218270	0.047388	2.857238
35	7	0	-7.182272	0.524612	2.023662
36	6	0	-8.116660	1.403172	2.492707
37	6	0	-8.098116	1.831417	3.823708
38	6	0	-7.101958	1.363703	4.695899
39	6	0	-0.004853	-4.051115	9.535002
40	6	0	-0.004455	-3.993396	10.946913
41	6	0	-0.001973	-2.751678	11.609838
42	6	0	0.000149	-1.546437	10.872156
43	6	0	0.000385	1.548753	-10.872045
44	6	0	0.002383	2.754212	-11.609370
45	6	0	0.004862	3.995734	-10.946080
46	6	0	0.005381	4.053037	-9.534152
47	6	0	-7.109136	-1.336976	-4.692634
48	6	0	-8.106594	-1.801121	-3.820022
49	6	0	-8.122938	-1.372950	-2.488969
50	7	0	-7.185084	-0.497902	-2.020275
51	6	0	-6.219735	-0.024116	-2.854256
52	6	0	6.218806	-0.047349	-2.857509
53	7	0	7.182562	-0.524977	-2.023883
54	6	0	8.116749	-1.403759	-2.492910
55	6	0	8.098239	-1.831836	-3.823965
56	6	0	7.102326	-1.363719	-4.696217
57	6	0	-6.142489	-0.431282	-4.204497
58	6	0	6.139439	-0.454219	-4.207719
59	8	0	-4.824258	2.224794	-4.167923
60	8	0	-4.758796	-1.932501	-6.342667
61	8	0	4.831349	2.206902	-4.170673
62	8	0	4.749162	-1.950179	-6.345263
63	7	0	5.077394	0.006858	-5.027071
64	7	0	-5.078997	0.025720	-5.024253
65	6	0	-4.409568	-0.789280	-6.016002
66	6	0	0.000910	1.611100	-9.474817
67	6	0	0.003394	2.857020	-8.809074
68	6	0	-4.434827	1.310676	-4.913574
69	6	0	4.404459	-0.805606	-6.018528
70	6	0	4.438186	1.294273	-4.916190
71	6	0	2.242893	-0.341531	-7.392960
72	6	0	1.220947	0.598343	-7.597220
73	6	0	-0.001025	0.412291	-8.508245
74	6	0	-1.221769	0.602862	-7.596509
75	6	0	-2.247070	-0.333220	-7.391655
76	6	0	-3.260696	0.020305	-6.492122
77	6	0	-3.272930	1.266836	-5.839061
78	6	0	-2.263417	2.216487	-6.053254
79	6	0	-1.224548	1.860323	-6.928830
80	6	0	0.003607	2.719289	-7.274603
81	6	0	1.228799	1.855804	-6.929581
82	6	0	2.269510	2.208137	-6.054643
83	6	0	3.275613	1.254746	-5.841024
84	6	0	3.258359	0.008251	-6.494039
85	6	0	3.233516	-6.498718	-0.011955
86	6	0	3.253879	-5.864667	-1.268233
87	6	0	2.252244	-6.097910	-2.222152
88	6	0	1.210666	-6.968277	-1.859453
89	6	0	-0.017516	-7.324569	-2.716133
90	6	0	-1.244740	-6.965086	-1.859434
91	6	0	-2.283971	-6.091917	-2.222087
92	6	0	-3.284651	-5.855593	-1.267938
93	6	0	-3.265812	-6.489477	-0.011551
94	6	0	-2.255003	-7.389329	0.348099
95	6	0	-1.237660	-7.613600	-0.591876
96	6	0	-0.019061	-8.525633	-0.392169
97	6	0	1.201971	-7.616877	-0.591948
98	6	0	2.220120	-7.395589	0.347857
99	6	0	4.412931	-4.934057	-1.314419
100	6	0	4.375219	-6.009505	0.799509
101	6	0	-4.440673	-4.921236	-1.313795
102	6	0	-0.019540	-8.860642	-2.832392
103	6	0	-0.020403	-9.508617	-1.577181
104	6	0	-4.405518	-5.996323	0.800342
105	7	0	-5.074239	-5.011715	-0.022440
106	7	0	5.047470	-5.027708	-0.023753
107	8	0	4.719360	-6.322001	1.948163
108	8	0	4.806978	-4.198105	-2.234483
109	8	0	-4.749743	-6.306919	1.949487
110	8	0	-4.832382	-4.183728	-2.233609
111	6	0	6.113917	-4.210491	0.429455
112	6	0	-6.136075	-4.189104	0.431782
113	6	0	7.091238	-4.711943	1.316056
114	6	0	8.097898	-3.849023	1.777724
115	6	0	8.114727	-2.514562	1.360972
116	7	0	7.166682	-2.032646	0.504645
117	6	0	6.186516	-2.855100	0.039488
118	6	0	-6.201841	-2.833353	0.041906
119	7	0	-7.177013	-2.005631	0.508169

120	6	0	-8.126737	-2.482471	1.365476	178	1	0	8.865860	2.494563	4.166049
121	6	0	-8.116650	-3.817037	1.782147	179	1	0	8.869910	1.724369	1.787129
122	6	0	-7.115106	-4.685344	1.319431	180	1	0	5.516516	-0.684396	2.445490
123	6	0	-0.020544	-9.602618	-4.018026	181	1	0	-5.517288	-0.663844	2.448163
124	6	0	-0.022431	-11.013580	-3.940710	182	1	0	-8.861585	1.758092	1.791761
125	6	0	-0.023289	-11.659201	-2.689904	183	1	0	-8.853059	2.528315	4.170658
126	6	0	-0.022270	-10.904846	-1.495032	184	1	0	-7.063804	1.704294	5.722995
127	6	0	0.021847	10.904069	1.496005	185	1	0	-0.006781	-5.012627	9.027297
128	6	0	0.023238	11.658197	2.691020	186	1	0	-0.006078	-4.913276	11.525131
129	6	0	0.022382	11.012336	3.941702	187	1	0	-0.001686	-2.719807	12.695841
130	6	0	0.020122	9.601360	4.018750	188	1	0	0.002064	-0.589696	11.388618
131	6	0	-7.092674	4.711546	-1.316088	189	1	0	-0.001532	0.592165	-11.388788
132	6	0	-8.098977	3.848285	-1.777901	190	1	0	0.002000	2.722661	-12.695383
133	6	0	-8.115373	2.513790	-1.361225	191	1	0	0.006389	4.915785	-11.524026
134	7	0	-7.167252	2.032184	-0.504807	192	1	0	0.007309	5.014399	-9.026163
135	6	0	-6.187450	2.854967	-0.039497	193	1	0	-7.072743	-1.677567	-5.719793
136	6	0	6.200873	2.832449	-0.042371	194	1	0	-8.864276	-2.495178	-4.166697
137	7	0	7.176494	2.005150	-0.508434	195	1	0	-8.868857	-1.725169	-1.787719
138	6	0	8.126176	2.482384	-1.365567	196	1	0	-5.516050	0.684631	-2.445484
139	6	0	8.115617	3.816949	-1.782228	197	1	0	5.518017	0.664086	-2.448423
140	6	0	7.113638	4.684840	-1.319678	198	1	0	8.861490	-1.758972	-1.791919
141	6	0	-6.115271	4.210387	-0.429405	199	1	0	8.853021	-2.528910	-4.170912
142	6	0	6.134633	4.188175	-0.432236	200	1	0	7.064197	-1.704175	-5.723358
143	8	0	-4.808551	4.197826	2.234547	201	1	0	2.247886	-1.305536	-7.893182
144	8	0	-4.721019	6.322495	-1.947717	202	1	0	-0.002959	-0.551279	-9.023299
145	8	0	4.830373	4.181728	2.232824	203	1	0	-2.255942	-1.297185	-7.891902
146	8	0	4.747995	6.305975	-1.949750	204	1	0	-2.279852	3.173706	-5.540888
147	7	0	5.072444	5.010358	0.021921	205	1	0	0.005543	3.683184	-6.760015
148	7	0	-5.049098	5.027846	0.023984	206	1	0	2.289797	3.165292	-5.542298
149	6	0	-4.376902	6.009835	-0.799100	207	1	0	2.274478	-5.600084	-3.186928
150	6	0	0.019612	9.507826	1.577888	208	1	0	-0.016873	-6.823557	-3.687301
151	6	0	0.018750	8.859610	2.832975	209	1	0	-2.304910	-5.594055	-3.186872
152	6	0	-4.414618	4.934063	1.314662	210	1	0	-2.259209	-7.873987	1.319988
153	6	0	4.403619	5.994985	-0.800757	211	1	0	-0.019701	-9.026856	0.578645
154	6	0	4.438690	4.919424	1.313149	212	1	0	2.223221	-7.880494	1.319626
155	6	0	2.253409	7.388321	-0.348066	213	1	0	7.056446	-5.743626	1.643231
156	6	0	1.236227	7.612662	0.592065	214	1	0	8.863146	-4.205986	2.458104
157	6	0	0.017852	8.525069	0.392690	215	1	0	8.869602	-1.820011	1.707610
158	6	0	-1.203386	7.616586	0.592448	216	1	0	5.469068	-2.435517	-0.649799
159	6	0	-2.221663	7.395661	-0.347304	217	1	0	-5.482826	-2.417584	-0.648061
160	6	0	-3.235150	6.498854	0.012412	218	1	0	-8.877447	-1.783861	1.713002
161	6	0	-3.255499	5.864575	1.268576	219	1	0	-8.883061	-4.169894	2.463359
162	6	0	-2.253771	6.097496	2.222465	220	1	0	-7.085460	-5.717188	1.646603
163	6	0	-1.212085	6.967752	1.859833	221	1	0	-0.019891	-9.108312	-4.986498
164	6	0	0.016283	7.323559	2.716425	222	1	0	-0.023224	-11.604506	-4.852476
165	6	0	1.243267	6.963867	1.859481	223	1	0	-0.024739	-12.744654	-2.642951
166	6	0	2.282264	6.090292	2.221815	224	1	0	-0.022931	-11.407967	-0.531208
167	6	0	3.282811	5.853960	1.267533	225	1	0	0.022511	11.407375	0.532276
168	6	0	3.264033	6.488147	0.011299	226	1	0	0.024978	12.743658	2.644274
169	46	0	-7.172392	0.013284	0.001697	227	1	0	0.023462	11.603088	4.853582
170	46	0	7.172646	-0.013739	-0.001921	228	1	0	0.019466	9.106869	4.987128
171	1	0	2.280773	-3.173082	5.541693	229	1	0	-7.058208	5.743253	-1.643219
172	1	0	-0.004740	-3.682083	6.760757	230	1	0	-8.864272	4.205006	-2.458355
173	1	0	-2.288841	-3.164454	5.542667	231	1	0	-8.869946	1.818977	-1.707994
174	1	0	-2.247091	1.306981	7.892396	232	1	0	-5.469916	2.435606	0.649837
175	1	0	0.003743	0.553048	9.022789	233	1	0	5.481904	2.416382	0.647465
176	1	0	2.256924	1.298480	7.891426	234	1	0	8.877254	1.784091	-1.712936
177	1	0	7.074346	1.677514	5.719474	235	1	0	8.882020	4.170132	-2.463281

236	1	0	7.083649	5.716683	-1.646818	270	6	0	2.313740	-0.026402	-2.724313
237	1	0	2.257663	7.873217	-1.319835	271	6	0	0.726641	-1.921198	-2.940748
238	1	0	0.018504	9.026478	-0.578029	272	6	0	-2.313081	0.026452	2.724288
239	1	0	-2.224742	7.880712	-1.319001	273	6	0	2.607018	2.036500	1.312462
240	1	0	-2.275980	5.599460	3.187133	274	6	0	-2.615579	-2.434054	0.096034
241	1	0	0.015628	6.822360	3.687497	275	6	0	2.310968	1.381371	-2.327926
242	1	0	2.303184	5.592231	3.186499	276	6	0	1.178286	-0.589397	-3.336862
243	6	0	2.607212	-2.443874	0.094045	277	6	0	-0.735407	-1.918454	-2.940187
244	6	0	1.431797	-3.259358	0.337577	278	6	0	-1.182368	-0.584968	-3.335960
245	6	0	0.720873	-3.139773	1.552615	279	6	0	-2.606341	-2.036444	-1.312488
246	6	0	1.174428	-2.180703	2.564262	280	6	0	-3.051132	-1.508427	1.075182
247	6	0	2.307554	-1.389986	2.326146	281	6	0	-3.494710	-0.183432	0.681899
248	6	0	3.046960	-1.519872	1.072869	282	6	0	-0.000591	0.235799	-3.581272
249	6	0	0.693725	-3.374893	-0.922294	283	6	0	0.002090	1.594004	-3.201286
250	6	0	-0.730775	-3.137049	1.553172	284	6	0	-1.173772	2.180752	-2.564284
251	6	0	-0.001431	-1.593953	3.201267	285	6	0	1.180629	2.176333	-2.565168
252	6	0	2.315889	0.017772	2.722520	286	6	0	1.434467	2.629444	1.949496
253	6	0	3.495193	-0.196543	0.679242	287	6	0	-3.494535	0.196581	-0.679269
254	6	0	2.598382	-2.046228	-1.314476	288	6	0	2.616261	2.434108	-0.096063
255	6	0	1.183025	0.585021	3.335928	289	6	0	1.443733	3.254009	-0.338695
256	6	0	0.001249	-0.235746	3.581244	290	6	0	-3.038784	-0.758886	-1.694601
257	6	0	0.736066	1.918506	2.940154	291	6	0	-3.034646	0.770328	1.696897
258	6	0	-1.177627	0.589450	3.336834	292	6	0	-2.597737	2.046277	1.314451
259	6	0	-0.706388	-3.372261	-0.921758	293	6	0	-2.315236	-0.017720	-2.722553
260	6	0	-1.179968	-2.176285	2.565151	294	6	0	-2.306907	1.390039	-2.326177
261	6	0	-0.725982	1.921250	2.940717	295	6	0	0.731438	3.137097	-1.553192
262	6	0	-2.310303	-1.381322	2.327904	296	6	0	-0.720214	3.139820	-1.552636
263	6	0	-1.443060	-3.253953	0.338671	297	6	0	-3.046329	1.519924	-1.072903
264	6	0	3.039452	0.758935	1.694574	298	6	0	0.707053	3.372320	0.921732
265	6	0	3.495382	0.183467	-0.681929	299	6	0	-1.422473	2.634807	1.950587
266	6	0	-1.433800	-2.629388	-1.949524	300	6	0	-2.606569	2.443924	-0.094074
267	6	0	3.035292	-0.770284	-1.696918	301	6	0	-0.693067	3.374945	0.922268
268	6	0	1.423125	-2.634758	-1.950616	302	6	0	-1.431145	3.259407	-0.337602
269	6	0	3.051821	1.508478	-1.075214	---					

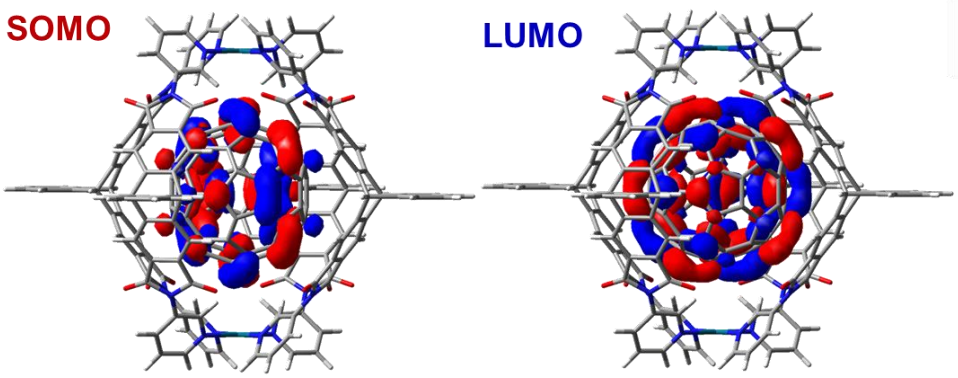

Figure 3.4.27 SOMO and LUMO of $[C_{60}^{\bullet-}@Pd_2\mathbf{L}^{\mathbf{P}}_4]^{3+}$ (UB3LYP/6-31G(d,p) for H, C, N, O atoms and Lanl2dz for Pd atom)

3.4.6.2.6 DFT-computed energies of host-guest complex formation with C_{60} and $C_{60}^{\bullet-}$

To gain information on the stabilization effect of $C_{60}^{-\bullet}$ inside the cage, DFT calculations were performed to estimate the energy changes by comparing the total electron energy difference for host-guest complex formation with C_{60} and $C_{60}^{\bullet-}$. First, the geometries of the host-guest complexes were optimized at B3LYP/Lanl2dz level. Then, each geometry of the guest and the host were extracted and single point calculations were conducted at B3LYP level of theory using basis-set 6-31G(d, p) for H, C, N, O atoms and Lanl2dz as basis-set for Pd atoms for the extracted geometries. As a result, the encapsulation of $C_{60}^{\bullet-}$@$Pd_2\mathbf{L}^{\mathbf{P}}_4$ was found to be significantly favored over the formation of C_{60}@$Pd_2\mathbf{L}^{\mathbf{P}}_4$ by 670 kJ/mol, a value that would certainly be lower in polar solution containing counter anions but still indicates strong interaction between the cationic host and anionic guest.

	Guest (Hartree)	Host (Hartree)	Host-Guest (Hartree)	ΔE(Hartree)	ΔE(kJ/mol)
C_{60}@$Pd_2\mathbf{L}^{\mathbf{P}}_4$	-2286.169553	-7558.295752	-9844.409798	0.05507	145.7
$C_{60}^{\bullet-}$@$Pd_2\mathbf{L}^{\mathbf{P}}_4$	-2286.245479	-7558.295430	-9844.741141	-0.20023	-525.7

Table 3.4.6.1 The summary of energy comparisons in gas-phase before and after encapsulation for $C_{60}^{\bullet-}$ and C_{60}

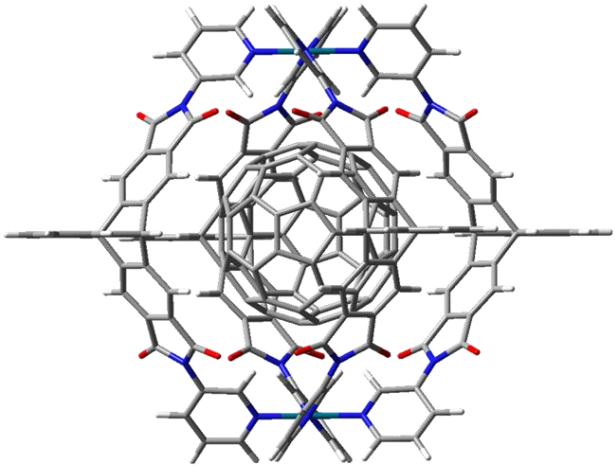

Figure 3.4.28 The gas-phase optimized geometry of $[C_{60}@Pd\mathbf{L}^{P}_{4}]^{4+}$(B3LYP/Lanl2dz)

Standard orientation:

Center Number	Atomic Number	Atomic Type	Coordinates (Angstroms) X	Y	Z
1	6	0	-3.275413	-2.878915	5.784974
2	6	0	-3.281422	-1.471512	5.764421
3	6	0	-2.267459	-0.725949	6.384654
4	6	0	-1.226292	-1.442811	6.997960
5	6	0	0.000089	-0.836877	7.700765
6	6	0	1.226505	-1.442768	6.997985
7	6	0	2.267654	-0.725871	6.384690
8	6	0	3.281657	-1.471402	5.764484
9	6	0	3.275709	-2.878804	5.785058
10	6	0	2.258430	-3.604871	6.418725
11	6	0	1.223432	-2.867149	7.016342
12	6	0	0.000133	-3.453573	7.736771
13	6	0	-1.223167	-2.867191	7.016309
14	6	0	-2.258121	-3.604947	6.418659
15	6	0	-4.437843	-1.008899	4.953034
16	6	0	-4.436168	-3.380172	5.006663
17	6	0	4.438058	-1.008752	4.953089
18	6	0	0.000083	-1.419952	9.127827
19	6	0	0.000105	-2.831991	9.146899
20	6	0	4.436500	-3.380022	5.006777
21	7	0	5.104552	-2.197741	4.493595
22	7	0	-5.104321	-2.197908	4.493573
23	8	0	-4.793692	-4.543028	4.779519
24	8	0	-4.789108	0.148161	4.660969
25	8	0	4.794046	-4.542867	4.779612
26	8	0	4.789226	0.148319	4.660949
27	6	0	-6.192538	-2.234119	3.581455
28	6	0	6.192709	-2.233936	3.581404
29	6	0	-7.176072	-3.245383	3.654092
30	6	0	-8.197831	-3.269389	2.691359
31	6	0	-8.221845	-2.308511	1.674346
32	7	0	-7.270160	-1.331737	1.607624
33	6	0	-6.282464	-1.281000	2.544071
34	6	0	6.282569	-1.280838	2.543993
35	7	0	7.270225	-1.331568	1.607507
36	6	0	8.221937	-2.308316	1.674204
37	6	0	8.197987	-3.269179	2.691234
38	6	0	7.176270	-3.245179	3.654012
39	6	0	0.000058	-0.689676	10.320715
40	6	0	0.000057	-1.389846	11.548116
41	6	0	0.000080	-2.797443	11.566966
42	6	0	0.000105	-3.530225	10.358800
43	6	0	-0.000164	3.529702	-10.358994
44	6	0	-0.000188	2.796829	-11.567103
45	6	0	-0.000173	1.389233	-11.548147
46	6	0	-0.000132	0.689157	-10.320692
47	6	0	7.176100	3.245306	-3.654206
48	6	0	8.197833	3.269349	-2.691445
49	6	0	8.221812	2.308518	-1.674385
50	7	0	7.270114	1.331757	-1.607642
51	6	0	6.282441	1.280993	-2.544105
52	6	0	-6.282512	1.280861	-2.543984
53	7	0	-7.270194	1.331594	-1.607527
54	6	0	-8.221921	2.308328	-1.674279
55	6	0	-8.197962	3.269156	-2.691343
56	6	0	-7.176221	3.245140	-3.654097
57	6	0	6.192550	2.234058	-3.581541
58	6	0	-6.192642	2.233923	-3.581420
59	8	0	4.789111	-0.148281	-4.660885
60	8	0	4.793786	4.542896	-4.779851
61	8	0	-4.789105	-0.148385	-4.660697
62	8	0	-4.793923	4.542792	-4.779733
63	7	0	-5.104450	2.197683	-4.493567
64	7	0	5.104369	2.197794	-4.493698
65	6	0	4.436230	3.380029	-5.006881
66	6	0	-0.000124	2.831561	-9.147039
67	6	0	-0.000106	1.419524	-9.127860

68	6	0	4.437892	1.008758	-4.953084	126	6	0	-0.000114	10.381254	3.553878
69	6	0	-4.436336	3.379931	-5.006750	127	6	0	0.000074	-10.381111	-3.553587
70	6	0	-4.437928	1.008661	-4.952926	128	6	0	0.000081	-11.596813	-2.833400
71	6	0	-2.258343	3.604662	-6.418840	129	6	0	0.000086	-11.592592	-1.425664
72	6	0	-1.223370	2.866891	-7.016439	130	6	0	0.000085	-10.372581	-0.712750
73	6	0	-0.000094	3.453253	-7.736960	131	6	0	7.161777	-3.675015	-3.215841
74	6	0	1.223231	2.866919	-7.016500	132	6	0	8.187271	-2.716954	-3.246562
75	6	0	2.258205	3.604713	-6.418931	133	6	0	8.210799	-1.691194	-2.295271
76	6	0	3.275491	2.878723	-5.785188	134	7	0	7.254493	-1.609542	-1.324550
77	6	0	3.281485	1.471321	-5.764519	135	6	0	6.258252	-2.537889	-1.270703
78	6	0	2.267511	0.725718	-6.384683	136	6	0	-6.258220	-2.538018	-1.270607
79	6	0	1.226343	1.442541	-6.998035	137	7	0	-7.254482	-1.609695	-1.324438
80	6	0	-0.000062	0.836560	-7.700751	138	6	0	-8.210791	-1.691361	-2.295157
81	6	0	-1.226447	1.442512	-6.997972	139	6	0	-8.187244	-2.717111	-3.246457
82	6	0	-2.267571	0.725665	-6.384575	140	6	0	-7.161724	-3.675145	-3.215754
83	6	0	-3.281547	1.471247	-5.764386	141	6	0	6.172579	-3.586880	-2.211281
84	6	0	-3.275594	2.878648	-5.785067	142	6	0	-6.172522	-3.586991	-2.211201
85	6	0	-3.262597	5.795514	2.860415	143	8	0	4.788130	-4.700117	0.171431
86	6	0	-3.275988	5.794366	1.452881	144	8	0	4.763400	-4.758640	-4.520609
87	6	0	-2.269698	6.433108	0.711863	145	8	0	-4.788030	-4.700222	0.171488
88	6	0	-1.227468	7.041863	1.432092	146	8	0	-4.763315	-4.758671	-4.520551
89	6	0	-0.000102	7.751558	0.833151	147	7	0	-5.084116	-4.498722	-2.174403
90	6	0	1.227283	7.041889	1.432082	148	7	0	5.084200	-4.498642	-2.174466
91	6	0	2.269523	6.433164	0.711840	149	6	0	4.414151	-5.002278	-3.358506
92	6	0	3.275833	5.794440	1.452847	150	6	0	0.000072	-9.176533	-2.842725
93	6	0	3.262447	5.795570	2.860381	151	6	0	0.000078	-9.172148	-1.430630
94	6	0	2.248104	6.428720	3.590662	152	6	0	4.429840	-4.978774	-0.986394
95	6	0	1.221103	7.043495	2.856846	153	6	0	-4.414058	-5.002322	-3.358453
96	6	0	-0.000090	7.760702	3.450108	154	6	0	-4.429736	-4.978849	-0.986341
97	6	0	-1.221275	7.043475	2.856856	155	6	0	-2.248162	-6.428626	-3.590563
98	6	0	-2.248262	6.428689	3.590684	156	6	0	-1.221134	-7.043322	-2.856717
99	6	0	-4.429635	4.978684	0.986424	157	6	0	0.000061	-7.760552	-3.449945
100	6	0	-4.414019	5.002184	3.358536	158	6	0	1.221255	-7.043310	-2.856729
101	6	0	4.429501	4.978794	0.986375	159	6	0	2.248273	-6.428613	-3.590586
102	6	0	-0.000113	9.172394	1.430862	160	6	0	3.262670	-5.795501	-2.860346
103	6	0	-0.000106	9.176710	2.842957	161	6	0	3.276079	-5.794316	-1.452812
104	6	0	4.413886	5.002252	3.358486	162	6	0	2.269726	-6.432925	-0.711764
105	7	0	5.083929	4.498684	2.174418	163	6	0	1.227449	-7.041634	-1.431965
106	7	0	-5.084059	4.498590	2.174476	164	6	0	0.000075	-7.751283	-0.832989
107	8	0	-4.763320	4.758564	4.520628	165	6	0	-1.227312	-7.041646	-1.431953
108	8	0	-4.787946	4.700117	-0.171415	166	6	0	-2.269589	-6.432950	-0.711740
109	8	0	4.763199	4.758622	4.520573	167	6	0	-3.275960	-5.794359	-1.452776
110	8	0	4.787832	4.700274	-0.171469	168	6	0	-3.262562	-5.795532	-2.860310
111	6	0	-6.172477	3.586873	2.211273	169	46	0	7.264907	0.000097	-0.000063
112	6	0	6.172373	3.586996	2.211195	170	46	0	-7.264956	-0.000062	0.000058
113	6	0	-7.161655	3.675030	3.215849	171	1	0	-2.287643	0.359943	6.375321
114	6	0	-8.187178	2.717001	3.246578	172	1	0	0.000071	0.255884	7.688669
115	6	0	-8.210751	1.691248	2.295284	173	1	0	2.287797	0.360022	6.375350
116	7	0	-7.254460	1.609572	1.324546	174	1	0	2.273804	-4.690842	6.433329
117	6	0	-6.258193	2.537887	1.270690	175	1	0	0.000151	-4.545937	7.752381
118	6	0	6.258087	2.538012	1.270608	176	1	0	-2.273452	-4.690919	6.433250
119	7	0	7.254385	1.609727	1.324430	177	1	0	-7.137375	-3.996011	4.433833
120	6	0	8.210705	1.691430	2.295137	178	1	0	-8.970029	-4.030068	2.724947
121	6	0	8.187133	2.717183	3.246431	179	1	0	-8.987563	-2.311938	0.908694
122	6	0	7.161581	3.675183	3.215737	180	1	0	-5.574598	-0.470284	2.471177
123	6	0	-0.000129	10.372862	0.713041	181	1	0	5.574687	-0.470137	2.471084
124	6	0	-0.000137	11.592837	1.426013	182	1	0	8.987618	-2.311741	0.908516
125	6	0	-0.000130	11.596990	2.833749	183	1	0	8.970204	-4.029839	2.724801

184	1	0	7.137628	-3.995791	4.433772	242	1	0	-2.293202	-6.436009	0.374137
185	1	0	0.000040	0.397545	10.312575	243	6	0	-2.609953	2.128189	1.173337
186	1	0	0.000038	-0.838694	12.484213	244	6	0	-1.430693	2.759436	1.762791
187	1	0	0.000079	-3.323899	12.517108	245	6	0	-0.731511	2.110003	2.790805
188	1	0	0.000123	-4.617126	10.379618	246	6	0	-1.181833	0.805354	3.273228
189	1	0	-0.000177	4.616602	-10.379895	247	6	0	-2.312204	0.201728	2.706285
190	1	0	-0.000220	3.323212	-12.517286	248	6	0	-3.041524	0.877270	1.638042
191	1	0	-0.000192	0.838009	-12.484201	249	6	0	-0.700002	3.432237	0.689554
192	1	0	-0.000121	-0.398063	-10.312469	250	6	0	0.731204	2.110039	2.790861
193	1	0	7.137436	3.995890	-4.433993	251	6	0	-0.000133	-0.001601	3.572293
194	1	0	8.970041	4.030017	-2.725048	252	6	0	-2.314865	-1.231958	2.421814
195	1	0	8.987513	2.311972	-0.908717	253	6	0	-3.493019	-0.138182	0.687697
196	1	0	5.574565	0.470290	-2.471160	254	6	0	-2.607331	2.413096	-0.260851
197	1	0	-5.574607	0.470183	-2.471047	255	6	0	-1.182189	-2.007379	2.711099
198	1	0	-8.987622	2.311769	-0.908611	256	6	0	-0.000093	-1.379104	3.299490
199	1	0	-8.970189	4.029804	-2.724954	257	6	0	-0.731479	-3.023636	1.761071
200	1	0	-7.137575	3.995722	-4.433886	258	6	0	1.182072	-2.007323	2.711181
201	1	0	-2.273712	4.690631	-6.433523	259	6	0	0.699782	3.432269	0.689605
202	1	0	-0.000107	4.545616	-7.752656	260	6	0	1.181554	0.805412	3.273323
203	1	0	2.273540	4.690684	-6.433601	261	6	0	0.731480	-3.023602	1.761122
204	1	0	2.287678	-0.360174	-6.375254	262	6	0	2.311989	0.201837	2.706452
205	1	0	-0.000048	-0.256201	-7.688568	263	6	0	1.430426	2.759501	1.762894
206	1	0	-2.287711	-0.360227	-6.375143	264	6	0	-3.042476	-1.441664	1.171948
207	1	0	-2.293304	6.436184	-0.374015	265	6	0	-3.492967	0.138174	-0.687979
208	1	0	-0.000107	7.750838	-0.259735	266	6	0	1.429278	3.221268	-0.560456
209	1	0	2.293118	6.436241	-0.374038	267	6	0	-3.042450	1.441677	-1.172195
210	1	0	2.259345	6.428643	4.676753	268	6	0	-1.429400	3.221203	-0.560559
211	1	0	-0.000086	7.764886	4.542557	269	6	0	-3.041356	-0.877254	-1.638286
212	1	0	-2.259498	6.428625	4.676775	270	6	0	-2.314742	1.232007	-2.422010
213	1	0	-7.124631	4.464650	3.956249	271	6	0	-0.731492	3.023759	-1.761156
214	1	0	-8.963018	2.761762	4.002939	272	6	0	2.314727	-1.231847	2.421974
215	1	0	-8.980538	0.929640	2.301386	273	6	0	-2.607238	-2.413062	0.260633
216	1	0	-5.542832	2.452943	0.466159	274	6	0	2.609760	2.128313	1.173524
217	1	0	5.542706	2.453042	0.466097	275	6	0	-2.311996	-0.201679	-2.706480
218	1	0	8.980519	0.929849	2.301210	276	6	0	-1.182086	2.007483	-2.711220
219	1	0	8.963003	2.761967	4.002760	277	6	0	0.731466	3.023792	-1.761102
220	1	0	7.124560	4.464804	3.956136	278	6	0	1.182176	2.007537	-2.711132
221	1	0	-0.000135	10.376051	-0.374197	279	6	0	2.607230	2.413221	-0.260663
222	1	0	-0.000150	12.534632	0.884669	280	6	0	3.041356	0.877415	1.638262
223	1	0	-0.000137	12.541584	3.370088	281	6	0	3.492961	-0.138016	0.687949
224	1	0	-0.000109	10.390733	4.640939	282	6	0	0.000081	1.379264	-3.299526
225	1	0	0.000070	-10.390643	-4.640648	283	6	0	0.000122	0.001759	-3.572325
226	1	0	0.000082	-12.541432	-3.369693	284	6	0	1.181822	-0.805196	-3.273259
227	1	0	0.000091	-12.534360	-0.884273	285	6	0	-1.181563	-0.805254	-3.273351
228	1	0	0.000090	-10.375717	0.374487	286	6	0	-1.429289	-3.221113	0.560424
229	1	0	7.124793	-4.464645	-3.956231	287	6	0	3.493009	0.138339	-0.687729
230	1	0	8.963129	-2.761699	-4.002906	288	6	0	-2.609769	-2.128156	-1.173553
231	1	0	8.980574	-0.929572	-2.301357	289	6	0	-1.430437	-2.759346	-1.762925
232	1	0	5.542882	-2.452964	-0.466179	290	6	0	3.042465	1.441823	-1.171978
233	1	0	-5.542863	-2.453094	-0.466070	291	6	0	3.042442	-1.441519	1.172165
234	1	0	-8.980584	-0.929758	-2.301233	292	6	0	2.607318	-2.412938	0.260820
235	1	0	-8.963108	-2.761868	-4.002793	293	6	0	2.314851	1.232117	-2.421844
236	1	0	-7.124725	-4.464770	-3.956149	294	6	0	2.312191	-0.201569	-2.706315
237	1	0	-2.259406	-6.428604	-4.676654	295	6	0	-0.731214	-2.109882	-2.790892
238	1	0	0.000055	-7.764789	-4.542393	296	6	0	0.731500	-2.109847	-2.790838
239	1	0	2.259509	-6.428597	-4.676678	297	6	0	3.041506	-0.877110	-1.638070
240	1	0	2.293348	-6.435981	0.374114	298	6	0	-0.699793	-3.432119	-0.689638
241	1	0	0.000081	-7.750509	0.259897	299	6	0	1.429389	-3.221048	0.560527

```
300       6       0       2.609941   -2.128032   -1.173368
301       6       0       0.699993   -3.432086   -0.689588
302       6       0       1.430682   -2.759281   -1.762824
---------------------------------------------------------------------
```

3.4.7 Generation of $C_{60}^{\bullet-}$ inside $Pd_2L^P_4$

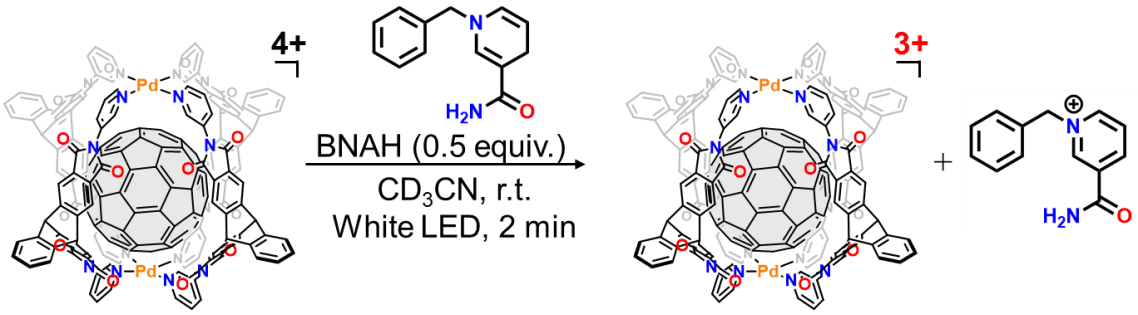

Figure 3.4.29 Photochemical reduction of encapsulated C_{60} inside $Pd_2\mathbf{L}^P_4$

To an acetonitrile solution of $C_{60}@Pd_2\mathbf{L}^P_4$ (0.70 mM, 0.60 mL, 0.42 µmol) 1-benzyl-1,4-dihydronicotinamide (BNAH) in acetonitrile (20.0 mM, 10.5 µL, 0.21 µmol) was added in the dark. The solution was irradiated with a white LED light source for 2 min after which the described measurements were carried out. For samples in inert atmosphere: the samples were handled and transferred to closed tubes/cuvettes for analysis in a glove box filled with N_2. To avoid oxygen contamination, the samples were sealed inside the glove box.

ESI MS found 1039.7808; calcd. for $[(C_{34}H_{18}N_4O_4)_4Pd_2C_{60}]^{3+}$ 1039.7816

3.4.7.1 ^{1}H NMR spectrum of $C_{60}^{\bullet-}@Pd_2L^P_4$

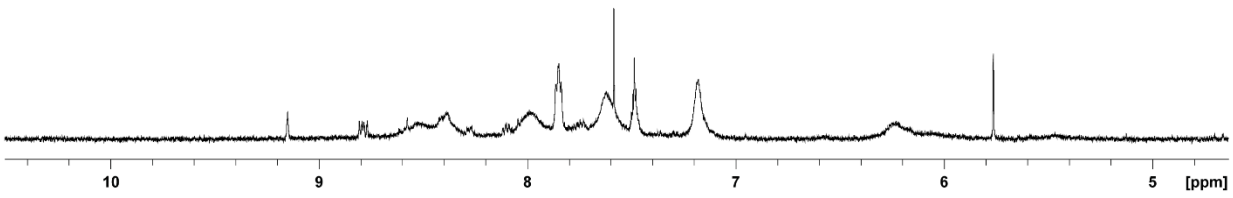

Figure 3.4.30 ^{1}H NMR spectrum of $C_{60}@Pd_2\mathbf{L}^P_4$ after photochemical reduction

3.4.7.2 ESI MS spectrum of $C_{60}^{\bullet-}$@$Pd_2L^P_4$

To an acetonitrile solution of C_{60}@$Pd_2\mathbf{L}^P_4$, 1-benzyl-1,4-dihydronicotinamide (BNAH) in acetonitrile was added in the dark. The solution was irradiated with a white LED light source for 2 mins and measurements were carried out immediately after irradiation. For the sample in inert atmosphere: the sample were prepared in glove box filled with N_2.

Sample prepared in air:

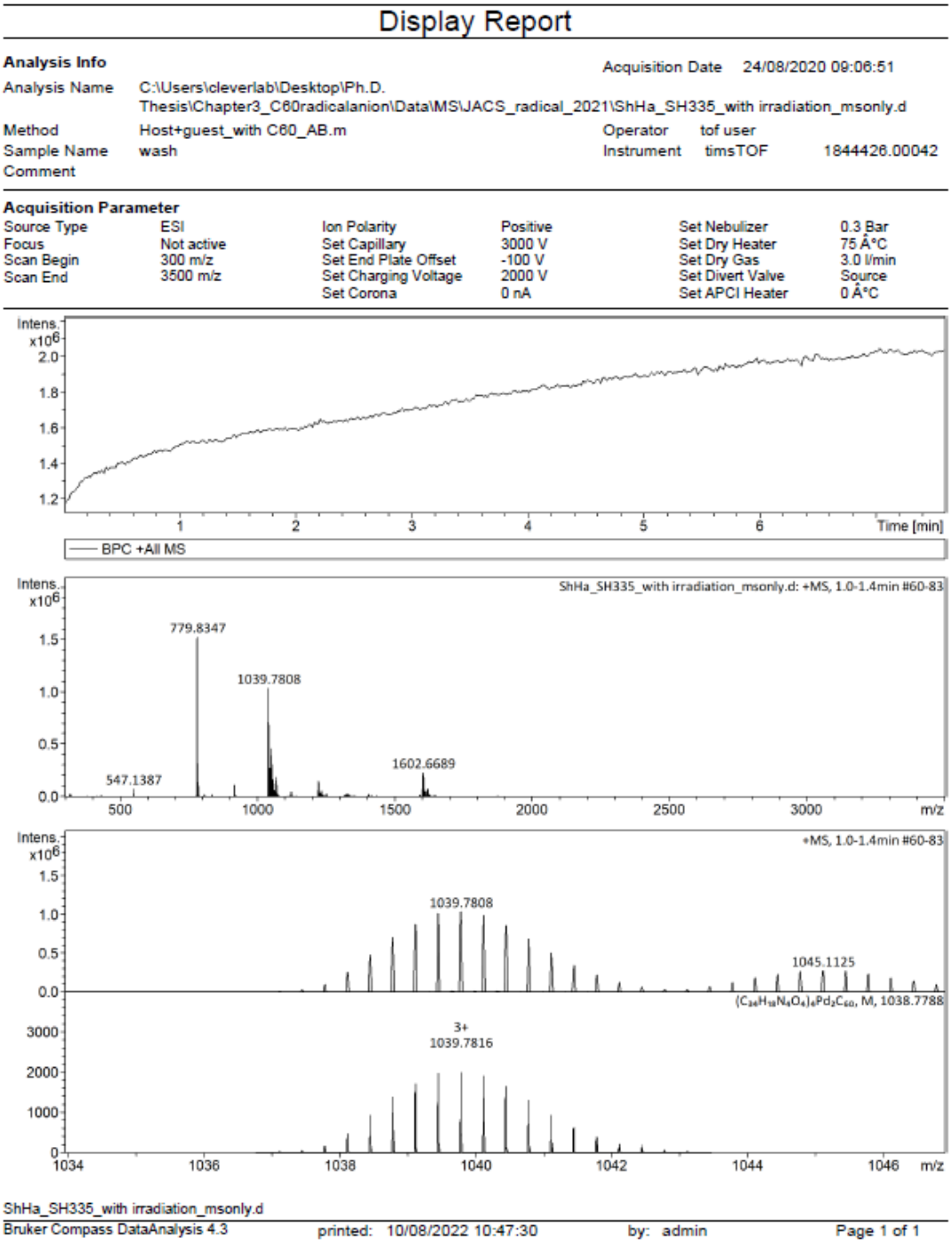

Figure 3.4.31 ESI-MS spectrum of $C_{60}^{\bullet-}$@$Pd_2\mathbf{L}^{\mathbf{P}}_4$ prepared under aerobic condition (positive mode)

Sample prepared in the glovebox:

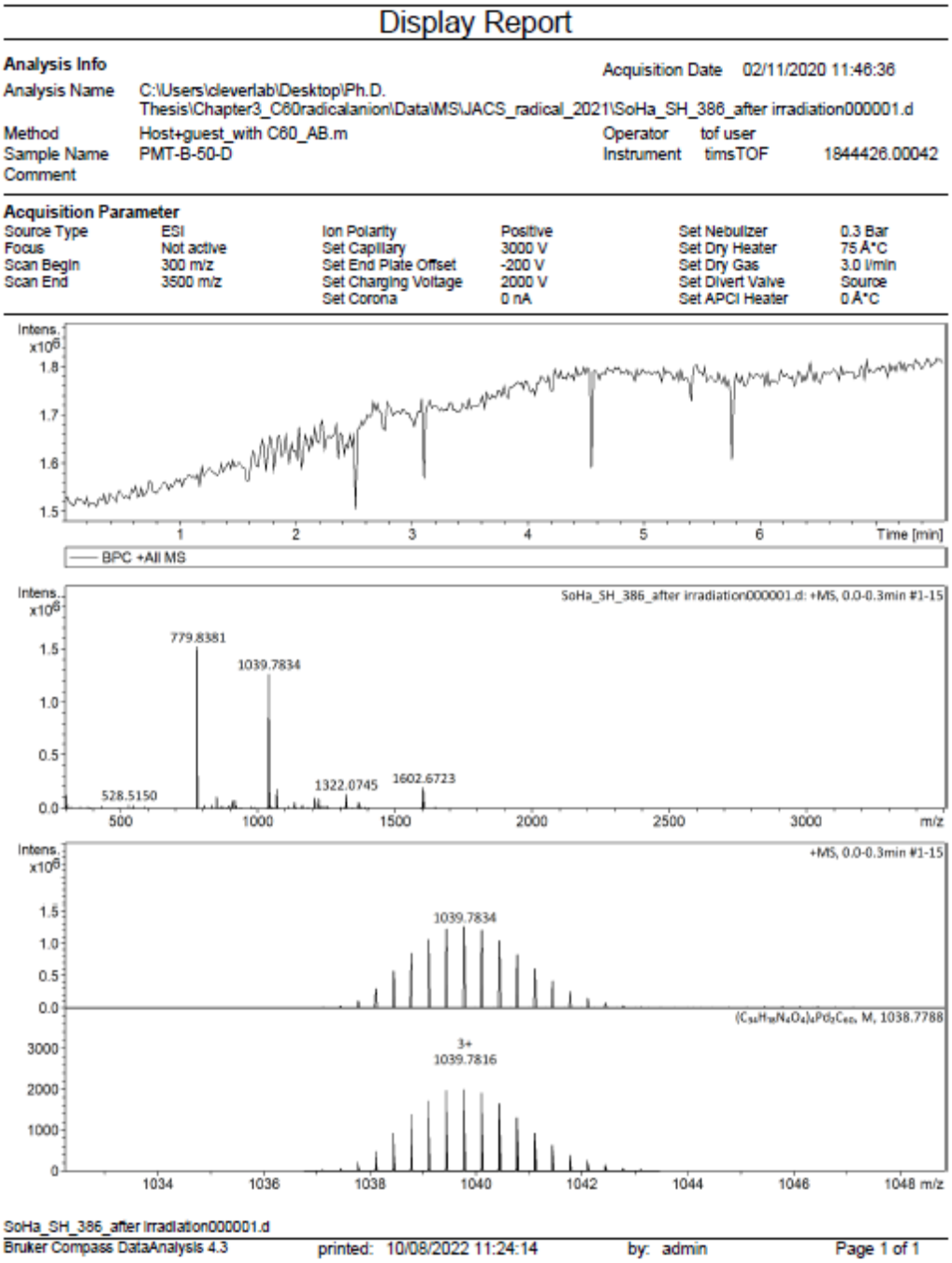

Figure 3.4.32 ESI-MS spectrum of $C_{60}^{\bullet-}$@$Pd_2\mathbf{L}^{\mathbf{P}}_4$ prepared under inert condition (positive mode)

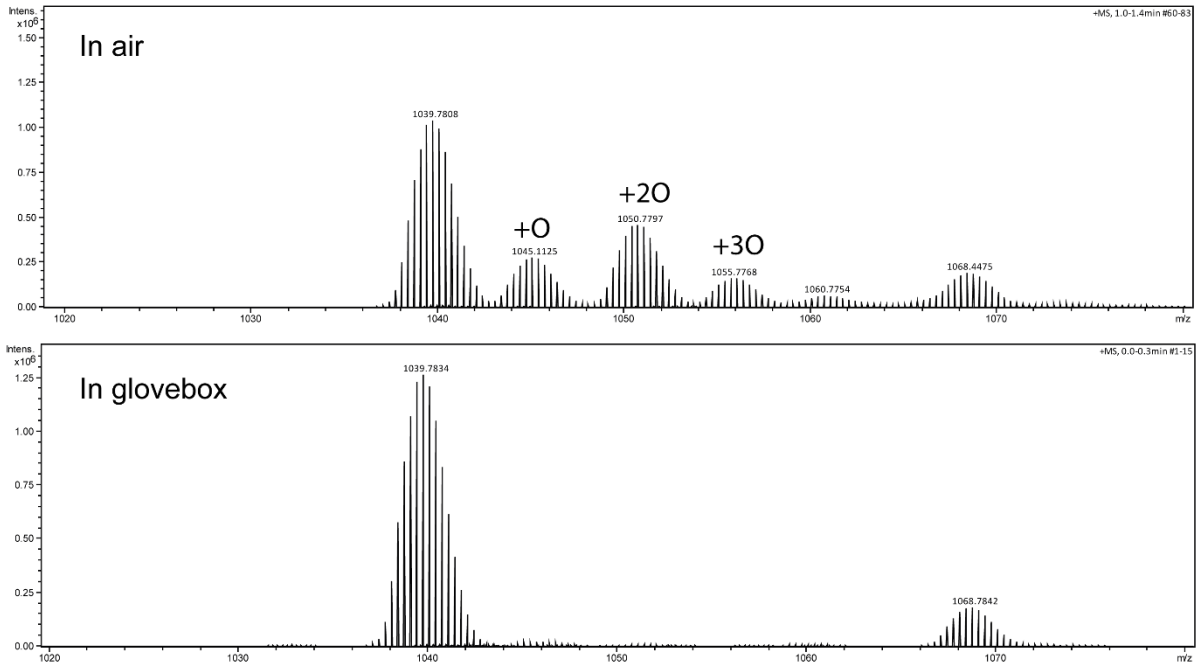

Figure 3.4.33 Comparison of ESI-MS spectra of $C_{60}^{\bullet-}$@$Pd_2\mathbf{L}^{\mathbf{P}}_4$ prepared in the air and the glovebox showing clear oxygenation for the sample prepared in the air (positive mode)

3.4.7.3 Control experiments

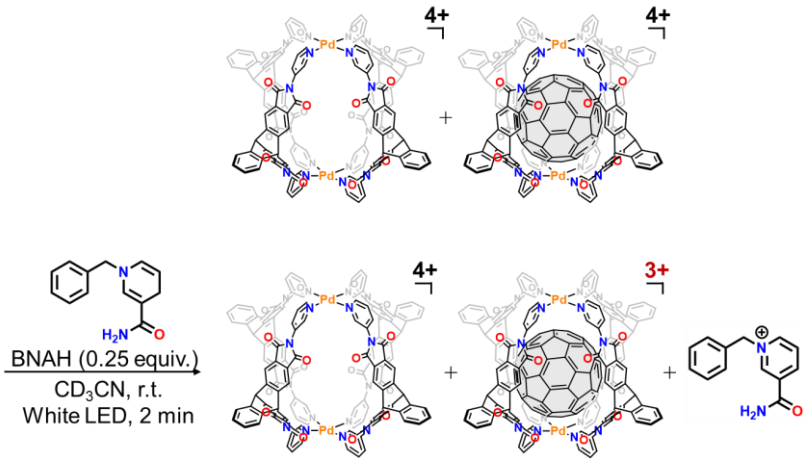

Figure 3.4.34 Photo chemical reduction of $C_{60}@Pd_2\mathbf{L}^{\mathbf{P}}_4$ in the presence of empty $Pd_2\mathbf{L}^{\mathbf{P}}_4$

To a mixture of $Pd_2\mathbf{1}_4$ and $C_{60}@Pd_2\mathbf{L}^{\mathbf{P}}_4$ (0.35 mM for each complex, 0.60 mL) 1-benzyl-1,4-dihydronicotinamide (BNAH) in acetonitrile (10.5 µL, 10.0 mM, 0.1 µmol) was added in the dark. The solution was irradiated with a white LED light source for 2 mins and then measurements were carried out. As a result, only the fullerene-containing $C_{60}@Pd_2\mathbf{L}^{\mathbf{P}}_4$ host-guest complex gave broadened ^{1}H NMR signals while the signals of empty $Pd_2\mathbf{L}^{\mathbf{P}}_4$ did not change. This shows that the encapsulated fullerene is not only the photocatalyst but also the recipient of the electron.

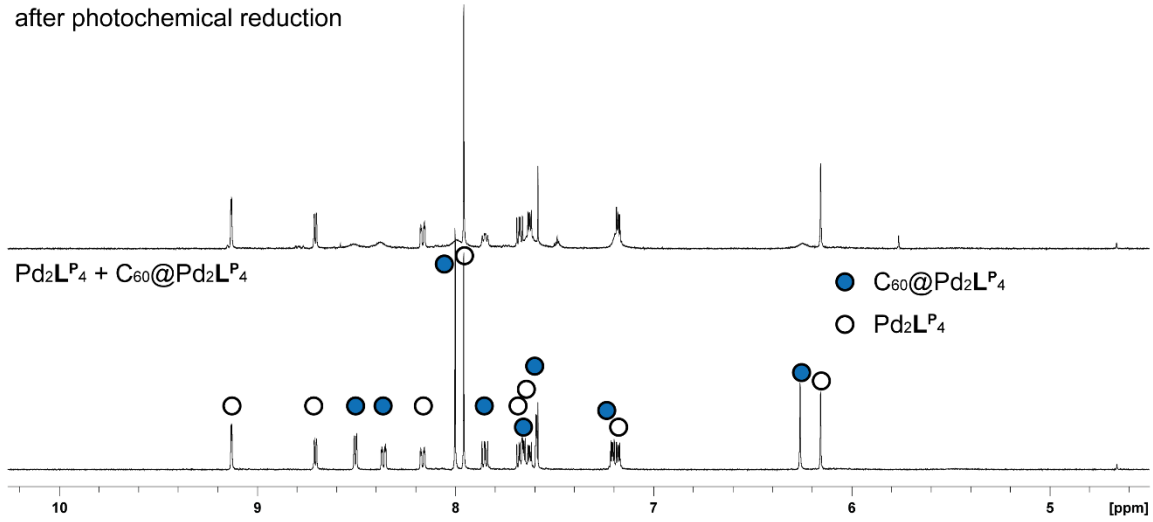

Figure 3.4.35 ^{1}H NMR spectra (CD_3CN, 500 MHz, 298 K) showing selective reduction of $C_{60}@Pd_2\mathbf{L}^{\mathbf{P}}_4$ by photochemical reduction

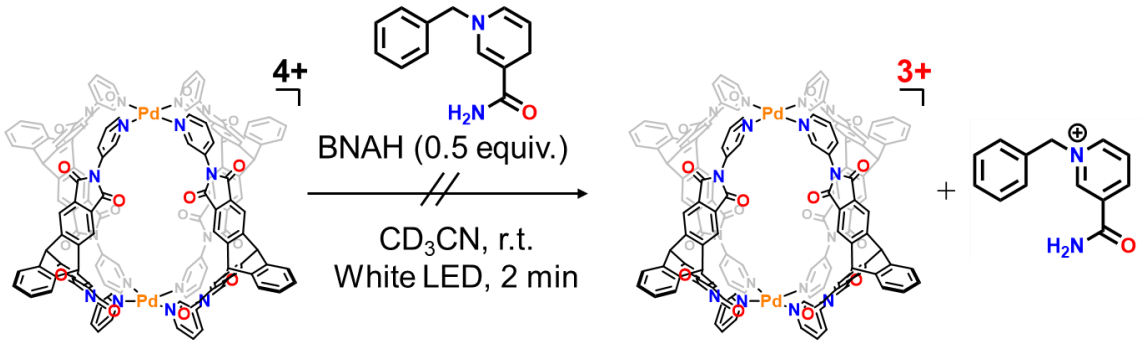

Figure 3.4.36 Attempted photochemical reduction of $Pd_2\mathbf{L}^{P}_4$

To a mixture of $Pd_2\mathbf{L}^{P}_4$ (0.70 mM, 0.60 mL) 1-benzyl-1,4-dihydronicotinamide (BNAH) in acetonitrile (10.5 µL, 20.0 mM, 0.2 µmol) was added in the dark. The solution was irradiated with a white LED light source for 2 mins and then measurements were carried out. However, no photochemical reduction took place.

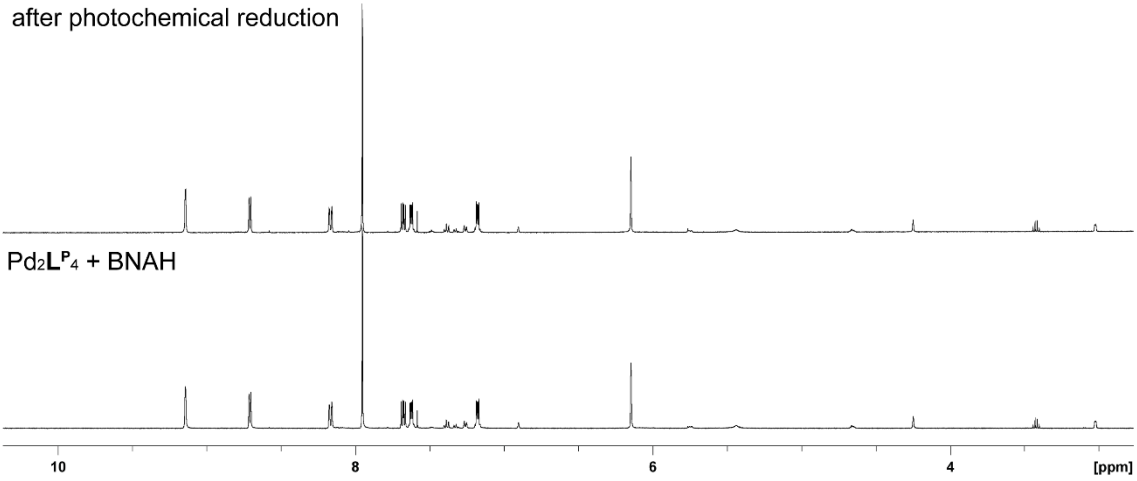

Figure 3.4.37 ^{1}H NMR spectra (CD_3CN, 500 MHz, 298 K) showing that no photochemical reduction occurred

3.4.7.4 UV-Vis NIR absorption

To an acetonitrile solution of $C_{60}@Pd_2\mathbf{L}^{\mathbf{P}}_4$ (0.35 mM, 2.00 mL, 0.70 µmol) 1-benzyl-1,4-dihydronicotinamide (BNAH) in acetonitrile (20.0 mM, 17.5 µL, 0.3 µmol) was added in the dark. The solution was irradiated with a white LED light source for 2 min and then measurements were carried out. For samples in inert atmosphere: the samples were prepared in a glove box filled with N_2. To avoid oxygen contamination, the samples were sealed in the glove box. After taking out from the glove box, the sample was irradiated with a white LED light source for 2 min and then measurements were carried out. All spectra were measured using an Agilent Cary 5000 double beam UV-vis-NIR spectrometer (175-3300 nm).

3.4.7.4.1 UV-Vis-NIR spectrum of $C_{60}@Pd_2L^P_4$

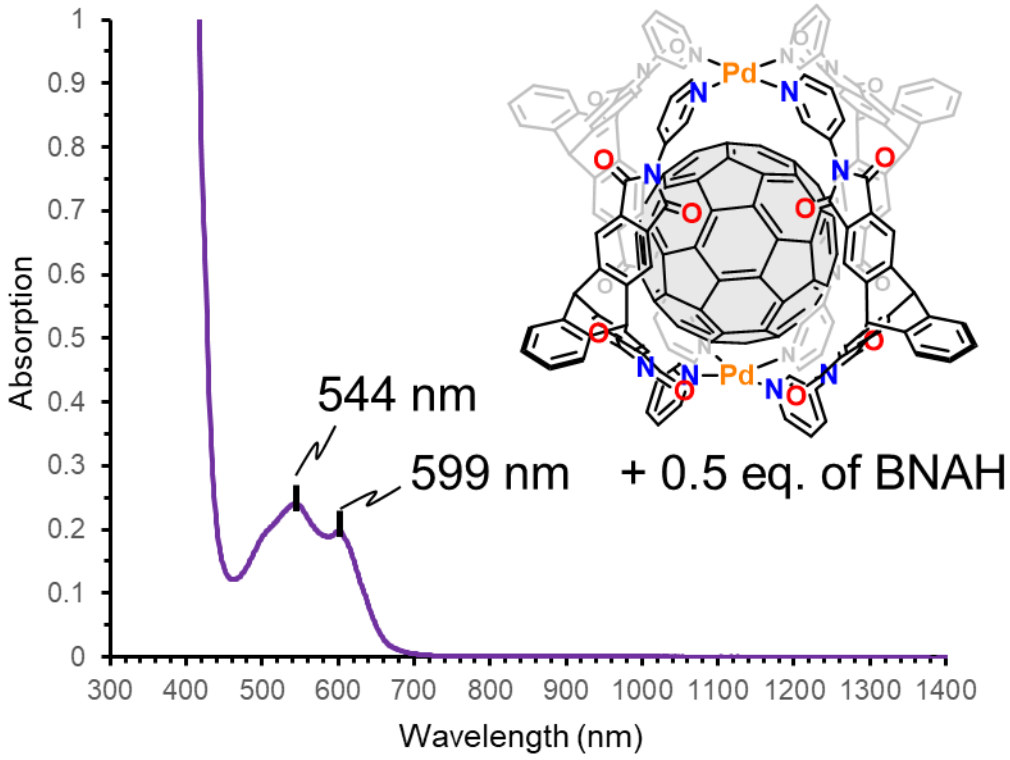

Figure 3.4.38 UV-Vis-NIR spectrum of $C_{60}@Pd_2\mathbf{L}^{\mathbf{P}}_4$ (0.35 mM, CD_3CN, 298 K, l = 1.0 cm) in the presence of BNAH in the dark

3.4.7.4.2 UV-Vis-NIR spectra of $C_{60}^{\bullet-}$@$Pd_2L^P_4$ under aerobic conditions

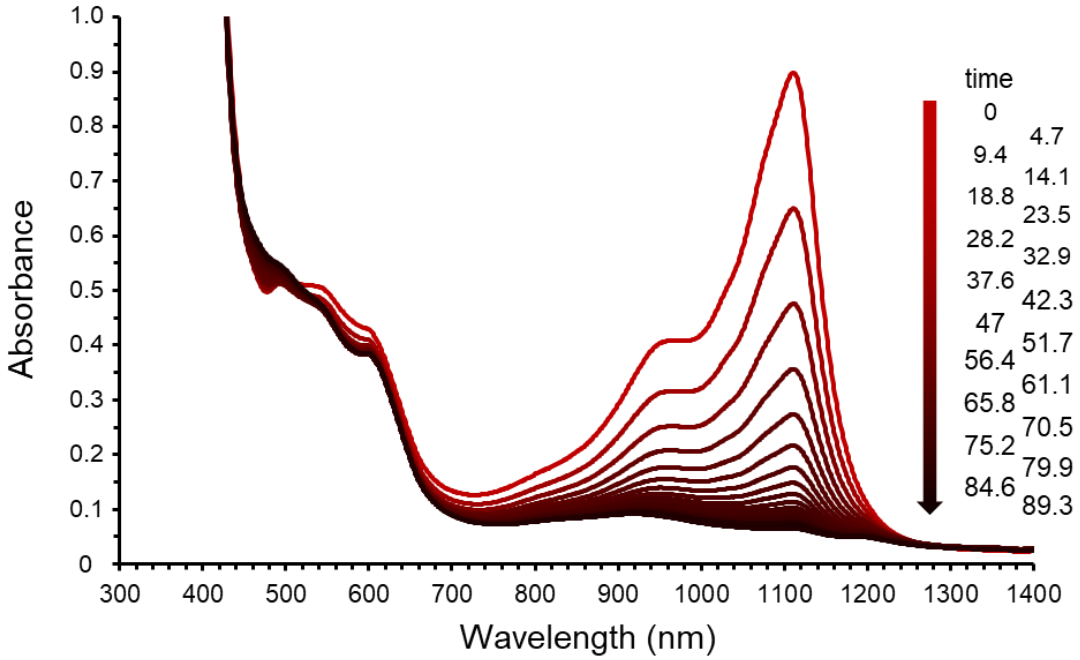

Figure 3.4.39 UV-Vis-NIR spectra of $C_{60}^{\bullet-}$@$Pd_2\mathbf{L}^P_4$ (0.35 mM, CD_3CN, 295 K, *l* = 1.0 cm) under aerobic conditions over time (ε_{1111}=5637 $M^{-1}cm^{-1}$, ε_{975}=2070 $M^{-1}cm^{-1}$).

The absorption decay at 1111 nm and 975 nm was analyzed to obtain kinetic parameters for the deactivation of $C_{60}^{\bullet-}$. We have attempted to fit the data as pseudo first order (eq. 1) and second order (eq. 2) reaction as shown below. To estimate the concentration of $C_{60}^{\bullet-}$@Pd_2**1**$_4$, absorption coefficient ε was calculated from the absorbance at 0 min measured in N_2 atmosphere for each wavelength (**4.3.3.**). The half lifetime estimated from second order reaction fitting was calculated using 3.5×10^{-4} M was used as [A0]. As a result, the pseudo first order fit for the signal at 1111 nm gave a similar half-lifetime of the radical (13 min) to the one estimated by EPR spectroscopy (14min) as shown in section **4.6.3.**

$$[A] = [A_0]e^{-kt} \quad \bullet\bullet\bullet (1)$$

$$\frac{1}{[A]} = \frac{1}{[A_0]} + kt \quad \bullet\bullet\bullet (2)$$

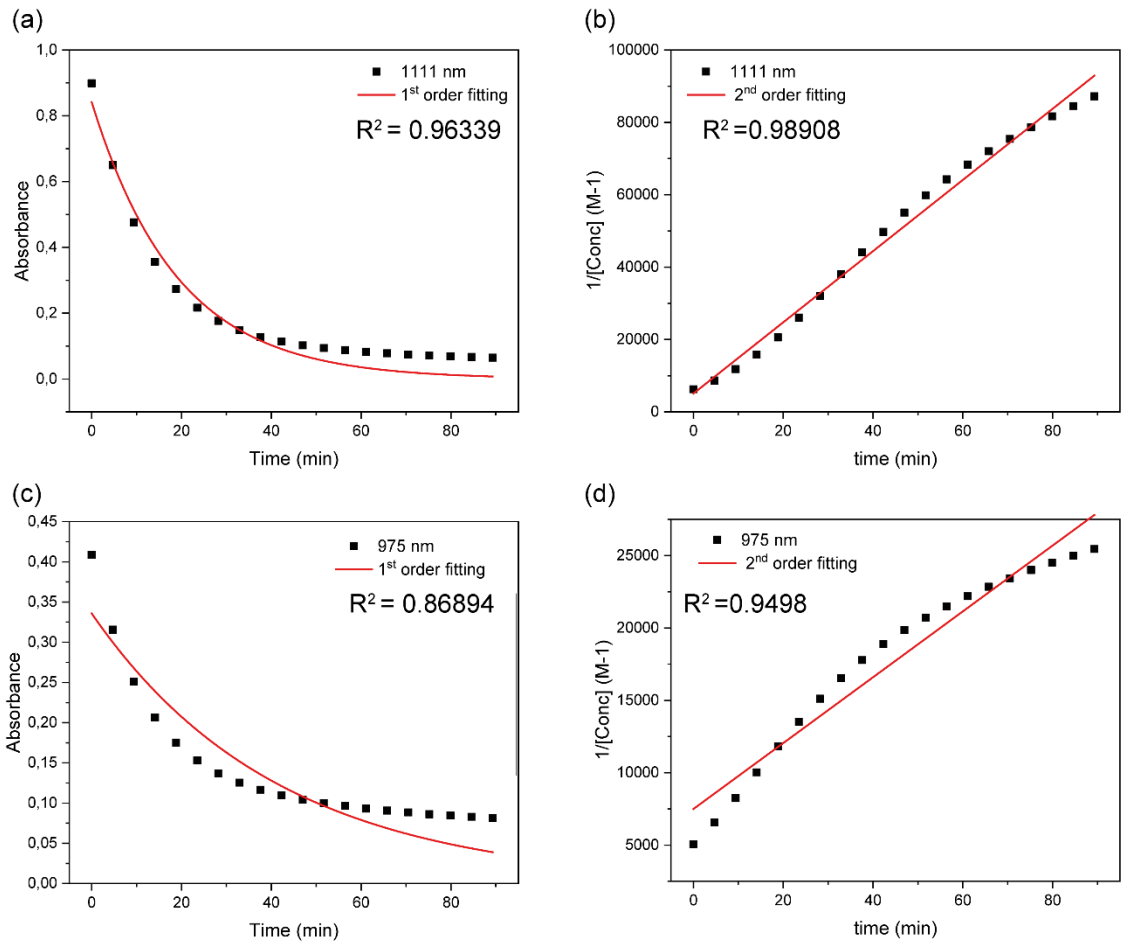

Figure 3.4.40 Absorbance decay of $C_{60}^{\bullet-}$@$Pd_2\mathbf{L}^{\mathbf{P}}_4$ (0.35 mM, CD_3CN, 295 K, *l* = 1.0 cm) under aerobic conditions over time (a) absorption change at 1111 nm fitted as pseudo first order reaction (b) as second order reaction (c) absorption change at 975 nm fitted as pseudo first order reaction (d) as second order reaction

Table 3.4.7.1. Summary of reaction rates and half-lifetimes under aerobic conditions obtained by the fittings of the absorption decay at 1111 nm, yielding a pseudo-first order half-lifetime of 13 min which is in good agreement with the EPR-derived result (14 min; see below). Fittings of the signal decay at 975 nm were too poor to result in trustworthy values.

	1111 nm	
	k	$t_{1/2}$ (min)
pseudo first order	5.2×10^{-2} (min^{-1})	13
second order	983.3 ($M^{-1}min^{-1}$)	3

3.4.7.4.3 UV-Vis-NIR spectra of $C_{60}^{\bullet-}$@$Pd_2L^P_4$ in inert atmosphere

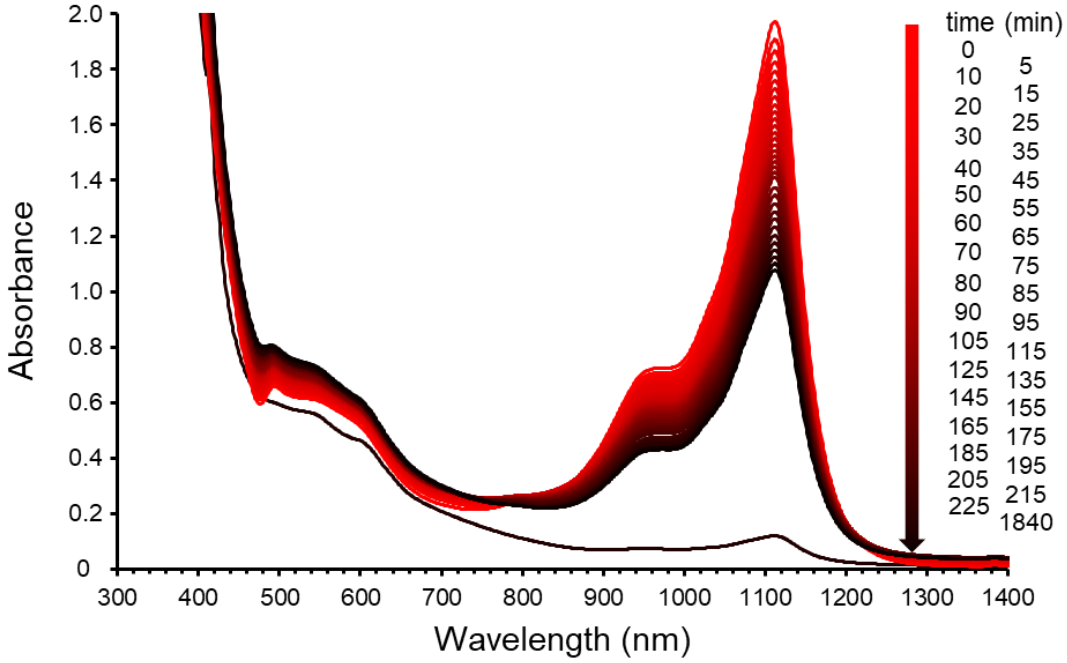

Figure 3.4.41 UV-Vis-NIR spectra of $C_{60}^{\bullet-}$@$Pd_2\mathbf{L}^P_4$ (0.35 mM, CD_3CN, 295 K, *l* = 1.0 cm) in N_2 atmosphere over time (ε_{1111}=5637 $M^{-1}cm^{-1}$, ε_{975}=2070 $M^{-1}cm^{-1}$)

Under anaerobic conditions, the absorption decay was again analyzed at 1111 nm and 975 nm to obtain kinetic parameters of the deactivation of $C_{60}^{\bullet-}$. We have attempted to fit the data as pseudo first order (eq. 1) and second order reaction (eq. 2) as shown above. Owing to the almost linearly appearing signal decay in the monitored time regime, all fittings gave half-lifetimes with similar magnitude around 300 min, which should therefore be considered as a rough estimate. To estimate the

concentration of $C_{60}^{\bullet-}$@$Pd_2\mathbf{L}^{\mathbf{P}}_4$, absorption coefficient ε was calculated from Absorbance at 0 min for each wavelength. The half lifetime estimated from second order reaction fitting was calculated using 3.5×10^{-4} M was used as [A_0].

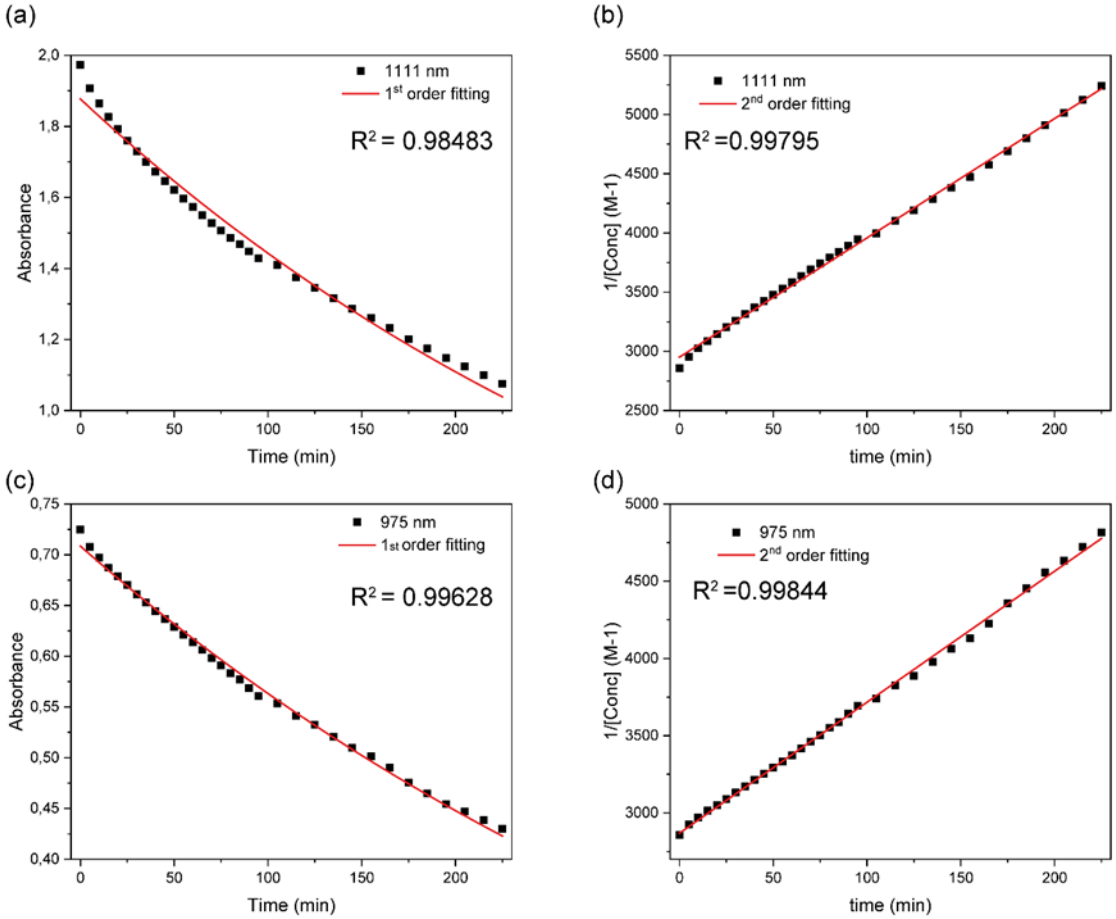

Figure 3.4.42 Absorbance decay of $C_{60}^{\bullet-}$@$Pd_2\mathbf{L}^{\mathbf{P}}_4$ (0.35 mM, CD_3CN, 295 K, *l* = 1.0 cm) under N_2 atmosphere over time: (a) absorption change at 1111 nm fitted as pseudo first order reaction (b) as second order reaction (c) absorption change at 975 nm fitted as pseudo first order reaction (b) as second order reaction

Table 3.4.7.2 Summary of reaction rates and half-lifetimes under N_2 atmosphere obtained by the fittings

	1111 nm		975 nm	
	k	$t_{1/2}$ (min)	*k*	$t_{1/2}$ (min)
pseudo first order	2.6×10^{-3} (min^{-1})	263	2.2×10^{-3} (min^{-1})	302
second order	10.0 ($M^{-1}min^{-1}$)	283	8.4 ($M^{-1}min^{-1}$)	337

3.4.7.5 Chemical oxidation of $C_{60}^{\bullet-}$@$Pd_2L^P_4$

To an acetonitrile solution of C_{60}@Pd_2**L**$^P_4$ (0.35 mM, 1.0 mL, 0.4 μmol) 1-benzyl-1,4-dihydronicotinamide (BNAH) in acetonitrile (17.5 μL, 10.0 mM, 0.17 μmol) was added in the dark. The solution was irradiated with a white LED light source for 2 mins and measurements were carried out immediately after irradiation. After measuring the absorption spectrum, tetracyanoethylene (TCNE) in acetonitrile (17.5 μL, 20.0 mM, 0.4 μmol) was quickly added under N_2 flow. Absorption spectra were measured immediately after addition of TCNE and 1h after the addition. The disappearance of absorption in NIR region indicates oxidation of $C_{60}^{\bullet-}$ inside the cage. The identical spectrum to C_{60}@Pd_2**1**$_4$ with less intensity was obtained after 1h. All the samples were prepared in the glove box filled with N_2. Absorption spectra were measured by using DAD HP-8453 UV-Vis.

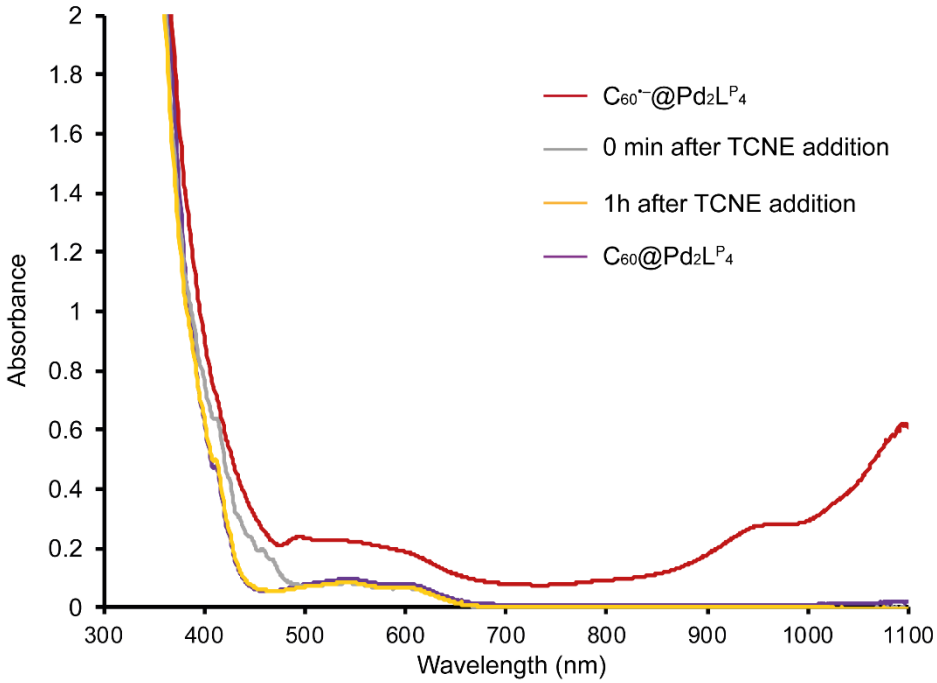

Figure 3.4.43 UV-Vis-NIR spectra (0.35 mM, CD3CN, 295 K, l = 0.2 cm) of $C_{60}^{\bullet-}$@Pd_2**L**$^P_4$ (red line), after TCNE addition (gray line), 1h after TCNE addition (yellow line), and C_{60}@Pd_2**L**$^P_4$ (purple line)

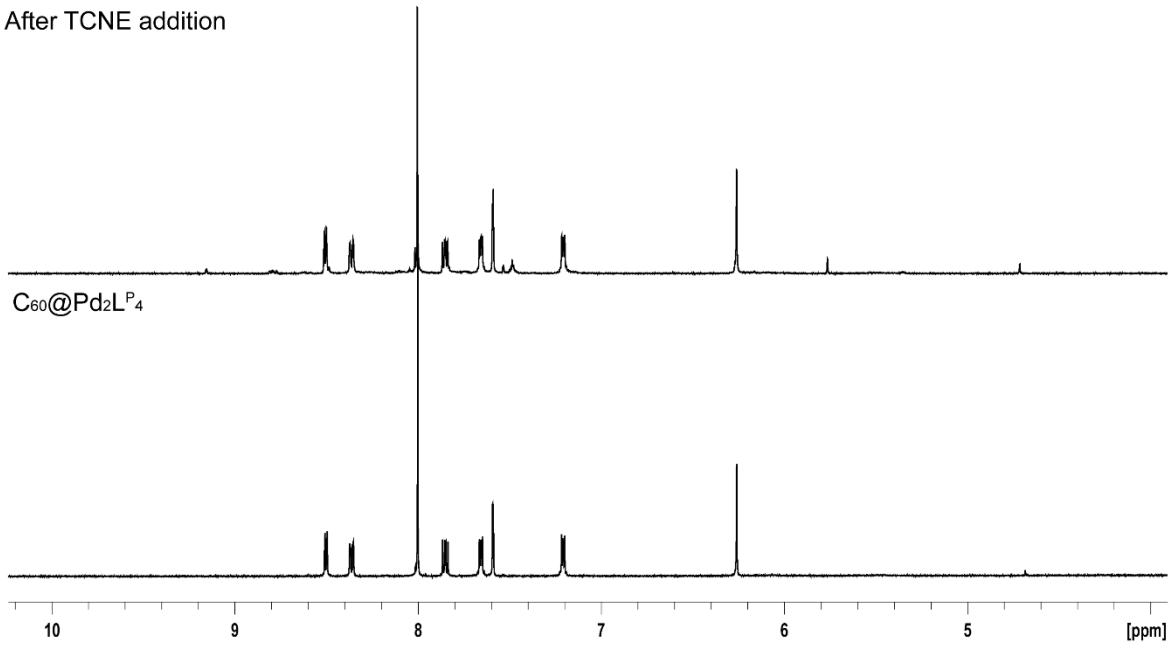

Figure 3.4.44 ^{1}H NMR spectra (0.70 mM, CD_3CN, 500 MHz) of $C_{60}@Pd_2\mathbf{L^P}_4$ (bottom) and after photochemical reduction and re-oxidation by using TCNE (top)

3.4.8 X-Band EPR spectra and simulations

3.4.8.1 EPR control experiments

The following experiments and analyses were performed by Shari L. Meichsner in the Kasanmascheff group. In addition, the following detail description of the experiments and analyses was contributed by Shari L. Meichsner. To ensure that the encapsulated $C_{60}^{\bullet-}$ is the only radical species detected, three control experiments were performed (**Figure 3.4.45**). The host-guest complex without BNAH was measured before (blue) and after (yellow) irradiation. These samples did not result in any detectable EPR signals. Similarly, irradiation of $Pd_2\mathbf{L}^{\mathbf{P}}_4$ together with BNAH showed no EPR signal (black). The irradiated host-guest assembly $C_{60}@Pd_2\mathbf{L}^{\mathbf{P}}_4$ was the only sample that displayed a sharp EPR signal (red).

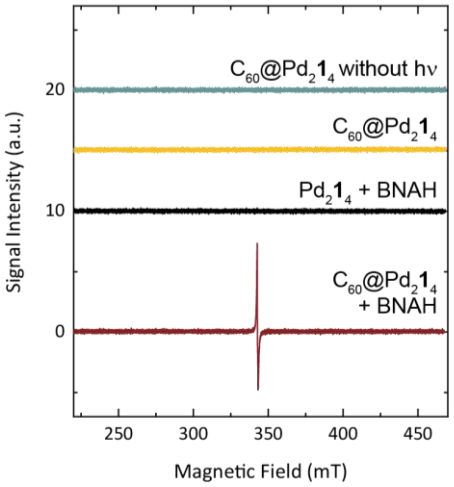

Figure 3.4.45 Control EPR experiments of different compounds, performed at X-Band under aerobic conditions. The only signal obtained arises after irradiation of $C_{60}@Pd_2\mathbf{1}_4$ in acetonitrile (0.35 mM, 0.50 mL, 0.17 µmol) in the presence of BNAH (10 mM, 8.8 µL, 0.08 µmol). Experimental conditions are: 0.32 mW power, 1 G modulation amplitude, 100 kHz modulation frequency, 1.28 ms as time constant, 15.0 ms conversion time, 1 scan.

3.4.8.2 Simulations of X-Band EPR spectra

X-band EPR measurements were carried out at T = 100 K using a Bruker EMX-Nano Benchtop spectrometer equipped with a continuous-flow nitrogen cryostat (**Figure 3.4.46**). Spectral simulations were performed with the EasySpin 5.2.28[50] 'pepper' routine.

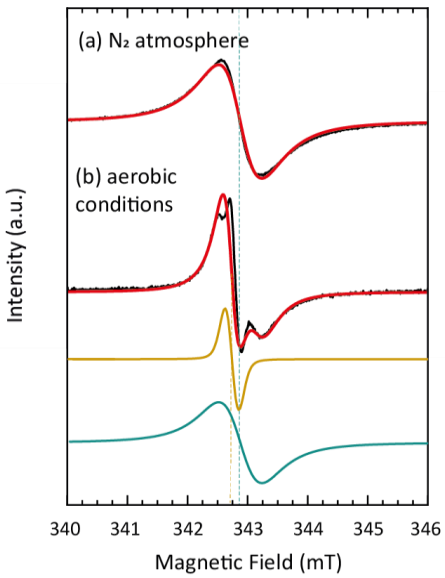

Figure 3.4.46 X-Band EPR spectra of $C_{60}^{\bullet-}$@$Pd_2\mathbf{L}^{\mathbf{P}}_4$ in acetonitrile (0.35 mM) prepared under N_2 atmosphere (a) and aerobic conditions (b) are shown with their corresponding simulations (red). Spectrum shown in (a) was simulated via using following parameters; S = ½ species with g_{iso} = 1.999 and 1.1 mT linewidth (red in (a) and blue in (b)). For simulations of (b) an additional second species (yellow) was taken into an account with g_{iso} = 2.001, 0.3 mT linewidth. A yellow-to-blue ratio of 1 resulted in the complete simulation of $C_{60}^{\bullet-}$@$Pd_2\mathbf{L}^{\mathbf{P}}_4$ prepared under aerobic conditions. Dotted lines indicate the positions of the *g*-values of the respective species. Experimental conditions are: 0.79 mW power, 1 G modulation amplitude, 100 kHz modulation frequency, 1.28 ms as time constant, 15.0 ms conversion time, and 20 scans.

3.4.8.3 Half-lifetime determination via X-Band EPR measurements

EPR signal intensity is dependent on the relaxation properties of the paramagnetic species under investigation and used microwave powers. Therefore, power saturation curves are plotted for $C_{60}^{\bullet-}$@$Pd_2\mathbf{1}_4$ in acetonitrile (0.35 mM) prepared under N_2 atmosphere and aerobic conditions (**Figure 3.4.47**). The results clearly demonstrated

the distinct relaxation properties of $C_{60}^{\bullet-}$ and the oxygenated species. Microwave powers higher than 0.8 mW led to saturation of the oxygenated species, whereas $C_{60}^{\bullet-}$ was not saturated in the observed range. This enabled us, firstly, to separate EPR signals of $C_{60}^{\bullet-}$ and the oxygenated species via measurements recorded at 0.79 and 79.43 mW (**Figure 3.4.47b**-**c**); and secondly, to determine the half-lifetime of both radicals by tracing the decay of the peak-to-peak amplitude of the EPR signals. The half-lifetime of encapsulated $C_{60}^{\bullet-}$ under aerobic conditions was estimated to be 14 mins, in excellent agreement with the UV-Vis-NIR results under the same aerobic conditions. The half-lifetime of encapsulated $C_{60}^{\bullet-}$ under anaerobic condition shows a significantly longer value of 893 mins. To determine this value, duplicates from two different sample preparations were measured for the encapsulated $C_{60}^{\bullet-}$ under anaerobic conditions and the mean values were plotted together with their standard deviation. We denote the longer half-lifetime determined by EPR as compared to UV-Vis-NIR measurements (~300min) to the different sample preparation conditions: In both cases, samples were prepared similarly in the glovebox. The UV-Vis-NIR measurements were performed in a stoppered cuvette outside the glovebox, keeping the sample at room temperature. Therefore, contamination from the surrounding air during the measurement period cannot be excluded, shortening the detected half-lifetime. In contrast, for the EPR measurement, the sample remained in the glovebox and aliquots were taken after indicated times, removed from the glovebox in sealed EPR tubes, immediately deep-frozen in liquid nitrogen and measured immediately, making additional radical degradation by oxygen contamination less likely.

It is worth noting that EPR was able to detect the signal of the encapsulated fullerene radical in the low micromolar range even after the solution was kept for four weeks at 303 K inside the glove box (**Figure 3.4.47c**).

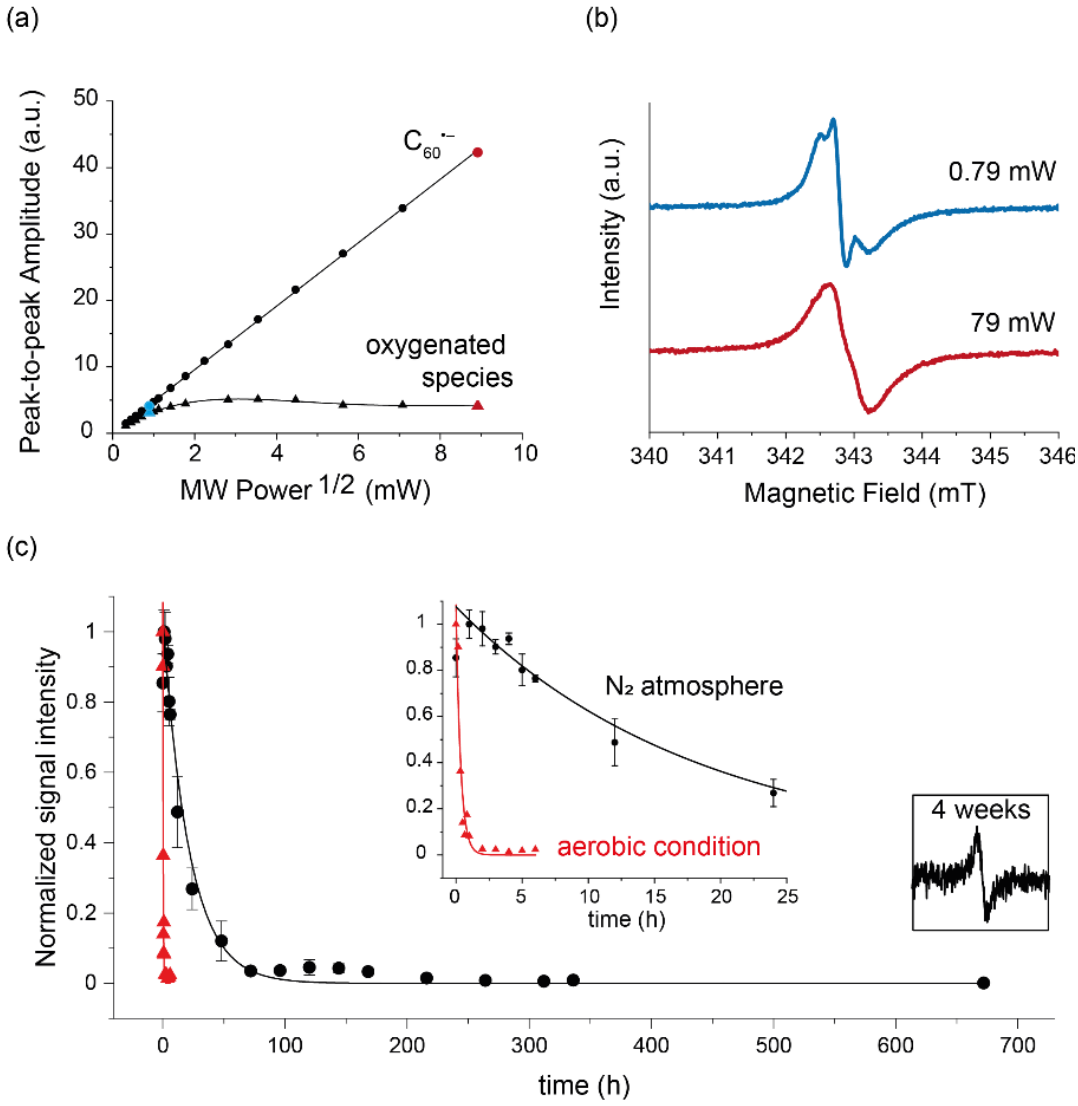

Figure 3.4.47 (a) Continuous-wave power saturation curves for $C_{60}^{\bullet-}$@$Pd_2\mathbf{L}^{P}_4$ in acetonitrile (0.35 µM) and its oxygenated species. Experiments shown in Figure 6 and S37 were recorded at 0.79 mW power (blue point in a), which is the ideal power for detecting both species. The lower spectrum shown in (b) was acquired with 79 mW power (red point in a) and shows the encapsulated $C_{60}^{\bullet-}$, only. The time-dependent EPR spectra of $C_{60}^{\bullet-}$@$Pd_2\mathbf{1}_4$ prepared under aerobic conditions and in N_2 atmosphere are used to calculate the half-lifetime (c) of the encapsulated $C_{60}^{\bullet-}$ radical anion (aerobic: 14 min, anaerobic 893 min). The data were normalized by dividing double integral values of each spectrum by the maximum obtained value. Experimental conditions are: 79.43 mW power, 1 G modulation amplitude, 100 kHz modulation frequency, 1.28 ms as time constant, 15.0 ms conversion time, 20 to 100 scans.

3.5 References

[1] H. W. Kroto, J. R. Heath, S. C. O'Brien, R. F. Curl, R. E. Smalley, *Nature* **1985**, *318*, 162–163.

[2] K. Komatsu, M. Murata, Y. Murata, *Science* **2005**, *307*, 238–240.

[3] K. Kurotobi, Y. Murata, *Science* **2011**, *333*, 613–616.

[4] S. Hasegawa, Y. Hashikawa, T. Kato, Y. Murata, *Angew. Chem. Int. Ed.* **2018**, *57*, 12804–12808.

[5] K. Itami, *Chem. Rec.* **2011**, *11*, 226–235.

[6] J.-F. Nierengarten, *New. J. Chem.* **2004**, *28*, 1177–1191.

[7] M. Sawamura, K. Kawai, Y. Matsuo, K. Kanie, T. Kato, E. Nakamura, *Nature* **2002**, *419*, 702–705.

[8] S. Collavini, J. L. Delgado, *Sustain. Energy Fuels* **2018**, *2*, 2480–2493.

[9] T.-M. Liu, J. Conde, T. Lipiński, A. Bednarkiewicz, C.-C. Huang, *NPG Asia Mater.* **2016**, *8*, e295–e295.

[10] T. Konishi, M. Fujitsuka, O. Ito, Y. Toba, Y. Usui, *Bull. Chem. Soc. Jpn.* **2001**, *74*, 39–45.

[11] T. Kato, T. Kodama, T. Shida, T. Nakagawa, Y. Matsui, S. Suzuki, H. Shiromaru, K. Yamauchi, Y. Achiba, *Chem. Phys. Lett*. **1991**, *180*, 446–450.

[12] T. Kato, T. Kodama, M. Oyama, S. Okazaki, T. Shida, T. Nakagawa, Y. Matsui, S. Suzuki, H. Shiromaru, K. Yamauchi, Y. Achiba, *Chem. Phys. Lett.* **1991**, *186*, 35–39.

[13] Z. Gasyna, L. Andrews, P. N. Schatz, *J. Phys. Chem.* **1992**, *96*, 1525–1527.

[14] J. Friedrich, P. Schweitzer, K.-P. Dinse, P. Rapta, A. Stasko, *Appl. Magn. Reson.* **1994**, *7*, 415–425.

[15] D. M. Guldi, R. E. Huie, P. Neta, H. Hungerbühler, K.-D. Asmus, *Chem. Phys. Lett.* **1994**, *223*, 511–516.

[16] M. Fujita, M. Tominaga, A. Hori, B. Therrien, *Acc. Chem. Res.* **2005**, *38*, 369–378.

[17] M. Yoshizawa, S. Miyagi, M. Kawano, K. Ishiguro, M. Fujita, *J. Am. Chem. Soc.* **2004**, *126*, 9172–9173.

[18] M. Yoshizawa, M. Tamura, M. Fujita, *Science* **2006**, *312*, 251–254.

[19] M. Yamashina, M. Akita, T. Hasegawa, S. Hayashi, M. Yoshizawa, *Sci. Adv.* **2017**, *3*, e1701126.

[20] M. Yamashina, T. Tsutsui, Y. Sei, M. Akita, M. Yoshizawa, *Sci. Adv.* **2019**, *5*, eaav3179.

[21] P. Mal, B. Breiner, K. Rissanen, J. R. Nitschke, *Science* **2009**, *324*, 1697–1699.

[22] M. Yamashina, Y. Sei, M. Akita, M. Yoshizawa, *Nat. Commun.* **2014**, *5*, 4662.

[23] M. Yamashina, Y. Tanaka, R. Lavendomme, T. K. Ronson, M. Pittelkow, J. R. Nitschke, *Nature* **2019**, *574*, 511–515.

[24] G. H. Clever, P. Punt, *Acc. Chem. Res.* **2017**, *50*, 2233–2243.

[25] F. J. Rizzuto, D. M. Wood, T. K. Ronson, J. R. Nitschke, *J. Am. Chem. Soc.* **2017**, *139*, 11008–11011.

[26] K. Matsumoto, S. Kusaba, Y. Tanaka, Y. Sei, M. Akita, K. Aritani, M. Haga, M. Yoshizawa, *Angew. Chem. Int. Ed.* **2019**, *58*, 8463–8467.

[27] P. M. Allemand, A. Koch, F. Wudl, Y. Rubin, F. Diederich, M. M. Alvarez, S. J. Anz, R. L. Whetten, *J. Am. Chem. Soc.* 1991, *113*, 1050–1051.

[28] B. Chen, J. J. Holstein, S. Horiuchi, W. G. Hiller, G. H. Clever, *J. Am. Chem. Soc.* **2019**, *141*, 8907–8913.

[29] B. Chen, S. Horiuchi, J. J. Holstein, J. Tessarolo, G. H. Clever, *Chem. Eur. J.* **2019**, 25, 14921–14927.

[30] B. Chen, J. J. Holstein, A. Platzek, L. Schneider, K. Wu, G. H. Clever, *Chem. Sci.* **2022**, *13*, 1829–1834.

[31] E. M. Veen, B. L. Feringa, P. M. Postma, H. T. Jonkman, A. L. Spek, *Chem. Commun.* **1999**, *0*, 1709–1710.

[32] Y.-H. Xiao, Y. Shao, X.-X. Ye, H. Cui, D.-L. Wang, X.-H. Zhou, S.-L. Sun, L. Cheng, *Chinese Chem Lett* **2016**, *27*, 454–458.

[33] M. Han, D. M. Engelhard, G. H. Clever, *Chem. Soc. Rev.* **2014**, *43*, 1848–1860.

[34] M. Frank, M. D. Johnstone, G. H. Clever, *Chem. Eur. J.* **2016**, *22*, 14104–14125.

[35] S. Fukuzumi, T. Suenobu, M. Patz, T. Hirasaka, S. Itoh, M. Fujitsuka, O. Ito, *J. Am. Chem. Soc.* **1998**, *120*, 8060–8068.

[36] G. N. L. Mar, F. A. Walker, *J. Am. Chem. Soc.* **1973**, *95*, 6950–6956.

[37] D. S. Bethune, G. Meijer, W. C. Tang, H. J. Rosen, *Chem. Phys. Lett.* **1990**, *174*, 219–222.

[38] P. Paul, K.-C. Kim, D. Sun, P. D. W. Boyd, C. A. Reed, *J. Am. Chem. Soc.* **2002**, *124*, 4394–4401.

[39] Gaussian 16, Revision B.01, M. J. Frisch, G. W. Trucks, H. B. Schlegel, G. E. Scuseria, M. A. Robb, J. R. Cheeseman, G. Scalmani, V. Barone, G. A. Petersson, H. Nakatsuji, X. Li, M. Caricato, A. V. Marenich, J. Bloino, B. G. Janesko, R. Gomperts, B. Mennucci, H. P. Hratchian, J. V. Ortiz, A. F. Izmaylov, J. L. Sonnenberg, D. Williams-Young, F. Ding, F. Lipparini, F. Egidi, J. Goings, B. Peng, A. Petrone, T. Henderson, D. Ranasinghe, V. G. Zakrzewski, J.

Gao, N. Rega, G. Zheng, W. Liang, M. Hada, M. Ehara, K. Toyota, R. Fukuda, J. Hasegawa, M. Ishida, T. Nakajima, Y. Honda, O. Kitao, H. Nakai, T. Vreven, K. Throssell, J. A. Montgomery, Jr., J. E. Peralta, F. Ogliaro, M. J. Bearpark, J. J. Heyd, E. N. Brothers, K. N. Kudin, V. N. Staroverov, T. A. Keith, R. Kobayashi, J. Normand, K. Raghavachari, A. P. Rendell, J. C. Burant, S. S. Iyengar, J. Tomasi, M. Cossi, J. M. Millam, M. Klene, C. Adamo, R. Cammi, J. W. Ochterski, R. L. Martin, K. Morokuma, O. Farkas, J. B. Foresman, and D. J. Fox, Gaussian, Inc., Wallingford CT, **2016**.

[40] A. Burkhardt, T. Pakendorf, B. Reime, J. Meyer, P. Fischer, N. Stübe, S. Panneerselvam, O. Lorbeer, K. Stachnik, M. Warmer, P. Rödig, D. Göries, A. Meents, *Eur. Phys. J. Plus* **2016**, *131*, 56.

[41] W. Kabsch, *Acta Crystallogr. D: Biol. Crystallogr.* **2010**, *66*, 125–132.

[42] G. M. Sheldrick, *Acta Crystallogr. A: Found. Adv.* **2015**, *71*, 3–8.

[43] G. M. Sheldrick, *Acta Crystallogr. C: Struct. Chem.* **2015**, *71*, 3–8.

[44] C. B. Hübschle, G. M. Sheldrick, B. Dittrich, *J. Appl. Crystallogr.* **2011**, *44*, 1281–1284.

[45] D. Kratzert, J. J. Holstein, I. Krossing, *J. Appl. Crystallogr.* **2015**, *48*, 933–938.

[46] D. Kratzert, I. Krossing, *J. Appl. Crystallogr.* 2018, *51*, 928–934.

[47] A. Thorn, B. Dittrich, G. M. Sheldrick, *Acta Crystallogr. A Found Crystallogr.* **2012**, *68*, 448–451.

[48] A. L. Spek, *Acta. Crystallogr. C: Struct. Chem.* **2015**, *71*, 9–18.

[49] A. L. Spek, *Acta Crystallogr. D: Biol. Crystallogr.* **2009**, *65*, 148–155.

[50] S. Stoll, A. Schweiger, *J. Magn. Reson.* **2006**, *178*, 42–55**.**

[51] S. Hasegawa, S. L. Meichsner, J. J. Holstein, M. Kasanmascheff, G. H. Clever, *J. Am. Chem. Soc.* **2021**, *143*, 9718–9723.

[52] T. Konishi, M. Fujitsuka, O. Ito, *Chem. Lett.* **2000**, *29*, 202–203.

4 Encapsulation Capability of a Triptycene-Based Pd_2L_4 Coordination Cage towards carbon-rich guests

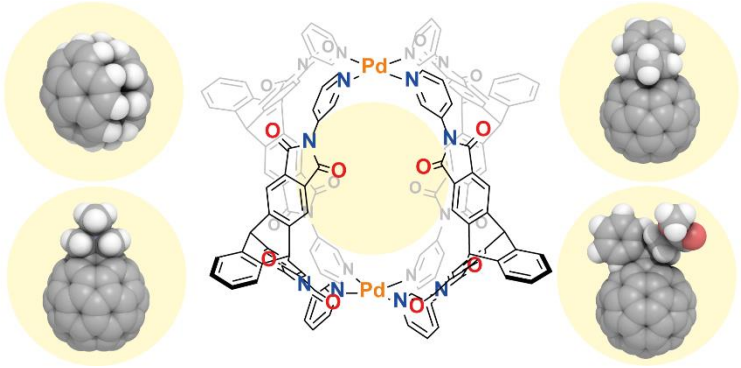

Abstract:

The encapsulation capability of a triptycene-based Pd_2L_4 coordination cage was investigated. The cage was found to encapsulate two molecules of corannulene and various C_{60} derivatives. Extraction of encapsulated $PC_{61}BM$, one of the most studied C_{60} derivative in organic photovoltaics, from the cage was performed by the addition of CS_2 into an acetonitrile solution of the $PC_{61}BM$ encapsulating cage. This extraction process can be performed in a layer-to-layer fashion. Thus, the recovered cage can be further used for $PC_{61}BM$ encapsulation and the following extraction process.

Contents of this chapter were published in:

S. Hasegawa, A. Baksi, B. Chen, G H. Clever, *Org. Mater*. **2022**, *4*, 222–227.

4.1 Introduction

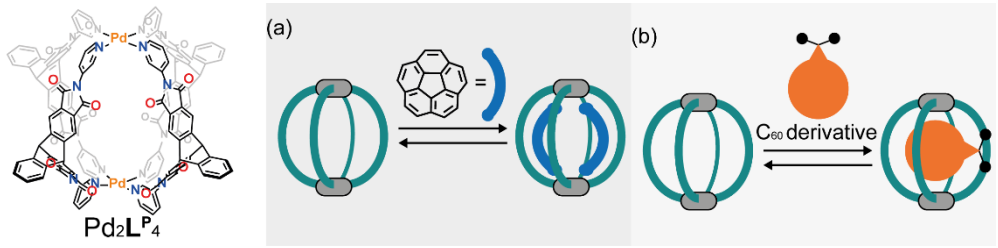

Figure 4.1.1 Schematic illustration of (a) encapsulation of two corannulene molecules and (b) encapsulation of a C_{60} derivative

Fullerene C_{60} is a globular-shaped allotrope of carbon utilized in a variety of fields.[1] For example, C_{60} and its derivatives have been used as an electron accepting material in organic solar cells.[2] Manipulation of the molecular orbital energies of fullerene derivatives is a crucial factor to tune the efficiency of charge transfer processes in such photovoltaic devices.[3] Many chemical reactions to modify C_{60} have been developed because such chemical modifications can tune its electronic properties, solubility, and packing manner in molecular composites.[4,5] For example, $PC_{61}BM$ is one of the most utilized C_{60} derivatives as an electron accepting and transporting material.[6] Although, covalent modification is a forthright method to manipulate the electronic properties of C_{60}, stereochemical control of chemical modifications of C_{60} is often difficult due to a similar reactivity of pristine C_{60} and its derivatives, resulting in the formation of multi-adduct isomers.[6,7] To facilitate chemical modification with regio-selectivity, a variety of strategies have been developed such as tether-directed syntheses and supramolecular-mask methods.[8–15] In the first strategy, the choice of substrate which has more than two reactive sites with C_{60} is a key point. First, the substrate reacts with C_{60} via one of the reactive sites. The length and the flexibility of the substrate defines the regio-selectivity of the following intramolecular addition. In the latter strategy, chemical modification of encapsulated C_{60} inside a host molecule facilitates regio-selectivity. The host molecule provides steric bulk to the confined C_{60} preventing it from random addition of multiple substrates on to the C_{60}. The encapsulation of C_{60} derivative inside coordination cages has been reported.[16–18] Amongst them, the coordination cages reported by Ribas and Yoshizawa display encapsulation and release of C_{60} derivatives.[16,18]

Well-established purification methods for C_{60} derivatives are largely limited to chromatographic separation, and thus, there is a space to be explored. Recently, the Clever group has reported several coordination cages based on organic ligands having a curved π-surface as shown in the chapters above.[19–21] These hosts provide a suitable cavity to accommodate C_{60} or C_{70} through π−π interactions. Strong encapsulation of fullerenes inside these coordination cages allows for a variety of applications as shown in *Chapters 1 & 3*.[22]

Some coordination cages composed of ligands with curved π-surfaces show unique guest binding behaviors.[23] Therefore, it can be presumed that $Pd_2\mathbf{L^P}_4$ should be able to encapsulate not only C_{60}, but also other guest compounds such as polyaromatic hydrocarbons and C_{60} derivatives. Based on this idea, the encapsulation capability of $Pd_2\mathbf{L^P}_4$ was investigated (**Figure 4.1.1**). As a result, $Pd_2\mathbf{L^P}_4$ was found to be able to encapsulate two molecules of corannulene (**Figure 4.1.1a**). In addition, $Pd_2\mathbf{L^P}_4$ showed an accommodation capability towards various C_{60} derivatives such as $PC_{61}BM$ (**Figure 4.1.1b**). Encouraged by the observation that $Pd_2\mathbf{L^P}_4$ can encapsulate $PC_{61}BM$ but not $PC_{62}BM$, a bis-adduct of $PC_{61}BM$, a facile yet non-disruptive method to liberate encapsulated $PC_{61}BM$ from $Pd_2\mathbf{L^P}_4$ was explored.

4.2 Results and discussion

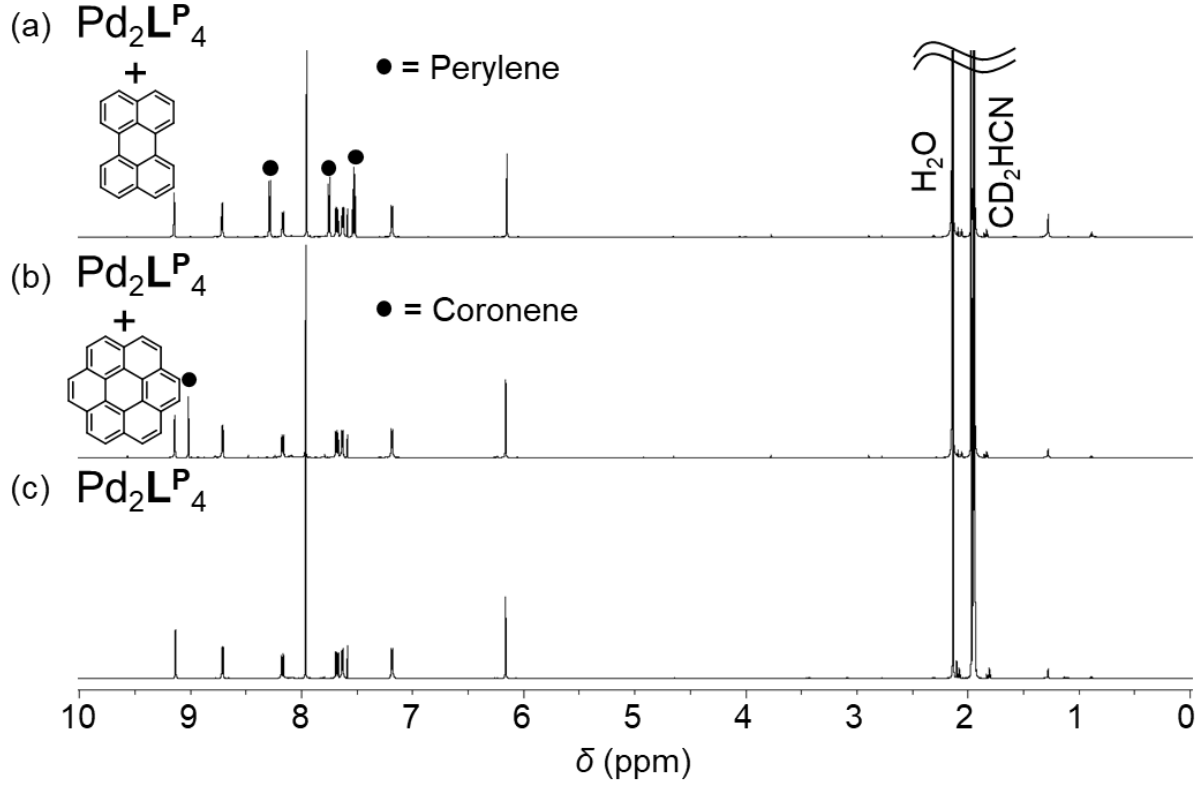

Figure 4.2.1 ^{1}H NMR spectrum of (a) $Pd_2\mathbf{L}^{\mathbf{P}}_4$ with perylene (CD_3CN, 0.70 mM, 600 MHz, 298 K) (b) $Pd_2\mathbf{L}^{\mathbf{P}}_4$ with coronene (CD_3CN, 0.70 mM, 600 MHz, 298 K) and (c) $Pd_2\mathbf{L}^{\mathbf{P}}_4$ (CD_3CN, 0.70 mM, 500 MHz, 298 K)

The triptycene-based Pd_2L_4 coordination cage was synthesized following the previous work aforementioned in *Chapter 3*.[22] The investigation of the guest scope of $Pd_2\mathbf{L}^{\mathbf{P}}_4$ started with small polyaromatic hydrocarbons (PAHs; **Figure 4.2.1**). Perylene, coronene and corannulene were tested for encapsulation. Among those molecules, only corannulene, known as a substructure of C_{60}, was incarcerated within the cage (**Figure 4.2.2a**) while coronene and perylene cannot be encapsulated. Specifically, an excess amount of solid corannulene was added into an acetonitrile solution of $Pd_2\mathbf{L}^{\mathbf{P}}_4$ and heated at 70 °C for 24 h. In the ^{1}H NMR spectrum, a new set of signals assignable to $(Cor)_2@Pd_2\mathbf{L}^{\mathbf{P}}_4$ by NMR analyses was observed besides empty $Pd_2\mathbf{L}^{\mathbf{P}}_4$. It was found that encapsulation of corannulene takes place pairwise in a cooperative manner with an exchange rate slower than the NMR time scale (**Figure 4.2.2b**). Two molecules of corannulene were found to be encapsulated inside $Pd_2\mathbf{L}^{\mathbf{P}}_4$ according to the ^{1}H NMR signal integration ratio between the cage and the encapsulated corannulenes signals

as well as the results of an NOESY experiment (**Figure 4.2.2c**). Furthermore, a prominent signal assignable to $(Cor)_2@Pd_2\mathbf{L^P}_4$ was also observed in the ESI-MS spectrum (**Figure 4.4.33**). Note that, the signals of free $Pd_2\mathbf{L^P}_4$ showed slightly different chemical shifts compared with the cage measured without corannulene. It can be assumed that this is originated from encapsulation of single corannulene with fast exchange between free corannulene. The ^{1}H NMR signal of the encapsulated corannulene guests appeared at 5.47 ppm. Comparing to the free corannulene, the signal of the encapsulated corannulenes showed an upfield shift by 2.42 ppm in acetonitrile, similar to what was observed in other reports.[23,24] In addition, the H^a signal of the pyridine coordination-sites which are supposed to be pointing inward the cavity also showed an upfield shift by 3.12 ppm, most likely due to interactions between the encapsulated corannulenes and these hydrogens, further supporting the encapsulation of corannulenes inside the cavity, not outside.[22]

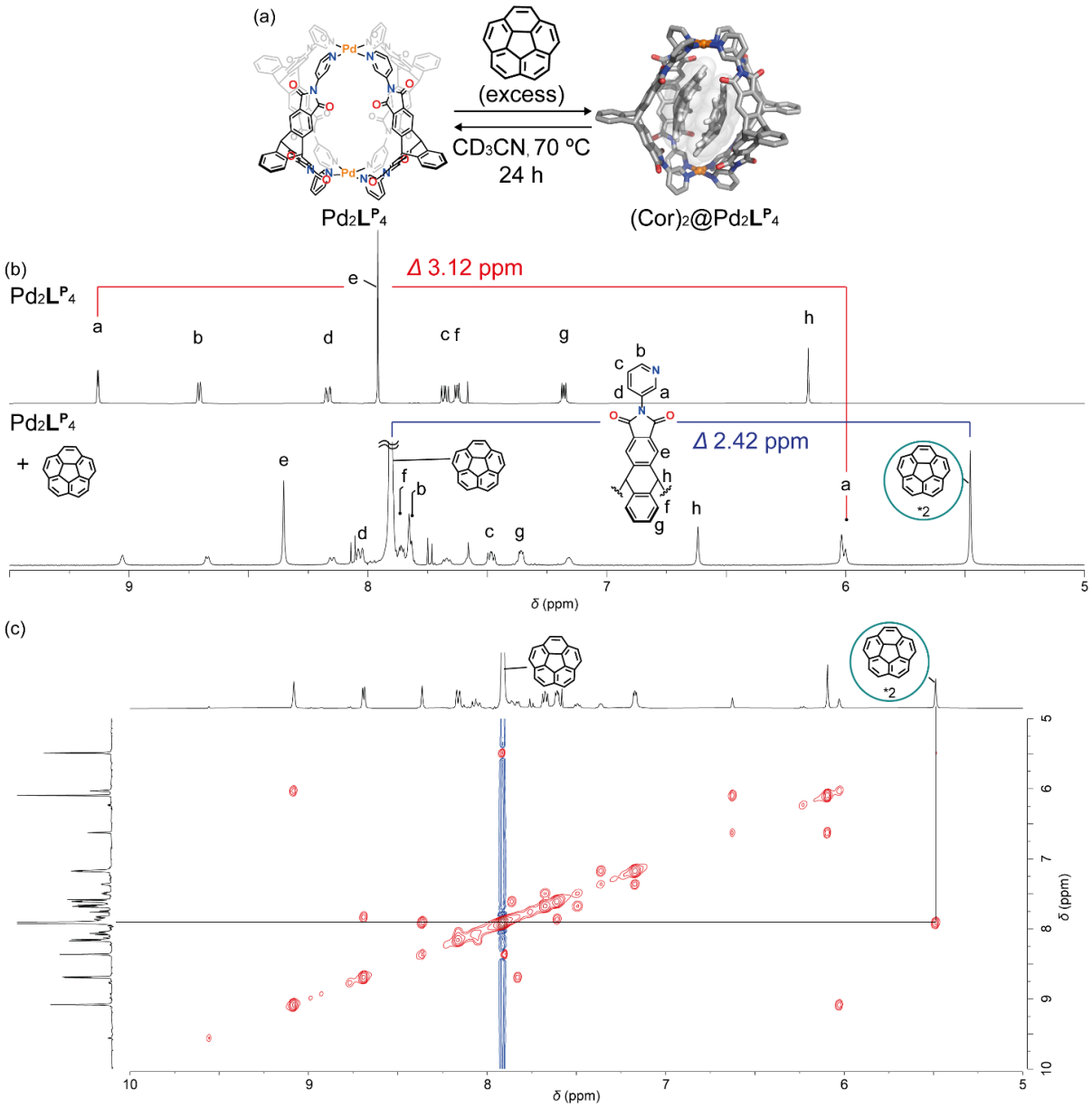

Figure 4.2.2 (a) Encapsulation of corannulene into $Pd_2\mathbf{L}^{\mathbf{P}}_4$ (b) ^{1}H NMR spectrum (CD_3CN, 500 MHz, 298 K) of $Pd_2\mathbf{L}^{\mathbf{P}}_4$ (top) and $(Cor)_2@Pd_2\mathbf{L}^{\mathbf{P}}_4$ (bottom) (c) ^{1}H-^{1}H NOESY spectrum (CD_3CN, 500 MHz, 298 K) of $(Cor)_2@Pd_2\mathbf{L}^{\mathbf{P}}_4$

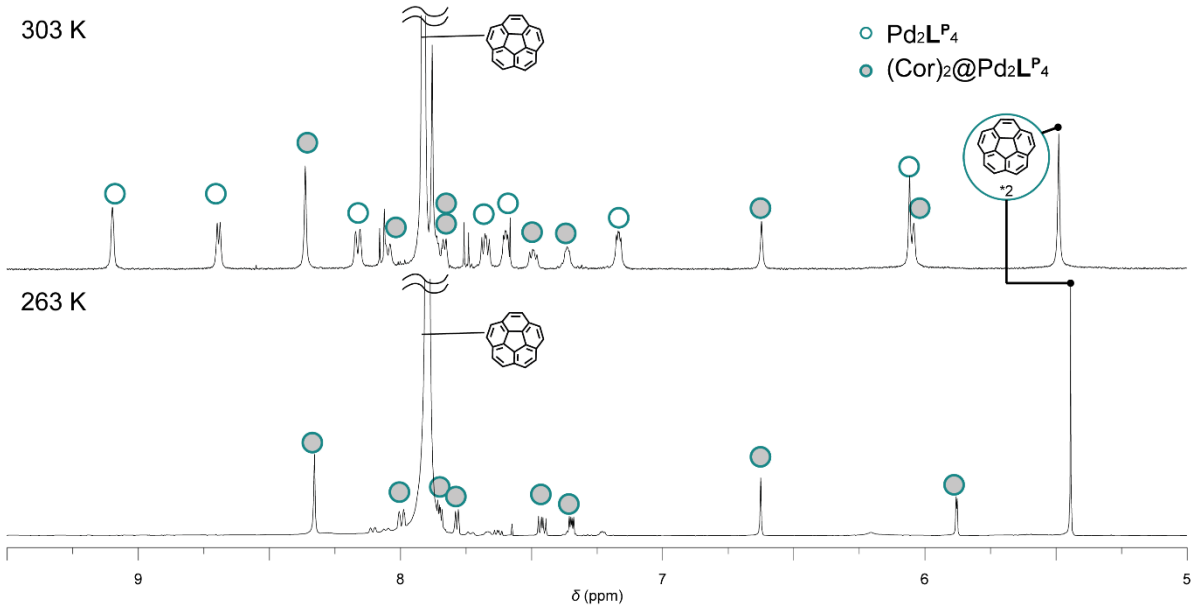

Figure 4.2.3 ^{1}H NMR spectrum (CD_3CN, 500 MHz) of $(Cor)_2@Pd_2\mathbf{L}^{P}_4$ at 303 K (top) and at 263 K (bottom)

In addition, DOSY analyses showed that the encapsulated corannulenes have a smaller diffusion coefficient compared with free corannulene in this acetonitrile solution (**Figure 4.4.31**). Furthermore, encapsulation of corannulenes was found to be temperature dependent. Upon cooling, the ratio of $(Cor)_2@Pd_2\mathbf{L}^{P}_4$ increased from 39 % (303 K) up to 77% (253 K, both at 0.70 mM cage concentration and excess of solid corannulene). During the VT-^{1}H NMR experiment, a host-guest complex of $Pd_2\mathbf{L}^{P}_4$ and single corannulene, $Cor@Pd_2\mathbf{L}^{P}_4$, was not independently observed on the NMR time scale (**Figure 4.2.3**). To further investigate the dynamic behavior of guest exchange, a ^{1}H NMR titration experiment was conducted. An acetonitrile solution of corannulene was titrated into an acetonitrile solution of $Pd_2\mathbf{L}^{P}_4$ in an NMR tube. As a result, all of the peaks from $Pd_2\mathbf{L}^{P}_4$ showed slight shifts ($\Delta\delta_{max}$ = 0.02 ppm) with the appearance of $(Cor)_2@Pd_2\mathbf{L}^{P}_4$ over the addition of 7 eq. of corannulene (**Figure 4.2.4**). These results indicate that encapsulation of single corannulene is in a fast equilibrium most likely due to the weak encapsulation of single corannulene, while a pair of corannulenes is bound in slow exchange (**Figure 4.2.5**).

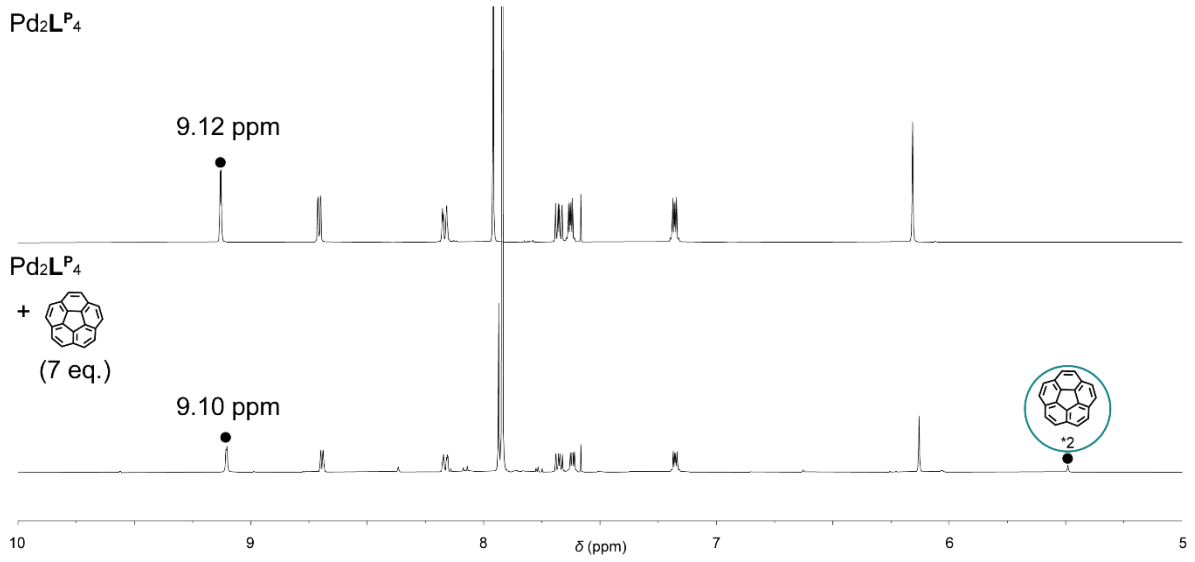

Figure 4.2.4 ^{1}H NMR spectrum (CD_3CN, 500 MHz, 298 K) of $Pd_2\mathbf{L}^{\mathbf{P}}_4$ without corannulene (top) and with 7 eq. of corannulene (bottom)

To gain additional insight into this process, DFT calculations at the M06-2X/Lanl2dz level of theory were performed. As a result, encapsulation of two corannulenes was implied to be a more favorable process than single corannulene encapsulation (**Table 4.4.2**). The energy gain of the two corannulenes encapsulation process was more than two-times larger than the single corannulene encapsulation in $Pd_2\mathbf{L}^{\mathbf{P}}_4$. In the obtained geometry, convex-concave interactions between the encapsulated corannulenes and the ligands were implied. As shown above, perylene and coronene cannot be encapsulated inside the cage. This is probably due to lack of such convex-concave interactions with the curved triptycene ligands.

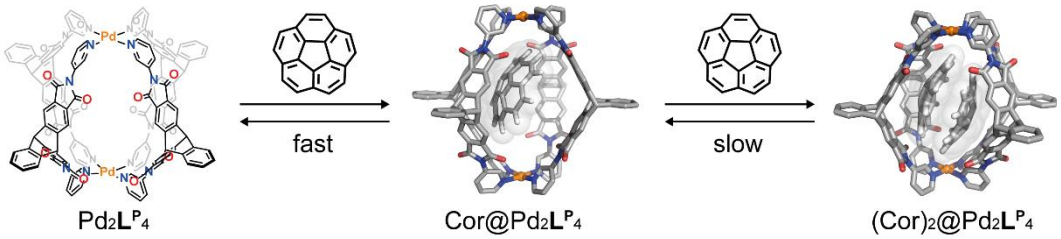

Figure 4.2.5 Schematic illustration of the kinetic of corannulene encapsulation into $Pd_2\mathbf{L}^{\mathbf{P}}_4$; the optimized geometries at M06-2X/Lanl2dz level of theory are shown for $Cor@Pd_2\mathbf{L}^{\mathbf{P}}_4$ and $(Cor)_2@Pd_2\mathbf{L}^{\mathbf{P}}_4$

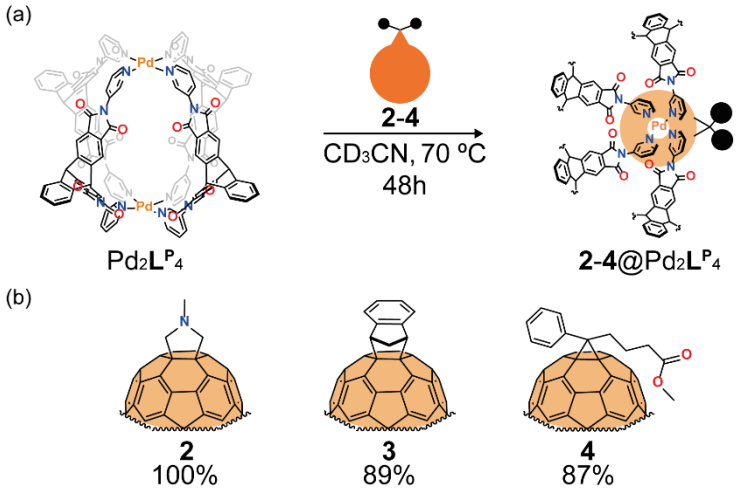

Figure 4.2.6 (a) Encapsulation of **2**-**4** into $Pd_2\mathbf{L}^{P}_4$ (b) chemical structure of **2**-**4** with encapsulation ratio

Next, encapsulation of a variety of C_{60} derivatives inside $Pd_2\mathbf{L}^{P}_4$ was investigated (**Figure 4.2.6**). C_{60} derivatives were added in an acetonitrile solution of $Pd_2\mathbf{L}^{P}_4$ and the suspension was stirred at 70 °C for 48 h. Afterwards, the residual solid C_{60} derivatives were removed by filtration. C_{60} derivatives **2**-**4** were encapsulated in 87-100% yield determined by ^{1}H NMR analyses measured at room temperature (**Figure 4.2.7a**). In the ^{1}H NMR spectra of the host-guest complexes, a new set of signals was observed in addition to empty $Pd_2\mathbf{L}^{P}_4$. The host-guest complexes should have a lower symmetry than the parental host because of the bulky substituent on the C_{60} derivatives. As shown in **Figure 4.2.7a**, as expected, in the ^{1}H NMR spectra of **2**-**4**@$Pd_2\mathbf{L}^{P}_4$, two sets and four sets of signals were observed for the pyridine coordination-site and the triptycene-backbone protons, respectively, which supports the encapsulation of the C_{60} derivatives (**Figure 4.4.2**, **Figure 4.4.8**, and **Figure 4.4.16**). In addition, ^{1}H DOSY NMR analyses showed that all of the new signals belong to a single species, having a comparable hydrodynamic radius to C_{60}@$Pd_2\mathbf{L}^{P}_4$ (**Figure 4.4.5, Figure 4.4.13** and **Figure 4.4.21**).[22] The formation of the **2**-**4**@$Pd_2\mathbf{L}^{P}_4$ host-guest complexes was further supported by ESI-MS analyses (**Figure 4.2.7b**, **Figure 4.4.7**, **Figure 4.4.15**, and **Figure 4.4.23**). Further, the small space in between the ligands found in the modelled geometry of **2**@$Pd_2\mathbf{L}^{P}_4$ implies that encapsulation of bis-adducts, which can be obtained as side-products of synthesis of C_{60} derivatives, should be sterically difficult (**Figure 4.2.8 a**-**b**). As can be seen in the DFT optimized molecular model, four ligands should be forced to gather to make the large enough window for the bulky substituent of **4** (**Figure 4.2.8c**), which should exclude encapsulation of $PC_{62}BM$. According to this

assumption, an excess amount of solid $PC_{62}BM$, a bis-adduct of **4** commercially available as a mixture of regio-isomers, was heterogeneously mixed in an acetonitrile solution of $Pd_2\mathbf{L}^{\mathbf{P}}_4$ for 24h at 70 °C. After heating, the residual solid $PC_{62}BM$ was removed by filtration. In the ^{1}H NMR spectrum of the resulting filtrate, only one set of signals of empty $Pd_2\mathbf{L}^{\mathbf{P}}_4$ was observed. (**Figure 4.4.43** and **Figure 4.4.45**) Therefore, probably due to steric reasons, encapsulation of $PC_{62}BM$ is not likely possible. This result implies that $Pd_2\mathbf{L}^{\mathbf{P}}_4$ preferably encapsulates C_{60} mono-adducts over their bis-adducts. Indeed, only **4**@$Pd_2\mathbf{L}^{\mathbf{P}}_4$ was obtained as a major species in 66% yield when 2.5 equivalent of **4** and $PC_{62}BM$ each were dispersed into an acetonitrile solution of $Pd_2\mathbf{L}^{\mathbf{P}}_4$ in the presence of minute amount of CS_2 (**Figure 4.4.46**).

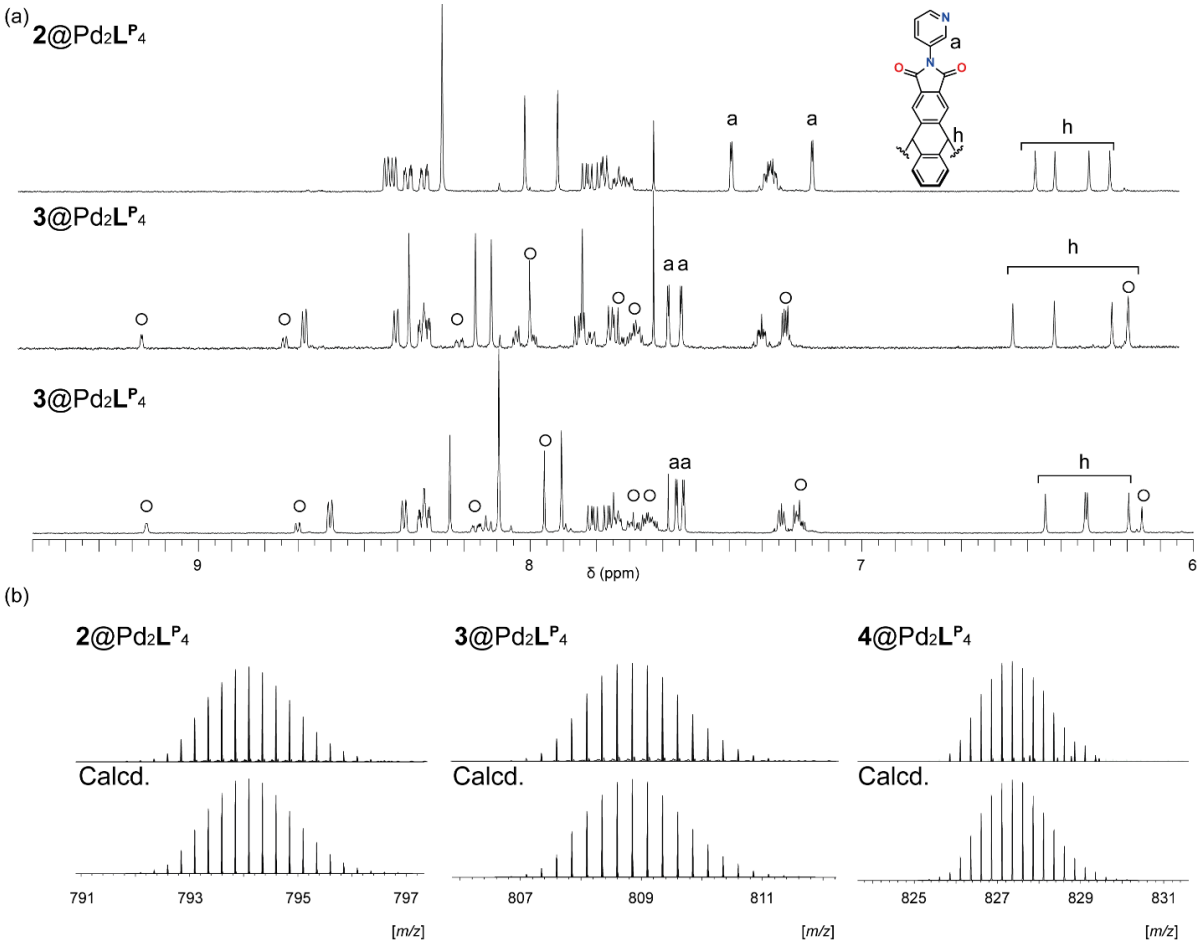

Figure 4.2.7 (a) ^{1}H NMR spectra (CD_3CN, 0.35 mM, 500 MHz, 298 K) of **2**-**4**@$Pd_2\mathbf{L}^{\mathbf{P}}_4$; (b) ESI-MS spectra (positive) of **2**-**4**@$Pd_2\mathbf{L}^{\mathbf{P}}_4$ with calculated isotopic patterns

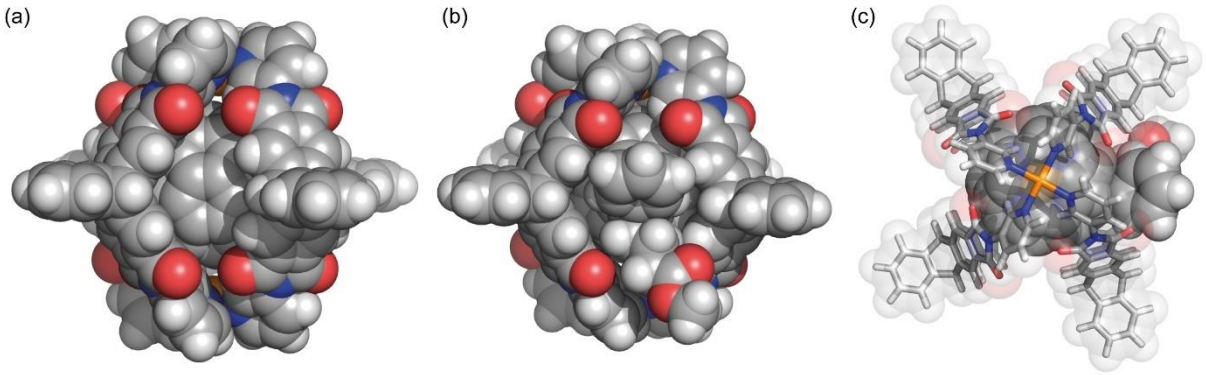

Figure 4.2.8 The optimized geometry of **4**@$Pd_2\mathbf{L^P}_4$ at B3LYP/6-31G(d) for the elements C, H, N, and O and B3LYP/Lanl2dz for Pd (a) the opposite side of the chemical appendix of $PC_{61}BM$ and (b) on the side of the chemical appendix and (c) the view from top

Take it into account that, the yield of **4**@$Pd_2\mathbf{L^P}_4$ was 87% while the quantitative formation of **2**@$Pd_2\mathbf{L^P}_4$ was observed, there should be an equilibrium between the encapsulated guest and the free guest slightly solubilized in the acetonitrile solution. In many cases, encapsulation of guest molecules in a very polar solvent are highly affected by solvophobic interactions. Hydrophobic organic guests tend to be captured inside a non-polar cavity rather than being solvated.[25] Thus, simple addition of a better solvent for the C_{60} derivatives to the host-guest complex solution was tested with the aim that the equilibrium between the confined guest and the free guest should lean towards releasing of the guest molecule into the mixed solvent.

Based on this hypothesis, we tried various organic solvents which are commonly employed to solubilize C_{60}. Among those organic solvents, addition of CS_2 was found to extract encapsulated guest **4** into the solvent from the cage. 26 vol% of CS_2 was added to an acetonitrile solution of **4**@$Pd_2\mathbf{L^P}_4$ and the mixture was shaken for several seconds and let stand for several minutes (**Figure 4.2.9**). After this resting time, two layers were obtained, where the upper layer is a transparent acetonitrile solution of the empty host and the bottom layer is a reddish CS_2 solution containing the extracted compound **4**. The purity of extracted **4** was confirmed by ^{1}H NMR measurement (**Figure 4.4.42**). The acetonitrile solution recovered from the upper layer was found to contain intact $Pd_2\mathbf{L^P}_4$, which shows that this method is non-disruptive (**Figure 4.2.9**).

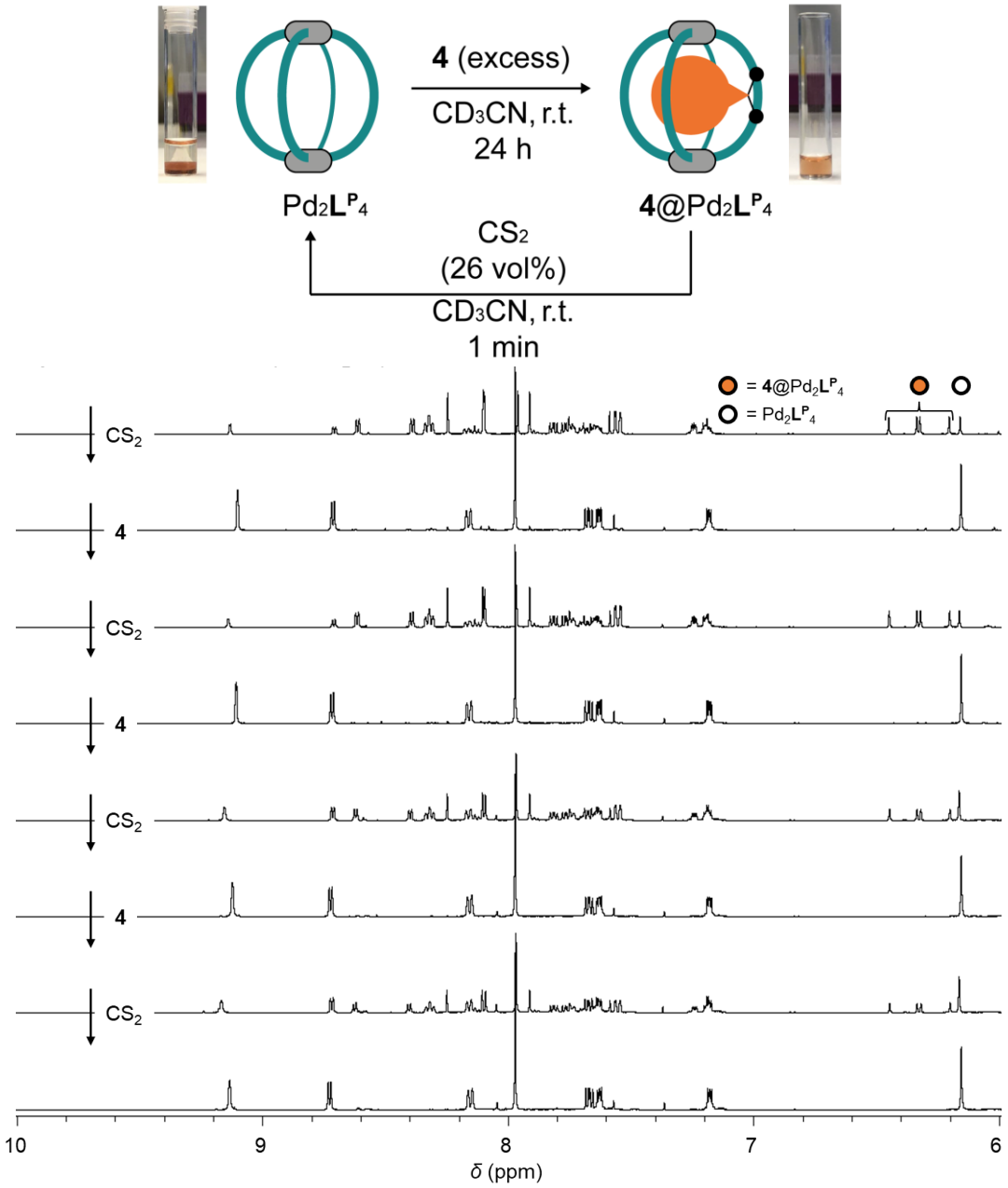

Figure 4.2.9 ^{1}H NMR spectra (CD_3CN, 500 MHz, 298 K) showing repetitive uptake and release of **4** using $Pd_2\mathbf{L}^{\mathbf{P}}_4$

Thus, we tackled repetitive encapsulation and extraction of **4** for 4 cycles (**Table 4.2.1**). After extracting **4** from **4**@$Pd_2\mathbf{L}^{\mathbf{P}}_4$, the mixture was cooled to –78 °C and the CS_2 layer was removed by decanting. The recovered acetonitrile solution of $Pd_2\mathbf{L}^{\mathbf{P}}_4$ was further tested for the further cycles. As a result, $Pd_2\mathbf{L}^{\mathbf{P}}_4$ was proven to encapsulate and liberate **4** in a recycling yet non-disruptive manner. However, the decline of the encapsulation ratio was observed over repetitive cycles. It is presumed that the

observed decrease of the encapsulation ratio can be attributed to a slight miscibility of CS_2 in the acetonitrile solution.

Table 4.2.1 Recycling encapsulation and release of **4** using $Pd_2\mathbf{L^P}_4$; the yields were determined by ^{1}H NMR analyses

Cycle	Yield (%)
1st	80.5
2nd	80.3
3rd	62.9
4th	52.2

4.3 Conclusion

The encapsulation capability of coordination cage $Pd_2\mathbf{L^P}_4$ towards corannulene and various C_{60}-derivatives has been investigated. The curved π–surface of the triptycene-backbone of $\mathbf{L^P}$ facilitates a nanoscopic cavity in which a variety of curved aromatic compounds can be encapsulated in high to quantitative yields. $Pd_2\mathbf{L^P}_4$ showcases the encapsulation of two molecules of corannulene in acetonitrile. In addition, $Pd_2\mathbf{L^P}_4$ encapsulates mono-adducts of C_{60} **2**-**4** leading to a host-guest complex having a lower symmetry. Uptake and extraction of **4** using $Pd_2\mathbf{L^P}_4$ were demonstrated in a recycling way. The uptake and extraction process can be accomplished in a layer-to-layer fashion by using two different solvents. Furthermore, $Pd_2\mathbf{L^P}_4$ was found not to encapsulate bis-adducts of fullerene derivatives such as $PC_{62}BM$, which should make $Pd_2\mathbf{L^P}_4$ a candidate for sustainable fullerene mono-adduct purification systems.

4.4 Appendix

4.4.1 Materials and methods

Unless otherwise stated, all chemicals were purchased from commercial sources and used as received. $[Pd(MeCN)_4](BF_4)_2$, **2**-**4**, and $PC_{62}BM$ as a mixture of isomers were purchased from Sigma-Aldrich. Corannulene was purchased from TCI.inc. Bruker ESI-timsTOF and compact mass spectrometers using Agilent tune mix as calibrant. NMR experiments were performed using Bruker AV 500 Avance NEO, Bruker AV 600 Avance FT-NMR, Bruker Avance III HD 700 MHz spectrometers. ^{1}H and ^{13}C signals were referenced to the residual solvent peak: acetonitrile (1.94 ppm,118.26 ppm), chloroform (7.26 ppm). DFT calculation were performed using Gaussian Gaussian 16, Revision B.01.[26] Hydrodynamic radii of compounds were calculated from Stokes-Einstein equation (eq 1) where D is a diffusion coefficient, k_B is Boltzman constant, T is a temperature, η is a viscosity of the solvent, and r_H is a hydrodynamic radius of interest. ^{1}H DOSY NMR spectra were recorded with a dstebpgp3s pulse sequence with diffusion delays D20 of 0.08 s and gradient powers P30 of 1200. T_1 analyses of the corresponding signals in the 1D spectra were performed to obtain the diffusion coefficients D using the STEJSKAL-TANNER-Equation.

$$D = \frac{k_B T}{6\pi\eta r_H} \quad \text{(eq 1)}$$

4.4.2 Encapsulation of C_{60} derivatives into $Pd_2L^P_4$

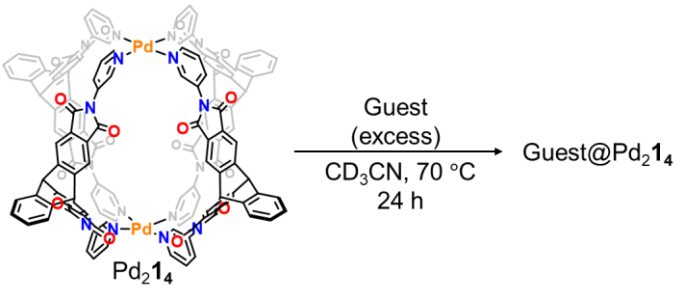

Figure 4.4.1 Encapsulation of guest molecules into $Pd_2\mathbf{L}^{\mathbf{P}}_4$

General procedure: To an acetonitrile solution of $Pd_2\mathbf{L}^{\mathbf{P}}_4$ (0.35 mM, 1.0 mL, 0.35 μmol), synthesized following the literature,[22] in a vial was added an excess amount of solid guest. The heterogenous mixture was stirred under heating at 70 °C for 24 h and NMR measurements were carried out. The encapsulation ratio was estimated from the ^{1}H NMR integral ratio.

4.4.2.1 Encapsulation of 2

^{1}H NMR (500 MHz, CD_3CN, 298 K): *δ* (ppm) **b** 8.38 (d, *J* = 5.2 Hz, 4H), **b** 8.37 (d, *J* = 5.2 Hz, 4H), **d** 8.32 (ddd, *J* = 8.5, 2.2, 1.2 Hz, 4H), **d** 8.27 (ddd, *J* = 8.5, 2.2, 1.2 Hz, 4H), **e*2** 8.22 (s, 8H), **e** 7.97 (s, 4H), **e** 7.87 (s, 4H), **c** 7.78 (dd, *J* = 8.5, 5.6 Hz, 4H), **c** 7.74 (dd, *J* = 8.5, 5.6 Hz, 4H), **f*4** 7.73-7.64 (m, 8H), **a** 7.34 (d, *J* = 2.1 Hz, 4H), **g*4** 7.26-7.20 (m, 8H), **a** 7.10 (d, *J* = 2.1 Hz, 4H), **h** 6.43 (s, 2H), **h** 6.37 (s, 2H), **h** 6.27 (s, 2H), **h** 6.20 (s, 2H), **i** 4.06 (s, 4H), **j** 3.57 (s, 3H)

^{13}C NMR (150 MHz, CD_3CN, 298 K): *δ* (ppm) 166.15, 166.00, 165.71, 165.60, 154.38, 153.71, 153.49, 153.44, 153.30, 152.23, 152.15, 147.56, 147.45, 146.51, 146.10, 145.73, 145.18, 144.80, 144.15, 144.02, 143.35, 143.01, 142.99, 142.83, 142.81, 142.27, 142.13, 142.03, 141.02, 140.74, 140.28, 140.16, 138.79, 135.51, 132.62, 132.13, 131.09, 131.06, 130.96, 130.61, 129.45, 129.04, 127.76, 127.74, 127.70, 127.69, 126.24, 126.20, 126.16, 126.01, 121.91, 121.76, 121.58, 121.55, 71.41, 69.57, 54.77, 54.70, 54.58, 42.11

DOSY: Diffusion coefficient $D = 5.26 \times 10^{-10}$ m^2s^{-1}, hydrodynamic radius r_H was calculated to be 12.4 Å

ESI MS (positive): found: 794.0997 and 1087.7986; calculated for $[(C_{34}H_{18}N_4O_4)_4Pd_2(C_{63}NH_7)]^{4+}$ and $[(C_{34}H_{18}N_4O_4)_4Pd_2(C_{63}NH_7)(BF_4)]^{3+}$ to be 794.1005 and 1087.8021 respectively

4.4.2.1.1 ^{1}H NMR spectra of 2@$Pd_2L^P_4$

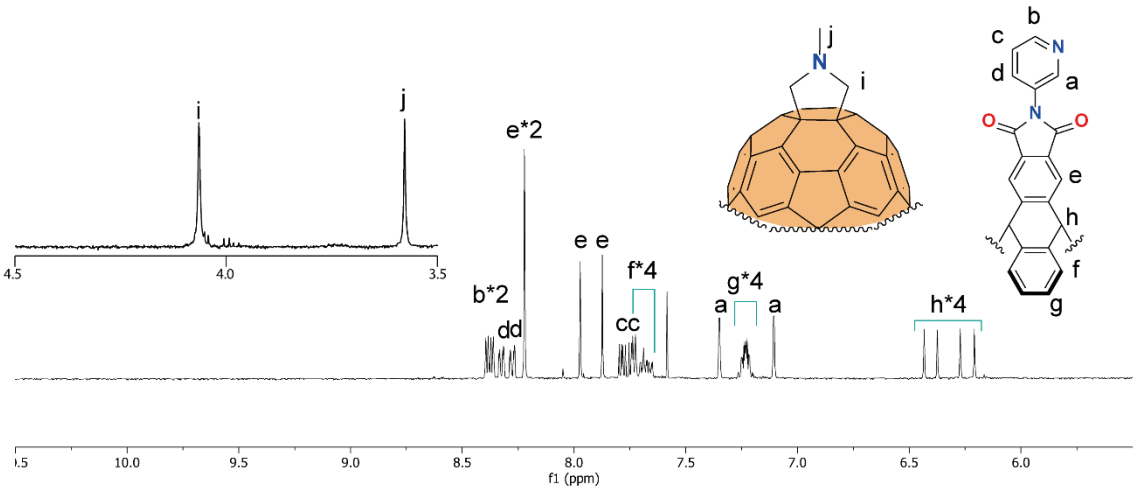

Figure 4.4.2 ^{1}H NMR spectrum of **2**@$Pd_2\mathbf{L}^{P}_4$ (CD_3CN, 500 MHz, 298 K)

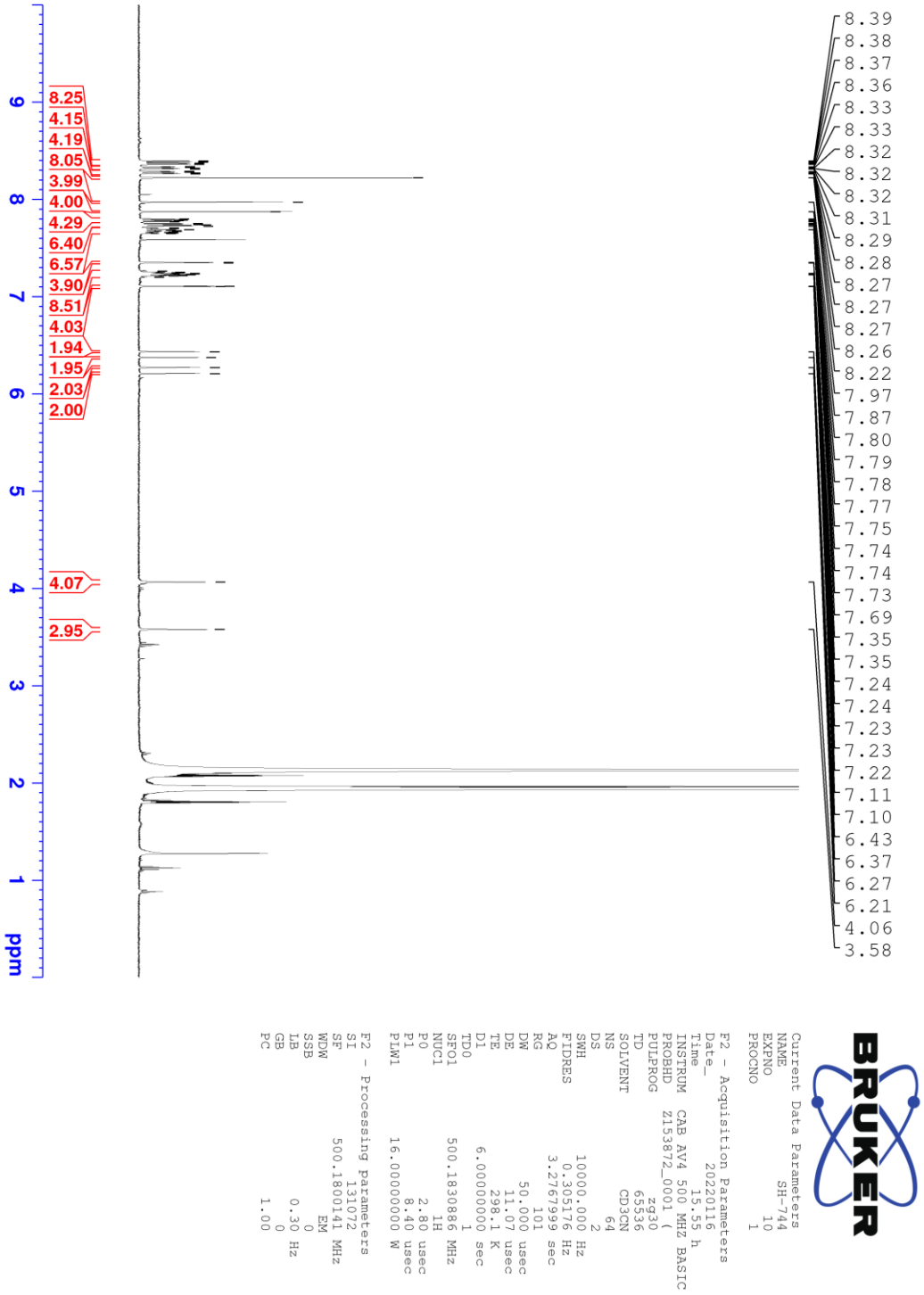

Figure 4.4.3 ^{1}H NMR spectrum of **2**@$Pd_2\mathbf{L}^{\mathbf{P}}_4$ (CD_3CN, 500 MHz, 298 K)

4.4.2.1.2 ^{1}H-^{1}H COSY NMR spectrum of 2@$Pd_2L^P_4$

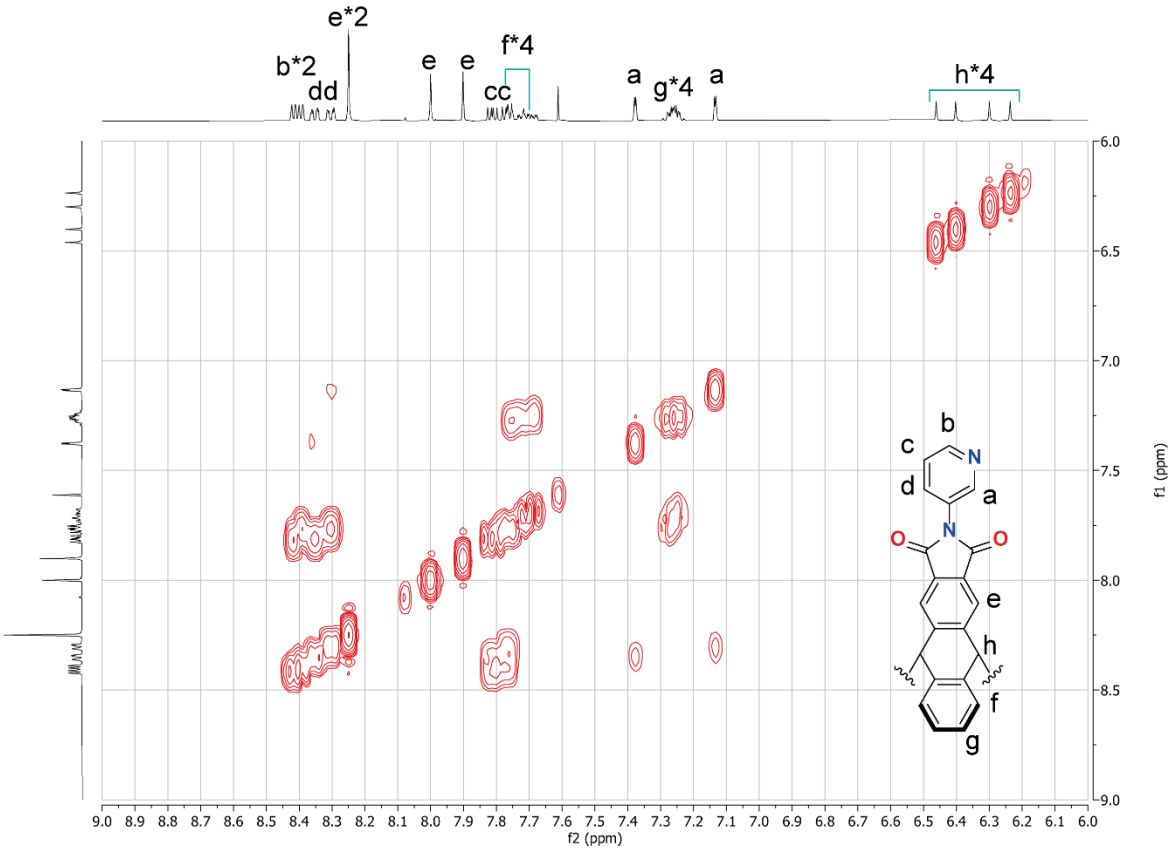

Figure 4.4.4 ^{1}H-^{1}H COSY NMR spectrum of **2**@$Pd_2\mathbf{L}^{P}_4$ (CD_3CN, 500 MHz, 298 K)

4.4.2.1.3 1H DOSY NMR spectrum of 2@Pd2LP4

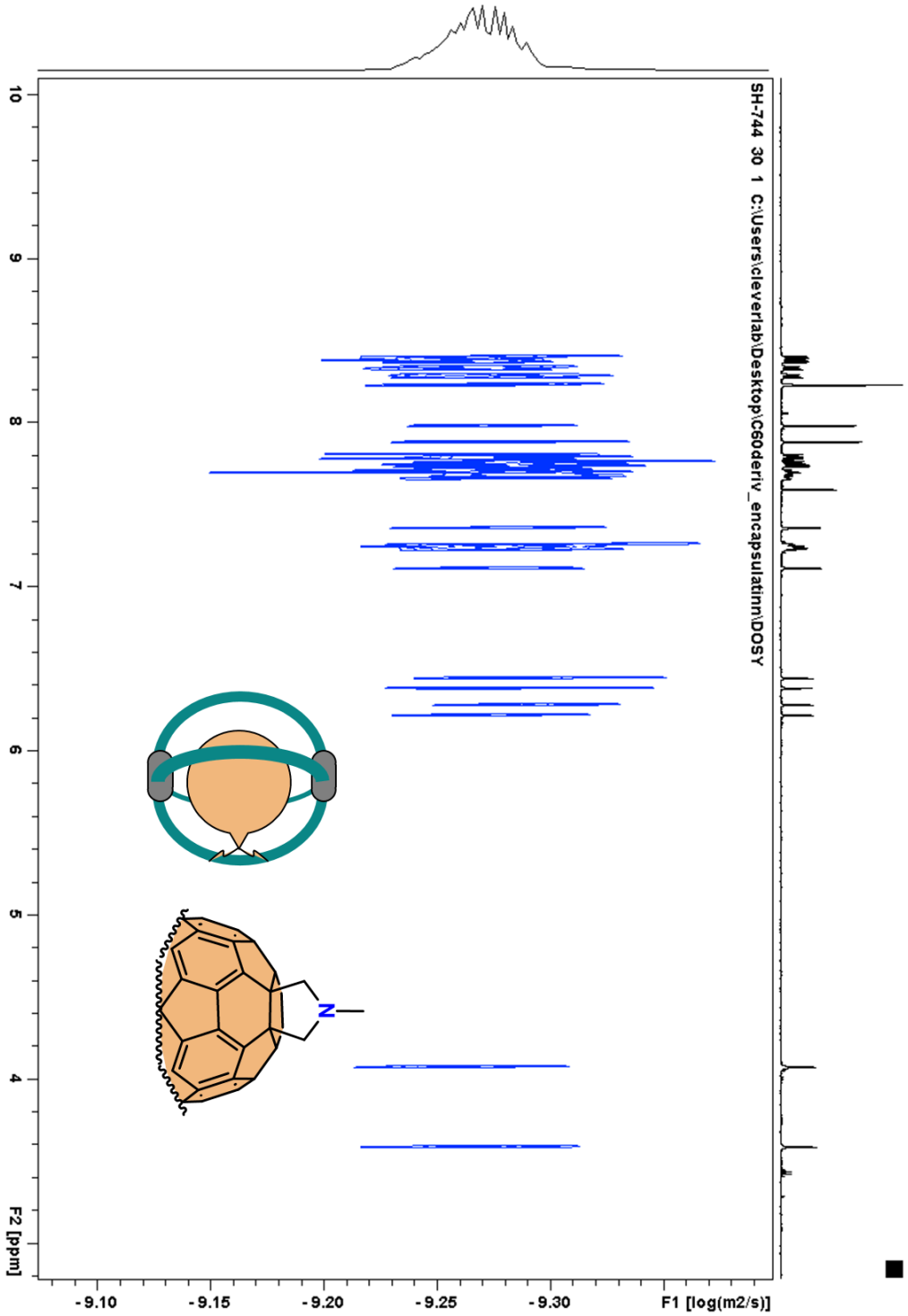

Figure 4.4.5 ^{1}H DOSY NMR spectrum of **2**@$Pd_2\mathbf{L}^{P}_4$ (CD_3CN, 500 MHz, 298 K)

4.4.2.1.4 ^{13}C NMR spectrum of 2@Pd$_2$L$^P_4$

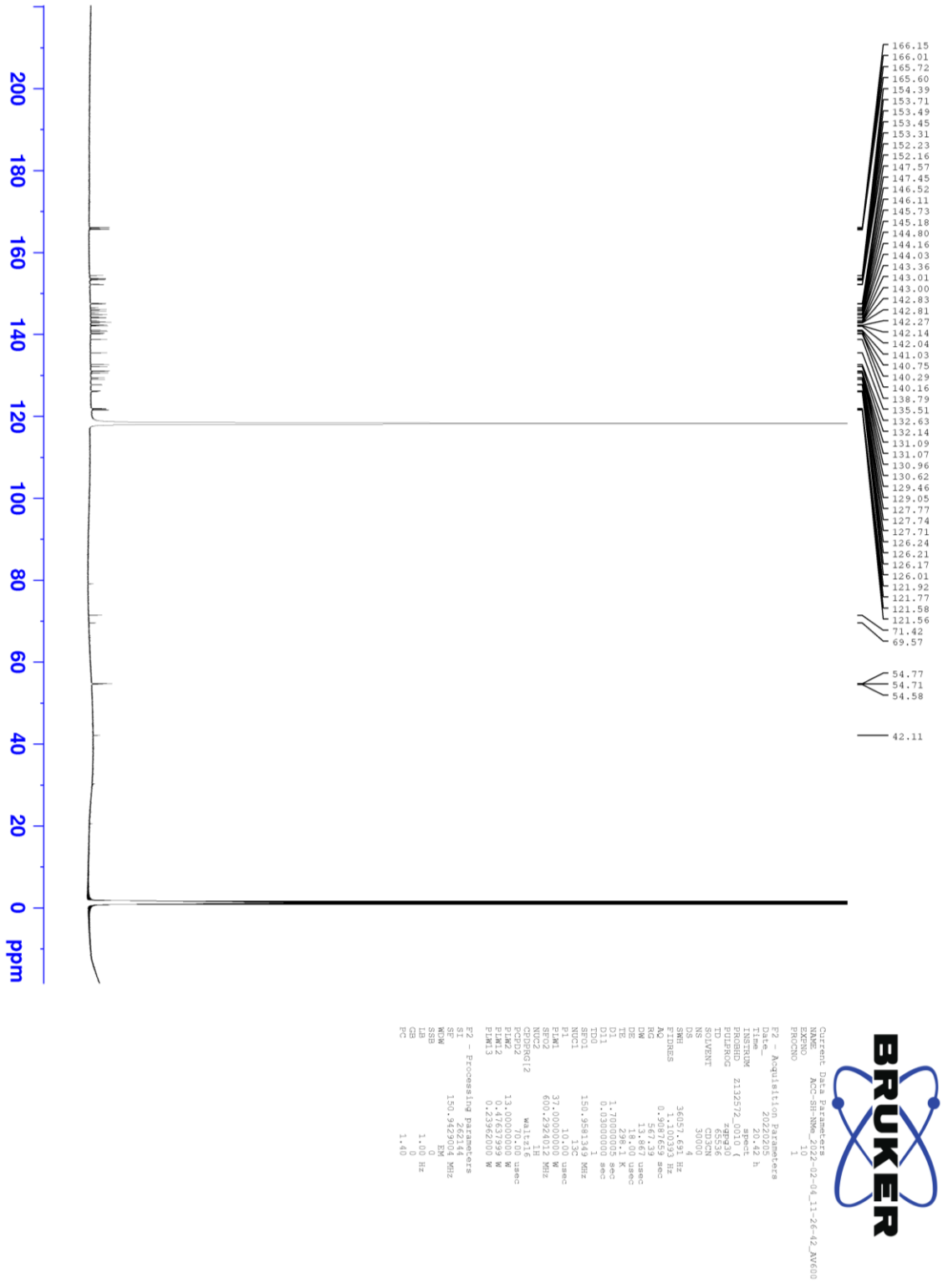

Figure 4.4.6 ^{13}C NMR spectrum of **2**@Pd$_2$**L**$^P_4$ (CD_3CN, 150 MHz, 298 K)

4.4.2.1.5 ESI MS spectrum of 2@$Pd_2L^P_4$

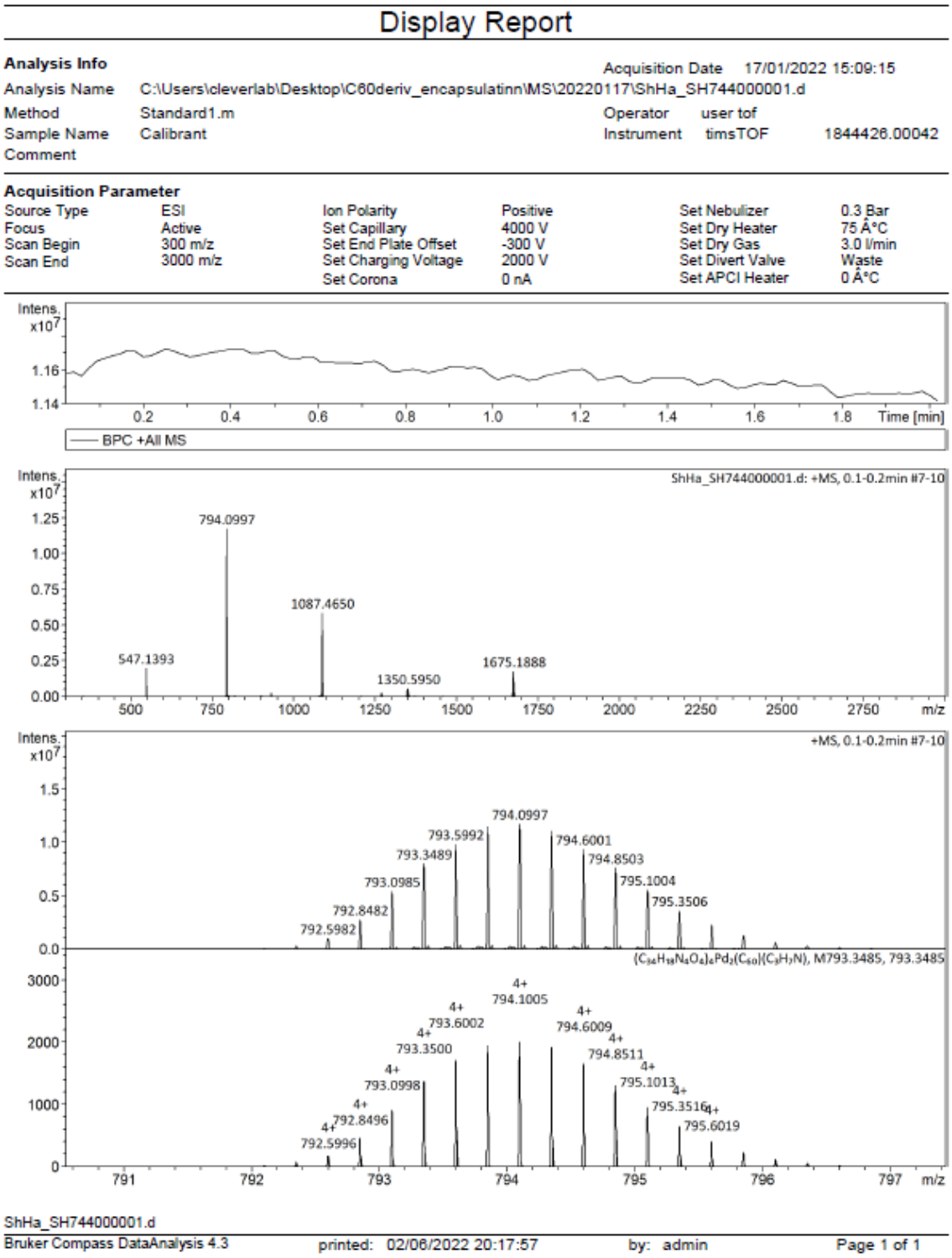

Figure 4.4.7 ESI MS spectrum of **2**@$Pd_2L^P_4$ (positive)

4.4.2.2 Encapsulation of 3

^{1}H NMR (500 MHz, CD_3CN, 298 K): *δ* (ppm) **b** 8.63 (d, *J* = 5.2 Hz, 4H), **b** 8.36 (d, *J* = 5.2 Hz, 4H), **e** 8.32 (s, 4H), **d** 8.28 (ddd, *J* = 8.5, 2.2, 1.2 Hz, 4H), **d** 8.26 (ddd, *J* = 8.5, 2.2, 1.2 Hz, 4H), **e** 8.12 (s, 4H), **e** 8.07 (s, 4H), **k/l** 7.99 (m, 2H), **k/l** 7.94 (m, 2H), **c** 7.80 (dd, *J* = 8.5, 5.6 Hz, 4H), **e** 7.79 (s, 4H), **c** 7.70 (dd, *J* = 8.5, 5.6 Hz, 4H), **f*4** 7.70-7.61 (m, 8H), **a** 7.53 (d, *J* = 2.1 Hz, 4H), **a** 7.50 (d, *J* = 2.1 Hz, 4H), **g*4** 7.26-7.17 (m, 8H), **h** 6.50 (s, 2H), **h** 6.37 (s, 2H), **h** 6.20 (s, 2H), **h** 6.15 (s, 2H), **i** 4.40(s, 2H), **j** 3.04 (m, 1H), **j** 2.70 (m, 1H)

^{13}C NMR (150 MHz, CD_3CN, 298 K): *δ* (ppm) 166.16, 166.13, 165.96, 165.68, 165.51, 156.20, 155.44, 153.78, 153.51, 153.36, 153.09, 153.01, 152.48, 151.80, 150.25, 148.66, 148.26, 147.15, 146.57, 146.51, 146.10, 145.71, 145.64, 145.52, 145.26, 145.01, 144.96, 144.76, 144.71, 144.19, 143.85, 143.84, 143.16, 143.11, 143.04, 143.02, 142.97, 142.85, 142.83, 142.61, 142.40, 142.34, 142.13, 142.03, 141.97, 141.13, 141.12, 140.99, 140.72, 140.48, 140.47, 139.29, 138.21, 138.04, 137.23, 136.41, 132.94, 132.63, 132.48, 131.07, 131.03, 130.90, 130.68, 130.37, 129.42, 129.26, 129.23, 128.37, 127.70, 127.69, 127.66, 127.53, 126.26, 126.24, 126.22, 126.02, 125.96, 125.19, 121.83, 121.63, 121.59, 121.30, 120.71, 76.22, 58.71, 54.85, 54.79, 54.64, 54.48, 48.10 (13 signals from empty $Pd_2\mathbf{L^P}_4$)

DOSY: Diffusion coefficient $D = 5.47 \times 10^{-10}$ m^2s^{-1}, hydrodynamic radius r_H was calculated to be 12.0 Å

ESI MS (positive): found: 808.8505 and 1107.4664; calculated for $[(C_{34}H_{18}N_4O_4)_4Pd_2(C_{69}H_8)]^{4+}$ and $[(C_{34}H_{18}N_4O_4)_4Pd_2(C_{69}H_8)(BF_4)]^{3+}$ to be 808.8518 and 1107.4704 respectively

4.4.2.2.1 ^{1}H NMR spectra of 3@$Pd_2L^P_4$

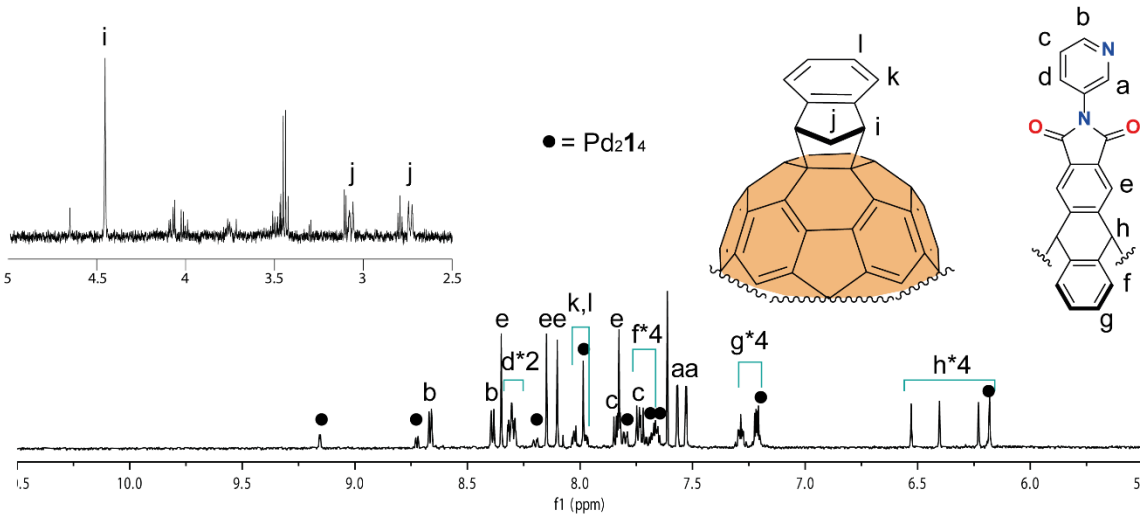

Figure 4.4.8 ^{1}H NMR spectrum of **3**@$Pd_2\mathbf{L}^{P}_4$ (CD_3CN, 500 MHz, 298 K)

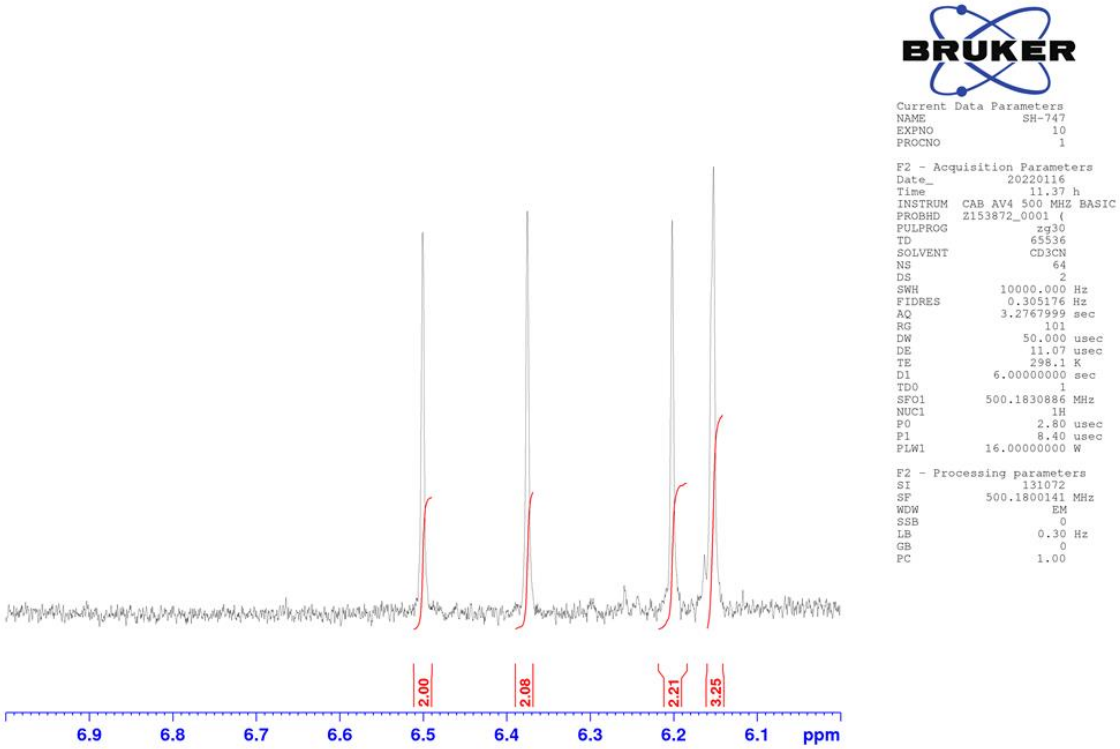

Figure 4.4.9 ^{1}H NMR integration ratio used to determine the encapsulation ratio of **3**@$Pd_2\mathbf{L}^{P}_4$ **100 * (2.21*4) / (2.21*4 + (3.25-2.21)) = 89.4 %**

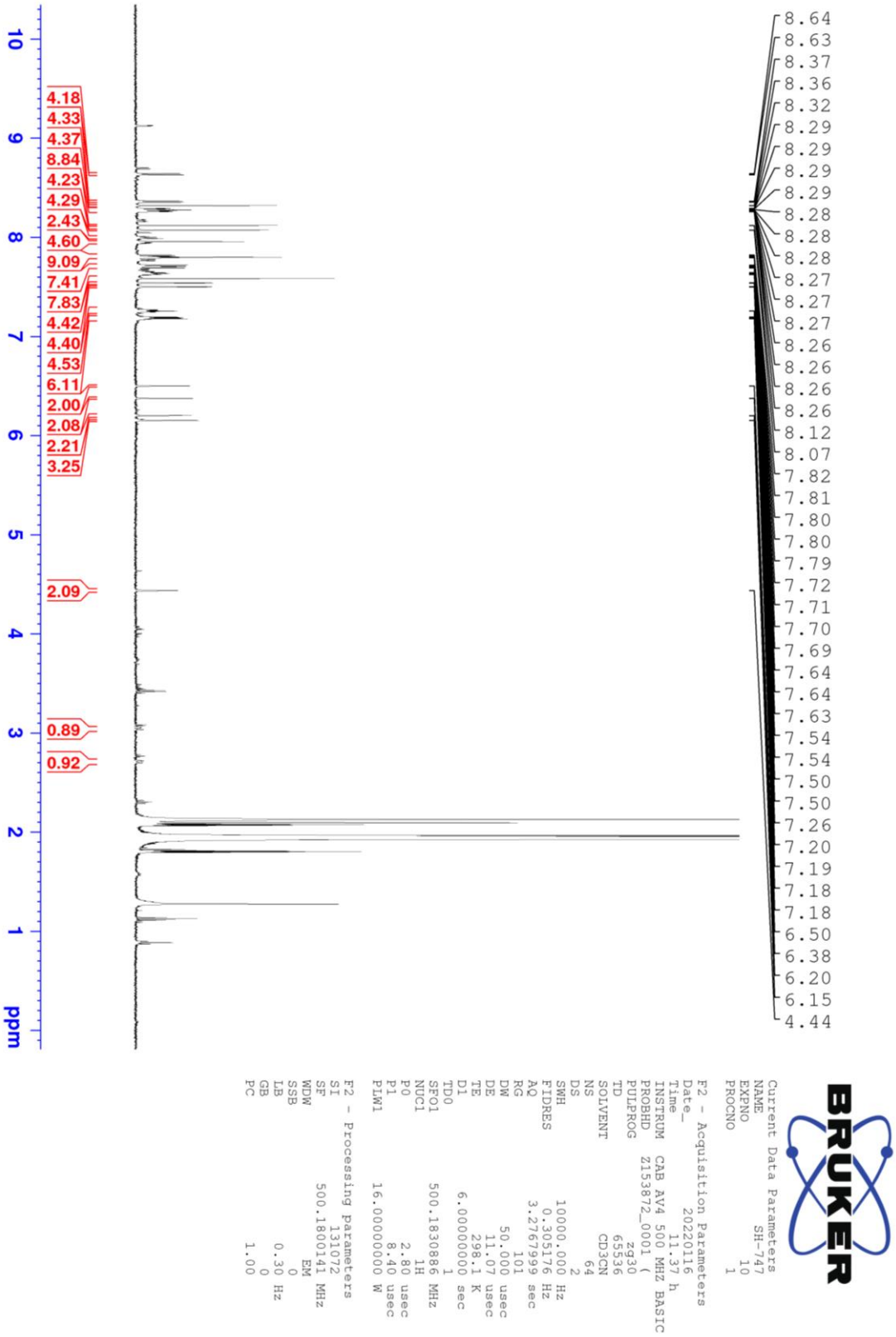

Figure 4.4.10 ^{1}H NMR spectrum of **3**@$Pd_2\mathbf{L}^{\mathbf{P}}_4$ (CD_3CN, 500 MHz, 298 K)

4.4.2.2.2 ^{1}H-^{1}H COSY NMR spectra of 3@Pd$_2$L$^{P}_4$

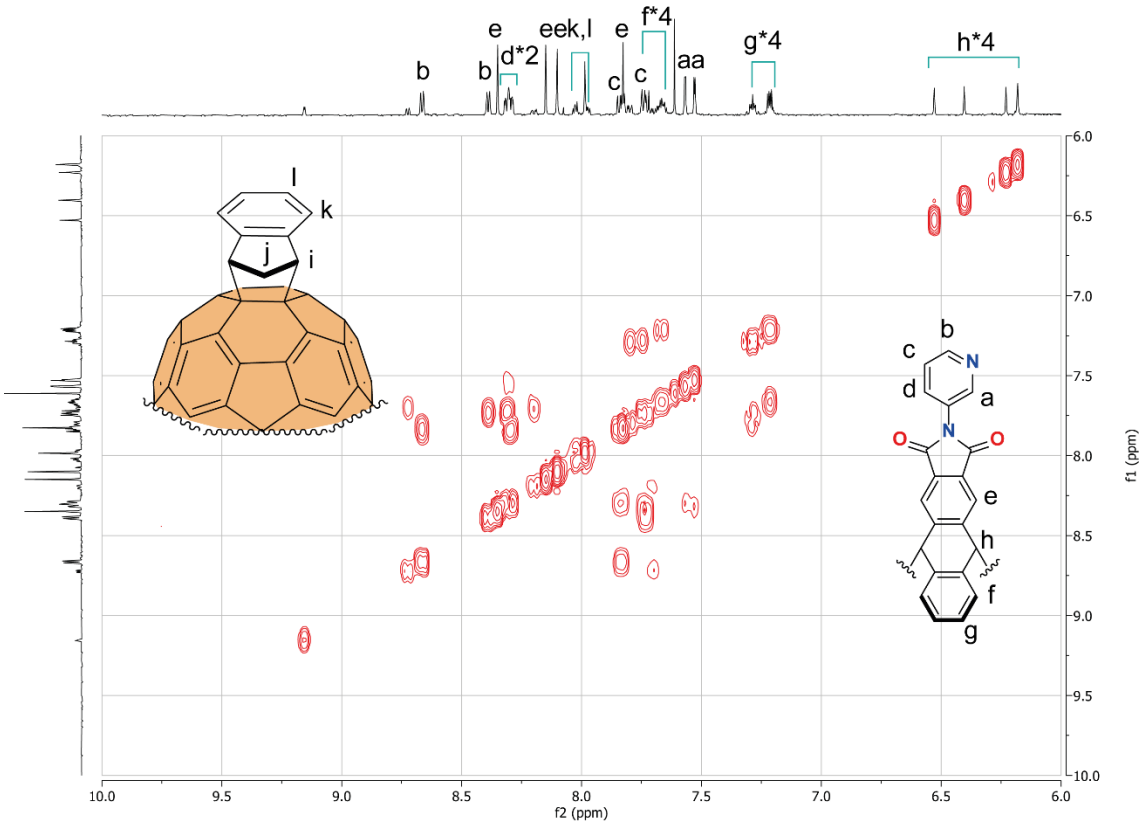

Figure 4.4.11 ^{1}H-^{1}H COSY NMR spectrum of **3**@Pd$_2$**L**$^{P}_4$ (CD$_3$CN, 500 MHz, 298 K) in a range of 10-6 ppm

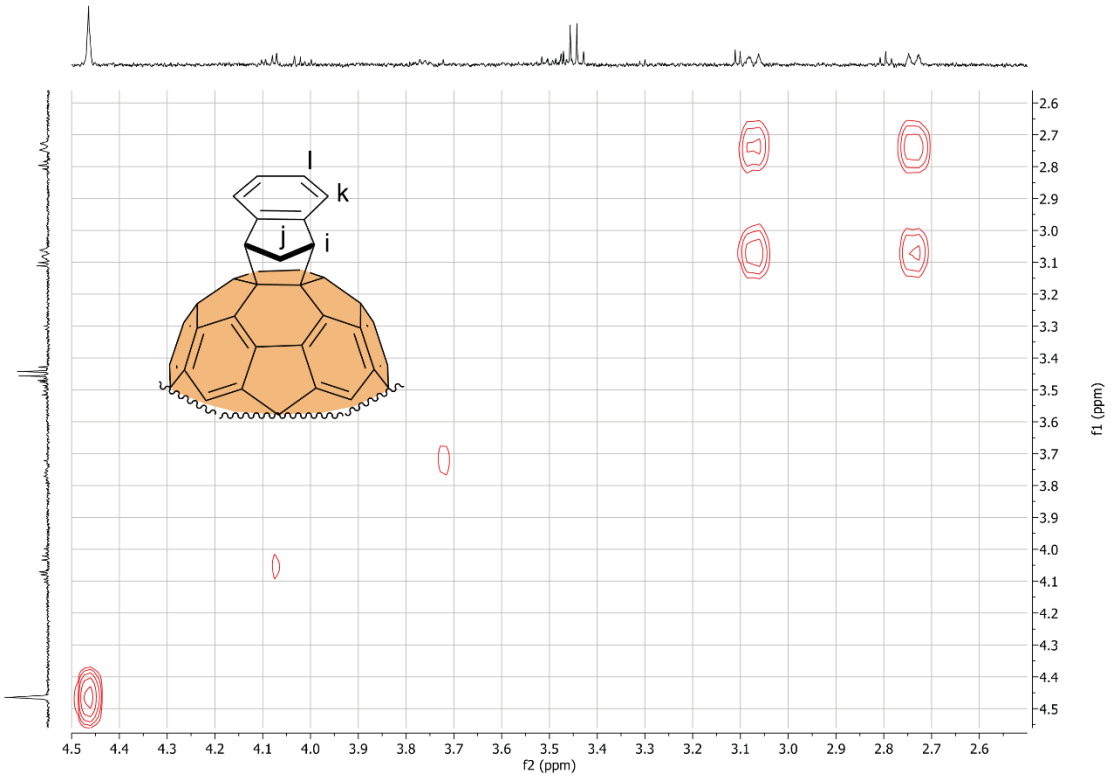

Figure 4.4.12 ^{1}H-^{1}H COSY NMR spectrum of **3**@$Pd_2\mathbf{L}^{\mathbf{P}}_4$ (CD_3CN, 500 MHz, 298 K) in a range of 4.5-2.5 ppm

4.4.2.2.3 ^{1}H DOSY NMR spectrum of 3@$Pd_2L^P_4$

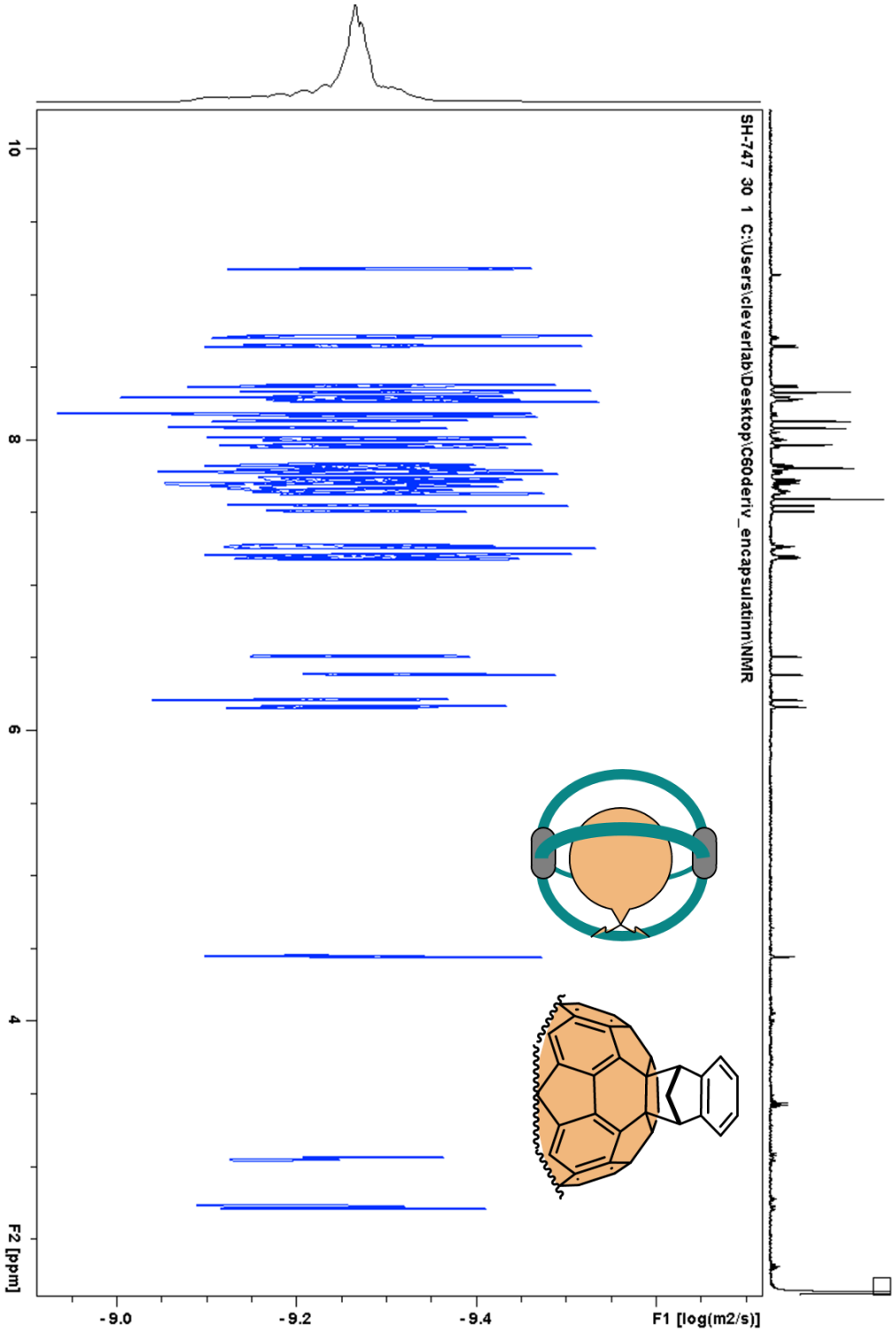

Figure 4.4.13 ^{1}H DOSY NMR spectrum of **3**@$Pd_2\mathbf{L}^P_4$ (CD_3CN, 500 MHz, 298 K)

4.4.2.2.4 ^{13}C NMR spectrum of 3@$Pd_2L^P_4$

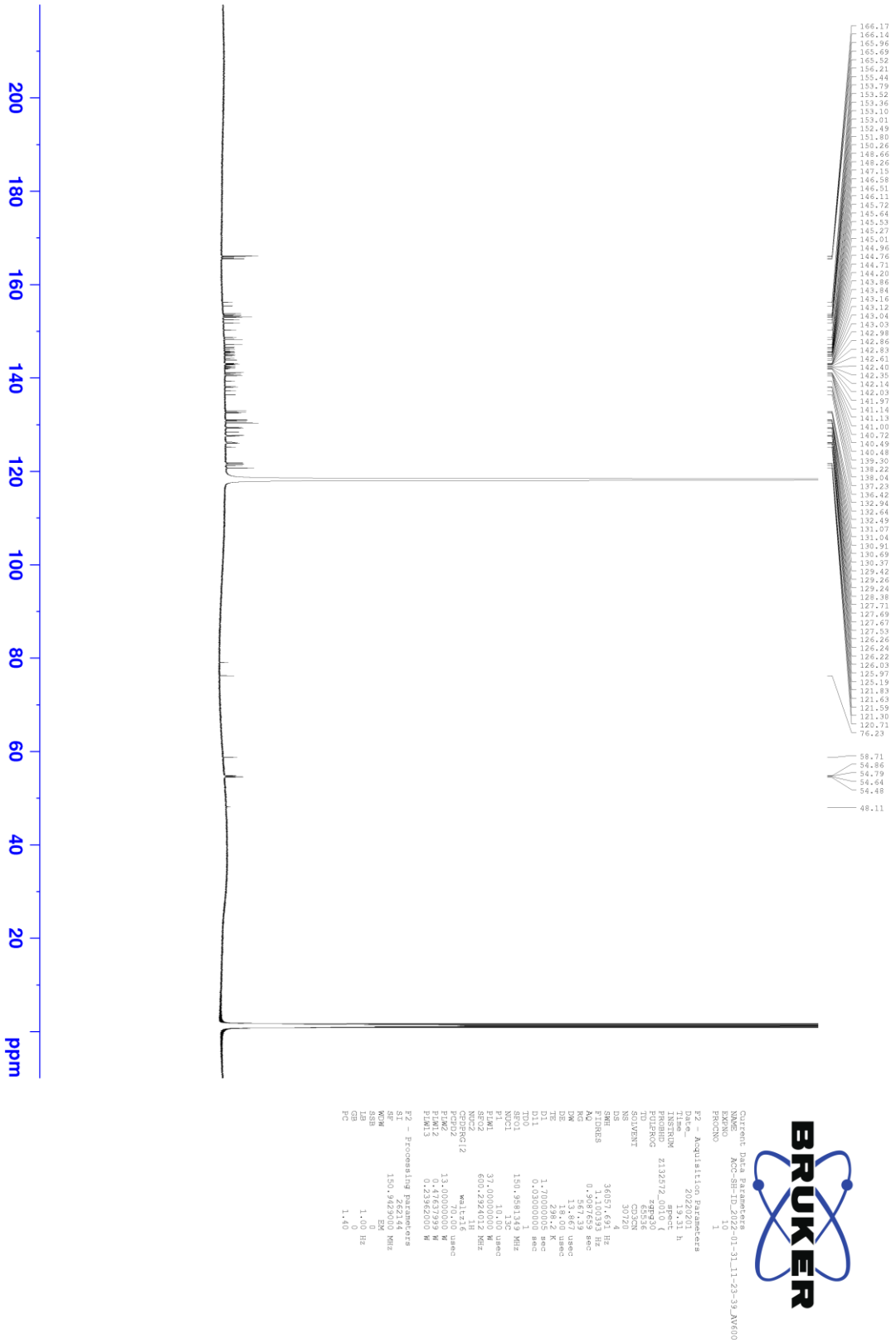

Figure 4.4.14 ^{13}C NMR spectrum of **3**@$Pd_2\mathbf{L}^P_4$ (CD_3CN, 150 MHz, 298 K)

4.4.2.2.5 ESI MS spectrum of 3@$Pd_2L^P_4$

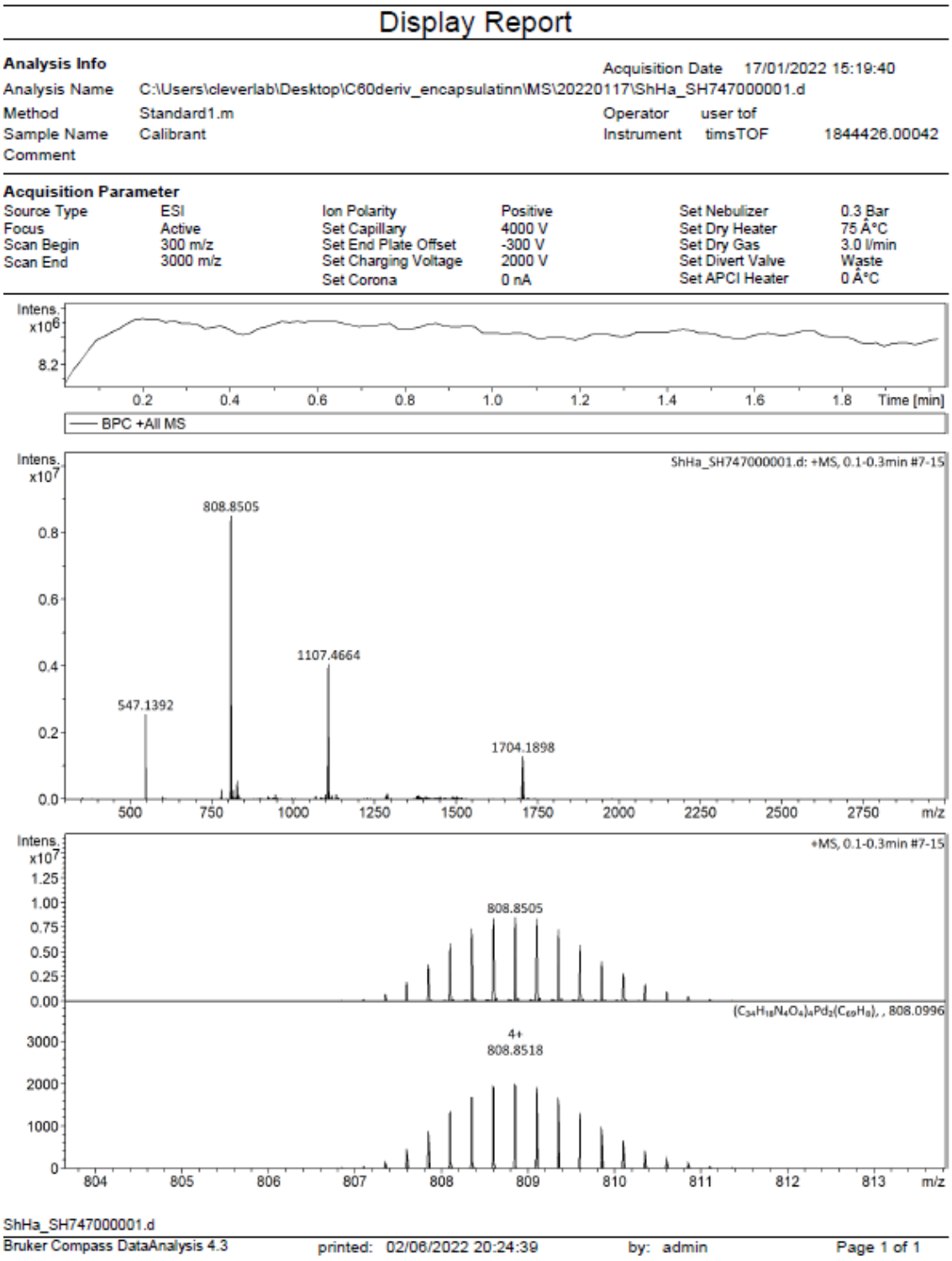

Figure 4.4.15 ESI-MS spectra (positive) of **3**@$Pd_2\mathbf{L}^P_4$

4.4.2.3 Encapsulation of 4

^{1}H NMR (500 MHz, CD_3CN, 298 K): *δ* (ppm) **b** 8.60 (d, *J* = 5.2 Hz, 4H), **b** 8.38 (d, *J* = 5.2 Hz, 4H), **d** 8.32 (ddd, *J* = 8.5, 2.2, 1.2 Hz, 4H), **d** 8.31 (ddd, *J* = 8.5, 2.2, 1.2 Hz, 4H), **e** 8.24 (s, 4H), **n** 8.12 (m, 2H), **e*2** 8.09 (s, 8H), **e** 7.90 (s, 4H), **o** 7.89 (m, 1H) **c** 7.88 (dd, *J* = 8.5, 5.6 Hz, 4H), **c** 7.76 (dd, *J* = 8.5, 5.6 Hz, 4H), **f*4**&**m** 7.74-7.61(m, 10H), **a** 7.55 (d, *J* = 2.1 Hz, 4H), **a** 7.53 (d, *J* = 2.1 Hz, 4H), **g*4** 7.25-7.18 (m, 8H), **h** 6.44 (s, 2H), **h** 6.32 (s, 2H), **h** 6.32 (s, 2H), **h** 6.19 (s, 2H), **i** 3.67 (s, 3H), **j** 2.52 (m, 2H), **l** 2.31 (m, 2H), **k** 2.00 (m, 2H)

^{13}C NMR (176 MHz, CD_3CN, 298 K): *δ* (ppm) 174.35, 166.17, 166.01, 165.96, 165.68, 165.57, 153.66, 153.65, 153.52, 153.45, 153.11, 152.61, 151.93, 150.26, 149.26, 148.70, 148.12, 147.44, 145.07, 144.91, 144.79, 144.33, 144.12, 144.09, 144.07, 143.96, 143.86, 143.48, 143.24, 143.18, 143.09, 142.99, 142.93, 142.82, 142.80, 142.72, 142.68, 142.62, 142.52, 142.21, 142.05, 141.86, 141.71, 141.59, 140.86, 140.72, 140.70, 140.54, 140.47, 140.41, 139.70, 138.05, 136.80, 136.62, 135.72, 132.88, 132.71, 132.63, 132.51, 131.11, 131.07, 131.03, 130.73, 130.39, 130.33, 130.11, 129.61, 129.24, 128.39, 127.76, 127.73, 127.55, 126.35, 126.25, 126.20, 125.98, 121.73, 121.59, 120.77, 120.72, 81.63, 54.81, 54.72, 54.66, 54.52, 54.50, 54.35, 52.21, 34.41, 33.80, 23.42 (13 signals from empty $Pd_2\mathbf{L^P}_4$)

DOSY: Diffusion coefficient $D = 5.38 \times 10^{-10}$ m^2s^{-1}, hydrodynamic radius r_H was calculated to be 12.1 Å

ESI MS (positive): found: 827.3599 and 1132.1460; calculated for $[(C_{34}H_{18}N_4O_4)_4Pd_2(C_{72}H_{14}O_2)]^{4+}$ and $[(C_{34}H_{18}N_4O_4)_4Pd_2(C_{72}H_{14}O_2)(BF_4)]^{3+}$ to be 827.3610 and 1132.1494 respectively

4.4.2.3.1 ^{1}H NMR spectra of 4@$Pd_2L^P_4$

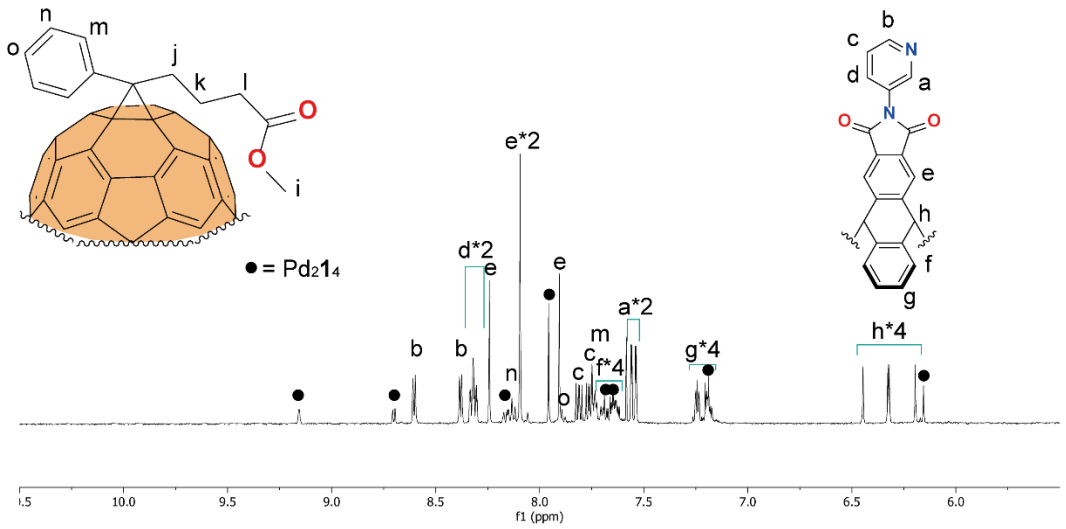

Figure 4.4.16 ^{1}H NMR spectrum (CD_3CN, 500 MHz, 298 K,) of **4**@$Pd_2\mathbf{L}^{\mathbf{P}}_4$

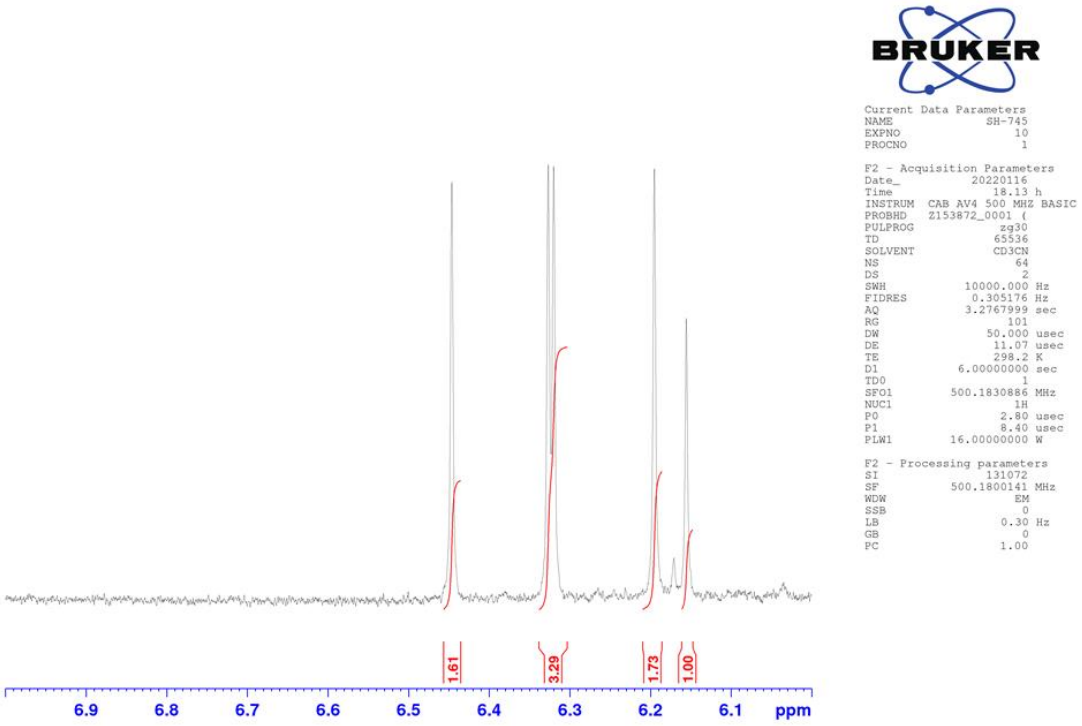

Figure 4.4.17 ^{1}H NMR integration ratio used to determine the encapsulation ratio of **4**@$Pd_2\mathbf{L}^{\mathbf{P}}_4$ **100 * (1.73*4) / (1.73*4 + 1.0) = 87.3 %**

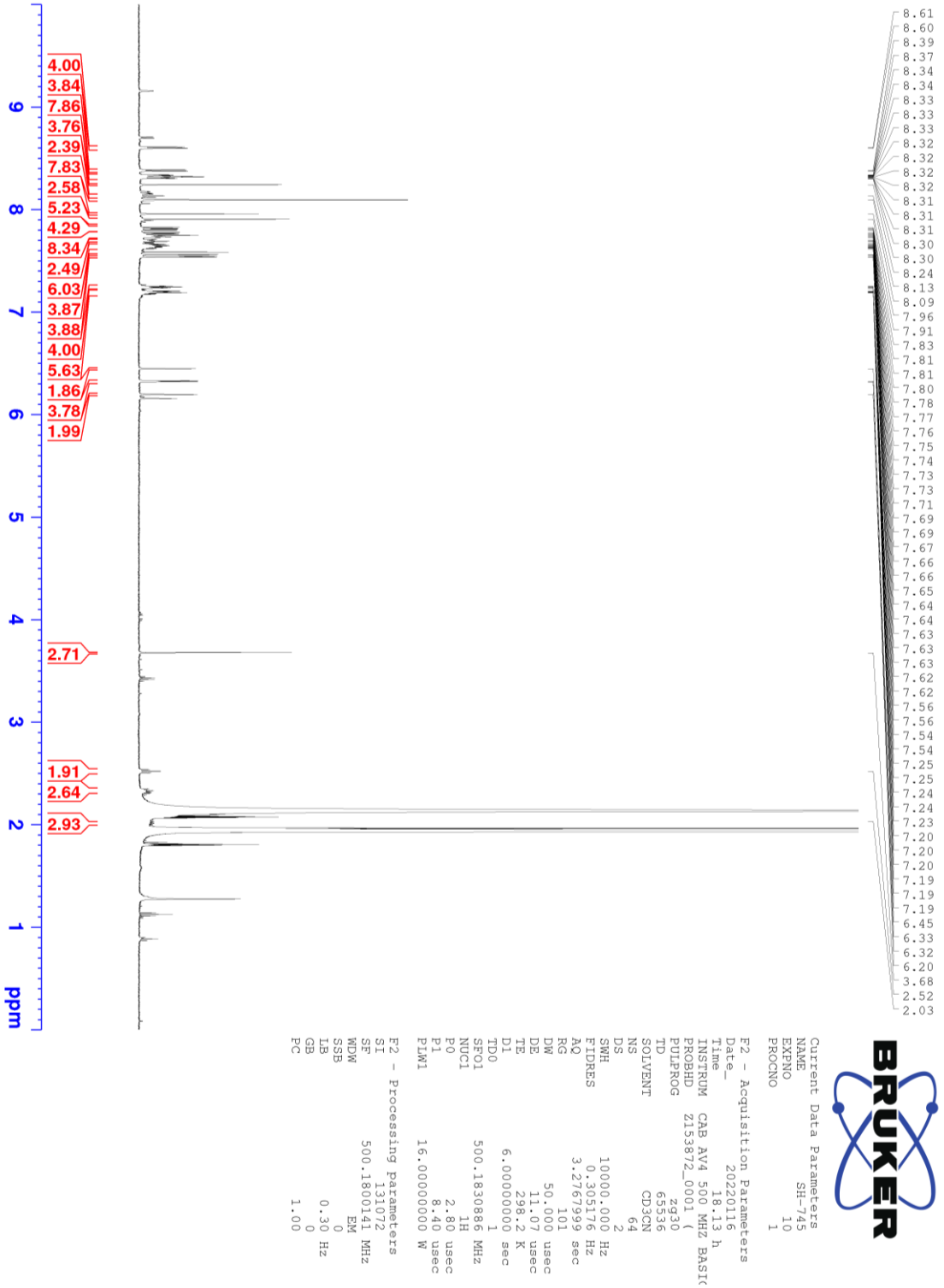

Figure 4.4.18 ^{1}H NMR spectrum of **4**@$Pd_2\mathbf{L}^{\mathbf{P}}_4$ (CD_3CN, 500 MHz, 298 K)

4.4.2.3.2 ^{1}H-^{1}H COSY NMR spectra of 4@$Pd_2L^P_4$

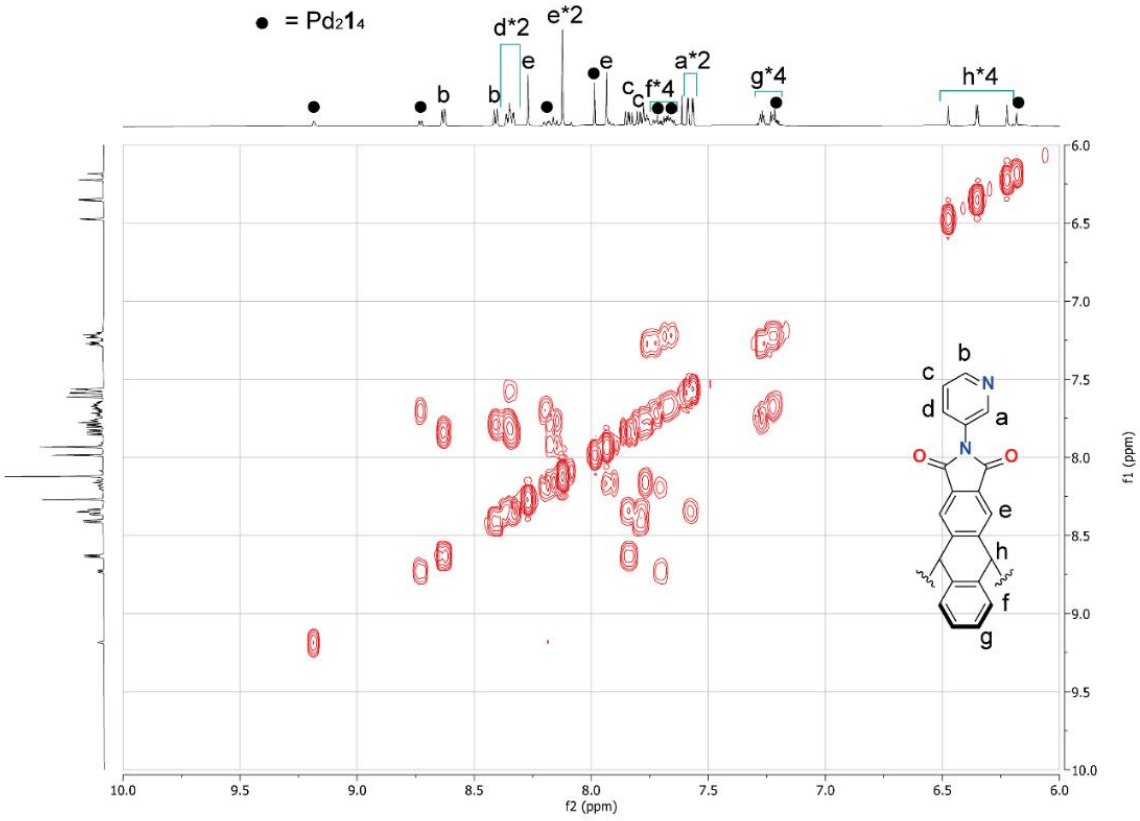

Figure 4.4.19 ^{1}H–^{1}H COSY NMR spectrum of **4**@$Pd_2\mathbf{L}^{P}_4$ (CD_3CN, 500 MHz, 298 K) in a range of 10-6 ppm

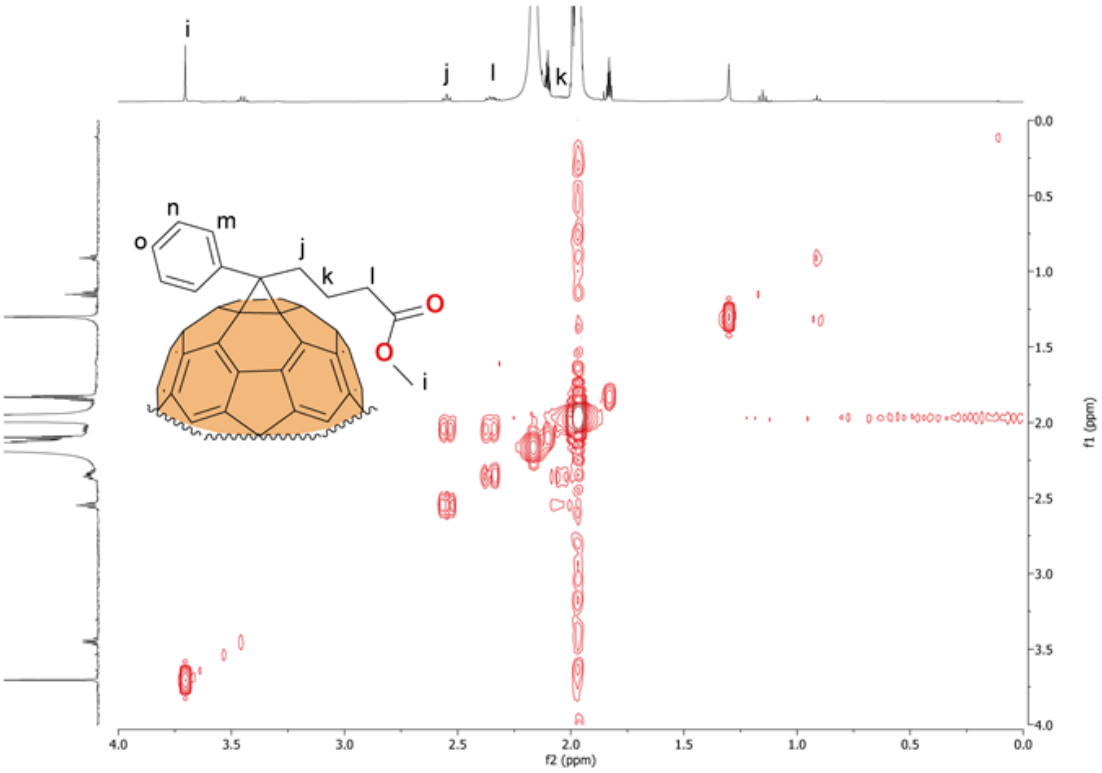

Figure 4.4.20 ^{1}H–^{1}H COSY NMR spectrum of **4**@$Pd_2\mathbf{L}^{\mathbf{P}}_4$ (CD_3CN, 500 MHz, 298 K) in a range of 4-0 ppm

4.4.2.3.3 ^{1}H DOSY NMR spectrum of 4@$Pd_2L^P_4$

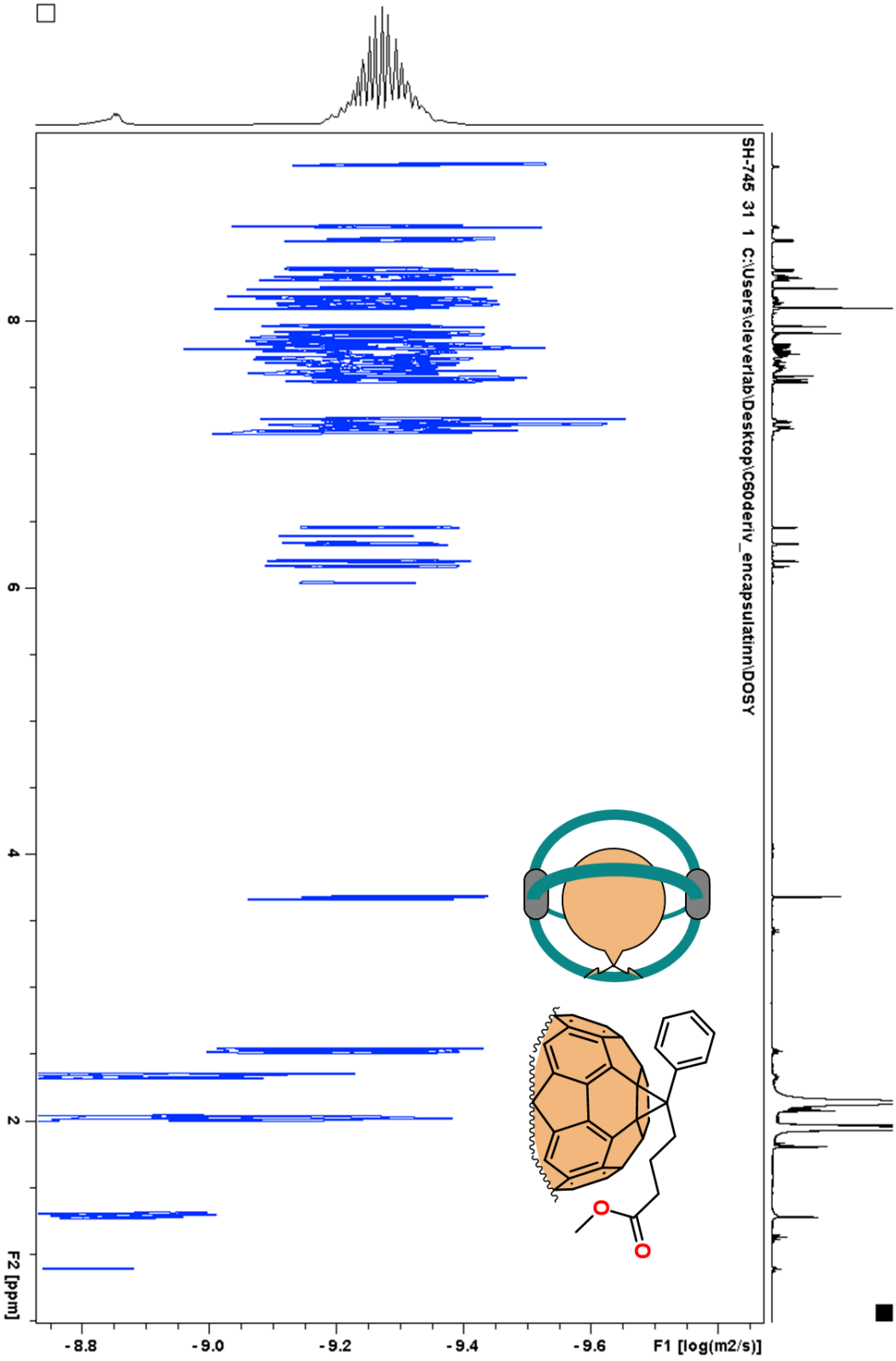

Figure 4.4.21 ^{1}H DOSY NMR spectrum of **4**@$Pd_2\mathbf{L}^{P}_4$ (CD_3CN, 500 MHz, 298 K)

4.4.2.3.4 ^{13}C NMR spectrum of 4@$Pd_2L^P_4$

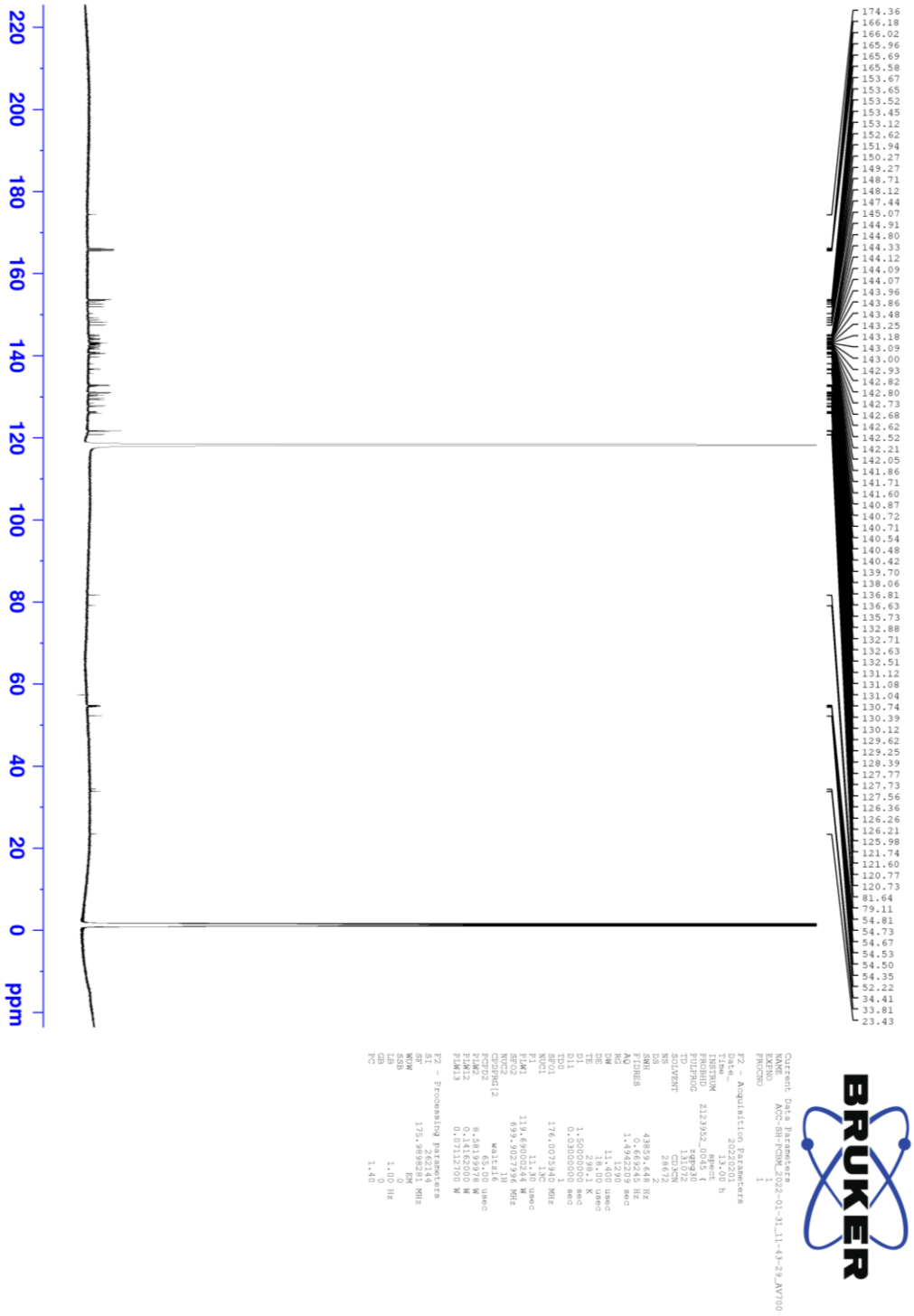

Figure 4.4.22 ^{13}C NMR spectrum of **4**@$Pd_2\mathbf{L}^P_4$ (CD_3CN, 176 MHz, 298 K)

4.4.2.3.5 ESI MS spectrum of 4@$Pd_2L^P_4$

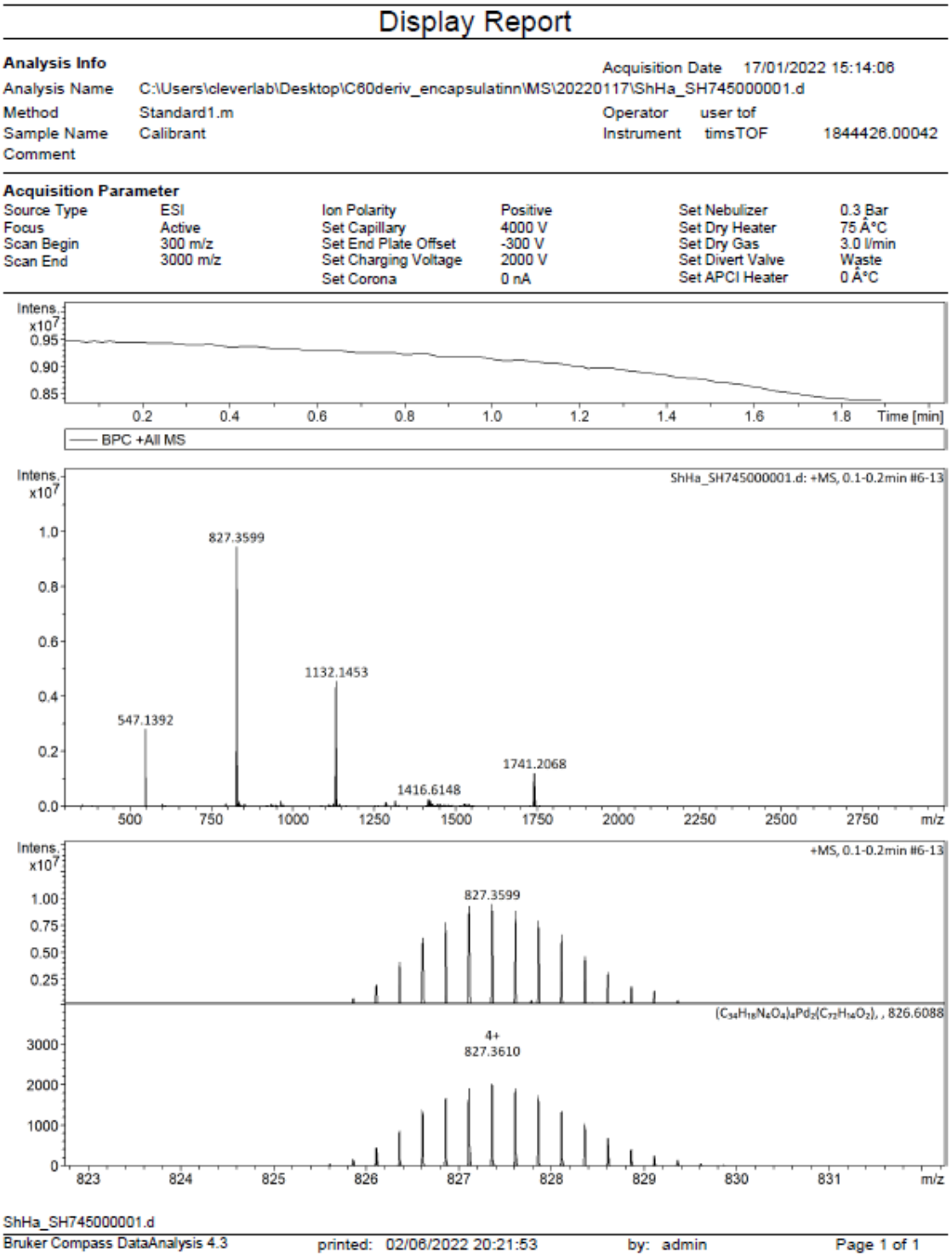

Figure 4.4.23 ESI-MS spectrum (positive) of **4**@$Pd_2L^P_4$

4.4.3 Encapsulation of corannulene

4.4.3.1 Scope of guests

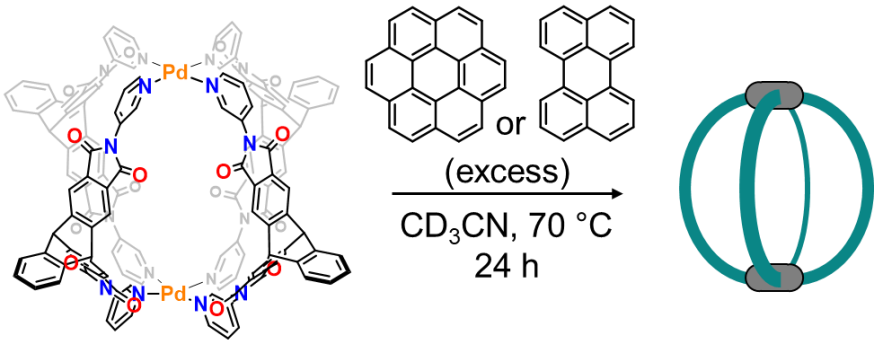

Figure 4.4.24 Encapsulation of coronene and perylene

To an acetonitrile solution of $Pd_2\mathbf{L}^{\mathbf{P}}_4$ (0.70 mM, 0.600 mL, 0.42 μmol) an excess amount of solid guest was added and heated at 70 °C for 24 h in an NMR tube. The resulting mixture was measured ^{1}H NMR. As a result, no guest encapsulation was observed.

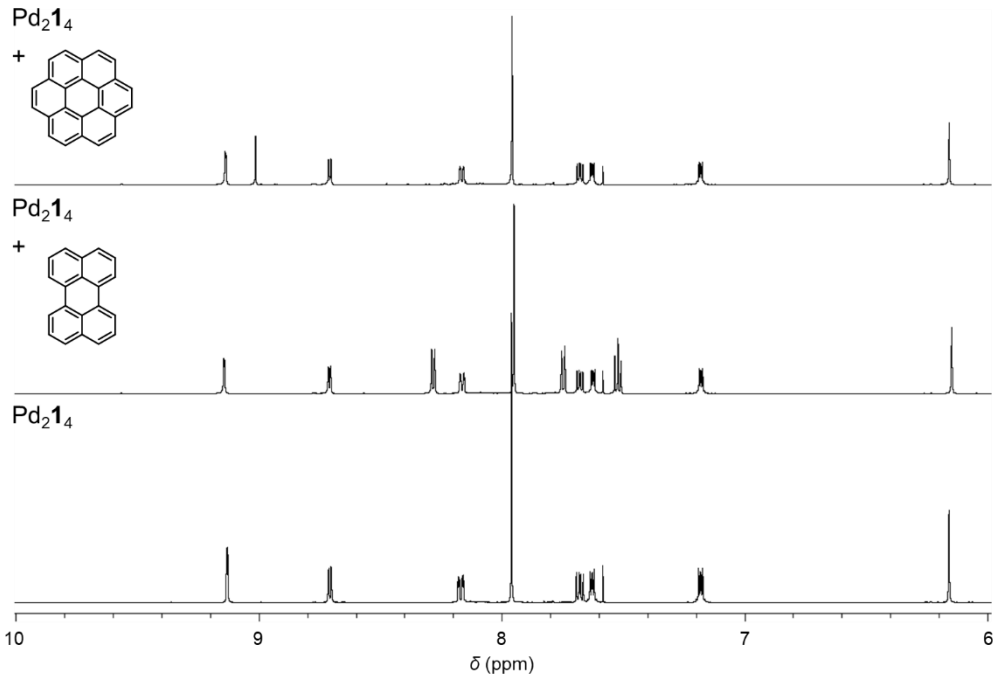

Figure 4.4.25 Comparison of ^{1}H NMR spectrum (CD_3CN, 0.70 mM, 500 MHz, 298 K) of $Pd_2\mathbf{L}^{\mathbf{P}}_4$ in the presence of coronene or perylene

4.4.3.2 Synthesis of $(Cor)_2@Pd_2L^P_4$

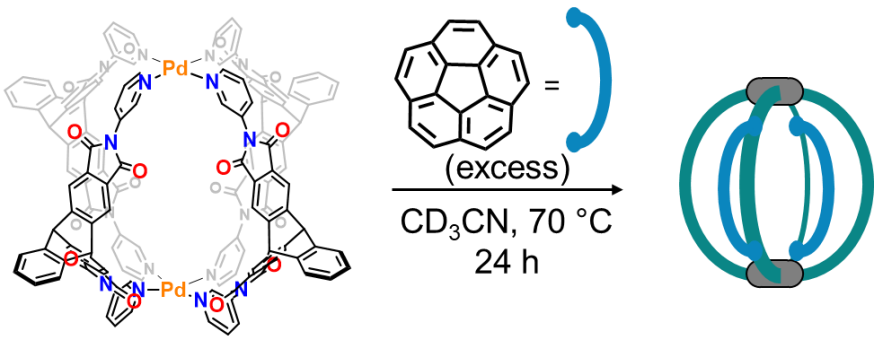

Figure 4.4.26 Synthesis of $(Cor)_2@Pd_2L^P_4$

To an NMR tube where an acetonitrile solution of $Pd_2L^P_4$ (0.70 mM, 0.600 mL, 0.42 μmol) was placed, solid-state corannulene (excess) was added and heated at 70 °C for 24 h.

^{1}H NMR (500 MHz, CD_3CN, 298 K): *δ* (ppm) **e** 8.35 (s, 16 H), **d** 8.03 (d, *J* = 8.8 Hz, 8H), **f** 7.86 (m, 8H), **b** 7.82 (m, 8H), **c** 7.48 (dd, *J* = 8.8, 5.7 Hz, 8H), **g** 7.35 (dd, *J* = 5.3, 3.3 Hz, 8H), **h** 6.61 (s, 8H), **a** 6.00 (s, 8H), **encapsulated corannulenes** 5.47 (s, 20H)

^{13}C NMR (125 MHz, CD_3CN, 298 K): *δ* (ppm) 166.12, 165.70, 154.15, 152.99, 151.33, 150.30, 148.64, 147.74, 142.88, 142.40, 139.94, 138.09, 133.29, 132.40, 131.49, 130.95, 130.35, 130.16, 128.66, 127.49, 126.89, 126.27, 125.91, 121.68, 120.64, 54.94, 54.54. (12 signals from empty $Pd_2L^P_4$ out of 13 signals, the missing signal must be overlapping)

DOSY: Diffusion coefficient *D* of corannulenes inside $Pd_2L^P_4$ and free corannulene in the solution were preliminary estimated to be 6.69×10^{-10} and 18.58×10^{-10} m^2s^{-1} respectively. Due to the equilibrium between the empty cage and the host-guest complex, determination of an accurate hydrodynamic radius of the host-guest complex was not possible.

ESI MS (positive): found: 724.6237; calculated for $[(C_{34}H_{18}N_4O_4)_4Pd_2(C_{20}H_{10})_2]^{4+}$ to be 724.6248

4.4.3.2.1 ^{1}H NMR spectra of $(Cor)_2@Pd_2L^P_4$

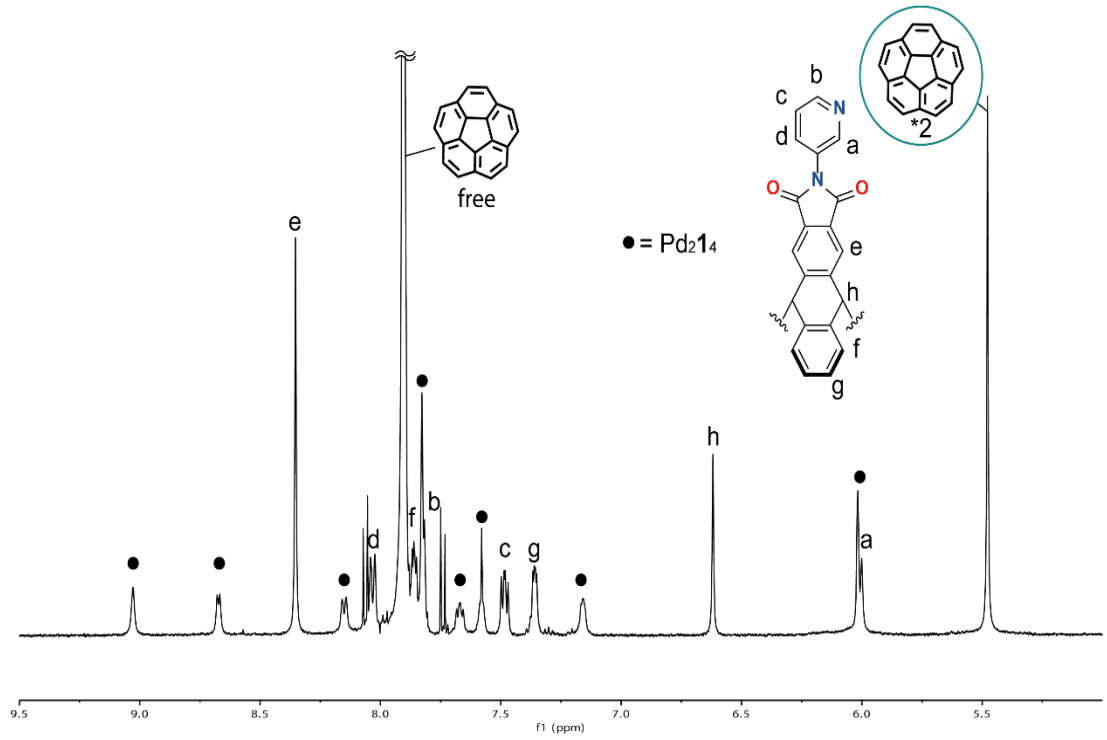

Figure 4.4.27 ^{1}H NMR spectrum of $(Cor)_2@Pd_2\mathbf{L}^P_4$ (CD_3CN, 500 MHz, 298 K)

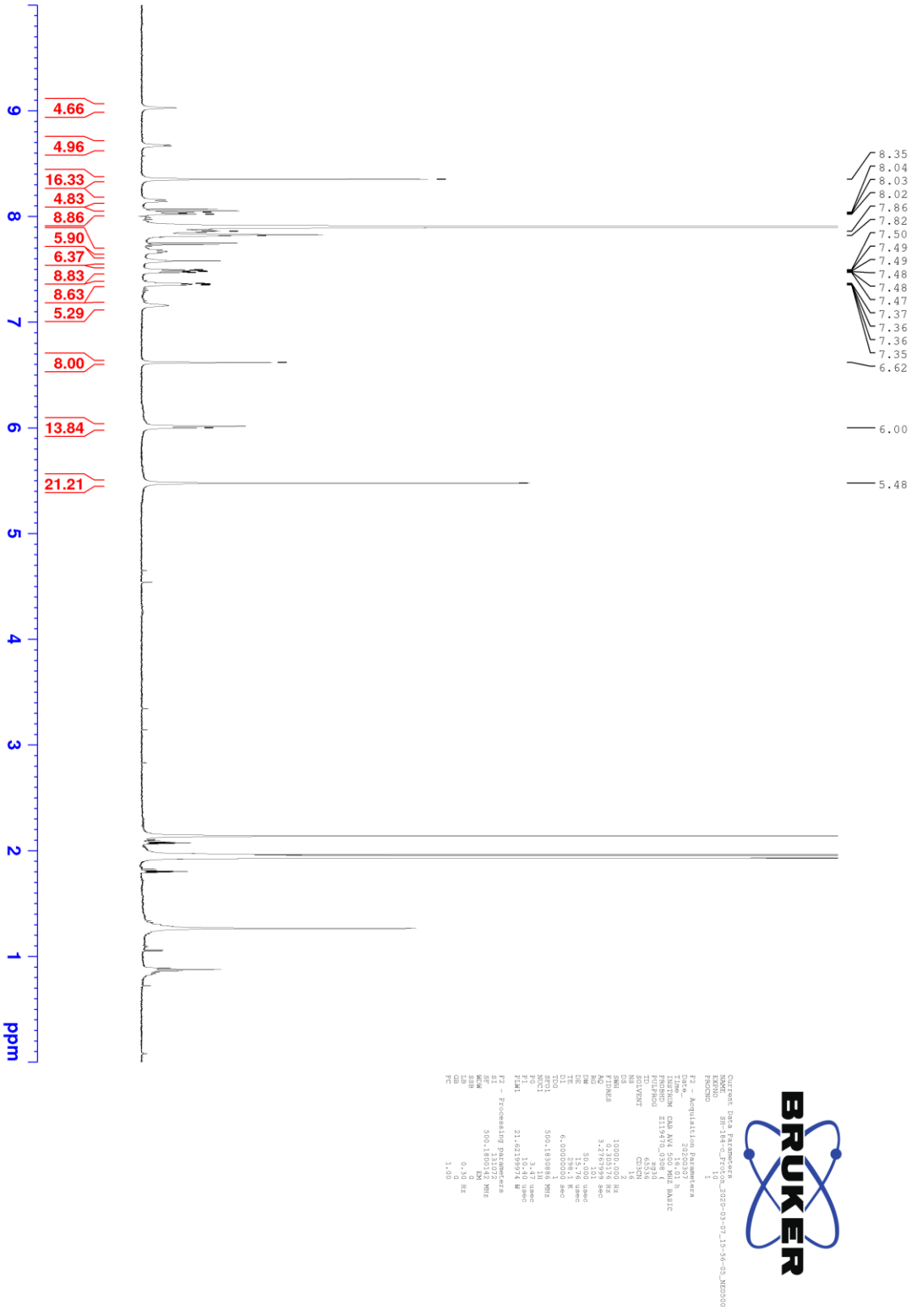

Figure 4.4.28 ^{1}H NMR spectrum of $(Cor)_2@Pd_2\mathbf{L}^{\mathbf{P}}_4$ (CD_3CN, 500 MHz, 298 K)

4.4.3.2.2 ^{1}H-^{1}H COSY NMR spectrum of $(Cor)_2@Pd_2L^P_4$

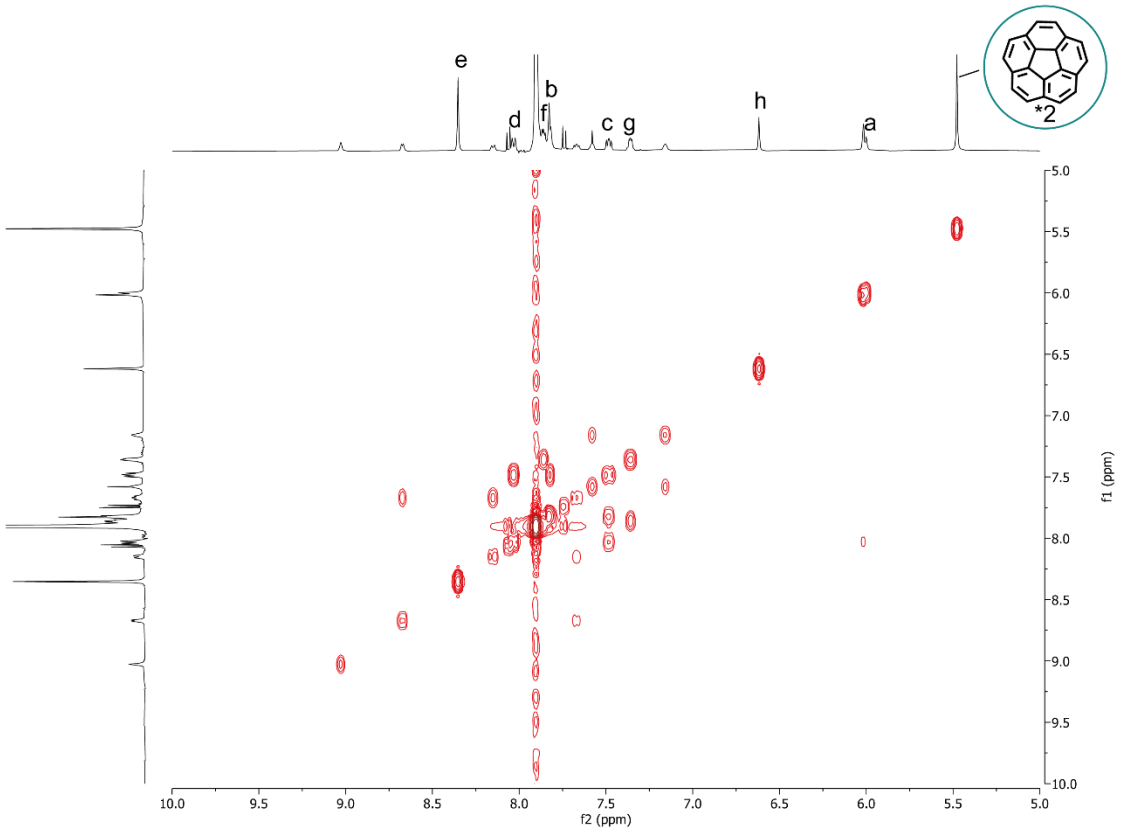

Figure 4.4.29 ^{1}H-^{1}H COSY NMR spectrum of $(Cor)_2@Pd_2\mathbf{L}^P_4$ (CD_3CN, 500 MHz, 298 K)

4.4.3.2.3 ^{1}H-^{1}H NOESY spectrum of (Cor)$_2$@Pd$_2$L$^{P}_4$

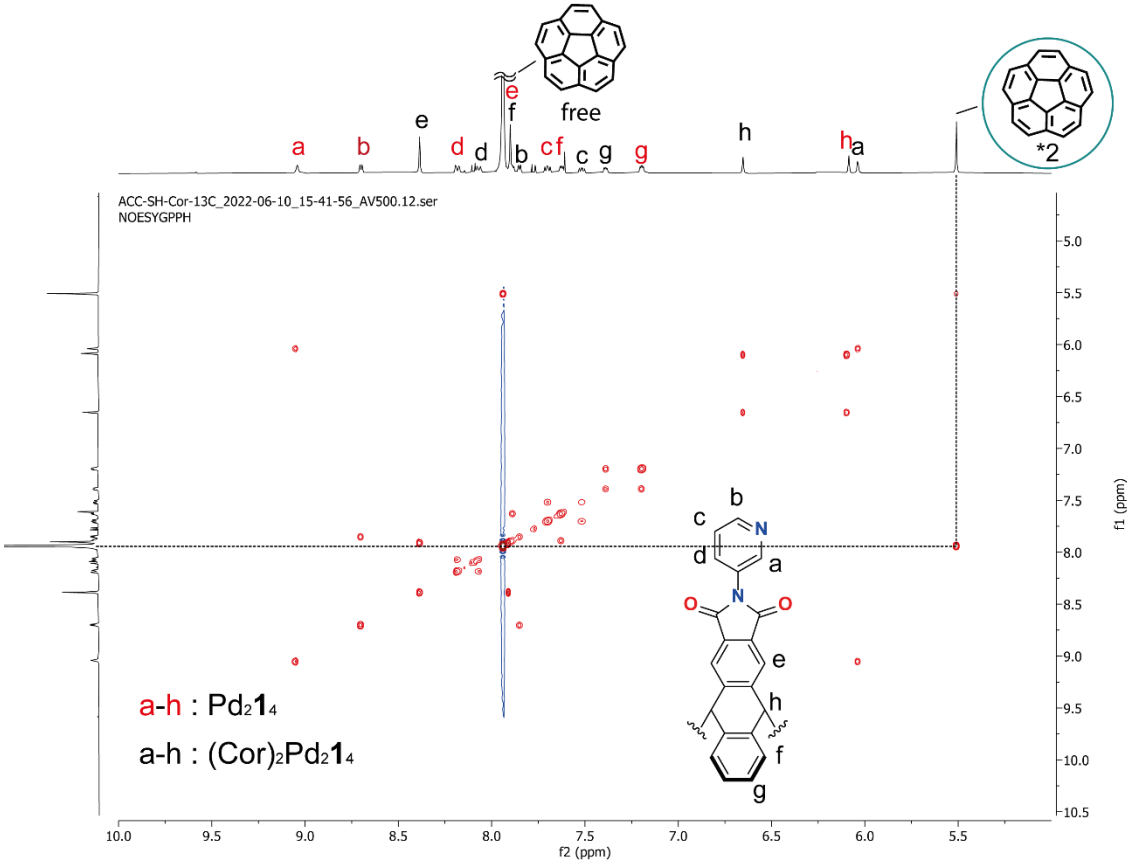

Figure 4.4.30 ^{1}H-^{1}H NOESY NMR spectrum of (Cor)$_2$@Pd$_2$**L**$^{P}_4$ (CD$_3$CN, 500 MHz, 298 K)

4.4.3.2.4 ^{1}H DOSY NMR spectrum of (Cor)$_2$@Pd$_2$L$^{P}_4$

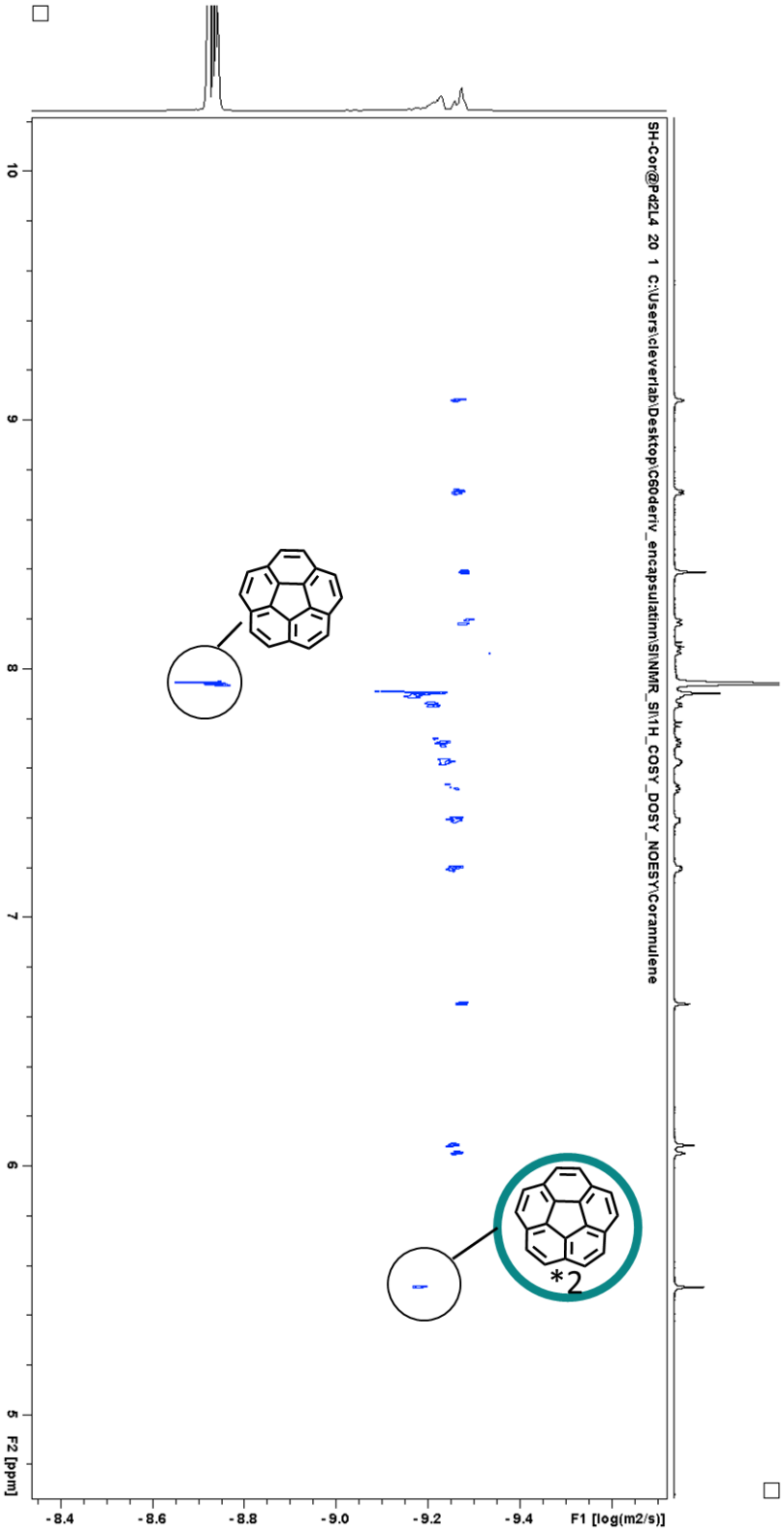

Figure 4.4.31 ^{1}H DOSY NMR spectrum of (Cor)$_2$@Pd$_2$**L**$^{P}_4$ (CD$_3$CN, 500 MHz, 298 K)

4.4.3.2.5 ^{13}C NMR spectrum of (Cor)$_2$@Pd$_2$L$^P_4$

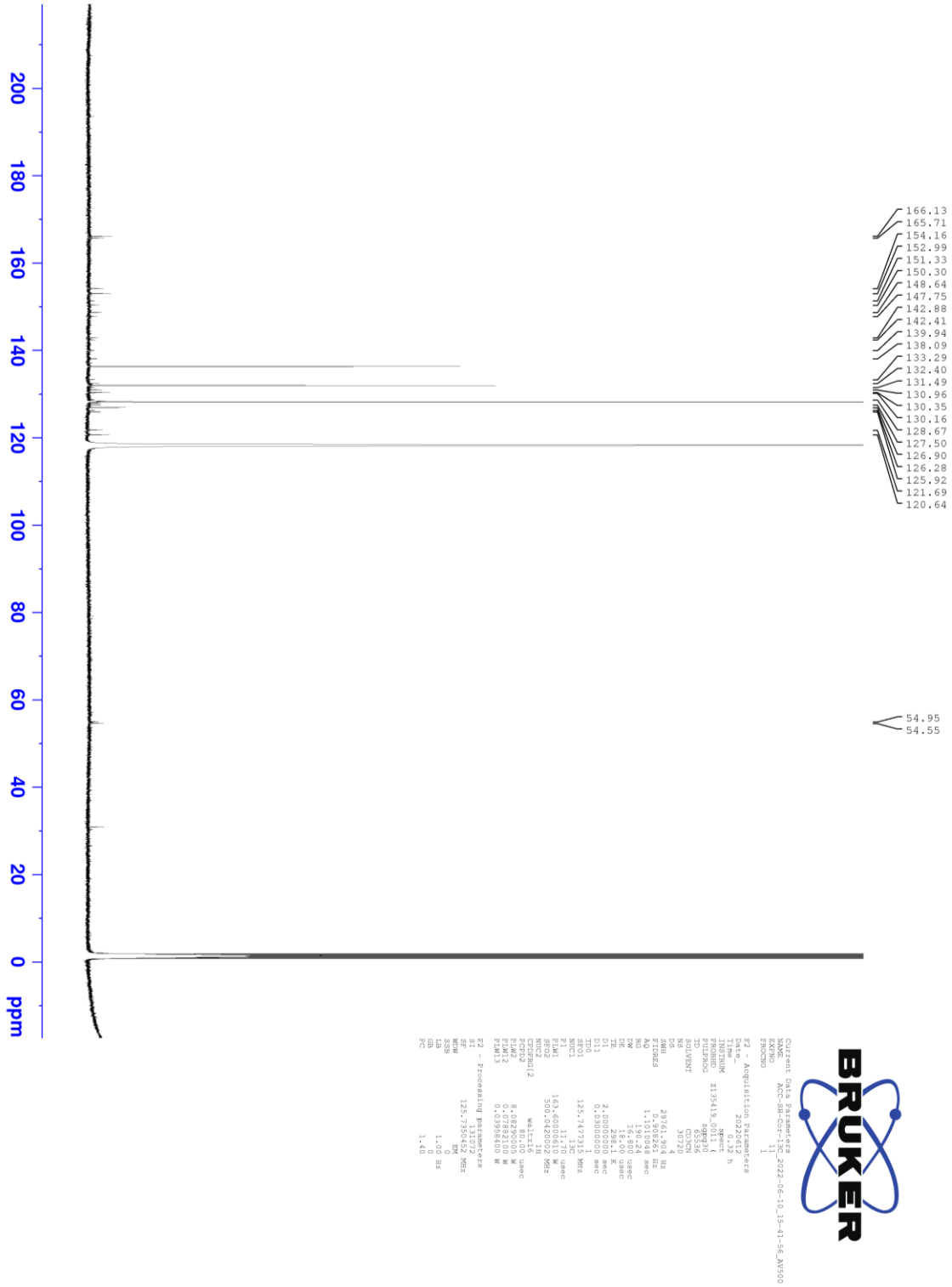

Figure 4.4.32 ^{13}C NMR spectrum of (Cor)$_2$@Pd$_2$**L**$^P_4$ (CD$_3$CN, 125 MHz, 298 K)

4.4.3.2.6 ESI MS spectrum of $(Cor)_2@Pd_2L^P_4$

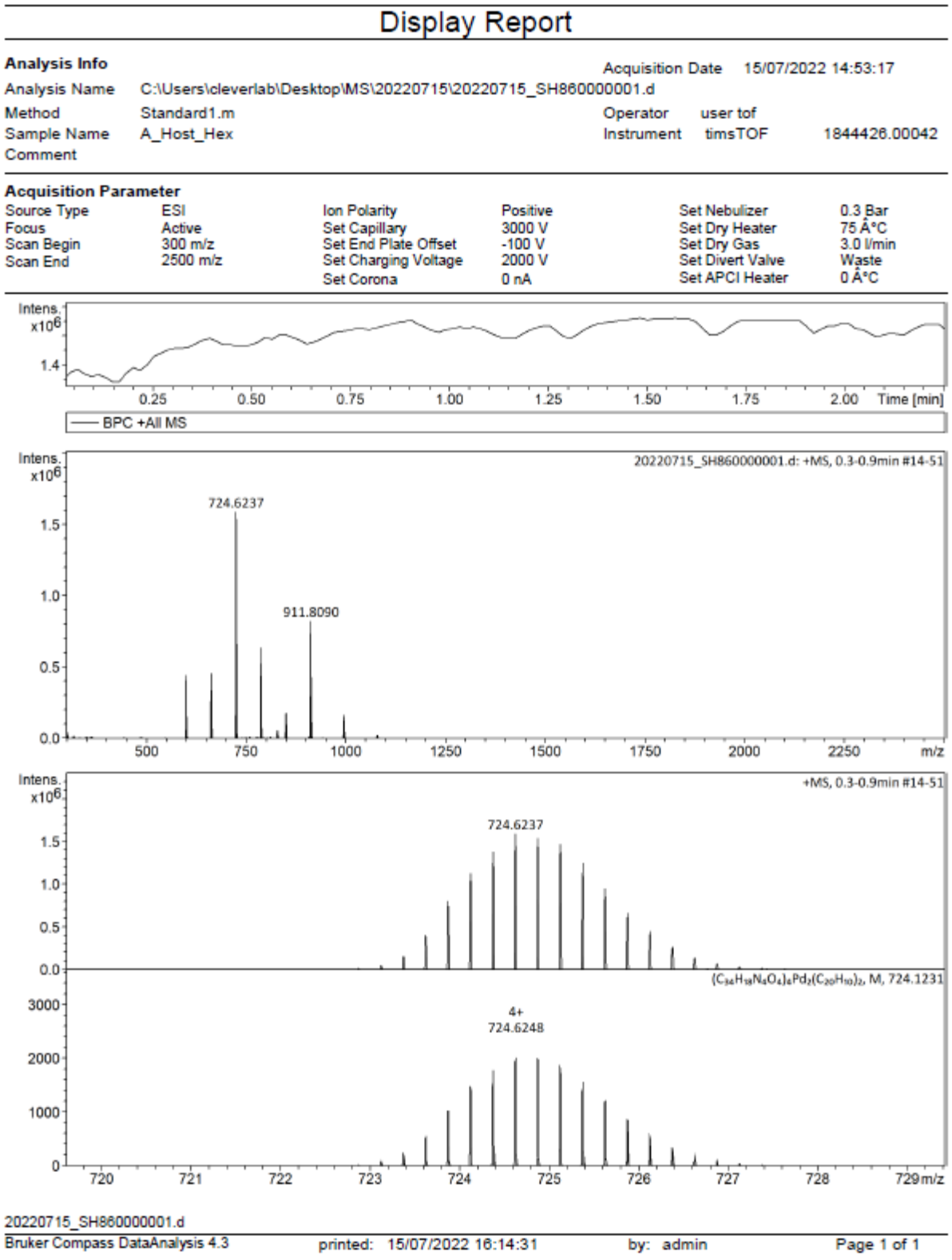

Figure 4.4.33 ESI-MS spectrum of $(Cor)_2@Pd_2L^P_4$ (positive)

4.4.3.2.7 VT-^{1}H NMR spectra of $(Cor)_2@Pd_2L^P_4$

VT-^{1}H NMR was carried out in a range of 253-343 K. Once temperature is set at a desired temperature, the sample was let stand for 10 mins in the NMR spectrometer to achieve an equilibrium state. The encapsulation ratio at each temperature was calculated from the ^{1}H NMR integral values of empty $Pd_2\mathbf{L}^{P}_4$ and $(Cor)_2@$ $Pd_2\mathbf{L}^{P}_4$. The results are summarized in the table below.

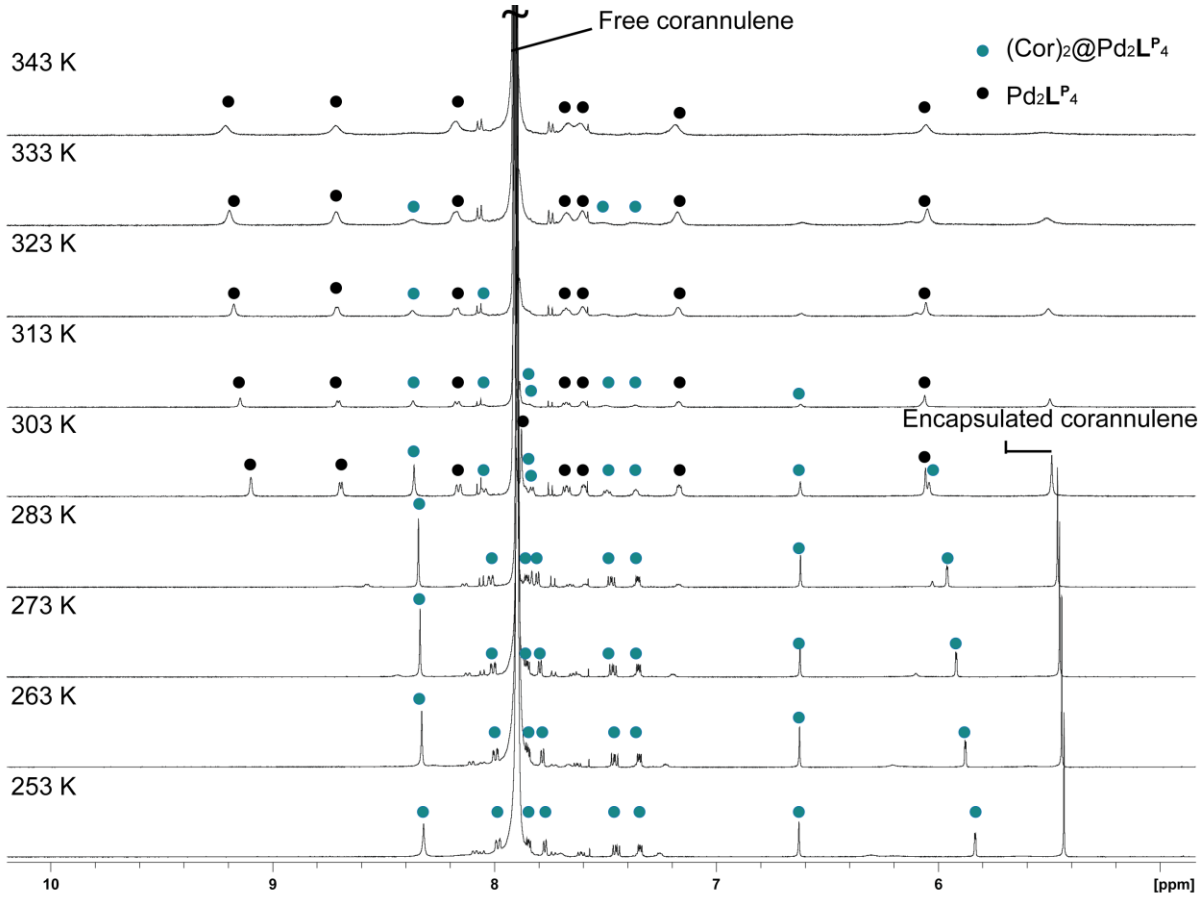

Figure 4.4.34 VT-^{1}H NMR spectra (CD_3CN, 500 MHz) of $(Cor)_2@Pd_2\mathbf{L}^{P}_4$ measured at various temperatures from 253-343 K

Table 4.4.1 Encapsulation ratio of corannulene in $Pd_2\mathbf{L}^{\mathbf{P}}_4$ at various temperatures

Temperature (K)	Ratio (HG complex)
343	**20%**
333	**25%**
323	**28%**
313	**31%**
303	**39%**
283	**66%**
273	**71%**
263	**75%**
253	**77%**

4.4.3.3 Titration experiment

To an acetonitrile solution of $Pd_2\mathbf{L}^{\mathbf{P}}_4$ (0.70 mM, 0.600 mL, 0.42 μmol) an acetonitrile solution of corannulene (10 mM) was titrated. An aliquot of the stock solution of corannulene was added in the NMR tube where the acetonitrile solution of the cage was placed and the NMR tube was shaken before measuring. The encapsulated corannulene's signal appeared over the titration with a subtle difference in the chemical shift of the empty cage ($\Delta\delta_{max}$ = -0.02 ppm).

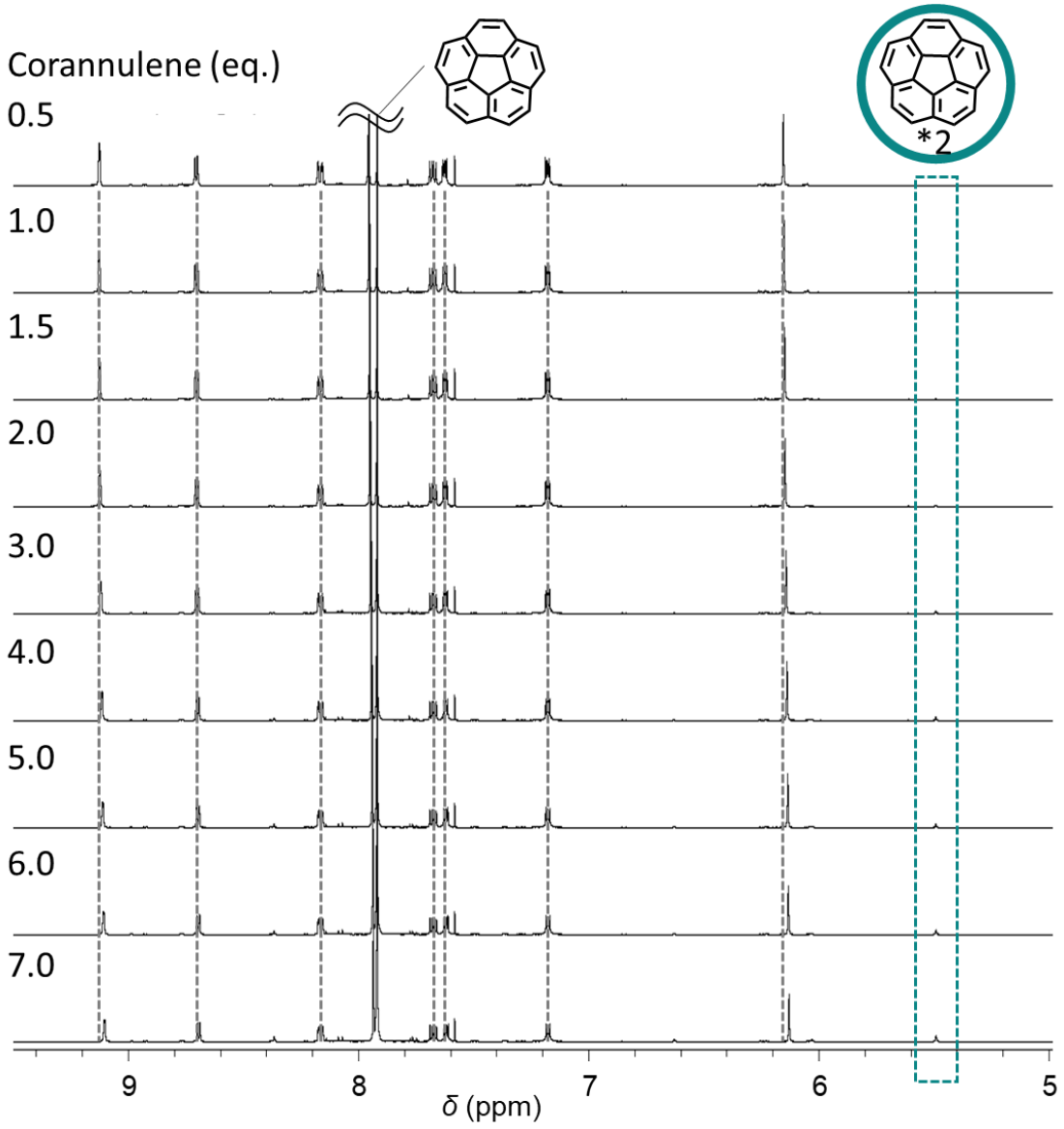

Figure 4.4.35 ^{1}H NMR spectra (CD_3CN, 500 MHz, 298 K) over titration of corannulene into $Pd_2\mathbf{L}^{\mathbf{P}}_4$

4.4.3.4 DFT calculations

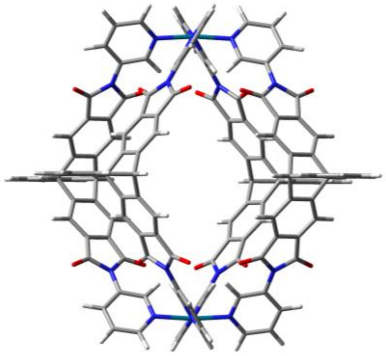

Figure 4.4.36 The optimized geometry of $Pd_2\mathbf{L^P}_4$ at M06-2X/Lanl2dz level of theory in the gas-phase

Standard orientation:

Center Number	Atomic Number	Atomic Type	Coordinates (Angstroms) X	Y	Z
1	6	0	3.236525	5.061884	3.323589
2	6	0	3.229923	3.760920	3.838018
3	6	0	2.227006	3.313730	4.699595
4	6	0	1.212447	4.225195	5.008248
5	6	0	0.000062	3.943742	5.897502
6	6	0	-1.212256	4.225274	5.008182
7	6	0	-2.226859	3.313875	4.699473
8	6	0	-3.229705	3.761134	3.837850
9	6	0	-3.236205	5.062104	3.323437
10	6	0	-2.236928	5.985485	3.633167
11	6	0	-1.213774	5.541943	4.478037
12	6	0	0.000166	6.362944	4.918069
13	6	0	1.214071	5.541860	4.478094
14	6	0	2.237288	5.985328	3.633260
15	6	0	4.390886	3.021272	3.284475
16	6	0	4.415670	5.218986	2.434971
17	6	0	-4.390690	3.021567	3.284247
18	6	0	0.000067	5.030754	6.979668
19	6	0	0.000126	6.334879	6.451572
20	6	0	-4.415299	5.219290	2.434765
21	7	0	-5.088923	3.945937	2.448341
22	7	0	5.089176	3.945579	2.448534
23	8	0	4.778200	6.196211	1.784501
24	8	0	4.711681	1.839003	3.459259
25	8	0	-4.777764	6.196579	1.784355
26	8	0	-4.711598	1.839328	3.459021
27	6	0	6.244869	3.645980	1.690043
28	6	0	-6.244660	3.646375	1.689902
29	6	0	7.165213	4.640178	1.302762
30	6	0	8.276864	4.272144	0.535497
31	6	0	8.463508	2.935699	0.174018
32	7	0	7.576506	1.987831	0.564081
33	6	0	6.487659	2.322094	1.297594
34	6	0	-6.487473	2.322480	1.297505
35	7	0	-7.576339	1.988205	0.564027
36	6	0	-8.463349	2.936067	0.173966
37	6	0	-8.276689	4.272520	0.535402
38	6	0	-7.165013	4.640571	1.302619
39	6	0	0.000019	4.821066	8.356990
40	6	0	0.000033	5.939243	9.213743
41	6	0	0.000092	7.238842	8.686997
42	6	0	0.000140	7.444831	7.293594
43	6	0	-0.000182	-7.444851	-7.292900
44	6	0	-0.000180	-7.238969	-8.686319
45	6	0	-0.000181	-5.939410	-9.213166
46	6	0	-0.000183	-4.821168	-8.356497
47	6	0	-7.164973	-4.639786	-1.301654
48	6	0	-8.276637	-4.271643	-0.534468
49	6	0	-8.463391	-2.935120	-0.173347
50	7	0	-7.576483	-1.987282	-0.563693
51	6	0	-6.487650	-2.321631	-1.297191
52	6	0	6.487441	-2.321820	-1.297082
53	7	0	7.576361	-1.987633	-0.563642
54	6	0	8.463223	-2.935587	-0.173472
55	6	0	8.276340	-4.272055	-0.534733
56	6	0	7.164597	-4.640019	-1.301896
57	6	0	-6.244744	-3.645609	-1.689278
58	6	0	6.244422	-3.645729	-1.689328
59	8	0	-4.711712	-1.838840	-3.458817

60	8	0	-4.777914	-6.195855	-1.783491	110	8	0	-4.712037	-3.459736	1.835551
61	8	0	4.711389	-1.838861	-3.458906	111	6	0	6.244556	-1.692297	3.644619
62	8	0	4.777527	-6.195805	-1.783414	112	6	0	-6.244731	-1.692070	3.644631
63	7	0	5.088681	-3.945295	-2.447762	113	6	0	7.164736	-1.305826	4.639310
64	7	0	-5.089075	-3.945294	-2.447775	114	6	0	8.276181	-0.537823	4.272190
65	6	0	-4.415541	-5.218693	-2.434147	115	6	0	8.462906	-0.174912	2.936139
66	6	0	-0.000186	-6.334836	-6.450961	116	7	0	7.576130	-0.564248	1.987779
67	6	0	-0.000186	-5.030753	-6.979159	117	6	0	6.487387	-1.298314	2.321199
68	6	0	-4.390875	-3.021075	-3.283886	118	6	0	-6.487465	-1.298076	2.321198
69	6	0	4.415076	-5.218642	-2.434022	119	7	0	-7.576122	-0.563909	1.987722
70	6	0	4.390466	-3.021054	-3.283844	120	6	0	-8.462912	-0.174488	2.936035
71	6	0	2.236831	-5.985095	-3.632498	121	6	0	-8.276290	-0.537415	4.272096
72	6	0	1.213710	-5.541696	-4.477482	122	6	0	-7.164928	-1.305514	4.639276
73	6	0	-0.000192	-6.362786	-4.917455	123	6	0	-0.000181	-8.360970	4.811562
74	6	0	-1.214104	-5.541702	-4.477498	124	6	0	-0.000181	-9.219023	5.928750
75	6	0	-2.237243	-5.985112	-3.632541	125	6	0	-0.000169	-8.693787	7.228960
76	6	0	-3.236466	-5.061654	-3.322868	126	6	0	-0.000156	-7.300625	7.436564
77	6	0	-3.229937	-3.760748	-3.837434	127	6	0	0.000232	7.299270	-7.438462
78	6	0	-2.227105	-3.313619	-4.699141	128	6	0	0.000246	8.692498	-7.231291
79	6	0	-1.212537	-4.225081	-5.007763	129	6	0	0.000253	9.218140	-5.931244
80	6	0	-0.000190	-3.943662	-5.897079	130	6	0	0.000247	8.360435	-4.813792
81	6	0	1.212152	-4.225081	-5.007759	131	6	0	-7.164594	1.305199	-4.639280
82	6	0	2.226723	-3.313620	-4.699139	132	6	0	-8.276064	0.537341	-4.271931
83	6	0	3.229533	-3.760736	-3.837399	133	6	0	-8.462889	0.174955	-2.935755
84	6	0	3.236041	-5.061632	-3.322803	134	7	0	-7.576187	0.564696	-1.987490
85	6	0	3.236218	-3.327796	5.058376	135	6	0	-6.487465	1.298709	-2.321102
86	6	0	3.229738	-3.840728	3.756824	136	6	0	6.487705	1.298419	-2.321050
87	6	0	2.226844	-4.701811	3.308595	137	7	0	7.576352	0.564286	-1.987450
88	6	0	1.212208	-5.011505	4.219637	138	6	0	8.462947	0.174364	-2.935740
89	6	0	-0.000170	-5.900439	3.937104	139	6	0	8.276081	0.536667	-4.271931
90	6	0	-1.212530	-5.011488	4.219653	140	6	0	7.164687	1.304636	-4.639272
91	6	0	-2.227169	-4.701770	3.308621	141	6	0	-6.244504	1.692132	-3.644678
92	6	0	-3.230053	-3.840685	3.756869	142	6	0	6.244712	1.691778	-3.644644
93	6	0	-3.236518	-3.327770	5.058427	143	8	0	-4.711529	3.460272	-1.836143
94	6	0	-2.237251	-3.638556	5.981450	144	8	0	-4.777782	1.789143	-6.194791
95	6	0	-1.214073	-4.482884	5.536936	145	8	0	4.711877	3.460152	-1.836145
96	6	0	-0.000146	-4.923851	6.357447	146	8	0	4.778031	1.788922	-6.194761
97	6	0	1.213775	-4.482898	5.536919	147	7	0	5.089218	2.450923	-3.943543
98	6	0	2.236964	-3.638574	5.981416	148	7	0	-5.088913	2.451127	-3.943561
99	6	0	4.390801	-3.286350	3.017934	149	6	0	-4.415296	2.438697	-5.216945
100	6	0	4.415278	-2.439274	5.216578	150	6	0	0.000225	6.456306	-6.329229
101	6	0	-4.391118	-3.286290	3.017995	151	6	0	0.000232	6.983293	-5.024655
102	6	0	-0.000170	-6.983894	5.022850	152	6	0	-4.390651	3.286326	-3.018523
103	6	0	-0.000157	-6.457319	6.327589	153	6	0	4.415646	2.438588	-5.216952
104	6	0	-4.415575	-2.439250	5.216654	154	6	0	4.391059	3.286266	-3.018550
105	7	0	-5.089225	-2.451268	3.943294	155	6	0	2.237310	3.637623	-5.982186
106	7	0	5.088969	-2.451390	3.943243	156	6	0	1.214126	4.482098	-5.537957
107	8	0	4.777765	-1.790030	6.194629	157	6	0	0.000205	4.922825	-6.358616
108	8	0	4.711772	-3.459905	1.835522	158	6	0	-1.213727	4.482131	-5.537955
109	8	0	-4.777996	-1.789952	6.194694	159	6	0	-2.236936	3.637688	-5.982184

160	6	0	-3.236187	3.327208	-5.059035
161	6	0	-3.229660	3.840521	-3.757640
162	6	0	-2.226776	4.701758	-3.309695
163	6	0	-1.212156	5.011167	-4.220844
164	6	0	0.000221	5.900181	-3.938582
165	6	0	1.212576	5.011139	-4.220847
166	6	0	2.227195	4.701711	-3.309704
167	6	0	3.230059	3.840454	-3.757655
168	6	0	3.236561	3.327127	-5.059043
169	46	0	-7.691900	0.000476	0.000136
170	46	0	7.692059	0.000105	0.000194
171	1	0	2.239843	2.306222	5.102299
172	1	0	0.000018	2.932892	6.309170
173	1	0	-2.239777	2.306364	5.102168
174	1	0	-2.258626	6.992765	3.229961
175	1	0	0.000212	7.374886	4.509928
176	1	0	2.259071	6.992604	3.230049
177	1	0	7.009441	5.674391	1.580412
178	1	0	8.998330	5.016304	0.223199
179	1	0	9.308536	2.614191	-0.421883
180	1	0	5.820201	1.524314	1.590245
181	1	0	-5.820000	1.524706	1.590153
182	1	0	-9.308391	2.614547	-0.421909
183	1	0	-8.998160	5.016675	0.223102
184	1	0	-7.009230	5.674791	1.580227
185	1	0	-0.000028	3.816466	8.768528
186	1	0	-0.000002	5.795007	10.288256
187	1	0	0.000101	8.091096	9.357011
188	1	0	0.000188	8.452139	6.889154
189	1	0	-0.000183	-8.452130	-6.888386
190	1	0	-0.000177	-8.091274	-9.356267
191	1	0	-0.000179	-5.795254	-10.287689
192	1	0	-0.000182	-3.816599	-8.768110
193	1	0	-7.009120	-5.674063	-1.579004
194	1	0	-8.998033	-5.015783	-0.221961
195	1	0	-9.308432	-2.613528	0.422490
196	1	0	-5.820314	-1.523855	-1.590135
197	1	0	5.820128	-1.523964	-1.589851
198	1	0	9.308336	-2.614126	0.422334
199	1	0	8.997697	-5.016286	-0.222355
200	1	0	7.008635	-5.674251	-1.579374
201	1	0	2.258548	-6.992327	-3.229173
202	1	0	-0.000192	-7.374699	-4.509244
203	1	0	-2.258972	-6.992349	-3.229231
204	1	0	-2.239989	-2.306145	-5.101930
205	1	0	-0.000188	-2.932842	-6.308824
206	1	0	2.239621	-2.306154	-5.101948
207	1	0	2.239752	-5.103387	2.300637
208	1	0	-0.000179	-6.310936	2.925777
209	1	0	-2.240088	-5.103335	2.300658
210	1	0	-2.258953	-3.236479	6.989180
211	1	0	-0.000134	-4.516915	7.369872
212	1	0	2.258682	-3.236490	6.989143
213	1	0	7.009002	-1.584638	5.673210
214	1	0	8.997461	-0.226072	5.016759
215	1	0	9.307817	0.421535	2.615336
216	1	0	5.820050	-1.590242	1.523059
217	1	0	-5.820111	-1.590068	1.523093
218	1	0	-9.307752	0.422033	2.615187
219	1	0	-8.997579	-0.225599	5.016629
220	1	0	-7.009271	-1.584331	5.673185
221	1	0	-0.000191	-8.771350	3.806489
222	1	0	-0.000190	-10.293367	5.783264
223	1	0	-0.000169	-9.364785	8.080439
224	1	0	-0.000145	-6.897350	8.444339
225	1	0	0.000226	6.895686	-8.446114
226	1	0	0.000251	9.363231	-8.082978
227	1	0	0.000264	10.292530	-5.786092
228	1	0	0.000252	8.771123	-3.808843
229	1	0	-7.008779	1.583563	-5.673287
230	1	0	-8.997287	0.225302	-5.016434
231	1	0	-9.307807	-0.421381	-2.614774
232	1	0	-5.820270	1.591057	-1.523002
233	1	0	5.820605	1.590914	-1.522927
234	1	0	9.307815	-0.422048	-2.614765
235	1	0	8.997214	0.224476	-5.016458
236	1	0	7.008842	1.582930	-5.673293
237	1	0	2.259028	3.235234	-6.989792
238	1	0	0.000199	4.515575	-7.370915
239	1	0	-2.258672	3.235307	-6.989792
240	1	0	-2.239656	5.103618	-2.301848
241	1	0	0.000226	6.310993	-2.927382
242	1	0	2.240094	5.103581	-2.301862

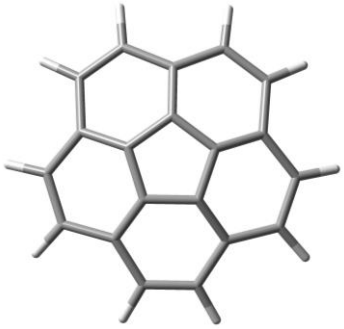

Figure 4.4.37 The optimized geometry of corannulene at M06-2X/Lanl2dz level of theory in the gas-phase

Standard orientation:

Center Number	Atomic Number	Atomic Type	Coordinates (Angstroms) X	Y	Z
1	6	0	3.084531	-1.118358	-0.250249
2	6	0	3.270333	0.264595	-0.250195
3	6	0	1.805322	-1.722306	0.093512
4	6	0	2.195890	1.184748	0.093547
5	6	0	0.875544	-0.835255	0.607205
6	6	0	2.016773	2.587928	-0.250269
7	6	0	0.758957	3.191968	-0.250344
8	6	0	1.064922	0.574561	0.607212
9	6	0	-0.523815	-1.090777	0.607233
10	6	0	1.262206	-3.028459	-0.250352
11	6	0	-0.110445	-3.279108	-0.250346
12	6	0	-0.217356	1.190361	0.607183
13	6	0	-1.080125	-2.249172	0.093543
14	6	0	-2.490203	-2.136285	-0.250295
15	6	0	-1.199274	0.161116	0.607277
16	6	0	-0.448191	2.454498	0.093442
17	6	0	-1.838073	2.717775	-0.250388
18	6	0	-2.801268	1.708197	-0.250283
19	6	0	-2.472955	0.332229	0.093699
20	6	0	-3.152807	-0.908281	-0.250163
21	1	0	3.895644	-1.751120	-0.600354
22	1	0	4.219638	0.660878	-0.600406
23	1	0	2.869247	3.163755	-0.600382
24	1	0	0.675449	4.217258	-0.600603
25	1	0	1.932383	-3.808778	-0.600824
26	1	0	-0.461603	-4.245932	-0.600794
27	1	0	-3.025271	-3.014828	-0.600632
28	1	0	-2.122276	3.706419	-0.600665
29	1	0	-3.802161	1.945594	-0.600601
30	1	0	-4.180847	-0.873088	-0.600552

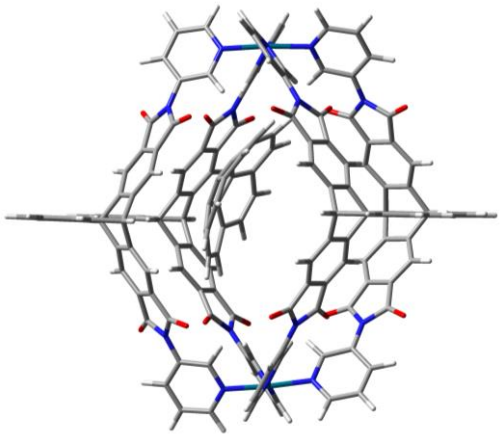

Figure 4.4.38 The optimized geometry of Cor@$Pd_2\mathbf{L^P}_4$ at M06-2X/Lanl2dz level of theory in the gas-phase

Standard orientation:

Center Number	Atomic Number	Atomic Type	Coordinates (Angstroms) X	Y	Z
1	6	0	2.466078	-5.385790	-1.834557
2	6	0	2.538102	-4.415845	-2.839690
3	6	0	1.512602	-4.242290	-3.769363
4	6	0	0.395743	-5.071141	-3.636218
5	6	0	-0.802602	-5.104434	-4.582950
6	6	0	-2.037709	-4.922533	-3.706753
7	6	0	-3.019587	-3.945585	-3.885517
8	6	0	-4.078321	-3.948665	-2.980238
9	6	0	-4.186258	-4.902632	-1.962277
10	6	0	-3.218985	-5.894061	-1.782766
11	6	0	-2.131387	-5.881388	-2.665050
12	6	0	-0.969746	-6.875279	-2.672797
13	6	0	0.309039	-6.038034	-2.600489
14	6	0	1.351113	-6.214480	-1.684911
15	6	0	3.848219	-3.718633	-2.734272
16	6	0	3.754416	-5.401860	-1.090474
17	6	0	-5.199078	-2.987225	-2.854570
18	6	0	-0.878020	-6.547041	-5.106209
19	6	0	-0.969902	-7.502320	-4.076161
20	6	0	-5.435548	-4.640716	-1.195402
21	7	0	-6.018786	-3.478680	-1.803567
22	7	0	4.562458	-4.394934	-1.704279
23	8	0	4.107852	-6.128072	-0.161923
24	8	0	4.285723	-2.760739	-3.378247
25	8	0	-5.916318	-5.247171	-0.240392
26	8	0	-5.392122	-1.929052	-3.465928
27	6	0	5.868817	-4.075179	-1.282905
28	6	0	-7.175578	-2.830576	-1.324104
29	6	0	6.785138	-5.083362	-0.946422
30	6	0	8.061107	-4.718707	-0.496092
31	6	0	8.382319	-3.367612	-0.369978
32	7	0	7.481925	-2.400949	-0.692284
33	6	0	6.254721	-2.733017	-1.159089
34	6	0	-7.179960	-1.433718	-1.216504
35	7	0	-8.242151	-0.769621	-0.708496
36	6	0	-9.352607	-1.450780	-0.318846
37	6	0	-9.412790	-2.841400	-0.418337
38	6	0	-8.308547	-3.549029	-0.915681
39	6	0	-0.863729	-6.940327	-6.442089
40	6	0	-0.942393	-8.313819	-6.746344
41	6	0	-1.033749	-9.265127	-5.720635
42	6	0	-1.047997	-8.861385	-4.370837
43	6	0	0.708010	7.644003	7.110253
44	6	0	0.645309	7.435897	8.502038
45	6	0	0.505611	6.141211	9.022012
46	6	0	0.426009	5.029751	8.160128
47	6	0	-6.640831	5.678850	1.185586
48	6	0	-7.833372	5.474094	0.482753
49	6	0	-8.224890	4.178465	0.141693
50	7	0	-7.462660	3.114002	0.494343
51	6	0	-6.303440	3.286307	1.173444
52	6	0	6.924510	1.925662	1.407377
53	7	0	7.956309	1.494276	0.642991
54	6	0	8.905607	2.361704	0.214469
55	6	0	8.836060	3.713747	0.559115
56	6	0	7.762179	4.188500	1.321407
57	6	0	-5.851955	4.565000	1.534877
58	6	0	6.772758	3.278893	1.745611
59	8	0	-4.466410	2.563945	3.215531
60	8	0	-4.061238	6.906961	1.553125
61	8	0	4.973140	1.625230	3.420664
62	8	0	5.561190	5.968641	1.811636
63	7	0	5.630605	3.693181	2.473482
64	7	0	-4.630980	4.710199	2.233321
65	6	0	-3.810721	5.893446	2.201489
66	6	0	0.628415	6.540919	6.263168
67	6	0	0.488366	5.241516	6.784598
68	6	0	-4.021281	3.705192	3.044099
69	6	0	5.079200	5.027056	2.435260
70	6	0	4.796986	2.840880	3.252697
71	6	0	2.923381	5.991756	3.534001
72	6	0	1.825065	5.641523	4.327801
73	6	0	0.678453	6.571534	4.729713
74	6	0	-0.596463	5.871481	4.252804
75	6	0	-1.559041	6.418067	3.397028
76	6	0	-2.646730	5.603864	3.077368
77	6	0	-2.778552	4.308036	3.586337
78	6	0	-1.832996	3.756269	4.451562
79	6	0	-0.736092	4.559910	4.777027
80	6	0	0.418033	4.161425	5.696932
81	6	0	1.678361	4.329175	4.848578
82	6	0	2.613492	3.327453	4.573492
83	6	0	3.690598	3.684046	3.761623
84	6	0	3.845893	4.980495	3.262307
85	6	0	3.750502	3.724478	-4.677653
86	6	0	3.786048	4.087271	-3.327155
87	6	0	2.826316	4.932849	-2.767573
88	6	0	1.818875	5.393734	-3.622433
89	6	0	0.667116	6.321340	-3.230176
90	6	0	-0.613948	5.583143	-3.625673
91	6	0	-1.683550	5.284832	-2.774152
92	6	0	-2.768652	4.612174	-3.340207
93	6	0	-2.793592	4.262260	-4.694614

94	6	0	-1.737648	4.558667	-5.556701	144	8	0	-5.340686	-2.037358	5.629676
95	6	0	-0.640125	5.222795	-4.998167	145	8	0	4.186241	-3.432449	1.010939
96	6	0	0.617942	5.654179	-5.752896	146	8	0	4.173265	-2.761001	5.629625
97	6	0	1.788896	5.029173	-4.993790	147	7	0	4.550184	-2.949447	3.301032
98	6	0	2.761789	4.188493	-5.545367	148	7	0	-5.651097	-2.085564	3.284911
99	6	0	4.931314	3.402201	-2.678747	149	6	0	-5.008192	-2.454343	4.524369
100	6	0	4.872469	2.794380	-4.953731	150	6	0	-0.905160	-6.937804	4.542511
101	6	0	-4.021189	4.135912	-2.700550	151	6	0	-0.918960	-7.107933	3.145333
102	6	0	0.762545	7.529244	-4.173722	152	6	0	-5.012177	-2.729535	2.187438
103	6	0	0.737199	7.169009	-5.533886	153	6	0	3.813407	-3.149704	4.519558
104	6	0	-4.069181	3.561742	-4.985398	154	6	0	3.821584	-3.482402	2.190632
105	7	0	-4.787123	3.515182	-3.735771	155	6	0	1.519679	-4.293097	4.940570
106	7	0	5.569366	2.630700	-3.701062	156	6	0	0.450165	-4.914960	4.289915
107	8	0	5.169143	2.224013	-6.000669	157	6	0	-0.802602	-5.467692	4.971279
108	8	0	5.278994	3.432807	-1.490341	158	6	0	-1.970315	-4.748256	4.299158
109	8	0	-4.473378	3.083272	-6.042043	159	6	0	-2.937230	-3.974773	4.953215
110	8	0	-4.363790	4.216456	-1.513397	160	6	0	-3.901996	-3.371201	4.146805
111	6	0	6.645891	1.727818	-3.505366	161	6	0	-3.922149	-3.550585	2.758838
112	6	0	-6.052218	2.900727	-3.566368	162	6	0	-2.984077	-4.347059	2.099883
113	6	0	7.458474	1.275318	-4.565703	163	6	0	-1.988074	-4.925530	2.891363
114	6	0	8.441320	0.313257	-4.302108	164	6	0	-0.829251	-5.780824	2.379708
115	6	0	8.604524	-0.188135	-3.007118	165	6	0	0.442376	-5.093837	2.882086
116	7	0	7.838679	0.278227	-1.992810	166	6	0	1.517544	-4.682223	2.088055
117	6	0	6.890924	1.218544	-2.222325	167	6	0	2.578015	-4.062919	2.749587
118	6	0	-6.422438	2.424767	-2.301527	168	6	0	2.573935	-3.866828	4.133346
119	7	0	-7.623612	1.833223	-2.083716	169	46	0	-7.917594	1.199183	-0.133857
120	6	0	-8.499816	1.659829	-3.101656	170	46	0	7.795762	-0.454909	-0.053999
121	6	0	-8.186951	2.108727	-4.388267	171	1	0	1.593356	-3.508177	-4.564521
122	6	0	-6.962791	2.742127	-4.632325	172	1	0	-0.733961	-4.362264	-5.380708
123	6	0	0.865531	8.865438	-3.793686	173	1	0	-2.968965	-3.221192	-4.691622
124	6	0	0.944597	9.852123	-4.796242	174	1	0	-3.323170	-6.645271	-1.005196
125	6	0	0.919924	9.492693	-6.151261	175	1	0	-1.038108	-7.620137	-1.877344
126	6	0	0.815219	8.139758	-6.529882	176	1	0	1.325917	-6.984737	-0.919177
127	6	0	-0.977738	-8.037945	5.393829	177	1	0	6.500887	-6.125912	-1.024580
128	6	0	-1.064928	-9.326995	4.832463	178	1	0	8.794778	-5.471005	-0.236177
129	6	0	-1.078409	-9.497007	3.440840	179	1	0	9.345573	-3.043401	0.004767
130	6	0	-1.005100	-8.380185	2.585416	180	1	0	5.567722	-1.931741	-1.412484
131	6	0	-7.616520	-0.901190	4.228286	181	1	0	-6.321299	-0.851292	-1.525641
132	6	0	-8.625013	0.051478	4.035104	182	1	0	-10.174936	-0.871782	0.083260
133	6	0	-8.737873	0.717849	2.809454	183	1	0	-10.308845	-3.361935	-0.105235
134	7	0	-7.863020	0.461825	1.809006	184	1	0	-8.321405	-4.630803	-0.977227
135	6	0	-6.854154	-0.424183	1.991110	185	1	0	-0.793144	-6.206463	-7.238912
136	6	0	6.216264	-1.748828	2.005427	186	1	0	-0.932666	-8.637837	-7.780882
137	7	0	7.425788	-1.154875	1.860807	187	1	0	-1.094217	-10.318899	-5.968113
138	6	0	8.273453	-1.051561	2.912086	188	1	0	-1.119025	-9.601331	-3.579676
139	6	0	7.917696	-1.574718	4.158468	189	1	0	0.816609	8.647683	6.711423
140	6	0	6.685484	-2.219120	4.324793	190	1	0	0.705779	8.282866	9.176003
141	6	0	-6.705769	-1.146532	3.180385	191	1	0	0.459062	5.995285	10.095269
142	6	0	5.810007	-2.309707	3.223194	192	1	0	0.318286	4.028869	8.566592
143	8	0	-5.300183	-2.561166	0.991731	193	1	0	-6.324184	6.680859	1.442682

194	1	0	-8.457216	6.313404	0.203114
195	1	0	-9.135187	3.980513	-0.410469
196	1	0	-5.745858	2.400571	1.442856
197	1	0	6.233999	1.178948	1.768900
198	1	0	9.704553	1.965424	-0.399433
199	1	0	9.612379	4.390668	0.226030
200	1	0	7.687873	5.239918	1.564788
201	1	0	3.058671	6.995493	3.144275
202	1	0	0.786743	7.579977	4.327245
203	1	0	-1.476655	7.425371	3.001675
204	1	0	-1.953691	2.755001	4.851655
205	1	0	0.309806	3.154369	6.103687
206	1	0	2.515541	2.321921	4.969775
207	1	0	2.867358	5.213580	-1.720305
208	1	0	0.687625	6.602696	-2.175784
209	1	0	-1.681371	5.565338	-1.725859
210	1	0	-1.777898	4.288630	-6.607033
211	1	0	0.597675	5.376455	-6.807873
212	1	0	2.756709	3.906190	-6.593237
213	1	0	7.315182	1.647180	-5.571396
214	1	0	9.073922	-0.053841	-5.100101
215	1	0	9.333266	-0.953729	-2.773608
216	1	0	6.337355	1.577825	-1.367653
217	1	0	-5.764072	2.543513	-1.453653
218	1	0	-9.436233	1.165230	-2.877206
219	1	0	-8.900173	1.968741	-5.190427
220	1	0	-6.716066	3.089199	-5.627043
221	1	0	0.885338	9.147666	-2.745566
222	1	0	1.025431	10.897109	-4.518998
223	1	0	0.982068	10.261273	-6.913266
224	1	0	0.796313	7.865210	-7.579857
225	1	0	-0.966948	-7.910727	6.471726
226	1	0	-1.121527	-10.193725	5.481118
227	1	0	-1.145193	-10.495087	3.022672
228	1	0	-1.014727	-8.515296	1.507621
229	1	0	-7.532047	-1.428081	5.170018
230	1	0	-9.332607	0.266719	4.825651
231	1	0	-9.516316	1.446307	2.620535
232	1	0	-6.176364	-0.581280	1.165345
233	1	0	5.572083	-1.793952	1.140921
234	1	0	9.221394	-0.555861	2.744642
235	1	0	8.606470	-1.488457	4.989145
236	1	0	6.408884	-2.629310	5.287079
237	1	0	1.540859	-4.149891	6.016149
238	1	0	-0.789157	-5.339733	6.054697
239	1	0	-2.938149	-3.839562	6.029944
240	1	0	-3.017549	-4.485397	1.023418
241	1	0	-0.842371	-5.903441	1.293895
242	1	0	1.528209	-4.820469	1.010631
243	6	0	1.607535	-1.707423	0.390113
244	6	0	2.325456	-1.345434	-0.784342
245	6	0	1.477333	-1.566167	-1.906924
246	6	0	0.233325	-2.065676	-1.425787
247	6	0	0.314750	-2.157863	-0.006488
248	6	0	3.590903	0.209520	-2.085477
249	6	0	-0.494685	-1.713272	2.204516
250	6	0	2.780945	-0.029852	-3.191034
251	6	0	3.040435	-0.303180	1.694057
252	6	0	1.597001	-0.863599	-3.094884
253	6	0	0.404230	-0.859189	-3.925807
254	6	0	-0.817843	-1.328595	-3.448087
255	6	0	-0.959385	-1.857847	-2.100482
256	6	0	-2.144967	-1.912987	-1.264462
257	6	0	-2.065167	-2.008564	0.122634
258	6	0	-0.792702	-2.055659	0.820854
259	6	0	0.770450	-1.276075	2.591314
260	6	0	1.858347	-1.145885	1.632976
261	6	0	3.725447	0.072275	0.535613
262	6	0	3.319972	-0.378911	-0.784486
263	1	0	4.397897	0.925759	-2.183207
264	1	0	-1.298935	-1.710532	2.938360
265	1	0	2.997384	0.483248	-4.124975
266	1	0	3.349050	0.137381	2.640191
267	1	0	0.437821	-0.389963	-4.905142
268	1	0	-1.704760	-1.194372	-4.062458
269	1	0	-3.119560	-1.751539	-1.717464
270	1	0	-2.986002	-1.930771	0.690835
271	1	0	0.919992	-0.945546	3.616222
272	1	0	4.509667	0.823175	0.618801

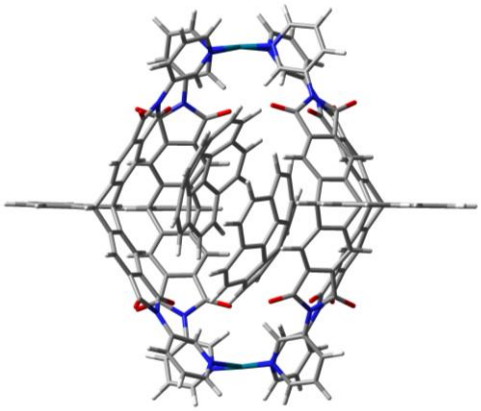

Figure 4.4.39 The optimized geometry of $(Cor)_2@Pd_2\mathbf{L^P}_4$ at M06-2X/Lanl2dz level of theory in the gas-phase

Standard orientation:

Center Number	Atomic Number	Atomic Type	Coordinates (Angstroms) X	Y	Z
1	6	0	-3.002680	5.544644	-1.746619
2	6	0	-2.982557	4.647368	-2.819495
3	6	0	-1.905414	4.580088	-3.702865
4	6	0	-0.825393	5.428165	-3.445455
5	6	0	0.412425	5.577670	-4.326928
6	6	0	1.621701	5.385744	-3.417135
7	6	0	2.673052	4.494354	-3.645691
8	6	0	3.721558	4.511409	-2.727761
9	6	0	3.745100	5.390738	-1.639435
10	6	0	2.701118	6.288605	-1.401763
11	6	0	1.629796	6.267068	-2.304554
12	6	0	0.419096	7.201370	-2.283939
13	6	0	-0.827477	6.315245	-2.337777
14	6	0	-1.926973	6.395484	-1.476415
15	6	0	-4.262263	3.887717	-2.828543
16	6	0	-4.329803	5.458915	-1.075561
17	6	0	4.935932	3.662077	-2.680607
18	6	0	0.446810	7.059454	-4.737486
19	6	0	0.451569	7.935534	-3.635148
20	6	0	5.018129	5.187414	-0.891879
21	7	0	5.708436	4.141796	-1.591682
22	7	0	-5.047654	4.443909	-1.780940
23	8	0	-4.774965	6.123050	-0.140371
24	8	0	-4.630274	2.969143	-3.565540
25	8	0	5.445224	5.758871	0.109247
26	8	0	5.241204	2.695948	-3.391245
27	6	0	-6.344983	4.010838	-1.433302
28	6	0	6.933379	3.578618	-1.168987
29	6	0	-7.362022	4.934880	-1.157490
30	6	0	-8.626706	4.458598	-0.783633
31	6	0	-8.831690	3.085435	-0.664964
32	7	0	-7.831134	2.196786	-0.918588
33	6	0	-6.615197	2.638281	-1.318869
34	6	0	7.060621	2.185193	-1.113978
35	7	0	8.184223	1.586547	-0.660287
36	6	0	9.248614	2.346533	-0.286596
37	6	0	9.192263	3.740842	-0.338122
38	6	0	8.016219	4.373979	-0.768056
39	6	0	0.471778	7.554359	-6.038972
40	6	0	0.501546	8.949649	-6.234418
41	6	0	0.506315	9.821585	-5.136770
42	6	0	0.481234	9.315139	-3.822003
43	6	0	-0.478541	-7.969563	5.974279
44	6	0	-0.482678	-7.982750	7.383136
45	6	0	-0.443361	-6.781942	8.105744
46	6	0	-0.399289	-5.544496	7.433531
47	6	0	7.243650	-4.919704	1.466712
48	6	0	8.482812	-4.586052	0.903372
49	6	0	8.745716	-3.262145	0.548756
50	7	0	7.817462	-2.293418	0.757049
51	6	0	6.622225	-2.590543	1.312059
52	6	0	-7.144312	-2.040915	1.332079
53	7	0	-8.240439	-1.627315	0.656374
54	6	0	-9.186946	-2.516909	0.267308
55	6	0	-9.039381	-3.877960	0.547922
56	6	0	-7.879447	-4.335788	1.186418
57	6	0	6.296811	-3.903342	1.669731
58	6	0	-6.902393	-3.399660	1.571865
59	8	0	4.652972	-2.175313	3.385468
60	8	0	4.637142	-6.263316	1.141078
61	8	0	-5.130711	-1.812386	3.314904
62	8	0	-5.418253	-5.878350	1.055369
63	7	0	-5.675644	-3.792708	2.146446

64	7	0	5.014863	-4.174740	2.185058	114	6	0	-8.403202	-1.337971	-4.244392
65	6	0	4.252691	-5.343108	1.859313	115	6	0	-8.632861	-0.556485	-3.106128
66	6	0	-0.434651	-6.743083	5.315468	116	7	0	-7.878359	-0.731313	-1.997571
67	6	0	-0.395317	-5.537559	6.040693	117	6	0	-6.870952	-1.641187	-1.990882
68	6	0	4.266275	-3.287321	3.006537	118	6	0	6.625079	-2.054054	-1.949261
69	6	0	-4.988117	-5.012469	1.813292	119	7	0	7.734035	-1.274309	-1.885253
70	6	0	-4.858893	-2.969928	2.965175	120	6	0	8.543463	-1.155075	-2.966033
71	6	0	-2.692796	-5.923946	2.658825	121	6	0	8.257720	-1.853220	-4.143647
72	6	0	-1.615850	-5.618910	3.499685	122	6	0	7.131505	-2.685151	-4.219231
73	6	0	-0.423158	-6.529527	3.793638	123	6	0	-0.233533	-8.956253	-1.671398
74	6	0	0.828314	-5.698564	3.504176	124	6	0	-0.232202	-10.169733	-2.387858
75	6	0	1.886387	-6.074941	2.670195	125	6	0	-0.236312	-10.166466	-3.789532
76	6	0	2.962891	-5.189996	2.585691	126	6	0	-0.241716	-8.950270	-4.501309
77	6	0	2.983941	-3.979808	3.286537	127	6	0	0.265767	8.195057	5.417665
78	6	0	1.940451	-3.597817	4.128643	128	6	0	0.308092	9.488840	4.861432
79	6	0	0.863106	-4.481031	4.232251	129	6	0	0.337790	9.664260	3.470904
80	6	0	-0.350459	-4.294901	5.139251	130	6	0	0.325969	8.547997	2.611371
81	6	0	-1.569155	-4.400731	4.227376	131	6	0	7.332430	1.536821	4.398133
82	6	0	-2.582569	-3.445851	4.115625	132	6	0	8.439721	0.697775	4.221477
83	6	0	-3.643615	-3.759197	3.267112	133	6	0	8.709495	0.133315	2.969232
84	6	0	-3.705380	-4.967119	2.565404	134	7	0	7.906706	0.402743	1.914411
85	6	0	-3.577102	-4.543228	-3.770384	135	6	0	6.825627	1.204583	2.067267
86	6	0	-3.561686	-4.510667	-2.371463	136	6	0	-6.667340	1.746352	1.880863
87	6	0	-2.518908	-5.079089	-1.636578	137	7	0	-7.857985	1.122725	1.704780
88	6	0	-1.467264	-5.649648	-2.366544	138	6	0	-8.753398	1.048554	2.718281
89	6	0	-0.234895	-6.341248	-1.778392	139	6	0	-8.465622	1.629169	3.957163
90	6	0	1.000130	-5.664610	-2.380175	140	6	0	-7.250196	2.296349	4.156773
91	6	0	2.100848	-5.183537	-1.660177	141	6	0	6.492517	1.794306	3.293203
92	6	0	3.151784	-4.648271	-2.404620	142	6	0	-6.325249	2.357222	3.094761
93	6	0	3.116166	-4.587084	-3.801122	143	8	0	4.920102	3.002500	1.069689
94	6	0	2.040749	-5.091543	-4.532842	144	8	0	4.991213	2.555405	5.720088
95	6	0	0.981132	-5.641424	-3.798001	145	8	0	-4.644824	3.455333	0.922984
96	6	0	-0.249120	-6.338405	-4.387095	146	8	0	-4.770546	2.856079	5.547512
97	6	0	-1.477014	-5.658522	-3.784322	147	7	0	-5.075742	3.011549	3.207105
98	6	0	-2.546383	-5.118368	-4.510705	148	7	0	5.332915	2.609567	3.374669
99	6	0	-4.710802	-3.698582	-1.904416	149	6	0	4.638037	2.926332	4.605071
100	6	0	-4.757724	-3.790873	-4.254661	150	6	0	0.253863	7.095820	4.562403
101	6	0	4.400772	-4.006737	-1.930884	151	6	0	0.284131	7.271266	3.165785
102	6	0	-0.239553	-7.757392	-2.379207	152	6	0	4.633270	3.170625	2.267445
103	6	0	-0.242302	-7.754752	-3.787411	153	6	0	-4.375595	3.230801	4.445105
104	6	0	4.342408	-3.895955	-4.278495	154	6	0	-4.319849	3.534410	2.112389
105	7	0	5.100105	-3.566350	-3.095305	155	6	0	-2.092994	4.391330	4.911701
106	7	0	-5.430153	-3.291568	-3.072624	156	6	0	-1.017960	5.026973	4.281561
107	8	0	-5.110705	-3.561426	-5.408621	157	6	0	0.205300	5.619602	4.985264
108	8	0	-4.987636	-3.359491	-0.741666	158	6	0	1.420400	4.961697	4.331747
109	8	0	4.684153	-3.615907	-5.425483	159	6	0	2.433277	4.261723	5.000941
110	8	0	4.784113	-3.848218	-0.764563	160	6	0	3.454481	3.733070	4.209764
111	6	0	-6.559151	-2.426783	-3.109853	161	6	0	3.476650	3.905099	2.822010
112	6	0	6.283388	-2.784363	-3.097326	162	6	0	2.493201	4.629993	2.148133
113	6	0	-7.371078	-2.283888	-4.257483	163	6	0	1.450677	5.142344	2.924586

164	6	0	0.263023	5.943191	2.395174	214	1	0	-9.028929	-1.203733	-5.117569
165	6	0	-0.989133	5.208618	2.874750	215	1	0	-9.408549	0.197739	-3.071928
166	6	0	-2.038587	4.773910	2.060047	216	1	0	-6.310110	-1.752458	-1.075759
167	6	0	-3.101168	4.137977	2.700150	217	1	0	6.001545	-2.105779	-1.072605
168	6	0	-3.127165	3.949916	4.084919	218	1	0	9.407127	-0.508672	-2.876359
169	46	0	8.029937	-0.397683	-0.009084	219	1	0	8.919843	-1.753250	-4.994292
170	46	0	-8.065809	0.267462	-0.170714	220	1	0	6.911675	-3.228434	-5.128886
171	1	0	-1.919737	3.908707	-4.555038	221	1	0	-0.228825	-8.962529	-0.585405
172	1	0	0.410097	4.897278	-5.180794	222	1	0	-0.227355	-11.112942	-1.853217
173	1	0	2.688155	3.832582	-4.505664	223	1	0	-0.234688	-11.106133	-4.330115
174	1	0	2.742663	6.989642	-0.572575	224	1	0	-0.243824	-8.952008	-5.586743
175	1	0	0.420760	7.885700	-1.432940	225	1	0	0.241894	8.063923	6.494867
176	1	0	-1.972261	7.111295	-0.659999	226	1	0	0.317123	10.354804	5.513498
177	1	0	-7.164215	5.998197	-1.226169	227	1	0	0.369193	10.665765	3.056758
178	1	0	-9.440113	5.142008	-0.576098	228	1	0	0.347448	8.687509	1.534171
179	1	0	-9.784686	2.680696	-0.346332	229	1	0	7.121248	1.964655	5.369109
180	1	0	-5.843931	1.903510	-1.524941	230	1	0	9.096659	0.481869	5.054464
181	1	0	6.246135	1.545356	-1.416176	231	1	0	9.552416	-0.525727	2.804550
182	1	0	10.128816	1.826615	0.070886	232	1	0	6.230827	1.402198	1.192484
183	1	0	10.054482	4.321285	-0.035506	233	1	0	-5.984019	1.770200	1.045628
184	1	0	7.938683	5.454924	-0.786322	234	1	0	-9.682977	0.526993	2.529096
185	1	0	0.467647	6.882480	-6.891625	235	1	0	-9.192507	1.565345	4.756819
186	1	0	0.520669	9.352184	-7.240879	236	1	0	-7.023646	2.746484	5.114521
187	1	0	0.529346	10.892984	-5.300744	237	1	0	-2.135180	4.252989	5.987329
188	1	0	0.484492	9.993811	-2.974686	238	1	0	0.179137	5.488165	6.068035
189	1	0	-0.509126	-8.901587	5.418620	239	1	0	2.431481	4.132277	6.078413
190	1	0	-0.516738	-8.928291	7.912325	240	1	0	2.531037	4.769122	1.071988
191	1	0	-0.447103	-6.806350	9.189589	241	1	0	0.288859	6.068195	1.309307
192	1	0	-0.368911	-4.616900	7.996751	242	1	0	-2.028295	4.909326	0.982442
193	1	0	7.010930	-5.945662	1.723760	243	6	0	1.341268	-2.083796	-2.610297
194	1	0	9.235756	-5.344984	0.733229	244	6	0	0.487062	-2.347253	-1.510107
195	1	0	9.679819	-2.966700	0.087200	245	6	0	1.196437	-2.054702	-0.314799
196	1	0	5.911498	-1.784182	1.447999	246	6	0	2.484697	-1.581240	-0.680644
197	1	0	-6.459285	-1.280334	1.677862	247	6	0	2.568505	-1.596811	-2.096882
198	1	0	-10.041568	-2.132407	-0.275172	248	6	0	-1.568233	-2.165311	-0.322698
199	1	0	-9.814852	-4.572468	0.250843	249	6	0	3.093221	-0.689236	-4.240723
200	1	0	-7.730266	-5.392890	1.365649	250	6	0	-0.870553	-1.887523	0.856192
201	1	0	-2.760637	-6.867306	2.125600	251	6	0	-0.535269	-2.004892	-4.060750
202	1	0	-0.452717	-7.466404	3.234402	252	6	0	0.577432	-1.720568	0.875142
203	1	0	1.897054	-7.021807	2.138763	253	6	0	1.451432	-1.044579	1.825854
204	1	0	1.987131	-2.673635	4.695477	254	6	0	2.715376	-0.574159	1.465847
205	1	0	-0.321127	-3.361697	5.704838	255	6	0	3.239593	-0.740179	0.116488
206	1	0	-2.567985	-2.518483	4.679706	256	6	0	4.248248	0.011885	-0.613218
207	1	0	-2.513649	-5.050125	-0.551075	257	6	0	4.341722	-0.018717	-2.010257
208	1	0	-0.228223	-6.337146	-0.685931	258	6	0	3.424661	-0.792902	-2.826018
209	1	0	2.137759	-5.210098	-0.575145	259	6	0	1.889868	-1.186530	-4.748110
210	1	0	2.036922	-5.060536	-5.617725	260	6	0	0.896791	-1.819419	-3.890392
211	1	0	-0.256156	-6.339125	-5.478207	261	6	0	-1.378212	-2.220459	-2.971383
212	1	0	-2.570871	-5.127758	-5.595692	262	6	0	-0.889776	-2.314148	-1.604172
213	1	0	-7.190786	-2.877216	-5.143422	263	1	0	-2.655682	-2.199854	-0.281810

264	1	0	3.762016	-0.154815	-4.909857
265	1	0	-1.443318	-1.709544	1.763324
266	1	0	-0.980675	-1.885722	-5.045677
267	1	0	1.078064	-0.817680	2.820410
268	1	0	3.290022	-0.019559	2.205035
269	1	0	4.857984	0.726959	-0.064765
270	1	0	5.039730	0.632591	-2.530408
271	1	0	1.667932	-1.024483	-5.799445
272	1	0	-2.446953	-2.228716	-3.151150
273	6	0	-2.019618	1.853032	0.411606
274	6	0	-2.714161	1.532176	-0.784964
275	6	0	-1.867199	1.846831	-1.884306
276	6	0	-0.646936	2.358912	-1.365006
277	6	0	-0.741407	2.368000	0.053625
278	6	0	-3.948765	0.057925	-2.194302
279	6	0	0.047147	1.882914	2.255634
280	6	0	-3.140958	0.395853	-3.276592
281	6	0	-3.438179	0.370929	1.631851
282	6	0	-1.964301	1.229798	-3.118172
283	6	0	-0.765860	1.317538	-3.935899
284	6	0	0.438624	1.794747	-3.419650
285	6	0	0.555825	2.241645	-2.040780
286	6	0	1.731040	2.306793	-1.191976
287	6	0	1.637843	2.320980	0.198181
288	6	0	0.359475	2.277799	0.888306
289	6	0	-1.207581	1.386791	2.608448
290	6	0	-2.275391	1.242690	1.627892
291	6	0	-4.098328	0.031305	0.445842
292	6	0	-3.690637	0.551318	-0.849172
293	1	0	-4.755384	-0.646045	-2.366564
294	1	0	0.835975	1.895221	3.006372
295	1	0	-3.360887	-0.038385	-4.248620
296	1	0	-3.752334	-0.116658	2.553527
297	1	0	-0.776821	0.915022	-4.945490
298	1	0	1.332066	1.726845	-4.035376
299	1	0	2.716533	2.218100	-1.640761
300	1	0	2.560445	2.250921	0.766616
301	1	0	-1.363474	1.031414	3.624602
302	1	0	-4.863541	-0.743052	0.488052

Table 4.4.2 Summary of the total electronic energies

	Cor	Cage	$(Cor)_2$@Cage	Cor@cage
E [Hartree]	-767.751686	-7554.40071	-9089.998854	-8322.195748
Δ*E* [Hartree]	-	-	-0.094772	-0.043352
Δ*E* kJ/mol	-	-	-248.82	-113.82

Δ*E* Hartree values were calculated for Cor@Cage and $(Cor)_2$@Cage as following:

$$\Delta E = E_{(Cor)n@Cage} - (E_{Cage} + n*E_{Cor})$$

where n = 1 and 2 stands for Cor@Cage and $(Cor)_2$@Cage respectively.

4.4.4 Uptake and release of 4 using $Pd_2L^P_4$

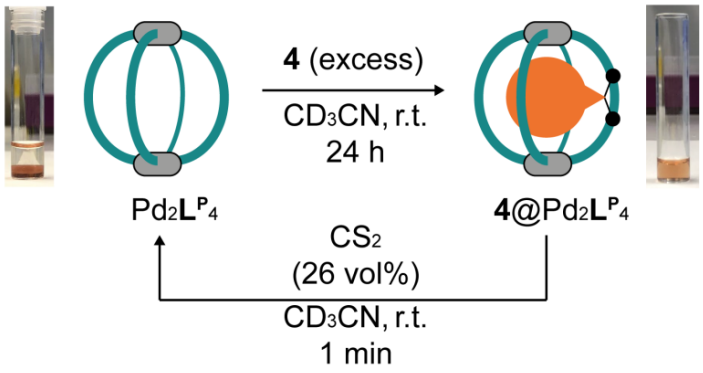

Figure 4.4.40 Uptake and release of **4** using $Pd_2L^P_4$

To an acetonitrile solution of **4**@$Pd_2L^P_4$ (0.7 mM, 2.0 mL, 1.4 µmol) 26 vol% of CS_2 (700 µL) was added. The mixture was shaken for 1 min and let it stand. Afterwards, ^{1}H NMR spectrum of the upper layer (CD_3CN) containing the cage was measured to confirm the liberation of **4**. The CS_2 layer at the bottom was removed by decantation at -78 °C. The recovered acetonitrile solution of $Pd_2L^P_4$ was stirred with solid-state **4** at ambient temperature. The same procedure was repeated 4 times. After 3rd cycle, the encapsulation yield was inclined most likely due to miscible CS_2 in the acetonitrile solution. The yields for each cycle are summarized in **Table 4.4.3.**

4.4.4.1 ^{1}H NMR spectra showing uptake and release of 4

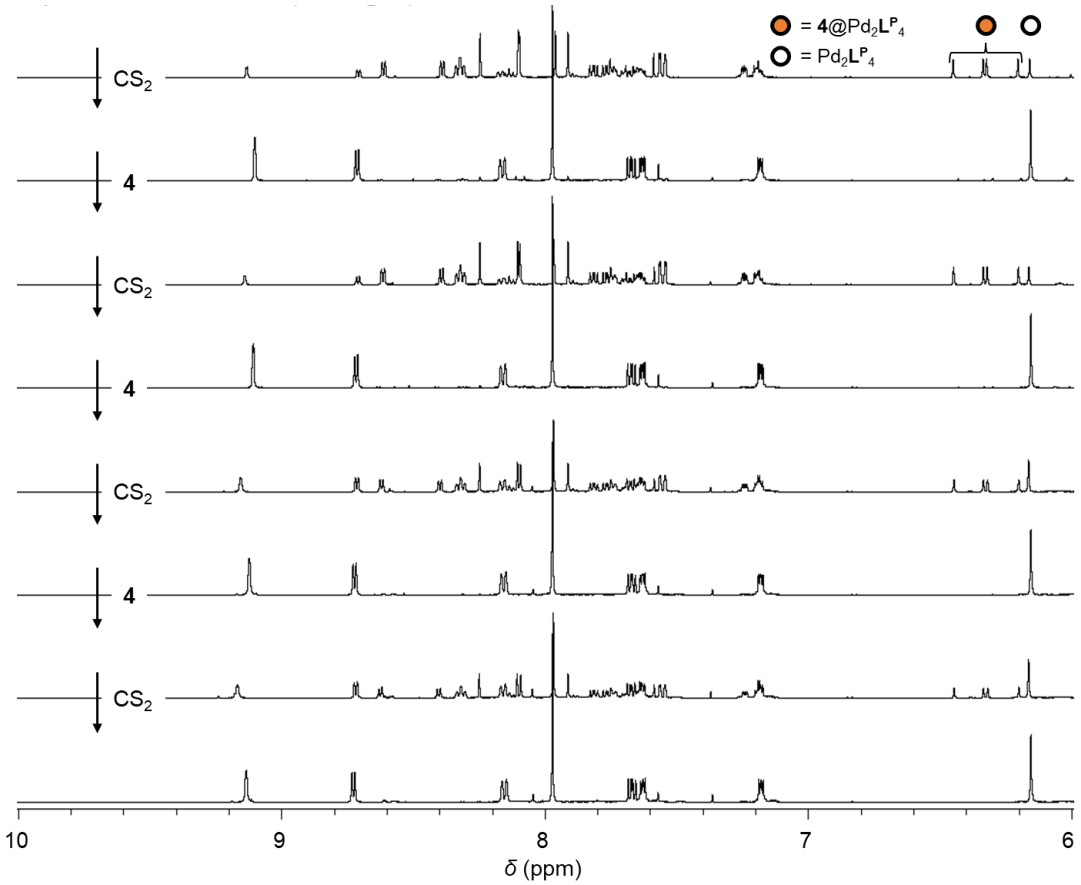

Figure 4.4.41 ^{1}H NMR spectra (CD_3CN, 500 MHz, 298 K) showing uptake and release of **4** by $Pd_2\mathbf{L}^{\mathbf{P}}{}_4$

Table 4.4.3 Encapsulation yield after each cycle

Cycle	Yields (%)
1st	**80.5**
2nd	**80.3**
3rd	**62.9**
4th	**52.2**

4.4.4.2 ^{1}H NMR spectrum of recovered 4

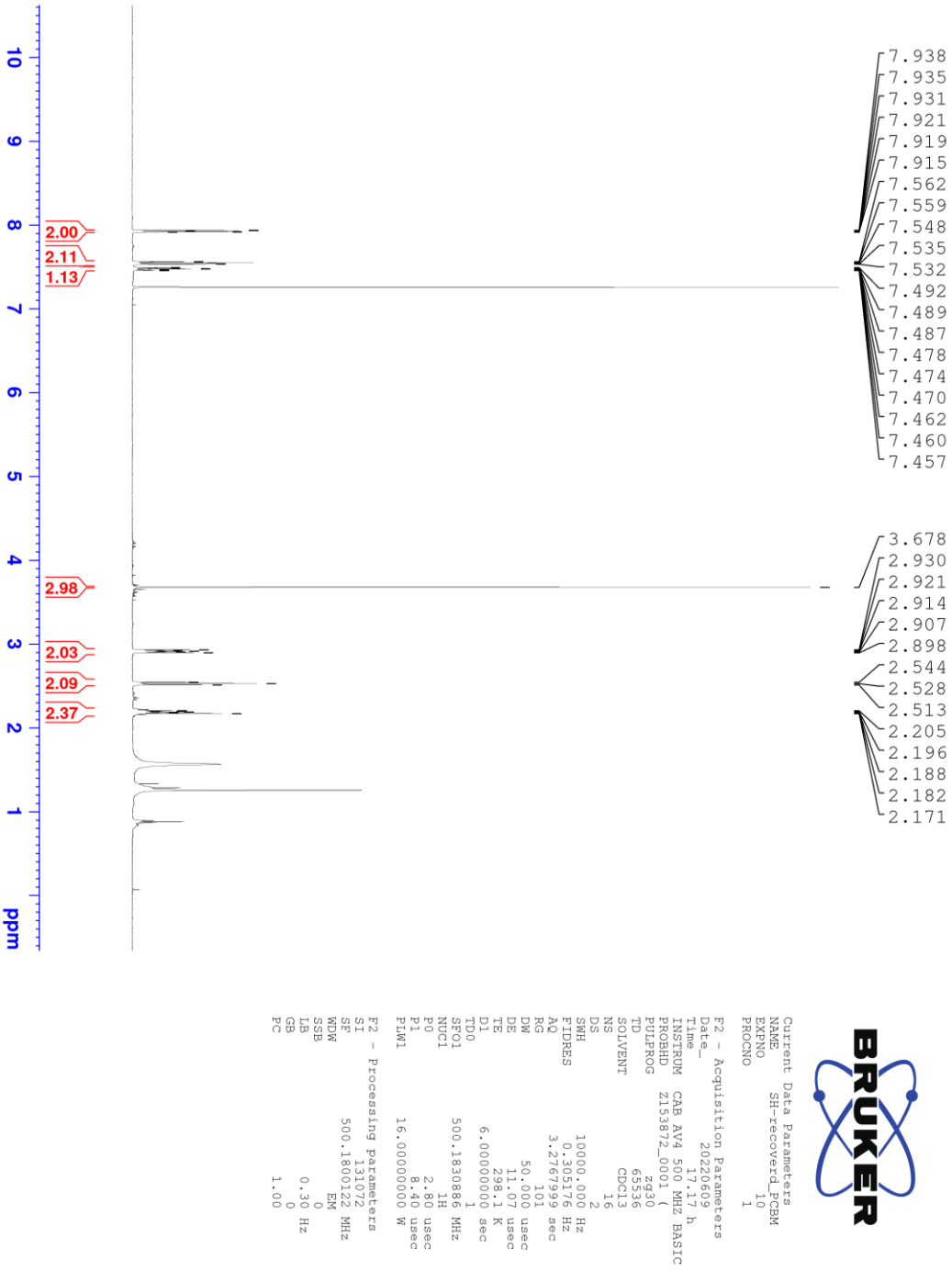

Figure 4.4.42 ^{1}H NMR spectrum ($CDCl_3$, 500 MHz, 298 K) of recovered **4**

4.4.5 Encapsulation of $PC_{62}BM$

To a vial where solid $PC_{62}BM$ (excess) as a mixture of isomers were placed an acetonitrile solution of $Pd_2\mathbf{L}^{\mathbf{P}}_4$ (0.600 mL, 0.70 mM, 0.42 μmol) were added. The mixture was stirred at 70 °C for 24 h and the resulting mixture was filtrated to remove the remaining solid guests.

4.4.5.1 ^{1}H NMR spectra

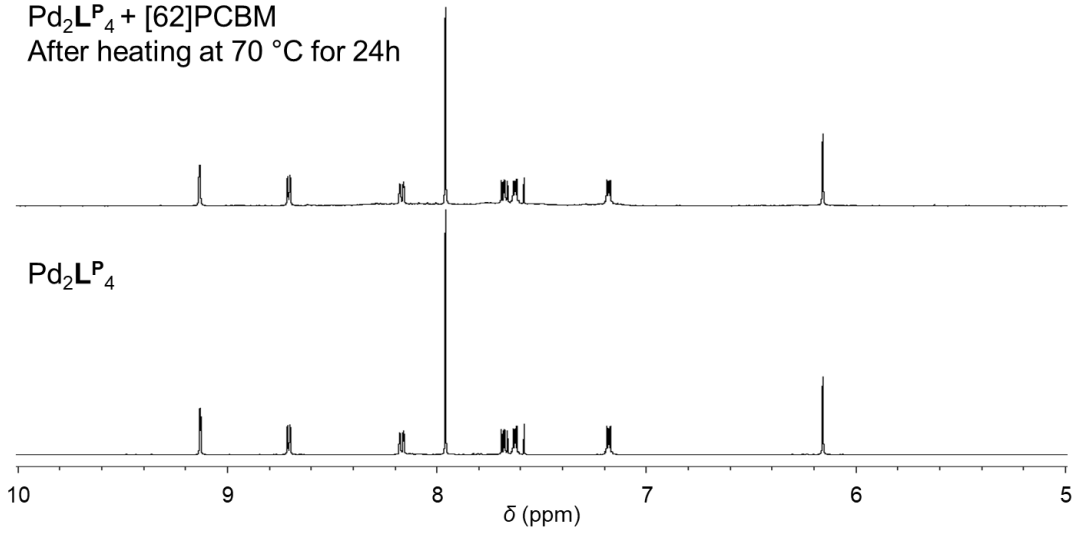

Figure 4.4.43 ^{1}H NMR spectra (CD_3CN, 500 MHz, 298 K) of the sample after heating with $PC_{62}BM$ for 24 h at 70 °C (top) and empty $Pd_2\mathbf{L}^{\mathbf{P}}_4$ (bottom, 0.70 mM)

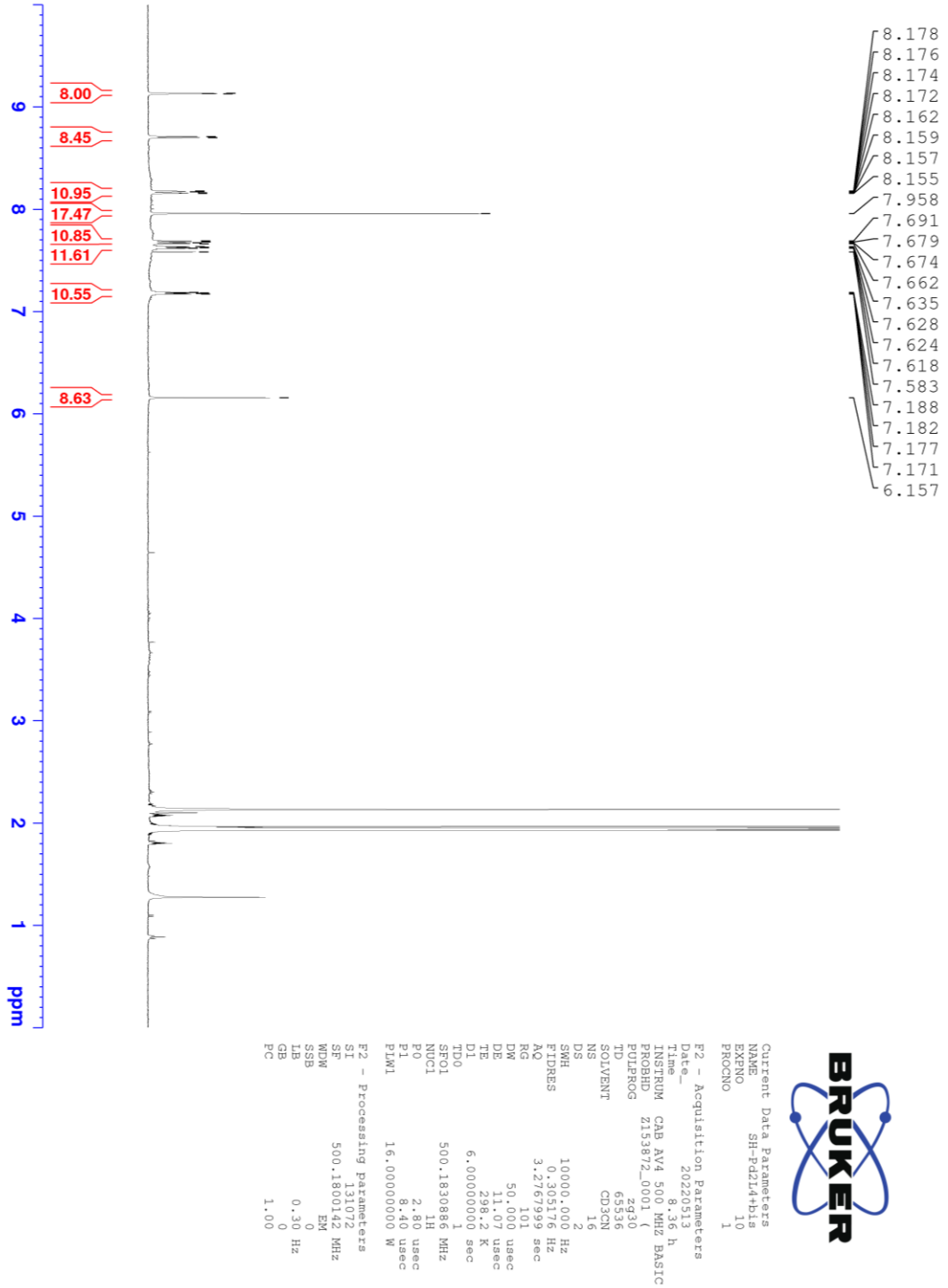

Figure 4.4.44 ^{1}H NMR spectrum (500 MHz, CD_3CN, 298 K) of the sample after heating with $PC_{62}BM$ for 24 h at 70 °C (top). Some of the ^{1}H NMR integration ratio of the cage differ from the theoretical values probably due to slightly solubilized $PC_{62}BM$

4.4.5.2 ESI MS spectrum

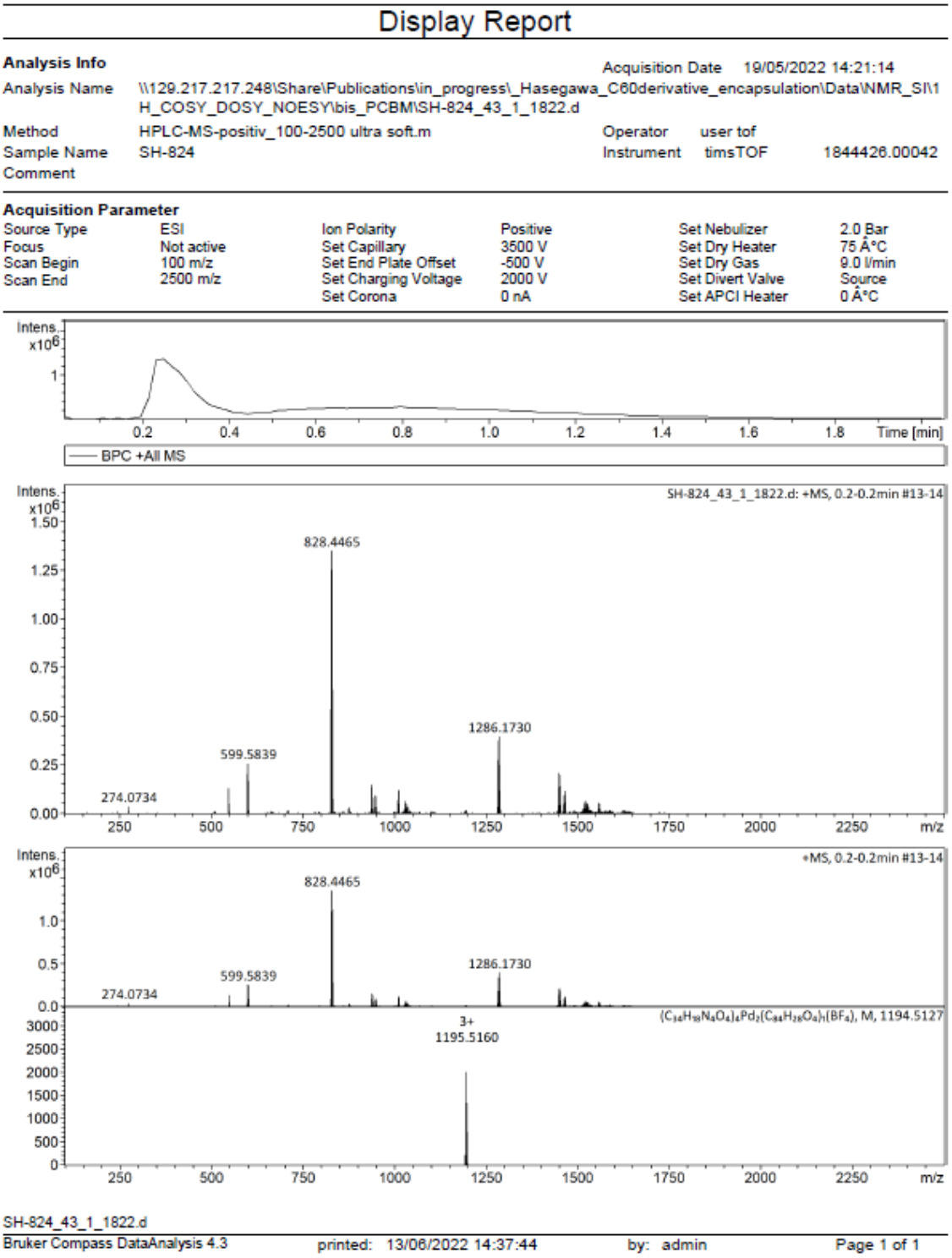

Figure 4.4.45 ESI MS spectrum (positive) of the sample after heating with $PC_{62}BM$ for 24 h. $Pd_2\mathbf{L}^{\mathbf{P}}_4$ was observed as a major species while $[(PC_{62}BM{\bullet}Pd_2\mathbf{L}^{\mathbf{P}}_4)BF_4]^{3+}$ was observed with a negligible intensity.

4.4.5.3 Competition experiment

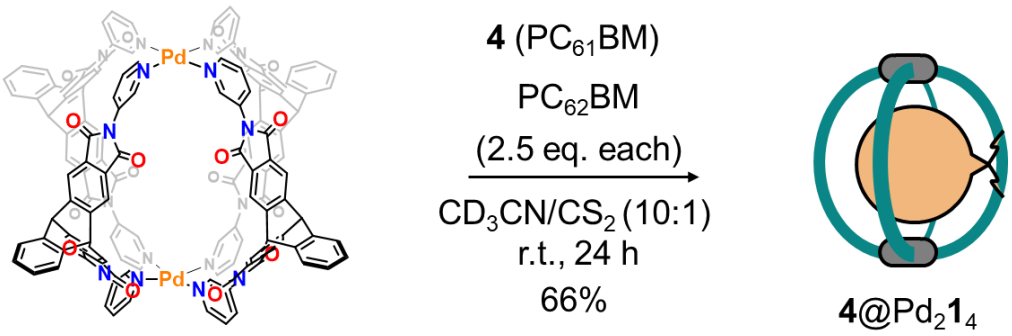

To a vial where solid **4** (1.1 mg, 1.2 μmol) and $PC_{62}BM$ (1.3 mg, 1.2 μmol) were placed an acetonitrile solution of $Pd_2\mathbf{L}^{P}_4$ (0.70 mL, 0.7 mM, 0.49 μmol) and CS_2 (70 μL) were added. The mixture was stirred at room temperature for 24 h and the resulting mixture was filtrated to remove the remaining solid guests. **4**@$Pd_2\mathbf{L}^{P}_4$ was obtained in 66% yield determined by ^{1}H NMR analysis.

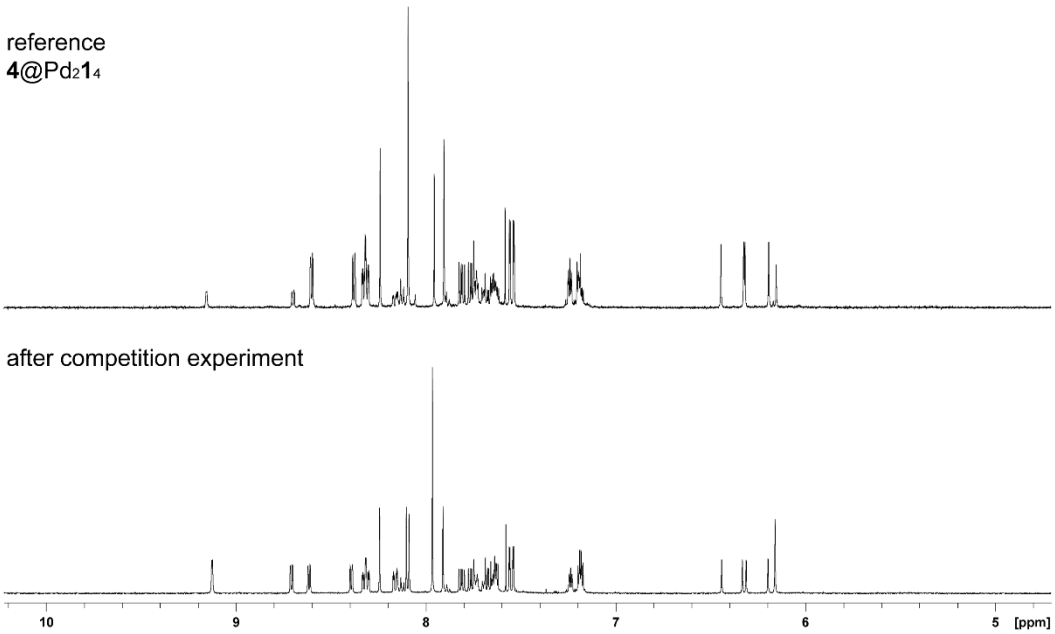

Figure 4.4.46 ^{1}H NMR spectrum of the sample after heating with **4** and $PC_{62}BM$ (CD_3CN/CS_2 = 10:1, 500 MHz, 298 K) for 24 h at r.t. (bottom) and **4**@$Pd_2\mathbf{L}_4$ (top) (CD_3CN, 500 MHz, 298 K)

4.4.5.4 Theoretical study

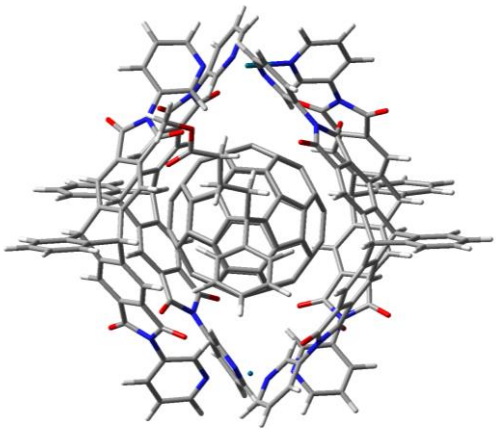

Figure 4.4.47 The optimized geometry of **4**@$Pd_2\mathbf{L}^{\mathbf{P}}_4$ at B3LYP/6-31G(d,p) for H, C, N, O atoms, Lanl2dz for Pd atoms in the gas-phase

Standard orientation:

Center Number	Atomic Number	Atomic Type	Coordinates (Angstroms) X	Y	Z
1	6	0	5.030147	-4.528852	2.154713
2	6	0	5.240487	-4.243045	0.803725
3	6	0	4.704412	-5.049156	-0.203659
4	6	0	3.892607	-6.112027	0.200175
5	6	0	3.157493	-7.085762	-0.727417
6	6	0	1.678001	-7.028954	-0.322921
7	6	0	0.596966	-6.730385	-1.157916
8	6	0	-0.676811	-6.733194	-0.583931
9	6	0	-0.864282	-7.048121	0.763403
10	6	0	0.203407	-7.353558	1.605507
11	6	0	1.481019	-7.328963	1.046166
12	6	0	2.786701	-7.622105	1.786760
13	6	0	3.677990	-6.397290	1.568606
14	6	0	4.260097	-5.615784	2.567699
15	6	0	5.977373	-2.954294	0.699535
16	6	0	5.693358	-3.491397	2.979843
17	6	0	-1.991741	-6.353197	-1.173273
18	6	0	3.647192	-8.485946	-0.336348
19	6	0	3.449970	-8.774229	1.021713
20	6	0	-2.305137	-6.933470	1.093845
21	7	0	-2.938992	-6.487597	-0.114408
22	7	0	6.242616	-2.550661	2.040407
23	8	0	5.772790	-3.384302	4.181141
24	8	0	6.271726	-2.296122	-0.278530
25	8	0	-2.880901	-7.133397	2.137910
26	8	0	-2.263304	-5.968420	-2.290406
27	6	0	6.847612	-1.339226	2.433974
28	6	0	-4.306389	-6.145125	-0.173402
29	6	0	7.763122	-1.310196	3.493710
30	6	0	8.292149	-0.085133	3.893664
31	6	0	7.886035	1.079058	3.256029
32	7	0	6.995776	1.054816	2.237706
33	6	0	6.500629	-0.127416	1.817590
34	6	0	-4.722271	-4.930282	-0.737921
35	7	0	-6.014463	-4.542389	-0.723201
36	6	0	-6.946386	-5.355699	-0.175838
37	6	0	-6.606531	-6.580033	0.383256
38	6	0	-5.273203	-6.982356	0.397394
39	6	0	4.237628	-9.420397	-1.179260
40	6	0	4.630366	-10.656811	-0.650163
41	6	0	4.432088	-10.944385	0.701237
42	6	0	3.838059	-10.000433	1.549174
43	6	0	-4.675088	10.105104	0.881138
44	6	0	-5.195846	10.777379	1.994405
45	6	0	-5.209961	10.165333	3.248953
46	6	0	-4.703631	8.869560	3.413597
47	6	0	-8.243947	1.753726	-2.793656
48	6	0	-8.712974	0.581351	-3.382729
49	6	0	-8.263296	-0.650254	-2.925043
50	7	0	-7.383513	-0.738882	-1.902851
51	6	0	-6.932620	0.383063	-1.310326
52	6	0	4.246372	5.134967	1.133942
53	7	0	5.535950	4.788267	0.956621
54	6	0	6.382906	5.644083	0.342936
55	6	0	5.950301	6.881498	-0.115548
56	6	0	4.618833	7.254726	0.052022
57	6	0	-7.327715	1.659297	-1.736937
58	6	0	3.741907	6.365393	0.688624
59	8	0	-6.537489	2.055733	1.063622
60	8	0	-6.588006	4.146622	-3.060750
61	8	0	1.979697	5.686357	2.932860
62	8	0	2.017226	7.757653	-1.200904
63	7	0	2.377256	6.672692	0.848423
64	7	0	-6.772529	2.808549	-1.140814
65	6	0	-6.384697	3.979309	-1.881191
66	6	0	-4.173212	8.819268	1.047364
67	6	0	-4.187429	8.204233	2.307375
68	6	0	-6.372371	2.917255	0.224379
69	6	0	1.585487	7.328092	-0.156707
70	6	0	1.569041	6.278351	1.955955
71	6	0	-0.974623	7.755999	-0.249675

72	6	0	-2.168093	7.549870	0.442977
73	6	0	-3.567415	7.930575	-0.045266
74	6	0	-4.373444	6.630261	-0.030877
75	6	0	-5.033212	6.063652	-1.121756
76	6	0	-5.686467	4.851151	-0.905700
77	6	0	-5.697277	4.233297	0.345212
78	6	0	-5.060773	4.803688	1.448223
79	6	0	-4.388182	6.008530	1.240515
80	6	0	-3.593040	6.790913	2.289471
81	6	0	-2.180407	6.932003	1.715905
82	6	0	-0.998633	6.509859	2.327189
83	6	0	0.187477	6.703718	1.618502
84	6	0	0.196755	7.313120	0.362591
85	6	0	3.834703	2.163528	-5.593487
86	6	0	3.251101	3.224715	-4.901508
87	6	0	2.003081	3.735218	-5.266666
88	6	0	1.349174	3.122116	-6.338085
89	6	0	-0.039356	3.481569	-6.883837
90	6	0	-0.864695	2.188743	-6.839100
91	6	0	-2.090444	2.006661	-6.194188
92	6	0	-2.648630	0.725619	-6.228408
93	6	0	-2.021798	-0.320991	-6.903200
94	6	0	-0.822542	-0.140696	-7.591158
95	6	0	-0.245498	1.127839	-7.541815
96	6	0	1.079644	1.534158	-8.189708
97	6	0	1.952260	2.054900	-7.046104
98	6	0	3.208987	1.564949	-6.687284
99	6	0	4.109528	3.563631	-3.735985
100	6	0	5.097189	1.781530	-4.917251
101	6	0	-3.848283	0.190167	-5.528662
102	6	0	0.165224	3.798337	-8.370763
103	6	0	0.769077	2.746828	-9.075008
104	6	0	-2.782071	-1.572662	-6.673961
105	7	0	-3.876420	-1.210107	-5.812910
106	7	0	5.216135	2.657562	-3.785598
107	8	0	5.876745	0.895499	-5.188497
108	8	0	3.938243	4.394905	-2.868932
109	8	0	-2.554895	-2.691668	-7.071441
110	8	0	-4.648452	0.766016	-4.821064
111	6	0	6.198505	2.500324	-2.782776
112	6	0	-4.744774	-2.155964	-5.224656
113	6	0	7.496532	2.067916	-3.095881
114	6	0	8.403980	1.855807	-2.060060
115	6	0	8.020375	2.082840	-0.743981
116	7	0	6.778871	2.521288	-0.443432
117	6	0	5.886765	2.729917	-1.433901
118	6	0	-5.211174	-1.989173	-3.910703
119	7	0	-5.981517	-2.914866	-3.300950
120	6	0	-6.328051	-4.039451	-3.963422
121	6	0	-5.919760	-4.258850	-5.272661
122	6	0	-5.126340	-3.314475	-5.919023
123	6	0	-0.184358	4.976408	-9.020908
124	6	0	0.076401	5.095914	-10.392191
125	6	0	0.677557	4.049008	-11.093037
126	6	0	1.029231	2.862847	-10.435735
127	6	0	-2.253414	-0.679169	10.854715
128	6	0	-2.003770	-1.710287	11.769661
129	6	0	-1.396031	-2.895743	11.352650
130	6	0	-1.026530	-3.072220	10.012878
131	6	0	-8.198525	-1.511167	3.168234
132	6	0	-9.080373	-1.540315	2.090401
133	6	0	-8.620759	-1.908325	0.832720
134	7	0	-7.330844	-2.256771	0.630752
135	6	0	-6.468166	-2.252989	1.666750
136	6	0	4.745380	2.592185	4.164471
137	7	0	5.657792	3.351564	3.525733
138	6	0	6.120259	4.478128	4.111399
139	6	0	5.671915	4.877499	5.363392
140	6	0	4.715678	4.115388	6.030179
141	6	0	-6.859370	-1.868974	2.958152
142	6	0	4.233621	2.948237	5.421351
143	8	0	-4.564232	-3.635556	3.479019
144	8	0	-6.684947	0.172888	5.019254
145	8	0	3.921145	0.026181	5.429223
146	8	0	1.923045	3.933293	6.884318
147	7	0	3.223621	2.176833	6.029541
148	7	0	-5.916444	-1.798499	4.003787
149	6	0	-5.875710	-0.722839	4.957814
150	6	0	-1.885651	-0.856886	9.525847
151	6	0	-1.275264	-2.047723	9.106650
152	6	0	-4.807076	-2.677697	4.183419
153	6	0	2.086724	2.750232	6.698338
154	6	0	3.113623	0.755605	5.966026
155	6	0	-0.050002	1.610633	7.637246
156	6	0	-0.688188	0.378344	7.784067
157	6	0	-2.077175	0.150574	8.385659
158	6	0	-2.882025	-0.579635	7.308257
159	6	0	-4.095618	-0.157669	6.764289
160	6	0	-4.654806	-0.956374	5.766931
161	6	0	-4.040791	-2.131924	5.333995
162	6	0	-2.842228	-2.578008	5.893359
163	6	0	-2.264842	-1.780133	6.882520
164	6	0	-0.944342	-2.054778	7.609163
165	6	0	-0.067758	-0.822509	7.365588
166	6	0	1.206294	-0.817929	6.794338
167	6	0	1.827747	0.421164	6.631989
168	6	0	1.213201	1.603849	7.046958
169	46	0	-6.648384	-2.618481	-1.326179
170	46	0	6.235786	2.903064	1.555777
171	1	0	4.941284	-4.870853	-1.247957
172	1	0	3.317668	-6.859748	-1.783835
173	1	0	0.733039	-6.489025	-2.208024
174	1	0	0.038687	-7.594443	2.651549
175	1	0	2.629186	-7.846096	2.843836
176	1	0	4.116601	-5.830394	3.622553
177	1	0	8.048043	-2.227312	3.994205
178	1	0	9.012043	-0.028994	4.702927
179	1	0	8.258530	2.049877	3.559535
180	1	0	5.807593	-0.105848	0.990207
181	1	0	-4.012699	-4.258330	-1.198838
182	1	0	-7.970633	-5.002932	-0.183412
183	1	0	-7.381517	-7.208241	0.808757
184	1	0	-4.982709	-7.924356	0.846091
185	1	0	4.395981	-9.198084	-2.231200
186	1	0	5.092873	-11.395432	-1.297711
187	1	0	4.740440	-11.905701	1.100632
188	1	0	3.685774	-10.226625	2.601177
189	1	0	-4.665585	10.584085	-0.094280
190	1	0	-5.591013	11.781872	1.878258
191	1	0	-5.616207	10.695961	4.104600
192	1	0	-4.716251	8.395608	4.391587
193	1	0	-8.571321	2.721733	-3.150306
194	1	0	-9.426058	0.620323	-4.199025
195	1	0	-8.594400	-1.580008	-3.371814
196	1	0	-6.246333	0.263328	-0.487213
197	1	0	3.610851	4.424310	1.640572
198	1	0	7.408976	5.318357	0.220875
199	1	0	6.655255	7.548960	-0.599187
200	1	0	4.262045	8.210884	-0.308689
201	1	0	-0.950953	8.231695	-1.225597
202	1	0	-3.555457	8.407913	-1.027199
203	1	0	-5.032216	6.532395	-2.101319
204	1	0	-5.077465	4.315833	2.418235
205	1	0	-3.603385	6.310770	3.270293
206	1	0	-0.996084	6.037724	3.304830
207	1	0	1.554415	4.557633	-4.717922
208	1	0	-0.508249	4.300184	-6.333702
209	1	0	-2.580958	2.815280	-5.660748
210	1	0	-0.358053	-0.961163	-8.128695
211	1	0	1.549200	0.714376	-8.737284
212	1	0	3.680604	0.747342	-7.224536
213	1	0	7.782615	1.889992	-4.124138
214	1	0	9.412781	1.518338	-2.271739
215	1	0	8.698447	1.918508	0.084424
216	1	0	4.911537	3.090828	-1.148861
217	1	0	-4.974437	-1.099065	-3.348870
218	1	0	-6.936306	-4.758195	-3.428249
219	1	0	-6.225677	-5.165323	-5.783534
220	1	0	-4.795553	-3.476689	-6.936179
221	1	0	-0.652561	5.793352	-8.478126

222	1	0	-0.191812	6.010474	-10.912146
223	1	0	0.875004	4.152536	-12.155537
224	1	0	1.497155	2.049654	-10.984095
225	1	0	-2.726823	0.242546	11.182270
226	1	0	-2.286027	-1.584263	12.810388
227	1	0	-1.207596	-3.688097	12.070572
228	1	0	-0.553607	-3.996430	9.691267
229	1	0	-8.536555	-1.209422	4.151278
230	1	0	-10.123708	-1.274872	2.222058
231	1	0	-9.275287	-1.921959	-0.030362
232	1	0	-5.453483	-2.560834	1.464639
233	1	0	4.419239	1.689978	3.669801
234	1	0	6.848996	5.057221	3.557170
235	1	0	6.068752	5.782484	5.810435
236	1	0	4.342107	4.420621	6.999189
237	1	0	-0.512474	2.539404	7.957862
238	1	0	-2.552670	1.078364	8.710175
239	1	0	-4.583857	0.756646	7.088228
240	1	0	-2.375015	-3.497345	5.553914
241	1	0	-0.468500	-2.981599	7.281646
242	1	0	1.692490	-1.733903	6.472915
243	6	0	-1.984667	-2.839428	1.217186
244	6	0	-1.180610	-3.401578	0.149962
245	6	0	-1.423017	-3.046097	-1.181290
246	6	0	-3.277008	-1.584822	-0.463782
247	6	0	-3.012455	-1.946851	0.917273
248	6	0	0.178907	-3.495655	0.618473
249	6	0	-0.333137	-2.807020	-2.102444
250	6	0	-3.653625	-0.181687	-0.495503
251	6	0	-3.214124	-0.764646	1.734060
252	6	0	-1.113568	-2.586444	2.352381
253	6	0	-3.245208	0.623597	-1.558209
254	6	0	-2.438434	0.059164	-2.622536
255	6	0	1.222230	-3.227904	-0.269327
256	6	0	-0.735211	-1.701713	-2.991262
257	6	0	0.972576	-2.918123	-1.656380
258	6	0	-3.612426	0.325105	0.861817
259	6	0	-2.375804	-0.516980	2.820274
260	6	0	-1.303457	-1.444915	3.131971
261	6	0	0.228416	-2.995929	1.981028
262	6	0	-1.899586	0.830139	3.076034
263	6	0	-0.159997	-0.670114	3.577623
264	6	0	1.326741	-2.252956	2.407053
265	6	0	-3.156016	1.620099	1.107391
266	6	0	2.090953	-2.072569	-2.167037
267	6	0	-0.528113	0.734965	3.543908
268	6	0	1.128585	-1.067942	3.220534
269	6	0	2.416980	-1.981929	1.485885
270	6	0	2.893540	-0.644307	1.731754
271	6	0	2.043243	0.508418	-2.683059
272	6	0	2.097995	-0.072584	2.800981
273	6	0	1.743221	1.275967	2.767129
274	6	0	2.169186	2.104859	1.653852
275	6	0	0.407118	1.691203	3.148077
276	6	0	-2.728839	2.459432	0.002583
277	6	0	2.862479	0.738722	-1.587876
278	6	0	-2.282221	1.878145	2.236459
279	6	0	-1.309116	2.876445	1.827469
280	6	0	3.268247	-0.366504	-0.702278
281	6	0	0.949528	1.416437	-2.932843
282	6	0	0.755643	2.565983	-2.161112
283	6	0	3.294932	0.148318	0.651601
284	6	0	2.925281	1.550464	0.618576
285	6	0	0.009266	2.782165	2.272940
286	6	0	1.098620	3.037274	1.351881
287	6	0	2.650996	1.909269	-0.758905
288	6	0	-1.586358	3.239131	0.447506
289	6	0	-0.585288	2.985615	-1.793663
290	6	0	1.629474	2.818804	-1.044150
291	6	0	-0.536222	3.495613	-0.434556
292	6	0	0.837564	3.391426	0.028104
293	6	0	1.649391	-0.855992	-3.148506
294	6	0	0.182752	-0.749089	-3.403140
295	6	0	-0.189336	0.644626	-3.376867
296	6	0	2.362439	-2.453782	0.171810
297	6	0	2.833560	-1.661561	-0.938947
298	6	0	-2.493600	-2.120572	-1.488558
299	6	0	-2.065259	-1.288033	-2.595454
300	6	0	-1.478056	1.051751	-3.026397
301	6	0	-2.778466	1.975587	-1.305839
302	6	0	-1.682709	2.241793	-2.220001
303	6	0	2.566365	-1.978386	-3.603821
304	6	0	2.008273	-2.980748	-4.591789
305	6	0	4.048014	-1.644820	-3.839233
306	6	0	1.526340	-2.550379	-5.834572
307	6	0	1.094928	-3.474017	-6.787826
308	6	0	1.145666	-4.842029	-6.515026
309	6	0	1.631318	-5.281261	-5.282736
310	6	0	2.056823	-4.356223	-4.327981
311	6	0	4.961128	-2.839883	-3.552052
312	6	0	6.450836	-2.532325	-3.697637
313	6	0	7.291605	-3.734405	-3.300485
314	8	0	6.865662	-4.719453	-2.726122
315	8	0	8.573195	-3.572090	-3.656183
316	6	0	9.466035	-4.660039	-3.334775
317	1	0	4.158317	-1.313602	-4.878275
318	1	0	4.349992	-0.801653	-3.210141
319	1	0	1.487697	-1.486121	-6.053733
320	1	0	0.718852	-3.132419	-7.747481
321	1	0	0.812743	-5.559302	-7.258857
322	1	0	1.685098	-6.344961	-5.068592
323	1	0	2.439215	-4.704880	-3.372778
324	1	0	4.784804	-3.174809	-2.526279
325	1	0	4.701672	-3.677438	-4.207301
326	1	0	6.714397	-2.233568	-4.718436
327	1	0	6.742190	-1.698042	-3.046335
328	1	0	10.443001	-4.353408	-3.706606
329	1	0	9.495856	-4.822016	-2.254469
330	1	0	9.137603	-5.577673	-3.827894

4.5 References

[1] H. W. Kroto, J. R. Heath, S. C. O'Brien, R. F. Curl, R. E. Smalley, *Nature* **1985**, *318*, 162–163.

[2] C. J. Brabec, S. Gowrisanker, J. J. M. Halls, D. Laird, S. Jia, S. P. Williams, *Adv. Mater.* **2010**, *22*, 3839–3856.

[3] T. Umeyama, H. Imahori, *Acc. Chem. Res.* **2019**, *52*, 2046–2055.

[4] J.-F. Nierengarten, *New. J. Chem.* **2004**, *28*, 1177–1191.

[5] K. Itami, *Chem. Rec.* **2011**, *11*, 226–235.

[6] J. C. Hummelen, B. W. Knight, F. LePeq, F. Wudl, J. Yao, C. L. Wilkins, *J. Org. Chem.* **1995**, *60*, 532–538.

[7] A. Puplovskis, J. Kacens, O. Neilands, *Tetrahedron Lett.* **1997**, *38*, 285–288.

[8] L. Isaacs, R. F. Haldimann, F. Diederich, *Angew. Chem. Int. Ed.* **1994**, *33*, 2339–2342.

[9] C. Thilgen, F. Diederich, *Chem. Rev.* **2006**, *106*, 5049–5135.

[10] K. L. Maxouti, A. Hirsch, *Eur J. Org. Chem.* **2018**, *2018*, 2579–2586.

[11] C. Fuertes-Espinosa, C. García-Simón, M. Pujals, M. Garcia-Borràs, L. Gómez, T. Parella, J. Juanhuix, I. Imaz, D. Maspoch, M. Costas, X. Ribas, *Chem* **2019**, *6*, 169–186.

[12] S. Hasegawa, G. H. Clever, *Chem* **2020**, *6*, 5–7.

[13] E. Ubasart, O. Borodin, C. Fuertes-Espinosa, Y. Xu, C. García-Simón, L. Gómez, J. Juanhuix, F. Gándara, I. Imaz, D. Maspoch, M. von Delius, X. Ribas, *Nat. Chem.* **2021**, *13*, 420–427.

[14] M. Wachter, L. Jurkiewicz, A. Hirsch, *Chem. Eur. J.* **2021**, *27*, 7677–7686.

[15] M. Pujals, T. Pèlachs, C. Fuertes-Espinosa, T. Parella, M. Garcia-Borràs, X. Ribas, DOI 10.26434/chemrxiv-2022-ckrjp.

[16] N. Kishi, M. Akita, M. Kamiya, S. Hayashi, H.-F. Hsu, M. Yoshizawa, *J. Am. Chem. Soc.* **2013**, *135*, 12976–9.

[17] M. Yamashina, T. Yuki, Y. Sei, M. Akita, M. Yoshizawa, *Chem. Eur. J.* **2015**, *21*, 4200–4204.

[18] C. García-Simón, A. Monferrer, M. Garcia-Borràs, I. Imaz, D. Maspoch, M. Costas, X. Ribas, *Chem. Commun.* **2019**, *55*, 798–801.

[19] B. Chen, J. J. Holstein, S. Horiuchi, W. G. Hiller, G. H. Clever, *J. Am. Chem. Soc.* **2019**, *141*, 8907–8913.

[20] B. Chen, S. Horiuchi, J. J. Holstein, J. Tessarolo, G. H. Clever, *Chem. Eur. J.* **2019**, *25*, 14921–14927.

[21] B. Chen, J. J. Holstein, A. Platzek, L. Schneider, K. Wu, G. H. Clever, *Chem. Sci.* **2022**, *13*, 1829–1834.

[22] S. Hasegawa, S. L. Meichsner, J. J. Holstein, A. Baksi, M. Kasanmascheff, G. H. Clever, *J. Am. Chem. Soc.* **2021**, *143*, 9718–9723.

[23] Y. Yang, T. K. Ronson, Z. Lu, J. Zheng, N. Vanthuyne, A. Martinez, J. R. Nitschke, *Nat. Commun.* **2021**, *12*, 4079.

[24] B. M. Schmidt, T. Osuga, T. Sawada, M. Hoshino, M. Fujita, *Angew. Chem. Int. Ed.* **2015**, *55*, 1561–1564.

[25] M. Yoshizawa, J. K. Klosterman, M. Fujita, *Angew. Chem. Int. Ed.* **2009**, *48*, 3418–3438.

[26] Gaussian 16, Revision B.01, M. J. Frisch, G. W. Trucks, H. B. Schlegel, G. E. Scuseria, M. A. Robb, J. R. Cheeseman, G. Scalmani, V. Barone, G. A. Petersson, H. Nakatsuji, X. Li, M. Caricato, A. V. Marenich, J. Bloino, B. G. Janesko, R. Gomperts, B. Mennucci, H. P. Hratchian, J. V. Ortiz, A. F. Izmaylov, J. L. Sonnenberg, D. Williams-Young, F. Ding, F. Lipparini, F. Egidi, J. Goings, B. Peng, A. Petrone, T. Henderson, D. Ranasinghe, V. G. Zakrzewski, J. Gao, N. Rega, G. Zheng, W. Liang, M. Hada, M. Ehara, K. Toyota, R. Fukuda, J. Hasegawa, M. Ishida, T. Nakajima, Y. Honda, O. Kitao, H. Nakai, T. Vreven, K. Throssell, J. A. Montgomery, Jr., J. E. Peralta, F. Ogliaro, M. J. Bearpark, J. J. Heyd, E. N. Brothers, K. N. Kudin, V. N. Staroverov, T. A. Keith, R. Kobayashi, J. Normand, K. Raghavachari, A. P. Rendell, J. C. Burant, S. S. Iyengar, J. Tomasi, M. Cossi, J. M. Millam, M. Klene, C. Adamo, R. Cammi, J. W. Ochterski, R. L. Martin, K. Morokuma, O. Farkas, J. B. Foresman, and D. J. Fox, Gaussian, Inc., Wallingford CT, **2016**.

5 Synthesis of [η^2-C_{60}(Pd(0)L)$_n$] by a supramolecular mask method

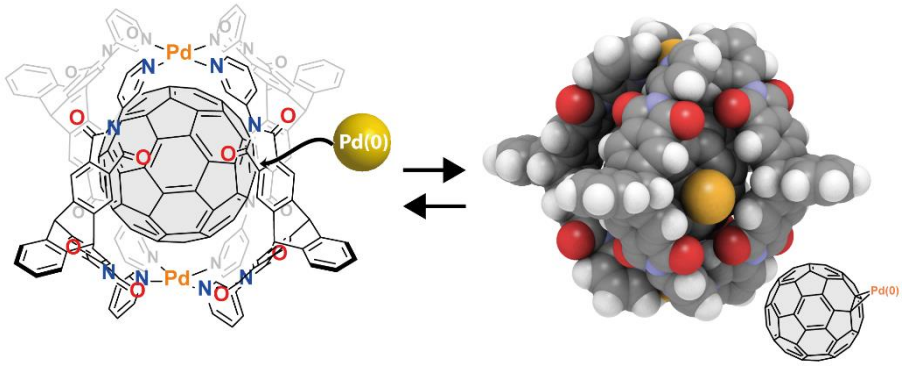

Abstract:

As shown in the previous chapters, triptycene-based coordination cage $Pd_2\mathbf{L}^{\mathbf{P}}{}_4$ encapsulates C_{60} derivatives in a high to quantitative yield thanks to the apertures between the ligands. It was also found that the synthesis of [η^2-C_{60}(Pd(0)L)$_n$] (n=1, 2) complexes is possible via coordination of the encapsulated C_{60} to Pd(0) through the window(s) by the simple addition of Pd(0)(dba)$_2$. In this complexation reaction, the cage serves as a bulky protecting group for the confined C_{60} to prevent the polymerization yielding [η^2-C_{60}(Pd(0)L)$_n$]. [η^2-C_{60}(Pd(0)L)$_2$] complex could also be synthesized in, potentially, a regio-selective manner by changing the equimolar amount of the Pd(0) source. Based on these observations, a thianthrene-based ligand was newly designed and synthesized for stabilizing the formed η^2-Pd(0)$_n$$C_{60}$ complex inside the cage. The thianthrene-based ligand shows a unique self-assembly behavior stemming from an intrinsic molecular inversion motion. Resulting from the self-assembly of the thianthrene-based ligand and Pd(II) cations was a Pd_3L_6 ring-shaped coordination ring, which represents an unprecedented homoleptic topology from ligands possessing an bite angle of ca. 0°. Upon encapsulation of C_{60}, the ring-shaped complex is partially transformed into C_{60}@Pd_2L_4 coordination cage most probably due to template-effect by C_{60}. The stabilization effect on the formed [η^2-C_{60}(Pd(0)L)$_n$] (n=1, 2) *in situ* inside the thianthrene-based coordination cage via coordination of the lone-pair of the sulfur atoms was not observed. However, the cage-to-cage transformation owing to the inversion motion of the thianthrene ligand can be a new concept for synthesis of functional coordination cages.

5.1 Introduction

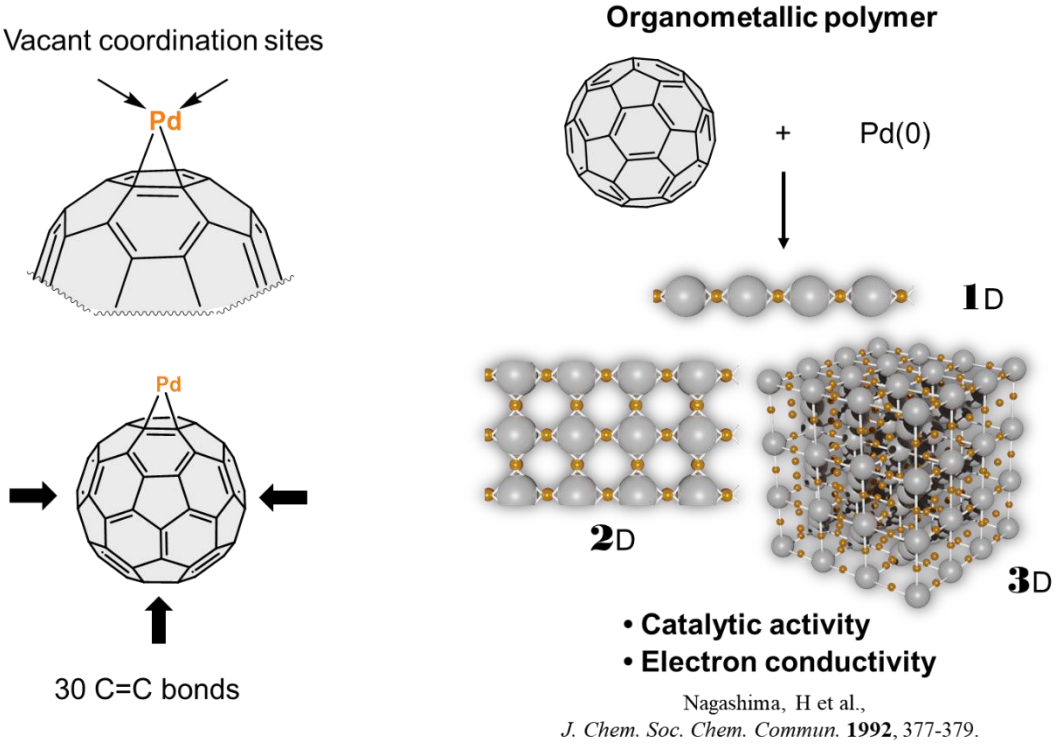

Figure 5.1.1 Coordination of C_{60} to Pd(0) resulting in organometallic polymers

C_{60} derivatives mentioned in the previous chapter are mainly covalently modified with organic residues, while coordination to transition metals through π–electrons from C=C bond can also modify the electronic property of C_{60}.[1] Among them, Pd(0)-C_{60} metalorganic polymers are of great interests owing to their catalytic activity in hydrogenation reaction, molecular absorption, and electron conductivity.[2] C_{60} is known to coordinate to Pd(0) as well as Pt(0) through C=C bond in an η^2 fashion (**Figure 5.1.1**).[3,4] The first example of Pd(0)-C_{60} metalorganic polymers was reported in 1992 by mixing Pd(0)(dba)$_3$ and C_{60} in toluene.[5] The composition between Pd(0) and C_{60} can be varied by changing the equivalent of the Pd(0) source. The topology of the polymer is thus believed to change depending on the stoichiometry of the Pd(0) source from 1D-polymer to 3D-network (**Figure 5.1.1**). Although C_{60}-Pd(0) polymers have been widely studied and are known to show interesting properties as mentioned above, investigations into the physical properties of [η^2-C_{60}Pd(0)$_n$] on unimolecular level is hindered due to the inevitable polymerization. The first unimolecular Pt(0)-C_{60} complex was synthesized in 1991[3] and its Pd(0) analogue in 1993.[4] In these reports, half of the vacant sites of the d^{10} square-planar metals are coordinated by

triphenylphosphines in a *cis*-fashion. The *cis*-protection prevents the complexes from polymerization and destabilization. As an alternative of the *cis*-protecting group, introduction of steric protection of unimolecular [η^2-$C_{60}Pd(0)_n$] (n=1,2) by, i.e. supramolecular mask method, seems to be able to realize synthesis of unimolecular C_{60}-Pd(0) complexes. In this chapter, synthesis of [η^2-$C_{60}Pd(0)_n$] (n=1,2) by a supramolecular mask method will be showcased. The apertures of $Pd_2\mathbf{L}^{\mathbf{P}}{}_4$ made it possible to render Pd(0) and the encapsulated C_{60} react to form the complex. An increase in the stoichiometry of the Pd(0) source yielded a regioselective formation of η^2-C_{60}-bis-Pd(0)-complex. Considering that the reaction between C_{60} and Pd(0) usually results in polymerization, the coordination cage serves as a protecting group to prevent polymerization by prohibiting further C_{60} addition onto the Pd(0) center. This method is strategically different from other unimolecular $C_{60}Pd(0)$ complexes in terms of the way of preventing polymerization.

5.2 Results and discussion

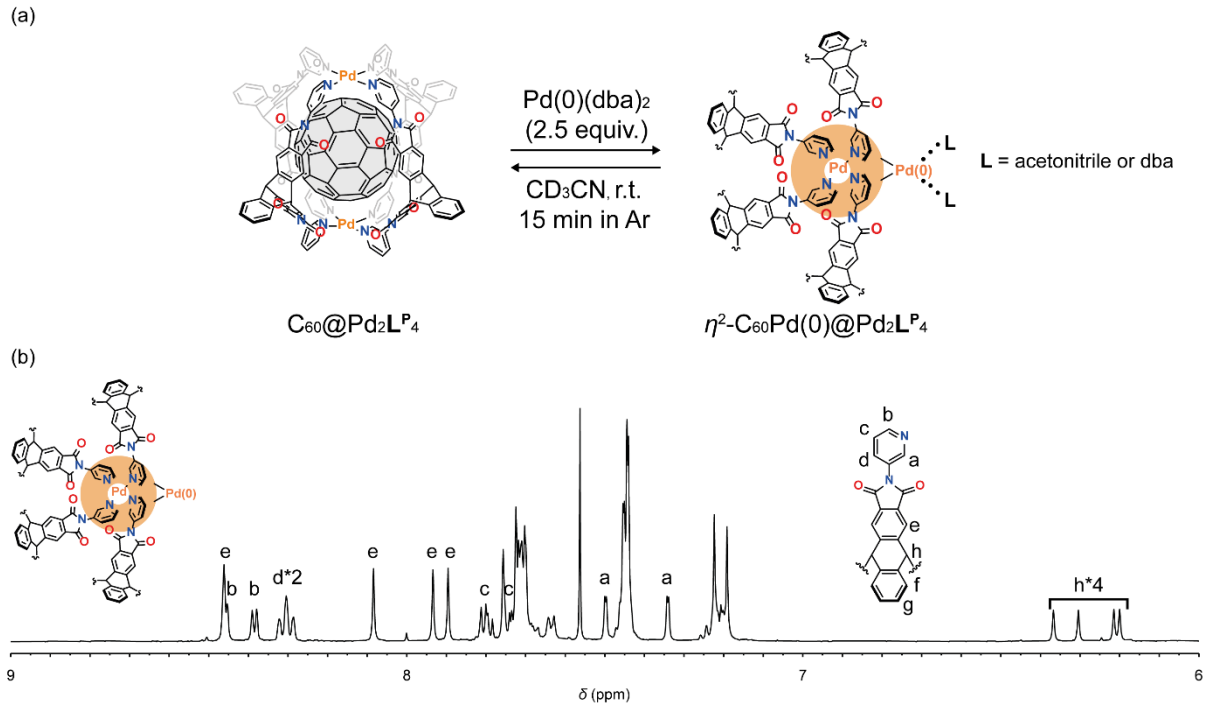

Figure 5.2.1 (a) Synthesis of η^2-$C_{60}Pd(0)@Pd_2\mathbf{L}^{\mathbf{P}}{}_4$ (b) ^{1}H NMR spectrum (CD_3CN, 500 MHz, 298 K) of η^2-$C_{60}Pd(0)@Pd_2\mathbf{L}^{\mathbf{P}}{}_4$

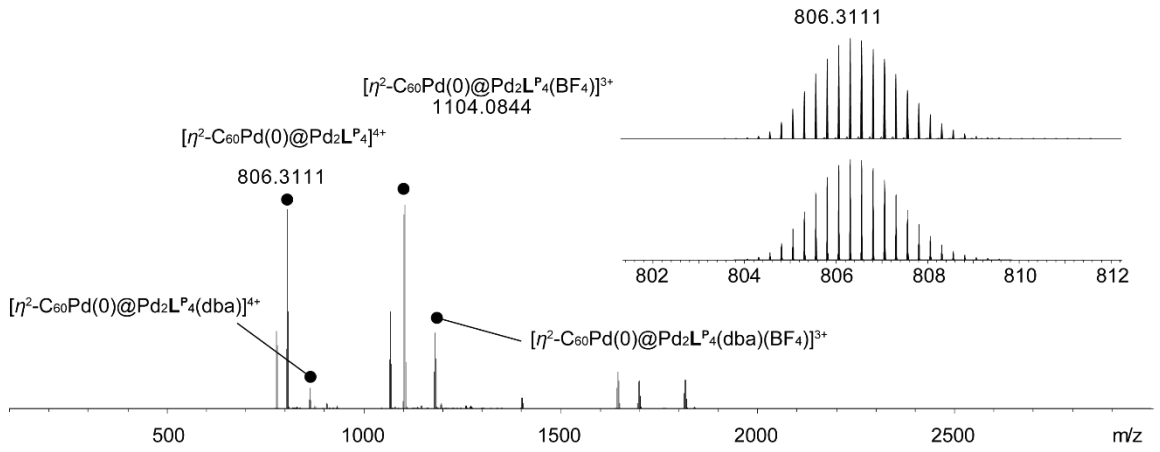

Figure 5.2.2 ESI MS spectrum (positive mode) of η^2-$C_{60}Pd(0)@Pd_2\mathbf{L^P}_4$

The first synthesis of η^2-$C_{60}Pd(0)$ complex inside $Pd_2\mathbf{L^P}_4$ was achieved serendipitously. While reproducing the result of the C_{60} radical anion generation inside $Pd_2\mathbf{L^P}_4$, an unusual greenish solution was obtained. ESI-MS analysis revealed a formation of η^2-$C_{60}Pd(0)@Pd_2\mathbf{L^P}_4$. This unprecedented result was assumed due to reduction of unreacted Pd(II) to Pd(0) by the generated C_{60} radical anion followed by the complexation between the encapsulated C_{60} and Pd(0) in the solution. This serendipitous finding stimulated further investigations of the complexation reaction. According to literature, when pristine C_{60} and Pd(0) are reacted in a toluene solution, organometallic $[C_{60}Pd(0)_n]_m$ polymers are formed.[5] In addition, the electronic reduction of the mixture of C_{60} and Pd(II) can also yield the organometallic polymers.[6] The latter example is a similar case to what was observed during C_{60} radical anion generation as mentioned above. According to these reports, we hypothesized that mere addition of a Pd(0) source should give the same complexation. Thus, $Pd(0)(dba)_2$ (dba = dibenzylidenaceton) in chloroform was added to $C_{60}@Pd_2\mathbf{L^P}_4$ in acetonitrile. In the ^{1}H NMR spectrum of the resulting mixture, desymmetrization of $Pd_2\mathbf{L^P}_4$ was observed, which is likely due to encapsulation of a C_{60} derivative as discussed in the last chapter (**Figure 5.2.1**). In the ESI-MS spectrum of the mixture, a prominent signal assignable to the expected $[\eta^2$-$C_{60}Pd(0)@Pd_2\mathbf{L^P}_4]^{4+}$ was observed (**Figure 5.2.2**). Additionally $[(\eta^2$-$C_{60}Pd(0)@Pd_2\mathbf{L^P}_4)(dba)]^{4+}$ was observed as well. This result indicates that Pd(0) is coordinating other ligands besides encapsulated C_{60} such as dba or acetonitrile in the solution. An increase of the amount of $Pd(0)(dba)_2$ added into $C_{60}@Pd_2\mathbf{L^P}_4$ resulted in a formation of η^2-$C_{60}Pd(0)_2$ inside the coordination cage.

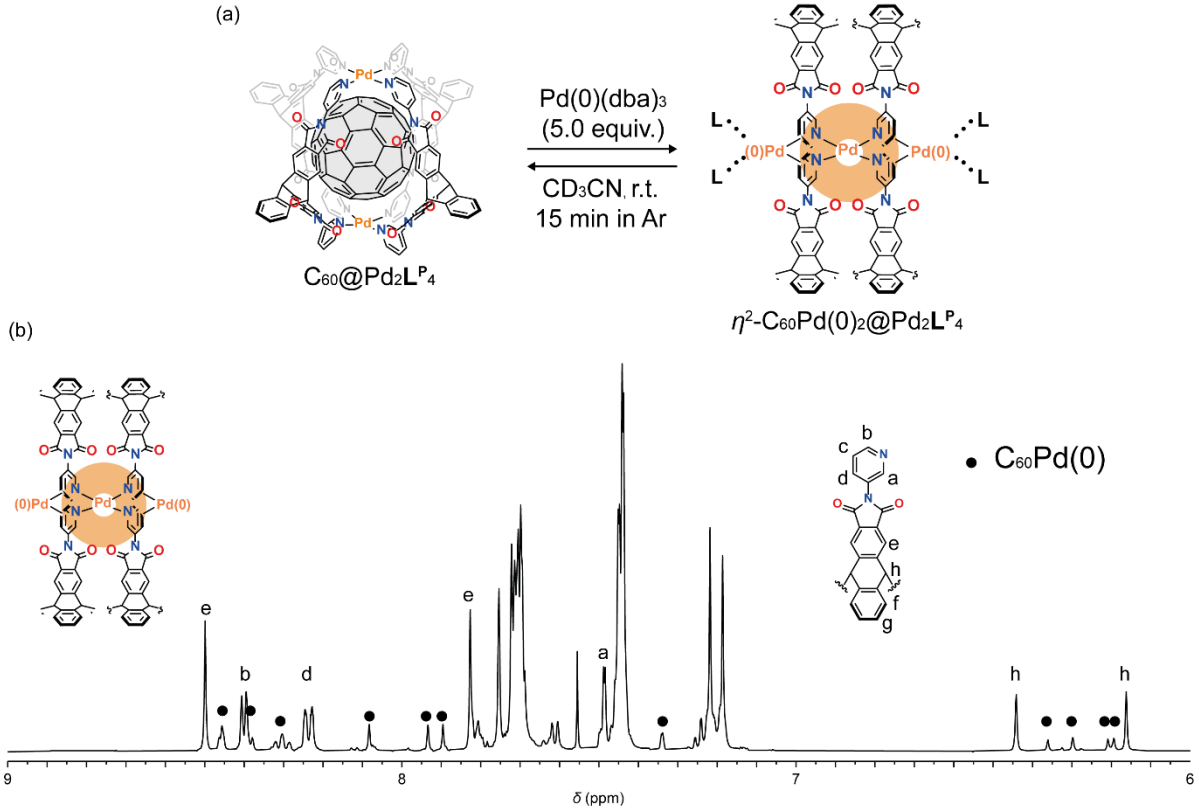

Figure 5.2.3 (a) Synthesis of η^2-$C_{60}Pd(0)_2$@$Pd_2\mathbf{L^P}_4$ (b) ^{1}H NMR spectrum (CD_3CN, 500 MHz, 298 K) of η^2-$C_{60}Pd(0)_2$@$Pd_2\mathbf{L^P}_4$

Addition of 5.0 equivalent of $Pd(0)(dba)_2$ into an acetonitrile solution of C_{60}@$Pd_2\mathbf{L^P}_4$ under inter atmosphere resulted in a simplified ^{1}H NMR spectrum compared to η^2-$C_{60}Pd(0)$@$Pd_2\mathbf{L^P}_4$ (**Figure 5.2.3**). New two sets of signals were observed in the ^{1}H NMR spectrum besides residual $C_{60}Pd(0)$@$Pd_2\mathbf{L^P}_4$. This result implies that a species having a higher symmetry was obtained. In the ESI-MS spectrum, [η^2-$C_{60}Pd(0)_2$@$Pd_2\mathbf{L^P}_4$]$^{4+}$ was found (**Figure 5.2.4**). Similar to η^2-$C_{60}Pd(0)$@$Pd_2\mathbf{L^P}_4$, a signal assignable to η^2-$C_{60}Pd(0)_2$@$Pd_2\mathbf{L^P}_4$ with one dba was also observed. Taking the higher symmetry implication from the ^{1}H NMR spectrum of η^2-$C_{60}Pd(0)_2$@$Pd_2\mathbf{L^P}_4$ into account, the addition of the second Pd(0) should occur in an antipodal fashion. A preference to the antipodal addition can be seen as a trend both in $C_{60}Pd(0)_n$ polymers and unimolecular $C_{60}Pd(0)$ complexes (**Figure 5.2.5**).[7,8] For instance, three dimensional $[C_{60}Pd_3]_n$ organometallic polymers are suggested to have an ordered body-centered-cubic (*bcc*) C_{60} units while Pd(0) atoms are locating in between aligned

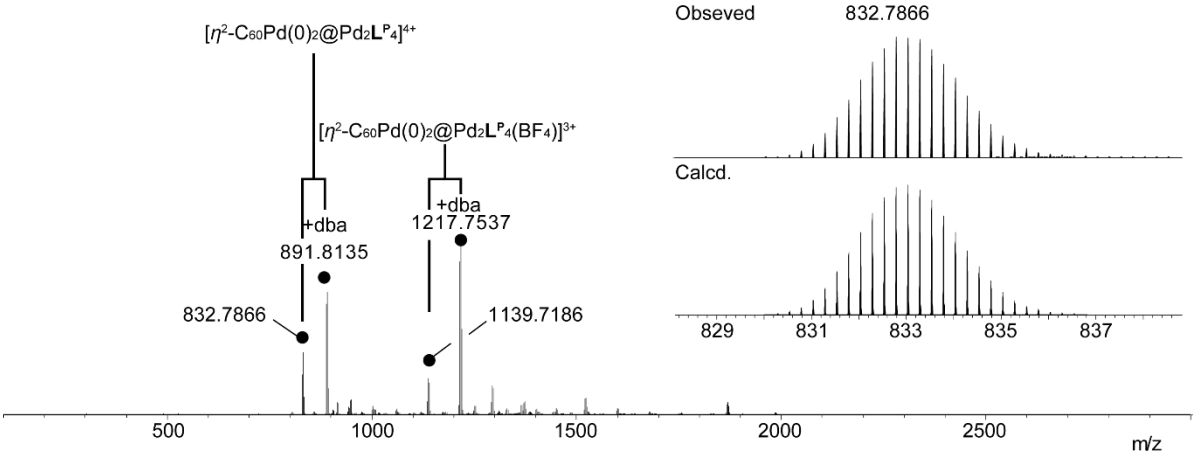

Figure 5.2.4 ESI MS spectrum (positive mode) of η^2-$C_{60}Pd(0)_2$@$Pd_2\mathbf{L}^{\mathbf{P}}_4$

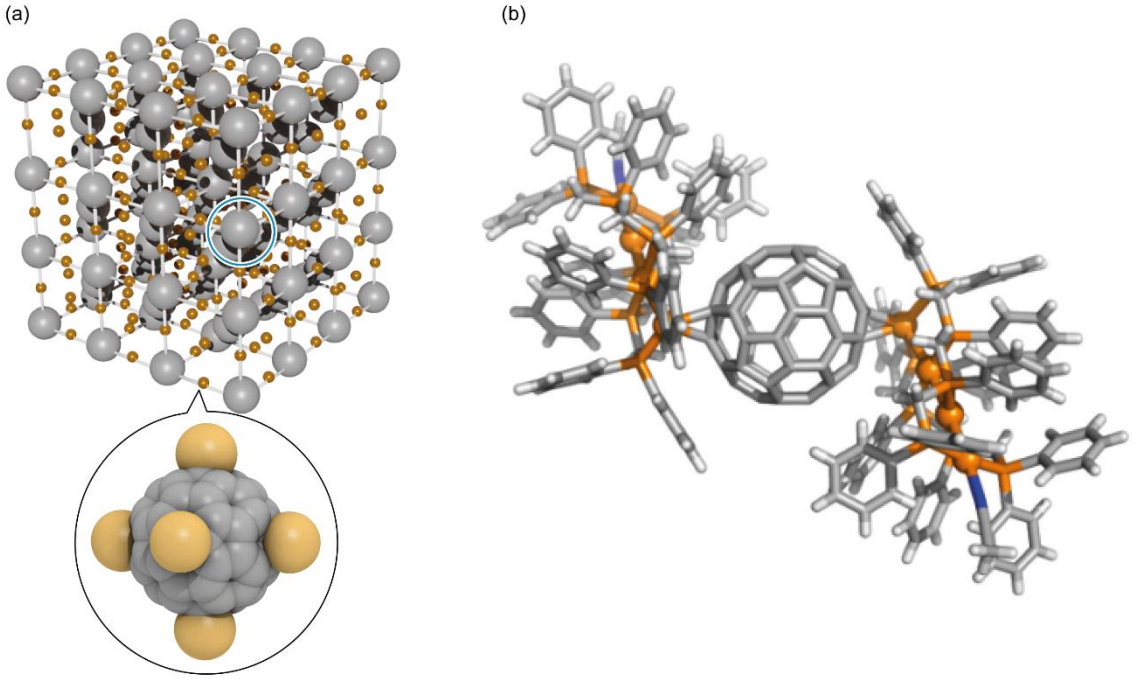

Figure 5.2.5 (a) Schematic structure of 3D $C_{60n}Pd_{3n}$ organometallic polymers (b) X-ray structure of η^2-$C_{60}Pd(0)_2$ complex reported by Tanase[8]

C_{60}s as depicted in **Figure 5.2.5a**.[7] As another example, Tanase and co-coworkers have reported an antipodal addition of an oligomeric Pd(0) complex to C_{60} (**Figure 5.2.5b**).[8] Based on the symmetry evidenced by the ^{1}H NMR experiment, the chemical structure of C_{60}, and steric hinderance from the cage, the second addition of Pd(0) onto the encapsulated η^2-$C_{60}Pd(0)$ under the confinement should be also in an antipodal fashion. The HOMO of the η^2-$C_{60}Pd(0)$ was suggested to be localized on the hexagons

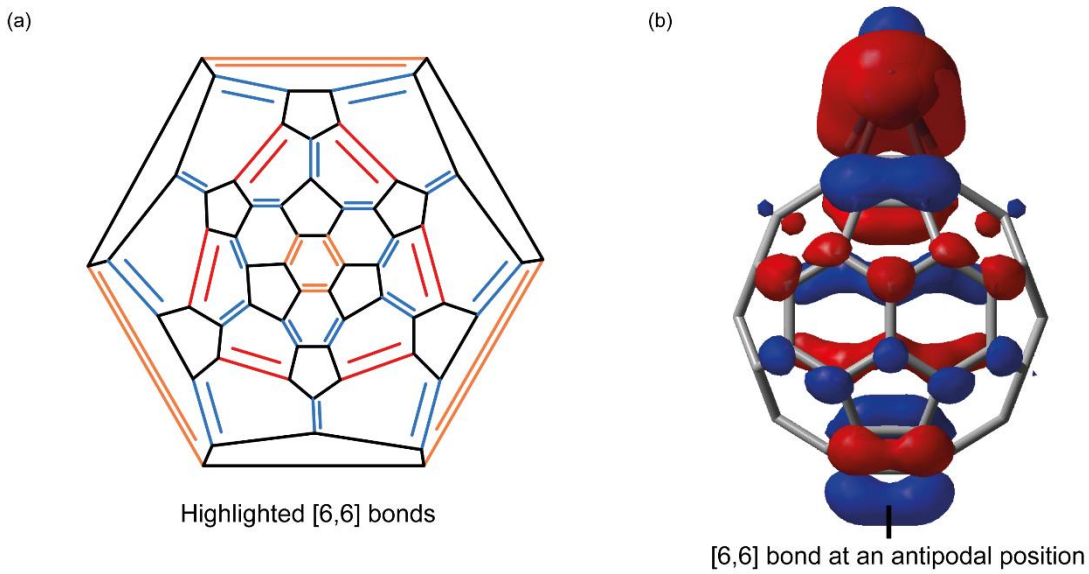

Figure 5.2.6 (a) Schegel diagram showing [6,6] bonds of C_{60} (b) Optimized geometry of η^2-$C_{60}Pd(0)$ with the HOMO calculated at B3LYP/6-31G(d) for C atoms and B3LYP/Lanl2dz for Pd atom in the gas-phase

at the antipodal position by DFT calculations, which further supports the antipodal addition of the second Pd(0) (**Figure 5.2.6**). Note that the reaction between C_{60} and $Pd(0)(dba)_3$ gives organometallic polymers, whereas $Pd_2\mathbf{L^P}_4$ served as a protecting group to yield the $C_{60}Pd(0)_n$ (n=1,2) complexes inside the cage. However, due to the possible coordination of acetonitrile and the absence of bulky ligands as a *cis*-protecting group, the obtained $C_{60}Pd(0)_n$ are rather unstable (**Figure 5.2.7**). In the ^{1}H NMR spectra measured over time, decomposition of η^2-$C_{60}Pd(0)_2$ to η^2-$C_{60}Pd(0)$ as well as η^2-$C_{60}Pd(0)$ to C_{60} inside the cage was clearly observed. After the experiment, dark precipitates were observed in the NMR tube, which are most likely polymerized Pd(0). In spite of several attempts to stabilize the obtained η^2-$C_{60}Pd(0)_n$ (n=1,2) complexes such as through addition of further ligands to stabilize, deoxygenation, dissolving in another solvent after precipitation, none of these strategies was successful. In addition, no further applications have been found yet such as functionalization of confined C_{60} using the η^2-$C_{60}Pd(0)_n$ complexes as an intermediate. A different molecular design for the cage may be required to stabilize the complexes for further investigations. Introduction of bulky substituents on the backbone to protect the coordinated Pd(0) could be a first step. Furthermore, different ligand designs could be potentially interesting, such as the synthesized thianthrene-based ligand $\mathbf{L^S}$ (

Figure 5.2.8a). The concept of this ligand is to stabilize the obtained η^2-$C_{60}Pd(0)_n$ complexes through coordination from the lone pairs on the sulfur atoms to the Pd(0) atom (**Figure 5.2.8b**).

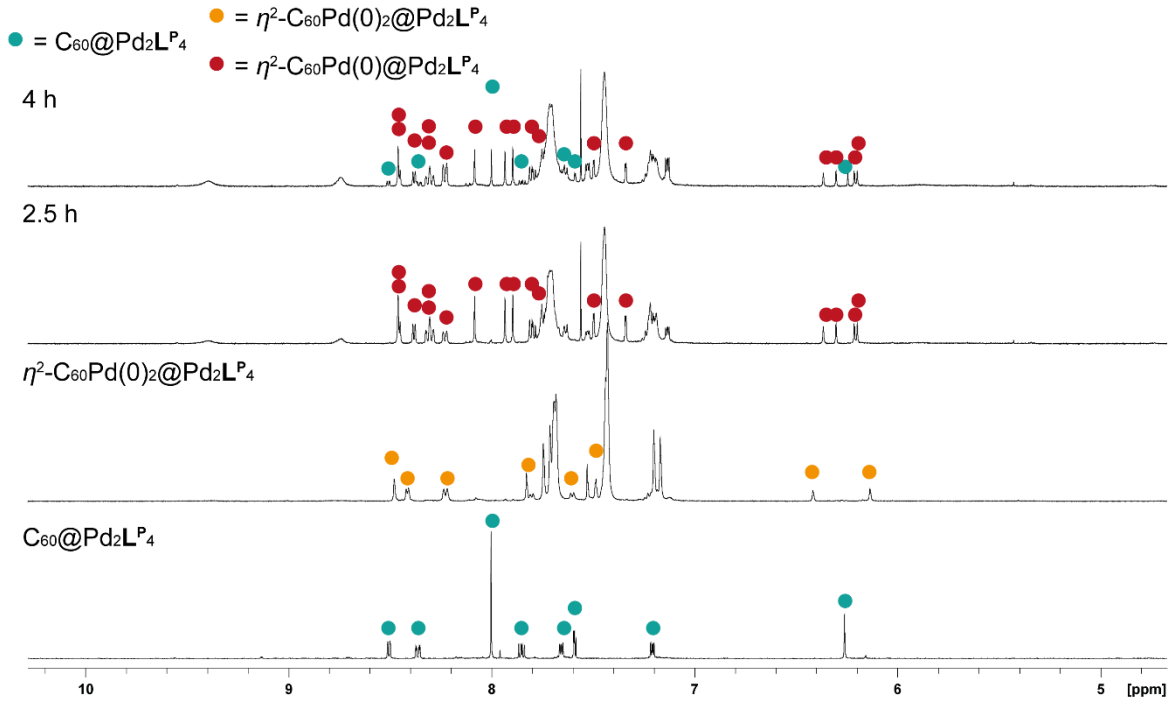

Figure 5.2.7 ^{1}H NMR spectra showing the decomposition of $C_{60}Pd(0)_2@Pd_2\mathbf{L}^{\mathbf{S}}_4$ (CD_3CN, 500 MHz, 298 K).

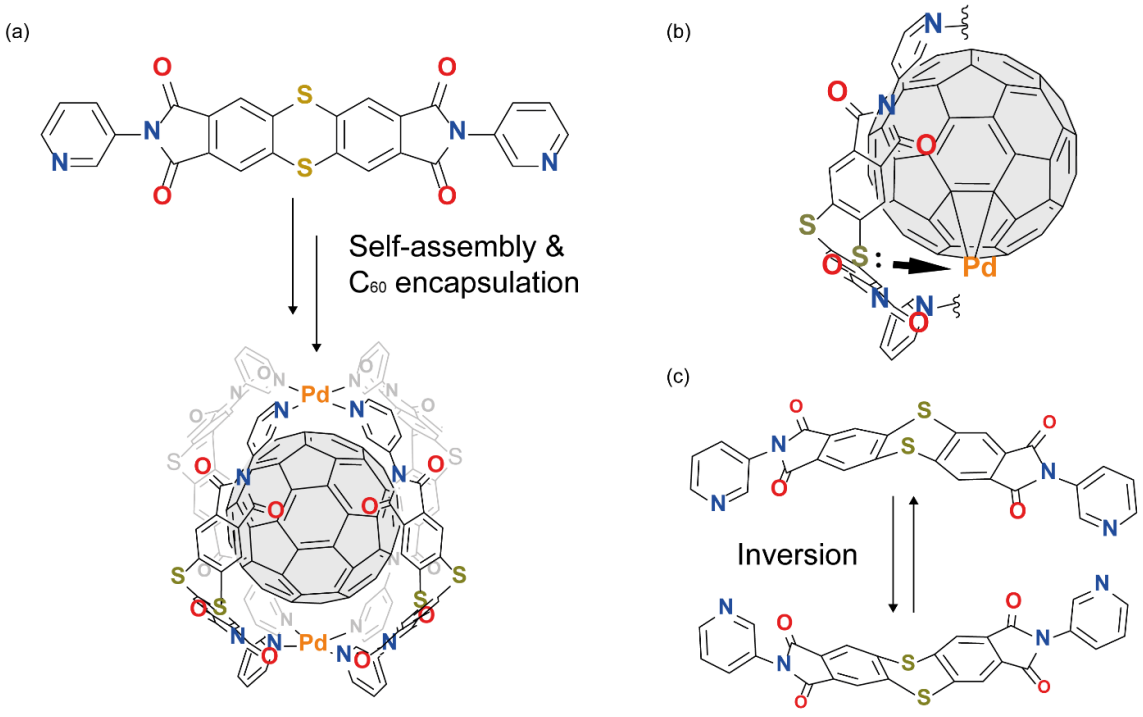

Figure 5.2.8 (a) Chemical structure of $\mathbf{L^S}$ and its expected self-assembly together with C_{60} as a guest (b) Simple illustration showing the concept of stabilization through coordination from the sulfur atoms (c) Inversion motion of $\mathbf{L^S}$

Thianthrene presents a similar bent angle to triptycene of approximately 120° due to the sulfur atoms on the center. Thus, an inner space surrounded by this ligand should be suitable to accommodate C_{60} similar to $Pd_2\mathbf{L^P}_4$. The ligand was synthesized following literature procedures.[9] The ligand is poorly soluble in organic solvents preventing spectroscopic analyses. The resulting suspension was soluble in acetonitrile after self-assembly with $[Pd(II)(MeCN)_4](BF_4)_2$ (**Figure 5.2.9a**). A single set of signals was observed in the ^{1}H NMR spectrum, which could be assigned as $Pd_n\mathbf{L^S}_{2n}$ (**Figure 5.2.9b**). ESI-MS analysis elucidated the chemical composition of the resulting complex to be $Pd_3\mathbf{L^S}_6$, an unexpected ring-shaped topology (**Figure 5.4.17**). In fact, a larger hydrodynamic radius of 14.9 Å was obtained by ^{1}H DOSY NMR experiment compared with $Pd_2\mathbf{L^P}_4$ having a hydrodynamic radius of 11.7 Å due to the higher nuclearity (**Figure 5.4.16**). On the other hand, cage-to-cage transformation from $Pd_3\mathbf{L^S}_6$ to $Pd_2\mathbf{L^S}_4$ was observed upon encapsulation of C_{60} in 21:79 ($Pd_3\mathbf{L^S}_6$:C_{60}@$Pd_2\mathbf{L^S}_4$) ratio (**Figure 5.2.9a** and **c**). Characterization was conducted by NMR and ESI MS spectroscopy. Furthermore, a characteristic upfield shift of proton **a**

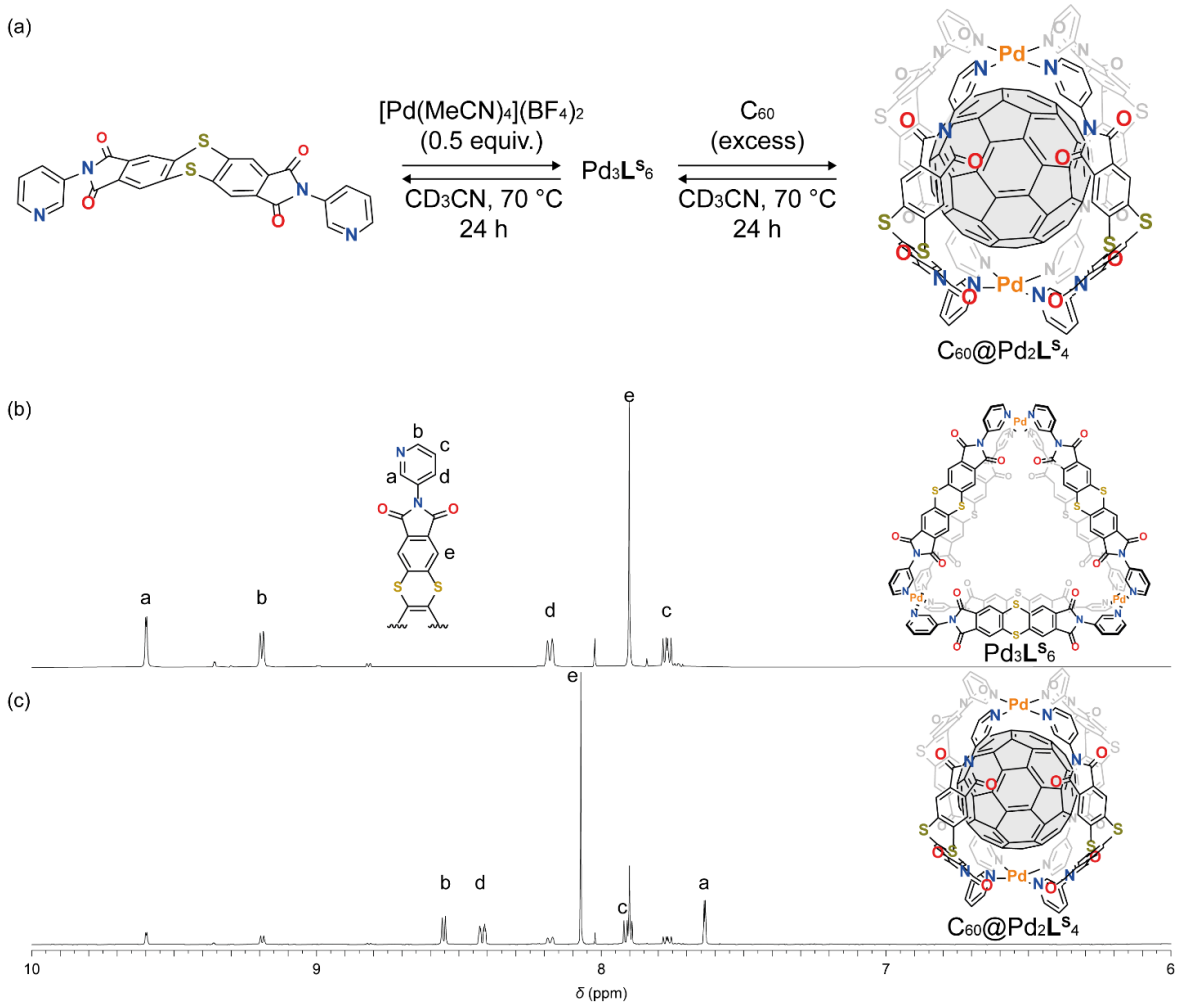

Figure 5.2.9 (a) Self-assembly of $\mathbf{L^s}$ with Pd(II) and C_{60} encapsulation (b) ^{1}H NMR spectrum (CD_3CN, 500 MHz, 298 K) of $Pd_3\mathbf{L^S}_6$ and (c) $C_{60}@Pd_2\mathbf{L^S}_4$

was observed upon C_{60} encapsulation supporting the assumption that encapsulation of C_{60} occurs inside the cavity. Despite the uncomplete conversion to $C_{60}@Pd_2\mathbf{L^S}_4$ even after longer heating with excess C_{60}, synthesis of η^2-$C_{60}Pd(0)_n$ (n=1,2) complex was carried out by addition of $Pd(0)(dba)_2$. After addition of $Pd(0)(dba)_2$ to an acetonitrile solution of $C_{60}@Pd_2\mathbf{L^S}_4$ in air gives a brownish solution. In the ^{1}H NMR spectrum of the solution, signals belonging to $C_{60}@Pd_2\mathbf{L^S}_4$ disappeared and a new set of signals indicating an identical symmetry to η^2-$C_{60}Pd(0)_2@Pd_2\mathbf{L^S}_4$ newly appeared. The formation of η^2-$C_{60}Pd(0)_2@Pd_2\mathbf{L^S}_4$ was further confirmed by ESI MS analysis. In spite of the lone pairs on the sulfur atoms which were expected to stabilize unstable η^2-$C_{60}Pd(0)_n$ (n=1,2) within the cage, the stabilization effect could not be observed in solution even in an inert condition (**Figure 5.2.10**).

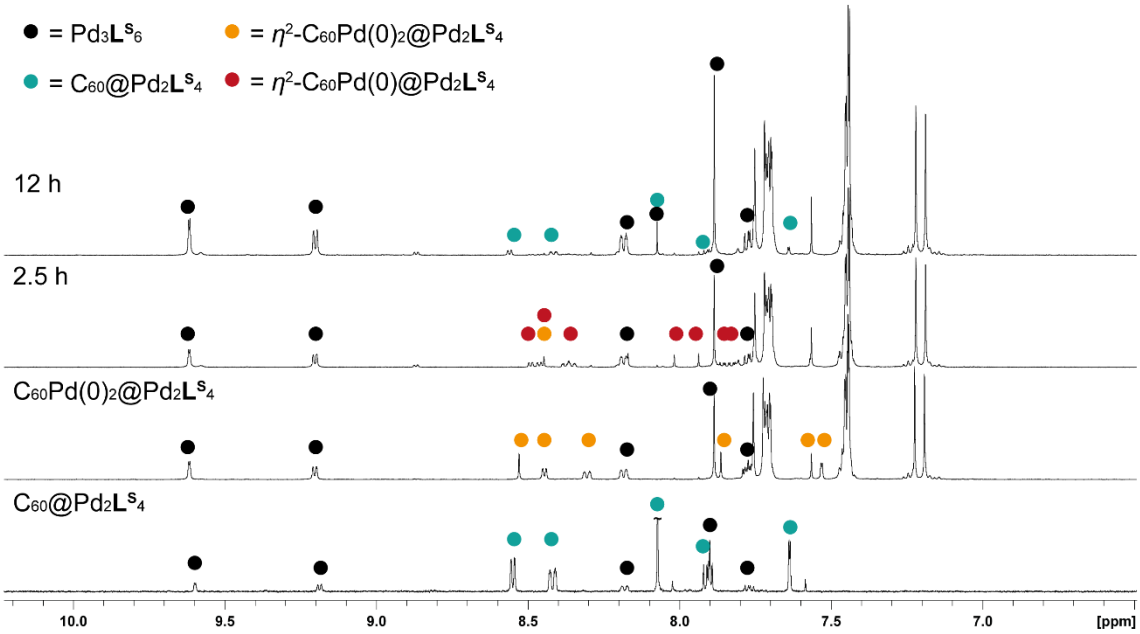

Figure 5.2.10 ^{1}H NMR spectra showing the decomposition of $C_{60}Pd(0)_2@Pd_2\mathbf{L}^{S}_4$ (CD_3CN, 500 MHz, 298 K).

Cage-to-cage transformation is facilitated by the template-effect of C_{60} encapsulation, stabilizing $Pd_2\mathbf{L}^{S}_4$ cage. In Ms. Alicia Dullweber´s bachelor thesis, synthesis and self-assembly with Pd(II) of ligand $\mathbf{L}^{A}$ having an anthracene backbone is described (**Figure 5.2.11**).[10] It was found that $\mathbf{L}^{A}$ forms a ring-shaped $Pd_3\mathbf{L}^{A}_6$ cage upon self-assembly. It is known that the bite angle of ligands plays a decisive role in the topology of coordination cages.[11,12] For instance, a ligand having a phenanthrene backbone forms Pd_3L_6 assembly upon Pd(II) addition.[10] The phenanthrene-based ligand has a bite angle of approximately 60° calculated based on a simple chemical structure. This trend is in a good accordance with the observed behavior of $\mathbf{L}^{A}$, having a bite angle of ca. 60°, in self-assembly with Pd(II). On the other hand, ligands having a bite angle of 0° favorably form Pd_2L_4 topology with square-planar Pd(II), which should be the case

for $\mathbf{L^P}$ and $\mathbf{L^S}$. However, $\mathbf{L^S}$ gives $Pd_3\mathbf{L^S}_6$ ring as a major species after self-assembly (**Figure 5.2.11**).

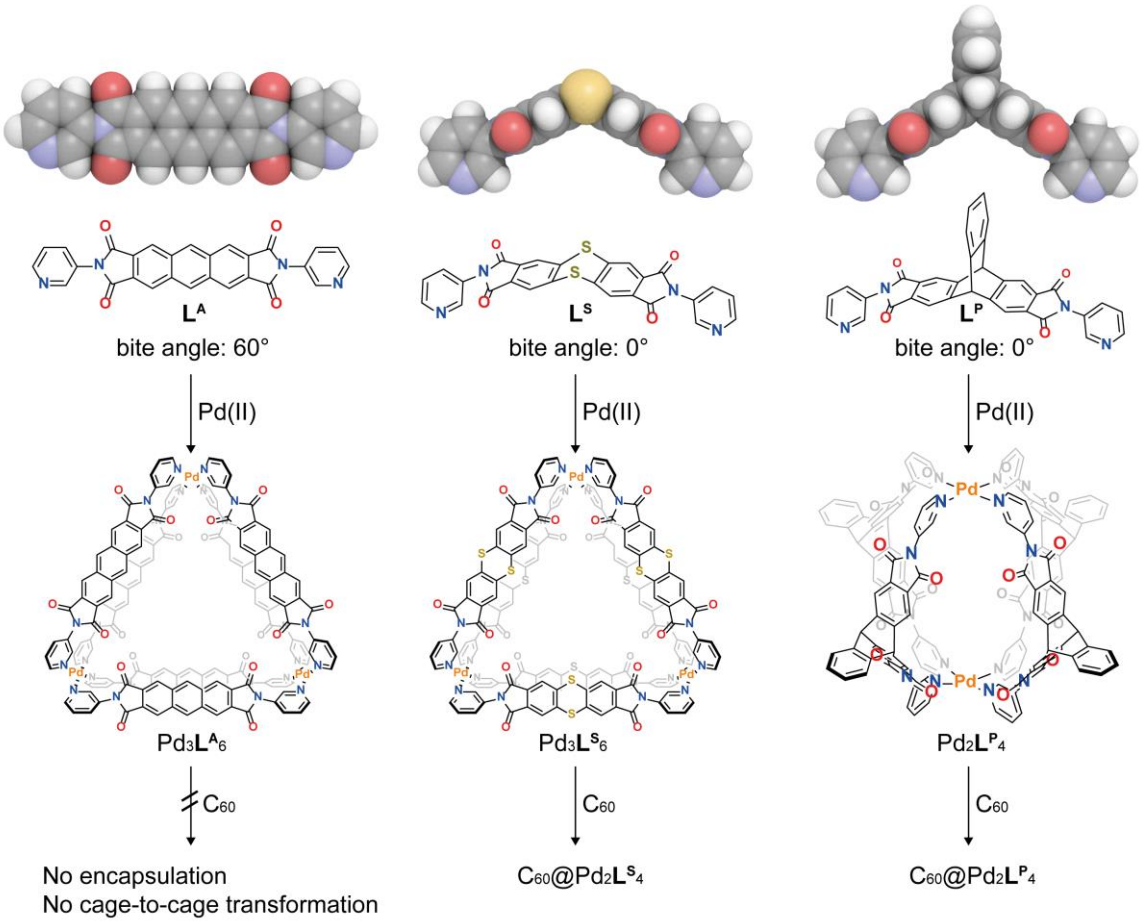

Figure 5.2.11 Bite angles of each ligand and the consequence of their assembly with Pd(II)

This should be related to an intrinsic inversion motion of the thianthrene-backbone (**Figure 5.2.8a**), having only around 6 kcal/mol of an energy barrier.[13] Therefore, the inversion motion may average the bite angle of the ligand to be close to 60° and thus, the resulting topology was $Pd_3\mathbf{L^S}_6$, while encapsulation of C_{60} inside $Pd_2\mathbf{L^S}_4$ probably suppresses the inversion motion of the ligand to maintain the bite angle to form the lantern-shaped topology.

5.3 Conclusion

In conclusion, synthesis of $C_{60}Pd(0)_n$ (n=1,2) could be achieved by preventing polymerization using coordination cages as a supramolecular mask. In addition, synthesis of thianthrene-based ligand $\mathbf{L^S}$ and its self-assembly behavior with Pd(II)

was investigated. Not only the bite-angle but also the flexibility of the ligand was found to play a role in deciding the topology of the resulting coordination cages. Due to the inversion motion of $\mathbf{L^S}$, coordination cages comprised of the ligand and Pd(II) showed cage-to-cage transformation upon encapsulation of C_{60}. Synthesized η^2-$C_{60}Pd(0)_n$ (n=1,2) complexes inside both $Pd_2\mathbf{L^S}_4$ and $Pd_2\mathbf{L^P}_4$ are a rather unstable species most likely due to acetonitrile which can act as a competing ligand. None of the attempts, such as *cis*-protection resulted in an increased stabilization of the system. Further investigations are required for stabilizing the formed complexes.

5.4 Appendix

5.4.1 Materials and methods

Unless otherwise stated, all chemicals were purchased from commercial sources and used as received. $[Pd(MeCN)_4](BF_4)_2$ and $Pd(0)(dba)_2$ were purchased from Sigma-Aldrich. Corannulene was purchased from TCI.inc. $\mathbf{L^P}$ was prepared according to literature procedures.[14] Bruker ESI-timsTOF and compact mass spectrometers using Agilent tune mix as calibrant. NMR experiments were performed using Bruker AV 500 Avance NEO, Bruker AV 600 Avance FT-NMR, Bruker Avance III HD 700 MHz spectrometers. ^1H and ^{13}C signals were referenced to the residual solvent peak: acetonitrile (1.94 ppm,118.26 ppm), chloroform (7.26 ppm, 77.16 ppm). DFT calculation were performed using Gaussian 16, Revision B.01.[15] Hydrodynamic radii of compounds were calculated from Stokes-Einstein equation (eq 1) where D is the diffusion coefficient, k_B is the Boltzman constant, T is the temperature, η is the viscosity of the solvent, and r_H is the hydrodynamic radius of interest. ^1H DOSY NMR spectra were recorded with a dstebpgp3s pulse sequence with diffusion delays D20 of 0.08 s and gradient powers P30 of 1200. T_1 analyses of the corresponding signals in the 1D spectra were performed to obtain the diffusion coefficients D using the STEJSKAL-TANNER-Equation.

5.4.2 Synthesis of η^2-$C_{60}Pd(0)@Pd_2L^P_4$

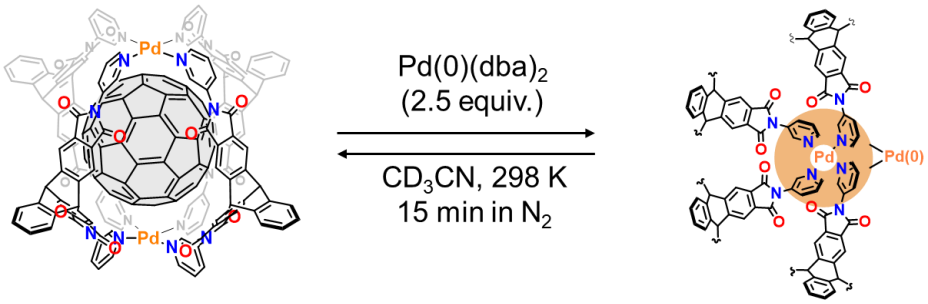

Figure 5.4.1 Synthesis of η^2-$C_{60}Pd(0)@Pd_2L^P_4$.

To an acetonitrile solution of $Pd_2L^P_4$ (0.70 mM, 0.600 mL, 0.42 μmol), synthesized following the literature,[13] in a NMR tube was added a stock solution of $Pd(0)(dba)_2$ (10 mM, 105 μL, 2.5 equiv.) in $CDCl_3$ in the glovebox. After shaking the NMR tube, measurements were carried out.

^{1}H NMR (CD_3CN, 500 MHz, 298 K): δ (ppm) **e** 8.46 (s, 4H), **b** 8.45 (m, 4H), **b** 8.38 (d, J = 5.4 Hz, 4H), **d*2** 8.307 (m, 8H), **e** 8.08 (s, 4H), **e** 7.93 (s, 4H), **e** 7.89 (s, 4H), **c** 7.79 (m, 4H), **c** 7.73 (m, 4H), **a** 7.49 (d, J = 2.3 Hz, 4H), **a** 7.34 (d, J = 2.3 Hz, 4H), **h** 6.36 (s, 2H), **h** 6.30 (s, 2H), **h** 6.21 (s, 2H), **h** 6.20 (s, 2H). **f**-**g** are overlapping with dba signals.

ESI MS (positive mode): found: 806.3109 and 1104.0842; calculated for $[(C_{34}H_{18}N_4O_4)_4Pd_2(C_{60})Pd]^{4+}$ and $[(C_{34}H_{18}N_4O_4)_4Pd_2(C_{60})Pd(BF_4)]^{3+}$ to be 806.3120 and 1104.0842 respectively

5.4.2.1 ^{1}H NMR spectra of η^2-$C_{60}Pd(0)@Pd_2L^P_4$

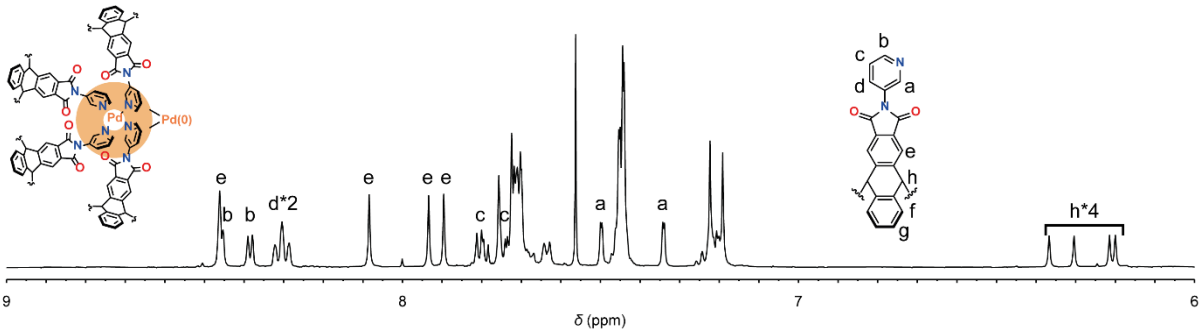

Figure 5.4.2 ^{1}H NMR spectrum of η^2-$C_{60}Pd(0)@Pd_2L^P_4$ (CD_3CN, 500 MHz, 298 K).

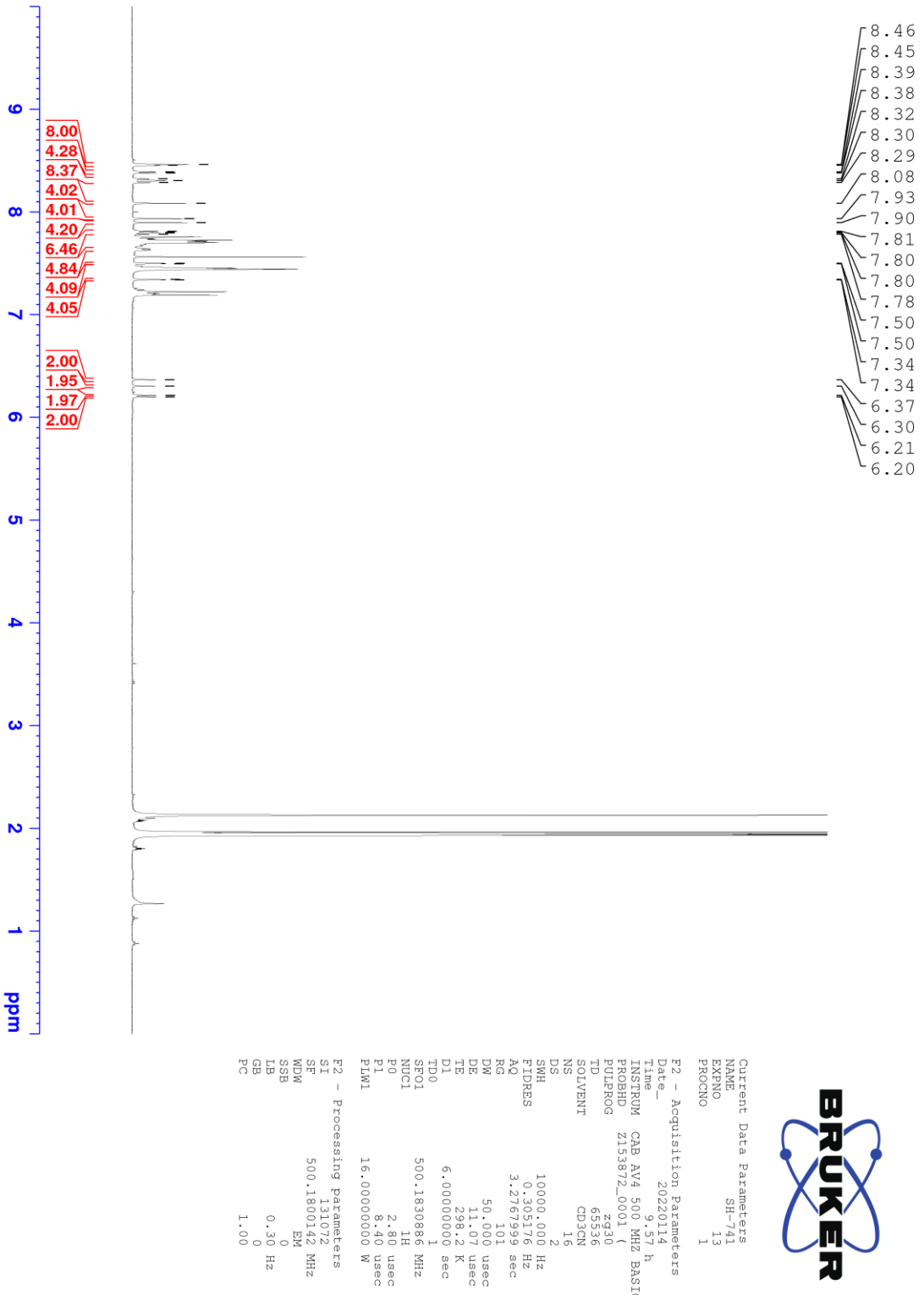

Figure 5.4.3 ^{1}H NMR spectrum of η^2-C_{60}Pd(0)@$Pd_2\mathbf{L^P}_4$ (CD_3CN, 500 MHz, 298 K).

5.4.2.2 ^{1}H-^{1}H COSY NMR spectrum of η^2-C_{60}Pd(0)@$Pd_2L^P_4$

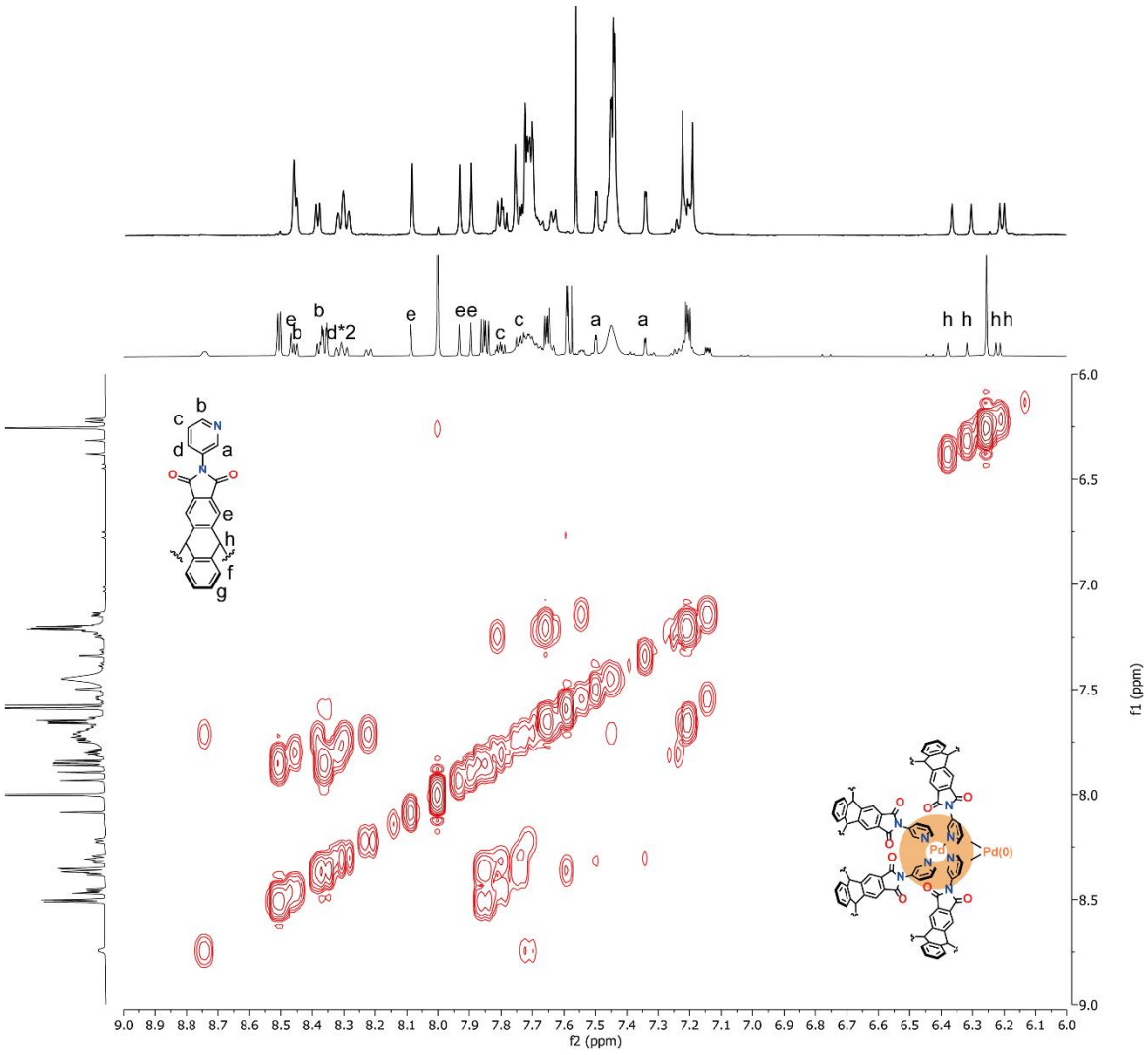

Figure 5.4.4 ^{1}H-^{1}H COSY NMR spectrum of η^2-C_{60}Pd(0)@$Pd_2\mathbf{L}^{\mathbf{P}}_4$ (CD_3CN, 600 MHz, 298 K).

5.4.2.3 ESI MS spectrum of η^2-$C_{60}Pd(0)@Pd_2L^P_4$

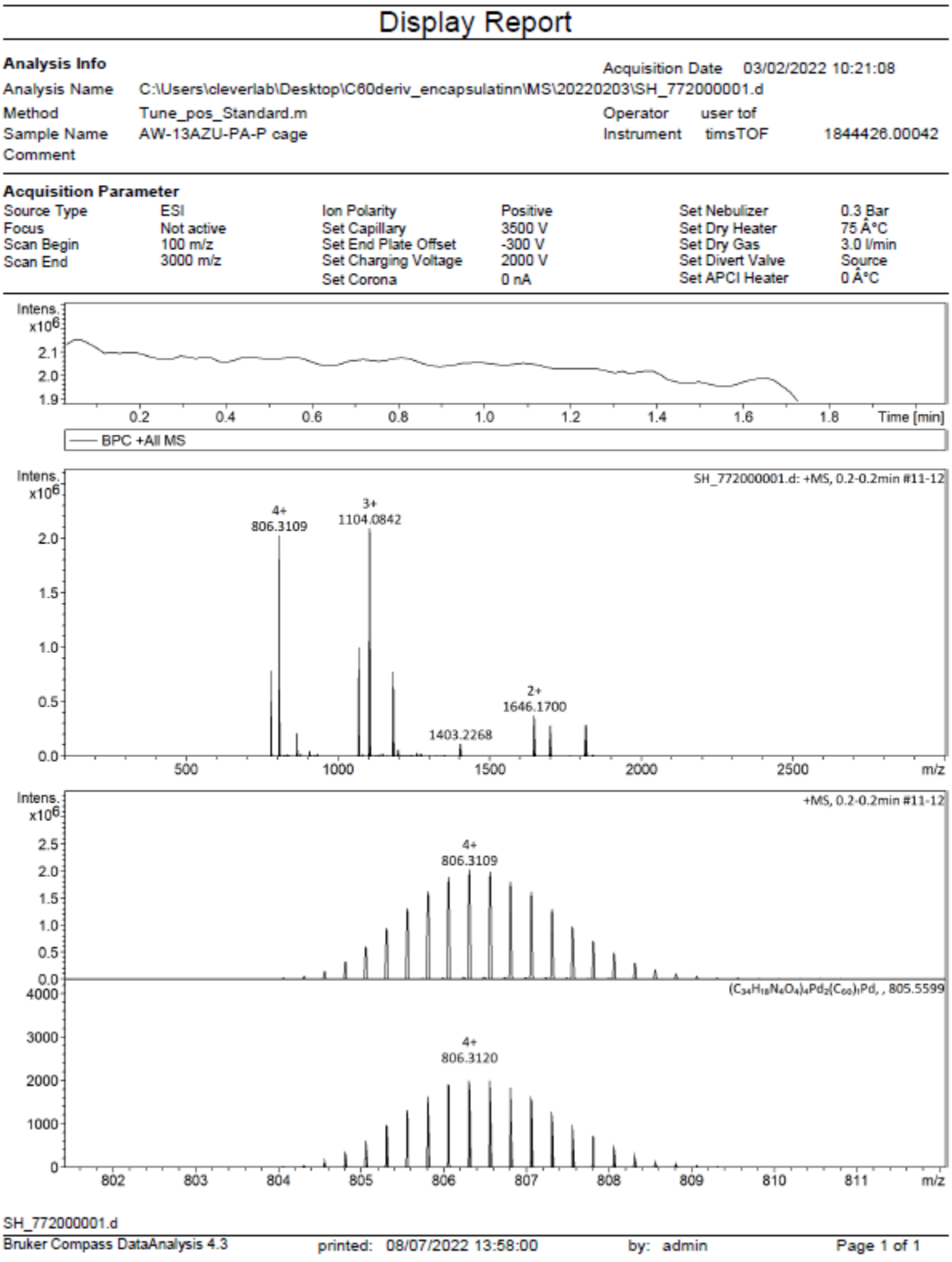

Figure 5.4.5 ESI MS spectrum of η^2-$C_{60}Pd(0)@Pd_2\mathbf{L}^P_4$ (positive mode).

5.4.3 Synthesis of η^2-$C_{60}Pd(0)_2$@$Pd_2L^P_4$

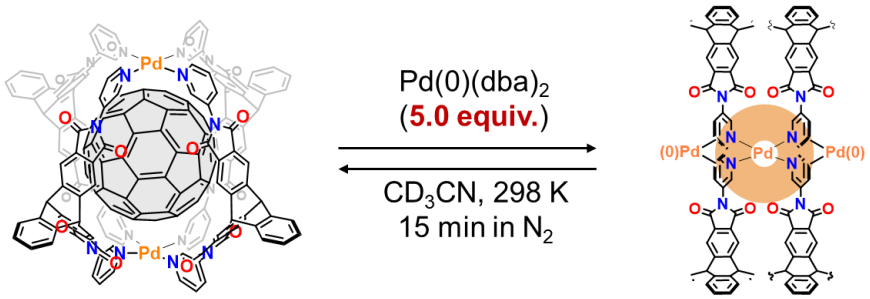

Figure 5.4.6 Synthesis of η^2-$C_{60}Pd(0)_2$@$Pd_2L^P_4$.

To an acetonitrile solution of $Pd_2L^P_4$ (0.70 mM, 0.600 mL, 0.42 μmol), synthesized following the literature,[13] in a NMR tube, was added a stock solution of $Pd(0)(dba)_2$ (10 mM, 210 μL, 2.1 μmol) in $CDCl_3$ in the glovebox. After shaking the NMR tube, measurements were carried out.

^{1}H NMR (CD_3CN, 500 MHz, 298 K): δ (ppm) **e** 8.49 (s, 8H), **b** 8.40 (d, J = 5.6 Hz, 8H), **d** 8.23 (ddd, J = 8.6, 2.3, 1.2 Hz, 8H), **e** 7.82 (s, 8H), **a** 7.48 (*d*, J = 2.3 Hz, 8H), **h** 6.44 (s, 4H), **h** 6.16 (s, 4H). **c**, **f**-**g** are overlapping with dba signals.

ESI MS (positive mode): found: 891.5633 and 1217.7537; calculated for $[(C_{34}H_{18}N_4O_4)_4Pd_2(C_{60})(C_{17}H_{14}O)]^{4+}$ and $[(C_{34}H_{18}N_4O_4)_4Pd_2(C_{60})(C_{17}H_{14}O)(BF_4)]^{3+}$ to be 891.5644 and 1217.7540 respectively

5.4.3.1 ^{1}H NMR spectra of η^2-$C_{60}Pd(0)_2$@$Pd_2L^P_4$

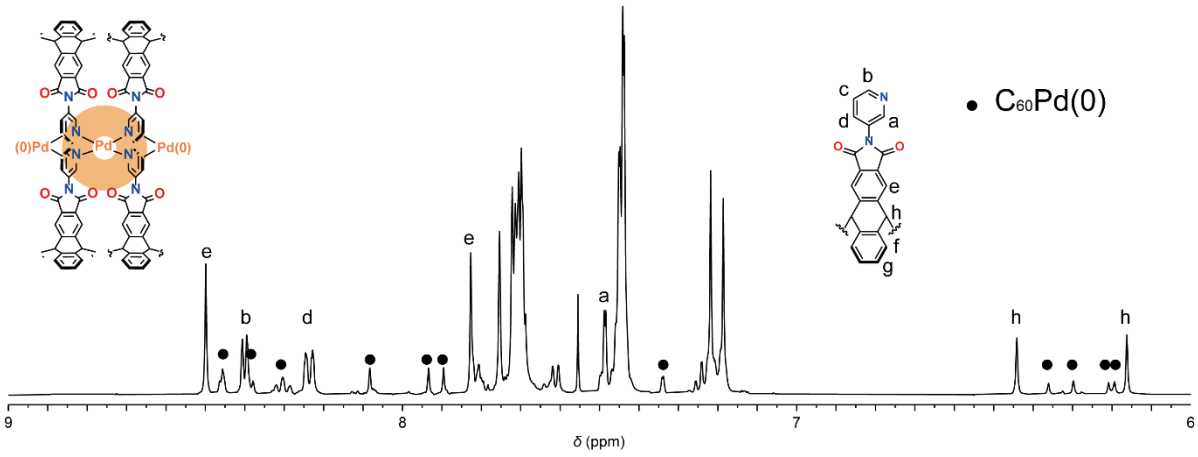

Figure 5.4.7 ^{1}H NMR spectrum of η^2-$C_{60}Pd(0)_2$@$Pd_2L^P_4$ (CD_3CN, 500 MHz, 298 K).

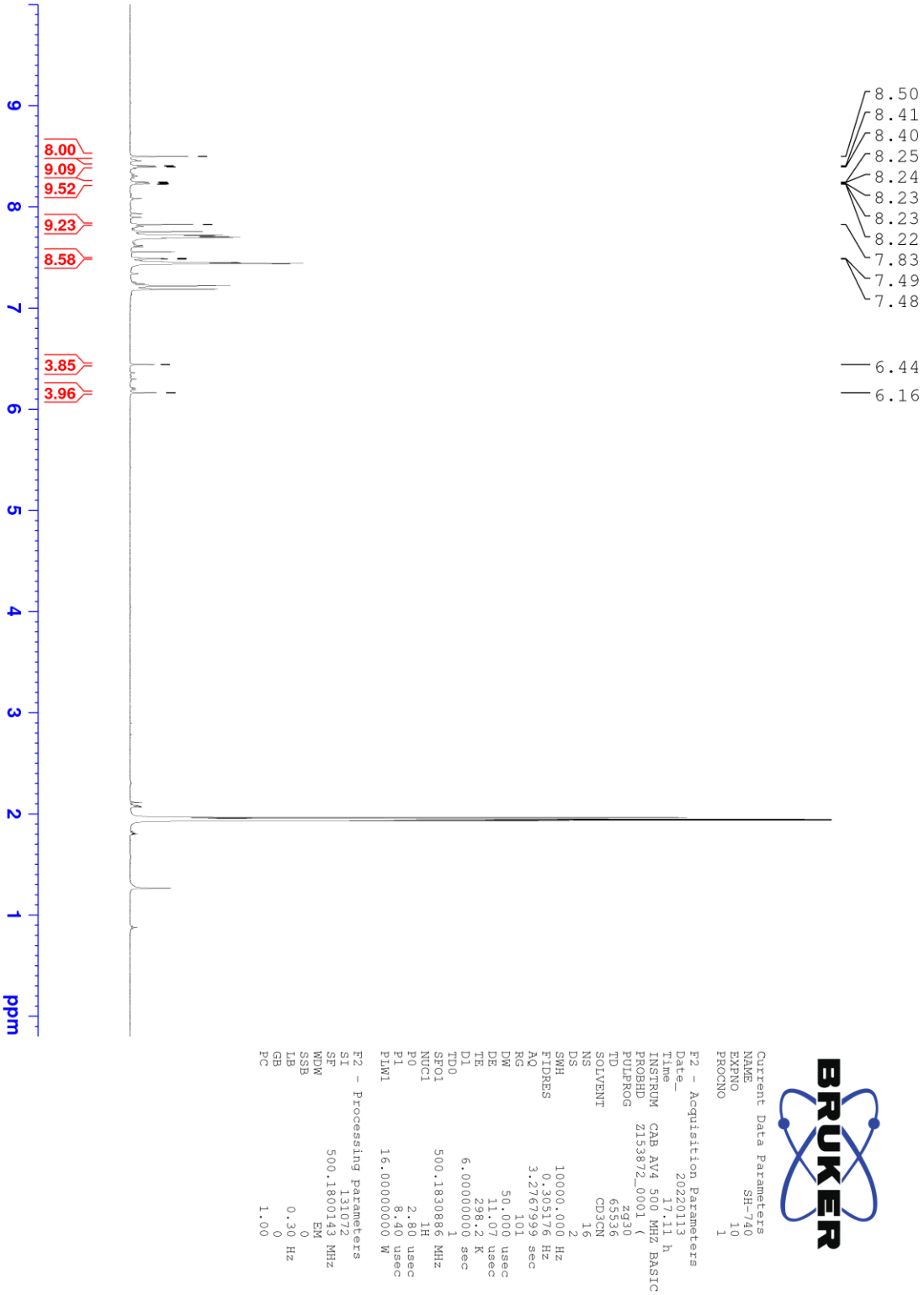

Figure 5.4.8 ^{1}H NMR spectrum of η^2-$C_{60}Pd(0)_2$@$Pd_2\mathbf{L}^{\mathbf{P}}_4$ (CD_3CN, 500 MHz, 298 K).

5.4.3.2 ^{1}H-^{1}H COSY NMR spectrum of η^2-$C_{60}Pd(0)_2$@$Pd_2L^P_4$

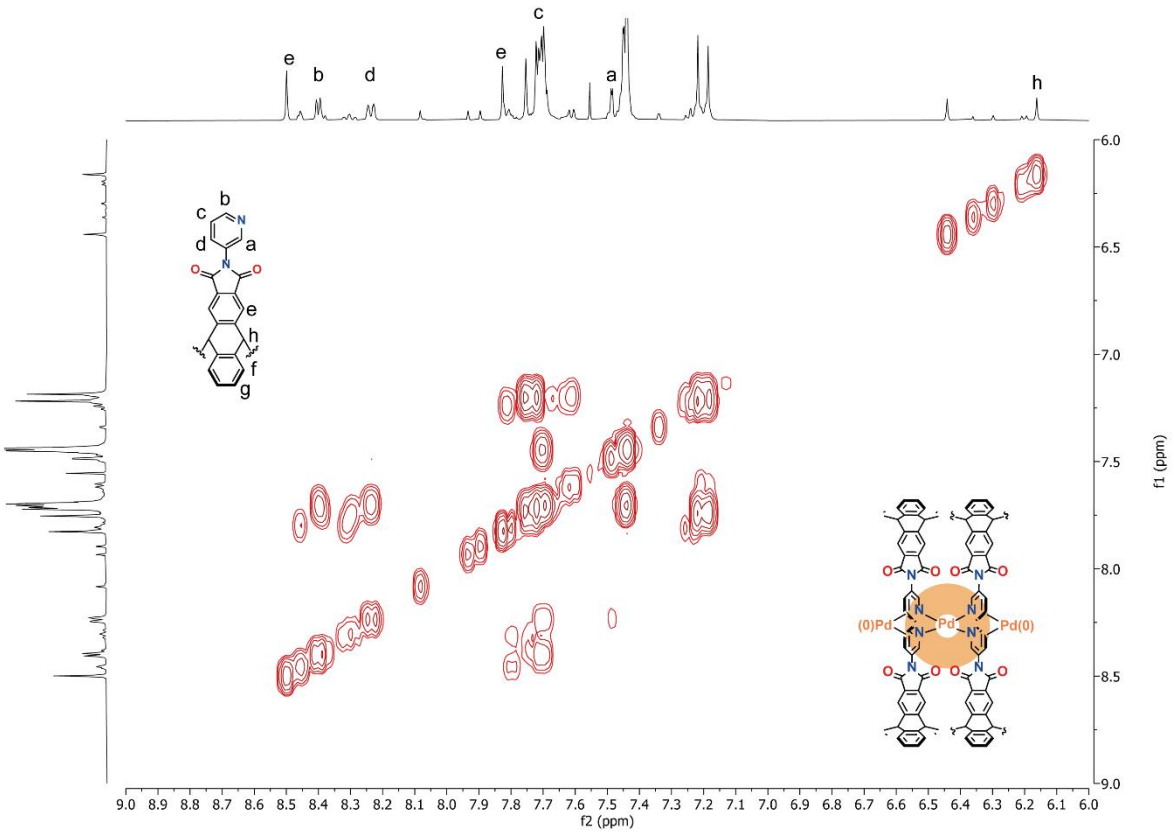

Figure 5.4.9 ^{1}H-^{1}H COSY NMR spectrum of η^2-$C_{60}Pd(0)_2$@$Pd_2\mathbf{L}^{\mathbf{P}}_4$ (CD_3CN, 500 MHz, 298 K).

5.4.3.3 ESI MS spectrum of η^2-$C_{60}Pd(0)_2$@$Pd_2L^P_4$

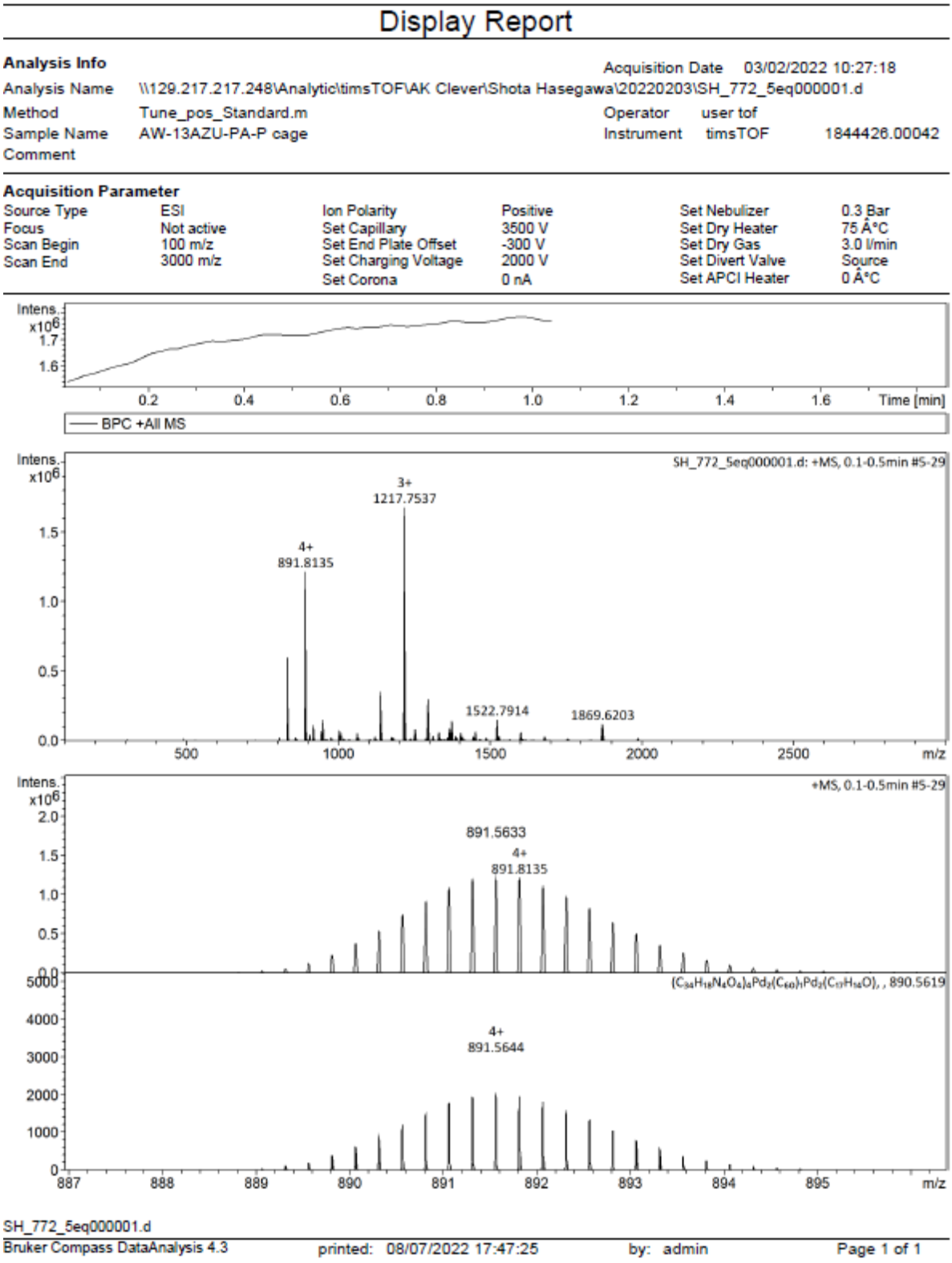

Figure 5.4.10 ESI-MS spectra (positive mode) of η^2-$C_{60}Pd(0)_2$@$Pd_2\mathbf{L^P}_4$.

5.4.4 Synthesis of $Pd_3L^S_6$

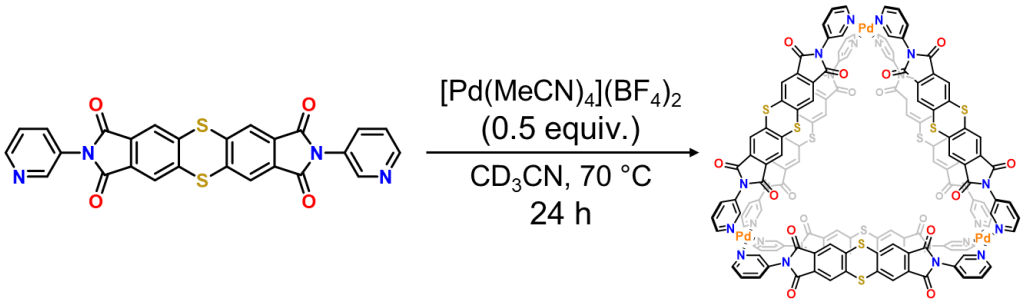

Figure 5.4.11 Synthesis of $Pd_3L^S_6$.

To a suspension of $\mathbf{L^S}$ (5.29 mg, 10.4 μmol) in CD_3CN (3.46 mL) $[Pd(MeCN)_4](BF_4)_2$ (20 mM, 260 μL, 5.2 μmol) was added and heated at 70 °C for 24 h while stirring. After filtrating the remaining solid, $Pd_3\mathbf{L^S}_6$ was obtained as a yellow solution (2.8 mM of ligand concentration).

^{1}H NMR (CD_3CN, 500 MHz, 298 K): *δ* (ppm) **a** 9.59 (d, *J* = 2.3 Hz, 12H), **b** 9.19 (d, *J* = 5.6 Hz, 12H), **d** 8.18 (ddd, *J* = 8.3, 2.3, 1.2 Hz, 12H), **e** 7.90 (s, 24H), **c** 7.76 (dd, *J* = 8.3, 5.6 Hz, 12H)

^{13}C NMR (CD_3CN, 176 MHz, 298 K): 165.71, 150.23, 148.20, 141.96, 138.02, 132.58, 132.44, 128.47, 124.06; While 9 peaks must be observed in theory, 9 peaks were observed.

DOSY: Diffusion coefficient $D = 4.38 \times 10^{-10}$ m^2s^{-1}, hydrodynamic radius r_H was calculated to be 14.9 Å

ESI MS (positive mode): found: 561.6489, 691.3797, and 885.9762; calculated for $[(C_{26}H_{12}N_4O_4)_6Pd_3]^{6+}$, $[(C_{26}H_{12}N_4O_4)_6Pd_3(BF_4)]^{5+}$, and $[(C_{26}H_{12}N_4O_4)_6Pd_3(BF_4)_2]^{4+}$ to be 561.6488, 691.3794, and 885.9753 respectively

5.4.4.1 ^{1}H NMR spectra of $Pd_3L^S_6$

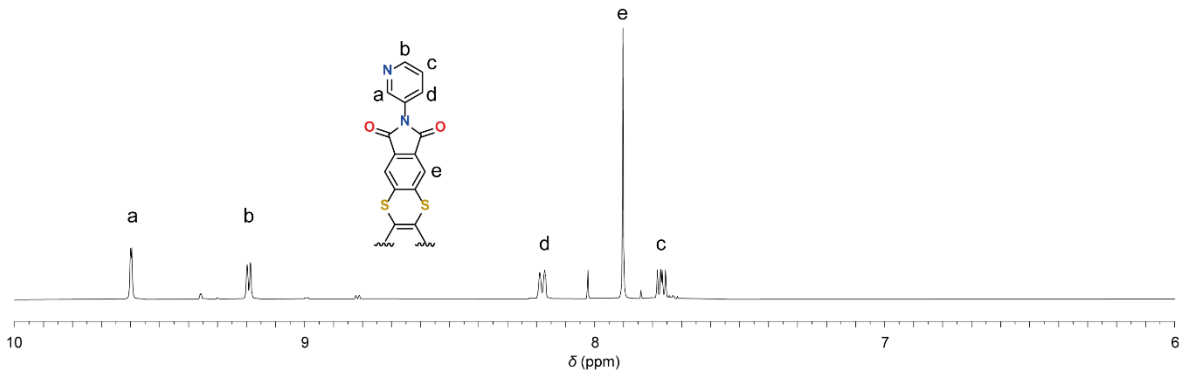

Figure 5.4.12 ^{1}H NMR spectrum of $Pd_3\mathbf{L}^S_6$ (CD_3CN, 500 MHz, 298 K).

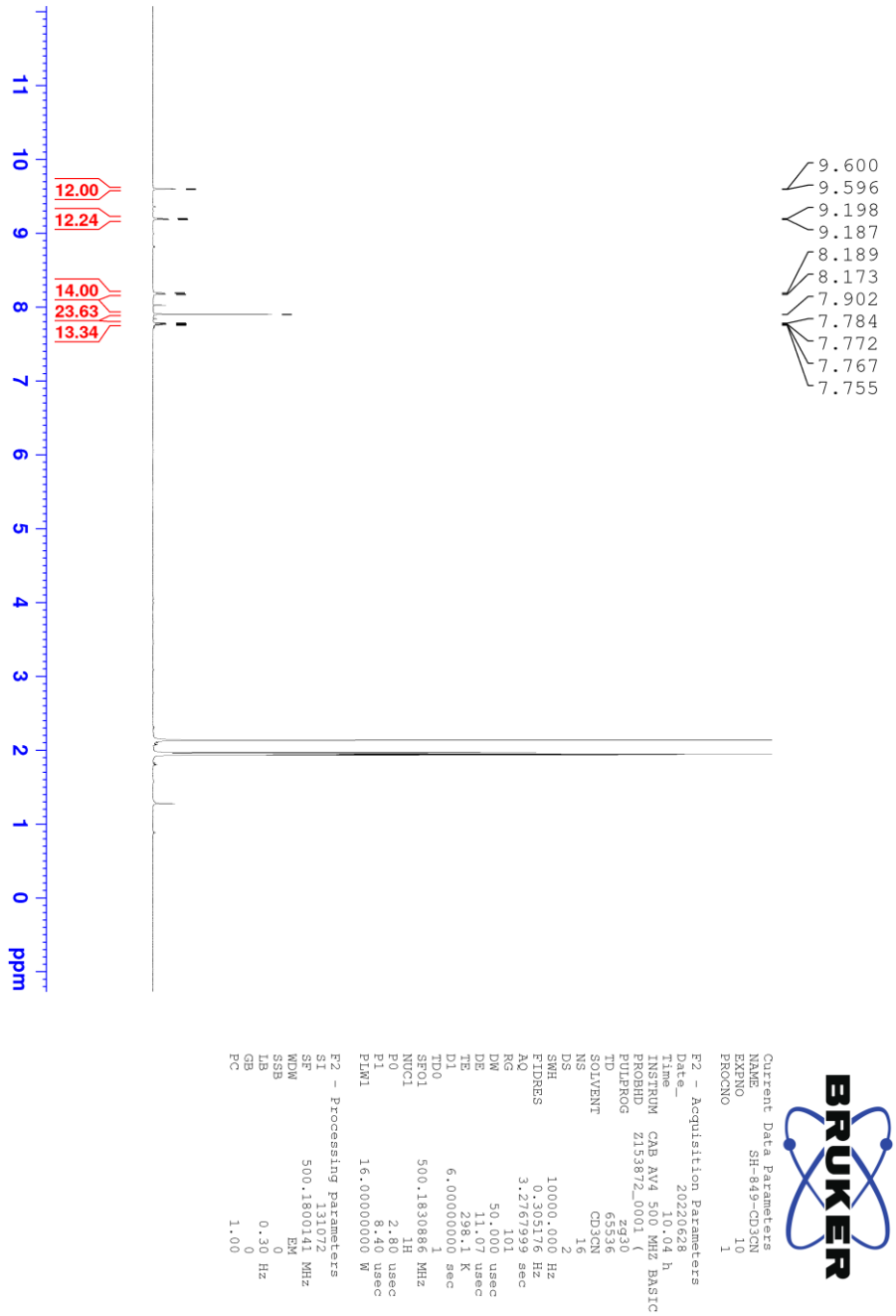

Figure 5.4.13 ^{1}H NMR spectrum of $Pd_3\mathbf{L}^{\mathbf{S}}_6$ (CD_3CN, 500 MHz, 298 K).

5.4.4.2 ^{1}H-^{1}H COSY NMR spectrum of $Pd_3L^S_6$

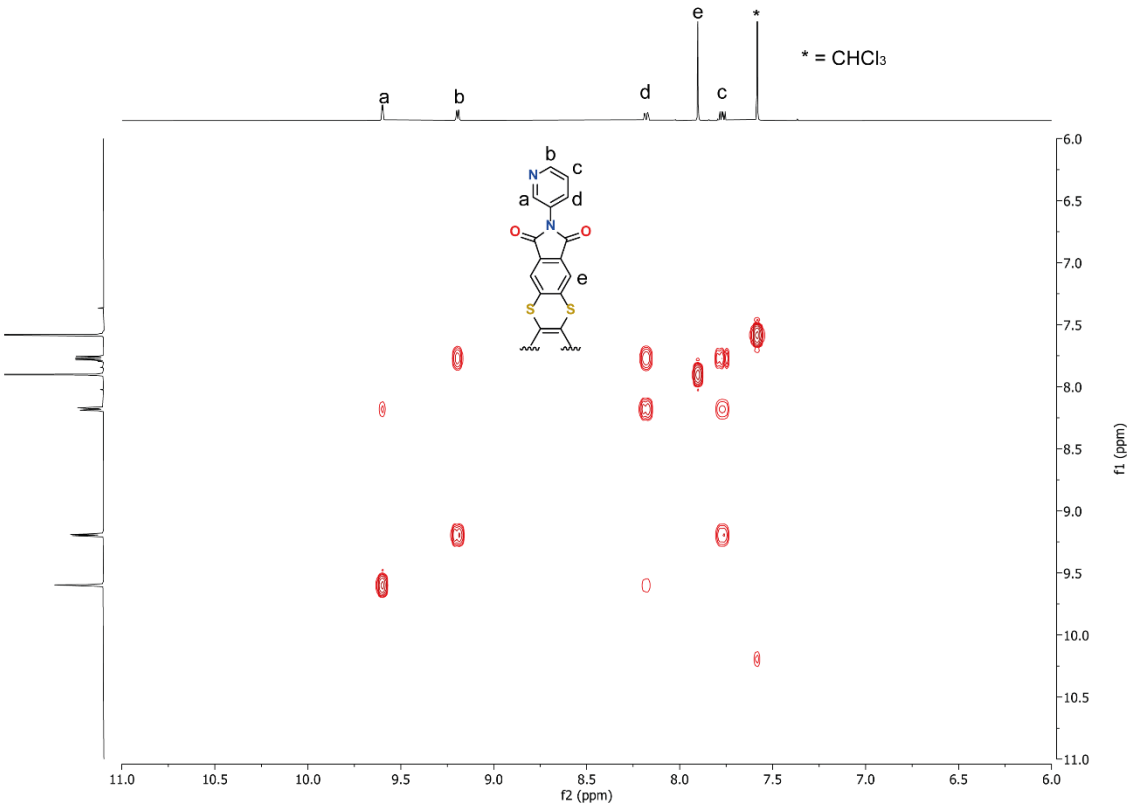

Figure 5.4.14 ^{1}H-^{1}H COSY NMR spectrum of $Pd_3\mathbf{L}^S_6$ (CD_3CN, 500 MHz, 298 K).

5.4.4.3 ^{13}C NMR spectrum of $Pd_3L^S_6$

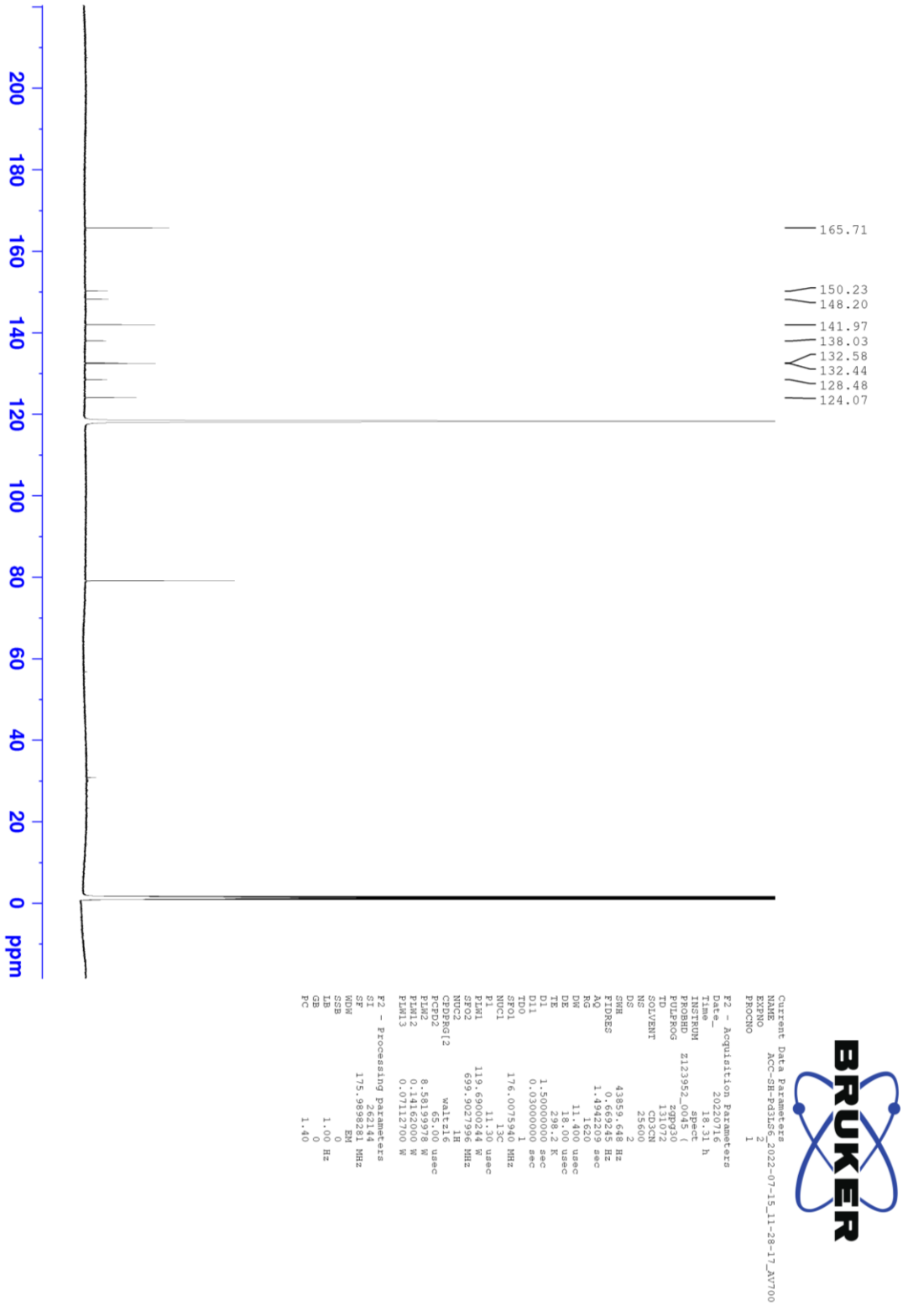

Figure 5.4.15 ^{13}C NMR spectrum of $Pd_3\mathbf{L}^S_6$ (CD_3CN, 176 MHz, 298 K).

5.4.4.4 ^{1}H DOSY NMR spectrum of $Pd_3L^S_6$

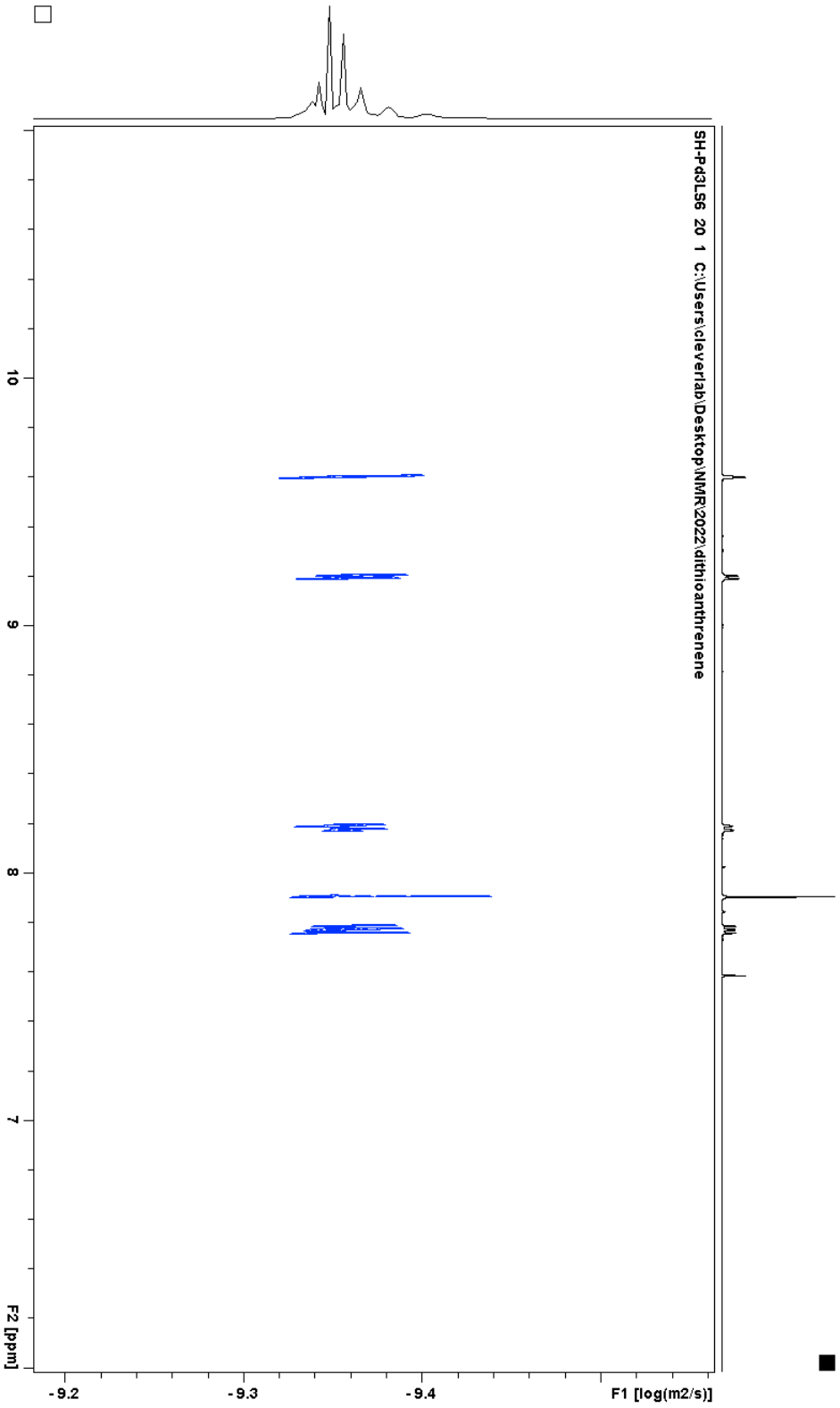

Figure 5.4.16 ^{1}H DOSY NMR spectrum of $Pd_3\mathbf{L}^S_6$ (CD_3CN, 500 MHz, 298 K).

5.4.4.5 ESI MS spectrum of $Pd_3L^S_6$

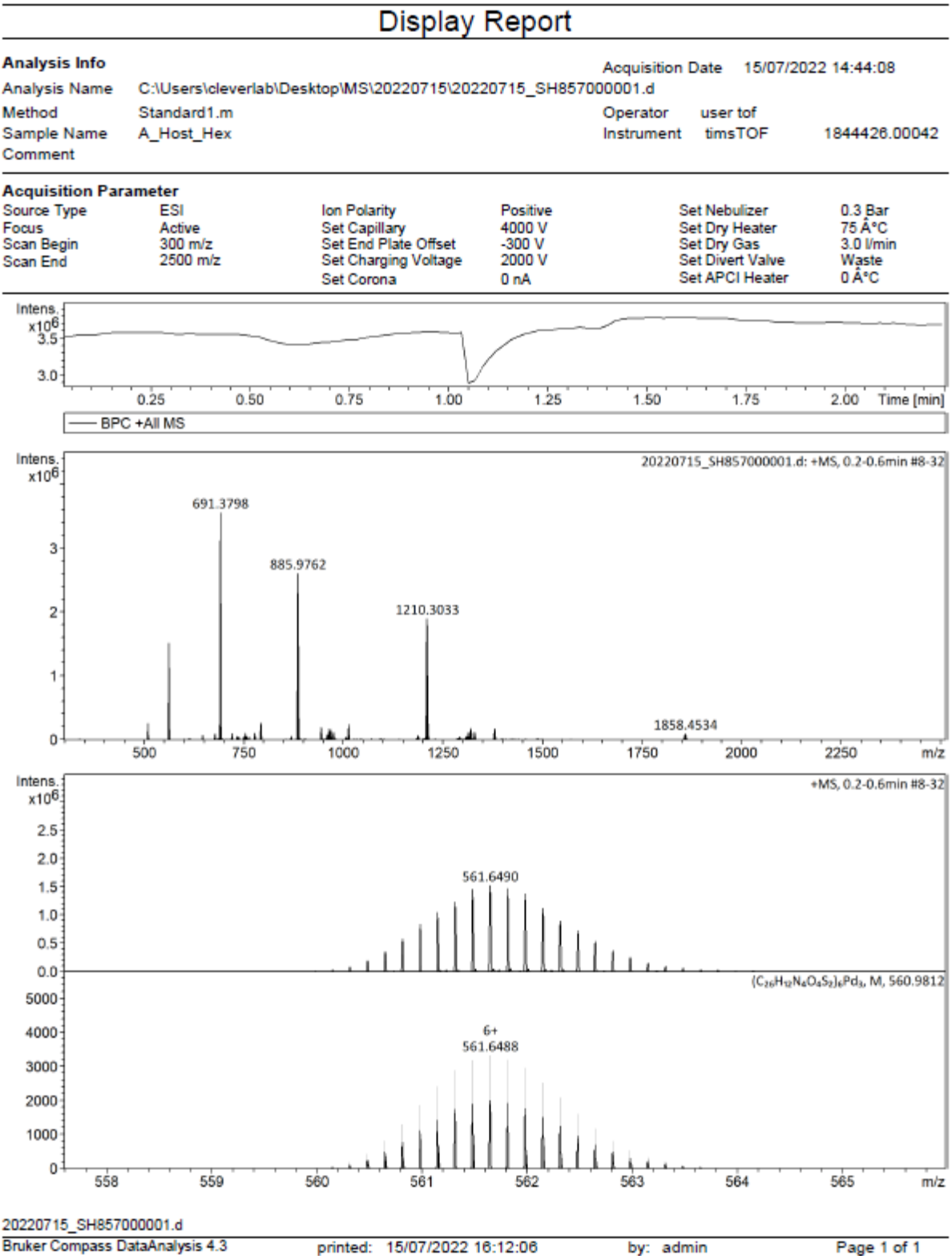

Figure 5.4.17 ESI-MS spectra (positive mode) of $Pd_3L^S_6$.

5.4.5 Synthesis of $C_{60}@Pd_2L^S_4$

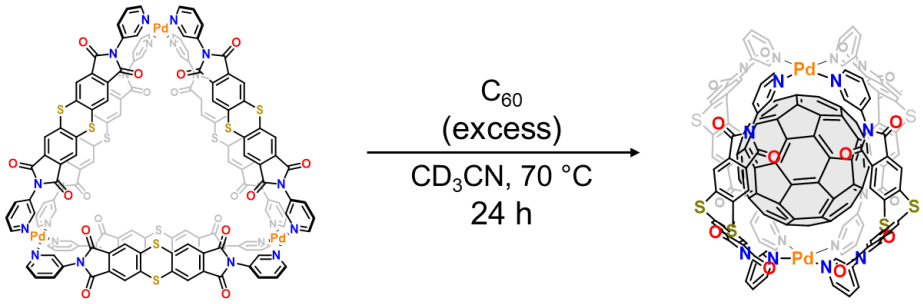

Figure 5.4.18 Synthesis of $C_{60}@Pd_2L^S_4$.

To a solution of $Pd_3L^S_6$ solid C_{60} (excess) was dispersed at 70 °C by stirring. The resulting suspension was filtrated to remove the remaining C_{60}. In the ^{1}H NMR spectrum of the filtrate, a new set of signals, which was assigned as $C_{60}@Pd_2L^S_4$ later, was observed besides another set of signals from $Pd_3L^S_6$.

^{1}H NMR (CD_3CN, 500 MHz, 298 K): δ (ppm) **b** 8.55 (d, J = 5.6 Hz, 8H), **d** 8.41 (ddd, J = 8.5, 2.3, 1.2 Hz, 8H), **e** 8.07 (s, 16H), **c** 7.76 (m, 8H), **a** 7.63 (d, J = 2.3 Hz, 8H)
^{13}C NMR (CD_3CN, 150 MHz, 298 K): 165.69, 164.87, 152.66, 150.21, 148.17, 147.15, 144.73, 142.06, 141.95, 140.44, 138.01, 132.55, 132.41, 132.38, 132.31, 129.89, 128.46, 127.40, 124.05; While 10 peaks must be observed in theory, 19 peaks were observed. 9 peaks belong to $Pd_3L^S_6$.
DOSY: Diffusion coefficient D = 5.57 × 10^{-10} m^2s^{-1}, hydrodynamic radius r_H was calculated to be 11.7 Å
ESI MS (positive mode): found: 741.7328 and 1017.9784; calculated for $[(C_{26}H_{12}N_4O_4S_2)_4Pd_2(C_{60})]^{4+}$ and $[(C_{34}H_{18}N_4O_4S_2)_4Pd_2(C_{60})(BF_4)]^{3+}$ to be 741.7326 and 1017.9782 respectively

5.4.5.1 ^{1}H NMR spectra of $C_{60}@Pd_2L^{S}_4$

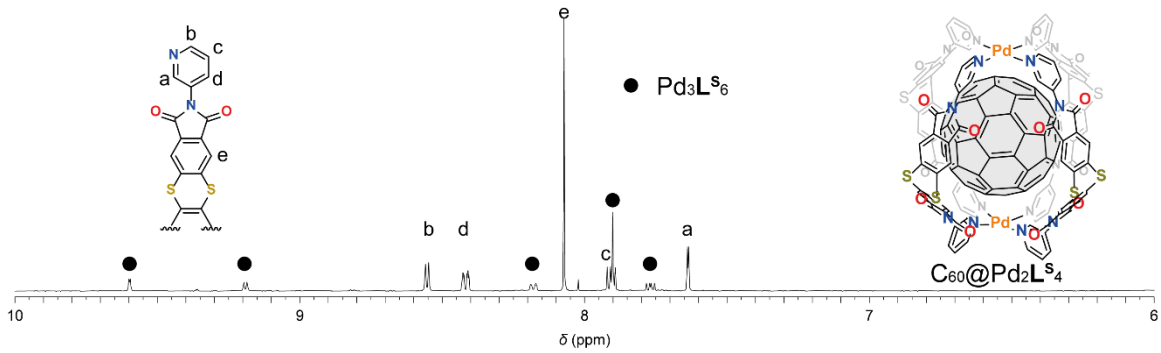

Figure 5.4.19 ^{1}H NMR spectrum of $C_{60}@Pd_2L^{S}_4$ (CD_3CN, 500 MHz, 298 K).

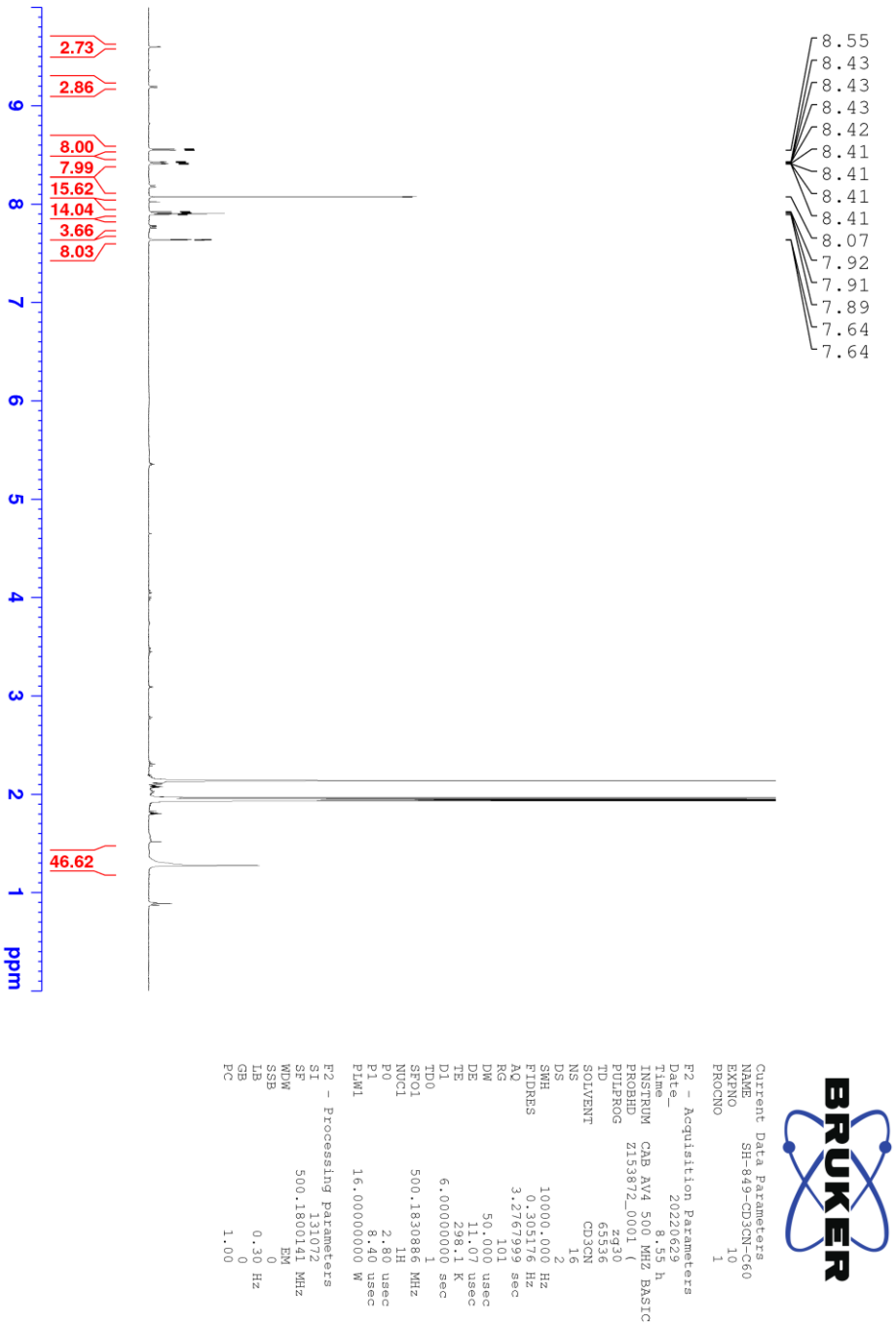

Figure 5.4.20 ^{1}H NMR spectrum of C_{60}@$Pd_2\mathbf{L}^{\mathbf{S}}_4$ (CD_3CN, 500 MHz, 298 K).

5.4.5.2 ^{1}H-^{1}H COSY NMR spectrum of $C_{60}@Pd_2L^S_4$

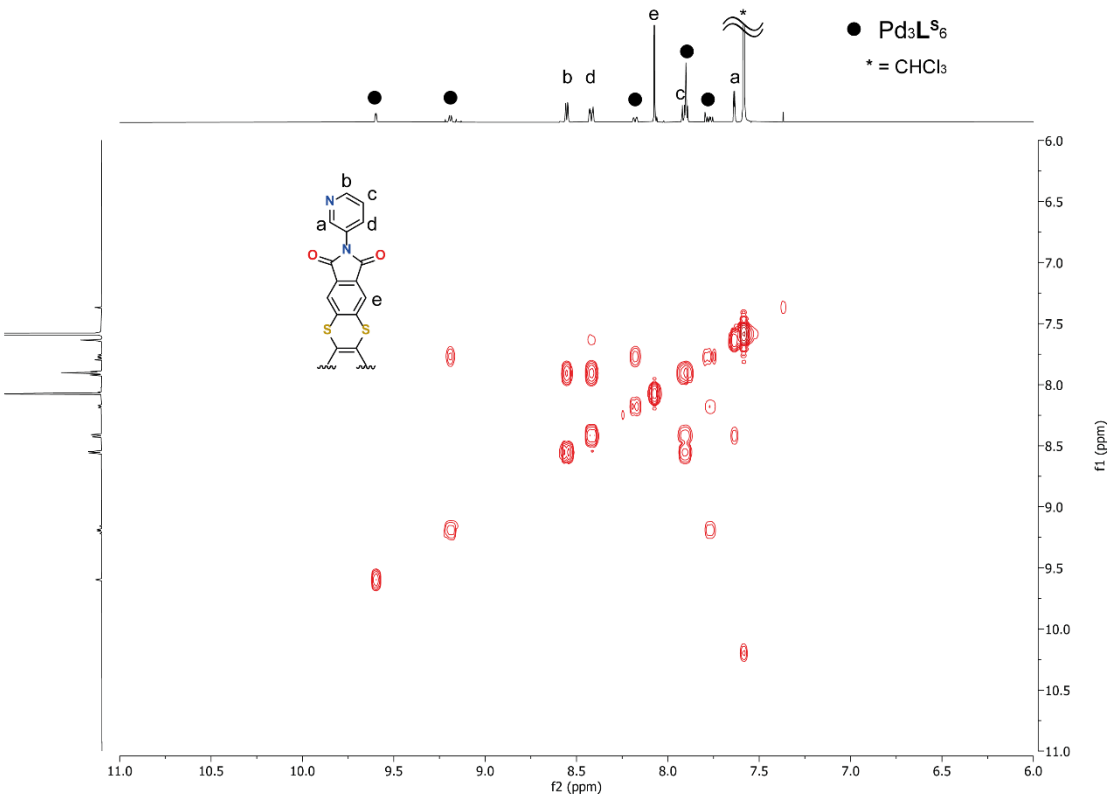

Figure 5.4.21 ^{1}H-^{1}H COSY NMR spectrum of $C_{60}@Pd_2\mathbf{L}^S_4$ (CD_3CN, 500 MHz, 298 K).

5.4.5.3 ^{13}C NMR spectrum of $C_{60}@Pd_2L^S_4$

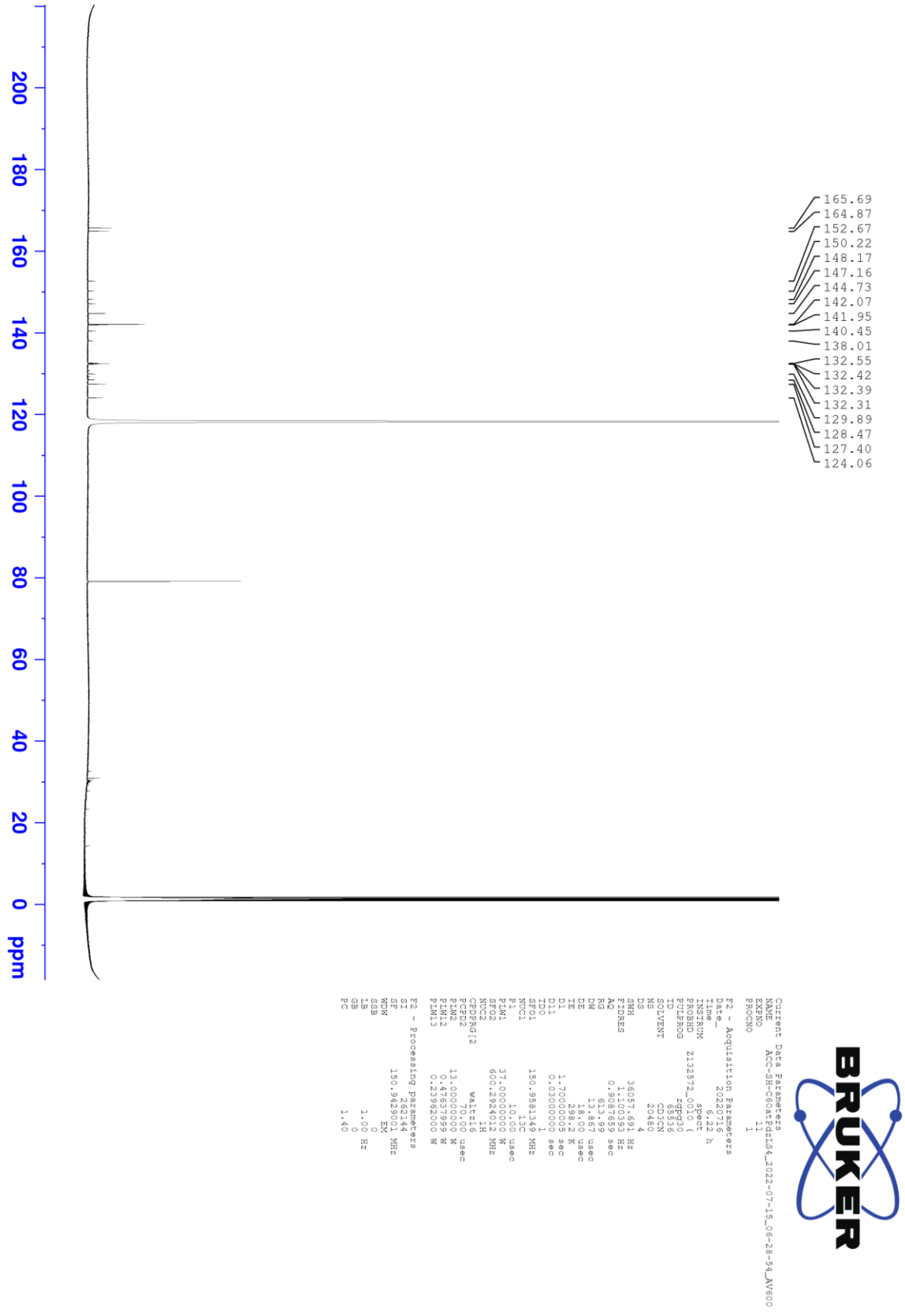

Figure 5.4.22 ^{13}C NMR spectrum of $C_{60}@Pd_2\mathbf{L}^{\mathbf{S}}_4$ (CD_3CN, 150 MHz, 298 K).

5.4.5.4 ^{1}H DOSY NMR spectrum of $C_{60}@Pd_2L^{S}_4$

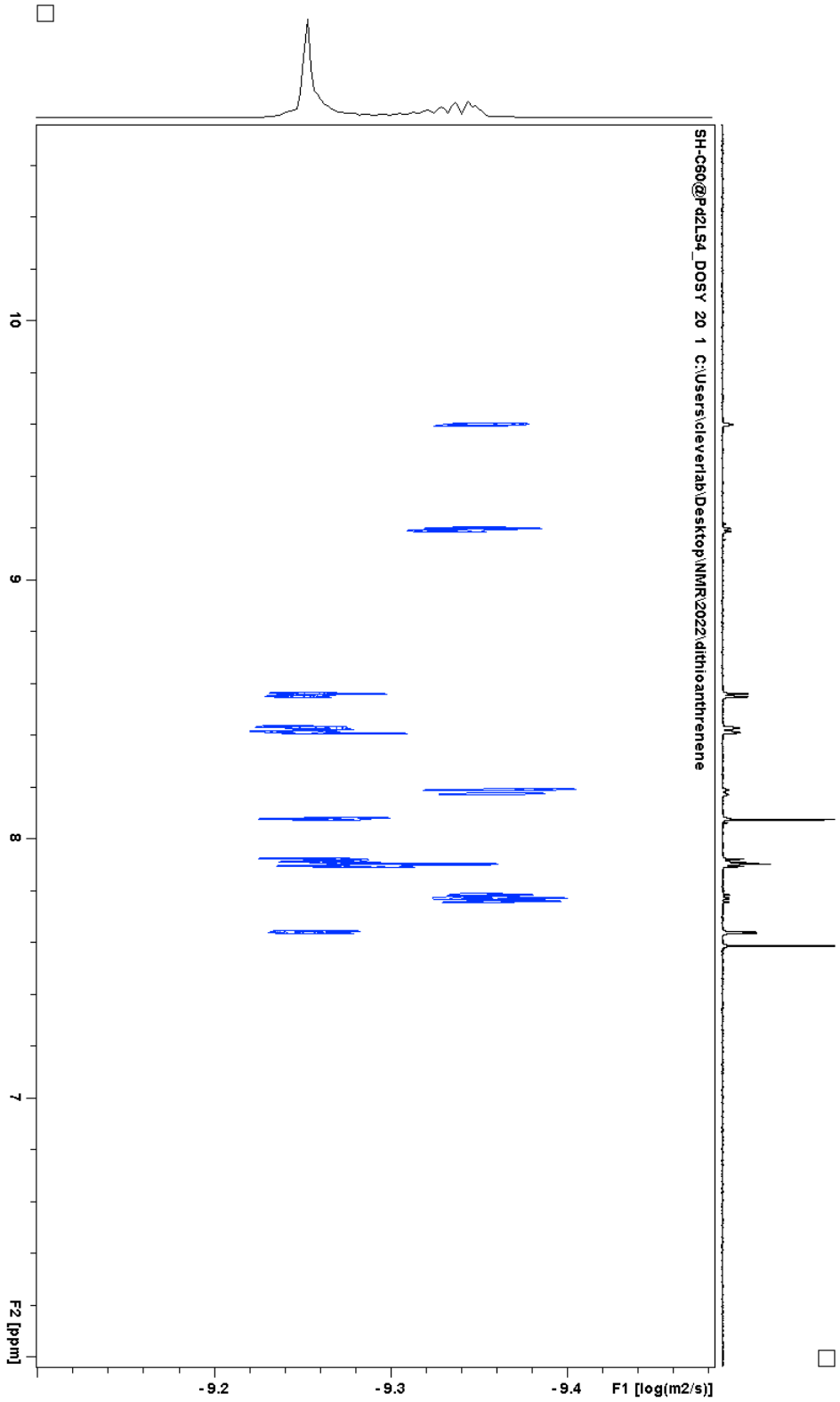

Figure 5.4.23 ^{1}H DOSY NMR spectrum of $C_{60}@Pd_2\mathbf{L}^{S}_4$ (CD_3CN, 500 MHz, 298 K).

5.4.5.5 ESI MS spectrum of $C_{60}@Pd_2L^S_4$

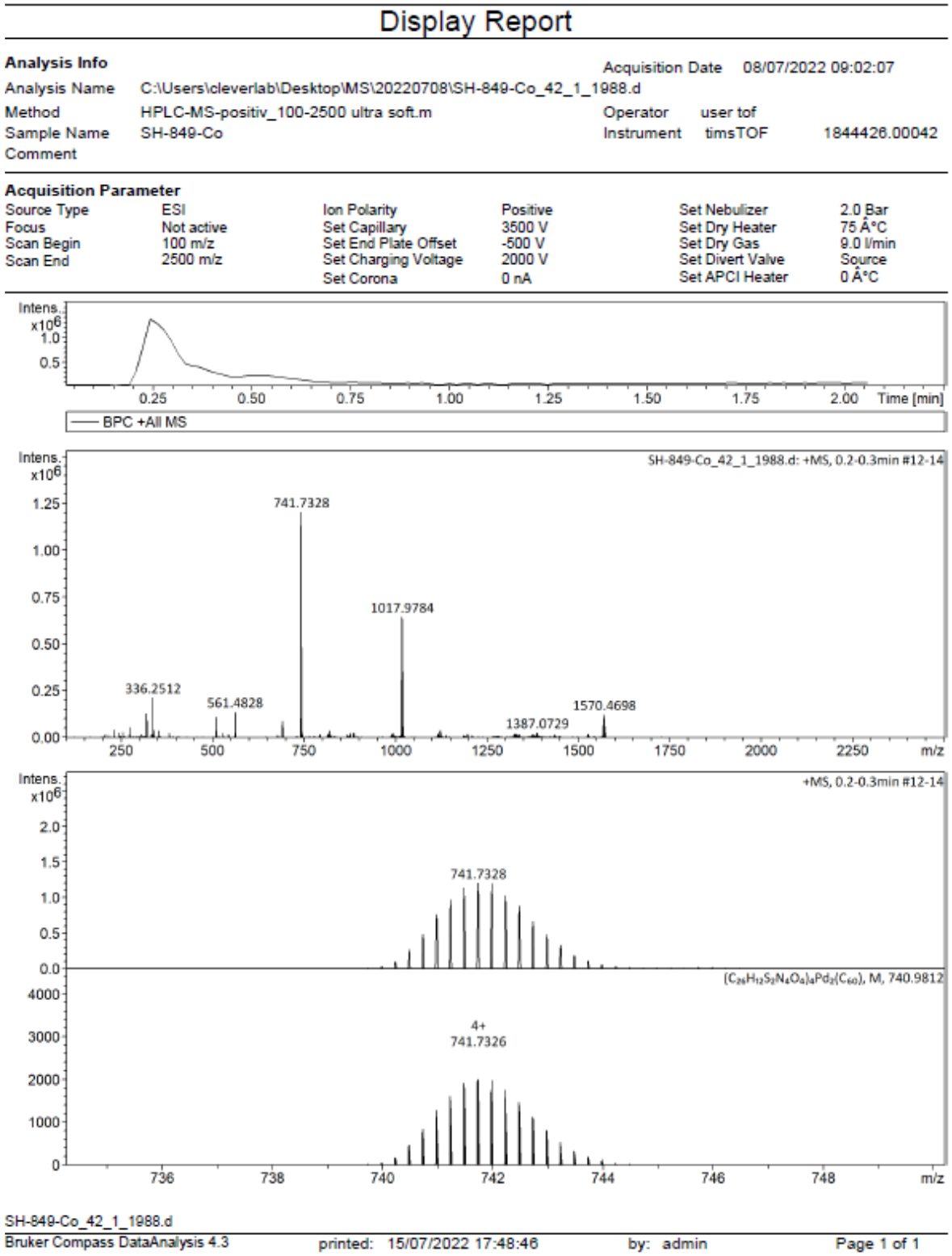

Figure 5.4.24 ESI-MS spectra (positive mode) of $C_{60}@Pd_2L^S_4$.

5.4.6 Synthesis of η^2-$C_{60}Pd(0)_2@Pd_2L^S_4$

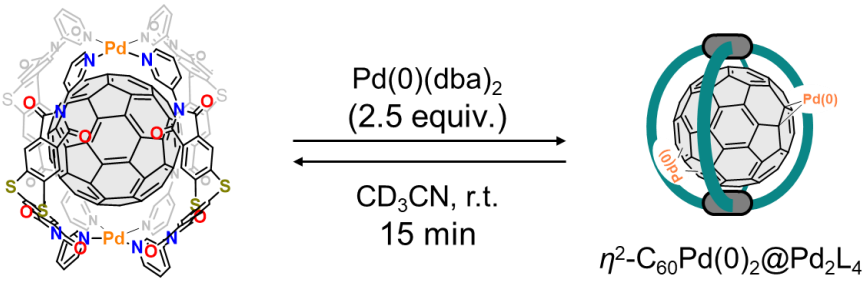

Figure 5.4.25 Synthesis of η^2-$C_{60}Pd(0)_2@Pd_2\mathbf{L}^S_4$.

To an acetonitrile solution containing $C_{60}@Pd_2\mathbf{L}^S_4$ and $Pd_3\mathbf{L}^S_6$ (2.8 mM of ligand concentration) in a NMR tube $Pd(0)(dba)_2$ (20 mM, 52.5 μL, 10.5 μmol) was added. The NMR tube was shaken after the addition and NMR experiments were carried out.

^{1}H NMR (CD_3CN, 500 MHz, 298 K): δ (ppm) **e** 8.53 (s, 8H), **b** 8.44 (d, J = 5.6 Hz, 8H), **d** (ddd, J = 8.3, 2.3, 1.2 Hz, 8H) **e** 7.86 (s, 8H), **c** 7.78 (m, 8H), **a** 7.53 (d, J = 2.3 Hz, 8H)

ESI MS (positive mode): found: 794.9331 and 853.7096; calculated for $[(C_{26}H_{12}N_4O_4S_2)_4Pd_2(C_{60})Pd_2]^{4+}$ and $[(C_{26}H_{12}N_4O_4S_2)_4Pd_2(C_{60})Pd_2(C_{17}H_{14}O)]^{4+}$ to be 794.9347 and 853.4610 respectively.

5.4.6.1 ^{1}H NMR spectra of η^2-$C_{60}Pd(0)_2@Pd_2L^S_4$

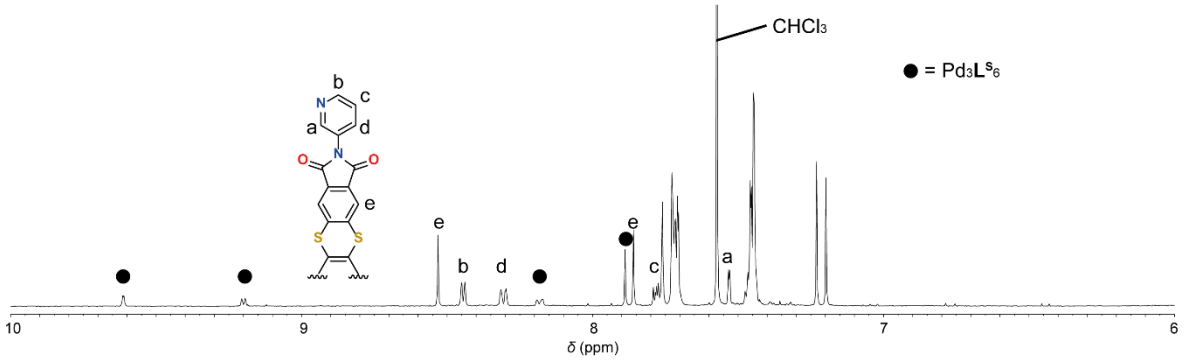

Figure 5.4.26 ^{1}H NMR spectrum of η^2-$C_{60}Pd(0)_2@Pd_2\mathbf{L}^S_4$ (CD_3CN, 500 MHz, 298 K).

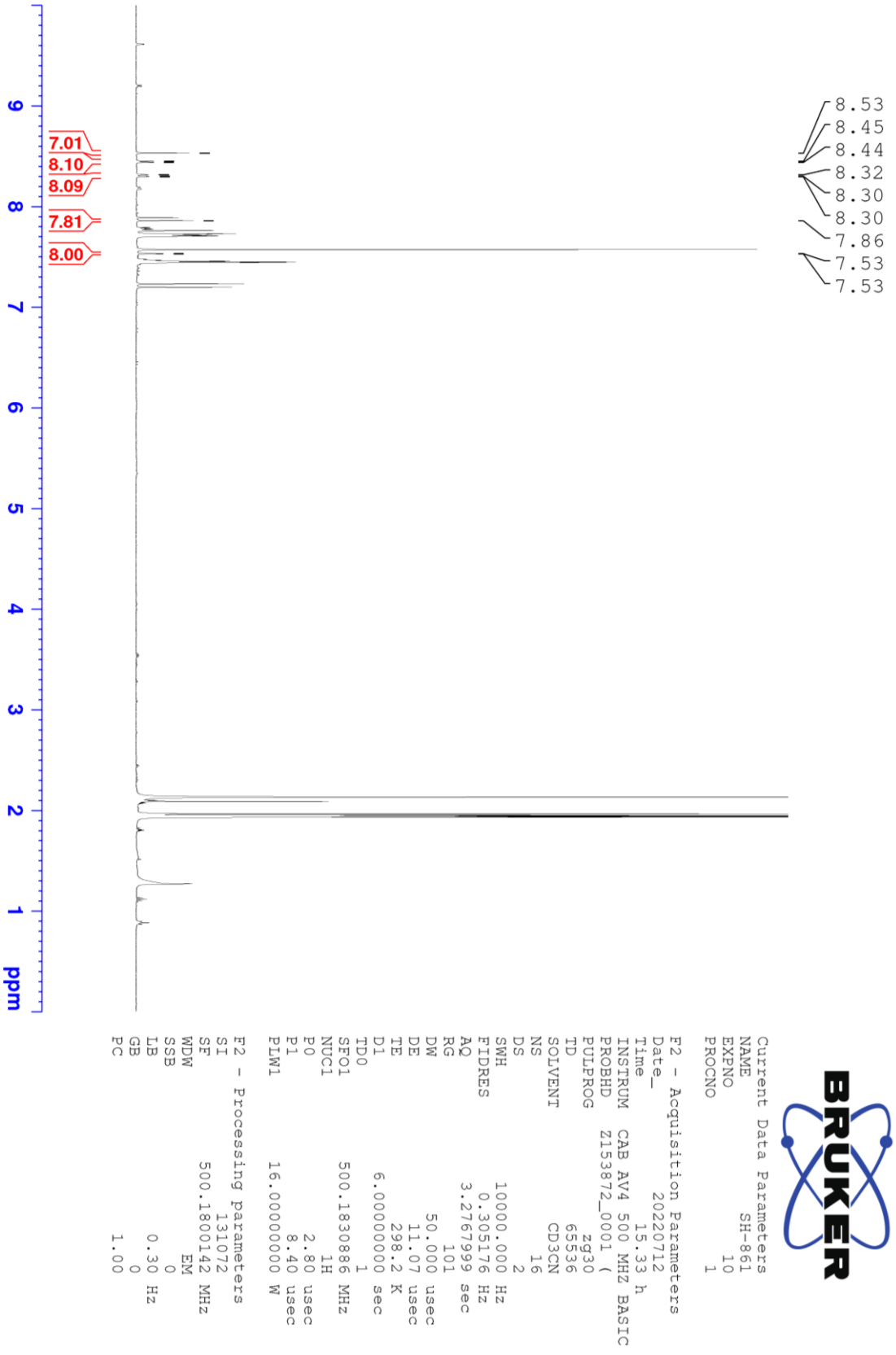

Figure 5.4.27 ^{1}H NMR spectrum of η^2-$C_{60}Pd(0)_2$@$Pd_2\mathbf{L}^{\mathbf{S}}_4$ (CD_3CN, 500 MHz, 298 K).

5.4.6.2 ^{1}H-^{1}H COSY NMR spectrum of η^2-$C_{60}Pd(0)_2$@$Pd_2L^S_4$

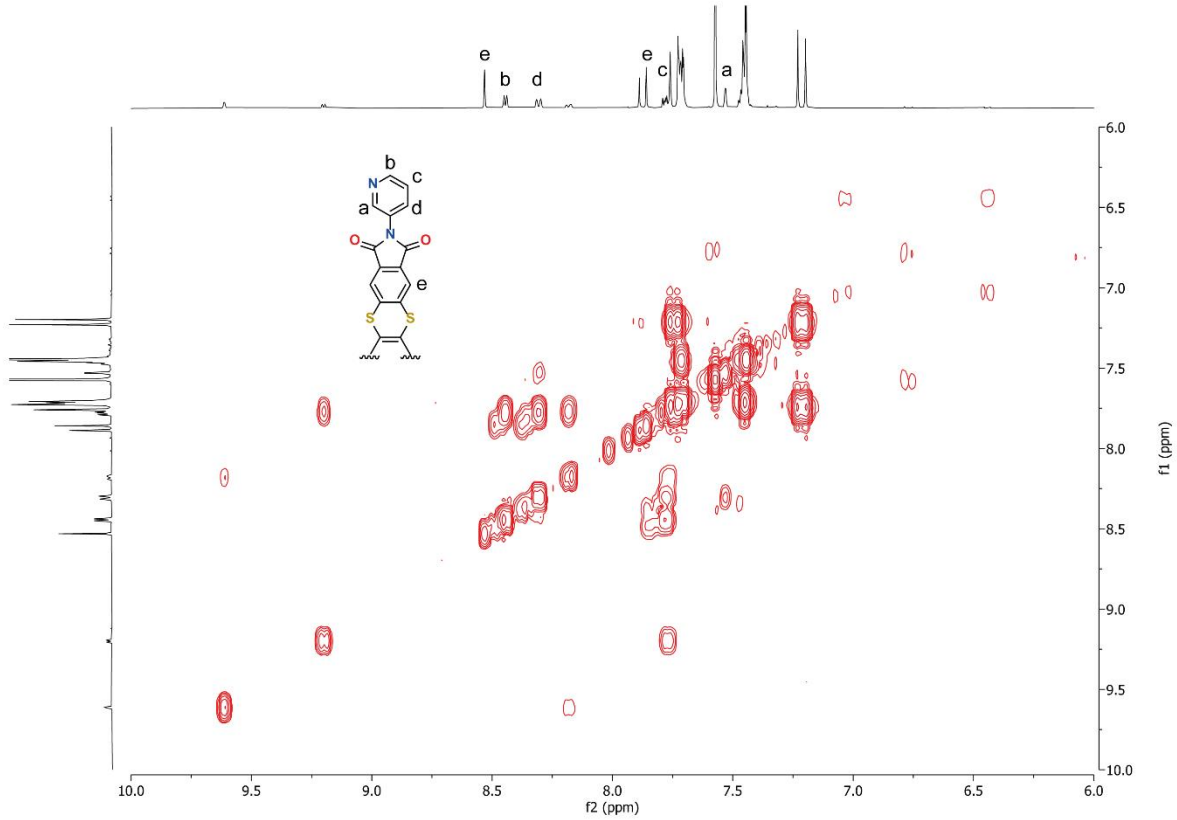

Figure 5.4.28 ^{1}H-^{1}H COSY NMR spectrum of η^2-$C_{60}Pd(0)_2$@$Pd_2\mathbf{L}^{\mathbf{S}}_4$ (CD_3CN, 500 MHz, 298 K).

5.4.6.3 ESI MS spectrum of η^2-$C_{60}Pd(0)_2$@$Pd_2L^S_4$

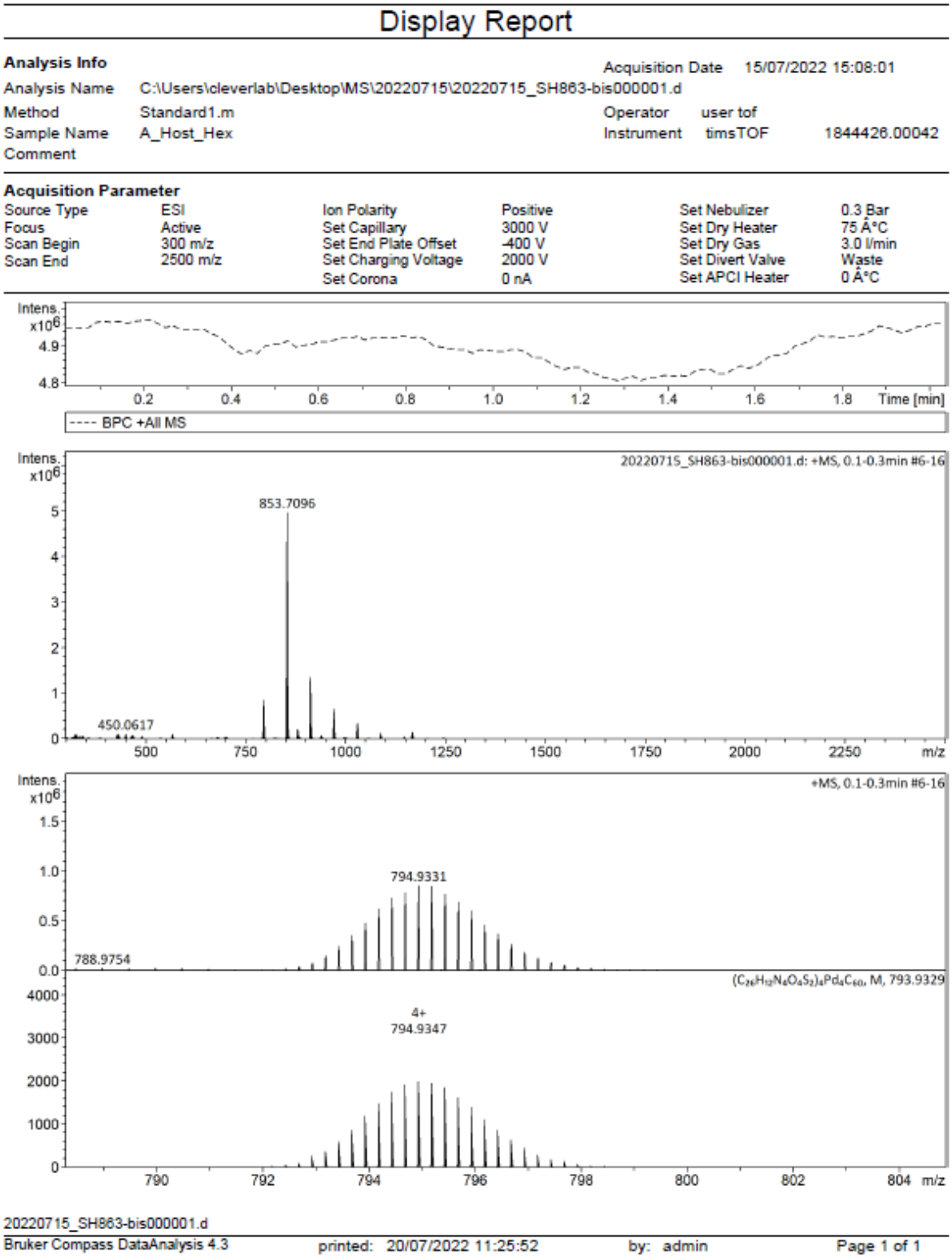

Figure 5.4.29 ESI MS spectrum of η^2-$C_{60}Pd(0)_2$@$Pd_2\mathbf{L}^S_4$ (positive mode).

5.4.7 DFT calculations

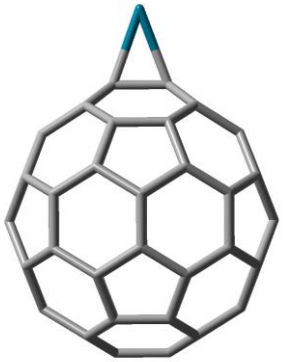

Figure 5.4.30 The optimized structure of η^2-$C_{60}Pd(0)$ at B3LYP/6-31G(d) for C atoms and B3LYP/Lanl2dz for Pd atom in the gas-phase in the gas-phase.

Standard orientation:

Center Number	Atomic Number	Atomic Type	Coordinates (Angstroms) X	Y	Z
1	6	0	-0.064678	0.001525	3.468348
2	6	0	-0.793706	1.175218	3.018623
3	6	0	-0.096061	2.309315	2.595848
4	6	0	1.357132	2.311333	2.598136
5	6	0	2.056327	1.182626	3.029316
6	6	0	1.330382	0.004689	3.476009
7	6	0	-1.968557	0.727463	2.294839
8	6	0	-0.544371	3.032164	1.421873
9	6	0	1.806551	3.038470	1.422297
10	6	0	3.232739	0.735182	2.304405
11	6	0	2.061647	-1.170743	3.031403
12	6	0	-0.788424	-1.176248	3.020688
13	6	0	3.664204	1.433078	1.174945
14	6	0	2.936486	2.607693	0.724923
15	6	0	4.114574	0.705726	-0.000164
16	6	0	2.936672	2.606389	-0.728969
17	6	0	-2.408819	1.428828	1.176187
18	6	0	0.630070	3.484347	0.694469
19	6	0	3.664506	1.430969	-1.176706
20	6	0	0.630204	3.483003	-0.700677
21	6	0	-1.671837	2.591300	0.723720
22	6	0	3.236023	-0.719284	2.305698
23	6	0	1.367556	-2.303360	2.602249
24	6	0	-2.946759	0.720947	-0.001114
25	6	0	-0.085634	-2.307935	2.599960
26	6	0	-1.965271	-0.735086	2.296116
27	6	0	1.820265	-3.030577	1.427721
28	6	0	-0.530672	-3.034914	1.427285
29	6	0	-2.402332	-1.440358	1.178593
30	6	0	1.806898	3.035863	-1.427400
31	6	0	3.670644	-1.417251	1.177493
32	6	0	-1.671657	2.589937	-0.728895
33	6	0	0.645826	-3.483091	0.700693
34	6	0	-1.660116	-2.600459	0.728345
35	6	0	-2.942537	-0.737023	0.000163
36	6	0	-2.402110	-1.442148	-1.176528
37	6	0	-2.408739	1.426293	-1.179248
38	6	0	-0.544111	3.029536	-1.427553
39	6	0	-0.095277	2.304544	-2.600131
40	6	0	-1.659855	-2.601722	-0.724246
41	6	0	-0.530361	-3.037433	-1.422144
42	6	0	-0.084829	-2.312490	-2.596001
43	6	0	0.645987	-3.484274	-0.694453
44	6	0	4.117714	-0.689973	0.001083
45	6	0	-0.792756	1.169810	-3.021102
46	6	0	2.948247	-2.595953	0.729577
47	6	0	2.948440	-2.597250	-0.724316
48	6	0	-1.967606	0.723121	-2.296453
49	6	0	1.357862	2.306667	-2.602083
50	6	0	2.057196	1.177164	-3.031049
51	6	0	-1.964314	-0.738981	-2.295138
52	6	0	-0.787457	-1.181658	-3.018962
53	6	0	1.820639	-3.033099	-1.421979
54	6	0	1.368302	-2.308029	-2.597956
55	6	0	-0.063640	-0.004686	-3.468527
56	6	0	3.670961	-1.419353	-1.174160
57	6	0	3.233420	0.731069	-2.305037
58	6	0	1.331452	-0.001538	-3.475894
59	6	0	3.236715	-0.723426	-2.303736
60	6	0	2.062520	-1.176140	-3.028930
61	46	0	-4.946827	0.000027	-0.000190

5.4.8 Decomposition of η^2-$C_{60}Pd(0)_2$

After preparing η^2-$C_{60}Pd(0)_2$@$Pd_2\mathbf{L}^{\mathbf{S}}_4$ or η^2-$C_{60}Pd(0)_2$@$Pd_2\mathbf{L}^{\mathbf{P}}_4$ in a J. Young NMR tube in the glovebox filled with N_2, the sample was left standing in the NMR spectrometer and ^{1}H NMR spectra were measured after a certain period of time to check decomposition of the encapsulated η^2-$C_{60}Pd(0)_2$ inside each cages.
η^2-$C_{60}Pd(0)_2$ and η^2-$C_{60}Pd(0)$ were found to have a short lifetime within the both cages in solution.

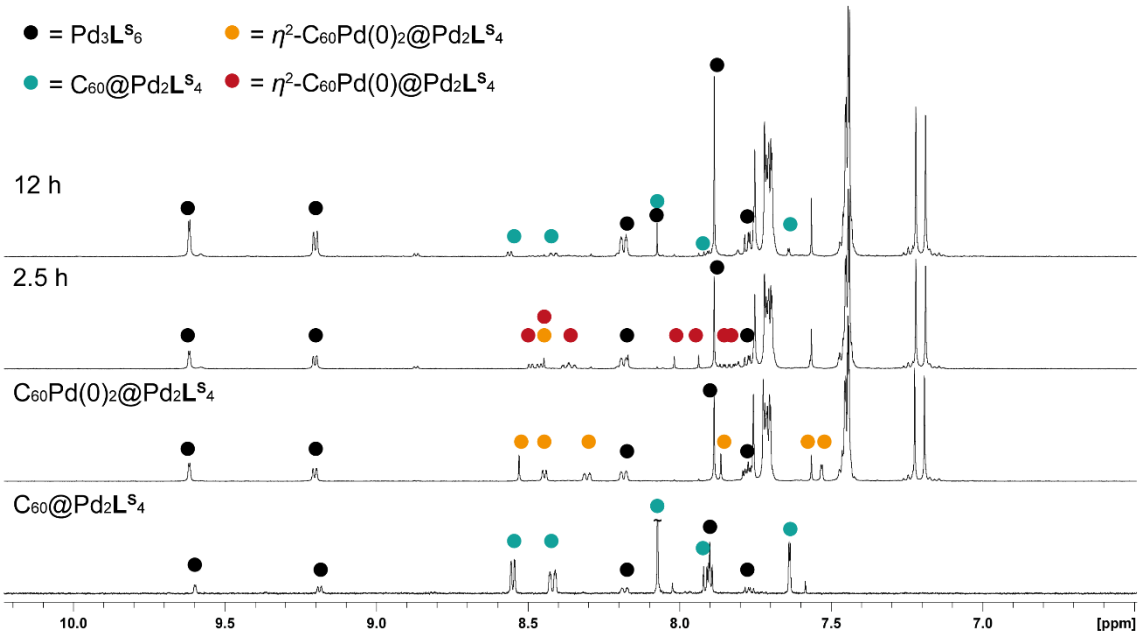

Figure 5.4.31 ^{1}H NMR spectra showing the decomposition of $C_{60}Pd(0)_2$@$Pd_2\mathbf{L}^{\mathbf{S}}_4$ (CD_3CN, 500 MHz, 298 K).

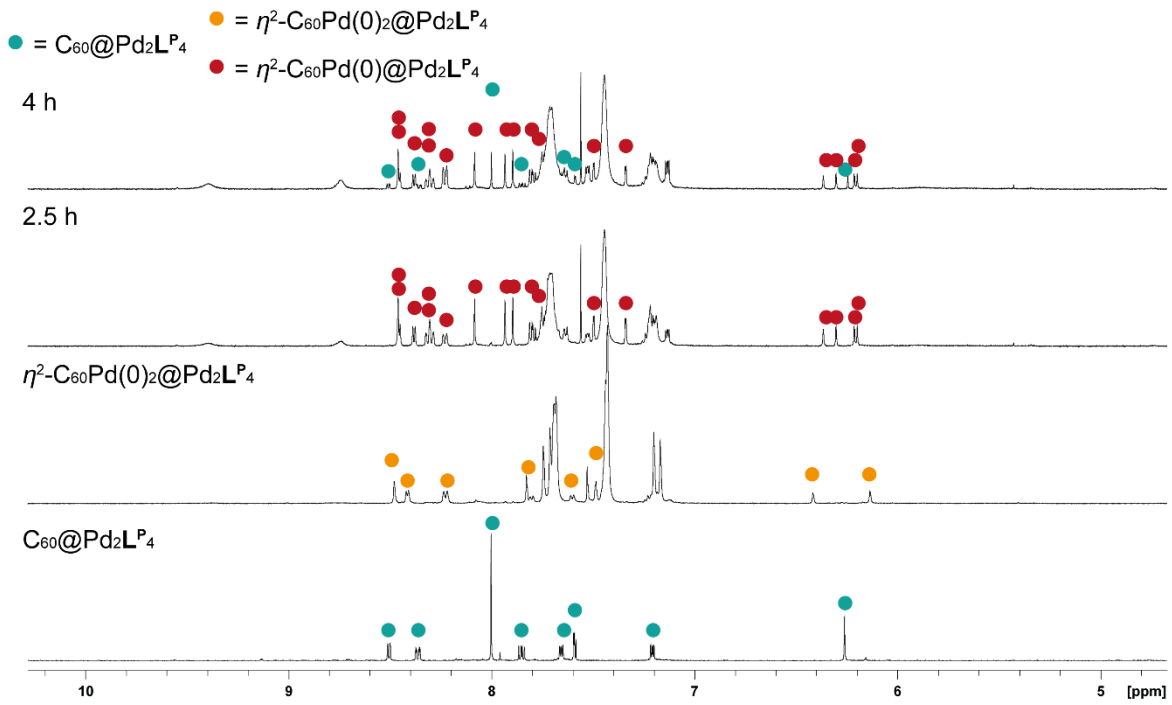

Figure 5.4.32 ^{1}H NMR spectra showing the decomposition of $C_{60}Pd(0)_2@Pd_2\mathbf{L}^{P}_4$ (CD_3CN, 500 MHz, 298 K).

5.5 References

[1] A. L. Balch, M. M. Olmstead, *Chem. Rev.* **1998**, *98*, 2123–2166.

[2] F. Giacalone, N. Martín, *Chem. Rev.* **2006**, *106*, 5136–5190.

[3] P. J. Fagan, J. C. Calabrese, B. Malone, *Science* **1991**, *252*, 1160–1161.

[4] V. V. Bashilov, P. V. Petrovskii, V. I. Sokolov, S. V. Lindeman, I. A. Guzey, Y. T. Struchkov, *Organometallics* **1993**, *12*, 991–992.

[5] H. Nagashima, A. Nakaoka, Y. Saito, M. Kato, T. Kawanishi, K. Itoh, *J. Chem. Soc. Chem. Commun.* **1992**, *0*, 377–379.

[6] A. L. Balch, D. A. Costa, K. Winkler, *J. Am. Chem. Soc.* **1998**, *120*, 9614–9620.

[7] J. M. Cowley, M.-Q. Liu, B. L. Ramakrishna, T. S. Peace, A. K. Wertsching, M. R. Pena, *Carbon* **1994**, *32*, 746–748.

[8] T. Tanase, K. Nakamae, Y. Kitagawa, T. Nakajima, *Chem. Eur. J.* **2021**, *27*, 12953–12958.

[9] M. Yoneyama, R. A. Johnson, L. J. Mathias, *J Polym. Sci. Part Polym. Chem.* **1995**, *33*, 1891–1899.

[10] A. Dullweber, **2021**, *Assembly and reactivity of anthracene based organic ligand for coordination cage formation*, TU Dortmund University.

[11] W. M. Bloch, J. J. Holstein, W. Hiller, G. H. Clever, *Angew. Chem. Int. Ed.* **2017**, *56*, 8285–8289.

[12] S. Saha, I. Regeni, G. H. Clever, *Coord. Chem. Rev.* **2018**, *374*, 1–14.

[13] D. Casarini, C. Coluccini, L. Lunazzi, A. Mazzanti, *J. Org. Chem.* 2006, *71*, 6248–6250.

[14] S. Hasegawa, S. L. Meichsner, J. J. Holstein, A. Baksi, M. Kasanmascheff, G. H. Clever, *J. Am. Chem. Soc.* **2021**, *143*, 9718–9723.

[15] Gaussian 16, Revision B.01, M. J. Frisch, G. W. Trucks, H. B. Schlegel, G. E. Scuseria, M. A. Robb, J. R. Cheeseman, G. Scalmani, V. Barone, G. A. Petersson, H. Nakatsuji, X. Li, M. Caricato, A. V. Marenich, J. Bloino, B. G. Janesko, R. Gomperts, B. Mennucci, H. P. Hratchian, J. V. Ortiz, A. F. Izmaylov, J. L. Sonnenberg, D. Williams-Young, F. Ding, F. Lipparini, F. Egidi, J. Goings, B. Peng, A. Petrone, T. Henderson, D. Ranasinghe, V. G. Zakrzewski, J. Gao, N. Rega, G. Zheng, W. Liang, M. Hada, M. Ehara, K. Toyota, R. Fukuda, J. Hasegawa, M. Ishida, T. Nakajima, Y. Honda, O. Kitao, H. Nakai, T. Vreven, K. Throssell, J. A. Montgomery, Jr., J. E. Peralta, F. Ogliaro, M. J. Bearpark, J. J. Heyd, E. N. Brothers, K. N. Kudin, V. N. Staroverov, T. A. Keith, R. Kobayashi, J. Normand, K. Raghavachari, A. P. Rendell, J. C. Burant, S. S. Iyengar, J. Tomasi, M. Cossi, J. M. Millam, M. Klene, C. Adamo, R. Cammi, J. W. Ochterski, R. L. Martin, K. Morokuma, O. Farkas, J. B. Foresman, and D. J. Fox, Gaussian, Inc., Wallingford CT, **2016**.

6 Guest Uptake and Observation of Topochemical-Like Reaction in between two Nano-Confined Fullerenes

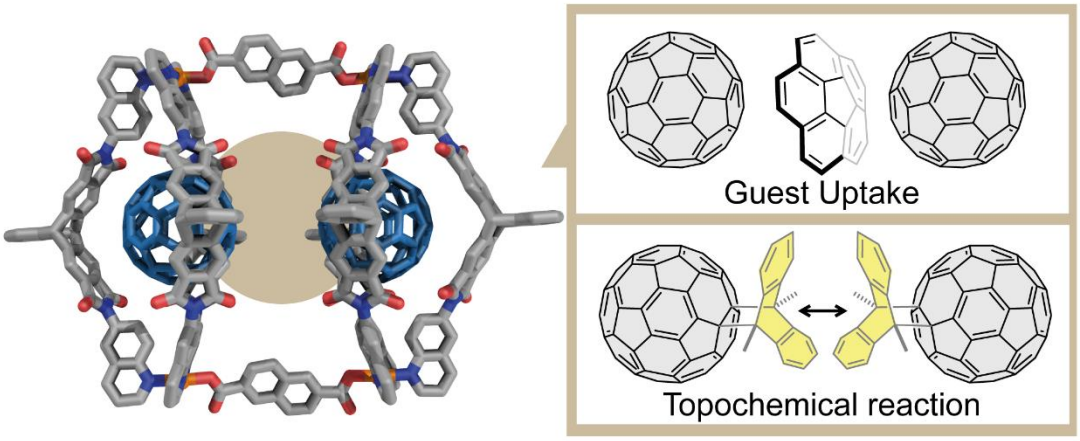

Chemistry in between multiple C_{60}s has been scarcely investigated due to the complexity to precisely align each C_{60} in appropriate positions. Herein, we report the synthesis of a pill-shaped coordination cage accommodating two fullerenes C_{60} in close proximity. The molecular design realizes a creation of a nanoscopic space surrounded by the curved π–conjugated surface of two C_{60}s. Inside the nanoscopic space, corannulene can be encapsulated with an association constant of a 10^3-order of magnitude resulting in the formation of a charge-transfer complex, while bulk C_{60} has a neglectable association constant with corannulene. Anthracene and its derivative reacts with one of the encapsulated C_{60}s inside the nanoscopic space yielding a coordination cage accommodating both C_{60} and its derivative in a quantitative manner. Exchange spectroscopy (EXSY) revealed an existence of repetitive Diels-Alder and retro Diels-Alder reactions, namely topochemical reaction, inside the coordination cage.

6.1 Introduction

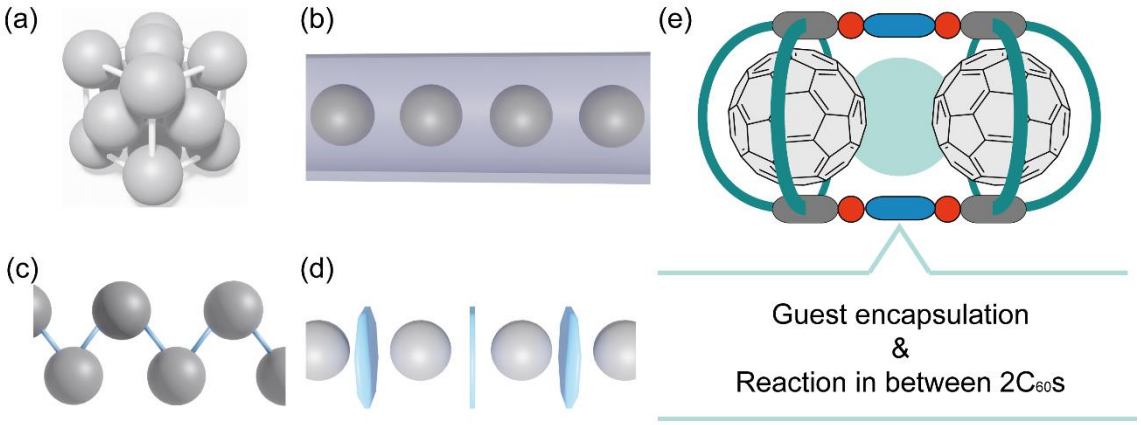

Figure 6.1.1 C_{60} array in (a) crystalline state (b) inside hosts (c) hydrogen bonded network and (d) supramolecular polymer (e) schematic illustration of a coordination cage possessing a nanoscopic space in between two C_{60}s

A countless number of sophisticatedly organized molecules work concertedly to maintain essential functions in livings.[1] What makes them function cooperatively is intermolecular interplay between the molecules. Molecular assemblies gathered by intermolecular forces, supramolecules, often show reversible and stimuli-responsive properties stemming from the dynamic and flexible bonds, which single molecules do not display.[2] Supramolecules show a different behavior from single molecules in a variety of fields such as molecular recognition, catalysis, and material development.[3–8] In this context, fullerene C_{60} is of great interest to be investigated since supramolecular arrays including C_{60} often result in change of the electronic properties of C_{60}.[9,10] Supramolecular polymerization of C_{60} derivatives is utilized in material development as well.[11] Furthermore, incorporation of guest molecules between the ordered C_{60}s can differ the electronic properties.[12] For instance, C_{60} is known to have a face-centered cubic (*fcc*) packing structure in the crystal structure.[13] Occupation by alkali metals in the gap between C_{60}s in the *fcc* packing results in formation of fullerides, salts of C_{60} radical anions and alkali metals, which show superconductivity at a relatively high temperature.[14] To investigate such molecular arrays of C_{60}, methods to control the arrangement are essential. To align multiple fullerenes, crystallization, encapsulation inside hosts, hydrogen bonds networks, and supramolecular polymerization are often utilized (**Figure 6.1.1a-d**).[15–17] In addition, incorporation of guests in between arranged pristine C_{60}s has been also investigated,

albeit most of the cases in the solid-state.[18] On the other hand, to align pristine C_{60}s in solution is still challenging because of neglectable interactions between spherical C_{60}s, Therefore, chemistry in between C_{60}s in solution has not been investigated well, rather never investigated to the best of our knowledge. One of the solutions to arrange pristine C_{60}s in an ordered manner in solution is encapsulation of C_{60}s inside hosts.[19–23] A few examples of hosts which can encapsulate multiple C_{60}s within their cavities have been reported, however, deeper investigations into their chemistry, e.g. host-guest chemistry, in between the encapsulated C_{60}s are still missing. Thus, construction of such molecular systems and investigation of the chemistry in between multiple C_{60}s will help build a fundamental basic knowledge for further development of futuristic materials.

Herein, we report a synthesis of a pill-shaped coordination cage dimer encapsulating two C_{60}s within each cavity. Thanks to the nanoscopic space surrounded by two C_{60}s, host-guest chemistry in between two C_{60}s could be investigated. We have employed a convergent method to construct such a pill-shaped coordination cage having an appropriately sized nano-space for accommodation of single molecule in between two C_{60}s (**Figure 6.1.1e**).

6.2 Results and discussion

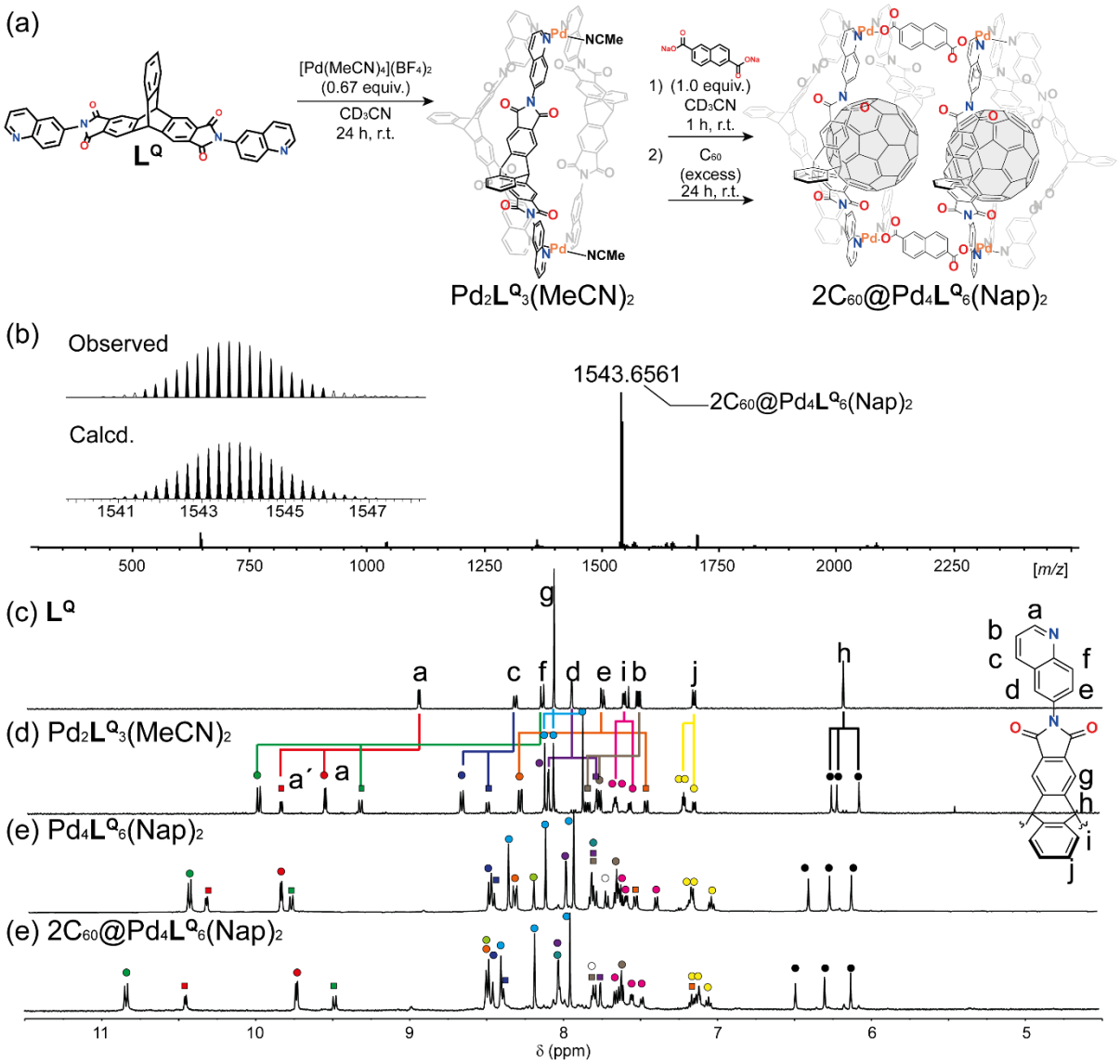

Figure 6.2.1 Synthesis of $Pd_2\mathbf{L}^{Q}_3(MeCN)_2$ and $(C_{60})_2@Pd_4\mathbf{L}^{Q}_6(Nap)_2$ (b) ESI-MS spectrum (positive) of $(C_{60})_2@Pd_4\mathbf{L}^{Q}_6(Nap)_2$ (c) ^{1}H NMR spectrum (CD_3CN, 500 MHz, 298 K) of $\mathbf{L}^{Q}$ (d) $Pd_2\mathbf{L}^{Q}_3(MeCN)_2$ (0.70 mM) (e) $Pd_4\mathbf{L}^{Q}_6(Nap)_2$ (0.34 mM) and (f) $(C_{60})_2@Pd_4\mathbf{L}^{Q}_6(Nap)_2$ (0.34 mM)

The triptycene-based ligand $\mathbf{L}^{Q}$ was synthesized in a moderate yield following the literature (**Figure 6.2.1a,c** and **Figure 6.4.1**).[23–25] Triptycene is known to have attractive interactions with C_{60} through convex-concave principle.[26] We have previously reported a synthesis of a bowl-shaped coordination cage via coordination sphere engineering.[23,27,28] Following the literature, $Pd_2\mathbf{L}^{Q}_3(MeCN)_2$ was synthesized via self-assembly by mixing $\mathbf{L}^{Q}$ and 0.67 equivalent of $[Pd(II)(MeCN)_4](BF_4)_2$ in CD_3CN

at ambient temperature (**Figure 6.2.1b**).[23] In the ^{1}H NMR spectrum of $Pd_2\mathbf{L}^{Q}_3(MeCN)_2$, most of the protons of the quinoline donor-sites showed downfield shifts upon coordination, which is a ubiquitous phenomenon found in coordination cages due to electron density transfer from ligands to metal centers.[23] In addition, two and three sets of signals were observed in 2:1 and 1:1:1 ratio for the quinoline donor-sites and the backbone of the ligand respectively, suggesting formation of the bowl-shaped structure (**Figure 6.2.1d**). Coordination of the fourth ligand is prohibited owing to the steric bulk around the Pd(II) centers. Recently, we have reported that addition of a terephtalate-linker yields a pill-shaped dimer by bridging two bowl-shaped coordination cages.[23] However, no host-guest capability of the pill-shaped coordination cage was found, most probably due to the too small space between the encapsulated C_{60}s. Therefore, 2,6-naphthalenedicarboxylate (Nap) was employed as a linker to expand the distance in between two C_{60}s. The pill-shaped coordination cage, $Pd_4\mathbf{L}^{Q}_6(Nap)_2$, was obtained after dropwise addition of an aqueous solution of Nap as a sodium salt into an acetonitrile solution of $Pd_2\mathbf{L}^{Q}_3(MeCN)_2$ while stirring (**Figure 6.2.1e**). Encapsulation of C_{60} was conducted by dispersing excess amount of C_{60}-solid into the acetonitrile solution of $Pd_4\mathbf{L}^{Q}_6(Nap)_2$ at room temperature for 24 h. The colorless solution turned purple which is the characteristic color of C_{60}, although C_{60} is insoluble in acetonitrile. Formation of $(C_{60})_2@Pd_4\mathbf{L}^{Q}_6(Nap)_2$ was confirmed by electrospray ionization mass spectrometry (ESI-MS) and NMR analysis (**Figure 6.2.1b** and **f**). The hydrodynamic radius of $(C_{60})_2@Pd_4\mathbf{L}^{Q}_6(Nap)_2$ was determined to be 17.0 Å by diffusion ordered spectroscopy (DOSY) which is larger than $C_{60}@Pd_2\mathbf{L}^{Q}_3(MeCN)_2$ (**Figure 6.4.28** and **Figure 6.4.68**).

The structure of $(C_{60})_2@Pd_4\mathbf{L}^{Q}_6(Nap)_2$ was unambiguously revealed by single crystal X-ray structure analysis using synchrotron radiation (**Figure 6.2.2a**-**b**).[29] Block-like single crystals suitable for crystallographic analysis was obtained by slow diffusion of benzene into an acetonitrile solution of $(C_{60})_2@Pd_4\mathbf{L}^{Q}_6(Nap)_2$. Two independent halves of the dimer were found in the unit cell (**Figure 6.4.45** and **Figure 6.4.46**). Only one of the dimers is showcased in **Figure 6.2.2**. The distance between the centers of mass of the encapsulated C_{60}s inside each dimer was determined to be 13.0 Å and 12.8 Å respectively. Subtraction of the diameter of C_{60} of 7 Å gives 6 Å and 5.8 Å of the distance of the surface of each confined C_{60}s, which should be large enough to accommodate a single guest molecule via π-π interactions(**Figure 6.2.2c**). The variation of the distances implies the flexibility of the molecular system even in the

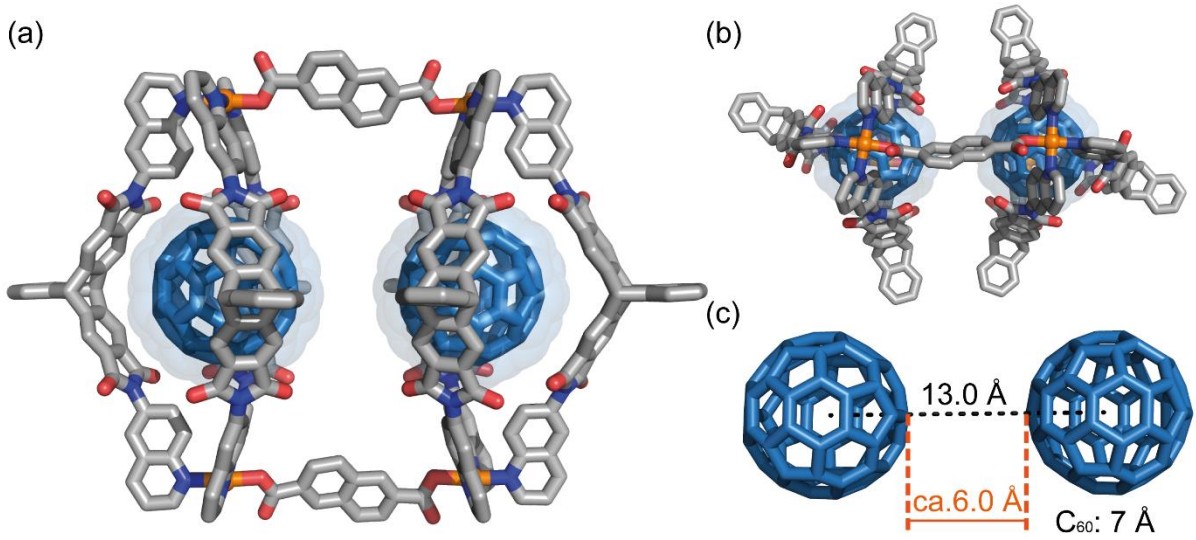

Figure 6.2.2. Single crystal X-ray structure of one of $(C_{60})_2$@Pd_4**1**$_6$$(Nap)_2$ co-exist (a) front view (b) top view (c) distance between the centers of mass of confined C_{60}s given the diameter of C_{60} is 7 Å. Hydrogen atoms, solvent molecules, and counter anions were omitted for clarity. Color legends: C: grey N: blue O: red Pd: orange C_{60}: sky blue

solid-state. Next, host-guest chemistry inside the nanoscopic space surrounded by two C_{60}s was investigated (**Figure 6.2.3a**).

Corannulene, known as a substructure of C_{60}, was employed as a suitable guest molecule. Thanks to the warped structure, corannulene has a moderately good solubility in acetonitrile, which is an important criterion for fine analyses. Besides, encapsulation of corannulene can be a good experiment to see an effect from the well alignment of C_{60}s in the cage because corannulene is known to have a neglectable association constant with pristine C_{60} in solution.[30] To determine a binding constant of corannulene inside the nano-space, a titration experiment was carried out using ^{1}H NMR and UV-Vis absorption spectroscopy. In addition to the change in the ^{1}H NMR chemical shifts, the emergence of an absorption band around 450 nm was also observed over the course of the titration, which is indicating of a formation of a charge-transfer complex between the encapsulated C_{60}s and the bound corannulene (**Figure 6.2.3c**).[30] Among the protons of the quinoline coordination-sites, protons *e*/*e'* which are supposed to be pointing towards the encapsulated C_{60} gave the large chemical shifts during the titration experiment, which indicates electronic perturbation on the confined C_{60}s by the charge-transfer complex formation (**Figure 6.2.3d**). The binding constant, K_a, was determined to be 4.4 ± 0.1× 10^3 M^{-1} by fitting the data using BindFit

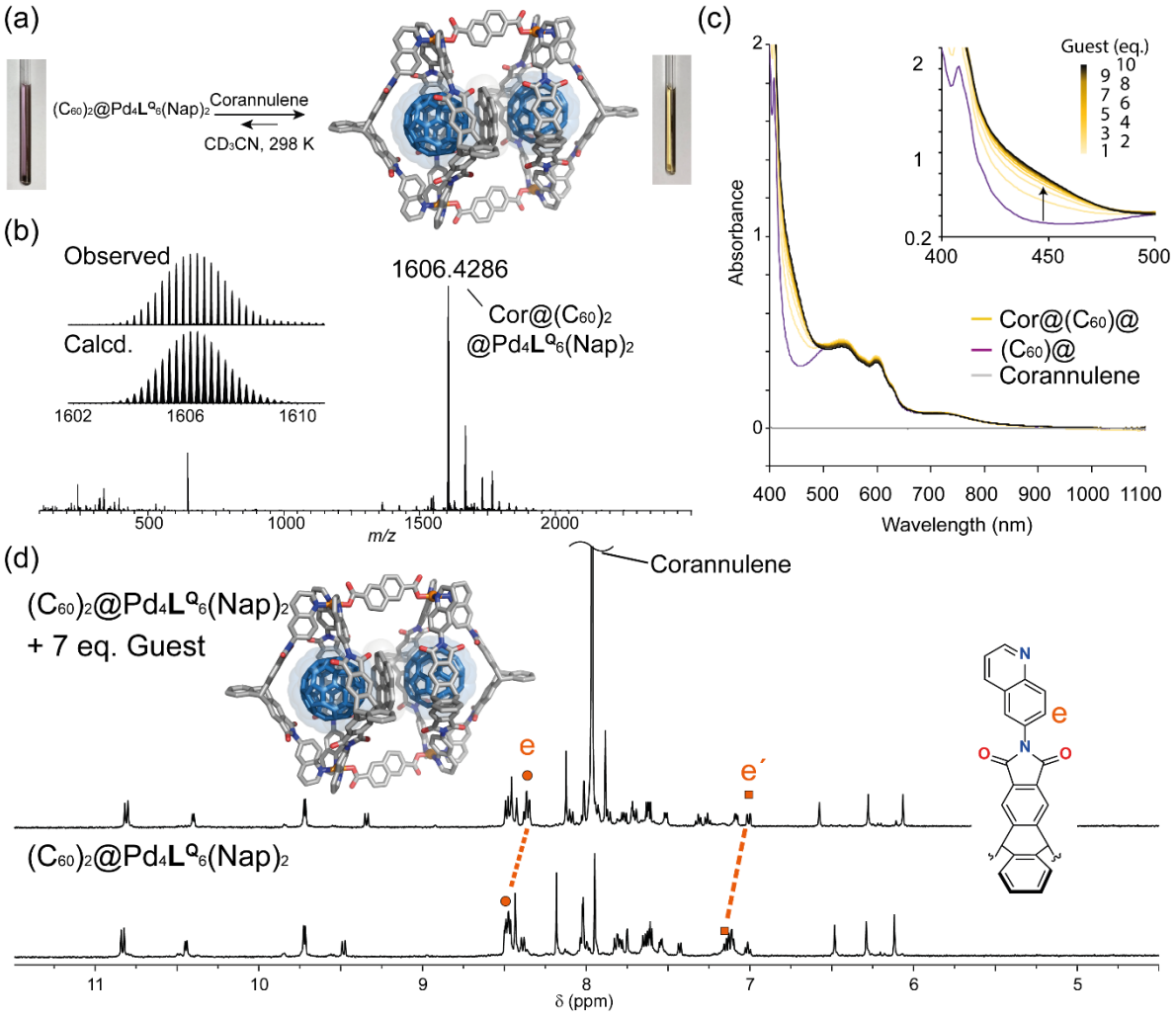

Figure 6.2.3 (a) Encapsulation of Corannulene into $(C_{60})_2$@$Pd_4\mathbf{L}^{Q}_6(Nap)_2$ (b) ESI-MS spectrum (positive) of 1:1 molecular complex of corannulene and $(C_{60})_2$@$Pd_4\mathbf{L}^{Q}_6(Nap)_2$ (c) UV-vis absorption spectrum of $(C_{60})_2$@$Pd_4\mathbf{L}^{Q}_6(Nap)_2$ (acetonitrile, 298 K, 0.34 mM) over corannulene titration (d) ^{1}H NMR spectrum (500 MHz, CD_3CN, 298 K) of $(C_{60})_2$@$Pd_4\mathbf{L}^{Q}_6(Nap)_2$ with and without corannulene

(**Figure 6.4.53 & Table 6.4.2**).[31] Furthermore, the formation of the 1:1 complex was also confirmed by ESI-MS (**Figure 6.2.3b**) The obtained K_a is comparable to other hosts showing binding capability toward corannulene.[32,33] Furthermore, considering that both naked C_{60} and the confined C_{60} inside $Pd_2\mathbf{L}^{Q}_3(MeCN)_2$ showed a neglectable association behavior with corannulene, the association constant was dramatically improved by having another C_{60} in close proximity. This observation suggests that the curved surface of C_{60} can be a building block to create a host-molecule despite of the scarce host-guest capability itself alone.

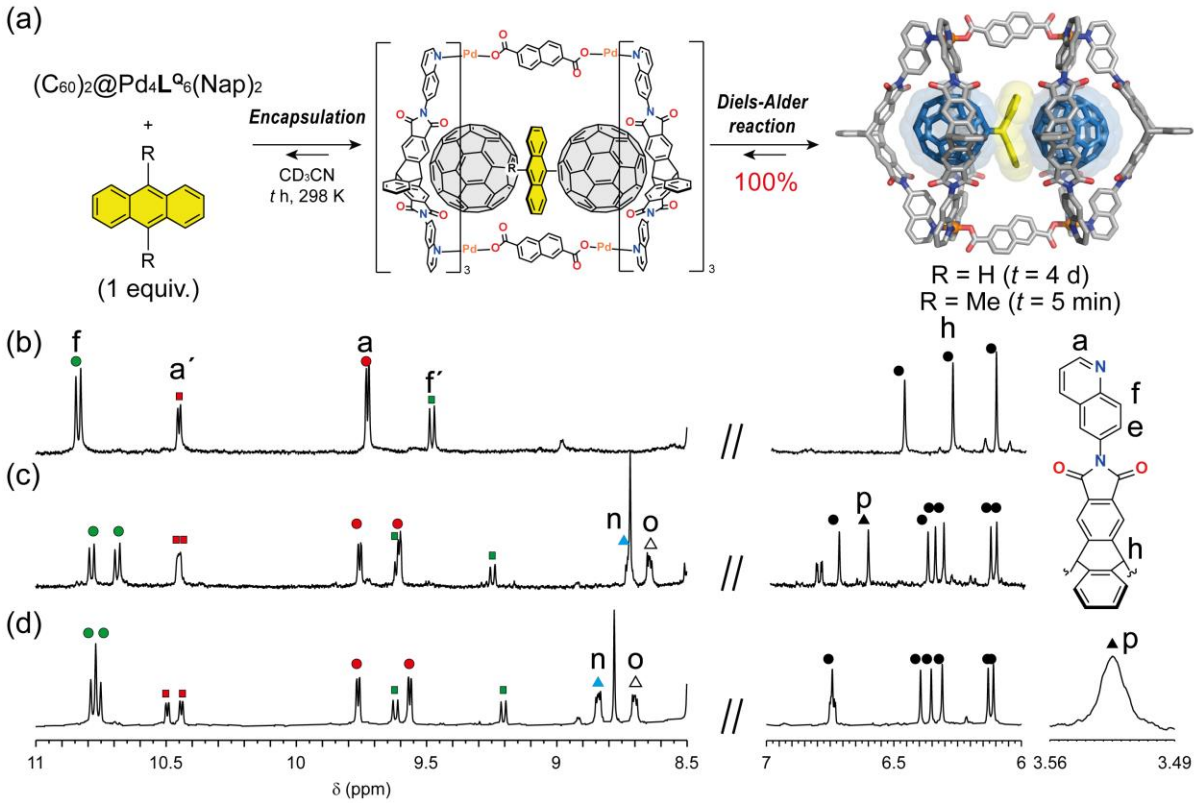

Figure 6.2.4 (a) Encapsulation and reaction of anthracene inside $(C_{60})_2$@Pd$_4$**L**$^{Q}_6$(Nap)$_2$ (b) ^{1}H NMR spectrum (500 MHz, CD_3CN, 298 K) of $(C_{60})_2$@Pd$_4$**L**$^{Q}_6$(Nap)$_2$ (0.34 mM) (c) C_{60}ant•C_{60}@Pd$_4$**L**$^{Q}_6$(Nap)$_2$ (0.33 mM) and (d) C_{60}DMA•C_{60}@Pd$_4$**L**$^{Q}_6$(Nap)$_2$ (0.33 mM)

We further explored the host-guest chemistry inside the nanoscopic space using anthracene (**Figure 6.2.4a**) In the course of the experiment, we found that anthracene shows an intriguing encapsulation behavior. Over the titration experiment of anthracene into an acetonitrile solution of $(C_{60})_2$@Pd$_4$**1**$_6$(Nap)$_2$, two sets of signals newly arose. We assumed that the entrapped anthracene reacted with one of the encapsulated C_{60}s and gave a Diels-Alder adduct inside the cage considering the symmetry. To prove the hypothesis, 1.0 equivalent of anthracene was added into acetonitrile solution of $(C_{60})_2$@Pd$_4$**1**$_6$(Nap)$_2$ and the mixture was let stand in the dark at ambient temperature for 4 days. A clean conversion from $(C_{60})_2$@Pd$_4$**1**$_6$(Nap)$_2$ to the new species was observed (**Figure 6.2.4b-c** and **Figure 6.4.31**). In the ^{1}H NMR spectrum, two sets of signals appeared stemming from the heteromultimeric encapsulation. ESI-MS analysis revealed the formation of C_{60}ant•C_{60}@Pd$_4$**1**$_6$(Nap)$_2$ as we assumed (**Figure 6.4.36**). Note that this is the first example of the rational synthesis of host-guest complex encapsulating two different fullerenes to the best of our

knowledge. Diels-Alder reaction in between two C_{60}s has been studied theoretically by Podewitz et al., however, most of molecular systems could not provide them with an appropriate model to explore experimentally.[34] In general, Diels-Alder reaction of C_{60} and anthracene yields an equilibrium together with multi-adducts formation. Thus, quantitative formation of C_{60}ant is challenging. However, this was not the case inside $(C_{60})_2$@Pd_4**1**$_6(Nap)_2$. According to the theoretical study, it is indicated that an activation Gibbs free energy ($\Delta G^{\ddagger}$) barrier for a Diels-Alder reaction with anthracene should be lowered thanks to the neighboring C_{60}.[34] In addition, the resulting C_{60}ant is indicated to be stabilized thanks to the neighboring C_{60} probably via convex-concave interactions. Thanks to those effects, the possibility of a topochemical reaction is implied.[34] Stimulated by that theoretical study, we investigated the topochemical-like reaction within the soluble dimer cage. In fact, a transfer of anthracene from C_{60}ant to neighboring C_{60} has been reported using a variety of anthracene derivatives, e.g., 9,10-dimethylanthracene (DMA) in the solid-state.[35] To deeply investigate the reaction, we have performed kinetic studies with our system in solution (**Figure 6.4.57** and **Figure 6.4.58**). As a result, the activation Gibbs free energy barrier $\Delta G^{\ddagger}$ was determined to be 79 kJ/mol at 298 K which is lower than the one for the Diels-Alder reaction between anthracene and naked C_{60} in a toluene solution by 14 kJ/mol (**Figure 6.4.58**).[36] Taking it into account that kinetics in Diels-Alder reactions are, in general, independent from solvents, the lower $\Delta G^{\ddagger}$ should be attributed to the effect of the neighboring C_{60}. The neighboring C_{60} should stabilize the transition-state via π-π interactions between the slightly bent anthracene. In fact, C_{60} encapsulated inside Pd_2**L**$^{Q}_3(MeCN)_2$ did not undergo Diels-Alder reaction with anthracene to yield C_{60}ant@Pd_2**L**$^{Q}_3(MeCN)_2$ even after seven days at room temperature. Next, we tackled to elucidate if a topochemical reaction takes place within the coordination cage. For this purpose, more reactive 9,10-dimethylanthracene (DMA) was employed as a diene. DMA is notorious for a fast retro-Diels-Alder reaction and a bis-adduct formation even at room temperature.[37,38] Mixing a stoichiometric amount of DMA and $(C_{60})_2$@Pd_4**L**$^{Q}_6(Nap)_2$ immediately yielded C_{60}DMA•C_{60}@Pd_4**L**$^{Q}_6(Nap)_2$ in a quantitative manner despite the possibility of falling apart again by a retro Diels-Alder reaction (**Figure 6.2.4d** and **Figure 6.4.37**).

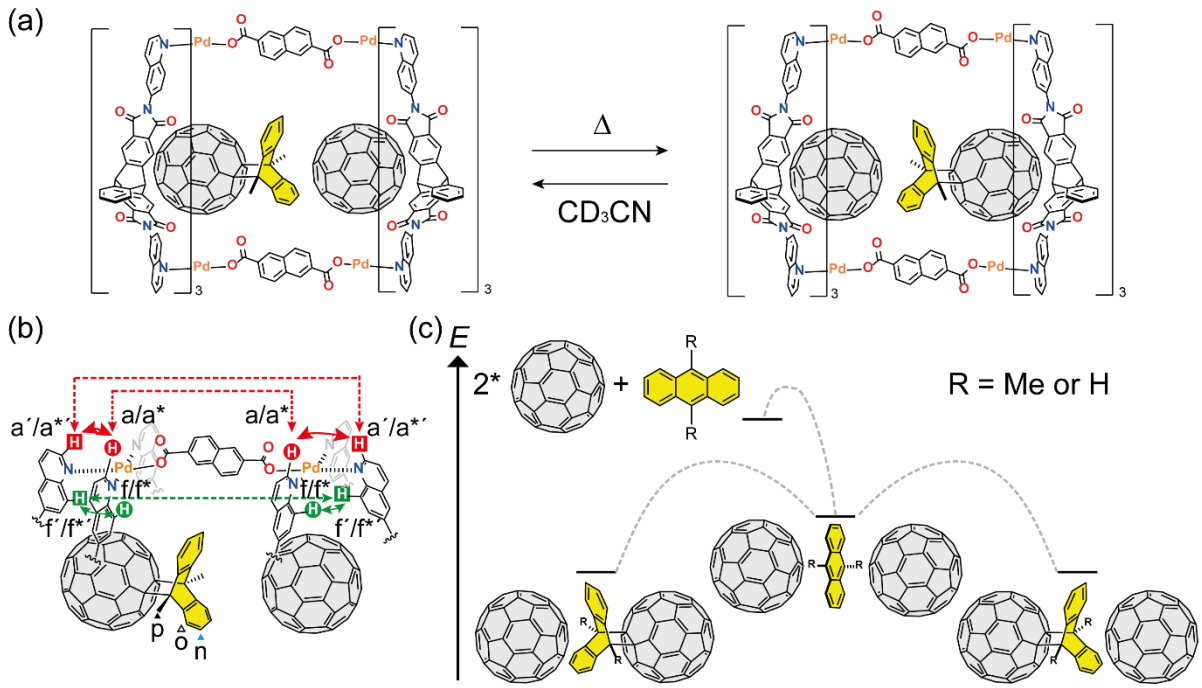

Figure 6.2.5 (a) Schematic illustration of the topochemical reaction within the cage (b) EXSY (dotted line) and NOESY (solid line) correlations (c) An energy diagram explaining encapsulation of anthracene/DMA between the encapsulated C_{60}s and the following topochemical reaction

To elucidate the dynamic behavior of the C_{60}-DMA adduct within the cage, EXSY experiments were performed at various mixing times. If there is a guest-exchange related to the expected topochemical reaction within the cage, pairs of protons of each cage halve should show EXSY correlation (**Figure 6.2.5a**). The signal pairs (a-a*), (a'-a*'), and (f'-f*') are suitable pairs owing to less overlapping with other signals. When the EXSY spectrum was measured at 57.8 °C with 1 s mixing time by Prof. Hiller, all the three pairs showed EXSY correlations (**Figure 6.2.5b** and **Figure 6.4.77**). Since the proton a/a* does not have EXSY correlation with one of a´/a*´, the possibility of ligand exchange can be excluded. Note that, the retro-Diels-Alder reaction was observed in the case of C_{60}@Pd_2**L**$^{Q}_3$$(MeCN)_2$ upon elevating the temperature (**Figure 6.4.73**). These results strongly support our hypothesis that the sequential retro-Diels-Alder/Diels-Alder reactions take place in between two C_{60}s inside the cage. The exchange rate was estimated to be 0.45-1.52 s^{-1} from the EXSY experiment. The activation Gibbs free energy barrier could be calculated from these rates to be 81.7 ± 1.5 kJ/mol at the experiment temperature. Considering that the equilibrium constant

of the Diels-Alder reaction between naked C_{60} and DMA is 110 M^{-1} at 325 K resulting in ΔG = -12.7 kJ/mol,[38] it can be concluded that the neighboring C_{60} stabilizes C_{60}DMA adduct inside $Pd_4\mathbf{L}^{Q}_6(Nap)_2$. This suggests that the second C_{60} in close proximity stabilizes both transition state and product probably via convex-concave interactions as suggested theoretically.[34] To further support this conclusion, the following control experiments were carried out. In the presence of excess amount of corannulene, C_{60}DMA•C_{60}@$Pd_4\mathbf{L}^{Q}_6(Nap)_2$ was let stand either in the dark or under the ambient light in the air for 3 days. If there is such a topochemical reaction within the cage, corannulene having the higher association constant (anthracene: ca. 199 M^{-1}) should replace DMA in an intermediate state (**Figure 6.4.56** and **Table 6.4.3**). A binding constant towards DMA could not be obtained due to the instant Diels-Alder reaction. As a result, only slight guest exchange was observed from the sample left in the dark while full guest exchange was observed together with the hetero-Diels-Alder product of DMA and singlet oxygen from the one left under the light (**Figure 6.4.79**). These results implied that the trapped DMA between two C_{60}s rather undergoes the Diels-Alder reaction with one of C_{60}s than being expelled from the nanoscopic space. An energy diagram based on the observations is summarized in Figure 6.2.5c. The DFT calculations suggest that the activation energy barrier for escape of the entrapped anthracene is higher than the one for the Diels-Alder reaction (**Figure 6.2.5c** and **Figure 6.4.80**). The entrapped DMA should keep staying in between two C_{60}s and proceed the topochemical reaction within the coordination cage.

6.3 Conclusion

In this report, the synthesis of a pill-shaped coordination cage having a nanoscopic space suitable to encapsulate a guest molecule in between two C_{60}s is reported. The association constant between corannulene and C_{60} was found to be dramatically increased due to the nano-confinement effects. Encapsulation of anthracene in the space lead to the first example of heteromultimeric encapsulation of two different fullerenes. The Gibbs activation free energy barrier for the Diels-Alder reaction between C_{60} and anthracene was lower than the one of naked C_{60} due to the close proximity to the other C_{60}. A quantitative formation of the heteromultimeric encapsulating cage was achieved even with 9,10-dimethylanthracene known to show

a retro-Diels-Alder reaction at ambient temperature, most likely due to the stabilization effect by the neighboring C_{60}. A clue of a topochemical-like reaction inside the cage was observed by EXSY experiments. The author believe that this result has paved the way toward a new concept of supramolecular chemistry.

6.4 Appendix

6.4.1 Materials and methods

Unless otherwise stated, all chemicals were purchased from commercial sources and used as received. $[Pd(MeCN)_4](BF_4)_2$ and 6-aminoquinoline purchased from Sigma-Aldrich. Corannulene was purchased from TCI.inc. $\mathbf{L^Q}$ was prepared according to literature procedures.[23,25] Electrospray ionization (ESI) mass spectra were recorded using Bruker ESI-timsTOF and compact mass spectrometers using Agilent tune mix as calibrant. NMR experiments were performed using Bruker AV 500 Avance NEO, Bruker AV 600 Avance FT-NMR and Bruker AV 700 Avance FT-NMR spectrometers. ^{1}H and ^{13}C signals were referenced to the residual solvent peak: acetonitrile (1.94 ppm,118.26 ppm), chloroform (7.26 ppm, 77.16 ppm). DFT calculation were performed using Gaussian Gaussian 16, Revision B.01.[2] Hydrodynamic radii of compounds were calculated from Stokes-Einstein equation (eq 1) where D is a diffusion coefficient, k_B is Boltzman constant, T is a temperature, η is a viscosity of the solvent, and r_H is a hydrodynamic radius of interest. ^{1}H DOSY NMR spectra were recorded with a dstebpgp3s pulse sequence with diffusion delays D20 of 0.08 s and gradient powers P30 of 1200. T_1 analyses of the corresponding signals in the 1D spectra were performed to obtain the diffusion coefficients D using the STEJSKAL-TANNER-Equation.

$$D = \frac{k_B T}{6\pi\eta r_H} \quad \text{(eq 1)}$$

6.4.2 Synthesis

6.4.2.1 Synthesis of L^Q

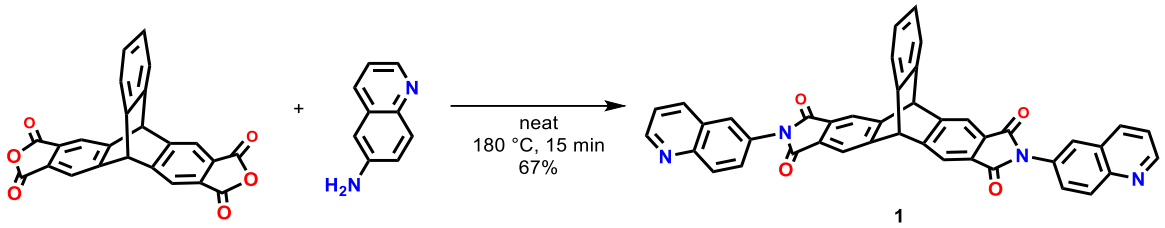

Figure 6.4.1 Synthesis of ligand 1

Triptycene-2,3,6,7-tetracarboxylic dianhydride (39.2 mg, 0.1 mmol) and 6-aminoquinoline (432.5 mg, 3 mmol) were placed in a vial and Ar gas was purged into the vial. The sealed vial was heated at 180 °C for 15 min while stirring and cooled to ambient temperature. The obtained crude material was purified by GPC ($CHCl_3$, 7.0 mL/min). After evaporating $CHCl_3$, the obtained solid was dried in vacuo. The desired compound was obtained as a yellow solid in 67% yield (43.3 mg, 0.067 mmol).

^{1}H NMR (500 MHz, CD_3CN, 298 K): δ (ppm) 8.94 (dd, J = 4.2, 1.7Hz, 2H), 8.32 (dd, J = 8.5, 1.7 Hz, 2H), 8.15 (d, 9.0 Hz, 2H), 8.06 (s, 4H), 7.95 (d, J = 2.3 Hz, 2H), 7.75 (dd, J = 9.0, 2.3 Hz, 2H), 7.61 (dd, J = 5.3, 3.3 Hz, 2H), b 7.52 (dd, J = 8.5, 4.2 Hz, 2H), 7.16 (dd, J = 5.3, 3.3, 2H), 6.18 (s, 2H);

^{13}C NMR (150 MHz, $CDCl_3$, 298 K): δ (ppm) 166.88, 151.36, 150.61, 146.42, 141.88, 137.19, 130.34, 130.16, 130.11, 128.34, 128.08, 126.96, 124.93, 124.78, 121.82, 119.72, 54.95, 17 signals were observed while 17 peaks must be observed in theory.

ESI MS calcd. for $[C_{42}H_{23}N_4O_4]^{1+}$ 647.1714 (100%), found 647.1683 [**1**+H]$^{1+}$.

6.4.2.1.1 ^{1}H NMR spectra of L^{Q}

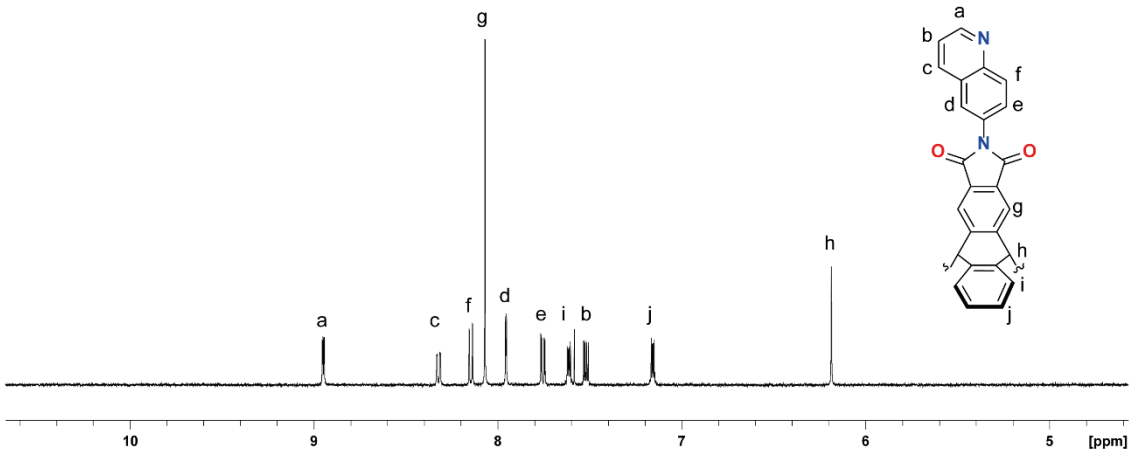

Figure 6.4.2 ^{1}H NMR spectrum (500 MHz, 298 K, CD_3CN) of L^{Q}

δ (ppm) 8.94 (dd, *J* = 4.2, 1.7Hz, 2H), 8.32 (dd, *J* = 8.5, 1.7 Hz, 2H), 8.15 (d, 9.0 Hz, 2H), 8.06 (s, 4H), 7.95 (d, *J* = 2.3 Hz, 2H), 7.75 (dd, *J* = 9.0, 2.3 Hz, 2H), 7.61 (dd, *J* = 5.3, 3.3 Hz, 2H), b 7.52 (dd, *J* = 8.5, 4.2 Hz, 2H), 7.16 (dd, *J* = 5.3, 3.3, 2H), 6.18 (s, 2H)

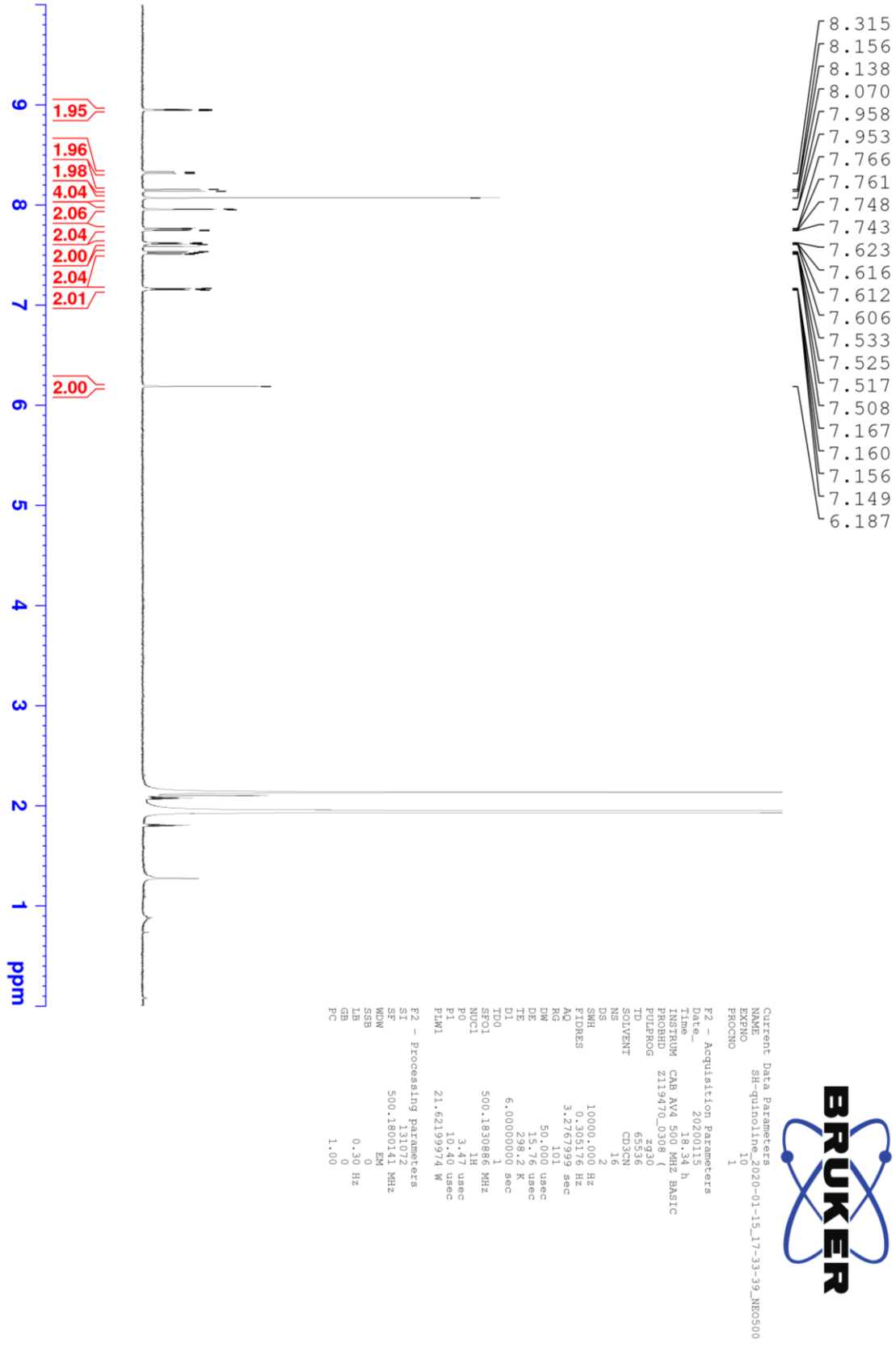

Figure 6.4.3 ^{1}H NMR spectrum (500 MHz, 298 K, CD_3CN) of **L^{Q}**

6.4.2.1.2 ^{1}H-^{1}H COSY spectrum of L^{Q}

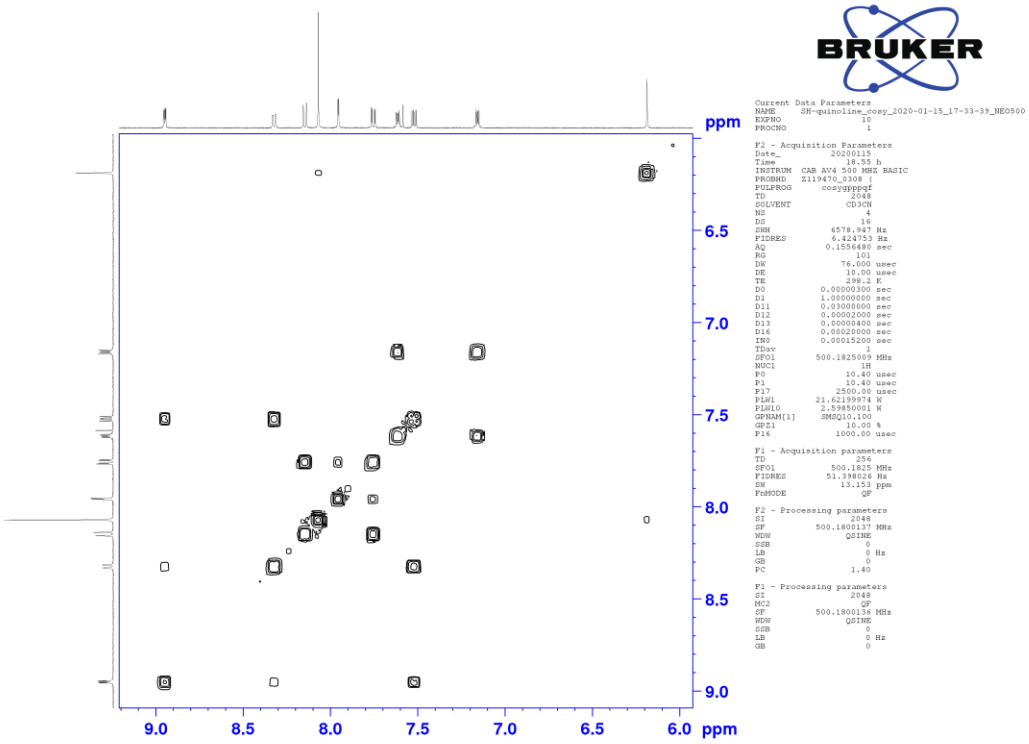

Figure 6.4.4 ^{1}H-^{1}H COSY spectrum (500 MHz, 298 K, CD_3CN) of **L^{Q}**

6.4.2.1.3 ^{13}C NMR spectrum of L^{Q}

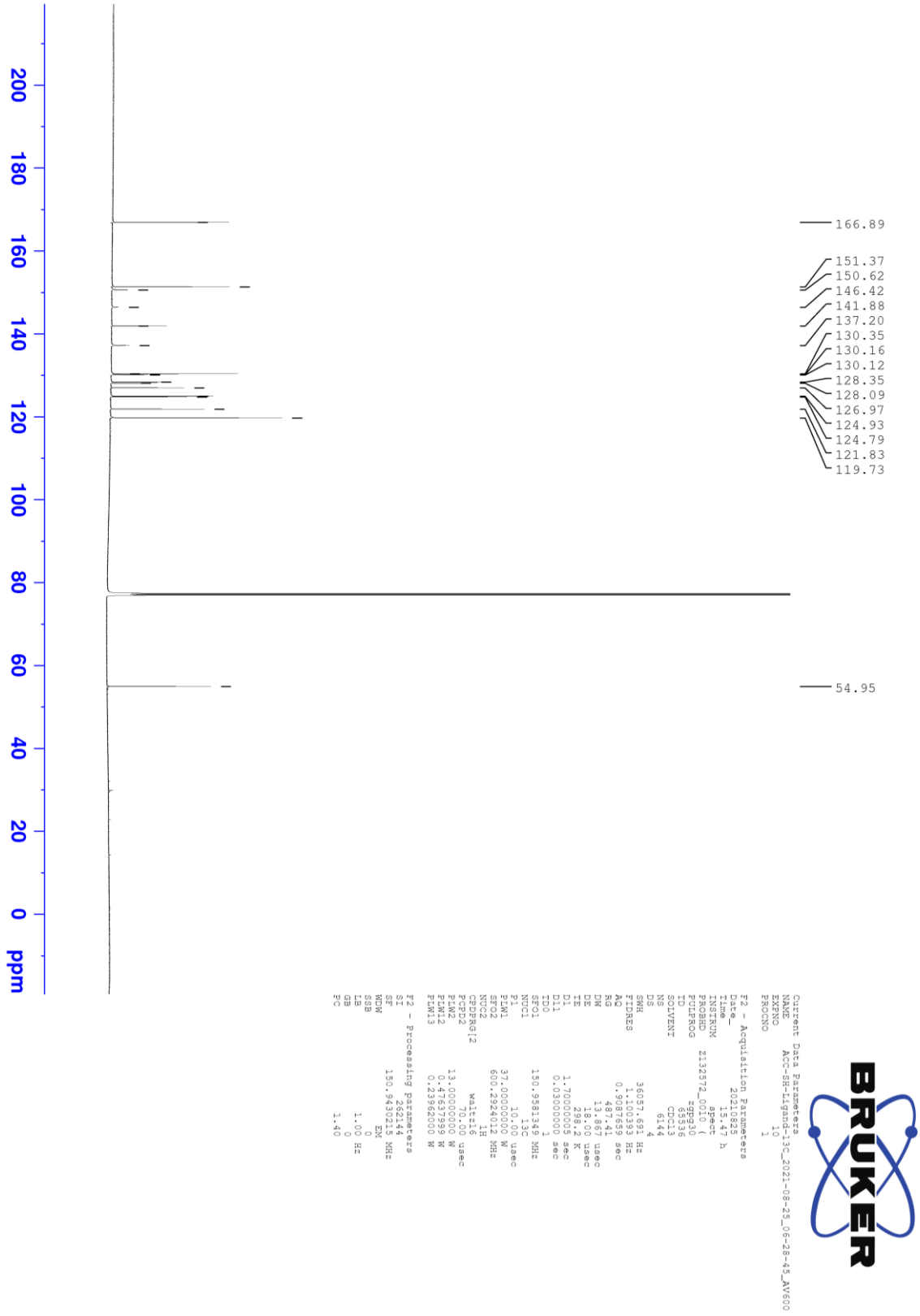

Figure 6.4.5 ^{13}C NMR spectrum (150 MHz, 298 K, $CDCl_3$) of **L^{Q}**

6.4.2.1.4 ESI MS spectrum of L^{Q}

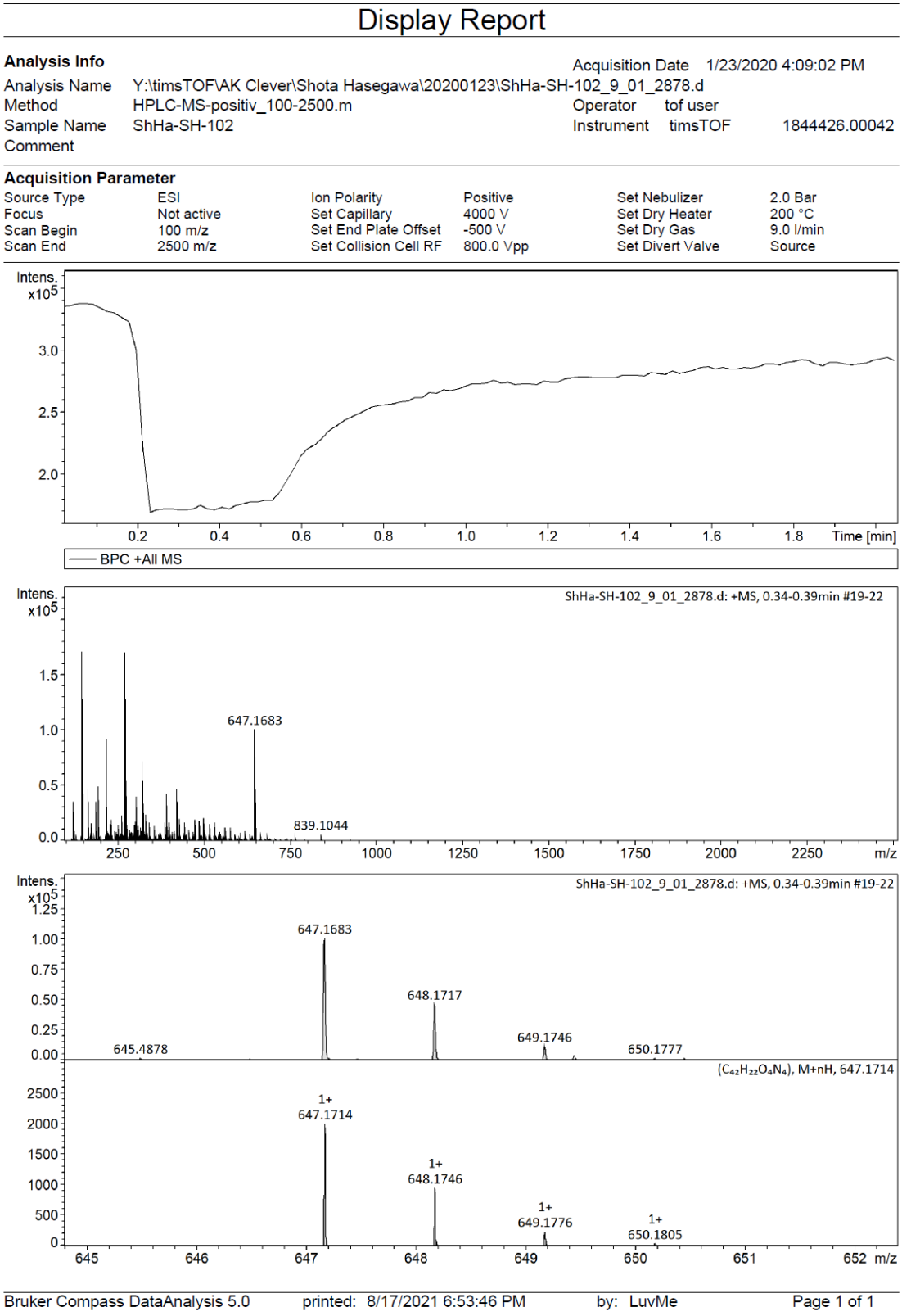

Figure 6.4.6 ESI MS spectrum of L^{Q} (positive mode).

6.4.2.2 Synthesis of $Pd_2L^Q{}_3(MeCN)_2$

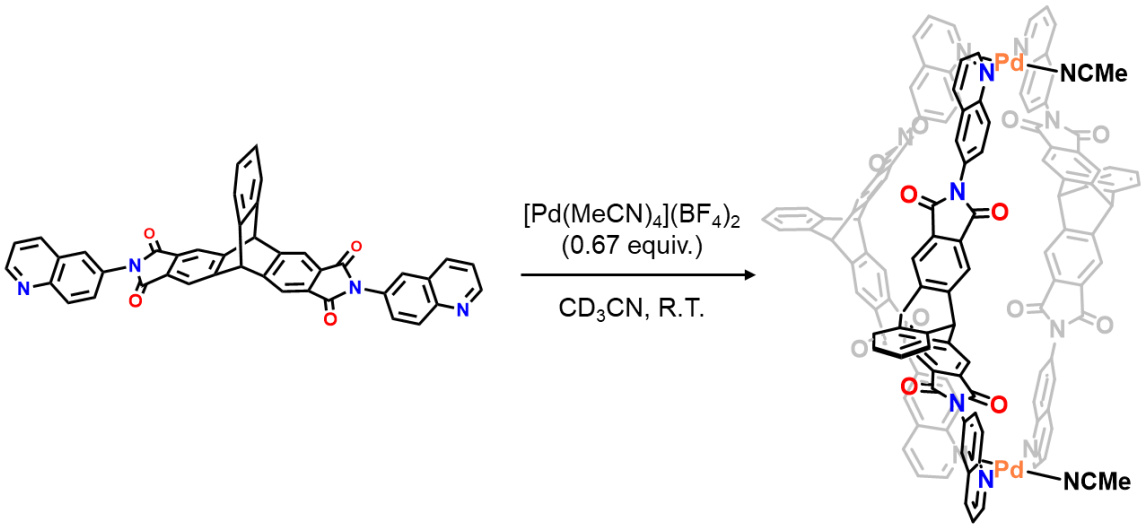

Figure 6.4.7 Synthesis of $Pd_2L^Q{}_3(MeCN)_2$

To a suspension of **L^Q** (11.37 mg, 17.6 μmol) in acetonitrile (7.80 mL), a solution of $[Pd(MeCN)_4](BF_4)_2$ in acetonitrile (586 μL, 20.0 mM, 11.7 μmol) was added. The mixture was stirred at ambient temperature for 24 h and the desired complex was obtained (0.7 mM).

^{1}H NMR (500 MHz, CD_3CN, 298 K): *δ* (ppm) 9.98 (d, *J* = 9.2 Hz, 4H), 9.84 (dd, *J* = 5.6, 1.2 Hz, 2H), 9.55 (dd, *J* = 5.6, 1.2 Hz, 4H), 9.32 (d, *J* = 9.2 Hz, 2H), 8.66 (d, *J* = 8.2 Hz, 4H), 8.49 (d, *J* = 8.2 Hz, 2H), 8.28 (dd, *J* = 9.2, 2.3 Hz, 4H), 8.12 (s, 4H), 8.09 (d, *J* = 2.3 Hz, 4H), 8.06 (s, 4H), 7.87 (s, 4H), 7.84 (dd, *J* = 8.2, 5.6 Hz, 2H), 7.78 (d, *J* = 2.3 Hz, 2H), 7.76 (dd, *J* = 8.2, 5.6 Hz, 4H), 7.66 (dd, *J* = 5.4, 3.3 Hz, 4H), 7.56 (dd, *J* = 5.4, 3.3 Hz, 2H), 7.46 (dd, *J* = 9.2, 2.3, 2H), 7.21 (dd, *J* = 5.4, 3.3 Hz, 4H), 7.14 (dd, *J* = 5.4, 3.3 Hz, 2H), 6.25 (s, 2H) , 6.21 (s, 2H) , 6.07 (s, 2H): **^{13}C NMR** (150 MHz, CD_3CN, 298 K): *δ* (ppm) 168.03, 167.76, 167.63, 156.29, 156.03, 152.90, 152.84, 152.72, 146.29, 146.27, 143.54, 143.34, 143.08, 143.05, 142.77, 134.09, 133.68, 133.09, 132.92, 131.35, 131.30, 131.23, 131.21, 131.07, 130.43, 128.79, 128.67, 128.18, 127.59, 127.54, 127.49, 125.96, 125.93, 125.85, 125.74, 125.57, 124.64, 120.54, 120.35, 120.21, 54.73, 54.57, 42 peaks were observed while 44 peaks must be observed in theory. 1 signal should be overlapped in sp3 region and 1 signal should be overlapped in aromatic region.

DOSY: Diffusion coefficient $D = 5.17 \times 10^{-10}$ m^2s^{-1}, hydrodynamic radius r_H was calculated to be 12.6 Å

ESI-MS calcd. for $[(C_{42}H_{22}N_4O_4)_3Pd_2(CH_3CN)_2]^{4+}$ 558.5889, found 558.5871 $[Pd_2L^Q{}_3(MeCN)_2]^{4+}$.

6.4.2.2.1 ^{1}H NMR spectra of $Pd_2L^{Q}_3(MeCN)_2$

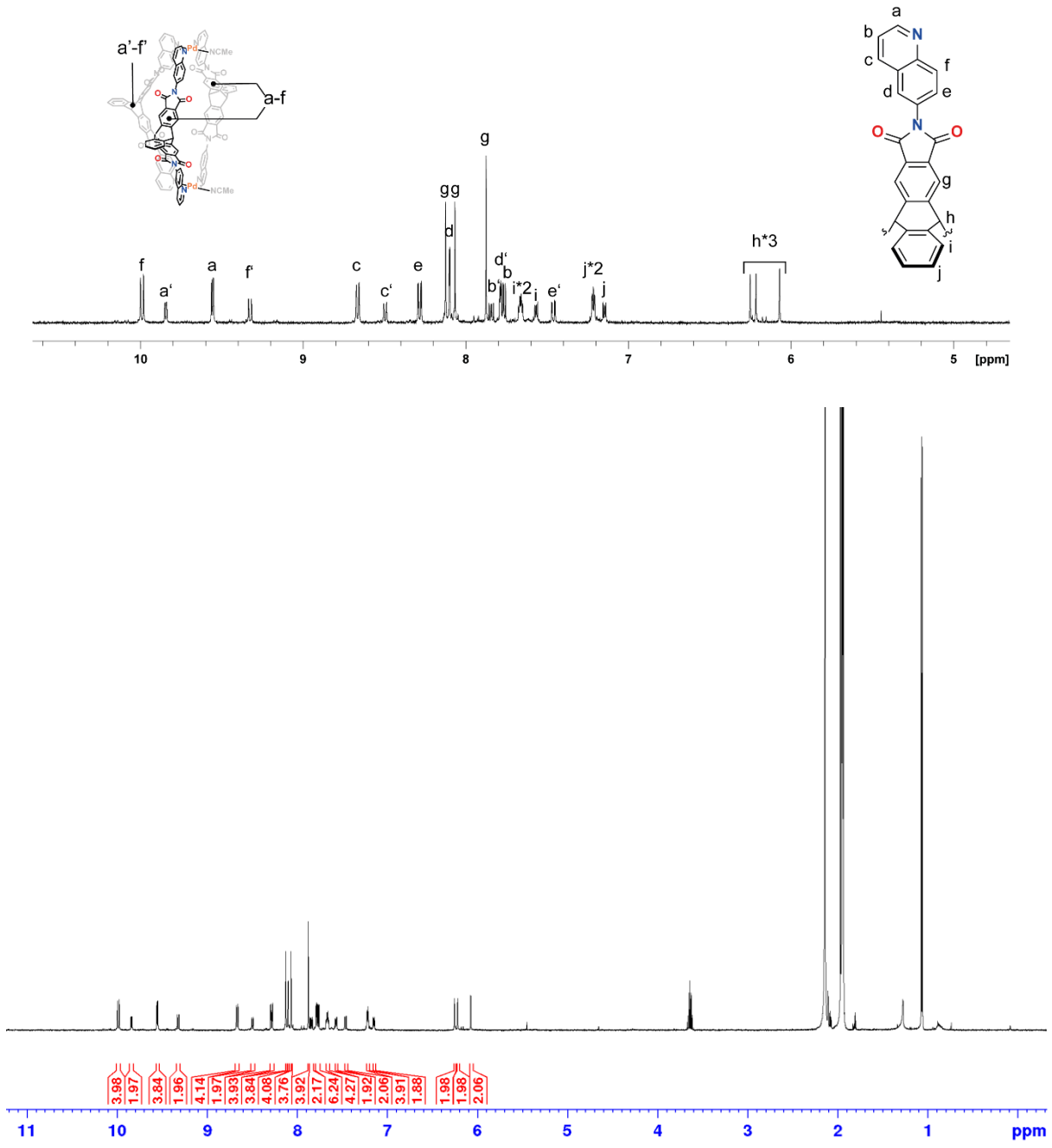

Figure 6.4.8 ^{1}H NMR spectra (500 MHz, 298 K, CD_3CN, 0.70 mM) of $Pd_2\mathbf{L}^{Q}_3(MeCN)_2$

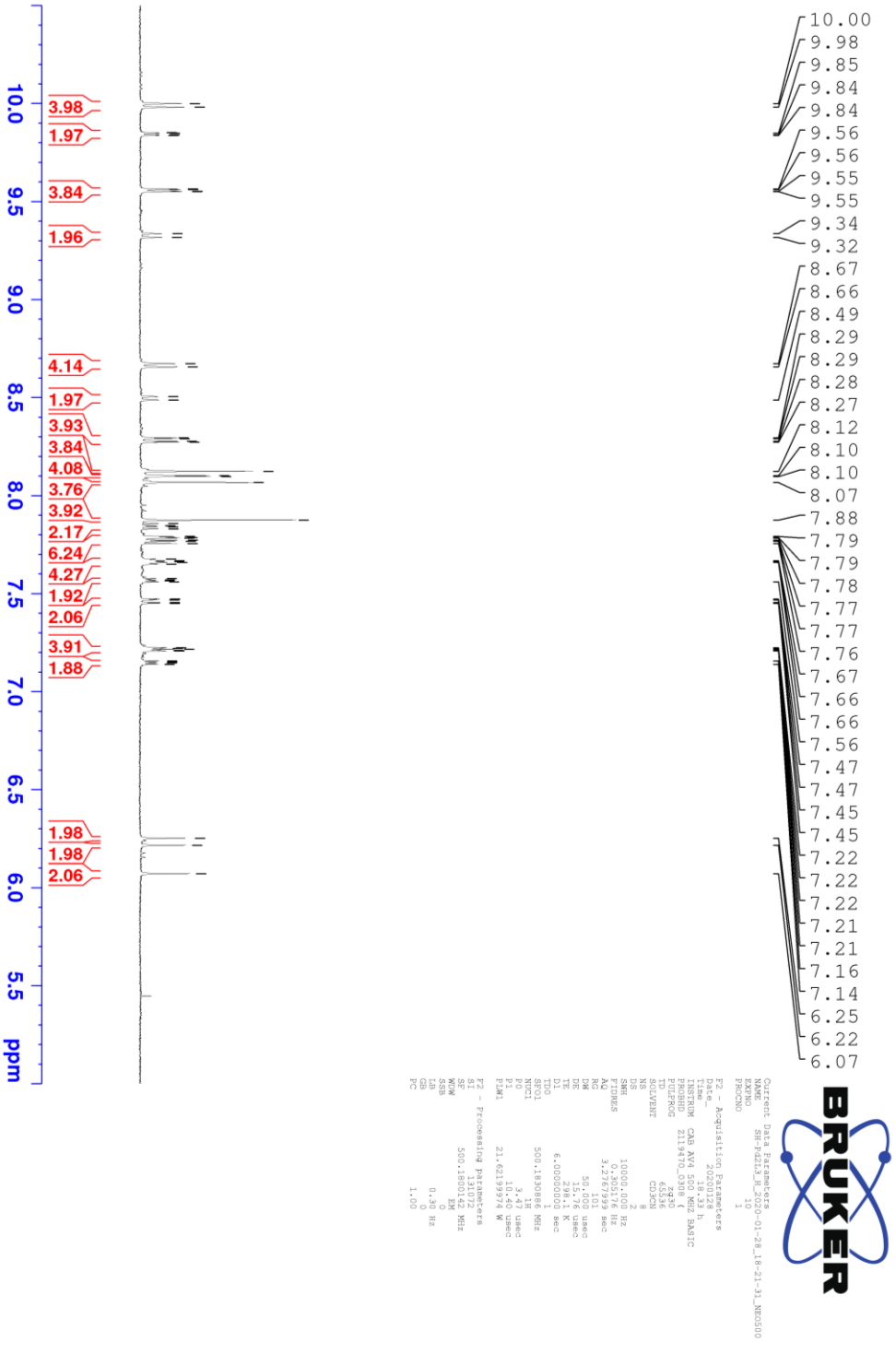

Figure 6.4.9 ^{1}H NMR spectrum (500 MHz, 298 K, CD_3CN, 0.70 mM) of $Pd_2\mathbf{L}^{Q}_3(MeCN)_2$

6.4.2.2.2 ^{1}H-^{1}H COSY NMR spectrum of $Pd_2L^{Q}_3(MeCN)_2$

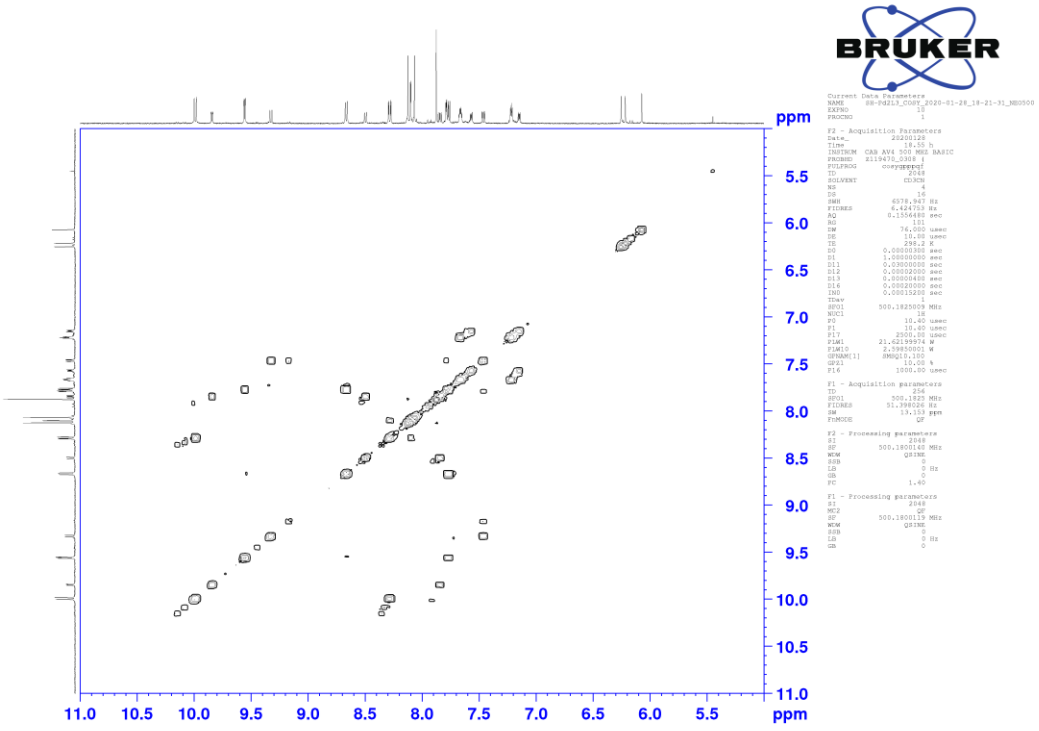

Figure 6.4.10 ^{1}H-^{1}H COSY NMR spectrum (500 MHz, 298 K, CD_3CN, 0.70 mM) of $Pd_2\mathbf{L}^{Q}_3(MeCN)_2$

6.4.2.2.3 ^{13}C NMR spectrum of $Pd_2L^Q_3(MeCN)_2$

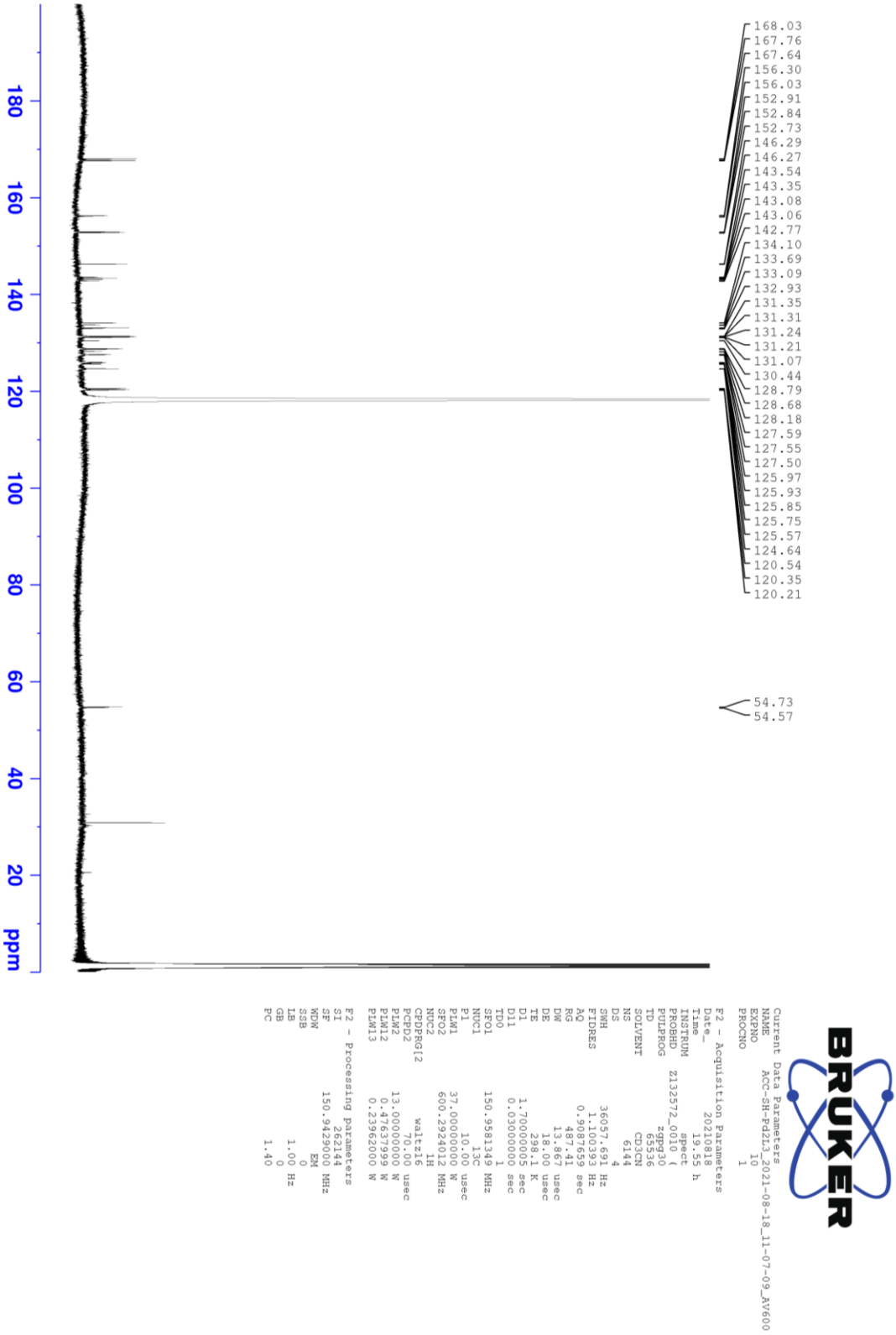

Figure 6.4.11 ^{13}C NMR spectra (150 MHz, 298 K, CD_3CN, 0.70 mM) of Pd_2**1**$_3(MeCN)_2$

6.4.2.2.4 ^{1}H DOSY NMR spectrum of $Pd_2L^{Q}_3(MeCN)_2$

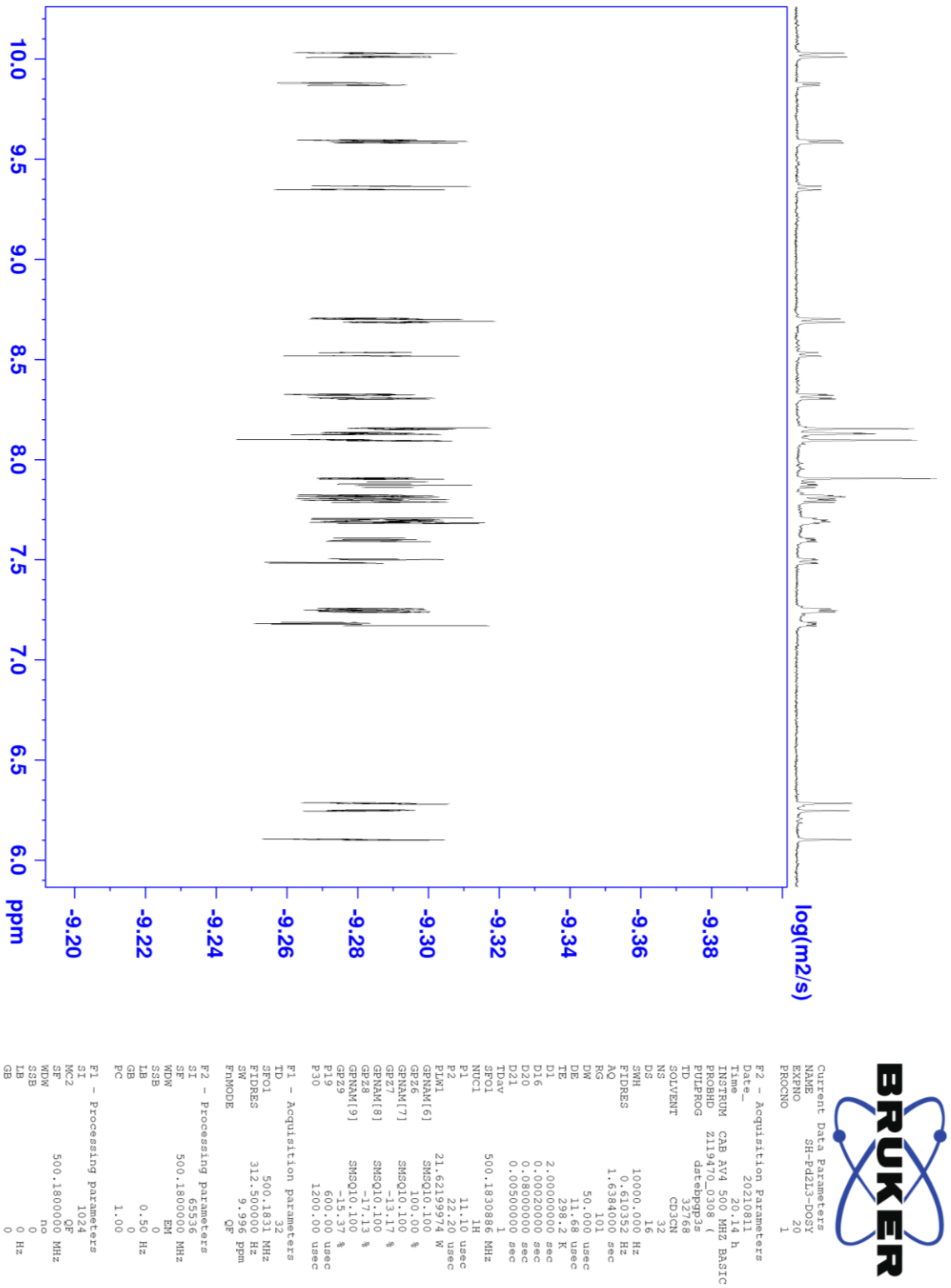

Figure 6.4.12 ^{1}H DOSY NMR spectrum (500 MHz, 298 K, CD_3CN, 0.70 mM) of $Pd_2\mathbf{L}^{Q}_3(MeCN)_2$

6.4.2.2.5 ESI-MS spectrum of $Pd_2L^Q_3(MeCN)_2$

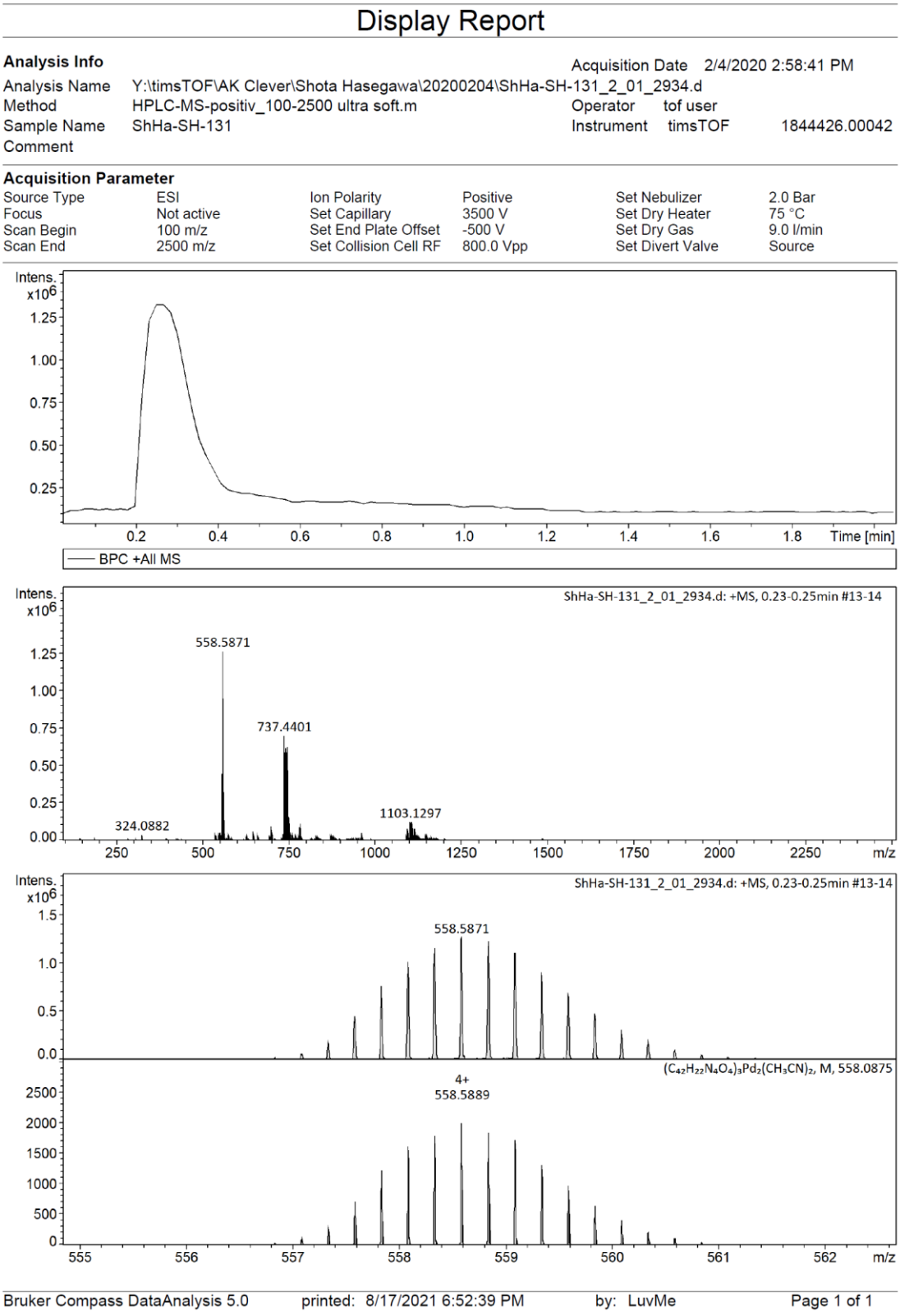

Figure 6.4.13 ESI-MS spectrum (positive) of $Pd_2L^Q_3(MeCN)_2$

6.4.2.2.6 Synthesis of $Pd_4L^{Q}_6(Nap)_2$

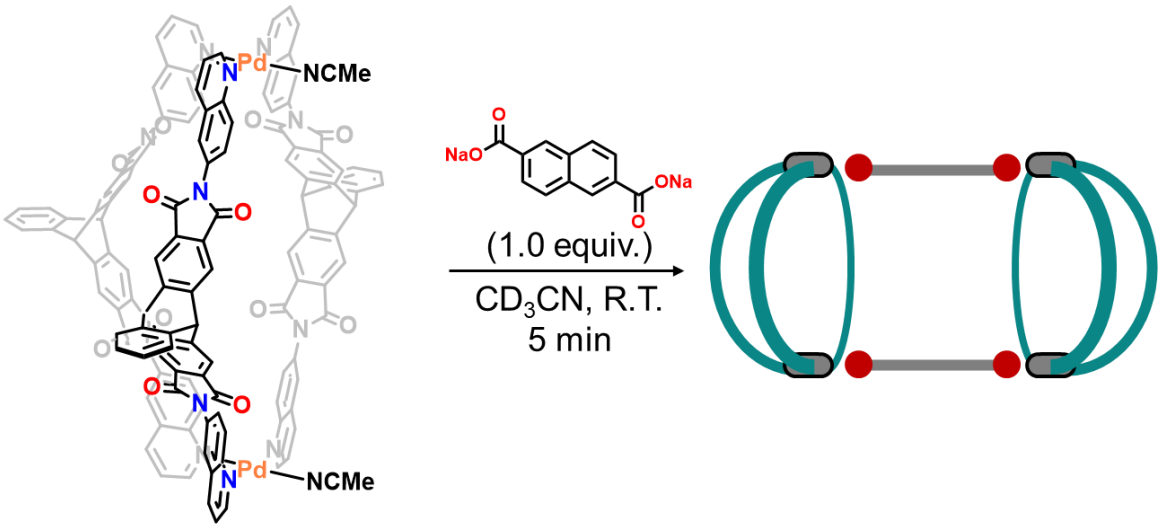

Figure 6.4.14 Synthesis of $Pd_4L^{Q}_6(Nap)_2$

To an acetonitrile solution of $Pd_2\mathbf{L}^{Q}_3(MeCN)_2$ (0.70 mM, 1.20 mL), 2,6-Naphthalnedicalboxylate sodium salt (20 mM in D_2O, 42 μL, 0.84 μmol) was added dropwise. The resulted solution was stirred at ambient temperature for 5 min. The desired complex was obtained.

^{1}H NMR (500 MHz, CD_3CN, 298 K): *δ* (ppm) 10.45 (d, *J* = 9.2 Hz, 8H), 10.33 (dd, *J* = 5.6, 1.2 Hz, 4H), 9.84 (dd, *J* = 5.6, 1.2 Hz, 4H), 9.77 (d, *J* = 9.2 Hz, 4H), 8.47 (d, *J* = 8.2 Hz, 8H), 8.45 (d, *J* = 8.2 Hz, 4H), 8.35 (s, 4H), 8.31 (dd, *J* = 9.2, 2.2 Hz, 8H), 8.19 (s, 4H), 8.11 (s, 4H), 7.97 (d, *J* = 2.2 Hz, 8H), 7.92 (s, 4H), 7.83-7.77 (m, 12H), 7.71 (d, *J* = 7.7 Hz, 4H) 7.63 (m, 12H), 7.58 (dd, *J* = 5.4, 3.3 Hz, 4H), 7.52 (dd, *J* = 9.2, 2.2 Hz, 4H), 7.38 (d, *J* = 7.5 Hz, 4H), 7.20-7.11 (m, 8H), 7.02 (dd, *J* = 7.5 Hz, 4H) 6.39 (s, 4H). 6.25 (s, 4H). 6.11 (s, 4H);

DOSY: Diffusion coefficient $D = 3.97 \times 10^{-10}$ m^2s^{-1}, hydrodynamic radius r_H was calculated to be 16.5 Å

^{13}C NMR (150 MHz, CD_3CN, 298 K): *δ* (ppm) 173.54, 168.10, 167.79, 167.62, 156.62, 152.73, 152.60, 146.72, 146.04, 142.94, 142.74, 142.69, 142.22, 142.12, 134.33, 133.09, 132.83, 132.75, 132.44, 132.35, 131.17, 131.12, 130.92, 130.72, 130.65, 129.99, 129.24, 129.01, 128.56, 128.42, 127.44, 127.34, 127.13, 126.92, 125.73, 125.70, 125.62, 124.93, 123.82, 120.49, 120.37, 120.12, 54.76, 54.59, 54.43; 45 peaks were observed while 48 peaks must be observed in theory. 3 peaks should be overlapped in aromatic region.

ESI MS calcd. for $[(C_{42}H_{22}N_4O_4)_6Pd_4(C_{12}H_6O_4)_2]^{4+}$ 1183.4156, found 1183.4024 $[Pd_4\mathbf{L}^{Q}_6(Nap)_2]^{4+}$

6.4.2.2.7 ^{1}H NMR spectra of $Pd_4L^{Q}_6(Nap)_2$

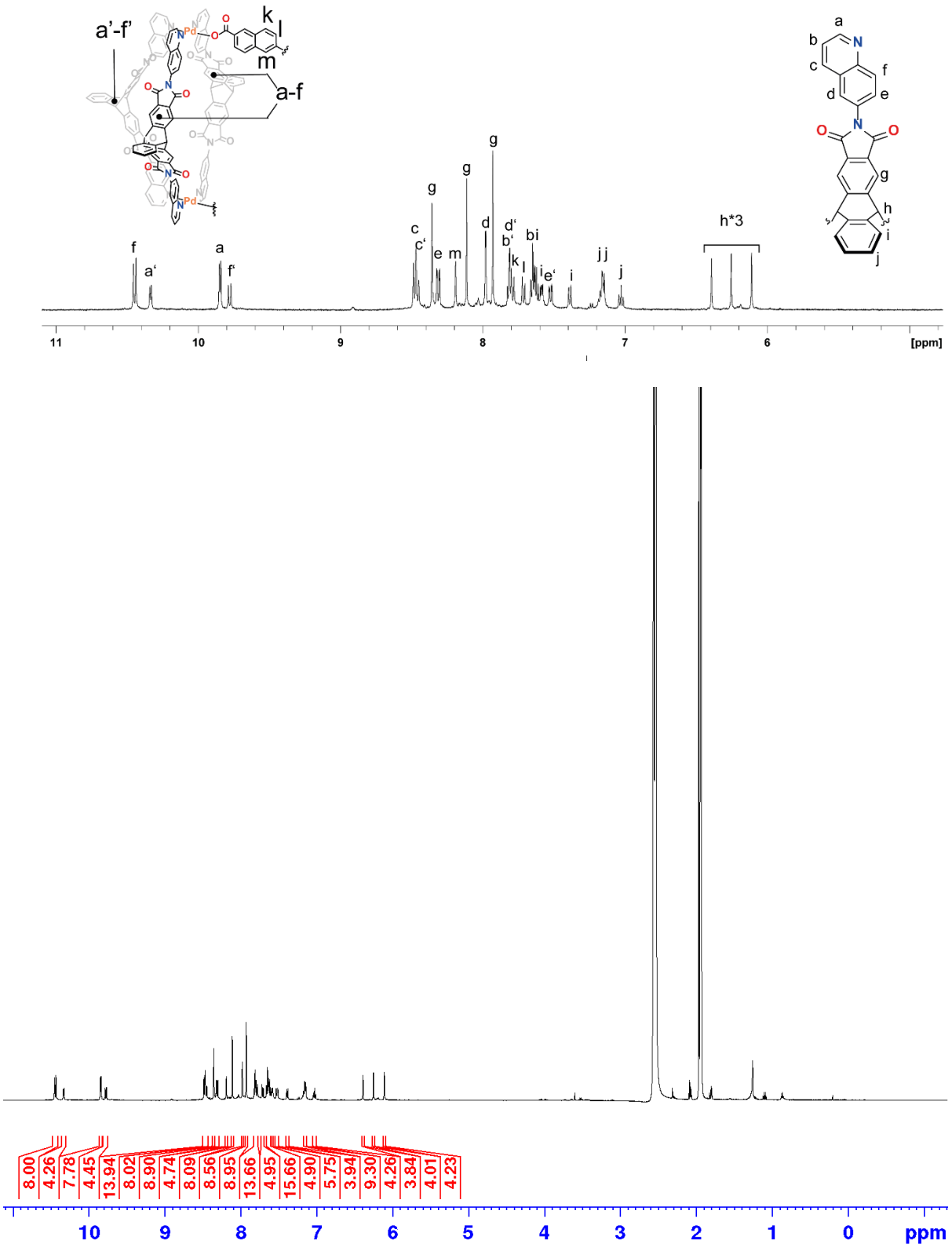

Figure 6.4.15 ^{1}H NMR spectra (500 MHz, 298 K, CD_3CN, 0.34 mM) of $Pd_4\mathbf{L}^{Q}_6(Nap)_2$

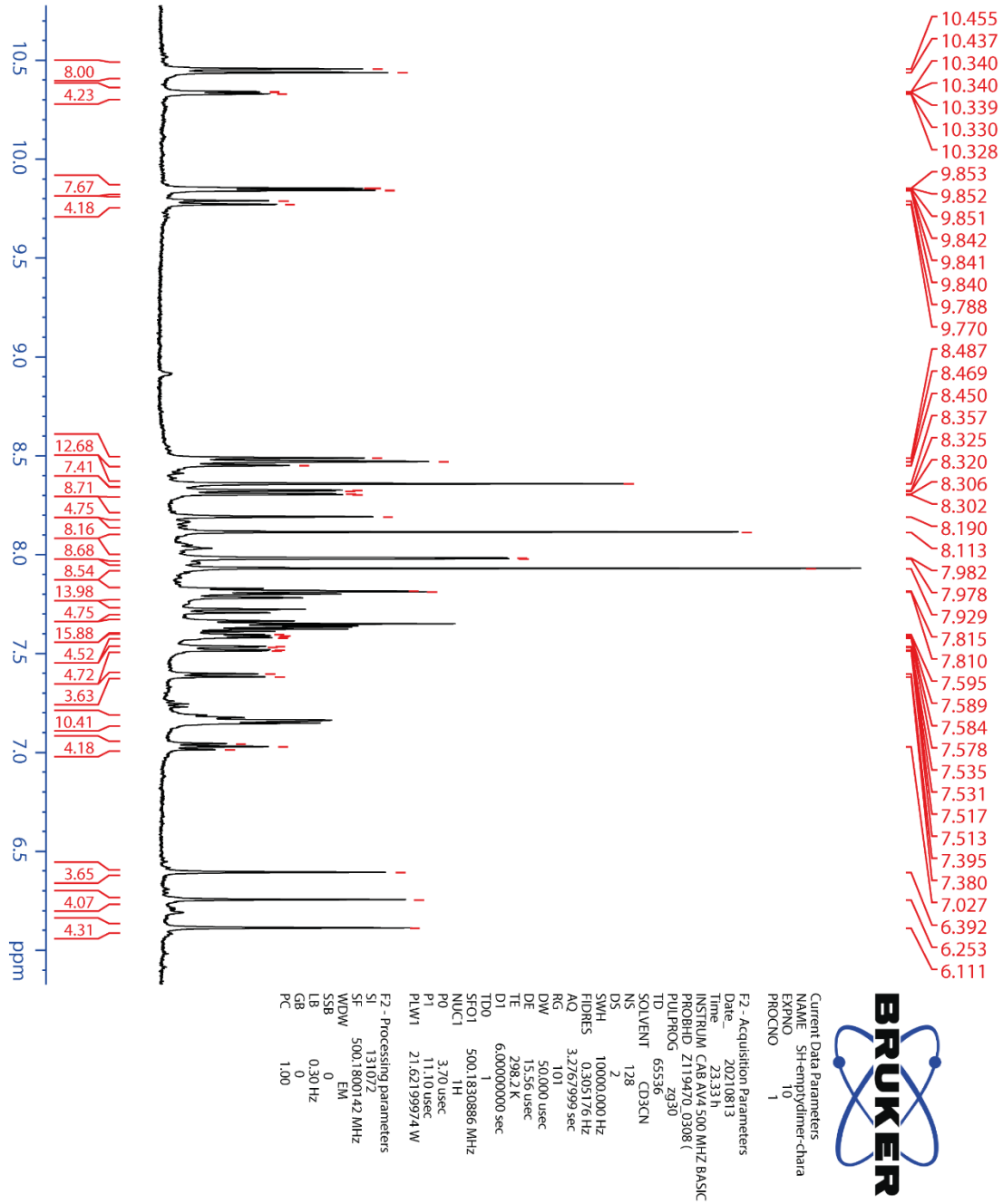

Figure 6.4.16 ^{1}H NMR spectrum (500 MHz, 298 K, CD_3CN, 0.34 mM) of $Pd_4\mathbf{L}^{Q}_6(Nap)_2$

6.4.2.2.8 ^{1}H-^{1}H COSY NMR spectrum of $Pd_4L^{Q}_6(Nap)_2$

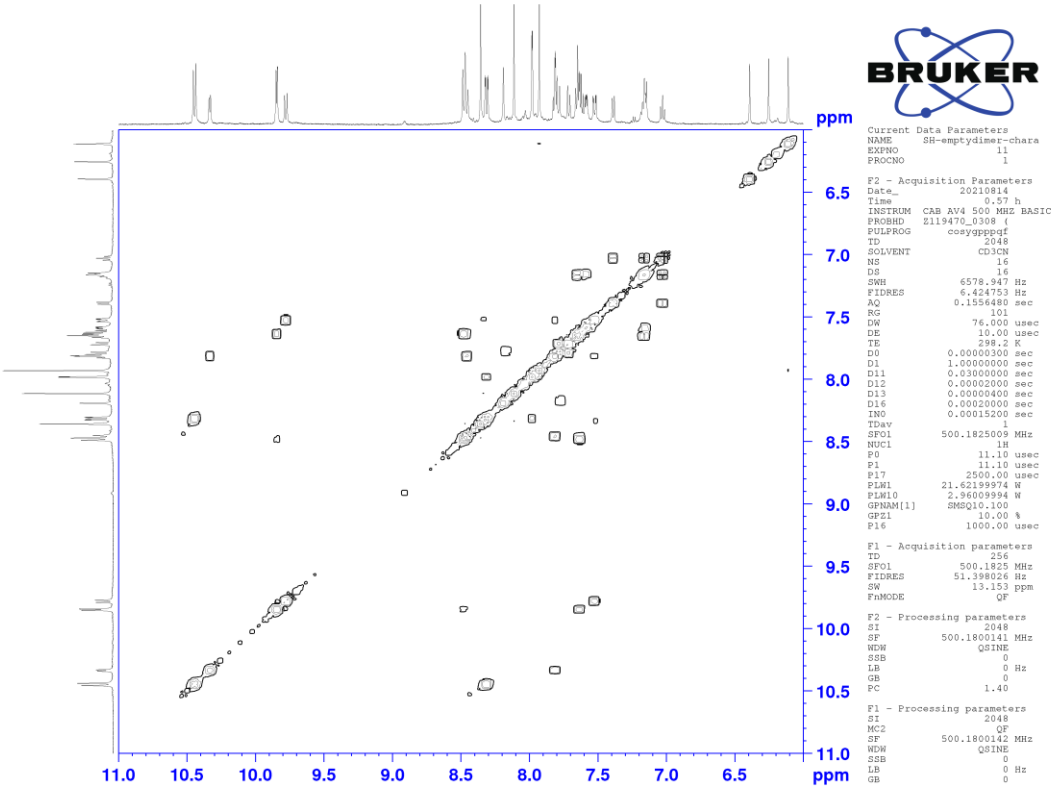

Figure 6.4.17 ^{1}H–^{1}H COSY NMR spectrum (500 MHz, 298 K, CD_3CN, 0.34 mM) of $Pd_4\mathbf{L}^{Q}_6(Nap)_2$

6.4.2.2.9 ^{1}H-^{1}H NOESY NMR spectrum of $Pd_4L^{Q}_6(Nap)_2$

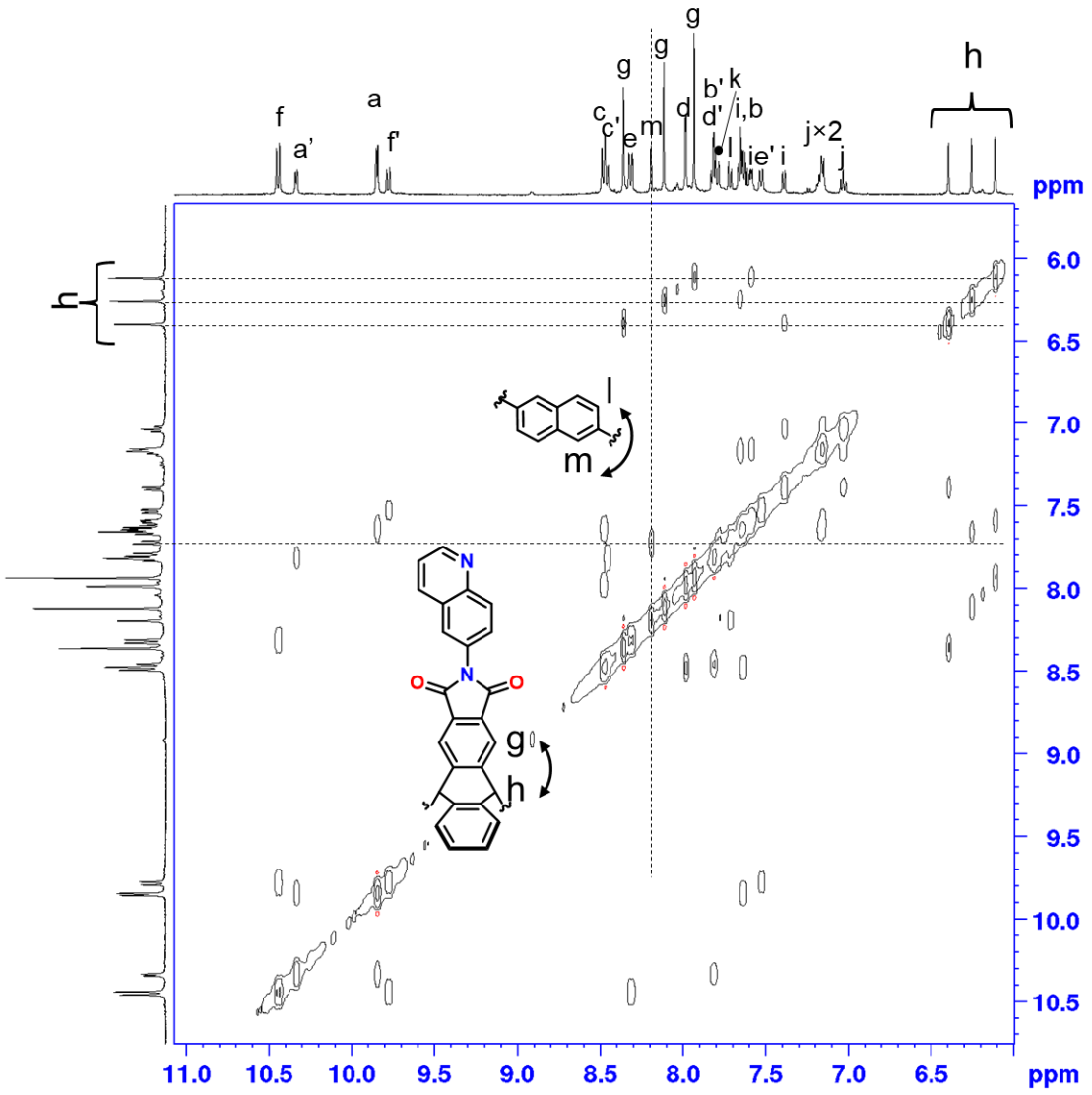

Figure 6.4.18 ^{1}H–^{1}H NOESY NMR spectrum (500 MHz, 298 K, CD_3CN, 0.34 mM) of $Pd_4\mathbf{L}^{Q}_6(Nap)_2$

6.4.2.2.10 ^{13}C NMR spectra of $Pd_4L^Q{}_6(Nap)_2$

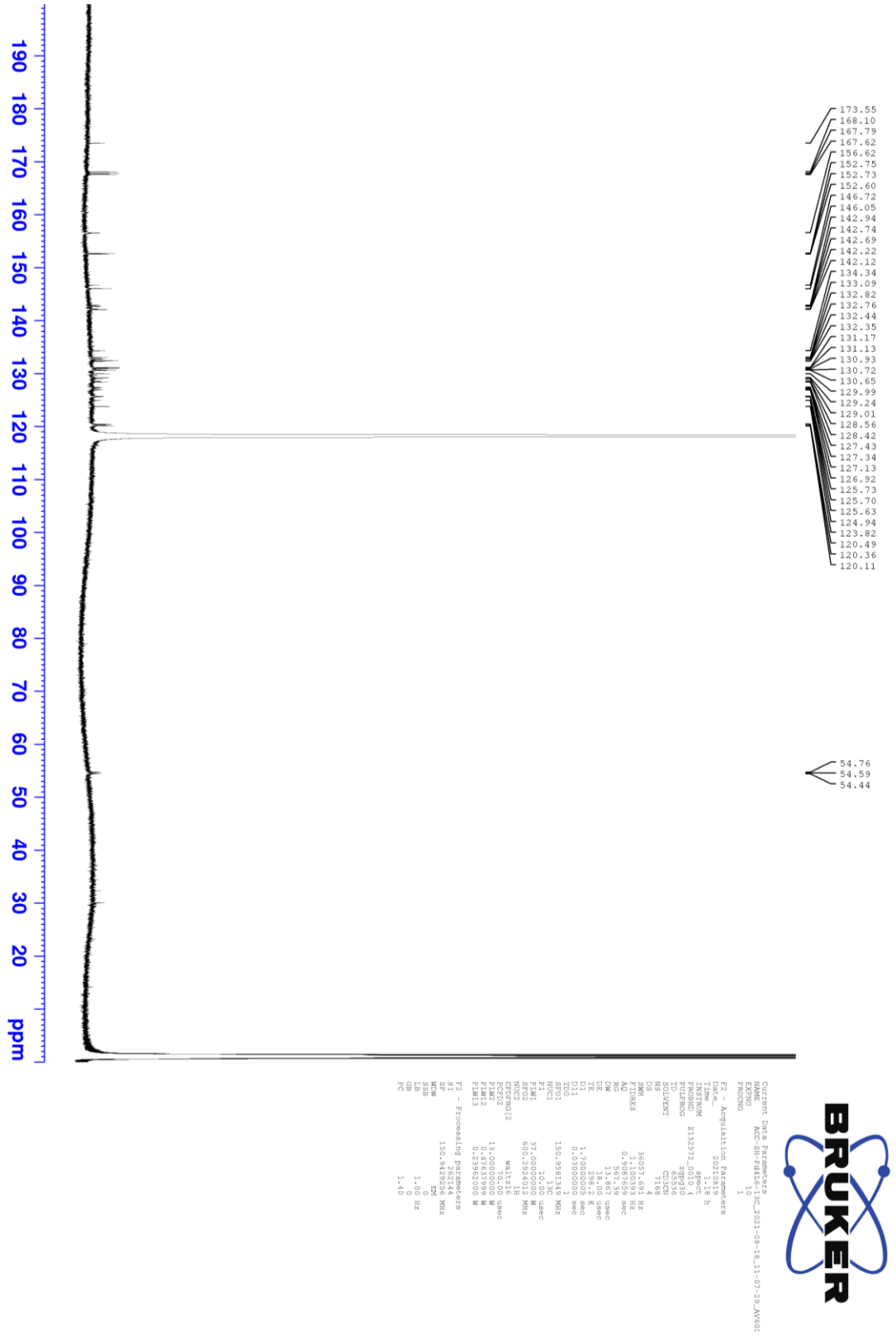

Figure 6.4.19 ^{13}C NMR spectra (150 MHz, 298 K, CD_3CN, 0.34 mM) of $Pd_4\mathbf{L}^Q{}_6(Nap)_2$

6.4.2.2.11 ^{1}H DOSY NMR spectrum of $Pd_4L^{Q}_6(Nap)_2$

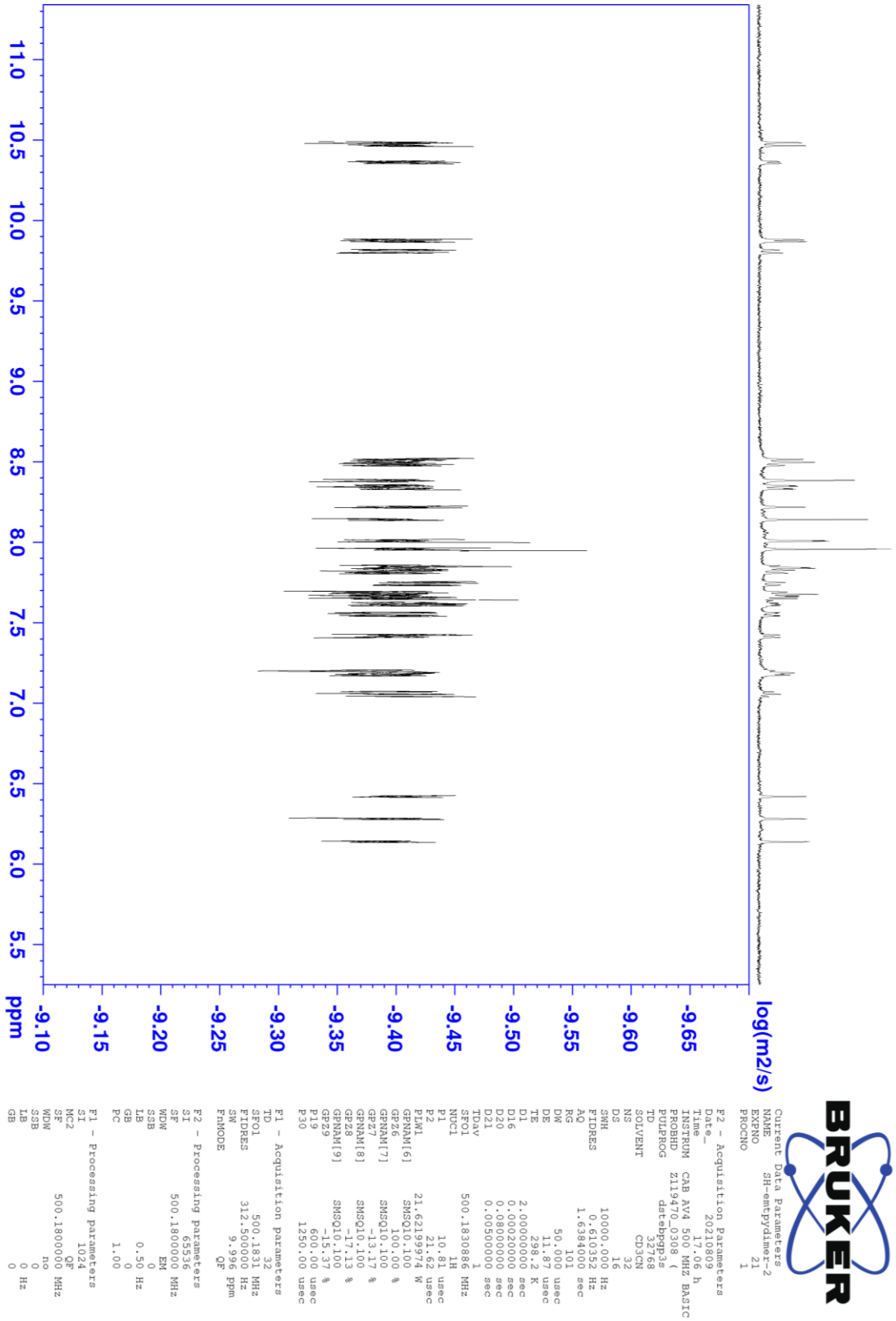

Figure 6.4.20 ^{1}H DOSY NMR spectrum (500 MHz, 298 K, CD_3CN, 0.34 mM) of $Pd_4L^{Q}_6(Nap)_2$

6.4.2.2.12 ESI-MS spectrum of $Pd_4L^Q_6(Nap)_2$

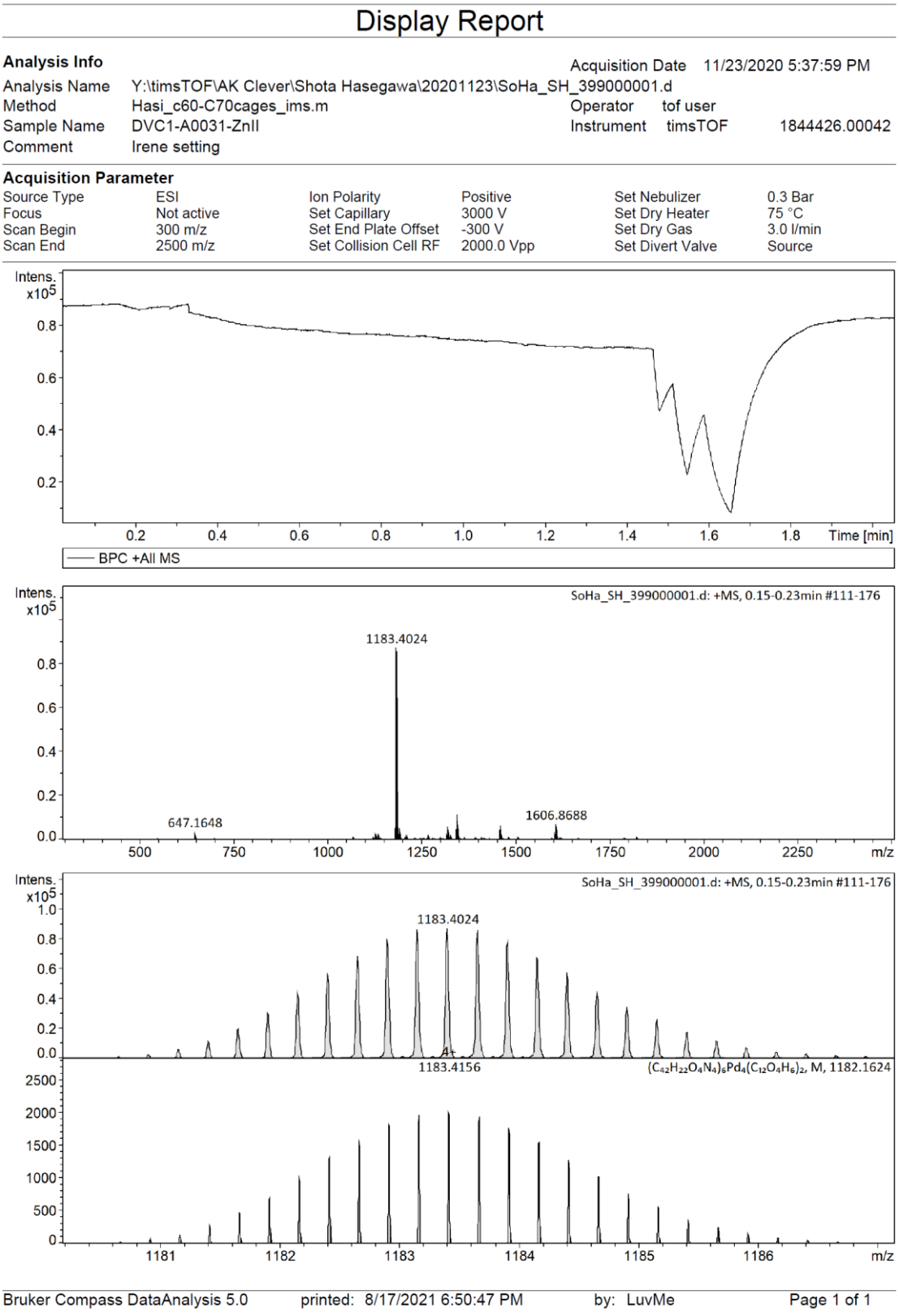

Figure 6.4.21 ESI-MS spectrum (positive) of $Pd_4L^Q_6(Nap)_2$

6.4.2.3 Synthesis of $(C_{60})_2$@$Pd_4L^Q_6(Nap)_2$

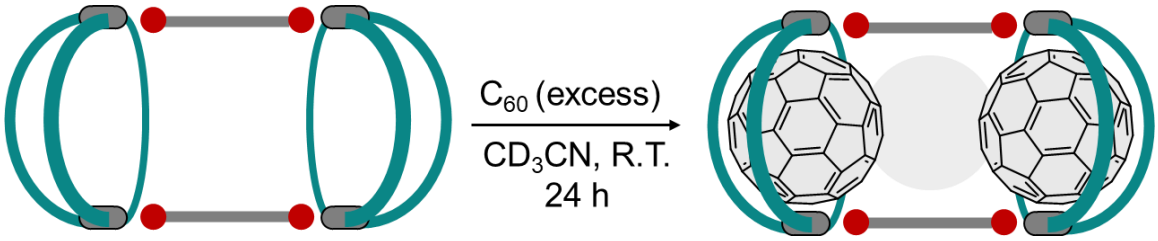

Figure 6.4.22 Synthesis of $(C_{60})_2$@$Pd_4\mathbf{L}^Q_6(Nap)_2$

To an acetonitrile solution of $Pd_4\mathbf{1}_6(Nap)_2$ (0.34 mM, 1.0 mL), 5 mg of powdery C_{60} was dispersed at ambient temperature for 24h. After filtrating the remained C_{60}, the desired complex was obtained (0.34 mM).

^{1}H NMR (500 MHz, CD_3CN, 298 K): *δ* (ppm) 10.83 (d, *J* = 9.2 Hz, 8H), 10.45 (dd, *J* = 5.6, 1.2 Hz, 4H), 9.72 (dd, *J* = 5.6, 1.2 Hz, 8H), 9.47 (d, *J* = 9.2 Hz, 4H), 8.50-8.44 (m, 20H), 8.41-8.37 (m, 12H). 8.17 (s, 8H), 8.04-8.00 (m, 12H) 7.94 (s, 8H), 7.80-7.77 (m, 8H), 7.74 (d, *J*= 2.2 Hz, 4H), 7.64 (d, *J* = 7.5 Hz, 4H), 7.63 (dd, *J* = 5.4, 3.3 Hz, 8H), 7.61 (dd, *J* = 5.4, 3.3 Hz, 4H). 7.54 (dd, *J* = 5.4, 3.3 Hz, 4H) 7.47 (d, *J* = 7.5 Hz, 4H), 7.18-7.10 (m, 12H), 7.04 (dd, *J* = 7.5 Hz, 4H), 6.47 (s, 4H), 6.28 (s, 4H), 6.11 (s, 4H); **^{13}C NMR** (150 MHz, CD_3CN, 298 K): *δ* (ppm) 173.78, 167.85, 167.54, 167.25, 153.38, 153.08, 146.21, 143.26, 143.09, 143.00, 142.64, 142.61, 142.47, 142.31, 142.15, 142.10, 134.55, 132.94, 132.03, 131.90, 131.66, 131.08, 131.01, 130.97, 130.93, 130.89, 130.77, 130.57, 130.34, 129.24, 128.83, 128.03, 127.87, 127.45, 127.30, 127.16, 125.90, 125.74, 125.18, 124.30, 120.89, 120.65, 54.83, 54.64, 54.42; 45 peaks were observed while 49 peaks must be observed in theory. 4 peaks should be overlapped in aromatic region.

DOSY: Diffusion coefficient D = 3.86 × 10^{-10} m^2s^{-1}, hydrodynamic radius r_H was calculated to be 17.0 Å

ESI MS calcd. for $[(C_{42}H_{22}N_4O_4)_6Pd_4(C_{60})_2(C_{12}H_6O_4)_2]^{4+}$ 1543.6666, found 1543.6559 $[(C_{60})_2$@$Pd_4\mathbf{L}^Q_6(Nap)_2]^{4+}$.

6.4.2.3.1 ^{1}H NMR spectra of $(C_{60})_2$@$Pd_4L^{Q}_6(Nap)_2$

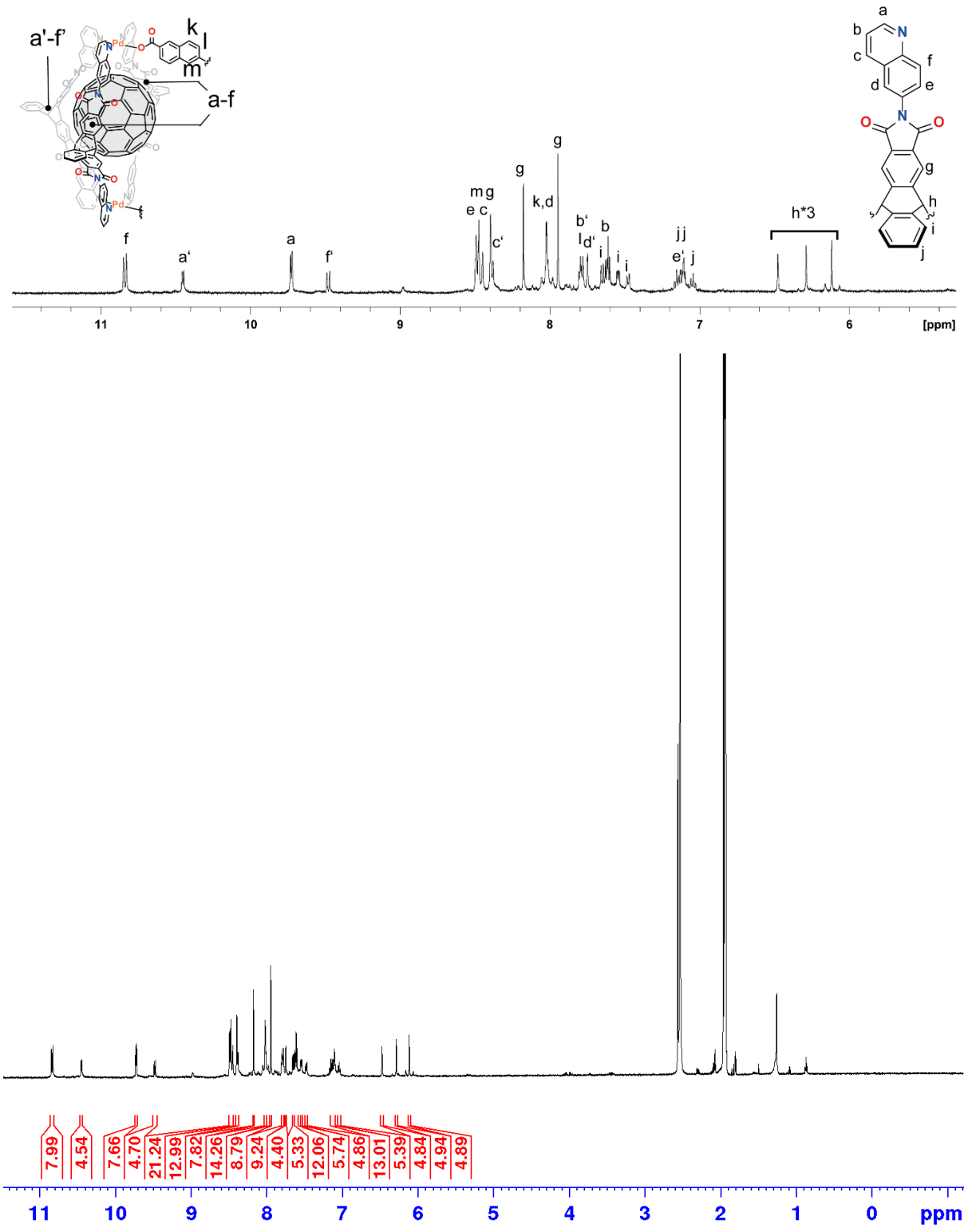

Figure 6.4.23 ^{1}H NMR spectra (500 MHz, 298 K, CD_3CN, 0.34 mM) of $(C_{60})_2$@$Pd_4L^{Q}_6(Nap)_2$

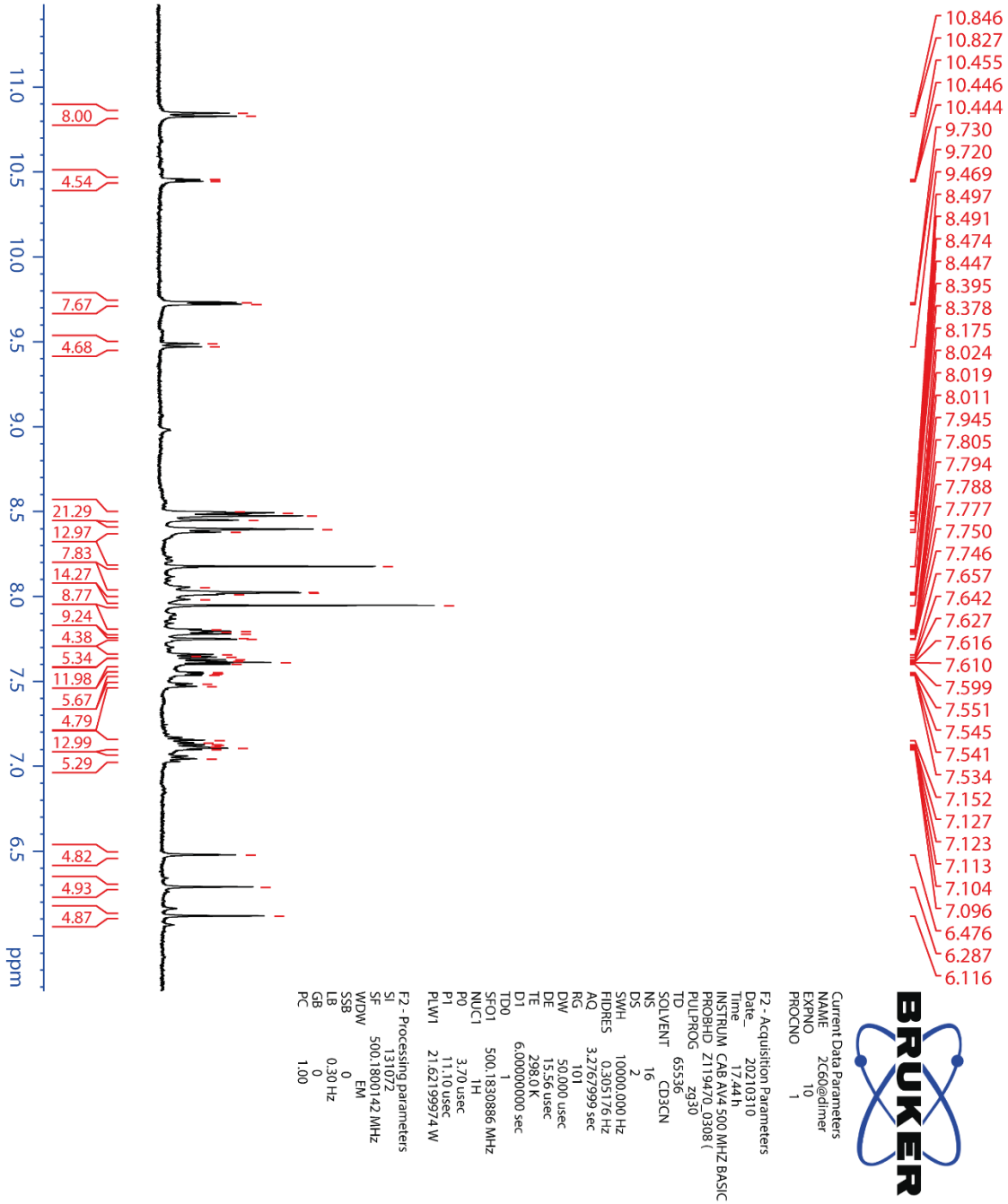

Figure 6.4.24 ^{1}H NMR spectrum (500 MHz, 298 K, CD_3CN, 0.34 mM) of $(C_{60})_2@Pd_4L^{Q}_6(Nap)_2$

6.4.2.3.2 ^{1}H-^{1}H COSY NMR spectrum of $(C_{60})_2$@$Pd_4L^{Q}_6(Nap)_2$

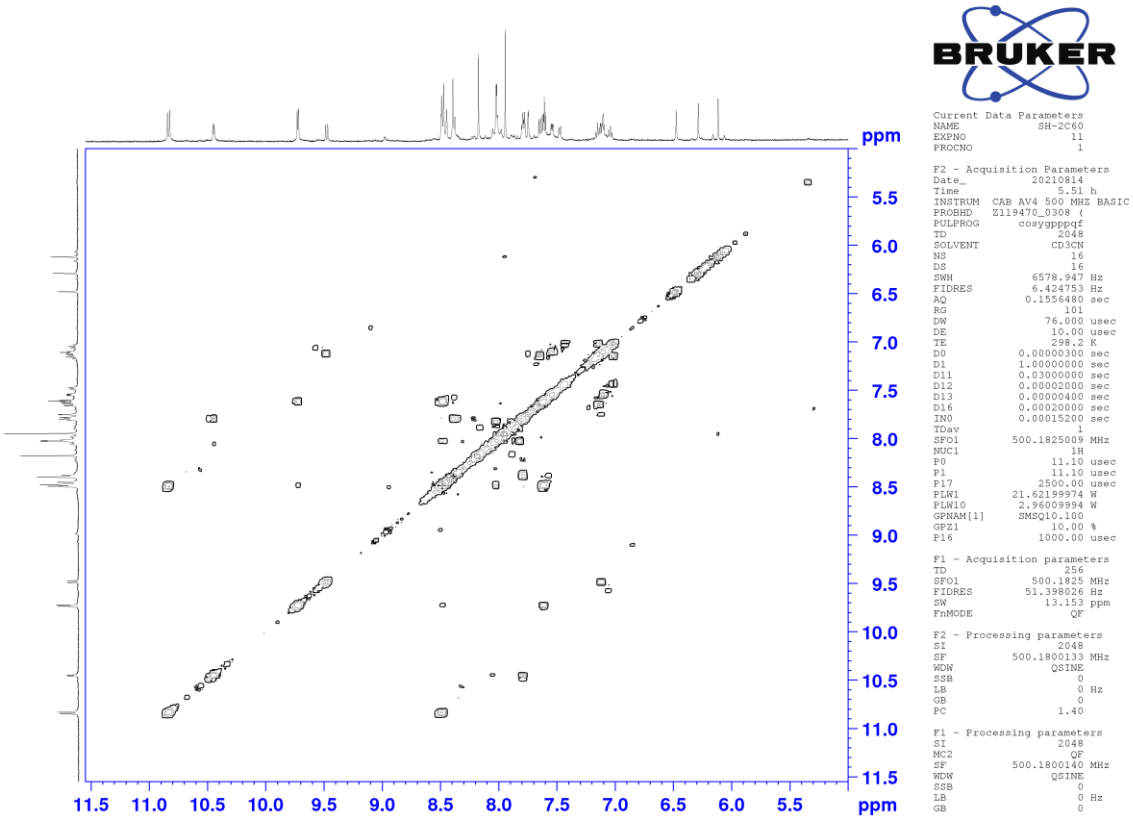

Figure 6.4.25 ^{1}H-^{1}H COSY NMR spectrum (500 MHz, 298 K, CD_3CN, 0.34 mM) of $(C_{60})_2$@$Pd_4L^{Q}_6(Nap)_2$

6.4.2.3.3 ^{1}H-^{1}H NOESY NMR spectrum of $(C_{60})_2$@$Pd_4L^{Q}_6(Nap)_2$

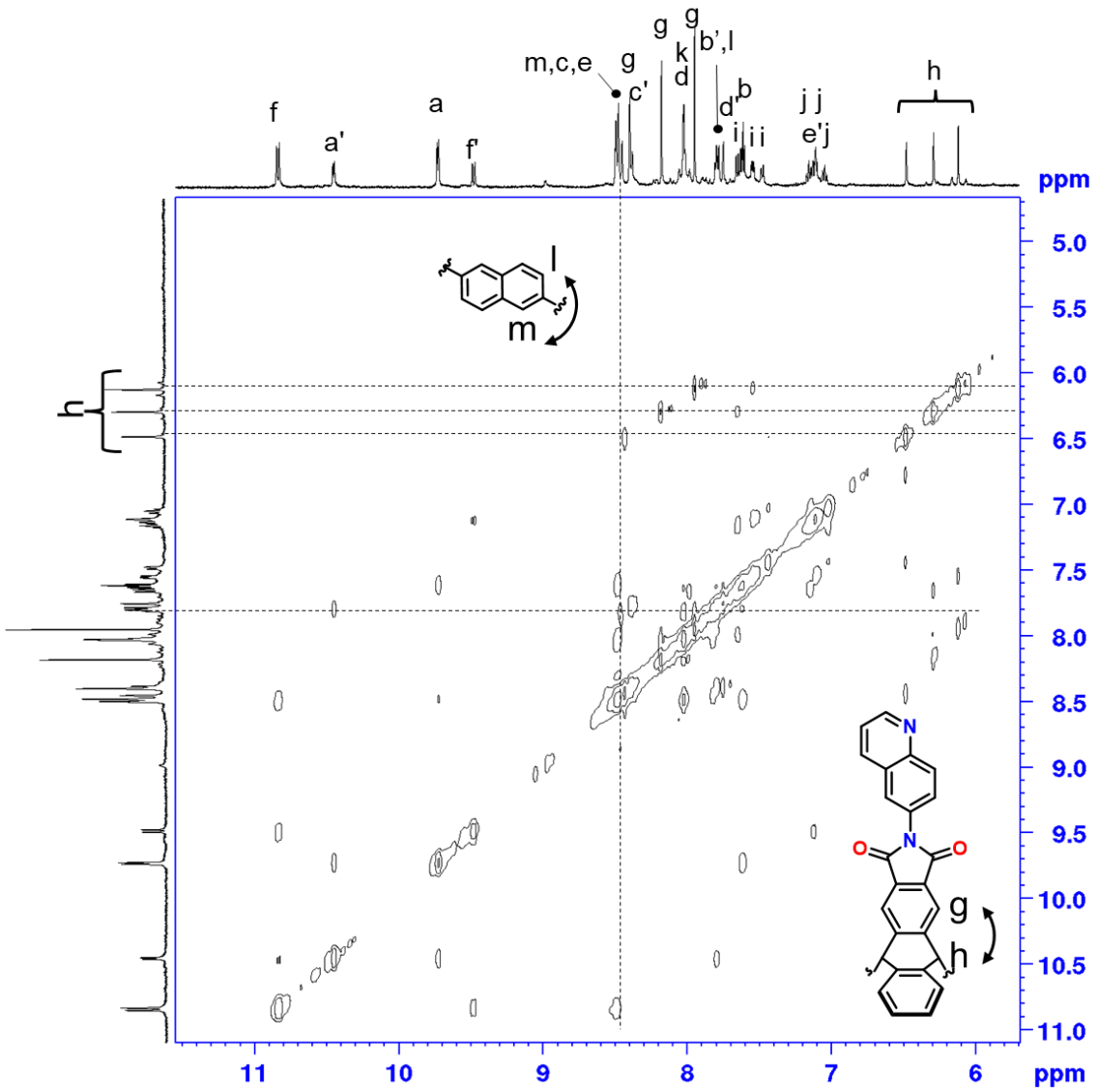

Figure 6.4.26 ^{1}H-^{1}H NOESY NMR spectrum (500 MHz, 298 K, CD_3CN, 0.34 mM) of $(C_{60})_2$@$Pd_4\mathbf{L}^{Q}_6(Nap)_2$

6.4.2.3.4 ^{13}C NMR spectrum of $(C_{60})_2@Pd_4L^Q_6(Nap)_2$

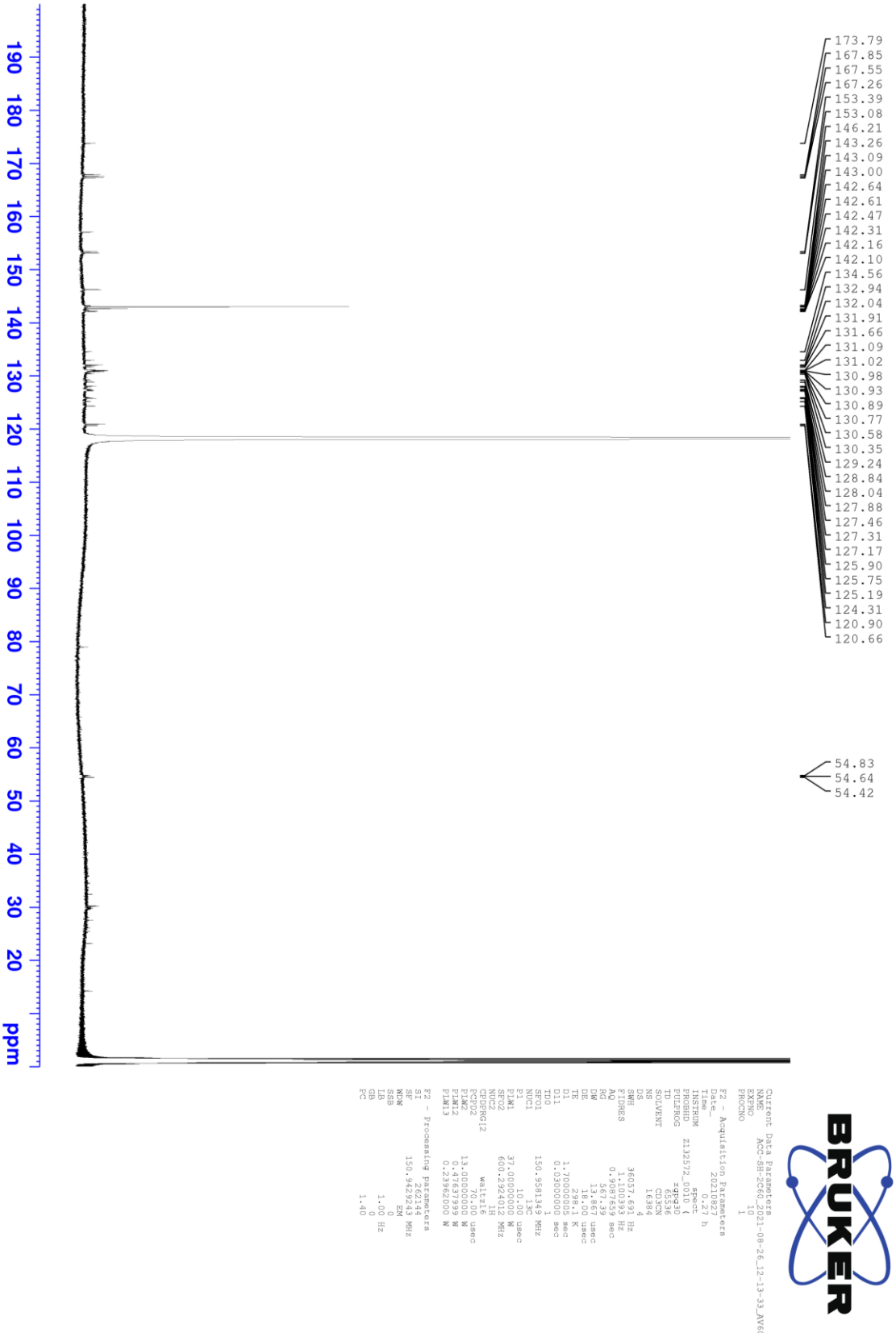

Figure 6.4.27 ^{13}C NMR spectrum (150 MHz, 298 K, CD_3CN, 0.34 mM) of $(C_{60})_2@Pd_4L^Q_6(Nap)_2$

6.4.2.3.5 ^{1}H DOSY NMR spectrum of $(C_{60})_2$@$Pd_4L^{Q}_6(Nap)_2$

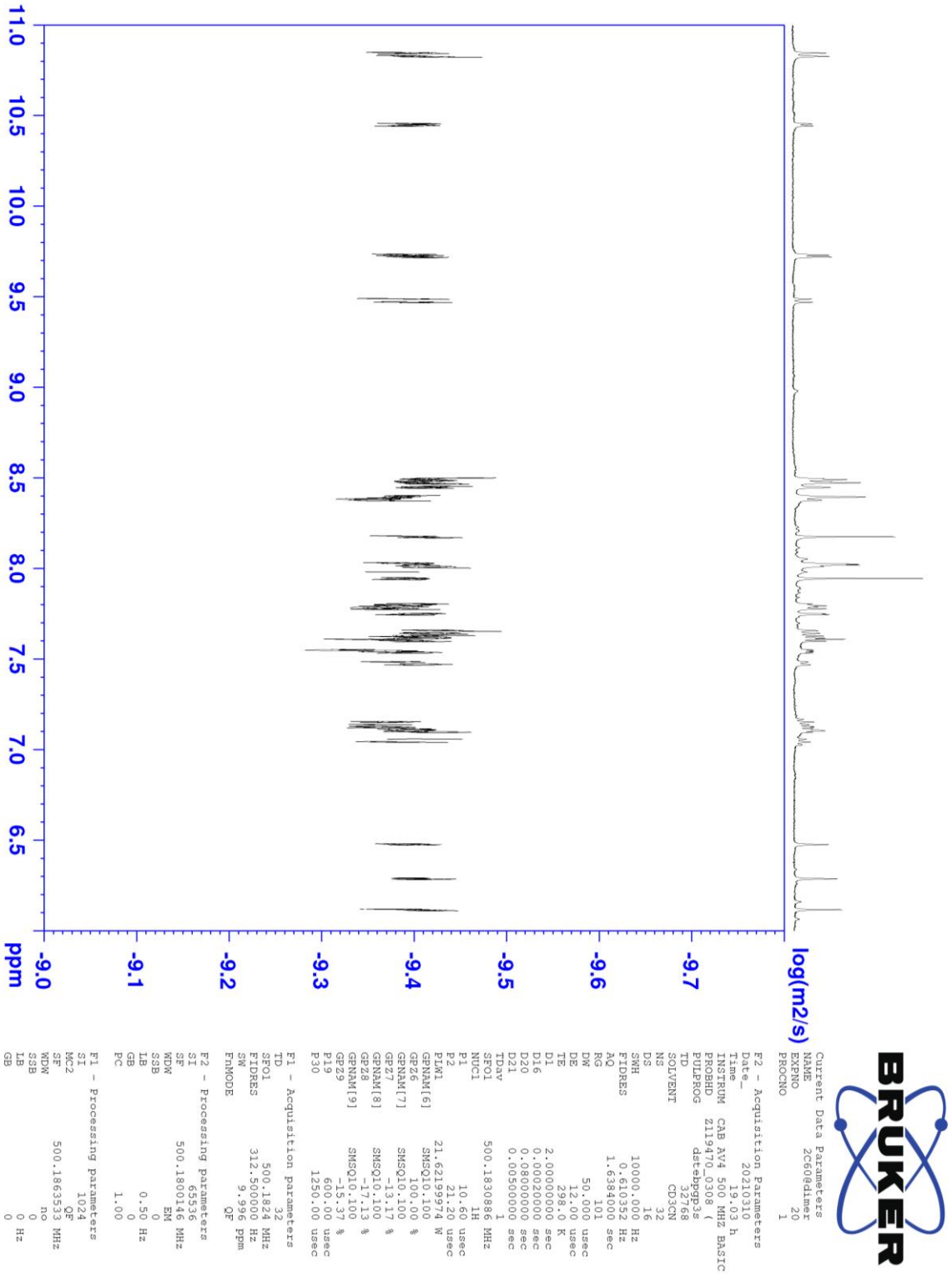

Figure 6.4.28 ^{1}H DOSY NMR spectrum (500 MHz, 298 K, CD_3CN, 0.34 mM) of $(C_{60})_2$@$Pd_4\mathbf{L}^{Q}_6(Nap)_2$

6.4.2.3.6 ESI-MS spectrum of $(C_{60})_2$@$Pd_4L^Q_6(Nap)_2$

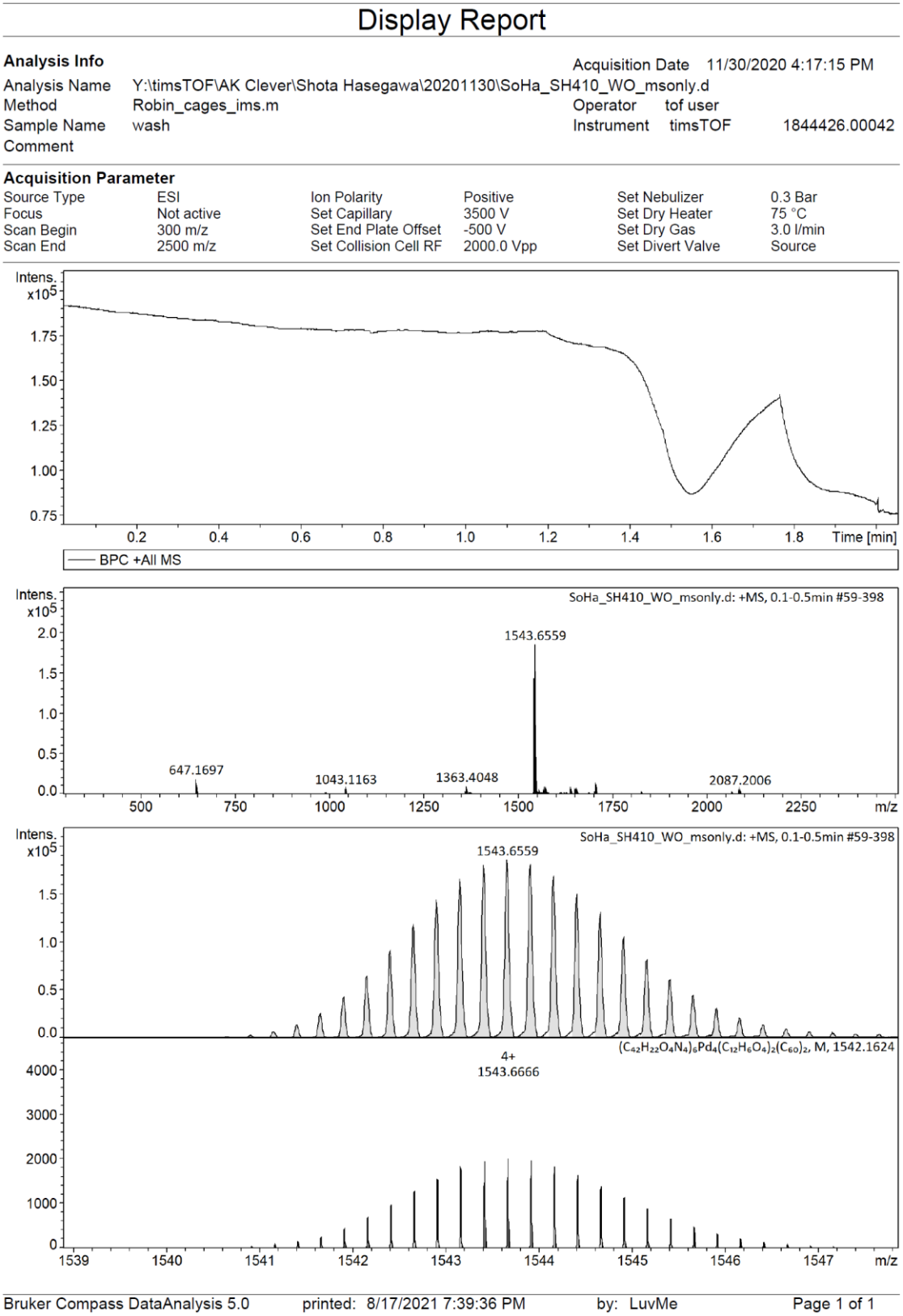

Figure 6.4.29 ESI-MS spectrum of $(C_{60})_2$@$Pd_4\mathbf{L}^Q_6(Nap)_2$ (positive)

6.4.2.4 Synthesis of C_{60}ant•C_{60}@$Pd_4L^Q_6(Nap)_2$

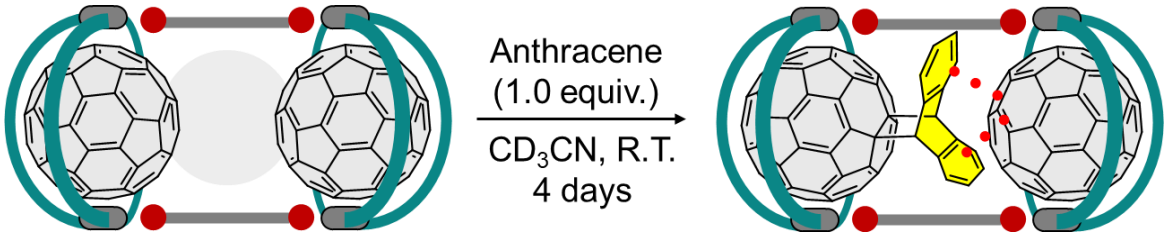

Figure 6.4.30 Synthesis of C_{60}ant•C_{60}@$Pd_4L^Q_6(Nap)_2$

To an acetonitrile solution of $(C_{60})_2$@$Pd_4L^Q_6(Nap)_2$ (0.34 mM, 621 μL, 0.21 μmol) in an NMR tube wrapped with alum foil, anthracene (20.0 mM in CD_3CN, 10.5 μL, 0.21 μmol) was added and the tube was shaken. The solution was let stand in dark for 4 days at ambient temperature. The desired heteromultimeric encapsulating cage dimer was obtained quantitatively.

^{1}H NMR (500 MHz, CD_3CN, 298 K): δ (ppm) 10.78 (d, J = 9.2 Hz, 4H) 10.68 (d, J = 9.2 Hz, 4H), 10.45 (br, 4H), 9.75 (dd, J = 5.6, 1.2 Hz, 4H), 9.61 (d, J = 9.2 Hz, 2H), 9.60 (dd, J = 5.6, 1.2 Hz, 4H), 9.24 (d, J = 9.2 Hz, 2H) 8.74-8.70 (m, 8H), 8.64 (dd, J = 5.6, 3.3 Hz, 4H),) 8.51-8.43 (m, 14H), 8.39-8.34 (m, 6H), 8.21 (s, 4H), 8.19-8.15 (m, 14H), 8.02 (d, J = 2.2 Hz, 4H) 7.99 (m, 2H), 7.96 (br, 8H), 7.93 (s, 4H), 7.90-7.87 (m, 4H), 7.83 (d, J = 8.0 Hz, 2H), 7.79-7.77 (m, 4H), 7.74-7.71 (m, 6H), 7.65-7.53 (m, 16H), 7.28-7.14 (m, 10H), 7.10 (m, 4H), 6.80 (dd, J = 9.2, 2.2 Hz, 2H), 6.72 (s, 2H), 6.61 (s, 2H), 6.38 (s, 2H), 6.35 (s, 2H), 6.31 (s, 2H), 6.13 (s, 2H), 6.11 (s, 2H);

^{13}C NMR Although we have tried to get the spectrum, a clear spectrum could not be observed even with 12000 scans due to the concentration of the sample.;

DOSY: Diffusion coefficient D = 3.66 × 10^{-10} m^2s^{-1}, hydrodynamic radius r_H was calculated to be 17.8 Å

ESI MS calcd. for $[(C_{42}H_{22}N_4O_4)_6Pd_4(C_{12}H_6O_4)_2(C_{60})_2(C_{14}H_{10})]^{4+}$ 1588.1862, found 1588.1630 $[C_{60}ant \cdot C_{60}@Pd_4L^Q_6(Nap)_2]^{4+}$.

6.4.2.4.1 ^{1}H NMR spectra of C_{60}ant•C_{60}@$Pd_4L^{Q}_6(Nap)_2$

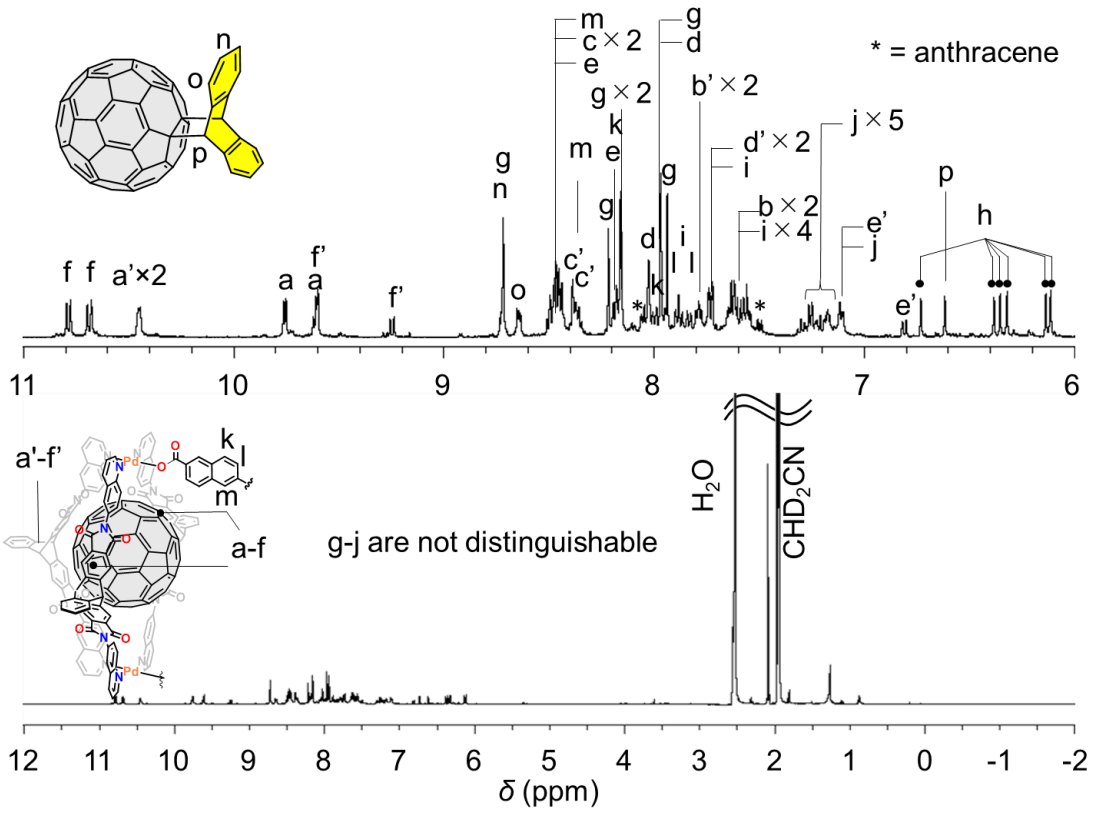

Figure 6.4.31 ^{1}H NMR spectra (500 MHz, 298 K, CD_3CN, 0.34 mM) of C_{60}ant•C_{60}@$Pd_4\mathbf{L}^{Q}_6(Nap)_2$

δ (ppm) 10.78 (d, *J* = 9.2 Hz, 4H) 10.68 (d, *J* = 9.2 Hz, 4H), 10.45 (br, 4H), 9.75 (dd, *J* = 5.6, 1.2 Hz, 4H), 9.61 (d, *J* = 9.2 Hz, 2H), 9.60 (dd, *J* = 5.6, 1.2 Hz, 4H), 9.24 (d, *J* = 9.2 Hz, 2H) 8.74-8.70 (m, 8H), 8.64 (dd, *J* = 5.6, 3.3 Hz, 4H), 8.51-8.43 (m, 14H), 8.39-8.34 (m, 6H), 8.21 (s, 4H), 8.19-8.14 (m, 14H), 8.02 (d, *J* = 2.2 Hz, 4H) 7.99 (m, 2H), 7.96 (br, 8H), 7.93 (s, 4H), 7.90-7.87 (m, 4H), 7.83 (d, *J* = 8.0 Hz, 2H), 7.79-7.77 (m, 4H), 7.74-7.71 (m, 6H), 7.65-7.53 (m, 16H), 7.28-7.14 (m, 10H), 7.10 (m, 4H), 6.80 (dd, *J* = 9.2, 2.2 Hz, 2H), 6.72 (s, 2H), 6.61 (s, 2H), 6.38 (s, 2H), 6.35 (s, 2H), 6.31 (s, 2H), 6.13 (s, 2H), 6.11 (s, 2H)

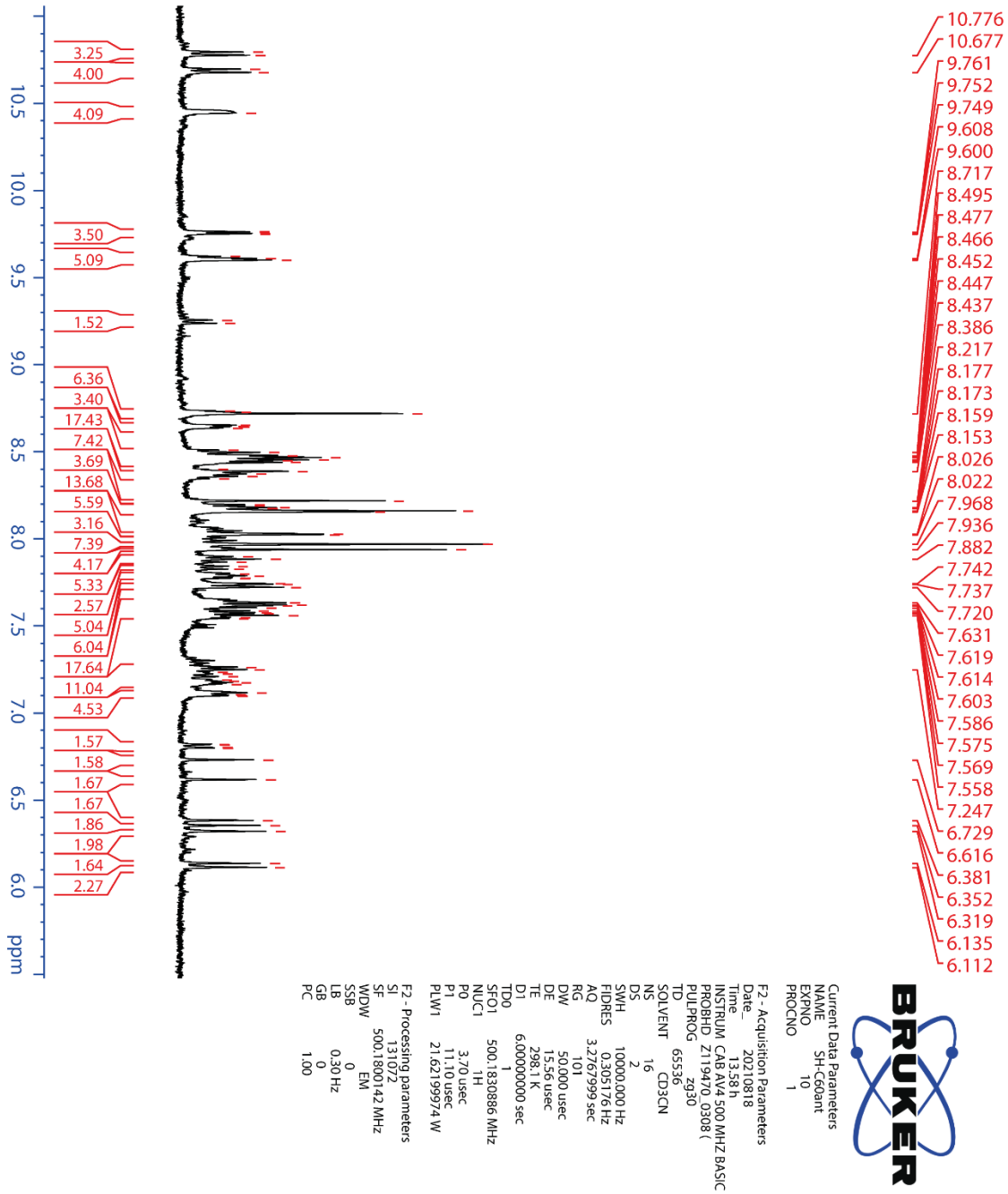

Figure 6.4.32 ^{1}H NMR spectrum (500 MHz, 298 K, CD_3CN, 0.34 mM) of C_{60}ant•C_{60}@$Pd_4L^{Q}_6(Nap)_2$

6.4.2.4.2 ^{1}H-^{1}H COSY NMR spectrum of C_{60}ant•C_{60}@$Pd_4L^{Q}_6(Nap)_2$

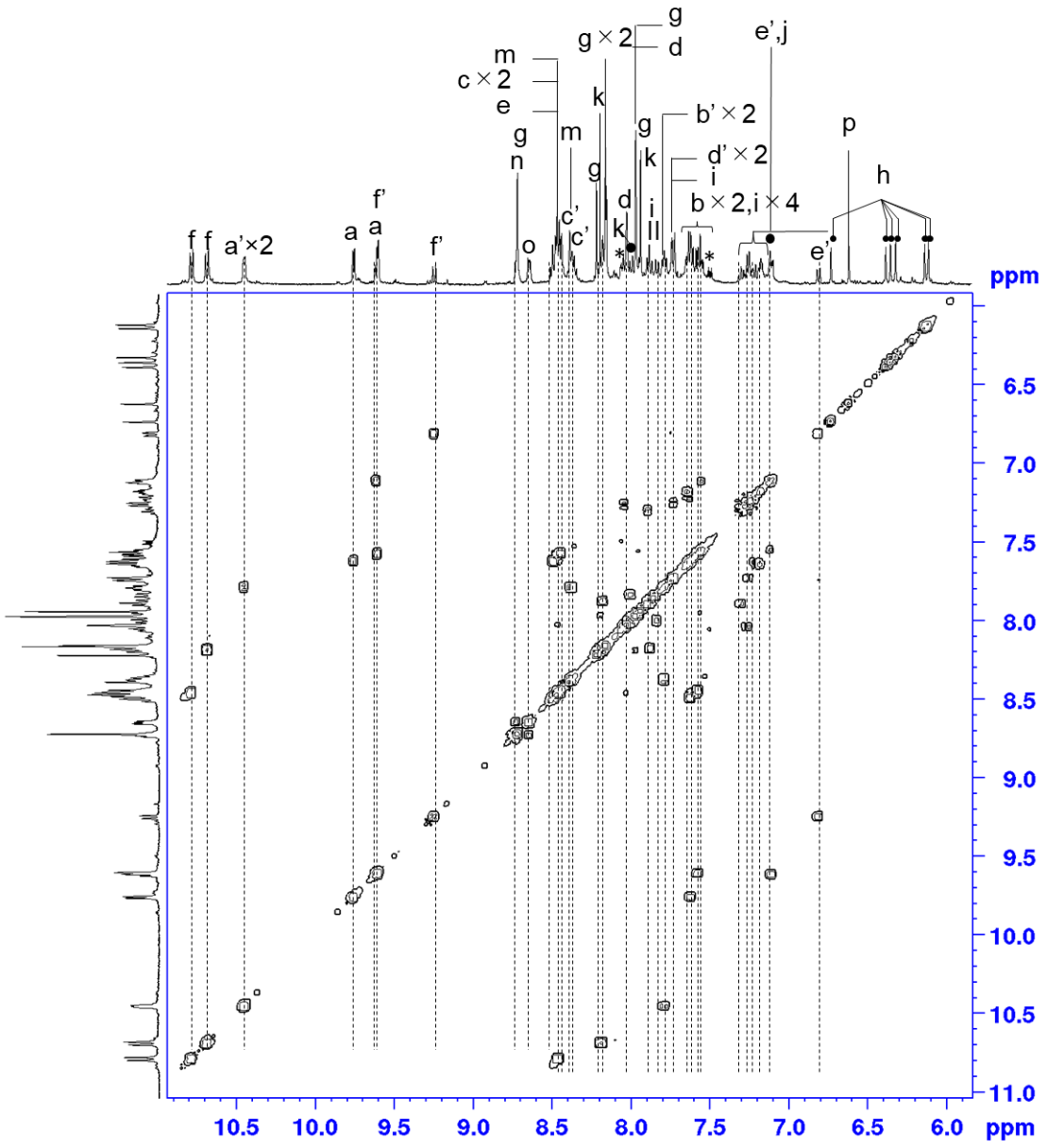

Figure 6.4.33 ^{1}H-^{1}H COSY NMR spectrum (500 MHz, 298 K, CD_3CN, 0.34 mM) of C_{60}ant•C_{60}@$Pd_4\mathbf{L}^{Q}_6(Nap)_2$

6.4.2.4.3 ^{1}H-^{1}H NOESY NMR spectrum of C_{60}ant•C_{60}@$Pd_4L^{Q}_6(Nap)_2$

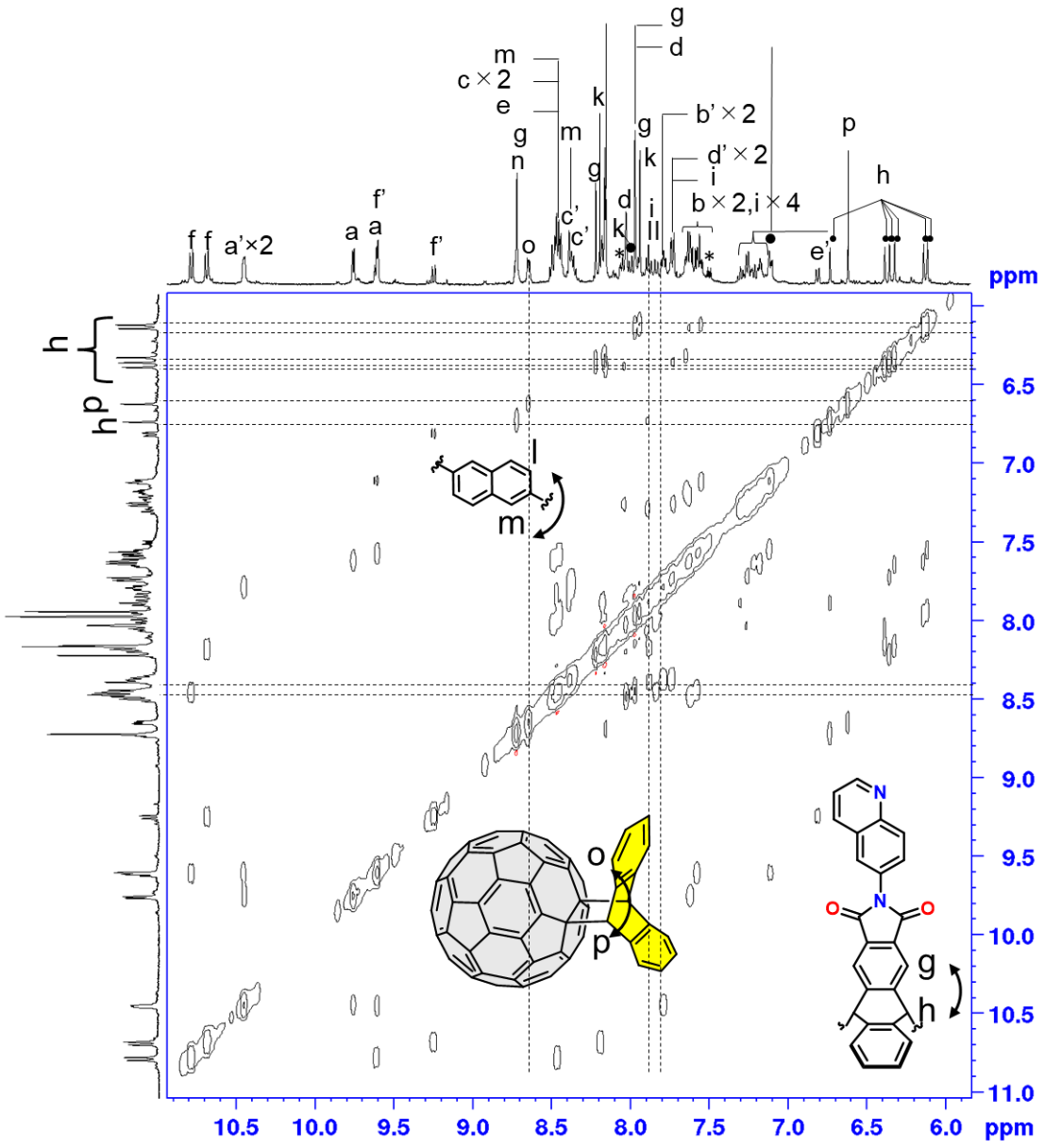

Figure 6.4.34 ^{1}H-^{1}H NOESY spectrum (500 MHz, 298 K, CD_3CN, 0.34 mM) of C_{60}ant•C_{60}@$Pd_4L^{Q}_6(Nap)_2$

6.4.2.4.4 ^{1}H DOSY NMR spectrum of C_{60}ant•C_{60}@$Pd_4L^{Q}_6(Nap)_2$

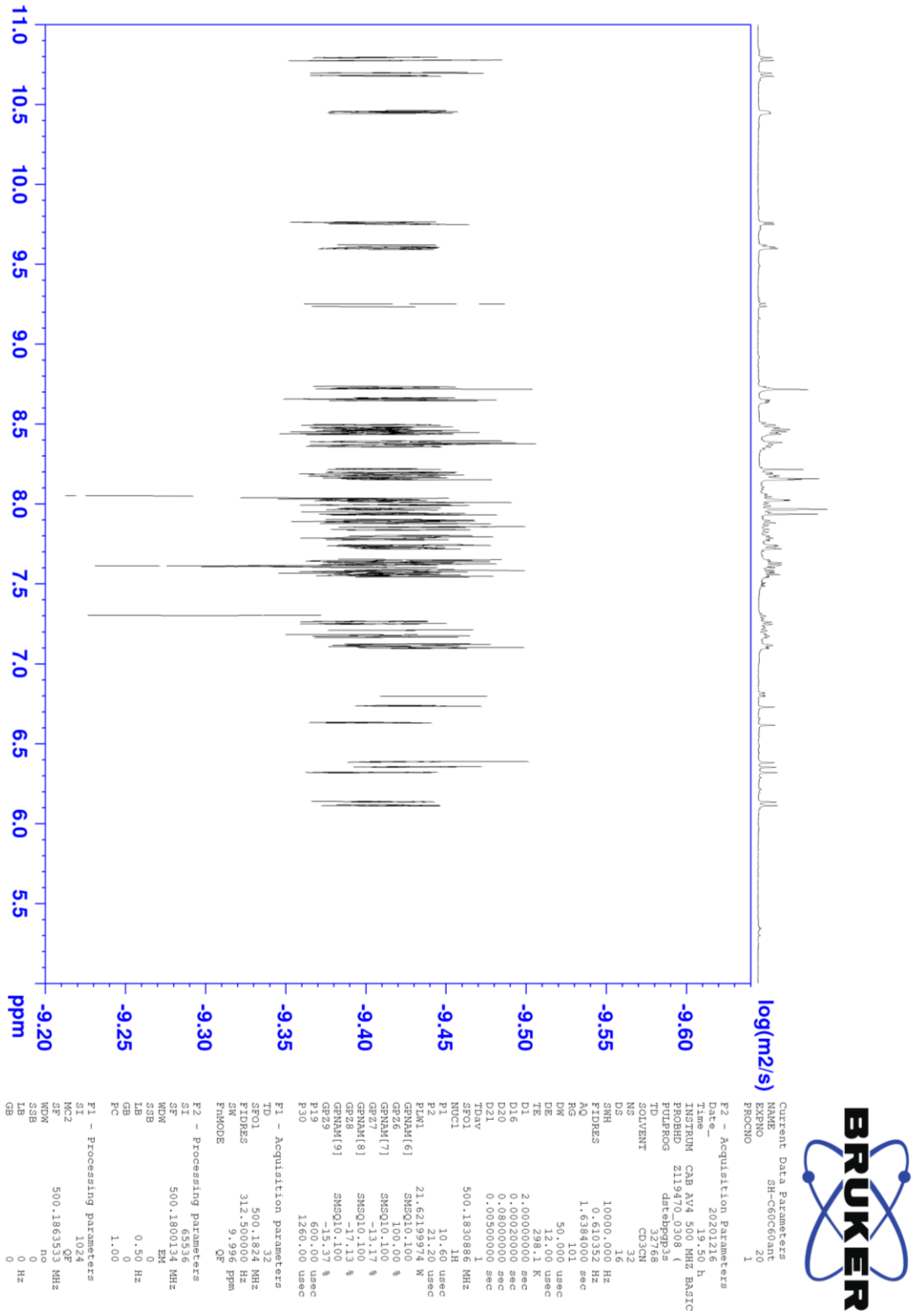

Figure 6.4.35 ^{1}H DOSY NMR spectrum (500 MHz, 298 K, CD_3CN, 0.34 mM) of C_{60}ant•C_{60}@$Pd_4L^{Q}_6(Nap)_2$

6.4.2.4.5 ESI-MS spectrum of C_{60}ant•C_{60}@$Pd_4L^Q_6(Nap)_2$

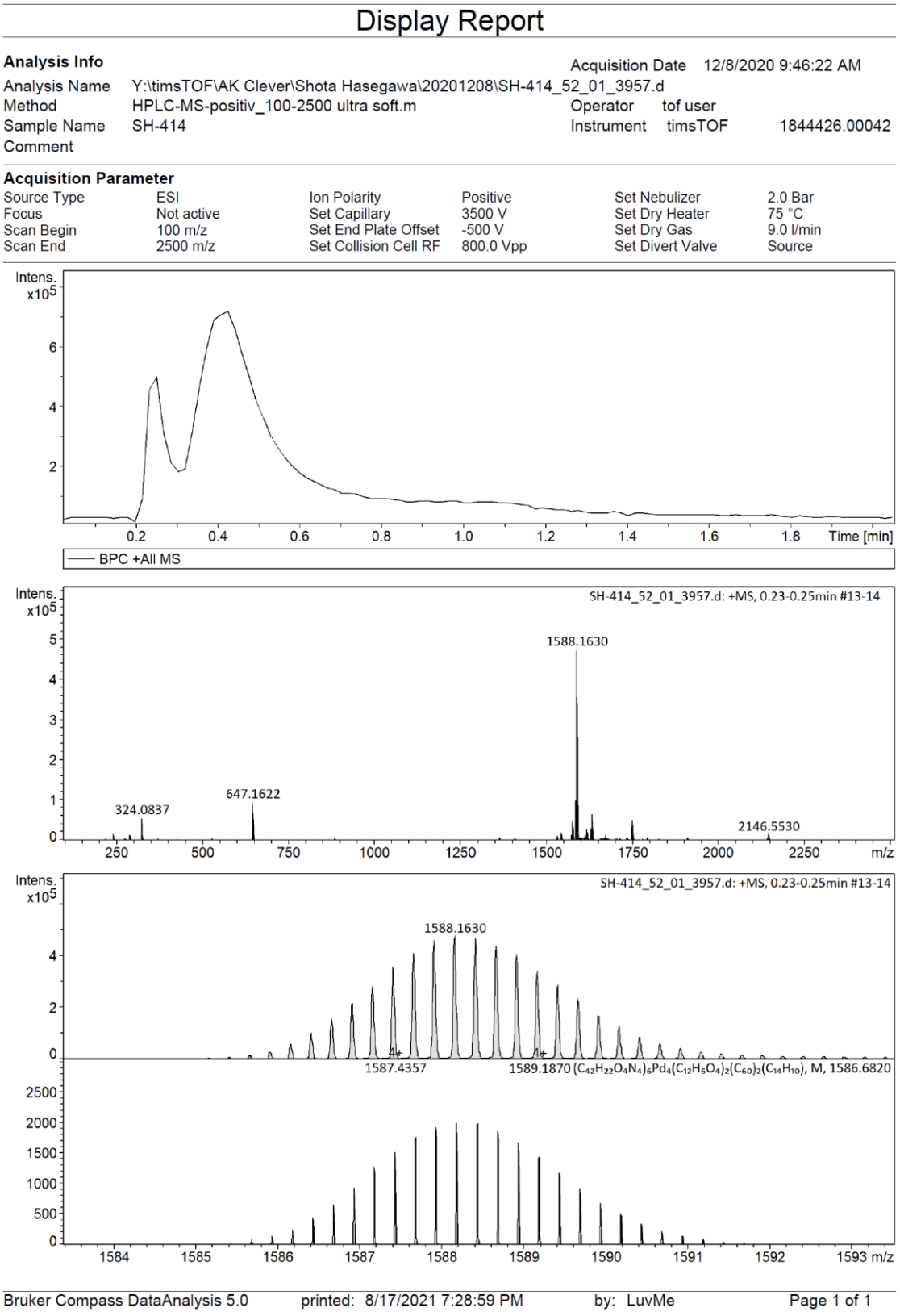

Figure 6.4.36 ESI-MS spectrum of C_{60}ant•C_{60}@$Pd_4\mathbf{L}^Q_6(Nap)_2$ (positive)

6.4.2.5 Synthesis of C_{60}DMA•C_{60}@$Pd_4L^Q_6(Nap)_2$

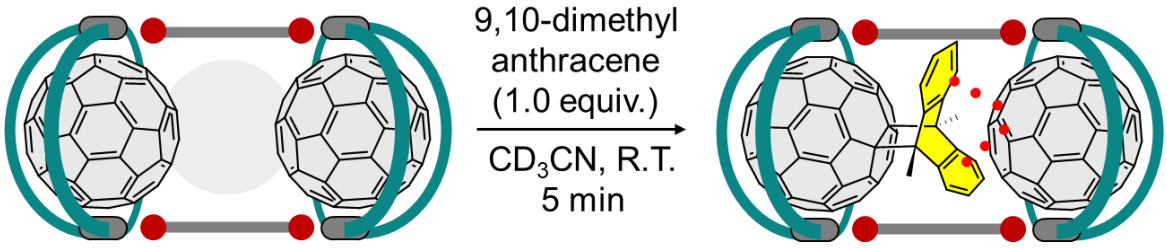

Figure 6.4.37 Synthesis of C_{60}DMA•C_{60}@$Pd_4L^Q_6(Nap)_2$

To an acetonitrile solution of $(C_{60})_2$@$Pd_4L^Q_6(Nap)_2$ (0.34 mM, 621 μL, 0.21 μmol) in an NMR tube wrapped with alum foil, 9,10-dimethylanthracene (20.0 mM in CD_3CN, 10.5 μL, 0.21 μmol) was added and the tube was shaken in the dark. The desired heteromultimeric encapsulating cage dimer was obtained quantitatively.

^{1}H NMR (500 MHz, CD_3CN, 298 K): δ (ppm) 10.77 (d, J = 9.2 Hz, 4H), 10.75 (d, J = 9.2 Hz, 4H), 10.49 (d, J = 5.6, 1.2 Hz, 2H), 10.44 (d, J = 5.6, 1.2 Hz, 2H), 9.76 (dd, J = 5.6, 1.2 Hz, 4H), 9.61 (d, J = 9.2 Hz, 2H), 9.56 (dd, J = 5.6, 1.2 Hz, 4H), 9.20 (d, J = 9.2 Hz, 2H), 8.83 (dd, J = 6.0, 3.1 Hz, 4H), 8.77 (s, 4H), 8.69 (dd, J = 6.0, 3.1 Hz, 4H), 8.50-8.42 (m, 14H), 8.39-8.34 (m, 6H), 8.24 (dd, 9.2, 2.3 H, 4H), 8.21 (s, 4H), 8.18 (d, J = 8.5 Hz, 2H), 8.16 (s, 4H), 8.15 (s, 4H), 8.06 (d, J = 7.5 Hz, 2H), 8.02 (d, J = 2.3 Hz, 4H), 7.98 (d, J = 2.3 Hz, 4H), 7.95 (s, 4H), 7.93 (s, 4H), 7.89 (d, J = 8.8 Hz, 2H), 7.87 (d, J = 7.5 Hz, 2H), 7.83 (d, J = 8.8 Hz, 2H), 7.79 (m, 4H), 7.74-7.70 (m, 4H), 7.65-7.60 (m, 8H), 7.58-7.53 (m, 6H) 7.28-7.15 (m, 10H), 7.13-7.09 (m, 4H). 6.74 (s, 2H), 6.73 (dd, 9.2, 2.3 H, 2H), 6.39 (s, 2H), 6.35 (s, 2H), 6.31 (s, 2H), 6.12 (s, 2H), 6.10 (s, 2H), 3.52 (s, 6H);

^{13}C NMR Although we have tried to get the spectrum, a clear spectrum could not be obtained due to the low concentration of the sample;

DOSY: Diffusion coefficient D = 3.98 × 10^{-10} m^2s^{-1}, hydrodynamic radius r_H was calculated to be 16.4 Å

ESI MS calcd. for $[(C_{42}H_{22}N_4O_4)_6Pd_4(C_{12}H_6O_4)_2(C_{60})_2(C_{16}H_{14})]^{4+}$ 1595.1941, found 1595.1870 [C_{60}DMA•C_{60}@$Pd_4L^Q_6(Nap)_2]^{4+}$.

6.4.2.5.1 ^{1}H NMR spectra of C_{60}DMA•C_{60}@$Pd_4L^{Q}_6(Nap)_2$

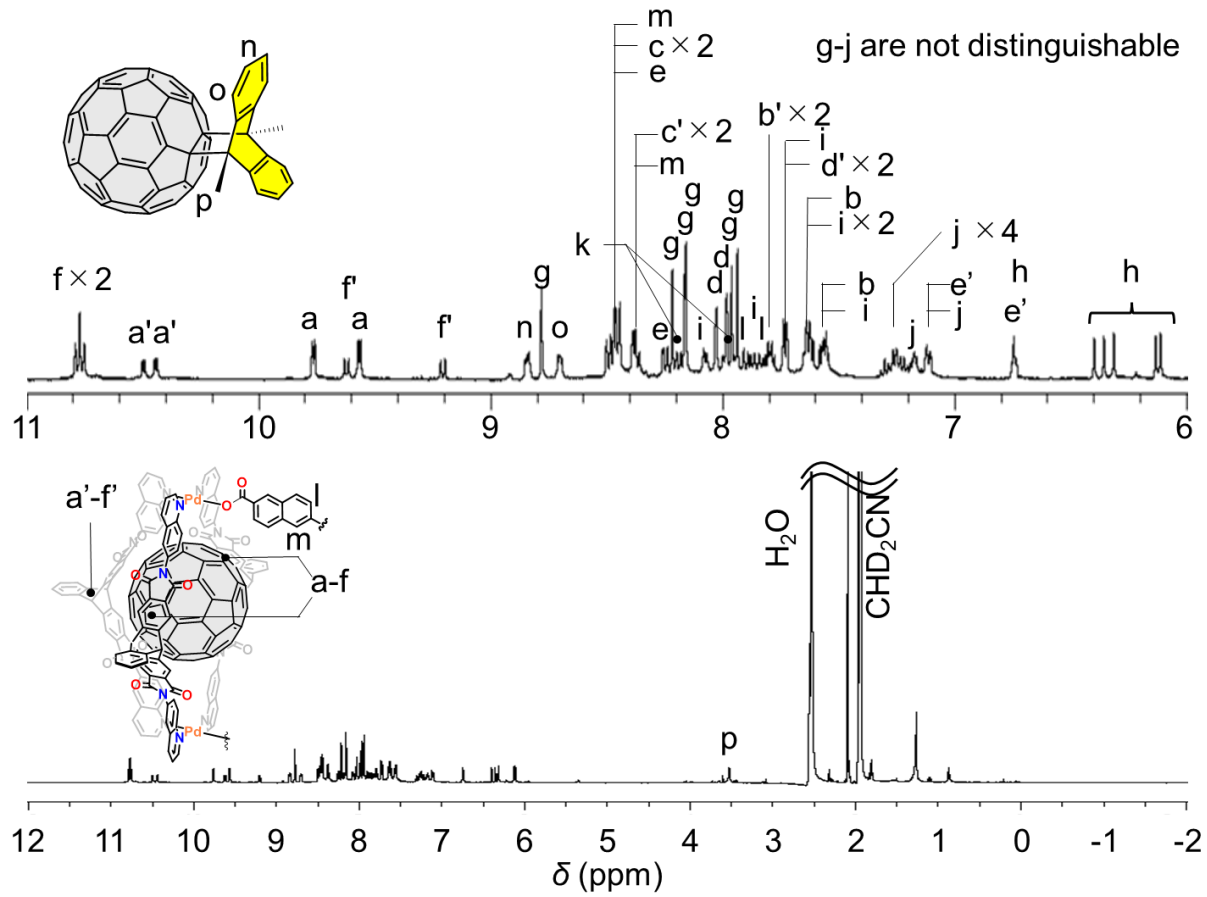

Figure 6.4.38 ^{1}H NMR spectra (500 MHz, 298 K, CD_3CN, 0.33 mM) of C_{60}DMA•C_{60}@$Pd_4L^{Q}_6(Nap)_2$

δ (ppm) 10.77 (d, *J* = 9.2 Hz, 4H), 10.75 (d, *J* = 9.2 Hz, 4H), 10.49 (d, *J* = 5.6, 1.2 Hz, 2H), 10.44 (d, *J* = 5.6, 1.2 Hz, 2H), 9.76 (dd, *J* = 5.6, 1.2 Hz, 4H), 9.61 (d, *J* = 9.2 Hz, 2H), 9.56 (dd, *J* = 5.6, 1.2 Hz, 4H), 9.20 (d, *J* = 9.2 Hz, 2H), 8.83 (dd, *J* = 6.0, 3.1 Hz, 4H), 8.77 (s, 4H), 8.69 (dd, *J* = 6.0, 3.1 Hz, 4H), 8.50-8.42 (m, 14H), 8.39-8.34 (m, 6H), 8.24 (dd, 9.2, 2.3 H, 4H), 8.21 (s, 4H), 8.18 (d, *J* = 8.5 Hz, 2H), 8.16 (s, 4H), 8.15 (s, 4H), 8.06 (d, *J* = 7.5 Hz, 2H), 8.02 (d, *J* = 2.3 Hz, 4H), 7.98 (d, *J* = 2.3 Hz, 4H), 7.95 (s, 4H), 7.93 (s, 4H), 7.89 (d, *J* = 8.8 Hz, 2H), 7.87 (d, *J* = 7.5 Hz, 2H), 7.83 (d, *J* = 8.8 Hz, 2H), 7.79 (m, 4H), 7.74-7.70 (m, 6H), 7.65-7.60 (m, 8H), 7.58-7.53 (m, 6H) 7.28-7.15 (m, 10H), 7.13-7.09 (m, 4H). 6.74 (s, 2H), 6.73 (dd, 9.2, 2.3 H, 2H), 6.39 (s, 2H), 6.35 (s, 2H), 6.31 (s, 2H), 6.12 (s, 2H), 6.10 (s, 2H), 3.52 (s, 6H)

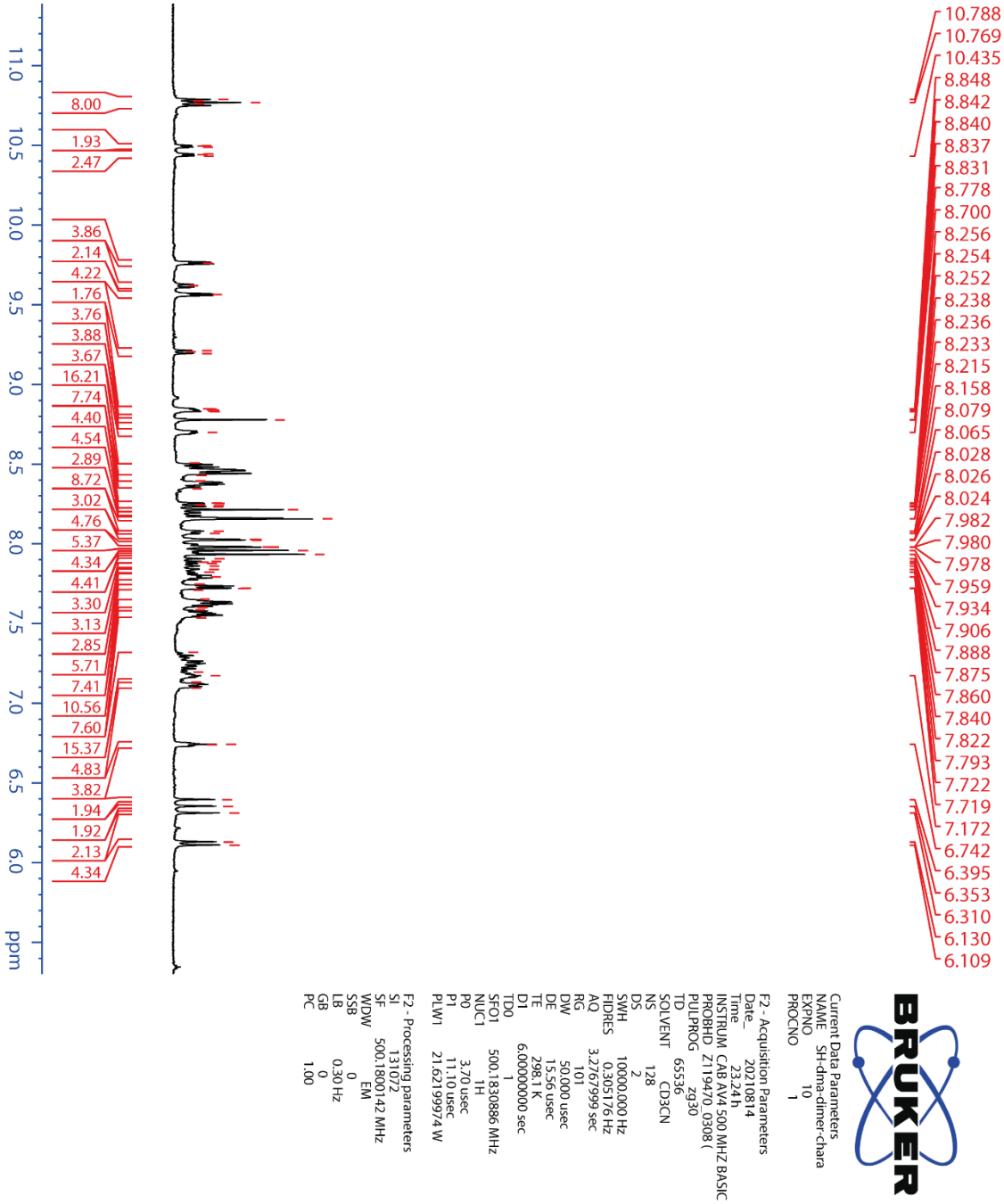

Figure 6.4.39 ^{1}H NMR spectrum (500 MHz, 298 K, CD_3CN, 0.33 mM) of $C_{60}DMA{\bullet}C_{60}@Pd_4\mathbf{L}^{Q}_6(Nap)_2$

6.4.2.5.2 ^{1}H-^{1}H COSY NMR spectrum of C_{60}DMA•C_{60}@$Pd_4L^{Q}_6(Nap)_2$

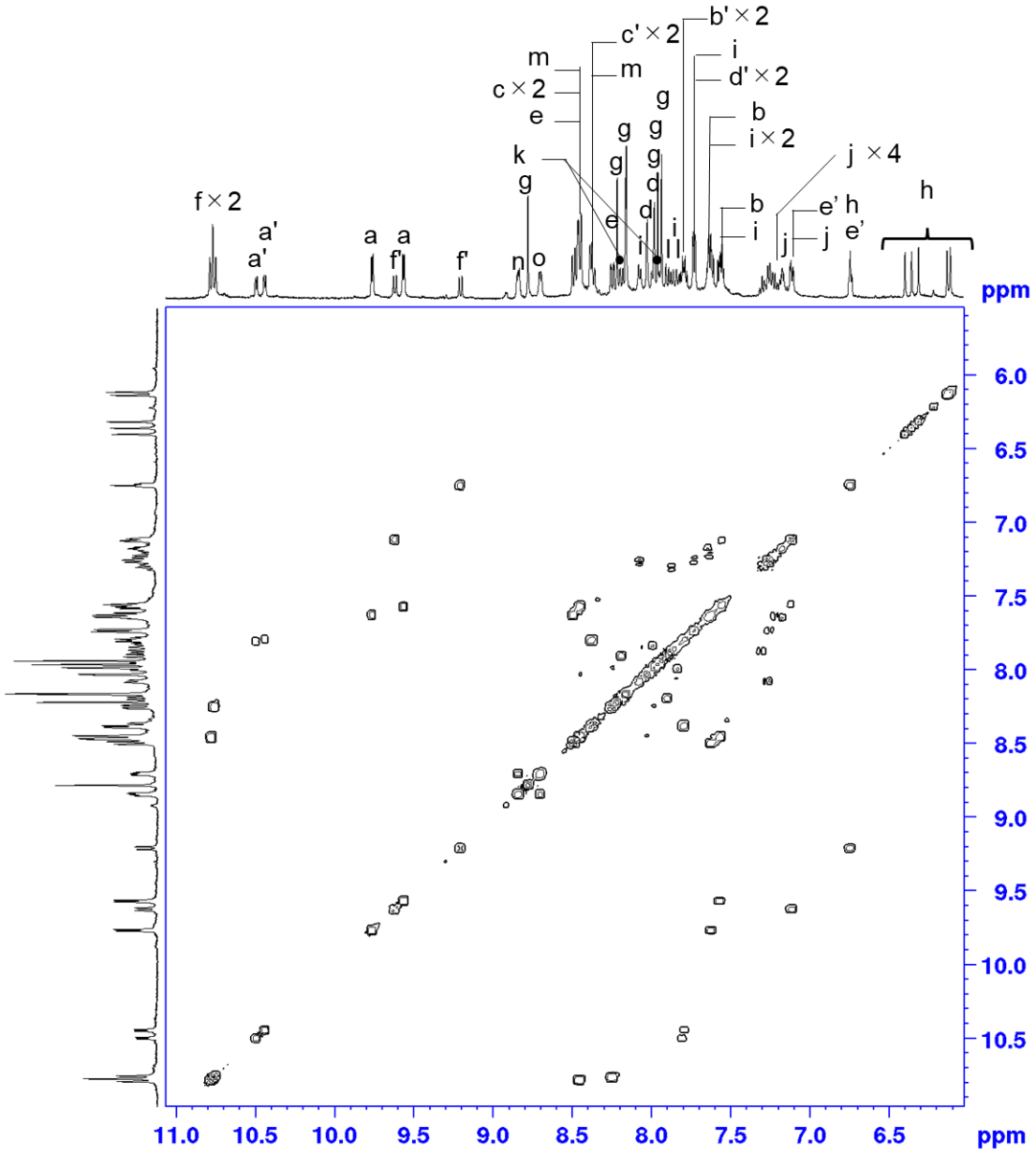

Figure 6.4.40 ^{1}H-^{1}H COSY NMR spectrum of C_{60}DMA•C_{60}@$Pd_4\mathbf{L}^{Q}_6(Nap)_2$ (500 MHz, 298 K, CD_3CN, 0.33 mM)

6.4.2.5.3 ^{1}H-^{1}H NOESY NMR spectrum of C_{60}ant•C_{60}@$Pd_4L^{Q}_6$(Nap)$_2$

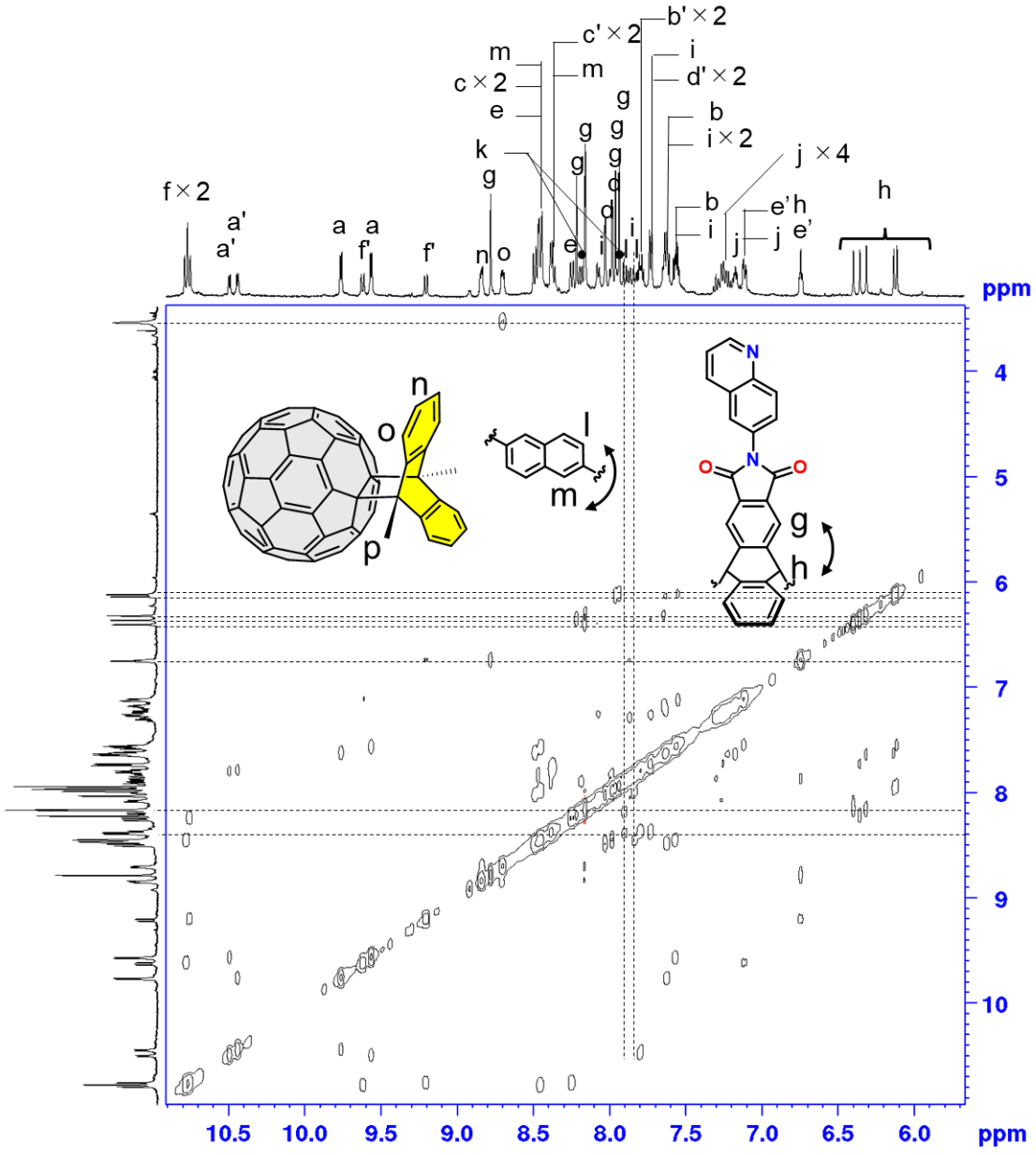

Figure 6.4.41 ^{1}H-^{1}H NOESY NMR spectrum of C_{60}DMA•C_{60}@$Pd_4L^{Q}_6$(Nap)$_2$ (500 MHz, 298 K, CD_3CN, 0.33 mM)

6.4.2.5.4 ^{1}H DOSY NMR spectrum of C_{60}DMA•C_{60}@$Pd_4L^{Q}_6(Nap)_2$

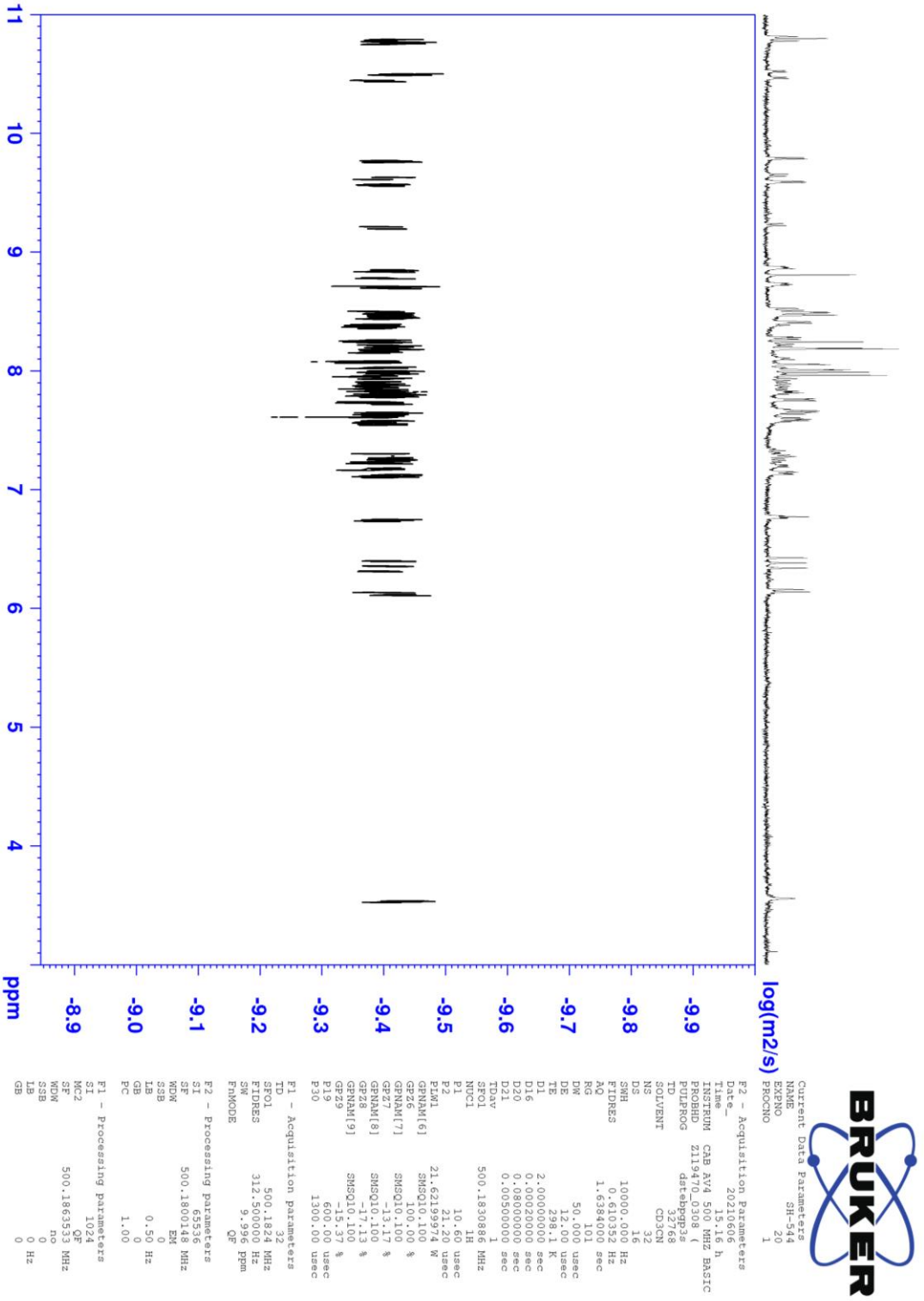

Figure 6.4.42 ^{1}H DOSY NMR spectrum (500 MHz, 298 K, CD_3CN, 0.33 mM) of C_{60}DMA•C_{60}@$Pd_4\mathbf{L}^{Q}_6(Nap)_2$

6.4.2.5.5 ESI-MS spectrum of $C_{60}DMA•C_{60}@Pd_4L^Q_6(Nap)_2$

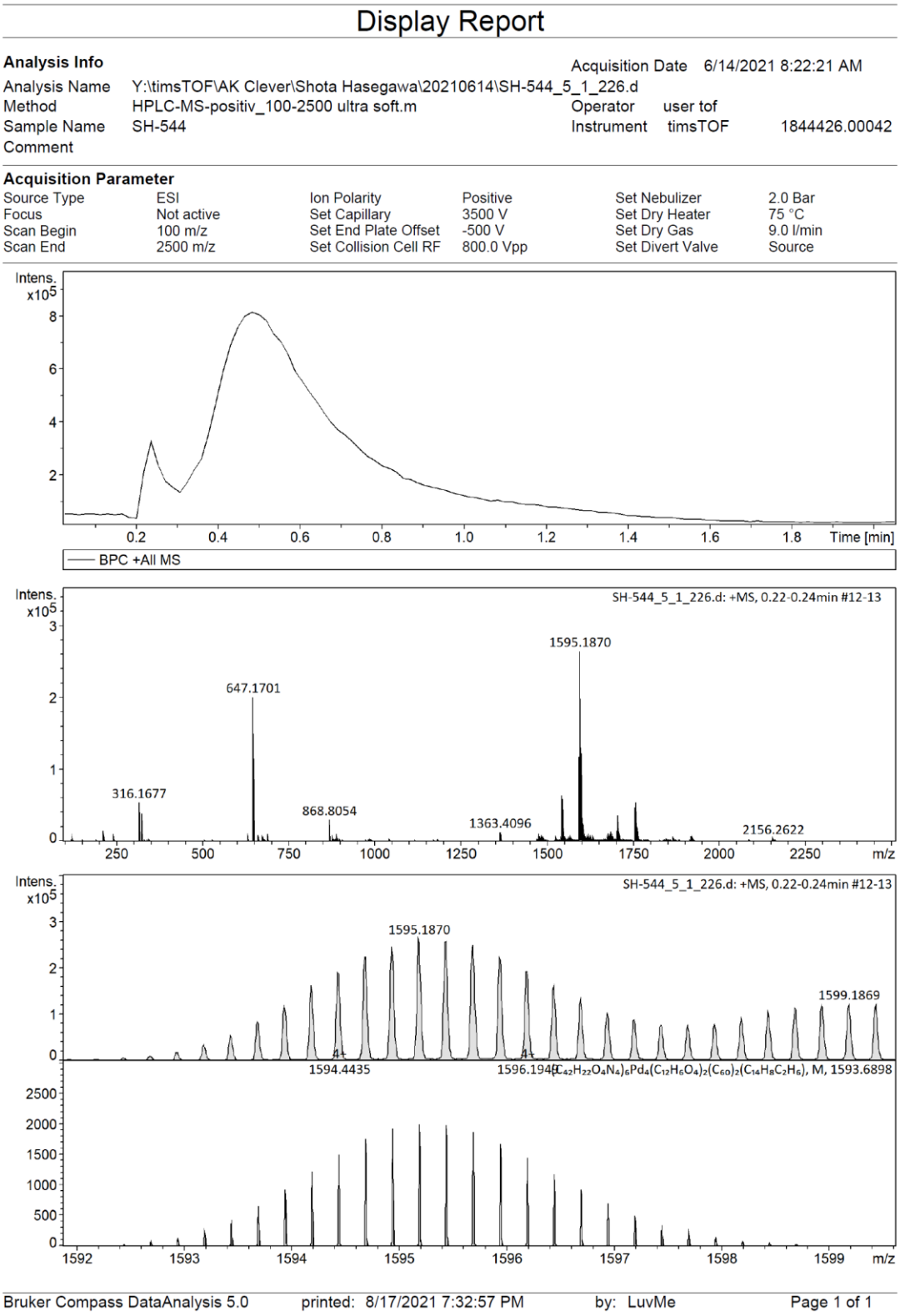

Figure 6.4.43 ESI-MS spectrum of $C_{60}DMA•C_{60}@Pd_4L^Q_6(Nap)_2$ (positive)

6.4.3 X-ray Crystallography

$(C_{60})_2$@Pd_4**L**$^{Q}_6$$(Nap)_2$ were studied using single-crystal X-ray diffraction. Due to very thin plate or needle-shaped crystals, the analysis was hampered by the limited scattering power of the samples not allowing to reach the desired (sub-)atomic resolution using our modern micro-focused X-ray Cu-K_α in-house source. Gaining detailed structural insight thus required cryogenic crystal handling and highly brilliant synchrotron radiation. Hence, diffraction data of was collected during at macromolecular synchrotron beamline P11, PETRA III, DESY.[29] Counterion and solvent flexibility required carefully adapted macromolecular refinement protocols employing geometrical restraint dictionaries, similarity restraints and restraints for anisotropic displacement parameters (ADPs). The crystal structures were refined and deposited on the CCDC database by Dr. Julian J. Holstein. In addition, the following detail description of the refinement was contributed by Dr. Julian J. Holstein.

Compound	$(C_{60})_2$@Pd_4**L**$^{Q}{}_6$$(Nap)_2$
CIF ID	**sha15b**
CCDC number	**2130013**
Empirical formula	$C_{452}H_{201}B_4F_{16}N_{25}O_{32}Pd_4$
Formula weight	7266.21
Temperature [K]	100(2)
Crystal system	triclinic
Space group (number)	$P\bar{1}$ (2)
a [Å]	18.797(4)
b [Å]	24.047(5)
c [Å]	42.680(9)
α [Å]	81.59(3)
β [Å]	77.30(3)
γ [Å]	74.29(3)
Volume [Å^3]	18040(7)
Z	2
ρ_{calc} [g/cm^3]	1.338
μ [mm^{-1}]	0.738
F(000)	7384
Crystal size [mm^3]	0.020×0.020×0.010
Crystal colour	purple
Crystal shape	block
Radiation	synchrotron (λ=1.0332 Å)
2Θ range [°]	1.43 to 55.60 (1.11 Å)
Index ranges	-16 ≤ h ≤ 16 -21 ≤ k ≤ 21 -36 ≤ l ≤ 36
Reflections collected	63819
Independent reflections	18379 R_{int} = 0.0425 R_{sigma} = 0.0396
Completeness	66.1 %
Data / Restraints / Parameters	18379/56046/5006
Goodness-of-fit on F^2	1.800
Final *R* indexes	R_1 = 0.1116
[I≥2σ(I)]	wR_2 = 0.3465
Final *R* indexes	R_1 = 0.1228
[all data]	wR_2 = 0.3610
Largest peak/hole [eÅ^3]	0.97/-0.48

6.4.3.1 $(C_{60})_2@Pd_4L^Q_6(Nap)_2$

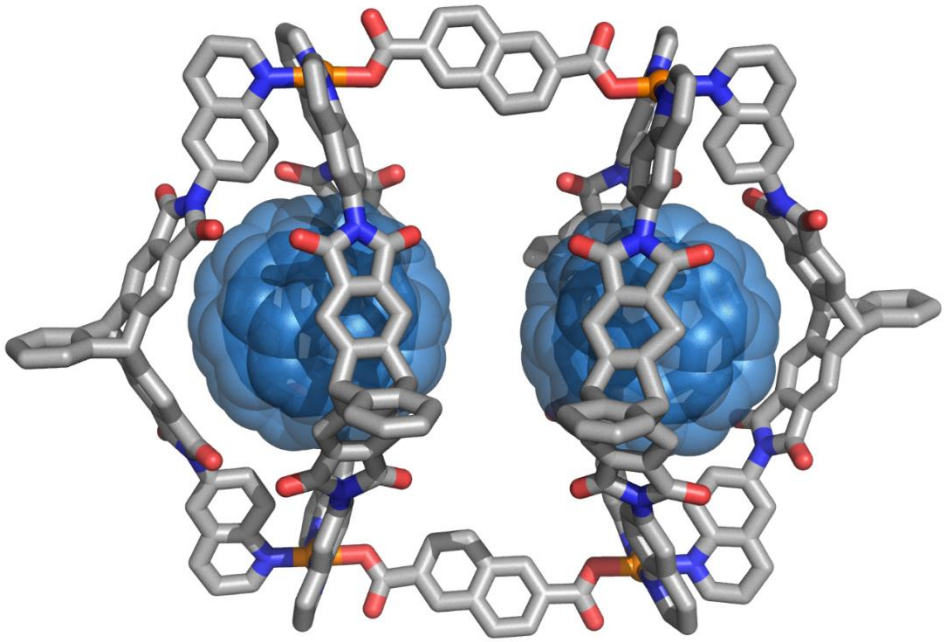

Figure 6.4.44 X-ray structure of $(C_{60})_2@Pd_4\mathbf{L}^Q_6(Nap)_2$. One of two independent supramolecular assemblies in the asymmetric unit is shown. Co-crystallised tetrafluoroborate counter anions, benzene and acetonitrile solvent molecules as well as hydrogen atoms are omitted for clarity. Color scheme: C (gray), N (blue), O (red), and Pd (orange)

Single crystals were grown by slow diffusion of benzene into a solution of $(C_{60})_2@Pd_4\mathbf{L}^Q_6(Nap)_2$ in acetonitrile. A single crystal of $(C_{60})_2@Pd_4\mathbf{L}^Q_6(Nap)_2$ in mother liquor was pipetted onto a glass slide containing NVH oil. Six crystals were quickly mounted onto nylon loops and immediately flash cooled in liquid nitrogen, to prevent cracking of the crystals due to loss of highly volatile organic solvents. Crystals were stored at cryogenic temperature in dry shippers, in which they were safely transported to macromolecular beamline P11 at Petra III,[29] DESY, Germany. A wavelength of λ = 1.03320 Å was chosen using a liquid N_2 cooled double crystal monochromator. Single crystal X-ray diffraction data was collected at 100(2) K on a single axis goniometer, equipped with an Oxford Cryostream 800 open flow cooling device and an Eiger 2x 16M detector. 3600 diffraction images were collected in a 360° φ sweep at a detector distance of 154 mm, 100% filter transmission, 0.1° step width and 30 ms (milliseconds) exposure time per image. Out of six crystals prepared only

one crystal yielded diffraction data of sufficient quality for indexing and structure solution, while the other five suffered from solvent loss resulting in a collapse of the crystal lattice, despite careful and quick crystal picking. Data integration and reduction were undertaken using XDS.[39] The structure was solved by intrinsic phasing/direct methods using SHELXT[40] and refined with SHELXL[41] using 22 CPU cores for full-matrix least-squares routines on F^2 and ShelXle[42] as a graphical user interface and the DSR program plugin was employed for modeling.[43,44]] The asymmetric unit contains two symmetry independent halves of the pill shaped supramolecular assembly $(C_{60})_2$@Pd_4**L**$^{Q}_6$$(Nap)_2$. One of the four co-crystallized tetrafluoroborate anions was modelled with two discrete positions refining their occupancy factor to 52:48 using a free variable. Co crystallized benzene molecules were modelled on twelve position, six of which only 50% occupied and one Acetonitrile molecule was modelled. Due to extremely small crystal size, disorder and poor crystal quality required stereochemical restraints to be employed for ensuring a sensible geometry of the organic part of the structure.

Stereochemical restraints for the ligands **L**^{Q} (residue class TRQ), bridging NAP ligands (residue class NAP) and co-crystallized benzene solvent molecules (residue class BEN) and acetonitrile molecule (residue class ACN) were generated by the GRADE program using the GRADE Web Server (http://grade.globalphasing.org) and applied in the refinement. A GRADE dictionary for SHELXL contains target values and standard deviations for 1,2-distances (DFIX) and 1,3-distances (DANG), as well as restraints for planar groups (FLAT). All displacements for non-hydrogen atoms were refined anisotropically. The refinement of ADPs for carbon, nitrogen and oxygen atoms was enabled by a combination of similarity restraints (SIMU) and rigid bond restraints (RIGU).[45] The contribution of the electron density from disordered counterions and solvent molecules, which could not be modeled with discrete atomic positions, were handled using the SQUEEZE[46] routine in PLATON.[47] The solvent mask file (.fab) computed by PLATON were included in the SHELXL refinement via the ABIN instruction leaving the measured intensities untouched.

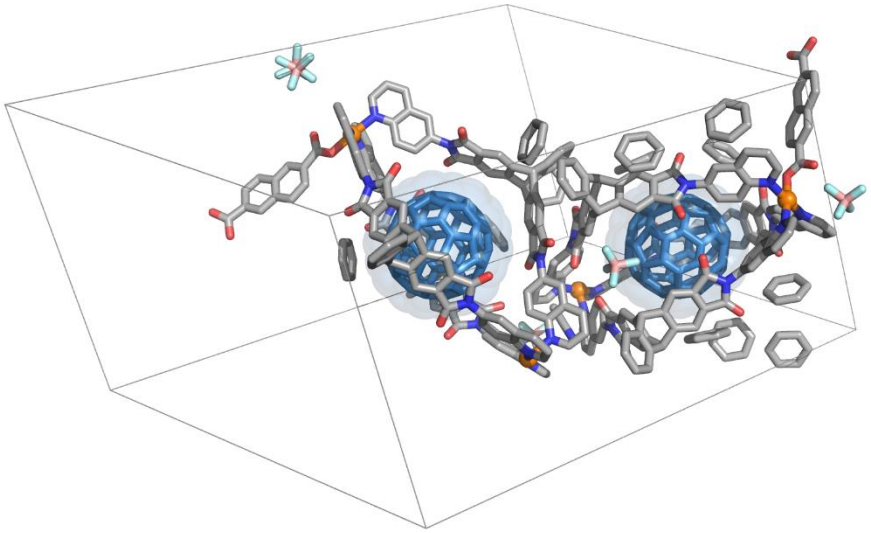

Figure 6.4.45 Unit cell of $(C_{60})_2$@$Pd_4\mathbf{L}^{Q}_6(Nap)_2$. Two halves of the dimer are filled in the unit cell. Hydrogen atoms are omitted for clarity. Color scheme: C (gray), C_{60} (skyblue), N (blue), O (red), and Pd (orange)

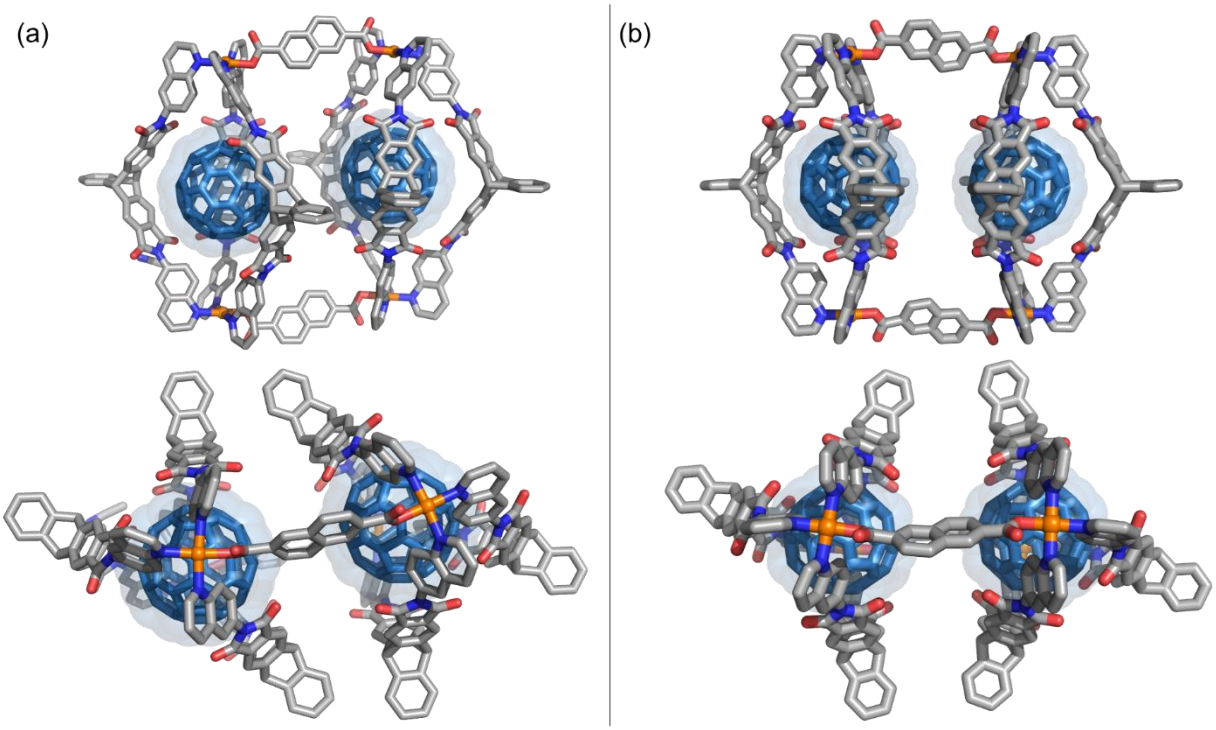

Figure 6.4.46 Single crystals X-ray structure of dimers co-exist (a) $(C_{60})_2$@$Pd_4\mathbf{L}^{Q}_6(Nap)_2$. and (b) the other pair. Color legends: C (gray), C_{60} (skyblue), N (blue), O (red), and Pd (orange)

Two independent halves of $(C_{60})_2$@Pd_2**L**$^{Q}_6$$(Nap)_2$ were found in the asymmetric unit cell. The distances of the center of mass of the encapsulated C_{60}s within each dimer and the values subtracted by the diameter of C_{60} are listed in **Table S1** below. The deviation of the distance implies the flexibility of the nanoscopic space inside the dimer.

Dimer	Distance [Å]	COM-C_{60} [Å]
1	12.8	5.8
2	13.0	6.0

Table 6.4.1 The distances of the center of mass of the encapsulated C_{60}s within each dimer

6.4.4 Host-Guest studies

6.4.4.1 Encapsulation of corannulene

6.4.4.1.1 ^{1}H NMR titration experiment

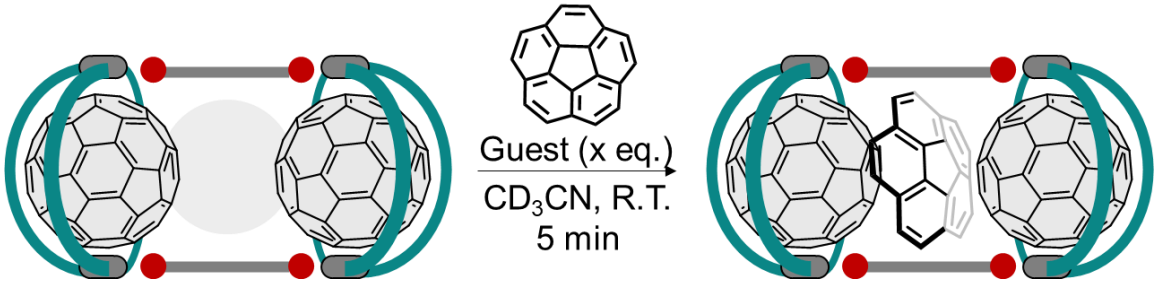

Figure 6.4.47 Encapsulation of corannulene in between two C_{60}s

To an acetonitrile solution of $(C_{60})_2$@Pd_4**L**$^{Q}_6$$(Nap)_2$ (0.34 mM, 600.0 μL, 0.21 μmol) in a NMR tube, corannulene solution in acetonitrile (20 mM, CD_3CN) was titrated. The NMR tube was shaken and ^{1}H NMR spectrum was measured immediately after shaking. The change of the chemical shifts was traced by NMR spectroscopy.

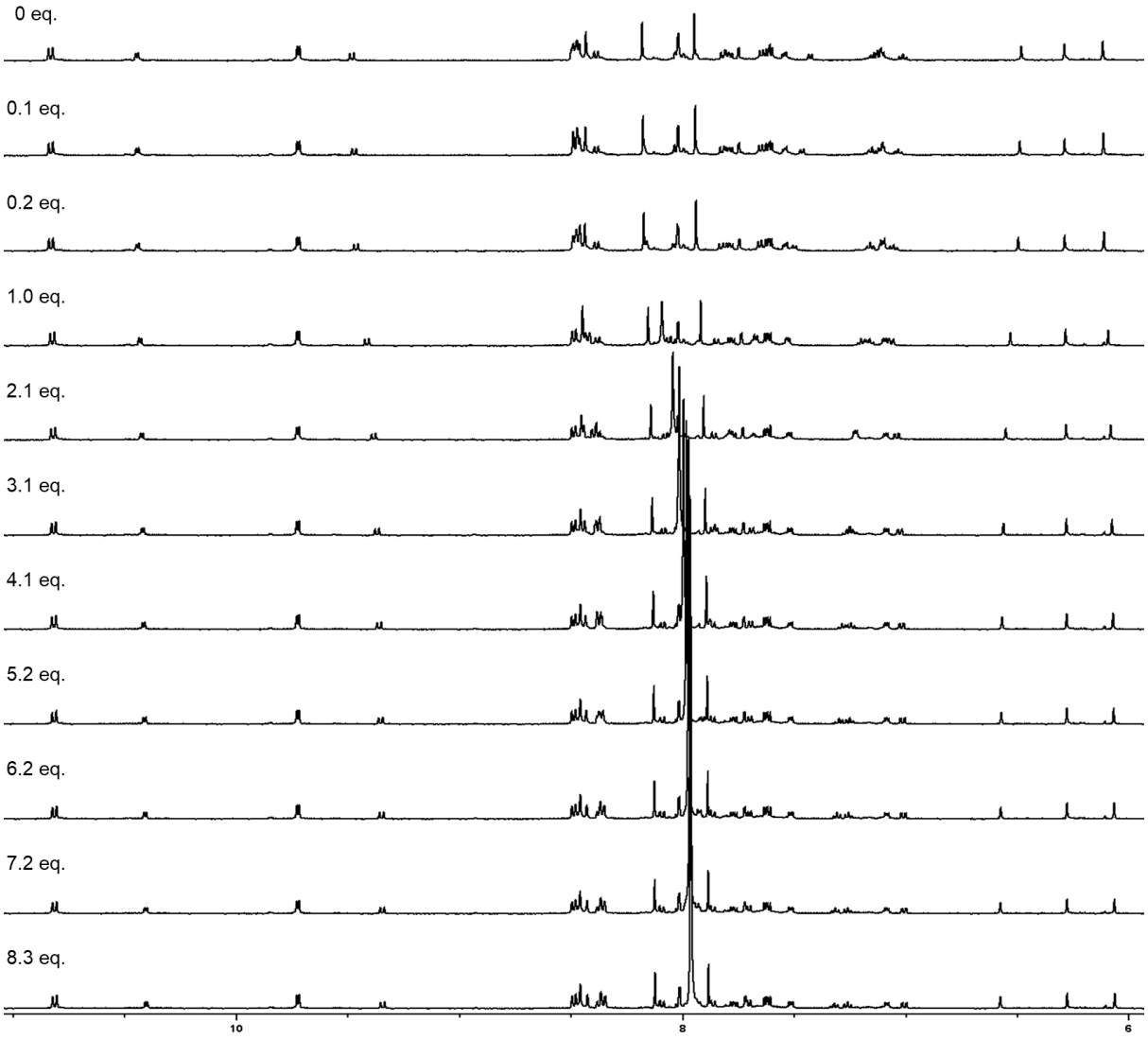

Figure 6.4.48 ^{1}H NMR spectra of $(C_{60})_2$@Pd_4**L**$^{Q}_6$$(Nap)_2$ in the presence of increasing equivalents of corannulene (500 MHz, 298 K, CD_3CN)

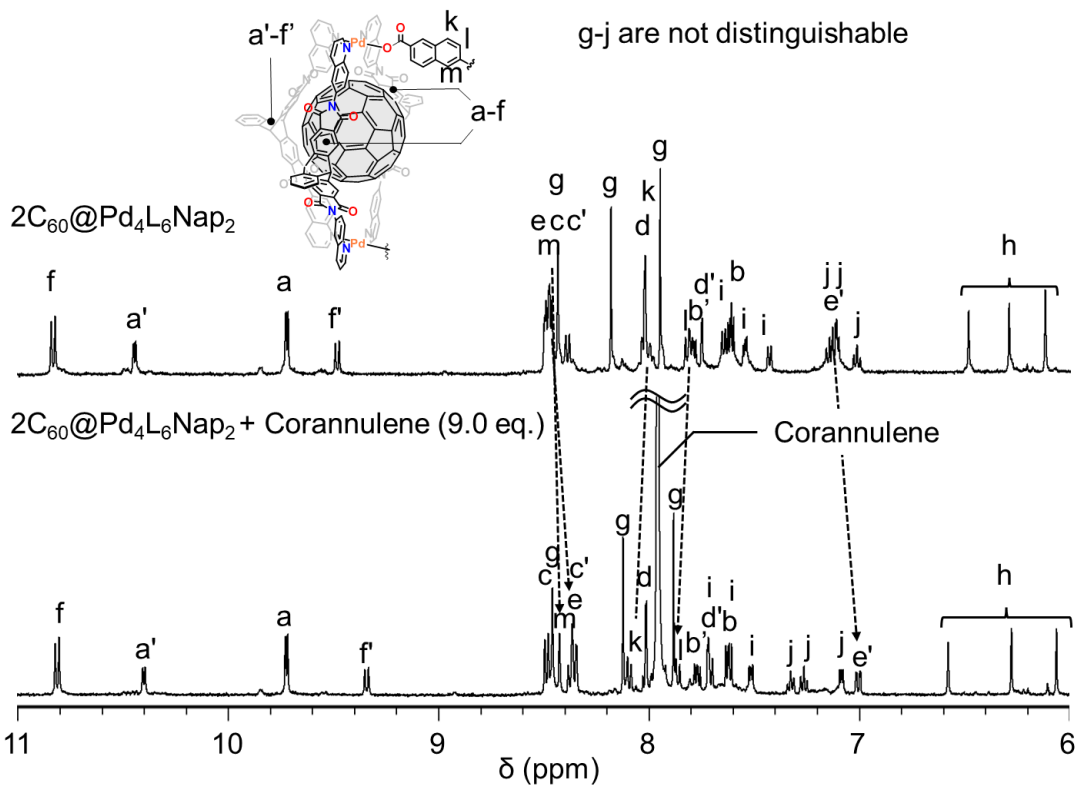

Figure 6.4.49 ^{1}H NMR spectra (500 MHz, 298 K, CD_3CN) of $(C_{60})_2$@Pd_4**L**$^{Q}_6$$(Nap)_2$ w.o. (0.34 mM) and w. corannulene (9 eq.) (0.30 mM)

6.4.4.1.2 ^{13}C NMR spectra

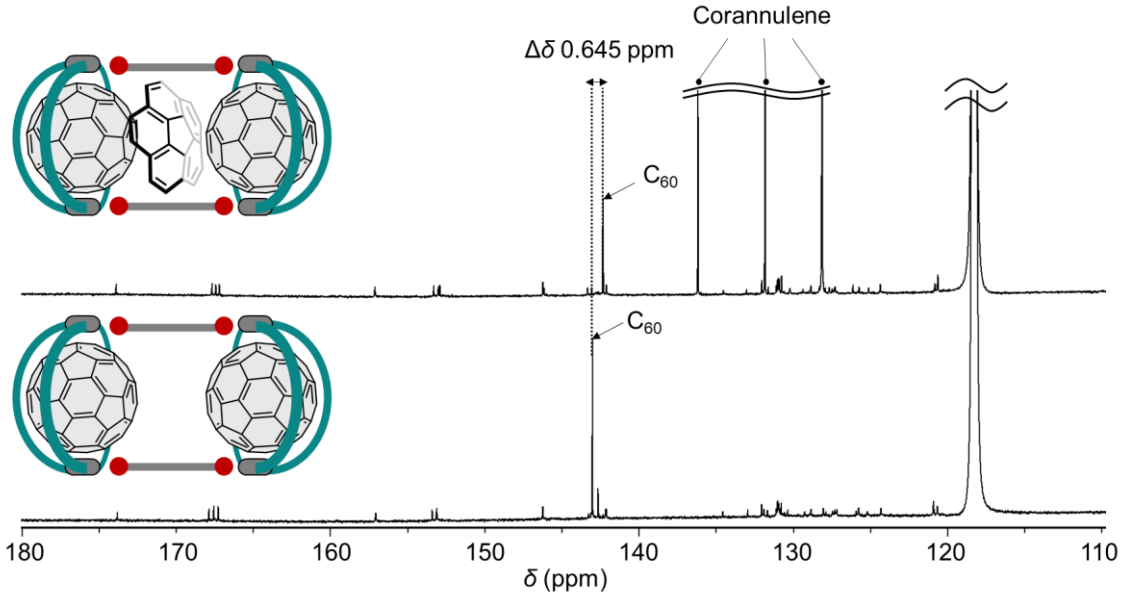

Figure 6.4.50 ^{13}C NMR spectra (150 MHz, 298 K, CD_3CN) of $(C_{60})_2$@Pd_4**L**$^{Q}_6$$(Nap)_2$ w.o. (0.34 mM) and w. corannulene (9 eq.) (0.30 mM)

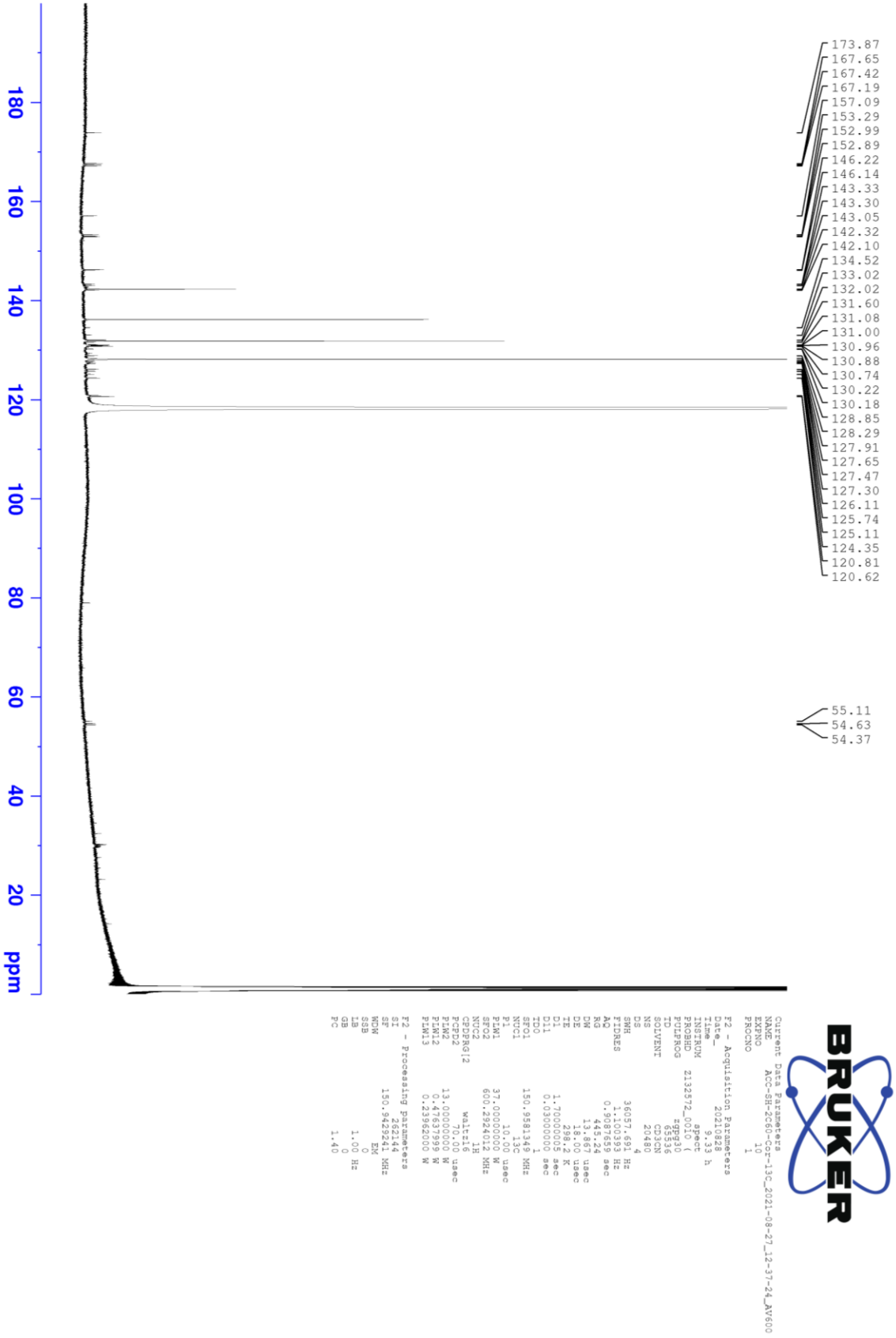

Figure 6.4.51 ^{13}C NMR spectrum (150 MHz, 298 K, CD_3CN) of $(C_{60})_2$@Pd_4**L**$^{Q}_6$$(Nap)_2$ w. corannulene (9 eq.) (0.30 mM)

6.4.4.1.3 Optical properties

To an acetonitrile solution of $(C_{60})_2$@Pd_4**L**$^{Q}_6$$(Nap)_2$, 9.0 equivalent of corannulene was added. Immediately after addition, the solution color changed from purple to yellow due to the charge transfer complex formation between the encapsulated C_{60} and the bound corannulene. The UV-Vis absorption spectra of the charge transfer complex were measured in acetonitrile (298 K, 0.34 mM, *l* = 1.0 cm). The intensity of the absorbance increased around 450 nm, which is in good accordance with the literature.[30]

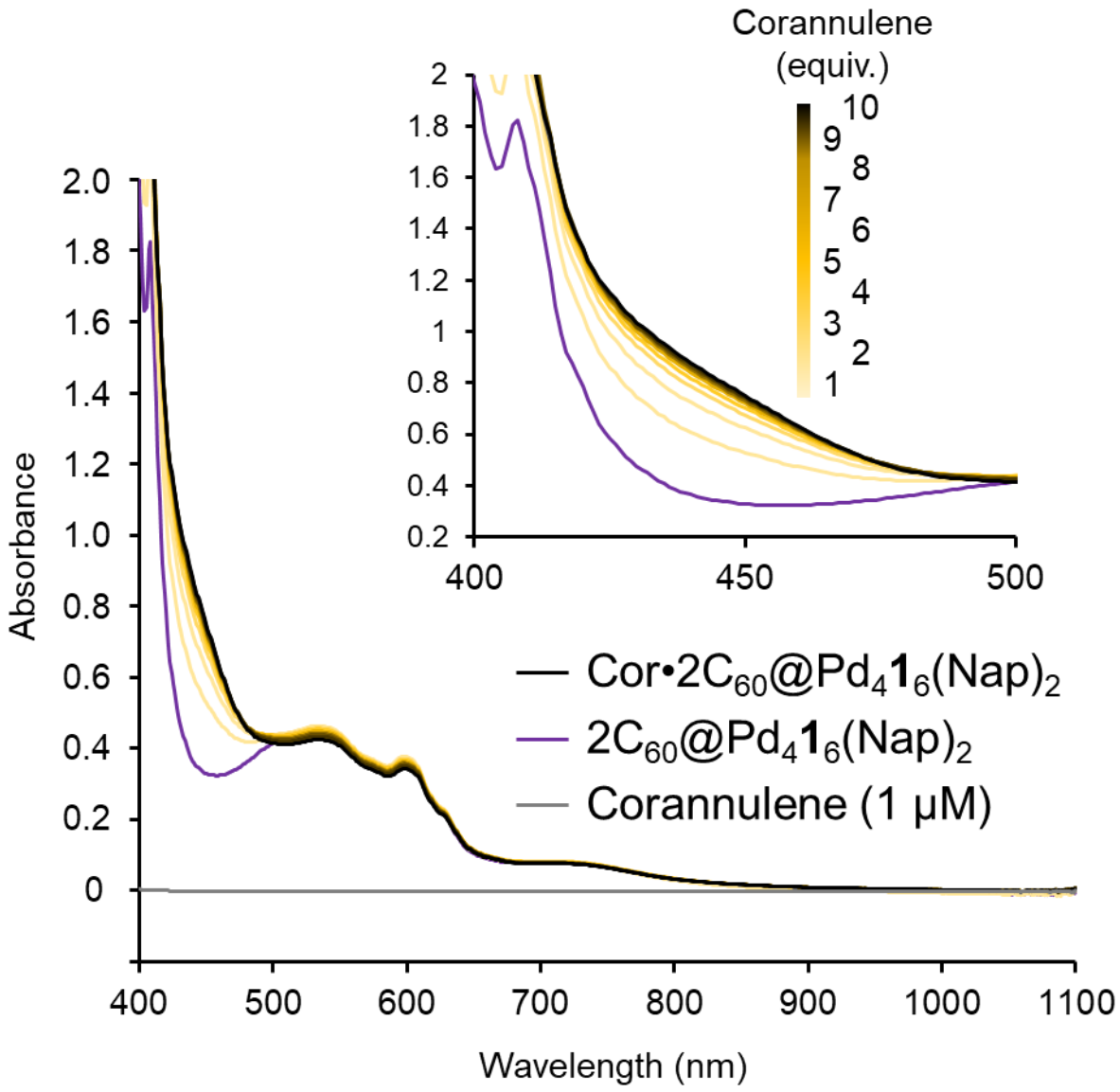

Figure 6.4.52 UV-Vis absorption spectra of yellow: Cor•$(C_{60})_2$@Pd_4**L**$^{Q}_6$$(Nap)_2$ (0.30 mM, *l* = 1 cm, 298 K, CD_3CN), purple: $(C_{60})_2$@Pd_4**L**$^{Q}_6$$(Nap)_2$ (0.34 mM, *l* = 1 cm, 298 K, CD_3CN), black: corannulene (1 µM, *l* = 1 cm, 298 K, CD_3CN)

6.4.4.1.4 Determination of binding constant

From the titration NMR experiment using $(C_{60})_2$@Pd_4**L**$^{Q}_6$$(Nap)_2$ as a host and corannulene as a guest, the binding constant was determined using BindFit ver.0.5.[48] The signals of proton h, which shows no overlap with other signals, was adopted for the analysis. The plot is shown in **Figure 6.4.53** and the outcome of the fitting is summarized in **Table 6.4.2**.

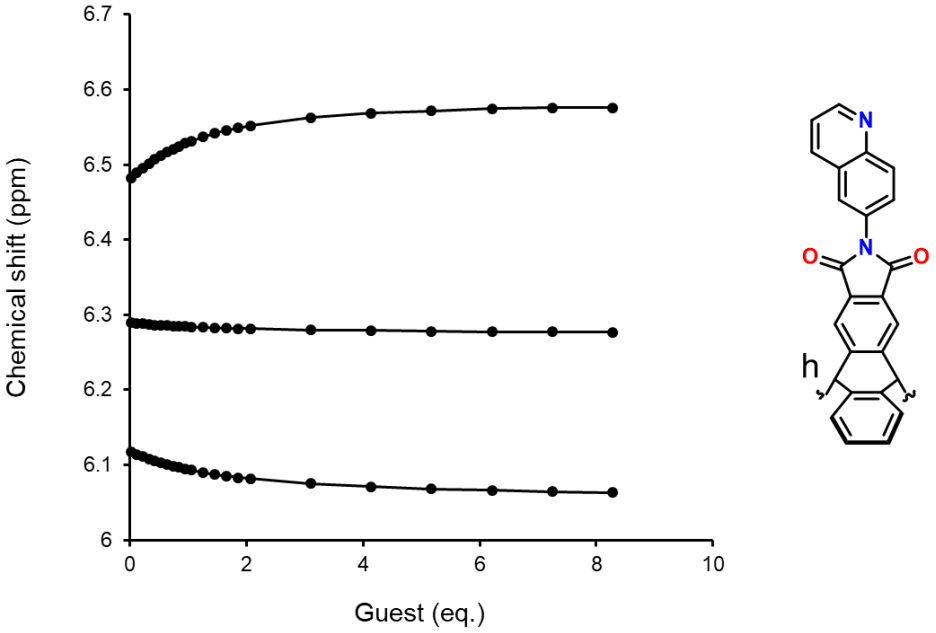

Figure 6.4.53 Plot of the chemical shifts over titration against the equivalent of the guest molecule

Table 6.4.2 Summary of the fitting

K_a (M^{-1})	error (%)	SSR
4410.671435	2.801771745	7.22434E-05

6.4.4.2 ESI-MS spectrum of Cor•$(C_{60})_2$@$Pd_4L^Q_6(Nap)_2$

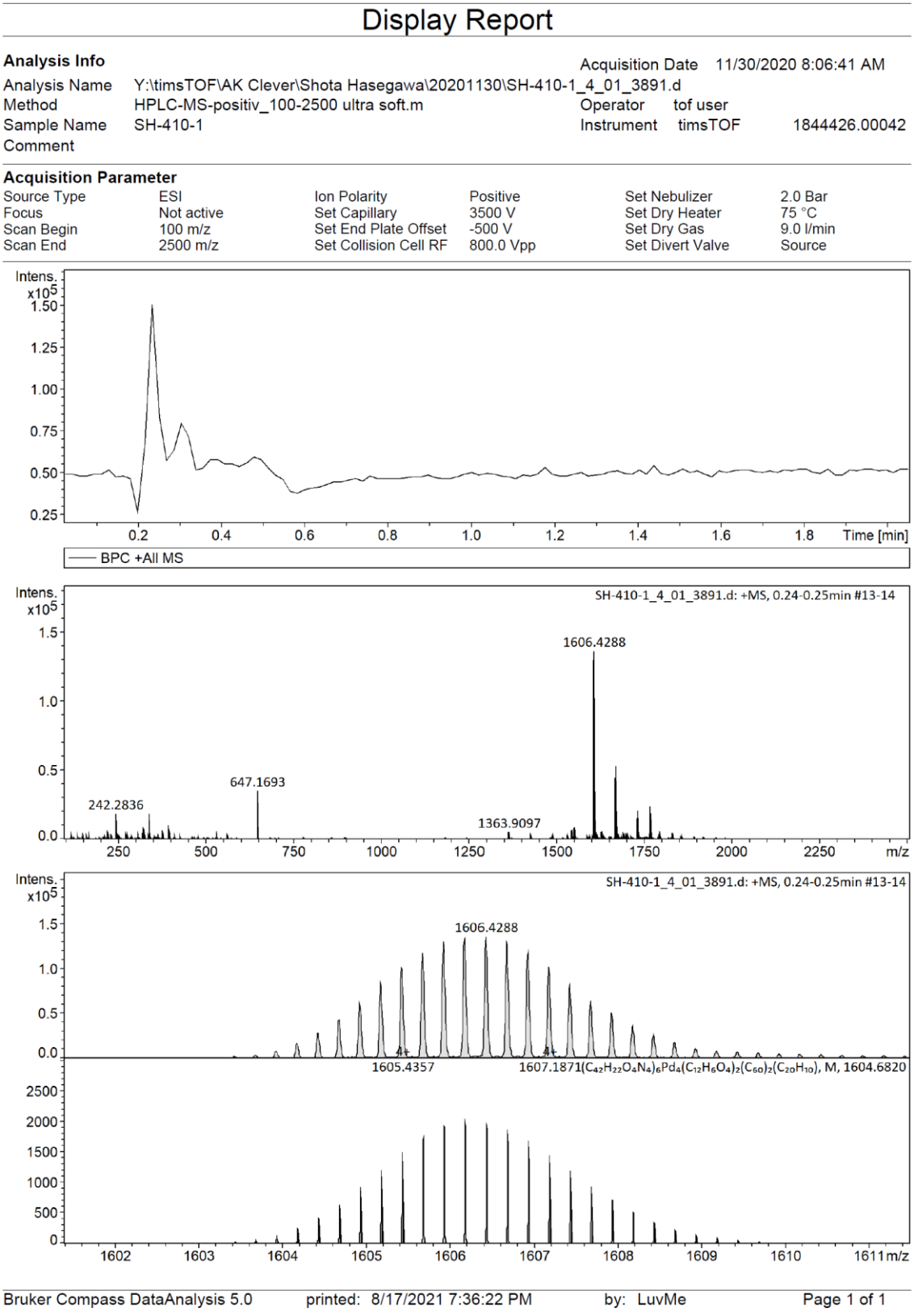

Figure 6.4.54 ESI-MS spectrum of Cor•$(C_{60})_2$@$Pd_4\mathbf{L}^Q_6(Nap)_2$ (positive)

6.4.4.3 Encapsulation of anthracene

6.4.4.3.1 ^{1}H NMR titration experiment

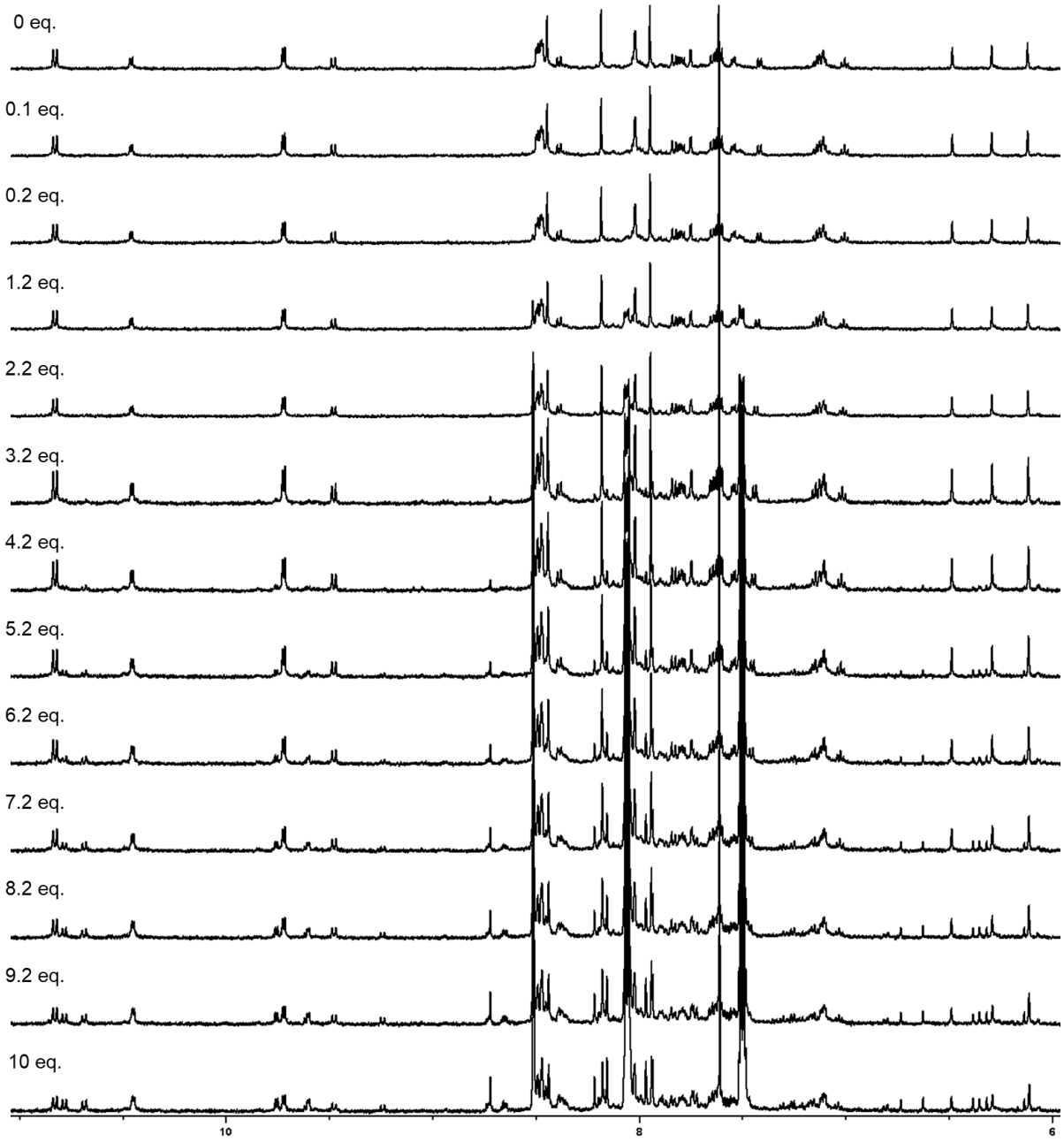

Figure 6.4.55 ^{1}H NMR spectra of $(C_{60})_2$@Pd_4**L**$^{Q}_6$$(Nap)_2$ in the presence of various equivalents of anthracene; the sum of titrated amounts of anthracene is written in the spectra (500 MHz, 298 K, CD_3CN)

6.4.4.3.2 Determination of binding constant

From the titration NMR experiment using $(C_{60})_2$@Pd_4**L**$^{Q}_6$$(Nap)_2$ as a host and anthracene as a guest, the binding constant was determined using BindFit v0.5.[48] For the sake of precise analysis, the chemical shifts of proton h, which show no overlap with other signals, were adopted for the analysis. The plot is shown in **Figure 6.4.56** and the outcome of the fitting is summarized in **Table 6.4.3**.

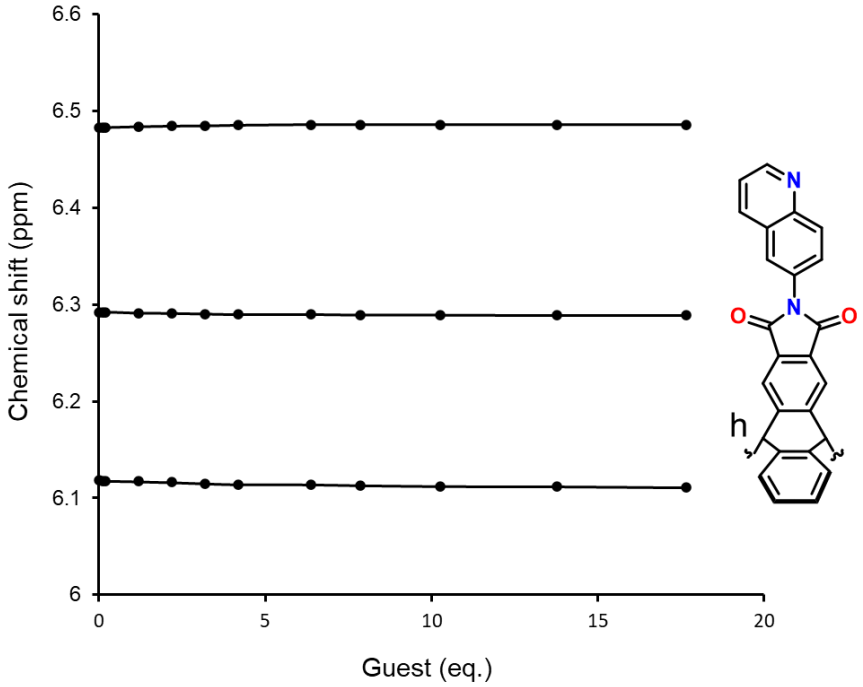

Figure 6.4.56 Plot of the chemical shifts over titration against the equivalent of the guest molecule

Table 6.4.3 Summary of the fitting

K_a (M^{-1})	error (%)	SSR
199.4497871	4.7805086155015	2.99439582318385E-06

6.4.5 Detail studies on Diels-Alder reaction

6.4.5.1 Kinetic analysis

The reaction rate of the Diels-Alder reaction of the encapsulated C_{60} inside the cage with anthracene was determined by ^{1}H NMR analysis at deferent temperatures (298 K, 303 K, 308 K). The analysis is limited in this range due to precipitation at higher temperature than this range. To an acetonitrile solution of $(C_{60})_2$@Pd_4**L**$^{Q}_6(Nap)_2$ (0.34 mM, 0.600 mL, 0.20 μmol) in an NMR tube, a certain amount of an acetonitrile solution of anthracene was added in the dark. The NMR tube was shaken and let stand for a certain time at a certain temperature till to be measured. The reaction was analyzed as a second order reaction following the equation below. The obtained *k* values at each temperature were plotted in an Eyring plot and the activation energy barrier was estimated. The experiment was repeated three times.

$$\ln\left(\frac{[B][A_0]}{[A][B_0]}\right) = ([B_0] - [A_0])kt$$

$$\ln\left(\frac{[\mathrm{B}]/[\mathrm{B}]_0}{[\mathrm{A}]/[\mathrm{A}]_0}\right) = ([\mathrm{B}]_0 - [\mathrm{A}]_0)k_2 t$$

A + B → C

A: $2C_{60}$@dimer
B: Anthracene
C: C_{60}ant•C_{60}@dimer

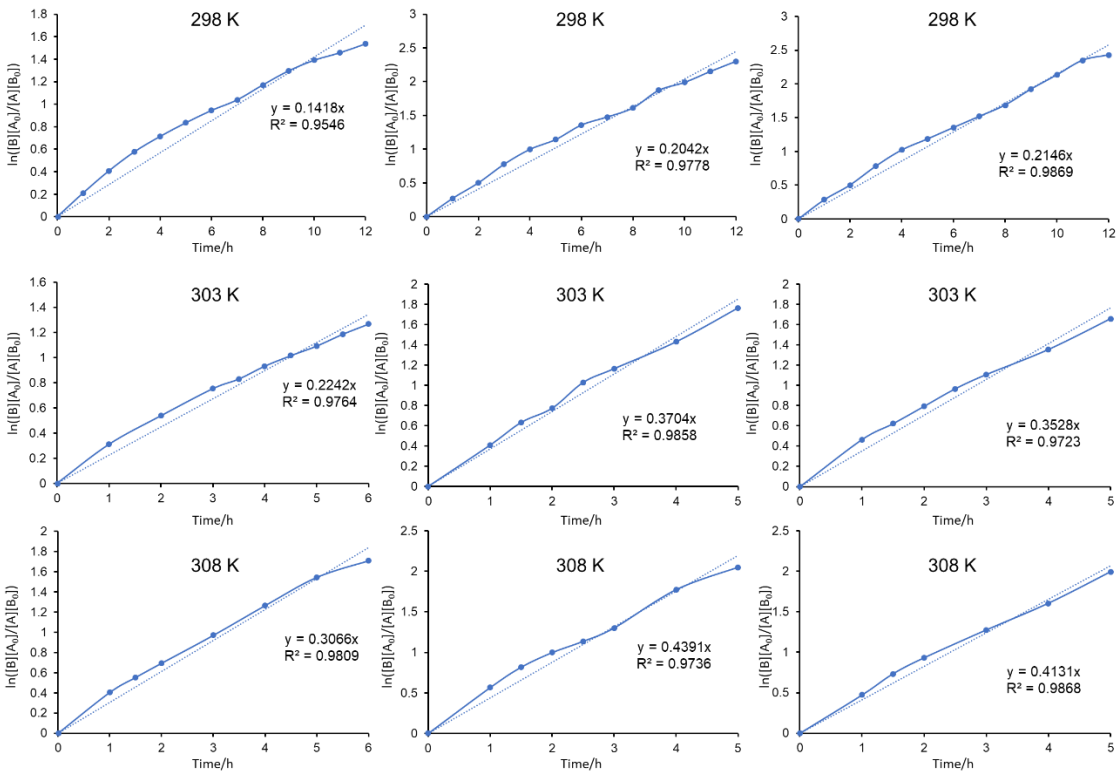

Figure 6.4.57 Plots over the Diels-Alder reaction as second order reactions measured at variable temperatures

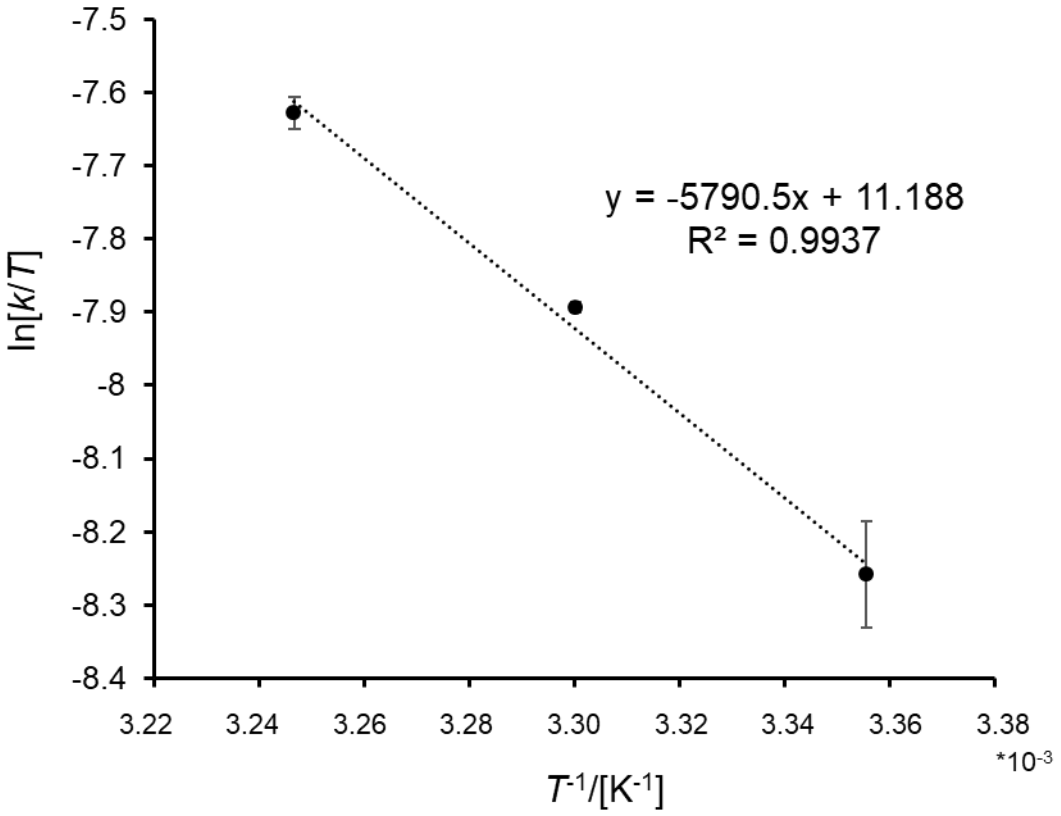

Figure 6.4.58 Eyring plot of the Diels-Alder reaction

An activation enthalpy $\Delta H^{\ddagger}$ was estimated from the value of the slope to be 48 kJ/mol. An activation entropy $\Delta S^{\ddagger}$ was calculated to be -104 J/mol from the intercept. An activation Gibbs free energy $\Delta G^{\ddagger}$ at 298 K was calculated to be 79 kJ/mol from the aforementioned values using the flowing equation (1)

$$\Delta G^{\ddagger} = \Delta H^{\ddagger} - T\,\Delta S^{\ddagger} \quad (1)$$

Temperature	298 K	303 K	308 K
Reaction rate	7.72 ± 0.54 × 10^{-2} M^{-1}/s	1.13 ± 0.08 × 10^{-1} M^{-1}/s	1.49 ± 0.03 × 10^{-1} M^{-1}/s

Table 6.4.4 Summary of the reaction rates at different temperatures

6.4.5.2 ^{1}H NMR spectra

6.4.5.2.1 298 K

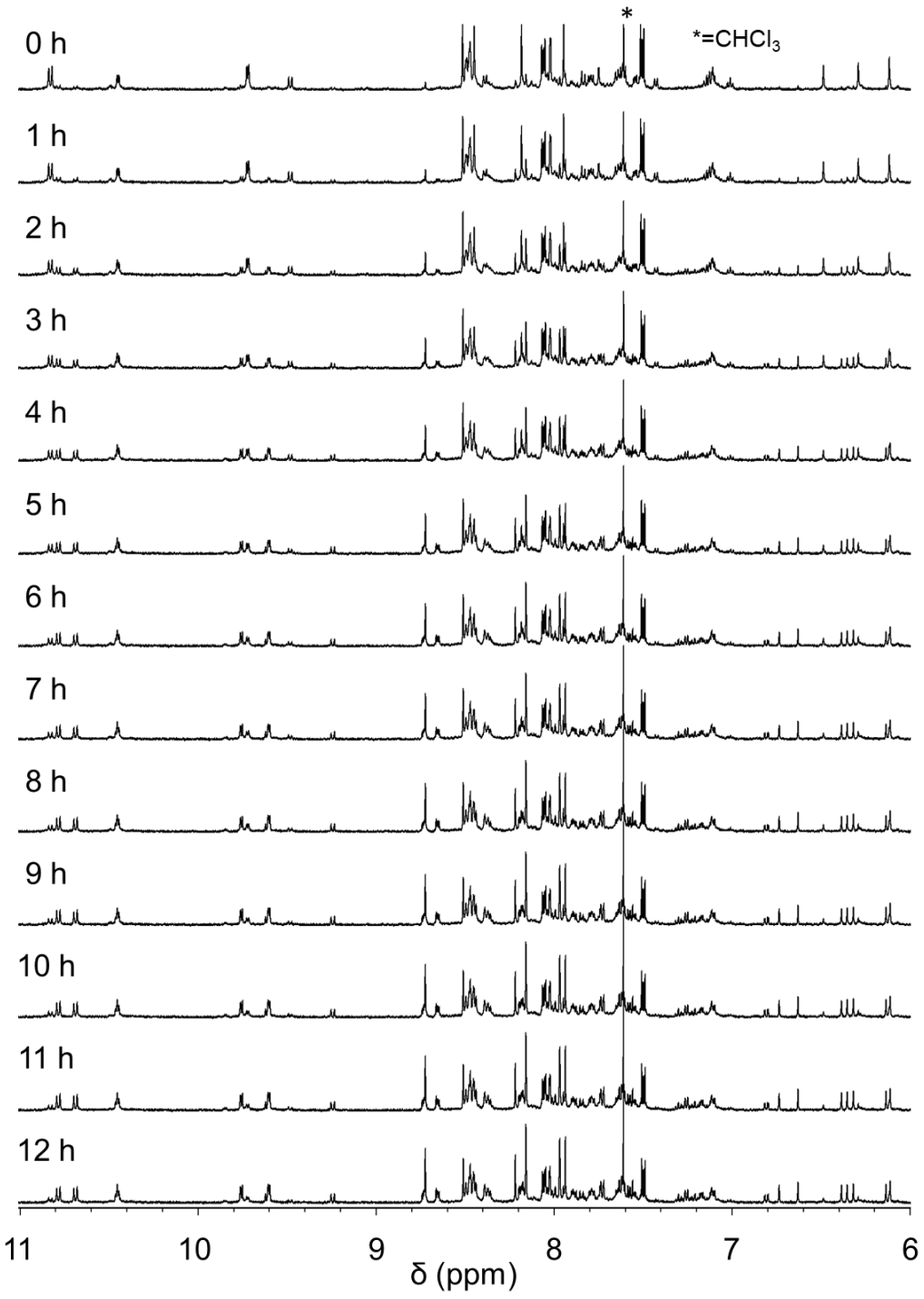

Figure 6.4.59 ^{1}H NMR spectra used to determine the reaction rate at 298 K (500 MHz, 298 K, CD_3CN)

6.4.5.2.2 303 K

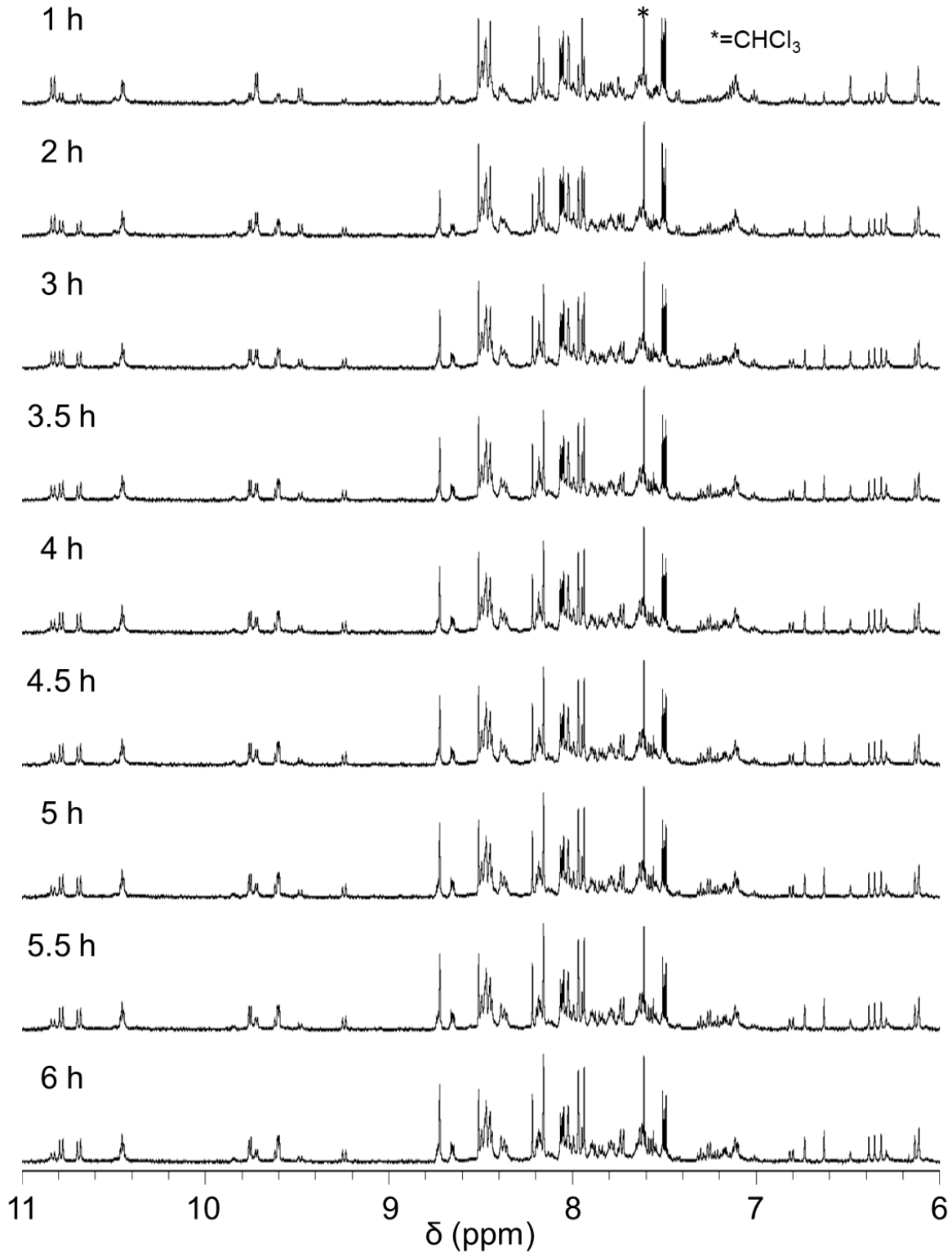

Figure 6.4.60 ^{1}H NMR spectra used to determine the reaction rate at 303 K (500 MHz, 298 K, CD_3CN)

6.4.5.2.3 308 K

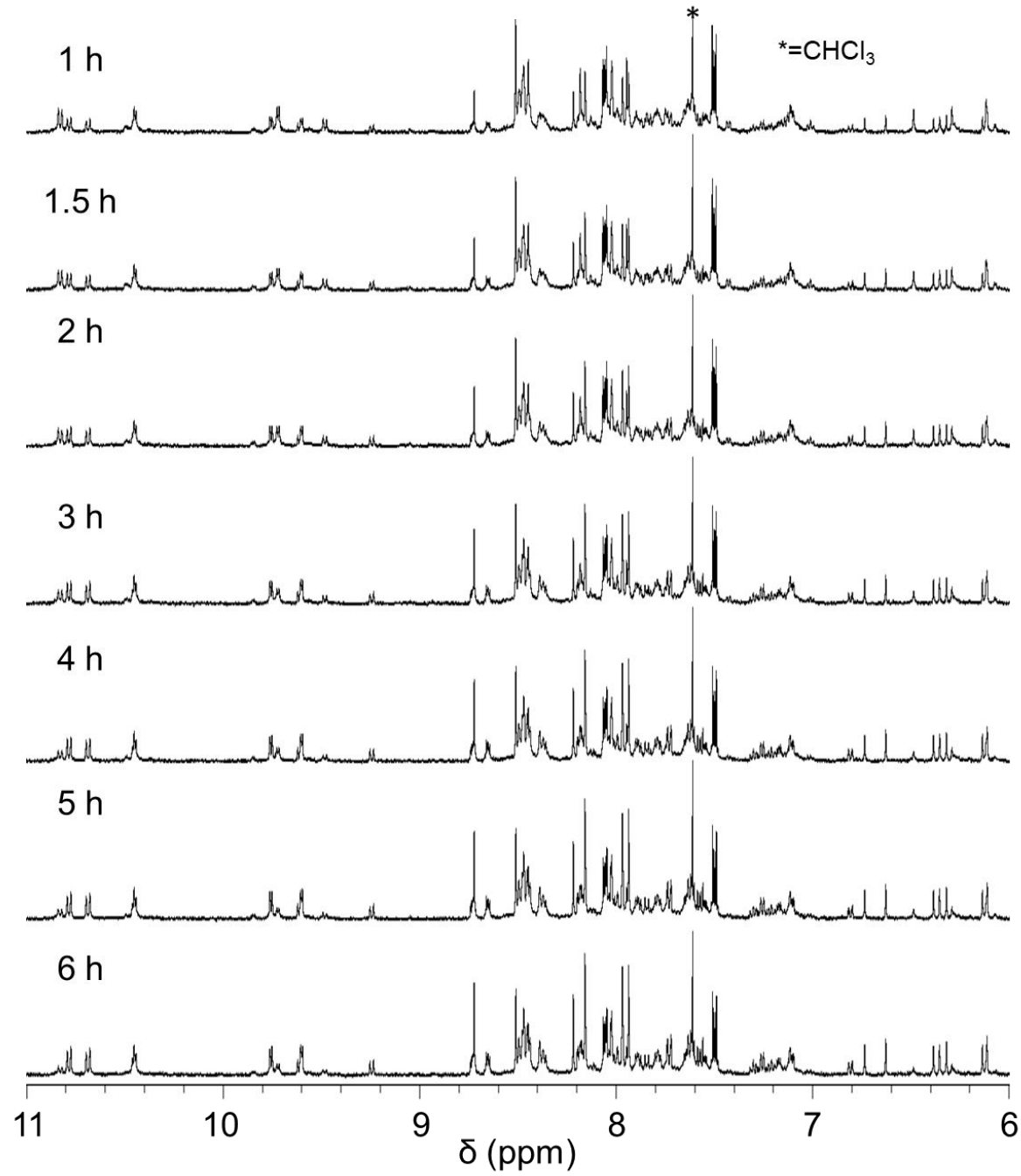

Figure 6.4.61 ^{1}H NMR spectra used to determine the reaction rate at 308 K (500 MHz, 298 K, CD_3CN)

6.4.5.3 Synthesis of $C_{60}@Pd_2L^Q_3(MeCN)_2$

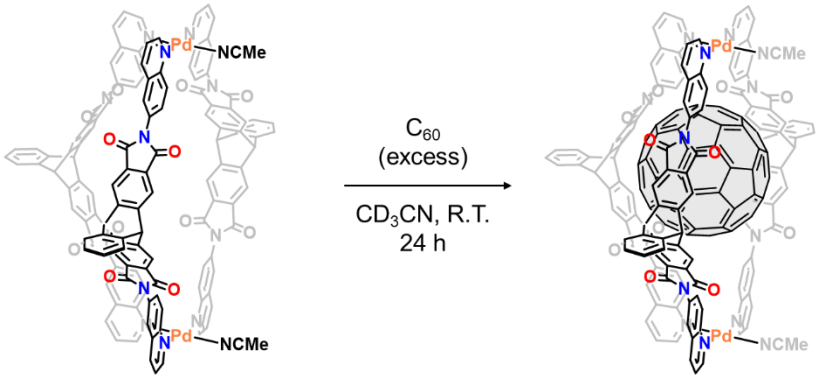

Figure 6.4.62 Synthesis of $C_{60}@Pd_2L^Q_3(MeCN)_2$

Solid C_{60} (excess) was dispersed in an acetonitrile solution of $Pd_2L^Q_3(MeCN)_2$ (1.00 mL, 0.70 mM, 0.7 μmol) at ambient temperature for 24 h. Filtration of the residual C_{60} yielded $C_{60}@Pd_2L^Q_3$.

^{1}H NMR (500 MHz, CD_3CN, 298 K): δ (ppm) 10.30 (d, J = 9.3 Hz, 4H), 9.82 (dd, J = 5.5, 1.2 Hz, 2H), 9.43 (dd, J = 5.4, 1.2 Hz, 4H), 9.04 (d, J = 9.2 Hz, 2H), 8.65 (d, J = 5.6, 8.4 Hz, 4H), 8.41 (d, J = 8.2 Hz, 2H), 8.35 (dd, J = 9.2, 2.1 Hz, 4H), 8.15 (s, 4H), 8.11-8.10 (m, 8H), 7.89 (s, 4H), 7.79 (dd, J = 8.2 Hz, 5.6 Hz, 2H), 7.76-7.72 (m, 6H), 7.63 (m, 4H), 7.52 (dd, J = 5.4, 3.2 H, 2H), 7.17 (m, 4H), 7.09 (dd, J = 5.4, 3.2 H, 2H), 7.02 (dd, J = 9.2, 2.1 Hz, 2H), 6.27 (s, 2H), 6.22 (s, 2H), 6.07 (s, 2H);
DOSY: Diffusion coefficient D = 5.00 × 10^{-10} m^2s^{-1}, hydrodynamic radius r_H was calculated to be 13.1 Å
ESI MS calcd. for $[(C_{42}H_{22}N_4O_4)_3Pd_2(CH_3CN)_2(C_{60})]^{4+}$ 738.8396 (100%), found 738.8356 $[Pd_2L^Q_3(MeCN)_2]^{4+}$.

6.4.5.3.1 ^{1}H NMR spectra of $C_{60}@Pd_2L^{Q}_3(MeCN)_2$

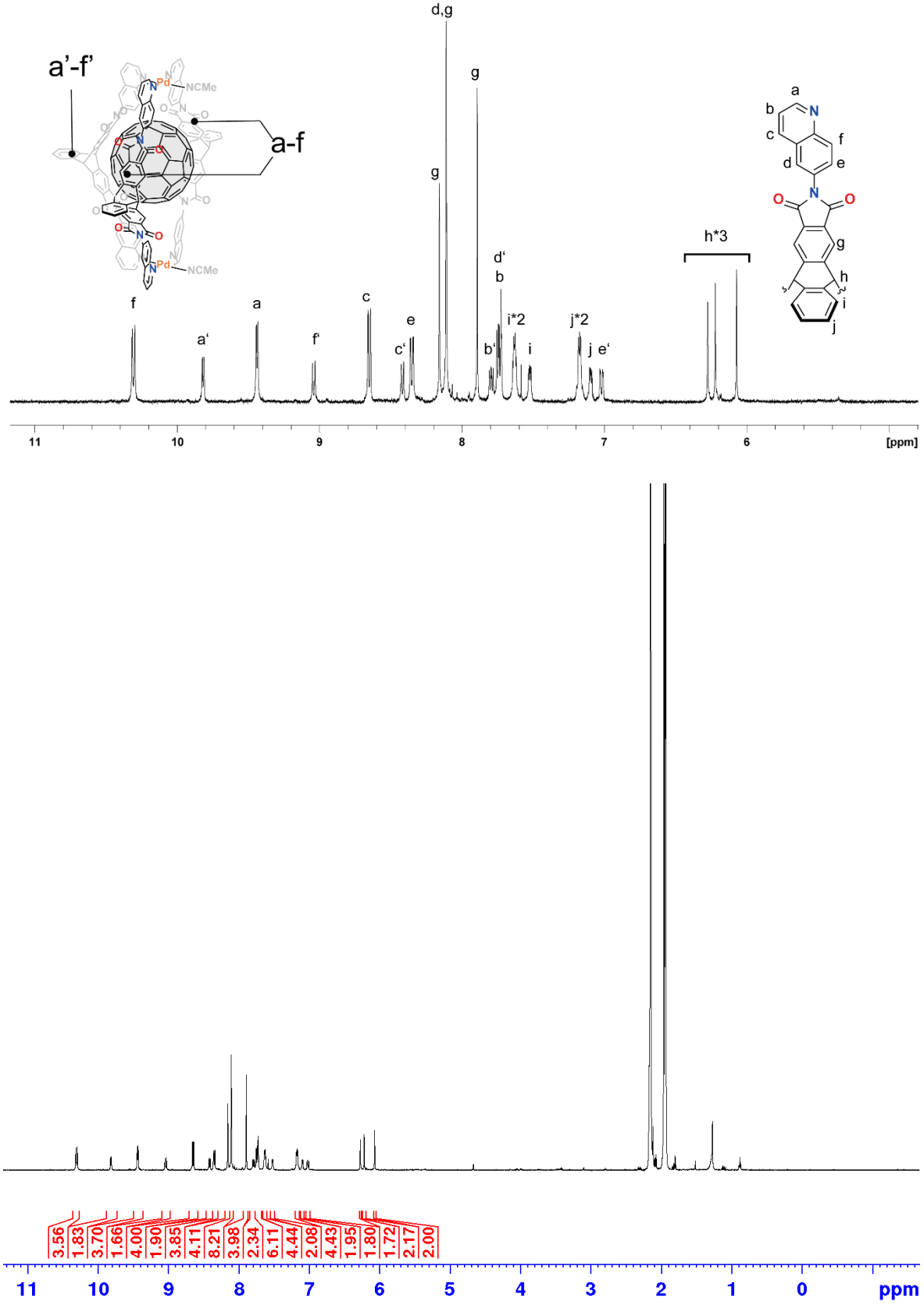

Figure 6.4.63 ^{1}H NMR spectra (500 MHz, 298 K, CD_3CN, 0.70 mM) of $C_{60}@Pd_2\mathbf{L}^{Q}_3(MeCN)_2$

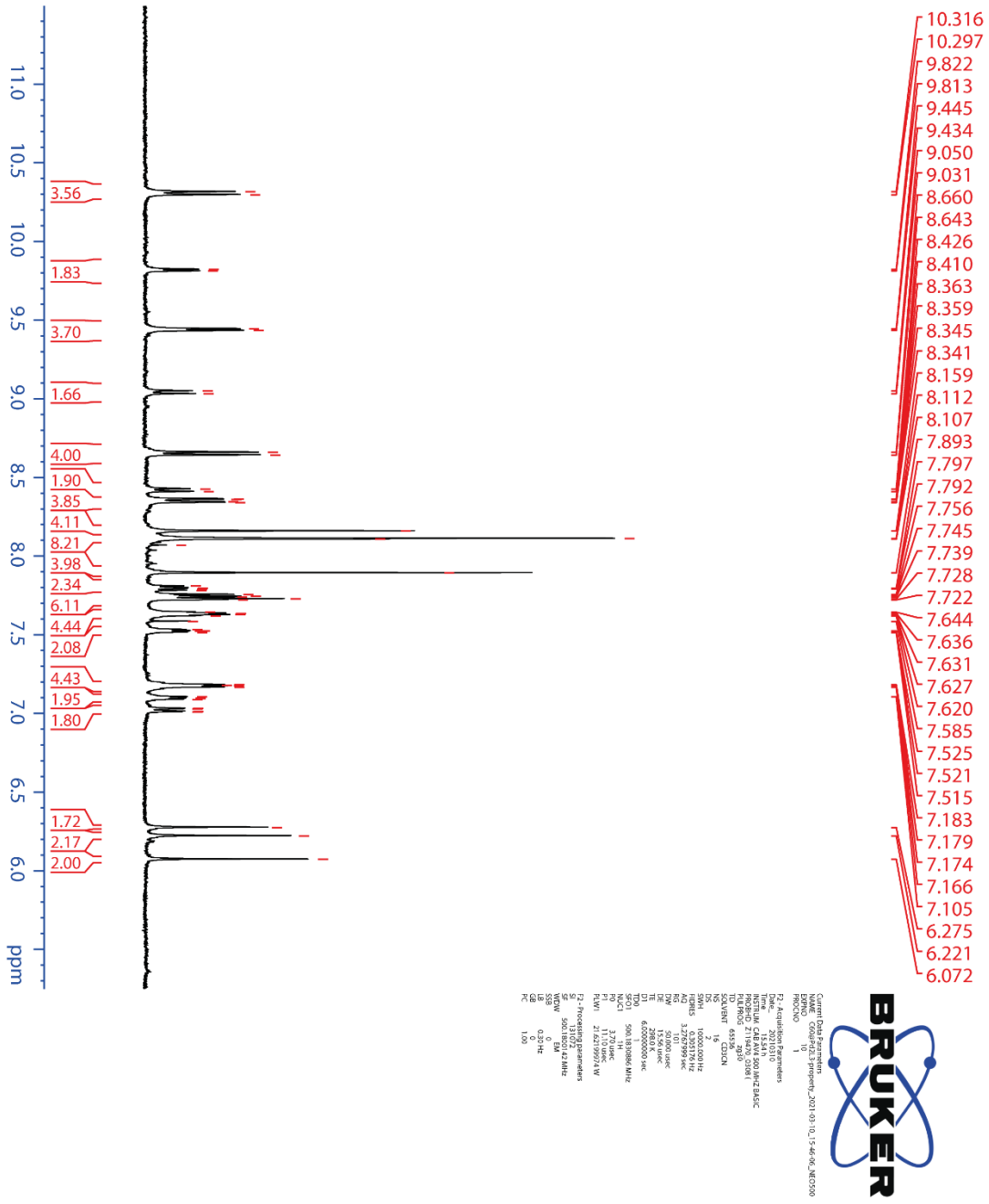

Figure 6.4.64 ^{1}H NMR spectrum (500 MHz, 298 K, CD_3CN, 0.70 mM) of $C_{60}@Pd_2\mathbf{L}^{Q}_3(MeCN)_2$

6.4.5.3.2 ^{1}H-^{1}H COSY NMR spectrum of C_{60}@$Pd_2L^{Q}_3(MeCN)_2$

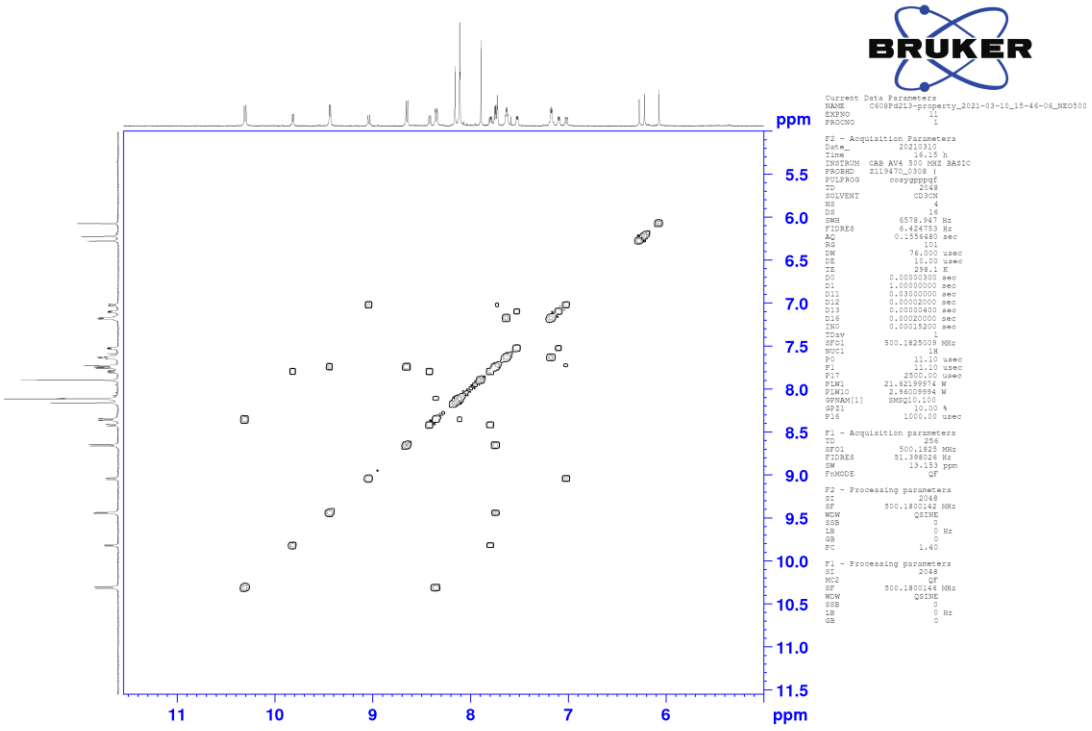

Figure 6.4.65 ^{1}H-^{1}H COSY NMR spectrum (500 MHz, 298 K, CD_3CN, 0.70 mM) of C_{60}@$Pd_2\mathbf{L}^{Q}_3(MeCN)_2$

6.4.5.3.3 ^{1}H-^{1}H NOESY NMR spectrum of $C_{60}@Pd_2L^{Q}_3(MeCN)_2$

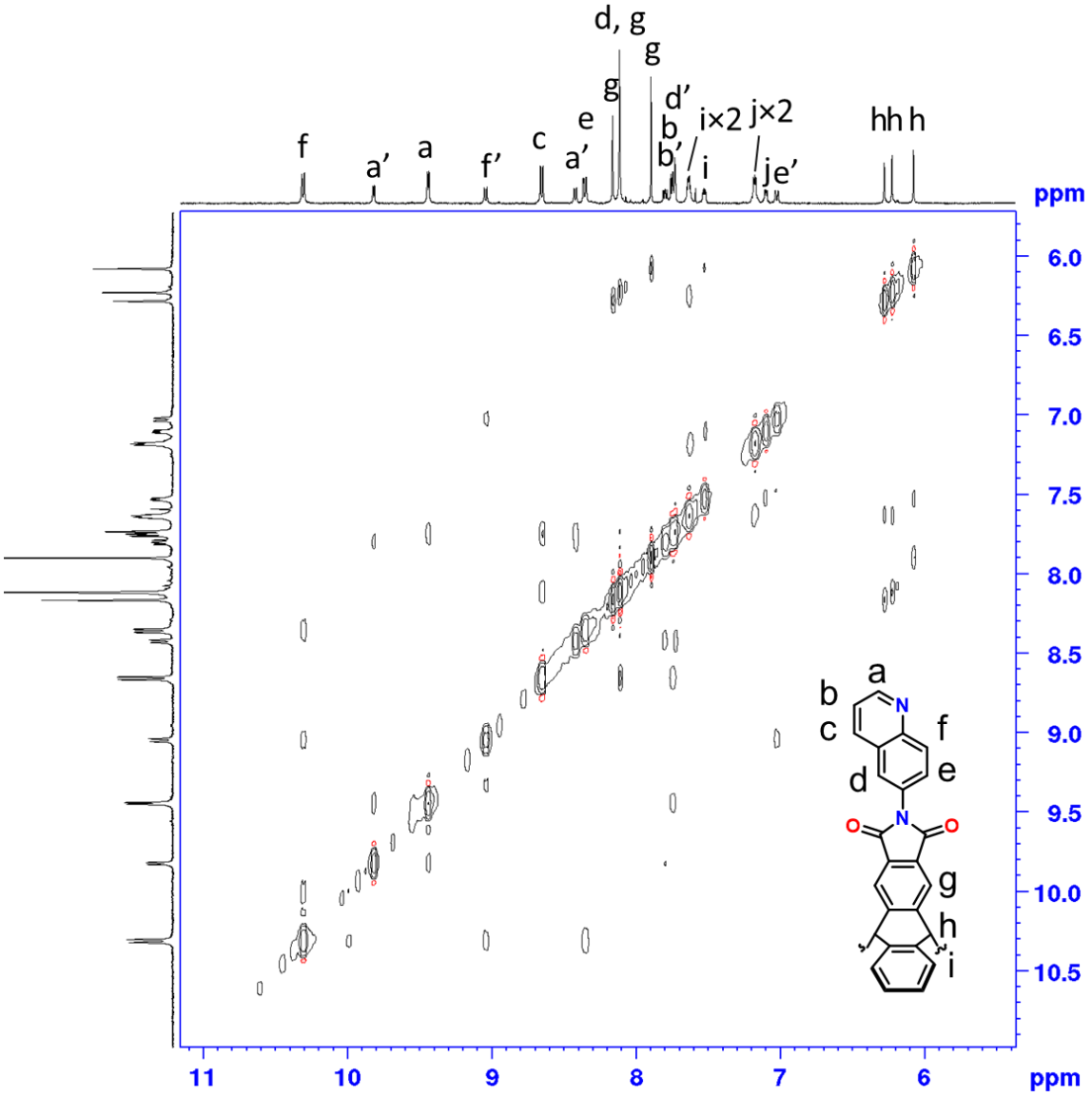

Figure 6.4.66 ^{1}H-^{1}H NOESY NMR spectrum (500 MHz, 298 K, CD_3CN, 0.70 mM) of $C_{60}@Pd_2\mathbf{L}^{Q}_3(MeCN)_2$

6.4.5.3.4 ^{13}C NMR spectrum of $C_{60}@Pd_2L^Q_3(MeCN)_2$

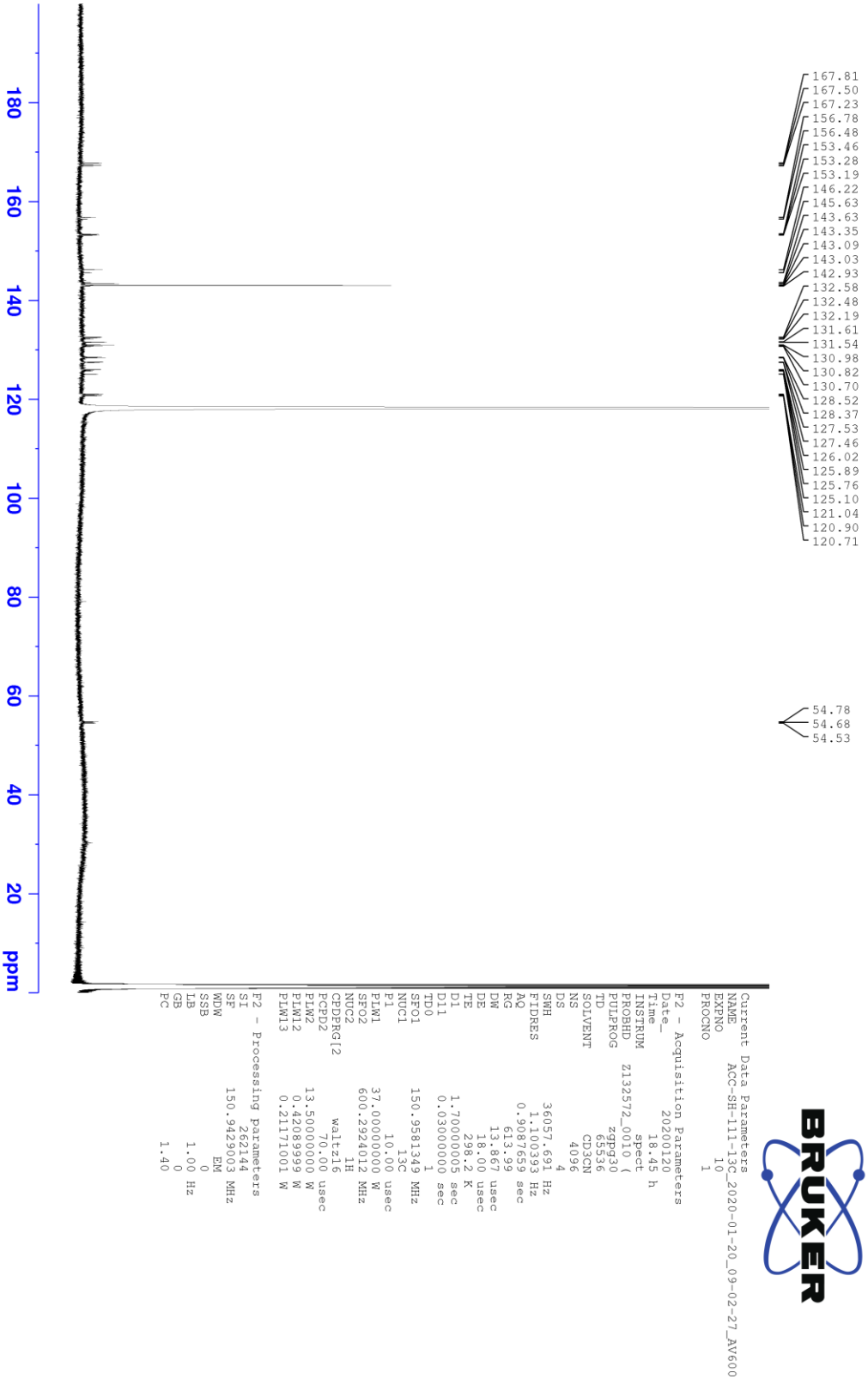

Figure 6.4.67 ^{13}C NMR spectrum (150 MHz, 298 K, CD_3CN, 0.70 mM) of $C_{60}@Pd_2L^Q_3(MeCN)_2$

6.4.5.3.5 ^{1}H DOSY NMR spectrum of $C_{60}@Pd_2L^{Q}_3(MeCN)_2$

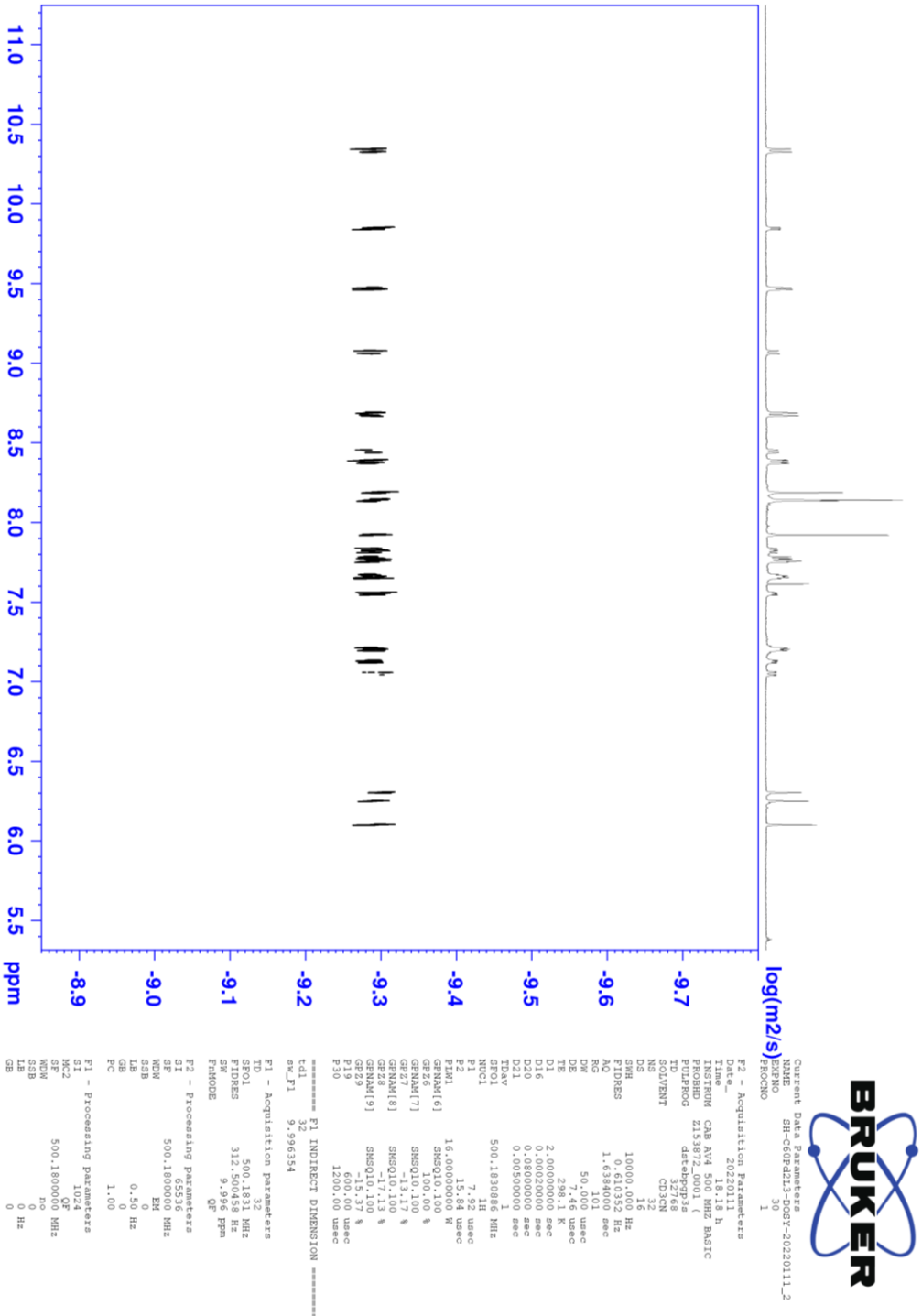

Figure 6.4.68 ^{1}H DOSY NMR spectrum (500 MHz, 298 K, CD_3CN, 0.70 mM) of $C_{60}@Pd_2\mathbf{L}^{Q}_3(MeCN)_2$

6.4.5.3.6 ESI-MS spectrum of $C_{60}@Pd_2L^{Q}_3(MeCN)_2$

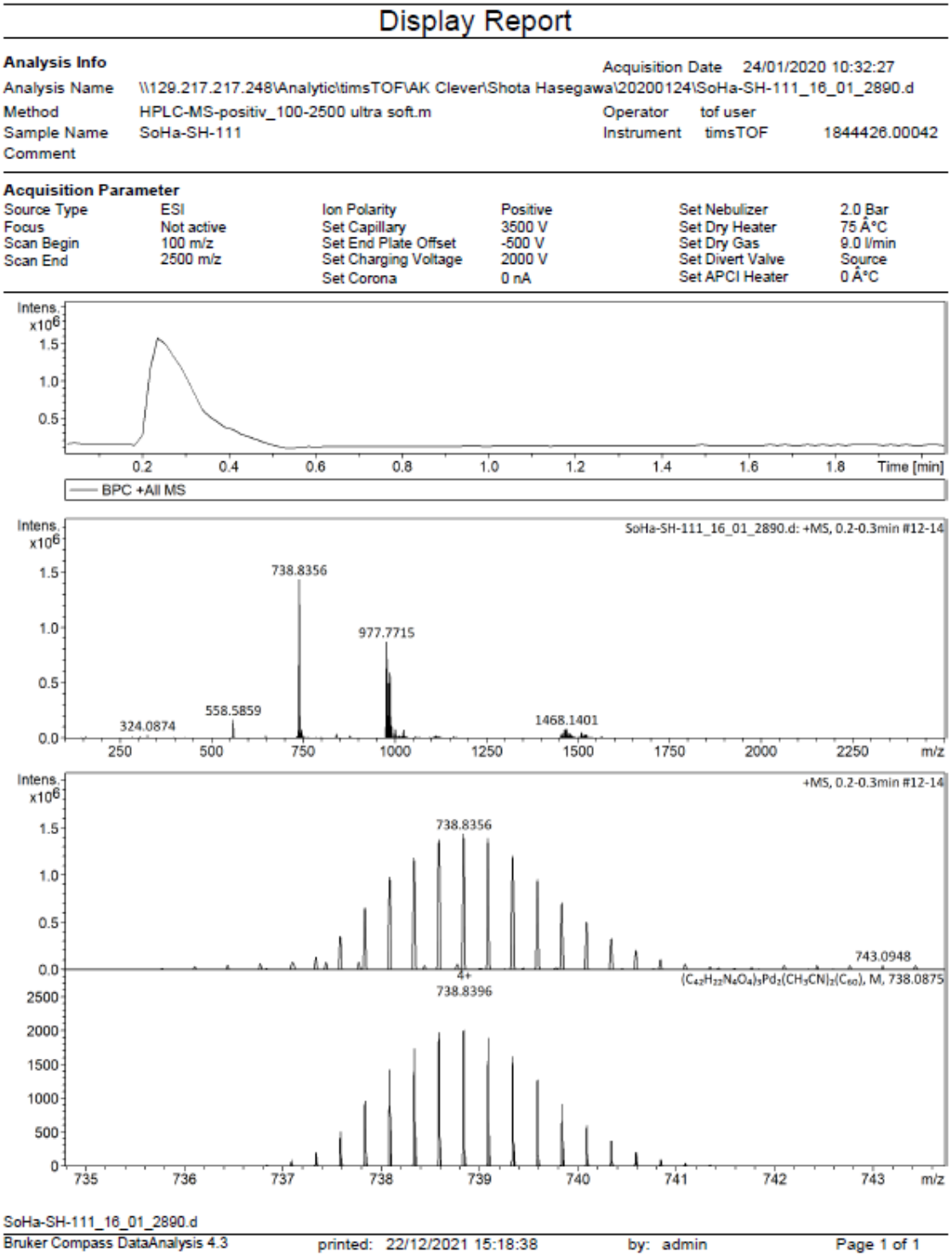

Figure 6.4.69 ESI-MS spectrum of $C_{60}@Pd_2L^{Q}_3(MeCN)_2$ (positive)

6.4.5.4 Diels-Alder reaction between anthracene and $C_{60}@Pd_2L^{Q}_3(MeCN)_2$

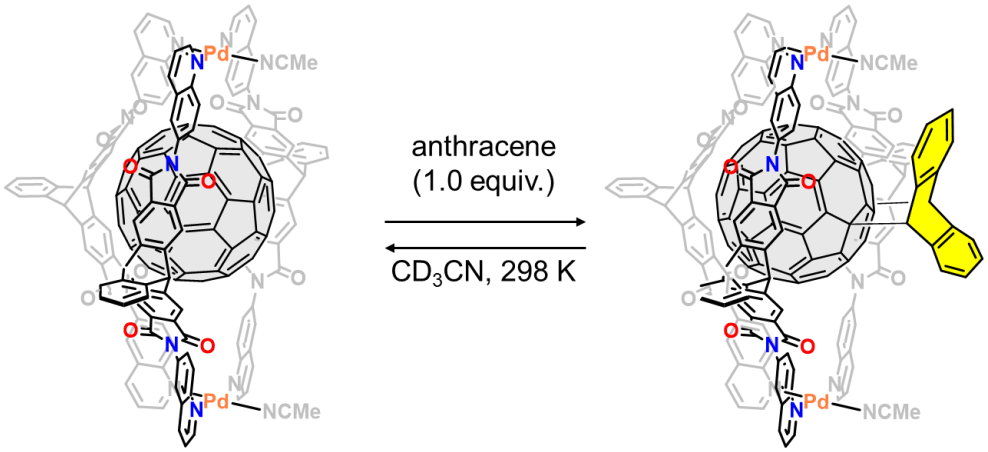

Figure 6.4.70 Diels-Alder reaction of $C_{60}@Pd_2\mathbf{L}^{Q}_3(MeCN)_2$ and anthracene

To an acetonitrile solution of $C_{60}@Pd_2\mathbf{L}^{Q}_3(MeCN)_2$ (0.35mM, 600 µL, 0.21 µmol) in a NMR tube wrapped with aluminium foil, anthracene (20.0 mM in CD_3CN, 10.5 µL, 0.21 µmol) was added and the tube was shaken in the dark. The mixture was let stand in the dark for 7 days at ambient temperature. Formation of $C_{60}ant@Pd_2\mathbf{L}^{Q}_3(MeCN)_2$ was not observed.

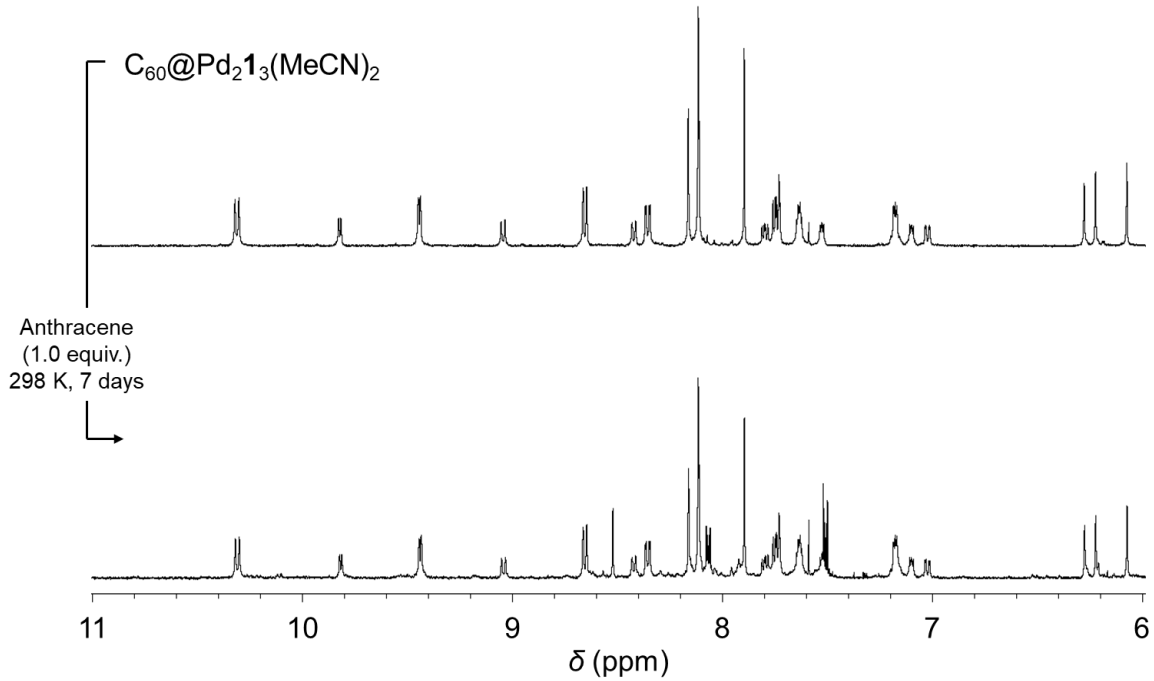

Figure 6.4.71 ^1H NMR spectra (500 MHz, 298 K, CD_3CN) of $C_{60}@Pd_2\mathbf{L}^{Q}_3(MeCN)_2$ (0.70 mM) mixture of $C_{60}@Pd_2\mathbf{L}^{Q}_3(MeCN)_2$ (0.35 mM) and 1 equivalent of anthracene after 7 days (bottom)

6.4.5.5 Diels-Alder reaction between DMA and $C_{60}@Pd_2L^{Q}_3(MeCN)_2$

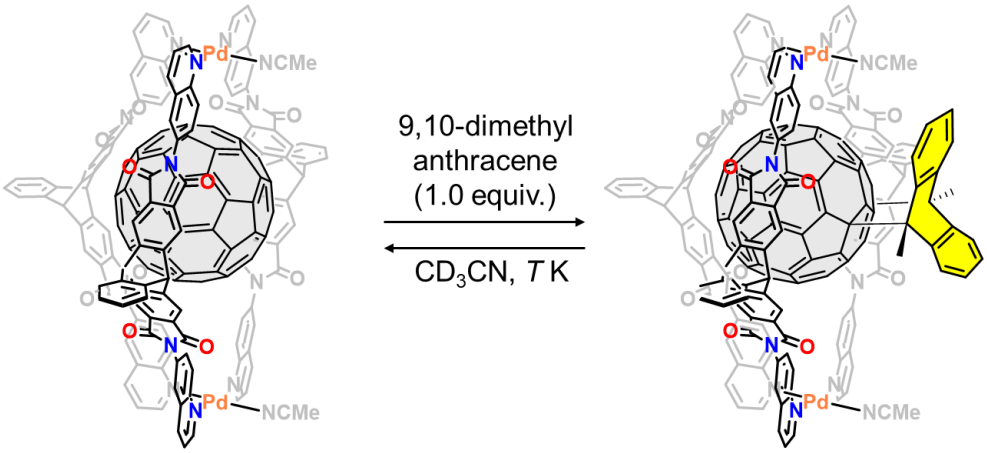

Figure 6.4.72 Diels-Alder reaction of $C_{60}@Pd_2\mathbf{L}^{Q}_3(MeCN)_2$ and DMA

To an acetonitrile solution of $C_{60}@Pd_2\mathbf{L}^{Q}_3(MeCN)_2$ (0.70 mM, 600 µL, 0.42 µmol) in a NMR tube wrapped with aluminium foil, 9,10-dimethylanthracene (20.0 mM in CD_3CN, 21.0 µL, 0.42 µmol) was added and the tube was shaken in the dark. The mixture was let stand in the dark for 1 h at ambient temperature. Besides the signals of $C_{60}@Pd_2\mathbf{L}^{Q}_3(MeCN)_2$, a new set of signals appeared which showed temperature dependency.

6.4.5.6 VT-^{1}H NMR measurements

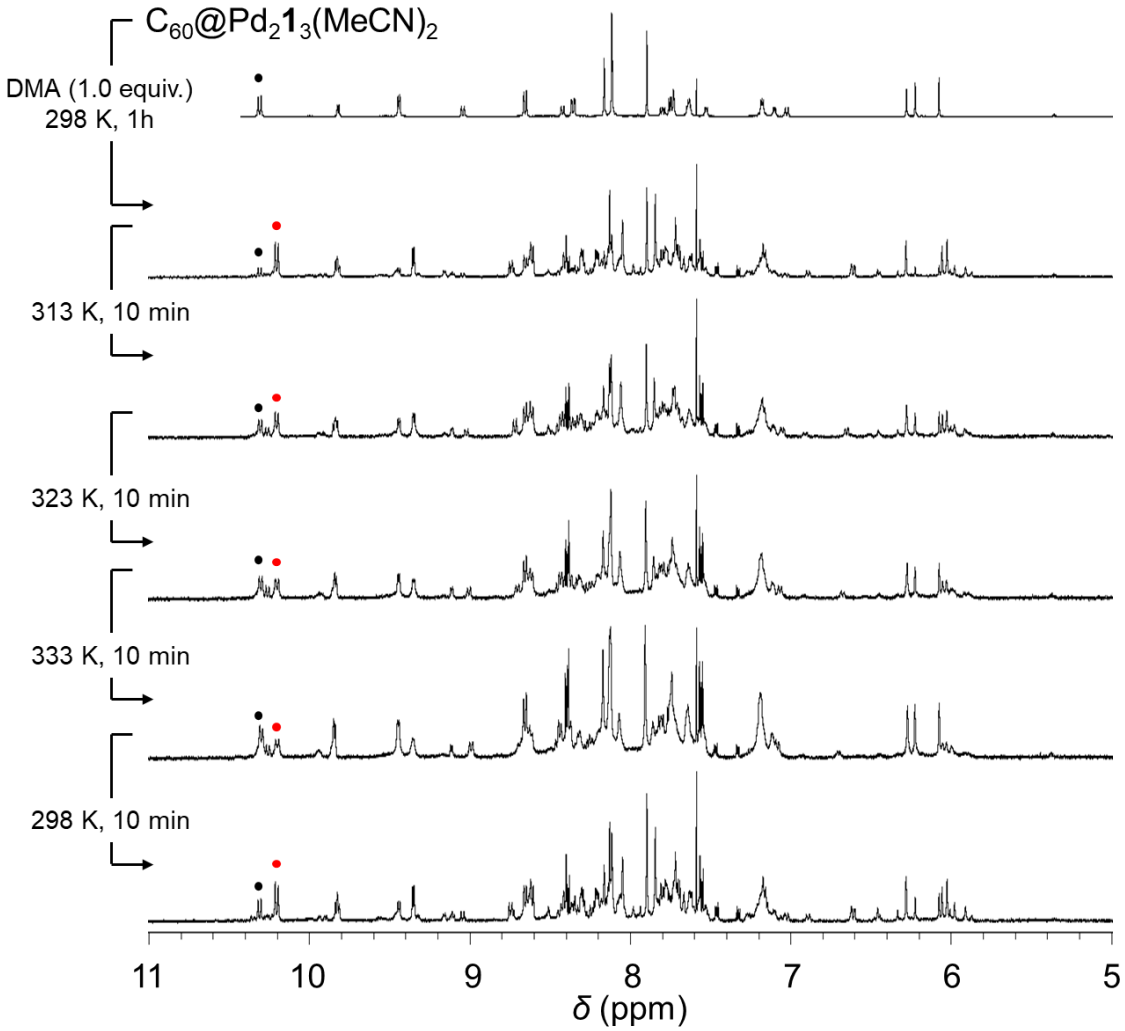

Figure 6.4.73 ^{1}H NMR spectra (500 MHz, 298 K, CD_3CN) of mixture of $C_{60}@Pd_2\mathbf{L}^{Q}_3(MeCN)_2$ and 1 equivalent of DMA

The sample was let stand for 10 min in the NMR spectrometer at each temperature to be sure that the temperature is stable during the measurement. Upon elevating the temperature, the ratio of $C_{60}DMA@Pd_2\mathbf{L}^{Q}_3(MeCN)_2$ to $Pd_2\mathbf{L}^{Q}_3(MeCN)_2$ decreased. To confirm that the process is reversible, the ^{1}H NMR spectrum was measured at 298 K again after the measurements at the higher temperature.

6.4.5.7 ESI MS spectrum of $C_{60}DMA@Pd_2L^Q_3$

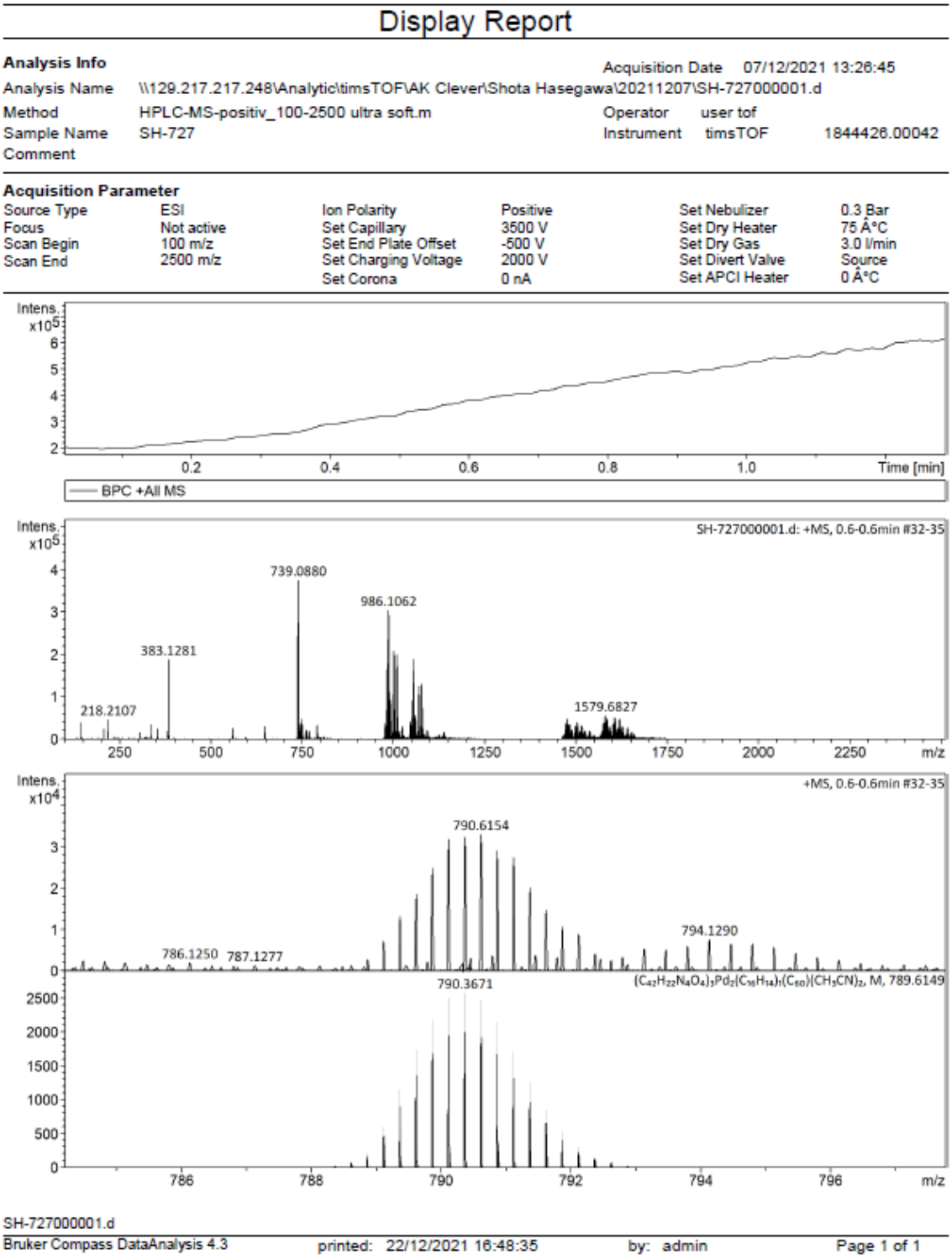

Figure 6.4.74 ESI-MS spectrum of $C_{60}DMA@Pd_2L^Q_3(MeCN)_2$ (positive)

6.4.6 Topochemical reaction

6.4.6.1 NMR experiments

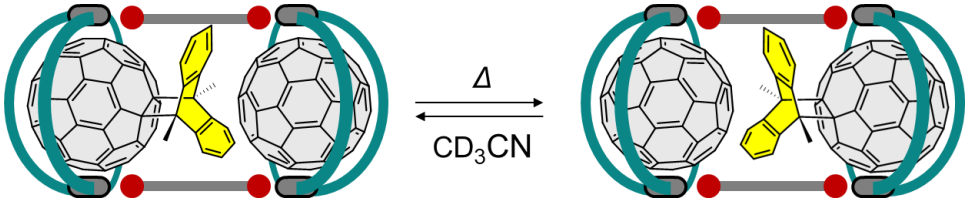

Figure 6.4.75 Topochemical-like reaction inside $Pd_4\mathbf{L}^{Q}_6(Nap)_2$

The EXSY experiments were performed by Prof. Dr. Wolf G. Hiller. The sample was prepared following **6.4.2.5**. The EXSY spectra were measured at various temperatures with various mixing time.

6.4.6.1.1 1D ^{1}H NOESY spectrum

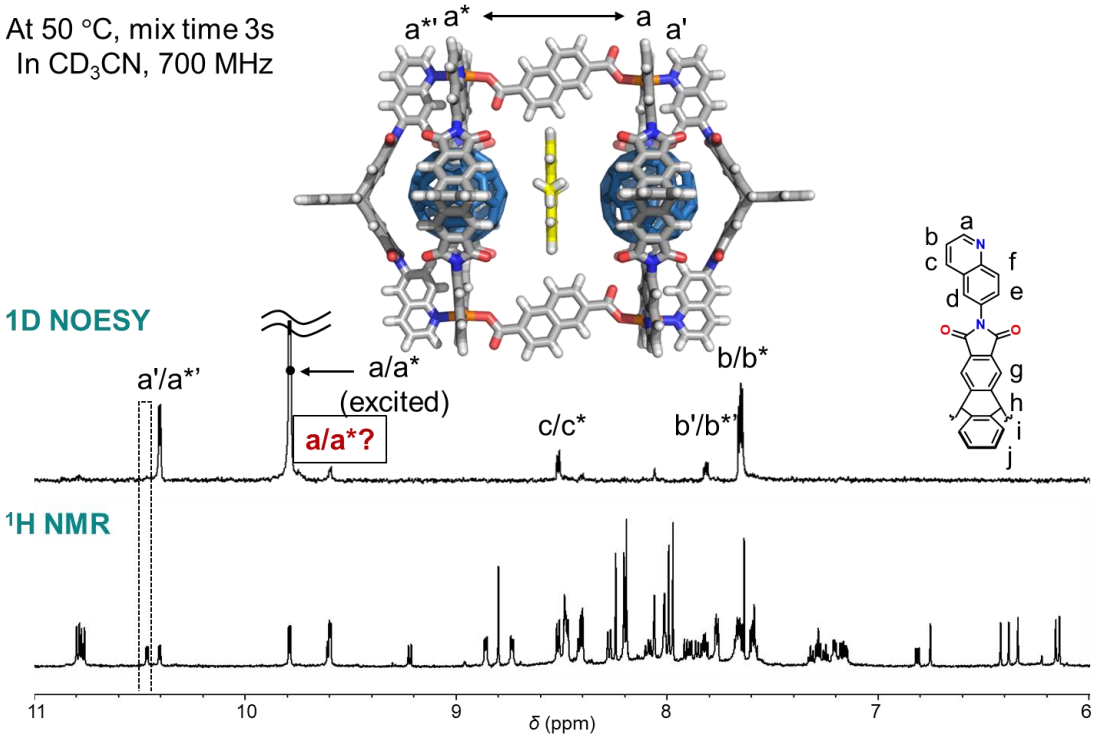

Figure 6.4.76 1D NOESY spectrum (mixing time = 3s) of C_{60}DMA•C_{60}@$Pd_4\mathbf{L}^{Q}_6(Nap)_2$ (0.33 mM, 642 μL, 0.21 μmol, CD_3CN, 700 MHz) (top) and ^{1}H NMR spectrum of C_{60}DMA•C_{60}@$Pd_4\mathbf{L}^{Q}_6(Nap)_2$ (0.33 mM, 642 μL, 0.21 μmol, CD_3CN) (bottom) at 50 °C

6.4.6.1.2 2D ^{1}H EXSY spectra

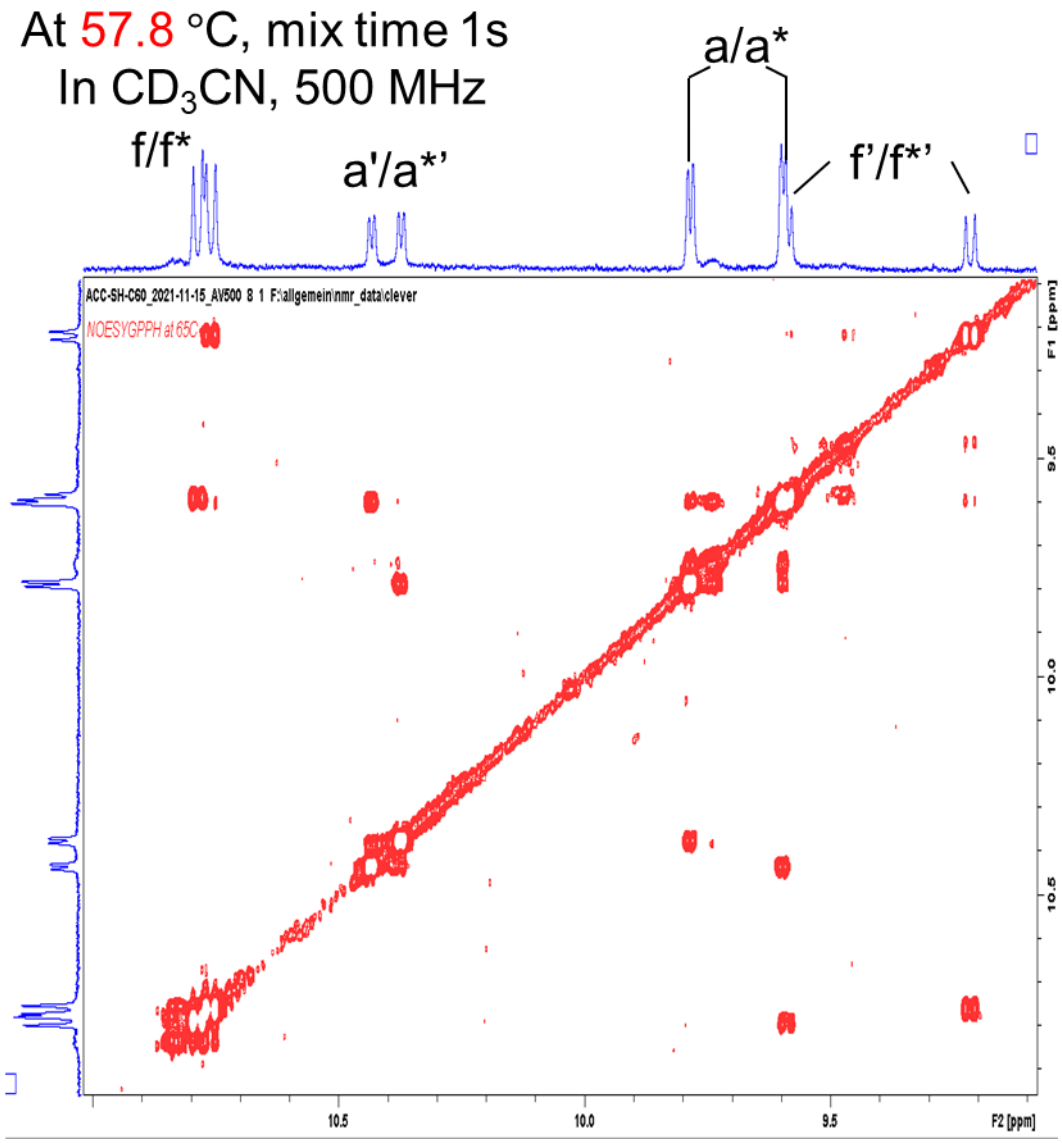

Figure 6.4.77 Overview of 2D EXSY spectrum (mixing time = 1s) of C_{60}DMA•C_{60}@Pd_4**L**$^{Q}_6$$(Nap)_2$ (0.33 mM, 642 µL, 0.21 µmol, CD_3CN, 500 MHz) at 57.8 °C

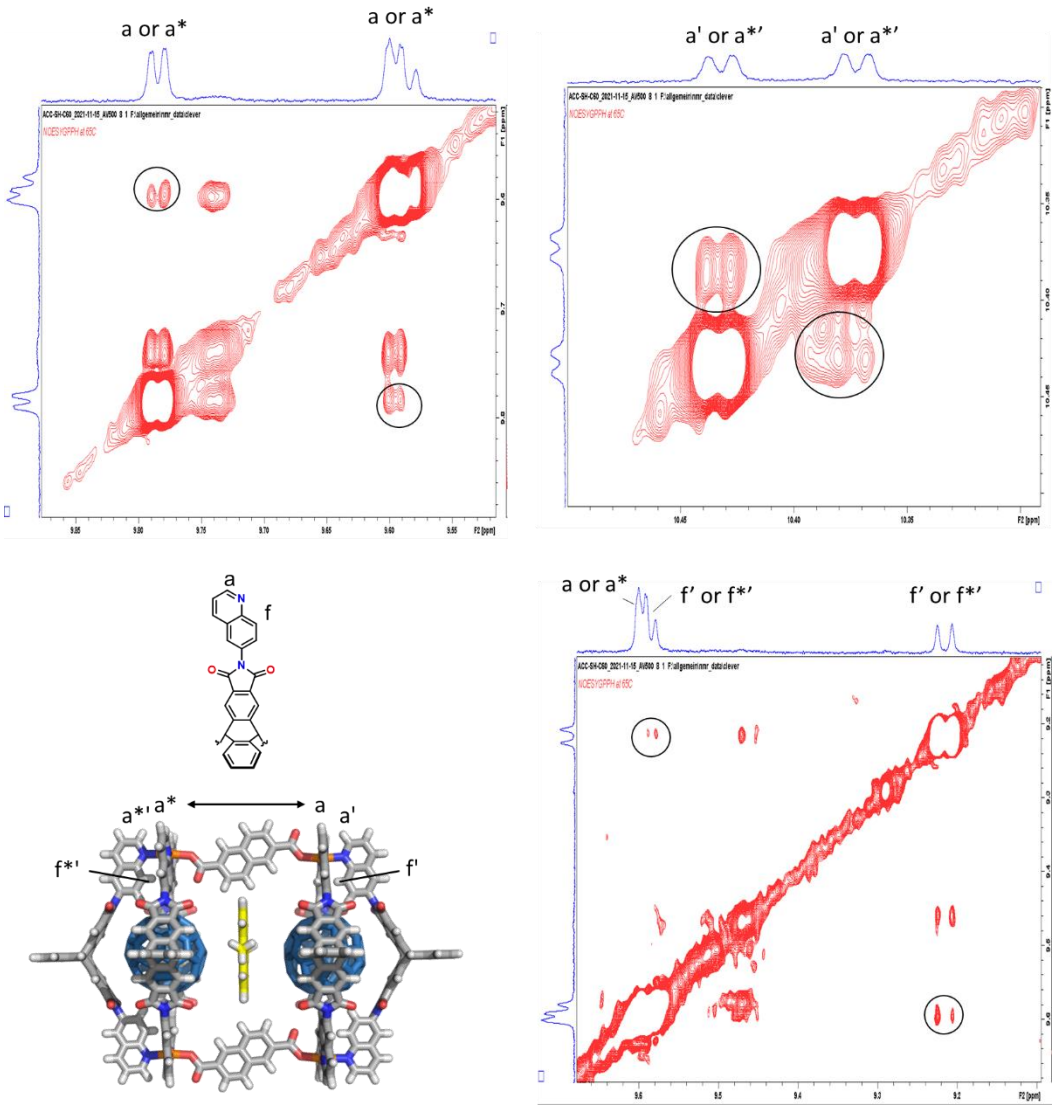

Figure 6.4.78 2D EXSY spectra (mixing time = 1s) of C_{60}DMA•C_{60}@Pd$_4$**L**$^{Q}_6$(Nap)$_2$ (0.33 mM, 642 µL, 0.21 µmol, CD_3CN, 500 MHz) at 57.8 °C

At 57.8 °C, mix time 1s
In CD_3CN, 500 MHz

$$k = \frac{\kappa k_B \cdot T}{h} \cdot e^{-\frac{\Delta G^{\ddagger}}{RT}}$$

Reaction rate (s^{-1})

a'-a*'	1.52	1.24	f'-f*'	0.45	0.66
$\Delta G^{\ddagger}$ (kJ/mol)	80.1	80.7	$\Delta G^{\ddagger}$ (kJ/mol)	83.5	82.4

6.4.6.1.3 Guest-exchange experiments

The sample was prepared as described in **6.4.2.5**. To two solutions in NMR tubes of C_{60}DMA•C_{60}@Pd_4**L**$^{Q}_6$$(Nap)_2$ (0.33 mM, 631 µL, 0.21 µmol), 10 equiv. of corannulene was added each. One of the NMR tube was darkened with alum foil and the other sample was exposed to daylight at room temperature for 3 days. In the darkened sample showed a neglectable guest exchange while the sample exposed to light showed guest-exchange from DMA to corannulene together with the observation of most probably the hetero Diels-Alder product of DMA and singlet oxygen.

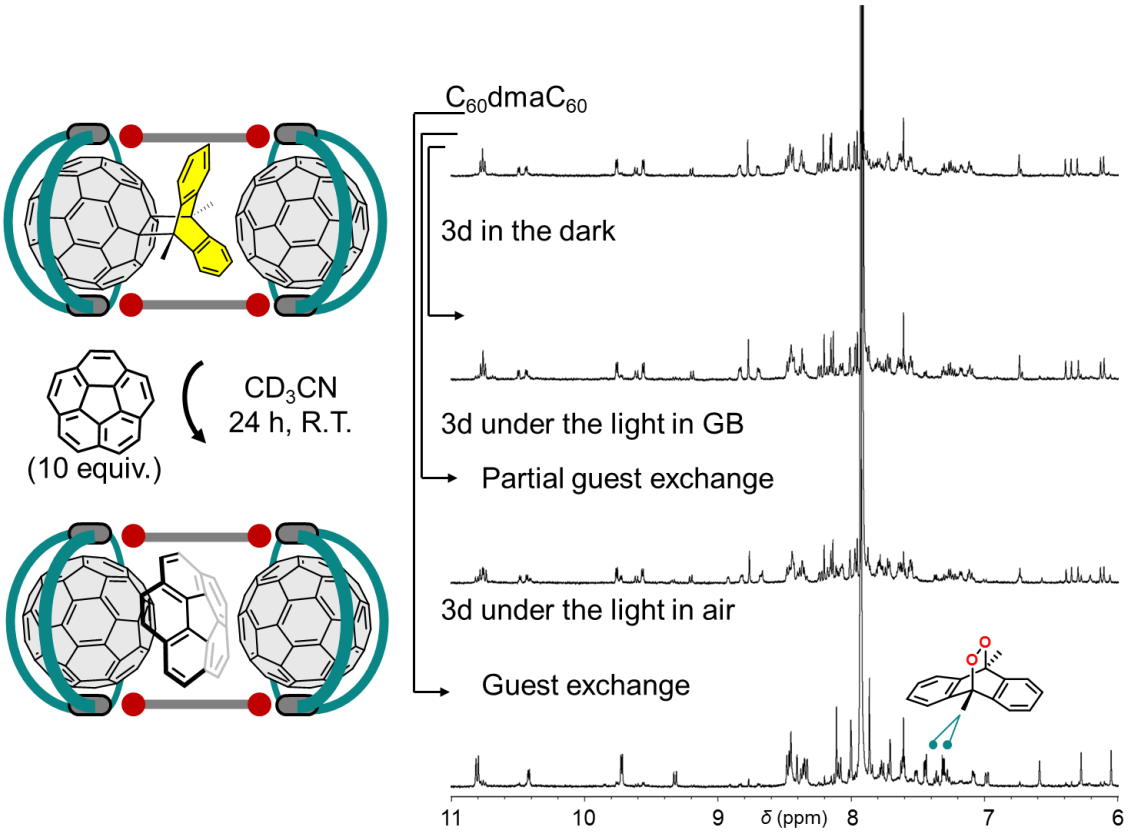

Figure 6.4.79 ^{1}H NMR spectra of C_{60}DMA•C_{60}@Pd_4**L**$^{Q}_6$$(Nap)_2$ (0.33 mM, 642 µL, 0.21 µmol, CD_3CN, 500 MHz, 298 K) after the guest-exchange experiments

6.4.7 Theoretical studies

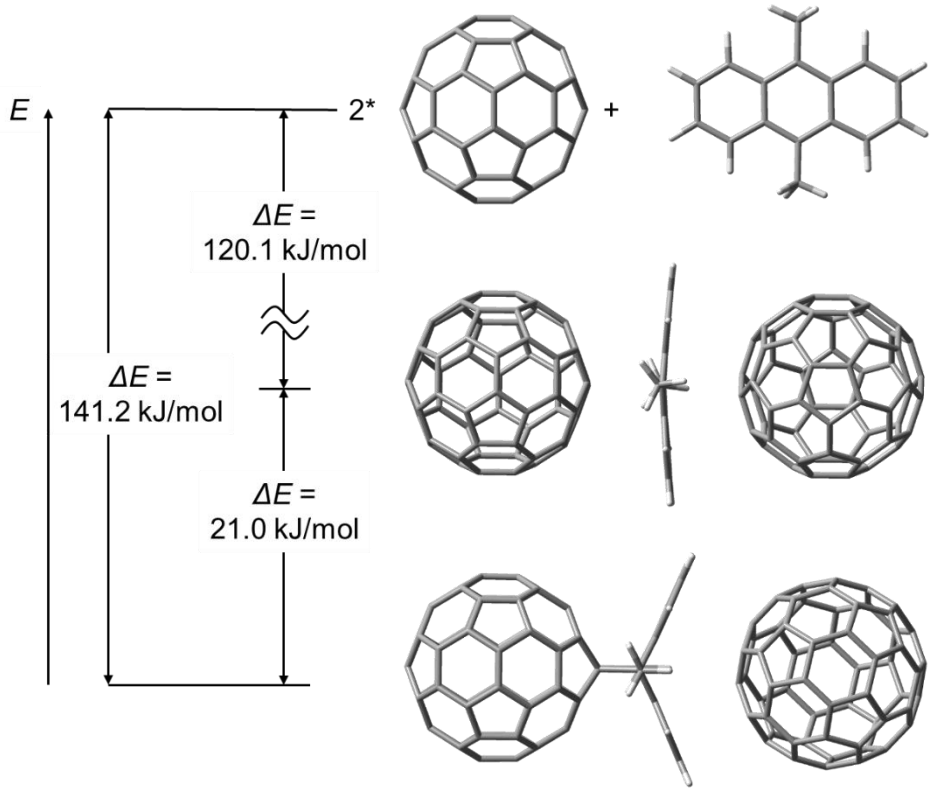

Figure 6.4.80 The energy diagram of each geometry based on the DFT calculations at B3LYP/6-31G(d,p)-D3 level of theory in the gas-phase

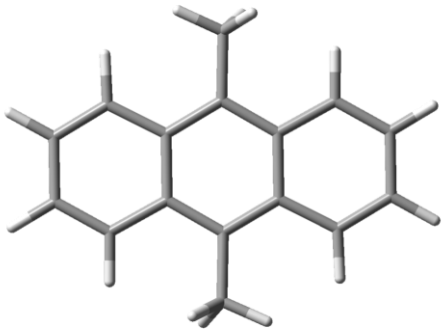

Figure 6.4.81 The optimized geometry of 9,10-Dimethy anthracene at B3LYP/6-31G(d,p)-D3 level of theory in the gas-phase

Standard orientation:

Center Number	Atomic Number	Atomic Type	Coordinates (Angstroms) X	Y	Z
1	6	0	-3.664802	0.744388	-0.053876
2	6	0	-3.676191	-0.675278	-0.046383
3	6	0	-2.496100	-1.367898	-0.013900
4	6	0	-1.225556	-0.703668	0.012790
5	6	0	-1.211799	0.745851	0.009497
6	6	0	-2.476139	1.422525	-0.026387
7	6	0	-0.019372	-1.438722	0.035536
8	6	0	1.211778	-0.745822	0.009458
9	6	0	1.225542	0.703668	0.012810
10	6	0	0.019333	1.438739	0.035413
11	6	0	2.476077	-1.422531	-0.026729
12	6	0	3.664759	-0.744404	-0.054125
13	6	0	3.676170	0.675247	-0.046132
14	6	0	2.496083	1.367890	-0.013558
15	6	0	0.087810	2.950961	0.075194
16	6	0	-0.087675	-2.950943	0.075617
17	1	0	-4.601843	1.292561	-0.085383
18	1	0	-4.621533	-1.209365	-0.070833
19	1	0	-2.526500	-2.450441	-0.019633
20	1	0	-2.500501	2.504643	-0.046184
21	1	0	2.500383	-2.504645	-0.046982
22	1	0	4.601786	-1.292585	-0.085910
23	1	0	4.621524	1.209329	-0.070282
24	1	0	2.526523	2.450433	-0.018809
25	1	0	-0.882775	3.419133	0.225113
26	1	0	0.729571	3.291716	0.894169
27	1	0	0.505840	3.356937	-0.853747
28	1	0	-0.503916	-3.357347	-0.853954
29	1	0	0.882752	-3.418820	0.227541
30	1	0	-0.730818	-3.291572	0.893533

Figure 6.4.82 The optimized geometry of C_{60} at B3LYP/6-31G(d,p)-D3 level of theory in the gas-phase

Standard orientation:

Center Number	Atomic Number	Atomic Type	Coordinates (Angstroms) X	Y	Z
1	6	0	3.304640	0.503772	1.195487
2	6	0	3.472589	-0.656381	0.336029
3	6	0	2.924313	-1.884793	0.706926
4	6	0	2.184779	-2.004038	1.952588
5	6	0	2.023466	-0.890331	2.777647
6	6	0	2.594757	0.389188	2.391358
7	6	0	3.386522	-0.209064	-1.044256
8	6	0	2.266892	-2.717024	-0.287108
9	6	0	1.070496	-2.910141	1.728540
10	6	0	0.741000	-0.636237	3.412899
11	6	0	1.665322	1.434045	2.787861
12	6	0	3.114766	1.668172	0.346330
13	6	0	-0.328712	-1.506024	3.197733
14	6	0	-0.160614	-2.666238	2.338430
15	6	0	-1.664335	-0.975501	2.979985
16	6	0	-1.392333	-2.852605	1.589480
17	6	0	2.755474	-1.007988	-1.998507
18	6	0	1.121173	-3.350672	0.344299
19	6	0	-2.321744	-1.807739	1.986041
20	6	0	-0.061245	-3.529727	-0.374683
21	6	0	2.184227	-2.287578	-1.612220
22	6	0	0.519686	0.800324	3.419262
23	6	0	1.482936	2.551699	1.972647
24	6	0	1.876773	-0.403591	-2.986083
25	6	0	2.222399	2.671169	0.726989
26	6	0	3.165391	1.227573	-1.037947
27	6	0	0.147346	3.082399	1.754999
28	6	0	1.343646	3.275464	-0.260630
29	6	0	2.321746	1.807739	-1.986042
30	6	0	-1.343646	-3.275462	0.260632
31	6	0	-0.762482	1.309646	3.210263
32	6	0	0.952428	-2.473919	-2.361078
33	6	0	0.061247	3.529728	0.374684
34	6	0	1.392331	2.852604	-1.589477
35	6	0	1.664337	0.975499	-2.979985
36	6	0	0.328709	1.506023	-3.197730
37	6	0	0.762482	-1.309648	-3.210265
38	6	0	-0.147343	-3.082394	-1.754998
39	6	0	-1.482936	-2.551696	-1.972646
40	6	0	0.160614	2.666238	-2.338430
41	6	0	-1.070494	2.910136	-1.728538
42	6	0	-2.184782	2.004041	-1.952590
43	6	0	-1.121173	3.350675	-0.344299
44	6	0	-1.876770	0.403589	2.986080
45	6	0	-1.665323	-1.434044	-2.787860
46	6	0	-0.952426	2.473920	2.361078
47	6	0	-2.184227	2.287576	1.612218
48	6	0	-0.519685	-0.800325	-3.419262
49	6	0	-2.222399	-2.671166	-0.726991
50	6	0	-3.114767	-1.668169	-0.346330
51	6	0	-0.741001	0.636236	-3.412900
52	6	0	-2.023464	0.890330	-2.777646
53	6	0	-2.266892	2.717025	0.287108
54	6	0	-2.924312	1.884791	-0.706925
55	6	0	-2.594759	-0.389191	-2.391360
56	6	0	-2.755475	1.007988	1.998505
57	6	0	-3.165393	-1.227573	1.037947
58	6	0	-3.304641	-0.503772	-1.195486
59	6	0	-3.386520	0.209063	1.044254
60	6	0	-3.472594	0.656382	-0.336028

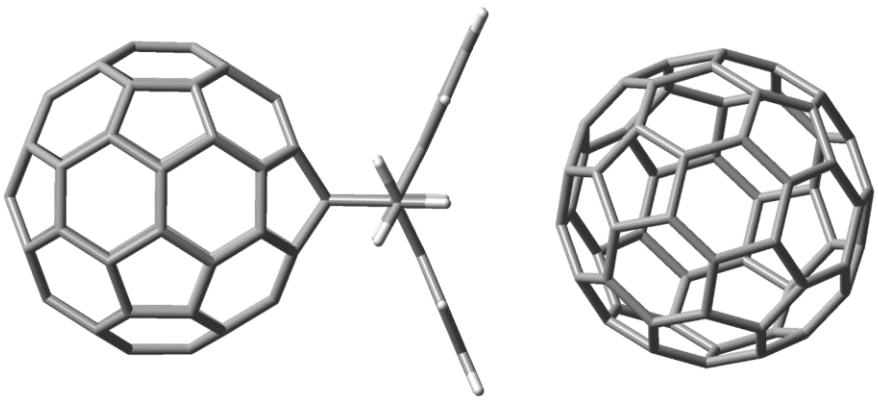

Figure 6.4.83 The optimized geometry of C_{60}DMA•C_{60} at B3LYP/6-31G(d,p)-D3 level of theory in the gas-phase

Standard orientation:

Center Number	Atomic Number	Atomic Type	Coordinates (Angstroms) X	Y	Z
1	6	0	9.426406	1.153463	-1.253719
2	6	0	9.833625	-0.030650	-0.516258
3	6	0	9.775669	-0.040123	0.878114
4	6	0	9.307852	1.134102	1.595202
5	6	0	8.910143	2.270681	0.888040
6	6	0	8.970633	2.280477	-0.566584
7	6	0	9.408200	-1.197699	-1.270438
8	6	0	9.289673	-1.217041	1.578503
9	6	0	8.534888	0.683485	2.739211
10	6	0	7.724613	3.000869	1.293285
11	6	0	7.822367	3.016537	-1.058960
12	6	0	8.751198	0.718814	-2.463896
13	6	0	6.980650	2.571510	2.394041
14	6	0	7.395048	1.387806	3.131736
15	6	0	5.530303	2.578558	2.335827
16	6	0	6.198141	0.665811	3.525798
17	6	0	8.934933	-2.327162	-0.599362
18	6	0	8.523646	-0.770821	2.728887
19	6	0	5.050132	1.406914	3.026439
20	6	0	7.372938	-1.462859	3.111400
21	6	0	8.874419	-2.337101	0.855252
22	6	0	7.046209	3.456160	0.089894
23	6	0	7.172662	2.602827	-2.223497
24	6	0	7.775485	-3.038320	-1.102034
25	6	0	7.647500	1.429029	-2.940157
26	6	0	8.739938	-0.735471	-2.474244
27	6	0	5.722431	2.609836	-2.285904
28	6	0	6.487798	0.713095	-3.441896
29	6	0	7.625453	-1.421651	-2.960468
30	6	0	6.187327	-0.728110	3.515884
31	6	0	5.652226	3.448939	0.031783
32	6	0	7.677712	-3.054563	1.250228
33	6	0	5.301759	1.447918	-3.029659
34	6	0	6.477039	-0.680758	-3.451830
35	6	0	7.132393	-2.598010	-2.260466
36	6	0	5.682252	-2.581633	-2.322793
37	6	0	6.992481	-3.482133	0.040551
38	6	0	6.940353	-2.629425	2.357055
39	6	0	5.490071	-2.613186	2.298941
40	6	0	5.279732	-1.402872	-3.049929
41	6	0	4.148200	-0.696797	-2.630219
42	6	0	3.346453	-1.147007	-1.524924
43	6	0	4.159225	0.753705	-2.620058
44	6	0	4.875028	3.001387	1.173723
45	6	0	4.828467	-3.009232	1.131005
46	6	0	4.972575	3.017461	-1.176770
47	6	0	3.772231	2.304071	-0.794761
48	6	0	5.598783	-3.452546	-0.017272
49	6	0	5.028025	-1.444178	3.006156
50	6	0	3.935156	-0.731737	2.503349
51	6	0	4.926092	-2.993394	-1.219482
52	6	0	3.736941	-2.267020	-0.827219
53	6	0	3.364040	1.200551	-1.508551
54	6	0	2.558623	0.028558	-0.929434
55	6	0	3.675619	-2.277039	0.651172
56	6	0	3.711053	2.294025	0.683628
57	6	0	3.946476	0.718689	2.513613
58	6	0	3.228329	-1.166357	1.329231
59	6	0	3.246717	1.180843	1.345827
60	6	0	2.492835	0.017796	0.686501
61	6	0	-0.592601	-3.402015	-0.964912
62	6	0	-0.641324	-3.413635	0.428457
63	6	0	-0.178522	-2.314498	1.154169
64	6	0	0.331522	-1.202450	0.483797
65	6	0	0.386456	-1.193478	-0.918315
66	6	0	-0.075527	-2.293491	-1.639506
67	6	0	0.935559	0.027484	1.146478
68	6	0	0.350656	1.274466	0.498401
69	6	0	0.403490	1.280933	-0.903572
70	6	0	1.043061	0.042854	-1.515237
71	6	0	-0.140159	2.387109	1.180545
72	6	0	-0.587365	3.501808	0.466832
73	6	0	-0.542518	3.505108	-0.925779
74	6	0	-0.044896	2.395309	-1.612366
75	6	0	0.771510	0.019349	2.666288
76	6	0	1.006762	0.052233	-3.043319
77	1	0	-0.961103	-4.252570	-1.530151
78	1	0	-1.050280	-4.271680	0.952536
79	1	0	-0.227113	-2.332846	2.236513
80	1	0	-0.041355	-2.298644	-2.722732
81	1	0	-0.186415	2.395622	2.263169
82	1	0	-0.980131	4.360825	1.001884
83	1	0	-0.899166	4.367106	-1.481097
84	1	0	-0.012966	2.410284	-2.695555
85	1	0	-0.293344	0.023564	2.916400
86	1	0	1.235993	0.893516	3.125125
87	1	0	1.225710	-0.865742	3.114398
88	1	0	-0.032857	0.062208	-3.383255
89	1	0	1.495692	-0.828825	-3.461942
90	1	0	1.508865	0.930933	-3.451195
91	6	0	-4.475721	1.845763	-2.343701
92	6	0	-3.533843	0.806838	-1.961839
93	6	0	-2.982922	0.804251	-0.679883

94	6	0	-3.347911	1.840540	0.269480
95	6	0	-4.246717	2.840709	-0.097279
96	6	0	-4.824464	2.842542	-1.430078
97	6	0	-3.974181	-0.441916	-2.563636
98	6	0	-2.841960	-0.443105	0.050809
99	6	0	-3.427301	1.236385	1.589171
100	6	0	-5.271298	3.273587	0.839313
101	6	0	-6.207971	3.274626	-1.317756
102	6	0	-5.498425	1.239520	-3.180787
103	6	0	-5.350566	2.693296	2.105735
104	6	0	-4.408642	1.652861	2.488593
105	6	0	-6.646303	2.353619	2.668604
106	6	0	-5.122460	0.672055	3.289079
107	6	0	-3.842063	-1.639409	-1.859290
108	6	0	-3.114378	-0.176893	1.454648
109	6	0	-6.505622	1.104878	3.399869
110	6	0	-3.797679	-1.118817	2.224824
111	6	0	-3.267414	-1.637289	-0.525600
112	6	0	-6.483720	3.541909	0.084691
113	6	0	-7.188538	2.693613	-2.122612
114	6	0	-4.914650	-2.620348	-1.882871
115	6	0	-6.826526	1.654958	-3.072818
116	6	0	-5.188306	-0.174360	-3.317074
117	6	0	-8.484681	2.354727	-1.558288
118	6	0	-7.899030	0.674210	-3.095657
119	6	0	-6.218737	-1.115830	-3.338841
120	6	0	-4.823835	-0.685483	3.158944
121	6	0	-7.728192	3.217005	0.626092
122	6	0	-3.979096	-2.619182	0.274586
123	6	0	-8.923829	1.106677	-2.159987
124	6	0	-7.601480	-0.682787	-3.226061
125	6	0	-6.078841	-2.364273	-2.607762
126	6	0	-7.375195	-2.703087	-2.043182
127	6	0	-4.998264	-3.226989	-0.563704
128	6	0	-4.238715	-2.367560	1.621723
129	6	0	-5.535420	-2.704999	2.184397
130	6	0	-8.316201	-1.663615	-2.425705
131	6	0	-9.299821	-1.248251	-1.527426
132	6	0	-9.382878	-1.854700	-0.209007
133	6	0	-9.609905	0.165240	-1.391920
134	6	0	-7.811222	2.610734	1.944301
135	6	0	-6.516600	-3.286644	1.379505
136	6	0	-8.749165	2.611156	-0.212465
137	6	0	-9.463402	1.630241	0.587812
138	6	0	-6.242282	-3.553366	-0.022575
139	6	0	-5.897053	-1.665881	3.134750
140	6	0	-7.224851	-1.249855	3.241372
141	6	0	-7.455384	-3.285639	-0.777781
142	6	0	-8.479451	-2.852575	0.158225
143	6	0	-9.884997	0.432237	0.010132
144	6	0	-9.744526	-0.816111	0.741264
145	6	0	-7.899183	-2.852785	1.491067
146	6	0	-8.883433	1.629738	1.920685
147	6	0	-7.535384	0.163619	3.377016
148	6	0	-8.246394	-1.855720	2.403370
149	6	0	-8.748665	0.431444	2.622660
150	6	0	-9.187832	-0.816576	2.020736

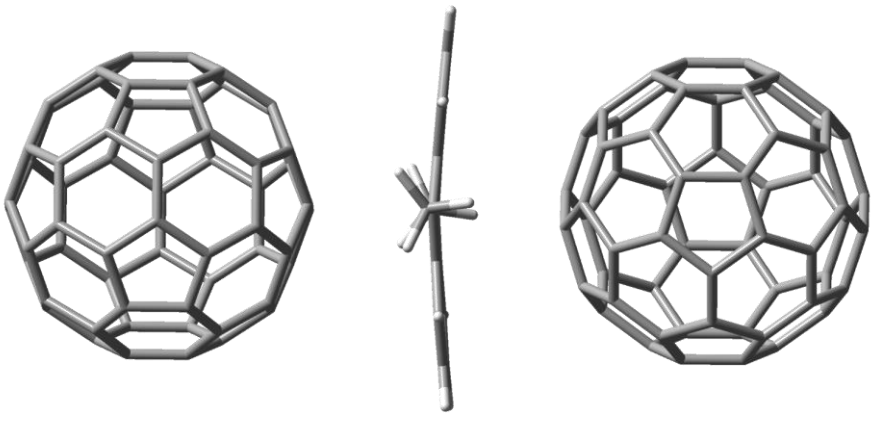

Figure 6.4.84 The optimized geometry of C_{60}•DMA•C_{60} at B3LYP/6-31G(d,p)-D3 level of theory in the gas-phase

Standard orientation:

Center Number	Atomic Number	Atomic Type	Coordinates (Angstroms) X	Y	Z
1	6	0	-8.776091	-0.430550	2.665398
2	6	0	-8.776148	1.013796	2.502371
3	6	0	-7.647342	1.755418	2.852898
4	6	0	-6.472052	1.083877	3.381894
5	6	0	-6.472102	-0.302766	3.538662

6	6	0	-7.647380	-1.075425	3.172626	56	6	0	-3.868374	-2.375059	-0.464321
7	6	0	-9.502658	1.328254	1.283439	57	6	0	-2.996695	-0.077980	-0.692908
8	6	0	-7.197442	2.842415	1.998698	58	6	0	-4.168116	0.431213	-2.665748
9	6	0	-5.295939	1.757200	2.854449	59	6	0	-3.443659	-1.328212	-1.282327
10	6	0	-5.295951	-1.076610	3.174296	60	6	0	-4.167645	-1.014746	-2.502730
11	6	0	-7.197314	-2.325310	2.581903	61	6	0	4.156264	-2.073944	1.730899
12	6	0	-9.502475	-1.008787	1.547204	62	6	0	4.156269	-0.875139	2.555651
13	6	0	-4.168226	-0.431128	2.665850	63	6	0	5.284607	-0.544386	3.306714
14	6	0	-4.167812	1.014831	2.502829	64	6	0	6.460711	-1.398324	3.264232
15	6	0	-3.444643	-1.008721	1.545954	65	6	0	6.460647	-2.548213	2.473471
16	6	0	-3.443781	1.328328	1.282461	66	6	0	5.284450	-2.893924	1.691548
17	6	0	-9.070829	2.371567	0.463706	67	6	0	3.431641	0.162456	1.839806
18	6	0	-5.744005	2.843814	2.000028	68	6	0	5.732911	0.836772	3.373450
19	6	0	-2.996733	0.078116	0.693066	69	6	0	7.635916	-0.544385	3.304847
20	6	0	-5.045302	3.145158	0.829022	70	6	0	7.636139	-2.891720	1.690804
21	6	0	-7.895085	3.144064	0.828546	71	6	0	5.732931	-3.450546	0.425762
22	6	0	-5.744024	-2.326411	2.583463	72	6	0	3.433441	-1.776022	0.506380
23	6	0	-7.895094	-2.880512	1.508585	73	6	0	8.764935	-2.072353	1.730694
24	6	0	-9.070712	2.208448	-0.980766	74	6	0	8.764930	-0.874751	2.554294
25	6	0	-9.070664	-2.208577	0.980620	75	6	0	9.491576	-1.776046	0.507261
26	6	0	-9.951669	0.078186	0.693125	76	6	0	9.491562	0.161764	1.840055
27	6	0	-7.167897	-3.458347	0.390360	77	6	0	3.857289	1.490179	1.907115
28	6	0	-9.070702	-2.371695	-0.463852	78	6	0	7.186323	0.836467	3.372198
29	6	0	-9.951631	-0.078353	-0.693315	79	6	0	9.940859	-0.395319	0.574884
30	6	0	-3.868502	2.375156	0.464433	80	6	0	7.884132	1.831420	2.686630
31	6	0	-5.045130	-2.881537	1.509361	81	6	0	5.034550	1.832540	2.687802
32	6	0	-7.168028	3.458301	-0.390412	82	6	0	7.186365	-3.448648	0.425407
33	6	0	-7.894907	-3.144141	-0.828634	83	6	0	5.034561	-3.165859	-0.749276
34	6	0	-9.502537	-1.328402	-1.283607	84	6	0	3.857647	2.314123	0.708148
35	6	0	-9.502442	1.008639	-1.547372	85	6	0	3.857717	-2.314187	-0.708307
36	6	0	-8.775978	0.430434	-2.665530	86	6	0	2.991695	-0.394606	0.573468
37	6	0	-7.895145	2.880435	-1.508673	87	6	0	5.761985	-2.869185	-1.972943
38	6	0	-5.772623	3.459227	-0.390464	88	6	0	3.857413	-1.490242	-1.907274
39	6	0	-5.045181	2.881584	-1.509309	89	6	0	2.991720	0.394531	-0.573673
40	6	0	-8.775979	-1.013911	-2.502503	90	6	0	9.059979	1.487088	1.904818
41	6	0	-7.647124	-1.755485	-2.852974	91	6	0	7.884301	-3.164365	-0.748964
42	6	0	-6.471837	-1.083893	-3.381911	92	6	0	5.761837	2.869150	1.972887
43	6	0	-7.197219	-2.842462	-1.998751	93	6	0	5.034721	-1.832586	-2.687897
44	6	0	-3.868152	-2.212217	0.982222	94	6	0	3.431740	-0.162525	-1.839990
45	6	0	-5.743998	2.326428	-2.583445	95	6	0	3.433441	1.775954	-0.506562
46	6	0	-5.772491	-3.459211	0.390481	96	6	0	4.156328	2.073886	-1.731042
47	6	0	-5.045123	-3.145112	-0.828968	97	6	0	5.034476	3.165813	0.749180
48	6	0	-7.197287	2.325263	-2.581956	98	6	0	7.157359	2.868169	1.972386
49	6	0	-3.868200	2.212316	-0.982110	99	6	0	7.884215	3.164358	0.749022
50	6	0	-3.444612	1.008835	-1.545815	100	6	0	4.156394	0.875081	-2.555793
51	6	0	-7.647269	1.075358	-3.172701	101	6	0	5.284778	0.544344	-3.306796
52	6	0	-6.471940	0.302750	-3.538677	102	6	0	6.460867	1.398299	-3.264250
53	6	0	-5.743782	-2.843798	-2.000009	103	6	0	5.733106	-0.836808	-3.373507
54	6	0	-5.295720	-1.757165	-2.854407	104	6	0	9.060035	-2.310771	-0.707060
55	6	0	-5.295840	1.076647	-3.174254	105	6	0	7.186339	3.448632	-0.425387

106	6	0	7.157507	-2.868187	-1.972368
107	6	0	7.884302	-1.831425	-2.686572
108	6	0	5.732905	3.450510	-0.425820
109	6	0	9.059965	2.310783	0.707181
110	6	0	9.491578	1.776063	-0.507116
111	6	0	5.284500	2.893882	-1.691630
112	6	0	6.460744	2.548187	-2.473489
113	6	0	7.186517	-0.836483	-3.372177
114	6	0	7.636086	0.544376	-3.304801
115	6	0	7.636189	2.891711	-1.690759
116	6	0	9.060102	-1.487077	-1.904696
117	6	0	9.940885	0.395342	-0.574715
118	6	0	8.765000	2.072361	-1.730588
119	6	0	9.491664	-0.161746	-1.839910
120	6	0	8.765055	0.874758	-2.554189
121	6	0	0.183205	3.658301	-0.724521
122	6	0	0.200423	3.662603	0.693473
123	6	0	0.109114	2.482827	1.384104
124	6	0	0.005230	1.222852	0.713862
125	6	0	-0.004107	1.216994	-0.731842
126	6	0	0.079342	2.475387	-1.408236
127	6	0	-0.076988	0.009112	1.434535
128	6	0	-0.004138	-1.216844	0.731953
129	6	0	0.005171	-1.222703	-0.713743
130	6	0	-0.077010	-0.008960	-1.434419
131	6	0	0.079276	-2.475232	1.408352
132	6	0	0.183086	-3.658152	0.724636
133	6	0	0.200267	-3.662457	-0.693358
134	6	0	0.108984	-2.482679	-1.383991
135	6	0	-0.191054	0.038942	2.941182
136	6	0	-0.191068	-0.038869	-2.941067
137	1	0	0.262226	4.594346	-1.268954
138	1	0	0.294454	4.601445	1.230563
139	1	0	0.145123	2.504365	2.466065
140	1	0	0.096387	2.495658	-2.490525
141	1	0	0.096333	-2.495495	2.490643
142	1	0	0.262084	-4.594199	1.269069
143	1	0	0.294248	-4.601304	-1.230447
144	1	0	0.144937	-2.504217	-2.465954
145	1	0	0.788721	0.176316	3.415645
146	1	0	-0.630728	-0.876506	3.336200
147	1	0	-0.837672	0.856192	3.268770
148	1	0	0.788644	-0.176912	-3.415459
149	1	0	-0.630166	0.876788	-3.336223
150	1	0	-0.838173	-0.855780	-3.268558

6.5 References

[1] J. A. Prescher, C. R. Bertozzi, *Nat. Chem. Biol.* **2005**, *1*, 13–21.

[2] J.-M. Lehn, *Supramolecular Chemistry*, **1995**, Weinheim, VCH Verlagsgesellschaft mbH

[3] E. Persch, O. Dumele, F. Diederich, *Angew. Chem. Int. Ed.* **2015**, *54*, 3290–3327.

[4] J. Meeuwissen, J. N. H. Reek, *Nat. Chem.* **2010**, *2*, 615.

[5] D. B. Amabilino, D. K. Smith, J. W. Steed, *Chem. Soc. Rev.* **2017**, *46*, 2404–2420.

[6] J. Lehn, *Angew. Chem. Int. Ed.* **1990**, *29*, 1304–1319.

[7] T. Aida, E. W. Meijer, S. I. Stupp, *Science* **2012**, *335*, 813–817.

[8] M. Yoshizawa, J. K. Klosterman, M. Fujita, *Angew. Chem. Int. Ed.* **2009**, *48*, 3418–3438.

[9] J. C. Barnes, E. J. Dale, A. Prokofjevs, A. Narayanan, I. C. Gibbs-Hall, M. Juríček, C. L. Stern, A. A. Sarjeant, Y. Y. Botros, S. I. Stupp, J. F. Stoddart, *J. Am. Chem. Soc.* 2015, *137*, 2392–2399.

[10] X. Yu, B. Wang, Y. Kim, J. Park, S. Ghosh, B. Dhara, R. D. Mukhopadhyay, J. Koo, I. Kim, S. Kim, I.-C. Hwang, S. Seki, D. M. Guldi, M.-H. Baik, K. Kim, *J. Am. Chem. Soc.* **2020**, *142*, 12596–12601.

[11] M. Sawamura, K. Kawai, Y. Matsuo, K. Kanie, T. Kato, E. Nakamura, *Nature* **2002**, *419*, 702–705.

[12] J. E. Fischer, P. A. Heiney, A. B. Smith, *Acc. Chem. Res.* **1992**, *25*, 112–118.

[13] S. Liu, Y.-J. Lu, M. M. Kappes, J. A. Ibers, *Science* **1991**, *254*, 408–410.

[14] Y. Takabayashi, K. Prassides, *Philos. Trans. Royal. Soc. A Math. Phys. Eng. Sci.* **2016**, *374*, 20150320.

[15] B. W. Smith, M. Monthioux, D. E. Luzzi, *Nature* **1998**, *396*, 323–324.

[16] L. Sánchez, N. Martín, D. M. Guldi, *Angew. Chem. Int. Ed.* **2005**, *44*, 5374–5382.

[17] F. Giacalone, N. Martín, *Chem. Rev.* **2006**, *106*, 5136–5190.

[18] B. Sundqvist, *Low Temp. Phys.* **2003**, *29*, 440–444.

[19] K. Mahata, P. D. Frischmann, F. Würthner, *J. Am. Chem. Soc.* **2013**, *135*, 15656–15661.

[20] K. Yazaki, M. Akita, S. Prusty, D. K. Chand, T. Kikuchi, H. Sato, M. Yoshizawa, *Nat. Commun.* **2017**, *8*, ncomms15914.

[21] F. J. Rizzuto, D. M. Wood, T. K. Ronson, J. R. Nitschke, *J. Am. Chem. Soc.* **2017**, *139*, 11008–11011.

[22] K. Matsumoto, S. Kusaba, Y. Tanaka, Y. Sei, M. Akita, K. Aritani, M. Haga, M. Yoshizawa, *Angew. Chem. Int. Ed.* **2019**, *58*, 8463–8467.

[23] B. Chen, J. J. Holstein, S. Horiuchi, W. G. Hiller, G. H. Clever, *J. Am. Chem. Soc.* **2019**, 141, 8907-8913.

[24] Y.-H. Xiao, Y. Shao, X.-X. Ye, H. Cui, D.-L. Wang, X.-H. Zhou, S.-L. Sun, L. Cheng, *Chin. Chem. Lett.* **2016**, *27*, 454–458.

[25] S. Hasegawa, S. L. Meichsner, J. J. Holstein, A. Baksi, M. Kasanmascheff, G. H. Clever, *J. Am. Chem. Soc.* **2021**, *143*, 9718–9723.

[26] E. M. Veen, B. L. Feringa, P. M. Postma, H. T. Jonkman, A. L. Spek, *Chem. Commun.* **1999**, *0*, 1709–1710.

[27] B. Chen, S. Horiuchi, J. J. Holstein, J. Tessarolo, G. H. Clever, *Chem. Eur. J.* **2019**, 25, 14921–14927.

[28] B. Chen, J. J. Holstein, A. Platzek, L. Schneider, K. Wu, G. H. Clever, *Chem. Sci.* **2022**, *13*, 1829–1834.

[29] A. Burkhardt, T. Pakendorf, B. Reime, J. Meyer, P. Fischer, N. Stübe, S. Panneerselvam, O. Lorbeer, K. Stachnik, M. Warmer, P. Rödig, D. Göries, A. Meents, *Eur. Phys. J. Plus* **2016**, *131*, 56.

[30] M. Yamada, K. Ohkubo, M. Shionoya, S. Fukuzumi, *J. Am. Chem. Soc.* **2014**, *136*, 13240–13248.

[31] P. Thordarson, *Chem. Soc. Rev.* **2010**, *40*, 1305–1323.

[32] M. Juríček, N. L. Strutt, J. C. Barnes, A. M. Butterfield, E. J. Dale, K. K. Baldridge, J. F. Stoddart, J. S. Siegel, *Nat. Chem.* **2014**, *6*, 222–228.

[33] H. Joshi, S. Sreejith, R. Dey, M. C. Stuparu, *RSC Adv.* **2016**, *6*, 110001–110003.

[34] R. A. Talmazan, K. R. Liedl, B. Kräutler, M. Podewitz, *Org. Biomol. Chem.* **2020**, *18*, 4090–4103.

[35] B. Kräutler, T. Müller, A. Duarte-Ruiz, *Chem. Eur. J.* **2001**, *7*, 3223–3235.

[36] G. H. Sarova, M. N. Berberan-Santos, *Chem. Phys. Lett.* **2004**, *397*, 402–407.

[37] I. Lamparth, C. Maichle–Mössmer, A. Hirsch, *Angew. Chem. Int. Ed.* **1995**, *34*, 1607–1609.

[38] G.-W. Wang, M. Saunders, R. J. Cross, *J. Am. Chem. Soc.* **2000**, *123*, 256–259.

[39] W. Kabsch, *Acta Crystallogr. D Biol. Crystallogr.* **2010**, *66*, 125–132.

[40] G. M. Sheldrick, *Acta Crystallogr. A Found Adv.* **2015**, *71*, 3–8.

[41] G. M. Sheldrick, *Acta Crystallogr. C Struct. Chem.* **2015**, *71*, 3–8.
[42] C. B. Hübschle, G. M. Sheldrick, B. Dittrich, *J. Appl. Crystallogr.* **2011**, *44*, 1281–1284.
[43] D. Kratzert, J. J. Holstein, I. Krossing, *J. Appl. Crystallogr.* **2015**, *48*, 933–938.
[44] D. Kratzert, I. Krossing, *J. Appl. Crystallogr.* **2018**, *51*, 928–934.
[45] A. Thorn, B. Dittrich, G. M. Sheldrick, *Acta Crystallogr. A Found Crystallogr.* **2012**, *68*, 448–451.
[46] A. L. Spek, *Acta Crystallogr. C Struct. Chem.* **2015**, *71*, 9–18.
[47] A. L. Spek, *Acta Crystallogr. D Biol. Crystallogr.* **2009**, *65*, 148–155.
[48] “Bindfit,” can be found under http://supramolecular.org,

7 Conclusion

Based on the molecular design previously established in our group, organic ligands having a curved π-surface have been synthesized. Self-assembly with Pd(II) yields coordination cages having a suitable cavity for C_{60} encapsulation. By using those coordination cages, the author had been investigating physical and chemical properties of C_{60} inside the cavities under the concepts of “Nano-confinement” and “Hierarchical assembly”. $Pd_2\mathbf{L}^{\mathbf{P}}_4$ can encapsulate C_{60} in a quantitative fashion and one-electron reduction of the confined C_{60} leads to generation of $C_{60}^{\bullet-}$ inside the cage. The generated $C_{60}^{\bullet-}$ was found to be stabilized within the cage due to nano-confinement effects. The encapsulation capability of $Pd_2\mathbf{L}^{\mathbf{P}}_4$ was further investigated towards carbon-rich aromatic molecules including C_{60} derivatives. Thanks to the curved π-surface of the ligand, two molecules of corannulene can be encapsulated inside the cavity with a temperature dependency. In addition, a variety of C_{60} derivatives can be also accommodated inside the coordination cage. The coordination cage was further proven to work as a supramolecular mask for synthesis of η^2-$C_{60}Pd(0)_n$ (n=1,2) complexes. Such complexes were found to be formed inside the coordination cage by simple addition of $Pd(0)(dba)_2$ to $C_{60}@Pd_2\mathbf{L}^{\mathbf{P}}_4$. Furthermore, a pill-shaped coordination cage, $Pd_4\mathbf{L}^{\mathbf{Q}}_6(Nap)_2$, has been synthesized. $Pd_4\mathbf{L}^{\mathbf{Q}}_6(Nap)_2$ has two pockets which allow encapsulation of two molecules of C_{60}. Thanks to the molecular design, there is a nanoscopic space in between the encapsulated C_{60}s, which can be further used for investigation of guest-incorporation in between the *outer* surfaces of two C_{60}s. Such host-guest studies have been investigated mostly in solid-state due to the difficulty of aligning C_{60} in an array. In the herein created nanoscopic space, single corannulene was found to be encapsulated via π-π interactions with the C_{60}s surrounding leading to formation of a charge-transfer complex. On the other hand, when anthracene or its derivative was entrapped in the nano-space, a Diels-Alder reaction took place yielding a host-guest complex holding C_{60} and its Diels-Alder adduct with anthracene (derivative) quantitatively. It was found that the Diels-Alder reaction has a faster reaction rate probably via stabilization of a transition state through π-π interactions with the neighboring C_{60}. Further, an evidence of the continuous Diels-Alder and its retro reaction inside the pill-shaped cage was found by 2D EXSY NMR measurements. To conclude, these results imply a potential of coordination cages as a host for the investigation of physical properties of C_{60}(s) under nano-confinement as well as in hierarchical assembly.

Abbreviations

Å	Ångström
°C	Celcius
BF_4	Tetrafluoroborate
CH_3CN	Acetonitrile
$CHCl_3$	Chloroform
COSY	Correlated spectroscopy
CS_2	Carbon disulfide
CV	Cyclic voltammetry
dba	Dibenzylidenaceton
DFT	Density Functional theory
DOSY	Diffusion ordered spectroscopy
EPR	Electron paramagnetic resonance
equiv.	equivalent
ESI-MS	Electrospray ionization mass spectroscopy
Et_2O	Diethyl ether
EXSY	Exchange spectroscopy
GPC	Gel permeation chromatography
h	Hour
HOMO	Highest occupied molecular orbital
K	Kelvin
LED	Light-emitting diode
LUMO	Lowest unoccupied molecular orbital
MeCN	Acetonitrile
MeOH	Methanol
MHz	Megahertz
m/z	Mass-to-charge ratio
mM	$mmol \bullet L^{-1}$
NIR	Near infrared region
nm	nanometer
NMR	Nuclear magnetic resonance
NOESY	Nuclear overhauser effect spectroscopy
$PC_{61}BM$	Phenyl-C_{61}-butyric acid methyl ester
ppm	Parts per million
r.t.	Room temperature
SOMO	Singly occupied molecular orbital
$TBAPF_6$	Tetrabutylammonium hexafluorophosphate
UV-Vis	Ultraviolet-visible
VT	Variable temperature

Acknowledgements:

To accomplish this Ph.D. dissertation, I have been provided countless help and support from a variety of perspectives. Here, I would like to show my acknowledgements to those people who kindly helped me.

The biggest gratitude goes to my supervisor, Prof. Dr. Guido H. Clever. He kindly accepted me as a Ph.D. student and let me follow my curiosity as a form of research. We first met in Sendai, Japan, where he delivered a plenary lecture about the beautiful “Clever chemistry”. My English was very poor at that moment, however, he listened to me attentively and gave me a lot of suggestions and advices varied from scholarship application to life in Germany. Similarly, he has given me many opportunities to talk about my research, helped me greatly with my career, shared his experience with me and so forth since I have joined this group. Although, most of my stay in Germany was under the Corona pandemic, I could fully perform my research thanks to his fine and continuous supports.

Second, I appreciate Prof. Dr. Max M. Hansmann for taking a part of the examination committee. Since I have talked with him at Tag der Chemie about my research, I had been willing to ask him to be my second examiner.

If one of the people that I have met during this study would have been lacking, I could not have accomplished this dissertation. I would like to thank Birgit Thormann and Dr. Gabriele Trötscher-Kaus for all the support and help they gave me. Thanks to them, I could spend the time in this group quite comfortably.

I would like to thank Dr. Ananya Baksi and Laura Schneider for the ESI MS measurements. I thank Prof. Dr. Wolf G. Hiller and André Platzek for help with the NMR measurements. I thank Dr. Julian J. Holstein for crystallographic analysis. I learned a lot from him. I appreciate Shari L. Meichsner and Prof. Dr. Müge Kasanmascheff for the EPR measurements and discussion. I also appreciate DESY for the access to synchrotron beam time. I thank Prof. Dr. Steffen for the access to the UV-Vis NIR absorption spectrometer. I appreciate DAAD for financial support. I am grateful to Christoph Drechsler for discussion about theoretical studies. I thank Armin Durmisevic, Christoph Drechsler, Elie Benchimol, Laura Neukirich, and Dr. Gabriele Trötscher-Kaus for polishing this thesis. I would like to thank Laura Neukirch and Dr. Gabriele Trötscher-Kaus for the contribution of the abstract in German.

I would like to thank Dr. Jacopo Tessarolo and Dr. Pedro Montes-Tolentino for staying together with me most of the time in Germany. They are colleagues, friends, brothers, and very valuable to me. If they would not have been with me, I would have left much

earlier. I would like to thank Elie Benchimol for caring me whenever I was down. The environment of the group became much brighter since he has joined this group. I really appreciate my roomies Dr. Irene Regeni and Dr. Lukas Stratmann for accommodating me for several months while I was homeless. I really enjoyed the time staying with them. I am thankful to André Platzek and Kristina Ebbert for providing food with me. I could maintain my weight thanks to them. When I would be asked what my favorite German food is someday, Kristina's Eintopf would be my answer. I would like to thank Dr. Qianqian Yan for taking a good care of me since we have started sharing our office. She always (unintentionally) made me laugh. We have also cheered each other while we had been writing dissertation.

I would like to thank my students Alicia Dullweber and Thomas Kembügler for working with me.

I appreciate everybody in the Clever group for their friendship and support.

Last but not least, I would like to thank my family for their selfless devotion since I was born. I am happier than others just because I am a child of my parents